Characterization of novel small molecule potentiators of oncolytic virotherapy

By

Ramya Krishnan

A thesis submitted to the Faculty of Graduate and Postdoctoral Studies

in partial fulfillment of the requirements for the degree of

Doctorate of Philosophy in Biochemistry

Department of Biochemistry, Microbiology and Immunology

Faculty of Medicine

University of Ottawa

Supervisors:

Dr. Jean-Simon Diallo

Dr. John C. Bell

Abstract

The use of oncolytic viruses (OVs) to selectively destroy cancer cells is poised to make a major impact in the clinic and potentially revolutionize cancer therapy. Pre-clinical and clinical studies have shown that OV therapy is safe, well-tolerated and effective in a broad range of cancers. Still, resistance due to tumour heterogeneity highlights areas for improvement in OV based therapeutics. Combining OVs and small molecules is a promising strategy to selectively enhance OV-mediated anti-tumour effects. To this end, we have previously identified the synthetic compound Viral Sensitizer 1 (VSe1) that enhances the spread of oncolytic vesicular stomatitis virus (VSVΔ51) in resistant cancer cell lines up to 1000-fold, resulting in synergistic cell killing and improved efficacy *in vitro* and *in vivo*. The electrophilic nature of VSe1 prompted us to investigate the scaffold to identify active analogs with more favourable physiochemical properties and explore structure-activity relationships (SAR). *In vitro* assays and a rational approach in the design of VSe1 analogs allowed us to identify functional groups that can be modified without hampering activity. Lead compounds created in this study based on a pyrrole scaffold increase OV growth up to 2000-fold *in vitro* and demonstrate remarkable selectivity for cancer cells over normal tissue *ex vivo* and *in vivo*. Compared to the parental VSe1, these small molecules also possess enhanced stability with reduced electrophilicity and are well-tolerated in animals, leading to reduced tumour burden and prolonged survival *in vivo* when used in combination with VSVΔ51.

It was known from previous studies that VSe1 suppresses the type I interferon response generated by cancer cells to defend against viral infection. In this study, further

investigation revealed that VSe1 and its analogs inhibit the nuclear translocation of nuclear factor kappa-light-chain-enhancer of activated B cells (NFκB), resulting in dampened transcriptional expression and secretion of IFN-β and interferon stimulated genes, thereby increasing viral replication and spread. While these findings further elucidated the effect these compounds have on the innate antiviral response, the molecular mechanisms leading to NFκB inhibition remained unclear. We used the newly generated VSe1 analogs to perform ligand-based affinity capture studies leading to the identification of glutathione-s-transferases as interacting proteins, catalytically inhibited by VSe1 and to a lesser extent by its pyrrole analogs. Further inquiry revealed that VSe1 and its analogs cause an imbalance in cellular glutathione homeostasis and increase oxidative stress, which is associated with inhibition of the nuclear translocation of NFκB. However, further studies are required to assess whether these phenomena are directly or indirectly linked.

Overall, this study highlights a novel approach to improving OV therapy by using a previously uncharacterized class of compounds that ultimately alter the innate cellular antiviral response through inhibition of NFκB.

Acknowledgements

First and foremost I would like to sincerely thank Dr. Jean-Simon Diallo for the opportunity to do a graduate degree in his lab, and for his support and mentorship over the past six years. Thank-you for always being available to talk, whether it was to discuss experiments, or offer career guidance, and for having faith in me and my abilities, especially when I did not.

I am also very grateful to Dr. John Bell for providing the opportunity to begin research in his lab as a summer student over ten years ago, which is what initiated my interest in this field and passion for scientific research.

There are several people without whom the work presented here would not be possible. I would like to thank Nader El Sayes for his invaluable contributions to the mechanism of action studies. Thank-you also to Michael Phan, Mohammed Selman and Johanne Mathieu for their contributions to these studies. I would like to thank Andrew Chen for his help with *in vivo* experiments. Thank-you to Dr. Rozanne Arulanandam, Dr. Fanny Tzelepis and Dr. Nicole Forbes for their research insights, help with planning and conducting experiments, and motivational tête-à-têtes. I would also like to thank Rozanne for taking the time to review this thesis. To all my fellow current and past Diallo lab members, thank-you for your friendship and for creating a collegial work environment. I will definitely miss working with all of you on a day-to-day basis, as well as our extra-curricular social events and infamous Christmas gift exchanges. To my colleagues from the Cancer Centre, thank-you for your comments and input at lab meetings and work-in-progress meetings, as well as for fostering a friendly and collaborative work environment. Thank-you

also to the members of my thesis advisory committee, Dr. Christopher Boddy, Dr. Douglas Gray and Dr. Tommy Alain for their supportive advice and thought provoking discussions during meetings.

This body of work is the product of close collaborations with several labs. I was very fortunate to work with Dr. Mark Dornan and Andrew Macklin to develop this project. I would also like to thank their respective supervisors, Dr. Boddy and Dr. Jeffrey Smith for their indispensable insights into various aspects of this project. Thank-you to other members of the Boddy and Smith labs, including (but not limited to) Graham Heberlig, Jesse Brown, Kristy Scarfone, and Carlos Canez for their contributions to this project. The GST inhibition experiments and measurement of GSH/GSSG by HPLC would not have been possible without Hilary Groom from Dr. David Josephy's lab and Dr. David Patten from Dr. Mary-Ellen Harper's lab, respectively. Thank-you to Hilary, David, Dr. Josephy and Dr. Harper for helping us conduct these experiments and for their valuable discussions.

Finally I would like to thank my parents, Usha and Krishnan, and my brother, Anish for their love, patience, and support. My decision to pursue research can be attributed to your encouragement, the importance you have always given to education, fulfilling one's potential, and your faith in my abilities.

Table of Contents

List of Abbreviations Used

3-ATZ	3-amino-1,2,4-triazole
7-AAD	7-aminoactinomycin
AAV	adeno-associated virus
ABPP	activity-based protein profiling
αMEM	Minimum Essential Medium Alpha modification
AP-1	activator protein 1
ARE	antioxidant response element
ATCC	American Type Culture Collection
ATF-2	activating transcription factor-2
ATP	adenosine triphosphate
Blimp1	B lymphocyte-induced maturation protein 1
BSA	bovine serum albumin
BSO	buthionine sulfoximine
CBP	CREB-binding protein
CDDO-Me	bardoxolone methyl ester
CDNB	1-chloro-2,4-dinitrobenzene
C-H_2DCFDA	6-carboxy-2',7'-dichlorodihydrofluorescein diacetate
ChIP	chromatin immunoprecipitation
CREB	cyclic-AMP-response element-binding protein
CTL	cytotoxic T-lymphocytes
CTLA-4	CTL-associated protein 4
Cys	cysteine
DEF	diethyl fumarate
DEM	diethyl maleate
DMEM	Dulbecco's Modified Eagle's Medium
DMF	dimethyl fumarate
DMM	dimethyl maleate
DMSO	dimethyl sulfoxide
DNA	deoxyribonucleic acid
DTT	dithiothreitol
ECMV	encephalomyocarditis virus
ELISA	enzyme-linked immunosorbent assay
EMSA	electromobility shift assay
FACS	fluorescence-activated cell sorting
FBS	fetal bovine serum
FLuc	firefly luciferase
GAPDH	glyceraldehyde-3-phosphate dehydrogenase
GBP3	guanylate binding protein 3
GCL	g-glutamyl cysteine synthetase/ligase

GCLC	g-glutamyl cysteine synthetase/ligase catalytic subunit
GCLM	g-glutamyl cysteine synthetase/ligase modifier subunit
GFP	green fluorescent protein
GMCSF	granulocyte-monocyte colony stimulating factor
GPx	glutathione peroxidase
GR	glutathione reductase
Grx	glutaredoxin
GS	glutathione synthase
GSH	glutathione
GSSG	glutathione disulfide
GST	glutathione S-transferase
H_2O_2	hydrogen peroxide
HDAC	histone deacetylase
hDCT	human dopachrome tautomerase
HEPES	4-(2-hydroxyethyl)-1-piperazineethanesulfonic acid
HER2	human epithelial growth factor receptor 2
HIV	human immunodeficiency virus
HMOX-1	heme oxygenase 1
$HO^{\bullet}$	hydroxyl radical
HPLC	high-performance liquid chromatography
HSV-1	herpes simplex virus, type 1
IVC	infected cell vaccine
IFI44	interferon induced protein 44
IFIT3	interferon-induced protein with tetratricopeptide repeats 3
IFITM	interferon-induced transmembrane protein
IFN	interferon
IFNAR	interferon α/β receptor
IκB	inhibitor of κB
IKK	inhibitor of IκB
IL-6	interleukin-6
IL-12	interleukin-12
IP	intraperitoneal / immunoprecipitation
IRF	interferon regulatory factor
ISG	interferon stimulated gene
ISGF3	interferon stimulated gene factor 3
ISRE	interferon stimulated response element
IT	intratumoural
JAK	janus kinase
JNK	c-Jun N-terminal kinase
Keap1	Kelch-like ECH-associated protein-1
LC-MRM	liquid chromatography-mass spectrometric multiple reaction

	monitoring
LC-MS	liquid chromatography-mass spectrometry
LDLR	low density lipoprotein receptor
LGP2	laboratory of genetics and physiology 2
mAB	monoclonal antibody
MAPK	mitogen-activated protein kinases
MDA5	melanoma differentiation-associated antigen 5
MG1	Maraba MG1 virus
MMF	monomethyl fumarate
MOI	multiplicity of infection
MVA	modified Vaccinia Ankara virus
MX2	murine myxovirus resistance 2
NADPH	nicotinamide adenine dinucleotide phosphate
NFκB	nuclear factor kappa-light-chain-enhancer of activated B cells
NIH	National Institutes of Health
NK	natural killer
$NO^{\bullet}$	nitric oxide radical
NRF2	nuclear factor (erythroid-derived 2)-like 2
$O2^{\bullet-}$	superoxide anion
$ONOO^{-}$	peroxynitrite
OSGIN	oxidative stress induced growth inhibitor
OV	oncolytic virus
PAMP	pathogen-associated molecular patterns
PD-1	programmed cell death 1 protein
PD-L1	PD-1 ligand 1
PFU	plaque forming units
PRD1-BF1	positive regulatory domain I binding factor 1
RHD	Rel homology domain
RIG-I	retinoic acid-inducible gene I
RLR	RIG-I-like receptors
RLU	relative light units
RNA	ribonucleic acid
RNAi	RNA interference
RNS	reactive nitrogen species
ROS	reactive oxygen species
RPMI	Roswell Park Memorial Institute medium
RT-qPCR	quantitative real-time polymerase chain reaction
SDS-PAGE	sodium dodecyl sulfate - polyacrylamide gel electrophoresis
siRNA	small interfering RNA
SLC7A11	solute carrier family 7 member 11
STAT	signal transducer and activator of transcription

TAA	tumour-associated antigen
TIL	tumour infiltrating leukocytes
TK	thymidine kinase
TKi	tyrosine kinase inhibitor
TLR	Toll-like receptor
TNF-α	tumour necrosis factor alpha
TNFR	tumour necrosis factor receptor
T-VEC	Talimogene laherparepvec
TYK	tyrosine kinase
UV	ultraviolet
UV-Vis	ultraviolet–visible spectroscopy
VEGF	Vascular endothelial growth factor
VEU	viral expression unit
VHL	von-Hippel Lindau
VSe	viral sensitizer
VSV	vesicular stomatitis virus
WT	wild-type

List of Figures

List of Tables

Copyright Statement

This thesis contains published and unpublished work.

Parts of the Introduction, Materials and Methods, Figures 6, 7, 9-22, 25, 26, Table 5,

associated figure legends and text, and Discussion are included in the following publication:

> Dornan MH[1], **Krishnan R[1]**, Macklin AM[1], Selman M, El Sayes N, Son HH, Davis C, Chen A, Keillor K, Le PJ, Moi C, Ou P, Pardin C, Canez CR, Le Boeuf F, Bell JC, Smith JC, Diallo JS, Boddy CN. "First-in-class small molecule potentiators of cancer virotherapy." *Scientific Reports*. 26;6:26786 (2016) doi: 10.1038/srep26786.
>
> [1]Equal contribution

Some modifications to the text and formatting of figures and tables have been made in this

thesis. The original article is attached as Appendix D and is also available here:

https://www.nature.com/articles/srep26786.

Parts of the text from section 1.3.1 in the Introduction are taken from

> Forbes NE, **Krishnan R**, Diallo JS. "Pharmacological modulation of anti-tumor immunity induced by oncolytic viruses." *Frontiers in Oncology* 4, 191 (2014) doi: 10.3389/fonc.2014.00191.

Some minor modifications have been made to the text. The original article is attached as Appendix E and is also available here:

https://www.frontiersin.org/articles/10.3389/fonc.2014.00191/full

Introduction

1.1 Cancer

According to the Canadian Cancer Society, 1 in 2 Canadians will develop some form of cancer and 1 in 4 will eventually succumb to the disease making it the leading cause of death in Canada[1]. The impact of cancer goes beyond just that of patient mortality and morbidity, but also affects the lives of family members and caregivers, and is a significant burden on the health care system. Over the past 30 years, survival rates for many cancer types have significantly improved, due to advances in efforts to better prevent, detect, and diagnose malignancies[1]. Still, low survival rates for cancers such as lung, pancreatic and ovarian cancers[1], and high recurrence rates due to resistance to first and second-line therapies[1] demonstrate the need for more effective therapeutic agents.

Cancer has been traditionally characterized as the rapid and uncontrolled growth of cells. While the start of the modern era of cancer research can be traced back to the late 19th century[2], our understanding of this complex and multifactorial disease is continuously being revised. The fundamental properties of this disease are perhaps best delineated by eight properties outlined by Dr. Hanahan and Dr. Weinberg called the Hallmarks of Cancer: (1) sustained proliferative signaling, (2) evasion of growth suppressors, (3) activation of invasion and metastasis, (4) replicative immortality, (5) induction of angiogenesis, (6) resistance to cell death, (7) dysregulated cellular energetics and metabolism and (8) evasion of detection and destruction by the immune system[3]. An underlying state of genomic instability, leads to mutations that drive the manifestation of these hallmarks. Activating mutations in genes that drive cellular transformation and proliferation can promote

tumourigenesis[4]. Such genes are termed proto-oncogenes and their mutated, pro-tumourigenic forms are known as oncogenes[4]. Conversely, inactivating mutations in tumour suppressor genes that normally restrict cellular proliferation can also support tumour development[4,5].

1.1.1. NFκB

The transcription factor nuclear factor kappa-light-chain-enhancer of activated B cells (NFκB) is activated by several oncogenes such as human epithelial growth factor receptor 2 (HER2/Neu), and is negatively regulated by tumour suppressors such as von-Hippel Lindau (VHL)[6,7]. NFκB plays an essential role in a variety of cellular processes, including the antiviral response, cell cycle regulation, proliferation, cell death, inflammation and response to oxidative stress[8]. It is a homo or hetero-dimer of five potential subunits: RelA/p65, p50 , RelB, p52 and c-Rel[8]. All subunits contain a Rel homology domain (RHD) that facilitates the formation of homo- or heterodimers prior to DNA binding[9]. P65, RelB and c-Rel also contain a transactivation domain that is required for transcriptional activity[9]. Activation of NFκB can occur through a canonical or non-canonical pathway. The canonical pathway leads to the activation of the p65-p50 dimer[8]. In the absence of stimuli, the dimer is sequestered in the cytoplasm by inhibitor of κBα (IκBα)[10]. Upon upstream activation of this pathway, IκBα is degraded and the p65-p50 dimer translocates to the nucleus to initiate transcription of target genes[8,10]. Activation of this pathway, as well as the role of NFκB in the antiviral response, is described in more detail in section 1.2.3. NFκB is found to be constitutively active in many tumours, in part due to the aberrant over-activation of

upstream regulators, and it has been implicated in the development of several Hallmarks of Cancer[11,12]. NFκB contributes to the pathogenesis of a diverse set of cancer types that include but are not limited to leukemia, lymphoma, multiple myeloma, glioblastoma, prostate cancer, breast cancer, colon cancer, and renal cell carcinoma (RCC)[11–13]. In RCC, the overexpression of NFκB can be attributed to its dysfunctional regulation conferred by mutations in the VHL gene[6,14]. Mutated VHL is a chief risk factor for developing clear cell RCC, which makes up 70-80% of all RCCs[6]. In a meta-analysis carried out on clear cell RCC gene expression datasets from human patients, loss of VHL expression correlated strongly with the appearance of NFκB gene signatures[15]. In addition to promoting tumour growth, NFκB is also involved in the development of resistance to chemotherapy by inducing the expression of the drug efflux pump multidrug resistance 1 (MDR1)[16,17]. Its undeniable role in promoting tumourigenesis and resistance to therapy has made NFκB a popular target in anti-cancer drug development. The drug bortezomib is a ubiquitin-proteasome inhibitor that is approved for the treatment of multiple myeloma and multiple mantle cell lymphoma[18]. While it is not a specific inhibitor of NFκB, one of its proposed mechanisms of action is that it abolishes NFκB signaling by inhibiting the degradation of IκBα[18,19]. This effect may not be applicable to all cell types and proteasome inhibitors, as some groups have shown that certain proteasome inhibitors can activate NFκB in some cell lines[20–22]. Numerous specific inhibitors of the NFκB pathway have been under pre-clinical development for decades, however none have yet been approved for clinical use[12,18].

1.1.2. Therapeutic challenges with current cancer treatments

Historically, radiation and cytotoxic chemotherapy have been the mainstay of non-surgical anti-cancer therapeutic modalities. The rationale for these therapies is that they interfere with DNA synthesis and repair, thus targeting genomically unstable, rapidly dividing cells[23,24]. Such therapies are effective to a certain extent. For example, survival rates for non-Hodgkin's lymphomas vary widely depending on the type of lymphoma, stage, and patient age. According to one systematic review, the standard cocktail of chemotherapy drugs known as CHOP 21 (cyclophosphamide, doxorubicin, vincristine and prednisolone, given at 21-day cycles) induced complete response rates between 37-85%, with overall survival at 5 years ranging from 38-51%[25]. A meta-analysis of adjuvant chemotherapy regimens for early-stage breast cancer in 100 000 women from 123 randomized trials found that on average, the use of chemotherapy was associated with a one-third reduction in 10-year mortality[26]. However, cancer recurrence and relapse can occur due to tumour heterogeneity and the selection pressure on residual cancer cells, leading to the formation of treatment-resistant tumours with mutations in DNA repair pathways[23]. It is also well documented that these therapies cause adverse reactions, primarily due to off-target effects on non-cancerous cells that also have rapid turnover, such as erythrocytes, leukocytes and epithelial cells that maintain mucosal membranes. Debilitating side effects that can occur include nausea, vomiting, diarrhea, myelosuppression, mucositis, alopecia and cutaneous reactions[23,24,27–29]. Efforts to develop more targeted therapies for certain types of cancers have led to game-changing treatments such as hormonal therapies for estrogen and progesterone receptor positive breast

cancers,[30,31] monoclonal antibodies (mAbs) against overexpressed tumour antigens[32], drug-conjugated mAbs[33], receptor tyrosine kinase inhibitors (TKis)[34], and angiogenesis inhibitors[35,36]. Still, resistance to these agents has been observed, mediated through similar mechanisms responsible for resistance to cytotoxic chemotherapy, such as alterations in target expression, increased drug efflux and metabolism, activation of cell survival pathways, and insensitivity to apoptosis[37]. These agents also cause significant adverse effects such as increased risk of thrombotic events, endocrine-related aberrations, myelosuppression, and edema, secondary to treatment with angiogenesis inhibitors or TKis[38–40]. Thus, a concerted effort is being made to find more effective anti-cancer therapies that are better tolerated.

More recently, research efforts have shifted focus towards harnessing the power of the immune system to control malignancies. The rise of cancer immunotherapy has been driven by progress in our understanding of how cancer evades the immune system and how it can be re-programmed to fight tumour growth[41]. The immune system plays a pivotal role in fighting cancer through the recognition and eradication of transformed cells. However, chronic inflammation and tumour immunoediting give rise to an immunosuppressive tumour microenvironment, promoting tumour progression and resistance to anti-tumour immune responses[41–44]. As our understanding of the mechanisms of cancer-related immunosuppression grows, so too does our ability to design therapies to combat these mechanisms. The cancer immunoediting hypothesis describes a process by which extrinsic immune pressure on tumours can block tumour growth, but in some cases can promote the formation of immune-resistant tumours[45]. Cancer immunoediting is characterized by three

phases: elimination, equilibrium and escape. In the first phase of elimination, transformed cells are detected and eliminated by components of the innate (e.g. natural killer (NK) cells) and adaptive (e.g. antigen-specific cytotoxic T-lymphocytes; CTLs) immune system[45]. The second phase, equilibrium, occurs as a result of the immune system being able to eliminate the entire population of transformed cells. The tumour enters a dormant phase, where the immune system is able to prevent tumour growth, yet a subpopulation of transformed cells persists[46]. The cells that persist are insensitive to the immune onslaught, often through evolved defects in antigen presentation or apoptotic pathways[47]. Eventually, the immune system is no longer able to keep tumour growth at bay, leading to the final phase, escape from immune surveillance and the appearance of clinically detectable tumours[45]. This can happen as a result of loss of antigen presentation, upregulation of inhibitors of CTL responses (e.g. CTL-associated protein 4 (CTLA-4), programmed cell death 1 protein (PD-1), and its ligand, PD-1 ligand 1 (PD-L1)) and the infiltration of immunosuppressive cells into the tumour microenvironment (e.g. myeloid derived suppressor cells (MDSCs) and regulatory T-cells)[47].

It is well documented that through processes such as cancer immunoediting, tumours can acquire mutations in the type I interferon (IFN) pathway[45]. Type I IFNs have very well-defined roles in the response to viral infection (described in sections 1.2.3 and 1.2.4). However, they also possess pleiotropic functions in controlling tumour growth by promoting cell growth arrest, inducing cell death, inhibiting angiogenesis, and stimulating innate and adaptive anti-tumour immune responses[48]. As tumours evolve to escape immune control, they often acquire defects in the type I IFN pathway, and this has been

associated with poor prognosis[49–52]. Several therapeutic modalities have been developed to exploit the anti-tumour properties of type I IFNs, including exogenous administration of type I IFN (IFN-α2b), treatment with inducers of endogenous IFN (e.g. polyribosinic-polyribocytidylic acid (Poly(I:C)), imiquimod), and gene therapy with viral vectors[48]. IFN-α2b and imiquimod are both approved for use in human patients[53,54].

Immune checkpoint inhibitors are drugs that target molecules that block T cell activation. Specifically, these are inhibitors of the aforementioned molecules CTLA-4, PD-1, and PD-L1. Clinical responses to these therapies have been remarkable, leading to complete tumour regression and improved survival in some solid tumour types and hematological malignancies[55]. Still, relapse and disease progression occurs in some patients, indicating that there is room for improvement, possibly through combinatorial strategies[56]. Another exciting development in this field is the recent FDA approval of chimeric antigen receptor T cells (CAR T cells) for diffuse large B-cell lymphoma and B-cell acute lymphoblastic leukemia[57,58]. In CAR T cell therapy, a patient's own T cells are engineered to target a specific tumour-associated-antigen and infused back into the patient (part of an overarching immunotherapy strategy known as adoptive cell transfer)[41]. The approved CAR T cell therapies target the CD19 receptor, which is highly expressed on B cells.

1.2 Oncolytic viruses for cancer therapy

Hallmark changes in cancer cells fuel cell growth via altered cellular energy metabolism and allow cancer cells to resist apoptosis and avoid detection and destruction by the immune system. Altogether, this makes tumours ideal microenvironments for viral

replication, rendering them uniquely vulnerable to viral infection and lysis[59,60]. Oncolytic viruses (OVs) are multi-mechanistic biotherapeutic agents that destroy tumours by inducing direct lysis of cancer cells, expression of therapeutic transgenes, vascular shutdown of tumour-associated blood vessels, and generation of an anti-tumour immune response[59–61].

The notion that viruses could be used to treat cancer stems from observations at the turn of the 20th century that cancer patients who naturally contracted viral infections went into temporary remission[62,63]. Since then, viruses have been investigated as anti-cancer agents with fluctuating interest, until a resurgence in the 1990s, following significant advancements in viral engineering[63]. A diverse set of viral platforms have been investigated for their oncolytic potential. Virus families of note include poxviridae, adenoviridae, herpesviridae, paramyxoviridae, reoviridae, rhabdoviridae, picornaviridae, and togaviridae[61]. In 2005, the oncolytic adenovirus H101 became the first oncolytic virus to be approved for use in humans, for the treatment of head and neck cancers in China[64]. Interest in the development of OVs as targeted cancer therapeutics has skyrocketed over the past few years, with the emergence of positive clinical trial data and the recent approval of the herpes simplex virus type 1 (HSV-1)-based talimogene laherparepvec (T-VEC; IMLYGIC®) in the United States[65–67]. An area of high interest is the use of OVs in combination with other modalities of cancer therapy, including cytotoxic chemotherapy, targeted therapies and novel immunotherapies. This is discussed further in section 1.3.1.

1.2.1 Selectivity of oncolytic viruses towards cancer cells

OVs preferentially target cancer by exploiting multiple tumour-specific defects. Some specificity for the preferential infection of tumours is conferred by the aberrant over-expression of cell surface receptors that facilitate viral entry. For example, measles virus binds to CD46 and nectin-4, both of which are upregulated in many types of cancers[68–72]. Dysregulated cellular metabolism prevalent in cancer cells also provides a supportive environment for viral replication. Due to high metabolic demands, cancer cells favour the generation of ATP through glycolysis, as opposed to mitochondrial oxidative phosphorylation, a phenomenon known as the Warbug effect[73]. The precise reason for this has not been clearly elucidated, but one theory is that switching to the glycolytic pathway also increases pools of precursors of nucleotides and amino acids, thus fueling tumour growth. This would also promote viral growth, and several viruses have been shown to induce this glycolytic switch, including measles and vaccinia virus[73,74].

Through engineering or experimental selection, OV tropism for cancerous tissue over normal tissue can be further enhanced compared to wild-type viruses. For example, T-VEC contains a deletion in the gene encoding for neurovirulence factor Infected cell protein 35.4 (ICP35.4). ICP35.4 prevents the shutdown of host cell translation induced by viral infection by promoting the dephosphorylation of eukaryotic initiation factor eIF2α, thus allowing the translation of viral proteins to continue[75]. In doing so, ICP35.4 also opposes the function of protein kinase R (PKR), an enzyme that is activated by the presence of double-stranded RNA and subsequently works to limit cell growth and initiate antiviral pathways, such as through the phosphorylation of eIF2α[75–77]. Without this gene, the replication of

HSV-1 is largely restricted to cells that overexpress eIF2α and have dysfunctional PKR signaling, which is common in tumour cells[78,79]. Increased specificity of HSV-1 towards cancer cells can also be conferred by targeting the viral ICP0 gene, a ubiquitin E3 ligase that targets host proteins for degradation[78]. Many ICP0-targeted proteins are involved in the induction of a type I IFN-mediated antiviral response, thus HSV-1 variants containing ICP0 mutations (such as oncolytic HSV-1 N212) are particularly sensitive to type I IFN[80]. As described in section 1.1.2, the type I IFN pathway is often dysregulated in cancer cells, thus ICP0 mutations confer enhanced selectivity for cancer cells over non-cancerous cells which retain intact type I IFN-mediated antiviral signaling[78].

The list of virulence genes that have been deleted or modified to improve the selectivity of OVs for cancer cells is extensive. By no means an exhaustive list, genes that have been modified in some of the OV platforms that have undergone clinical testing include viral thymidine kinase (TK; vaccinia virus, HSV-1), ICP6 (HSV-1), α47 (HSV-1), E3 and E1A (adenovirus)[67]. The rhabdovirus vesicular stomatitis virus (VSV) has undergone extensive pre-clinical testing for almost two decades and has also been genetically engineered in a variety of ways to specifically replicate in cancer cells[81–83].

1.2.2 Vesicular stomatitis virus

VSV is a bullet-shaped, single stranded negative-sense RNA virus with an 11 kilobase genome that encodes for five proteins: nucleocapsid (N), large protein (L), phosphoprotein (P), glycoprotein (G), and matrix protein (M)[84]. The RNA genome is encapsidated by N proteins and associated with the viral RNA dependent RNA polymerase (RdRp), comprised

of the L and P proteins[84]. This complex is surrounded by the M protein and host-derived lipid bilayer in which the transmembrane G protein is anchored[84]. The G protein plays a crucial role in viral entry and budding from host cells[84]. VSV enters target cells upon binding of the G protein to low-density lipoprotein receptors (LDLR) and LDLR family members on the cell surface, followed by clathrin-mediated endocytosis[85]. A drop in endosomal pH triggers fusion of the viral and endosomal membrane, uncoating and release of the viral genome into the cytoplasm[84]. Here, the RdRp uses the negative-sense viral RNA as a template for primary transcription of positive-sense mRNAs for each gene, which are translated by host ribosomes[84]. The resulting viral proteins synthesize complimentary negative-sense viral RNA genomes that are used as templates for further viral replication, secondary transcription or are assembled into infectious particles[84]. Infectious viral progeny are formed when virions bud out of the host at sites on the plasma membrane enriched in VSV G protein, with this host plasma membrane serving as a new viral envelope[84]. VSV M protein also facilitates viral budding and has several roles that are crucial to VSV replication. In particular, it blocks host gene expression by inhibiting the transcription and nuclear export of host mRNAs[84,86–90]. The early events of VSV's life cycle (binding, endocytosis, uncoating and primary transcription) occur within a few hours after infection[84]. The subsequent steps of genome replication, secondary transcription and progeny virion assembly occur over the next 12-18 hours[84].

1.2.3 The type I Interferon response: Induction of type I interferon

The innate immune response is the body's first line of defence against pathogens such as viruses. At the molecular level, type I interferon (IFN) plays a major role in the response to viral infection. Type I IFNs include IFN-β as well as multiple isoforms of IFN-α. The former is ubiquitously expressed, while the latter are primarily produced by hematopoietic cells and plasmacytoid dendritic cells[91–94]. The induction of type I IFNs is typically initiated through the stimulation of pattern recognition receptors (PRRs). PRRs are stimulated by the recognition of pathogen-associated molecular patterns (PAMPs), which include microbial glycoproteins, lipopolysaccharides, proteoglycans, and nucleic acid motifs[95]. PRRs can be separated into families according to ligand specificity and cellular localization. A major class of PRRs activated by viral infection are Toll-like receptors (TLRs). TLRs are transmembrane glycoprotein receptors that are stimulated by a variety of PAMPs and can be found in intracellular compartments as well as at the cell surface[96]. For example, TLR7 recognizes single-stranded viral RNA motifs and is primarily located in the endoplasmic reticulum. Upon stimulation, it migrates to endosomes and downstream signaling processes are initiated[96]. TLR7 is known to sense several RNA viruses, including influenza A virus, human immunodeficiency virus, Dengue virus and VSV[96]. VSV has also been shown to trigger TLR4 signaling through its G protein[97].

VSV is also recognized by another class of PRRs: retinoic acid-inducible gene I (RIG-I)-like receptors (RLRs). RLRs are located in the cytosol and include RIG-I, melanoma differentiation-associated antigen 5 (MDA5), and laboratory of genetics and physiology 2 (LGP2)[96]. Both RIG-I and MDA5 bind to viral RNA motifs, although it is thought that VSV is

preferentially recognized by RIG-I[96,98]. LGP2 is thought to modulate antiviral signaling by interacting with RIG-I and MDA5[96,99].

TLRs and RLRs differ in the manner and location in which they are stimulated, leading to the recruitment of various adapter molecules. Ultimately, these pathways converge to activate three key signaling pathways: mitogen-activated protein kinases (MAPKs), interferon regulatory factors (IRFs), and NFκB (**Figure 1**). Transcription factors activated in these pathways bind to the *IFNB* enhanceosome and are necessary for maximal induction of IFN-β expression[100,101]. Activation of the MAPK pathway via TLRs and RLRs can lead to the activation of c-Jun terminal kinase (JNK), which phosphorylates and activates activator protein 1 (AP-1), a heterodimeric transcription factor[102–104]. The AP-1 heterodimer is comprised of c-Jun and activating transcription factor-2 (ATF-2) and induces the transcription of pro-inflammatory cytokines as well as IFN-β[105,106]. IFN-β is also induced by IRFs. Of the nine IRF family members, IRF3 and IRF7 play key roles in initiating an antiviral response via TLR signaling[105]. IRF3 is constitutively expressed and thus largely responsible for the first wave of type I IFN production[107,108]. IRF7 is present at low levels in most cell types and is induced upon virus infection following the first wave of type I IFN production to induce various subtypes of IFN-α[108]. However, there is evidence in mouse embryonic fibroblasts that IRF7 is necessary for IFN-β production as well[109]. Once triggered, TLRs and RLRs will initiate molecular cascades resulting in the phosphorylation of IRF3 and IRF7, causing them to form hetero- or homodimers[91]. These dimers translocate to the nucleus, form a complex with the co-activators CBP (cyclic-AMP-response element-binding protein (CREB)-binding protein) or p300 and bind to the promoter regions of *IFNβ* and *IFNα*

isoforms to initiate their transcription in cooperation with other transcription factors or coactivators[105].

In addition to its role in cancer (explained previously in section 1.1.1), the transcription factor NFκB is a pivotal coordinator of the IFN response. As mentioned previously, NFκB transcription factors are hetero- or homodimers that are comprised of two of five possible subunits: RelA/p65, p50, RelB, p52 and cRel. Prior to activation, dimers are sequestered in the cytoplasm by the inhibitor of κB (IκB) family of proteins. IκBs are characterized by the presence of ankyrin repeats which facilitate binding to and inhibition of the DNA binding domains of NFκB[8,110]. Activation of NFκB-mediated transcription can occur through canonical or non-canonical pathways. The non-canonical pathway is mainly activated by stimuli involved in cell differentiation and development through the tumour necrosis factor receptor (TNFR) and affects lymphoid organ development and the adaptive immune response[111]. It may also negatively regulate the type I IFN response by regulating histone modifications and the recruitment of p65 to the IFN-β promoter[112]. Upon TNFR stimulation, NFκB kinase (NIK) phosphorylates IκB kinase alpha (IKKα), which in turn phosphorylates p100, the precursor to NFκB subunit p52 and inhibitor of RelB. Due to the presence of ankyrin repeats, p100 is considered to be an IκB protein as well[113]. Once p100 is phosphorylated, the ankyrin repeats are cleaved, yielding p52. The resulting p52-RelB dimer is transcriptionally active and translocates to the nucleus to initiate transcription of its targets[8].

The canonical pathway is responsible for the induction of type I IFN transcription and leads to the activation of a p65-p50 heterodimer[8]. As mentioned previously, in the

absence of stimuli, the p65-p50 heterodimer is sequestered in the cytoplasm by IκBα[10]. TLR and RLR stimulation activates the IκB kinase (IKK) complex, which consists of IKKα, IKKβ and IKKγ[114,115]. IKKα and IKKβ possess kinase activity and IKKγ (also known as NFκB essential modulator, or NEMO) is a regulatory subunit[116,117]. The activated IKK complex phosphorylates IκBα at serines S32 and S36, targeting it for ubiquitination and proteasomal degradation[114,115,118]. The liberated p65-p50 dimer is then able to translocate to the nucleus and initiate transcription of target genes. Following phosphorylation of IκBα, IKKβ also phosphorylates p65 at S536 in its transactivation domain, which enhances its transactivation[119].

NFκB activation and transcriptional activity as described above has been shown to occur as soon as 2 hours following virus inoculation at a high multiplicity of infection (MOI)[120–123]. There is also a low level of constitutive activity that is responsible for maintaining a basal level of IFN-β that is necessary for timely autocrine IFN-β signaling[124]. In $p65^{-/-}$ murine embryonic fibroblasts (MEFs), *Ifnb* and ISG induction and was significantly delayed in response to VSV or Newcastle disease virus infection[125,126]. NFκB is the primary driver of *IFNβ* transcription in the early stages of viral infection and stabilizes interaction of CBP/p300 at the enhanceosome[124]. Once IRF3 and IRF7 are present and interact with CBP/p300, these transcription factors power the expression of *IFNβ*. In this later stage of infection, NFκB is less important for IFN-β production and instead has a more important role in regulating the expression of chemokines, matrix metalloproteinases, proteins involved in antigen processing, and proteins with pro-inflammatory roles[124,126].

1.2.4 The type I interferon response: Induction of interferon stimulated genes

Once secreted, type I IFN elicits pleiotropic autocrine and paracrine effects through its cognate receptor. The type I IFN receptor (IFNAR) is composed of two subunits, IFNAR1 and IFNAR2[127]. IFNAR is associated with the protein tyrosine kinases Janus kinase 1 (JAK1) and tyrosine kinase 2 (TYK2). When type I IFN binds to IFNAR, it triggers the autophosphorylation of JAK1 and TYK2, causing the recruitment and phosphorylation of signal transducer and activator of transcription 1 and 2 (STAT1 and STAT2)[128]. STAT1 and STAT2 dimerize and associate with IRF9, forming a complex known as IFN-stimulated gene factor 3 (ISGF3)[105,129]. ISGF3 translocates to the nucleus and binds to DNA sequences known as IFN-stimulated response elements (ISREs)[91,130]. This leads to the expression of over a hundred different IFN-stimulated genes (ISGs) whose products combat viral infection by interfering with various stages of the virus life cycle, including viral entry, uncoating, endocytic trafficking, translation of viral mRNAs and budding[131]. For example, murine myxovirus resistance 2 (MX2) inhibits the capsid of human immunodeficiency virus-1 (HIV-1), limiting nuclear entry of the viral genome[132,133]. MX2 has also been shown to limit VSV infection[134]. IFN-induced transmembrane (IFITM) proteins limit the entry of viruses including VSV, possibly by altering membrane properties and the kinetics of endosome fusion[135,136]. The initial wave of type I IFN produced by most cells in response to virus consists of IFN-β and IFN-α4[100,105,108,137] (with the exception of plasmacytoid dendritic cells, which produce mostly IFN-α isoforms[100,138,139]). JAK-STAT signaling further induces these IFNs and various IFN-α subtypes, generating a positive feedback loop and a second wave of type I IFN production[140,141].

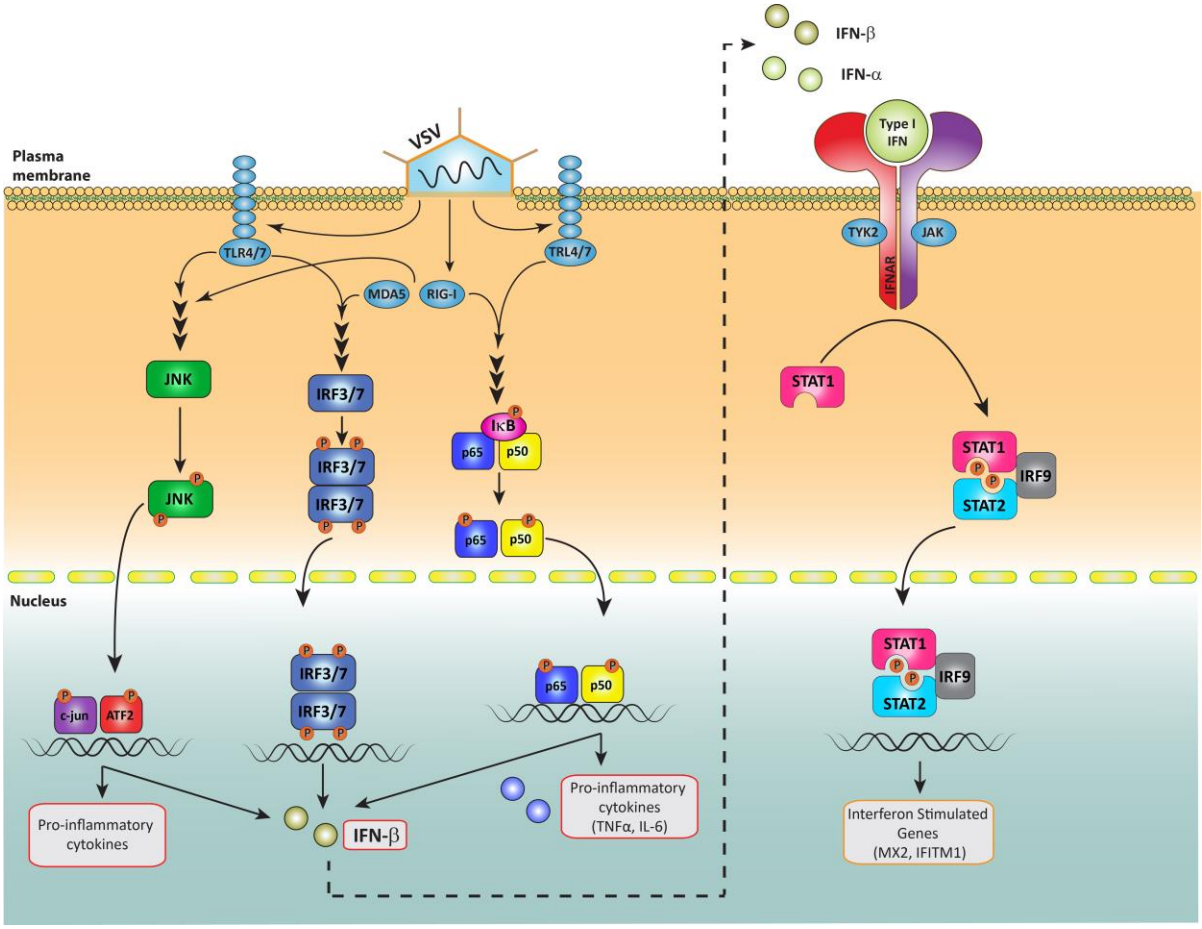

Figure 1. Pathways regulating the production and response to type I IFN. (Adapted from Nader El Sayes, MSc Thesis)

1.2.5 VSV as an OV candidate

VSV has broad tissue tropism, demonstrated by its ability to infect a wide range of cell types, giving it wide applicability as an anti-cancer therapeutic. This is likely due to the fact that its putative receptor, LDLR and its related family members, are expressed ubiquitously by mammalian cells, with the exception of quiescent T cells, B cells and hematopoietic stem cells[142]. This tropism makes it possible for VSV to infect non-cancerous tissues as well. While an effective oncolytic agent, wild-type VSV has been shown to cause neurotoxicity in animal models[81,143–145]. Efforts to attenuate VSV while maintaining its

oncolytic effect have largely focused on increasing its specificity for cells with defective type I IFN. VSV is a potent inducer of type I IFN and downstream signaling. Normally, this response is triggered in infected cells and rapidly spreads to neighbouring cells to protect them from infection. As previously stated, a large number of tumour types and cancer cell lines have defects in type I IFN signaling and are thus vulnerable to VSV oncolysis[146]. As mentioned above, VSV M blocks host gene expression, and in doing so blunts a non-cancerous cell's ability to produce and respond to type I IFN. The genetically attenuated variant known as VSVΔ51 contains a deletion of the 51st amino acid in the M protein which hinders its ability to block host antiviral gene expression[146]. Thus, VSVΔ51 has an improved safety profile over its wild-type counterpart[146], as normal cells with intact antiviral responses can resist infection and cancer cells with defective antiviral responses are more susceptible to viral infection and oncolysis.

Another mechanism of VSVΔ51-mediated tumour eradication is the induction of tumour vasculature collapse[147]. VSVΔ51 is able to limit tumour perfusion through direct infection of tumour-associated vasculature and recruitment of neutrophils, which leads to intratumoural coagulation[148,149]. Upon further examination, it was found that vascular endothelial growth factor (VEGF; a major driver of tumour neovascularization and metastasis that is overexpressed in many solid tumours[150,151]), sensitized endothelial cells to infection by several type I IFN-sensitive viruses, including VSVΔ51, through the upregulation of PRD1-BF1/Blimp1, which suppresses type I IFN-mediated signaling pathways[152]. Blimp1 expression was found to be significantly higher in tumour vasculature compared to vasculature from normal tissues, and was dependent on VEGF signaling[152].

In addition to causing cell lysis and destruction of tumour vasculature, VSVΔ51 induces a potent anti-tumour immune response that contributes to the eradication of tumours[153–157]. This is partly due to the type I IFN response induced following virus infection, which creates an immunostimulatory environment and recruits innate immune effector cells such as neutrophils and NK cells to the tumour site[158,159]. Additionally, virus-mediated cell lysis results in the release of tumour-associated antigens (TAAs), PAMPs, and danger-associated molecular patterns (DAMPs), resulting in the activation of antigen-presenting cells and the subsequent generation of tumour-specific $CD8^+$ T cells that drive an adaptive immune response against the tumour[153,160,161]. Due to its immunostimulatory properties, VSVΔ51 has been used to successfully eradicate tumours in pre-clinical models as part of two innovative therapeutic platforms: an infected-cell vaccine (ICV) and a heterologous prime-boost strategy. The ICV consists of irradiated tumour cells that are infected with a rhabdovirus, such as VSVΔ51[157,162,163]. Administration of the ICV to mice was able to robustly protect them from subsequent tumour challenge[157,162,163] and was also able to control the growth of pre-established tumours[157,163]. ICV treatment stimulates both an innate (e.g. NK cell-mediated) and adaptive (e.g. cytotoxic T-cell-mediated) immune response that is required for tumour eradication[157,163]. Efficacy was further enhanced by using a virus expressing granulocyte-monocyte colony stimulating factor (GMCSF)[157] and interleukin-12 (IL-12)[163]. The prime-boost strategy involves administration of a non-replicating viral vector (such as adenovirus) expressing a TAA, following by the administration of a replicating OV (such as VSVΔ51) expressing the same TAA. This strategy

leads to a skewing of the T-cell responses towards the TAA, leading to enhanced efficacy[164–166].

Rhabdoviruses were some of the earliest OV candidates tested pre-clinically and have emerged as promising OV platforms due to their ability to rapidly induce cell death and generate a strong anti-tumour immune response[83]. Furthermore, unlike many other platforms based on human pathogens or vaccines, pre-existing immunity in the human population is rare[83]. Oncolytic variants of VSV, as well as the closely related Maraba virus, are now undergoing phase I/II clinical evaluation in a number of malignancies as a monotherapy or as part of the prime-boost strategy in combination with immune checkpoint blockade (NCT02285816, NCT02879760). A Maraba virus-based OV known as MG1 contains 2 point mutations in its M and G proteins that impair its ability to block the production of type I IFN and attenuate its virulence selectively in non-cancerous cells and *in vivo*[167]. Two VSV variants based on the wild-type VSV backbone expressing human IFN-β alone or along with the sodium iodide symporter (VSV-IFN-β and VSV-IFN-β-NIS) are being evaluated in human phase I clinical trials (NCT02923466, NCT03120624, NCT03017820, NCT01628640). Expressing IFN-β from within VSV is intended to enhance the induction of anti-tumour immune responses and also limit viral replication to cells that are unable to generate an adequate type I IFN- response on their own (a property of many cancers, as mentioned above)[153]. This strategy is analogous to the Δ51 mutation in the matrix protein, but differs in that (1) it does not rely on the capacity of cells to produce type I IFN, and (2) the amount of type I IFN produced correlates with viral replication. The expression of NIS allows for non-invasive tracking of *in vivo* viral replication and distribution through

radioactive iodine (^{131}I) administration and imaging[168]. The combination of ^{131}I and NIS-encoding viruses has also been shown to synergistically improve therapeutic outcomes preclinical tumour models[169–173].

1.3 Heterogeneous response and resistance to OV therapy

While the deletion of methionine 51 improves VSVΔ51's safety profile considerably compared to its wild-type counterpart, patient-derived cancer cell lines and tumour samples show variable sensitivity to *in vitro* and *ex vivo* VSVΔ51 infection and approximately 30% of cancer cell lines in the NCI-60 Human Tumor Cell Line panel are IFN-responsive and thus resistant to infection with VSVΔ51[146,174,175]. Given that tumour heterogeneity may be one reason behind resistance to various types of OVs seen in clinical trials[176–178], significant efforts have been made to increase OV efficacy in resistant tumours. Some groups have resorted to further genetic manipulation of the virus to increase its virulence while others have incorporated prodrug converting enzymes to enhance virus-mediated tumour cell death in the presence of prodrugs[179–182]. Both engineering strategies have distinct pitfalls: the former could potentially compromise safety while the latter still requires productive infection of the tumour, which is limited in resistant tumours. One alternative strategy is to use small molecules to enhance the replication and spread of OVs in resistant tumours.

1.3.1 Pharmacological combinations to enhance OV therapy

The study of pharmacologic enhancement of OV therapy has led to the discovery of molecules that improve the efficacy of OVs by modulation of the anti-viral immune response to OVs and/or the anti-tumour immune response induced by OVs. The pharmacologic categories of drugs that have been used are widely varied, ranging from cytotoxic chemotherapy agents, epigenetic modifiers, microtubule destabilizers, targeted immunomodulators and novel, unclassified compounds[183].

Cyclophosphamide is DNA alkylating agent used as a first-line agent for many types of cancers, including leukemias and lymphomas[184]. It has been used in combination with various types of OVs, including HSV[177,185,186], adenovirus[187–190], vaccinia virus[191], reovirus[192], measles[193–195] and VSV[193], leading to improved efficacy *in vivo*. Cyclophosphamide may augment OV-related outcomes through inhibiting the production of anti-viral neutralizing antibodies as well as by decreasing levels of regulatory T cells, thus promoting adaptive anti-tumour immunity[177,186–189,196].

Due to their immune-stimulating effects, combining OVs with agents that modulate the immune system is a logical choice. In fact, it has been shown that OVs are able to modulate the expression of PD-1 and PD-L1 on cancer cells, providing rationale for the combination of OVs and checkpoint inhibitors[197,198]. Positive results from numerous pre-clinical studies legitimized this approach and several phase I and II trials testing the combination of checkpoint inhibitors with various OVs are underway (NCT03004183, NCT02620423, NCT03206073, NCT02977156, NCT03153085, NCT03294083, NCT02824965)[61,198–201].

Given that the type I IFN response plays a crucial role in limiting viral replication, targeting this pathway would theoretically lead to improved oncolysis in cancer cells with intact type I IFN signaling. Resistance to VSV in squamous cell carcinoma, sarcoma and bladder cancers was overcome through the use of JAK1 inhibitors and was associated with decreased ISG expression[202,203]. Inhibiting type I IFN further upstream through the use of IKK inhibitors *in vitro* was also able to sensitize cancer cells to infection with oncolytic VSV, HSV-1 and encephalomyocarditis virus (ECMV)[204–206]. Transcriptional activation of ISGs is known to require the activity of histone deacetylase (HDAC)[207]. HDAC inhibitors have been used in combination with a diverse set of OVs, leading to synergistic enhancements of oncolysis, decreased ISG expression and improved survival in a variety of pre-clinical cancer models[208–214]. Additionally, the HDAC inhibitor MS-275 was able to potentiate the anti-tumour immune response in the context of oncolytic VSV administered as part of a heterologous prime-boost vaccination strategy[214]. More specifically, oncolytic adenovirus expressing the TAA human dopachrome tautomerase (hDCT) was administered to mice bearing B16 tumours engineered to express this TAA. This was followed by oncolytic VSV also expressing hDCT, with or without concomitant administration of MS-275. The inclusion of MS-275 was shown to lead to a reduction of antiviral neutralizing antibodies, improvement of the T-cell response towards hDCT, and complete cures in approximately 60% of mice[214].

As demonstrated above, rationally selecting therapeutics to use in combination with OVs based on predictable mechanistic synergy has proven to be a successful method of improving OV therapy. However, there is value to be had in using an unbiased approach to

identify compounds that enhance OV activity through previously uncharacterized mechanisms. To this end, nearly a decade ago, a high-throughput small molecule screen was conducted to identify compounds that would sensitize resistant cells to infection with VSVΔ51[215]. The screen was conducted on 4T1 cells, a murine mammary carcinoma cell line that is highly resistant to infection with VSVΔ51. Unexpectedly, several compounds that were found to enhance VSVΔ51-mediated oncolysis turned out to be microtubule destabilizing agents (MDAs). MDAs were found to augment OV therapy *in vivo*, impede the translation of type I IFN and increase bystander killing of cancer cells pursuant to a boost in virus-induced cytokine production[216]. The combination of MG1 and paclitaxel, a microtubule targeting agent and first-line chemotherapy drug used in a variety of cancer types, lead to improved efficacy in multiple murine mammary carcinoma models, demonstrating the potential benefits of combining OV therapy with standard chemotherapy drugs[217].

1.3.2. Identification of VSe1 as a viral sensitizer

The compound 3.4-dichloro-5-phenyl-2,5-dihydrofuran-2-one (hereafter referred to as VSe1) was identified in the high-throughput small molecule screen described above and was the most effective at inducing synergistic cell death in combination with VSVΔ51, and augmenting *in vitro* infection in several VSVΔ51-resistant cell lines, in some cases up to 1000-fold[215]. VSe1 also enhanced *ex vivo* infection of human tumour samples[215]. Infection was not enhanced in normal GM38 fibroblast cells or normal tissue samples, indicating that VSe1's virus sensitizing effect is specific to cancer cells[215]. Additional data suggest that VSe1

may act by inhibiting antiviral signaling as it does not significantly increase infection of wild-type VSV in CT26.WT mouse colon carcinoma cells, which are resistant to infection with the Δ51 mutant[215]. In the IFN-responsive U251 human glioma cell line, VSe1 was able to partially suppress IFN-mediated protection from VSVΔ51 infection[215]. VSe1 treatment was also shown to repress the expression of approximately 96% of VSVΔ51-induced mRNA transcripts in CT26.WT cells, most of which were IFN-stimulated genes[215]. While these data insinuate that VSe1 has an impact on IFN signaling, the exact target(s) were unknown.

1.4 Covalent inhibitors as therapeutic candidates

A noteworthy feature of VSe1's structure is the presence of an α, β-unsaturated carbonyl moiety which can act as a Michael acceptor (**Figure 2**).

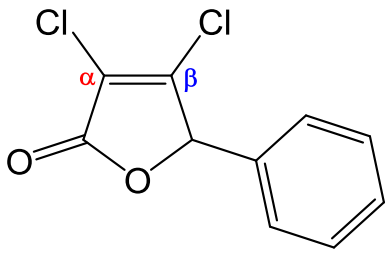

Figure 2. Structure of 3.4-dichloro-5-phenyl-2,5-dihydrofuran-2-one (VSe1). The α and β carbons in the Michael acceptor group are indicated.

Compounds with Michael acceptors are electrophilic and thus are susceptible to nucleophilic attack from other molecules. For this reason, they are thought to have the potential to react covalently and indiscriminately with biological molecules and are generally regarded as undesirable drug candidates by the pharmaceutical industry[218,219].

This largely stems from data connecting the formation of reactive electrophilic drug metabolites to organ toxicity and idiosyncratic adverse drug reactions[220]. Many marketed parent compounds that are covalent inhibitors were discovered serendipitously and identified as such only after approval and widespread clinical use[218,219]. A better understanding of the Michael addition reaction with biological molecules under physiological conditions can lead to the development of drug candidates that bind with high affinity to specific nucleophilic moieties, such as a particular cysteine on a target protein[218]. Such compounds are also reported to be less susceptible to drug resistance[218,221–224]. Covalent inhibition can be reversible or irreversible[218,219]. In the case of irreversible inhibitors, pharmacodynamic effects are driven by the turnover rate of targets (i.e. rate of *de novo* synthesis) as opposed to the pharmacokinetic parameters of the drug (absorption, distribution, metabolism and elimination) and target inhibition can persist after the drug has been cleared from the body[219,225]. Thus, depending on the rate of target turnover, an irreversible inhibitor could be administered less often than a non-covalent reversible inhibitor targeting the same protein[219,225]. Advances in *in silico* targeting of proteins and drug design have permitted the development of targeted covalent inhibitors (TCIs) that possess relatively weak electrophilic warheads designed to react with a specific residue, and will only do so after coming in close enough proximity to first interact non-covalently[219,226,227]. This strategy has recently led to the approval of several compounds that irreversibly or reversibly covalently modify their target. Several of these compounds contain acrylamide groups, which are weakly electrophilic and need to be in close proximity to the target cysteine[218]. As a result, off-target reactions are minimized. The success of telaprevir,

a covalent inhibitor of the NS3 protein from hepatitis C virus (HCV), spawned the development of numerous covalent inhibitors against HCV proteins[218]. Tyrosine kinase inhibitors used in cancer therapy (ibrutinib and spebrutinib, for example) also covalently modify their target, Bruton's tyrosine kinase[228,229].

Contrastingly, the therapeutic effect of some electrophilic compounds is attributed to their induction of antioxidant signaling pathways. Dimethyl fumarate (DMF) is a drug approved for the treatment of psoriasis (Europe) and multiple sclerosis (North America)[230] and is under investigation for the treatment of chronic lymphocytic leukemia and cutaneous T cell lymphoma (NCT02546440, NCT02784834). DMF is an electrophilic compound that contains an α, β-unsaturated carbonyl and is known to act as a Michael acceptor. One of the proposed mechanisms of actions of DMF is that it activates the nuclear factor (erythroid-derived 2)-like 2 (NRF2) antioxidant response pathway, a key mediator in the cellular response to oxidative stress[231,232]. The activation of this pathway leads to the upregulation of glutathione synthesis and other neuroprotective effects that are thought to have a beneficial effect in multiple sclerosis[233,234]. However, other mechanisms of DMF have been proposed more recently, in particular DMF's ability to covalently bind to a key cysteine on p65, which leads to inhibition of its nuclear translocation, DNA binding and transcriptional activity[235]. Interestingly, other key players of innate antiviral pathways, such as p50, IFNAR1 and JAK1 also contain cysteine moieties that have previously been shown to be prone to oxidation or reacting with electrophilic compounds, leading to inhibition of downstream activity[236–240].

1.4.1 Response to oxidative stress

In addition to covalently reacting with endogenous biomolecules, reactive electrophilic compounds can lead to the formation of reactive oxygen and nitrogen species (ROS and RNS). ROS encompass radical and non-radical species such as hydrogen peroxide (H_2O_2), superoxide anion ($O_2^{\bullet -}$), and hydroxyl radical ($HO^{\bullet}$) that contain reactive and reduced oxygen molecules[241,242]. RNS are various nitric oxide derived compounds, including nitric oxide radical ($NO^{\bullet}$) and peroxynitrite ($ONOO^-$)[241,242]. ROS/RNS are formed as by-products of normal metabolism, are known to regulate a variety of cell signaling pathways and are critical in antimicrobial defence mechanisms[241,243–245]. The formation of ROS/RNS is tightly regulated by the cell, as an imbalance can lead to oxidative stress and irreversible damage to cellular macromolecules. This has been implicated in pathogenic mechanisms of numerous diseases, including carcinogenesis, atherosclerosis and neurodegeneration[246–249]. As mentioned above, the transcription factor NRF2 has an integral role in the cell's response to oxidative stress. Under non-stressed conditions, NRF2 is sequestered in the cytoplasm by Kelch-like ECH-associated protein-1 (Keap1), which also targets NRF2 for proteasomal degradation via cullin-3 E3-ubiquitin ligase (Cul3)[250–252]. ROS oxidizes specific reactive cysteines on Keap1, resulting in its dissociation from NRF2. NRF2 then translocates to the nucleus and binds to the antioxidant responsive element (ARE) enhancer, initiating the transcription of genes whose protein products are required for phase II detoxification of electrophiles, glutathione synthesis, and also function as antioxidant themselves[241,250].

Glutathione (GSH) is a tripeptide molecule formed by glutamate, glycine and cysteine that is primarily responsible for the detoxification of endogenous electrophilic

compounds and xenobiotics[253]. GSH is an essential biological molecule. Homozygous deletion of the gene responsible for the rate limiting step of GSH synthesis, γ-glutamyl cysteine synthetase/ligase (GCL) is embryonic lethal in mice[254]. GSH is capable of scavenging ROS such as H_2O_2 via glutathione peroxidase (GPx), which reduces H_2O_2 to water and oxidizes two GSH molecules together to form glutathione disulfide (GSSG). GSH reductase (GR) is responsible for catalyzing the reduction of GSSG, replenishing GSH stores (**Figure 3A**). In view of its principal role as an antioxidant, the ratio of GSH to GSSG is often used as an indicator of oxidative stress[255].

GSH is also covalently conjugated directly to electrophilic substrates via the thiol group on its cysteine (**Figure 3B**).

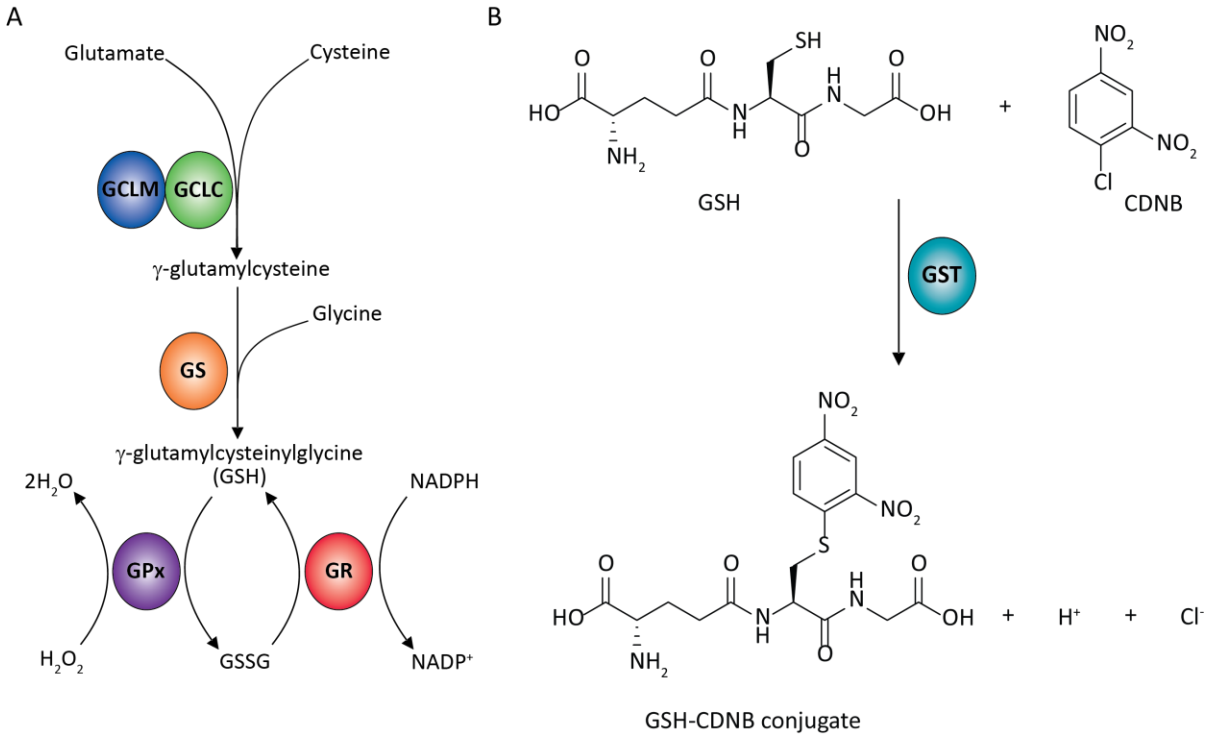

Figure 3. Glutathione synthesis, redox cycle and conjugation. (A) Synthesis of glutathione (GSH) is a two-step process. The first and rate-limiting step is the conjugation of glutamate with cysteine and is catalyzed by γ-glutamyl cysteine synthetase/ligase (GCL), which is composed of catalytic (C) and modifier (M) subunits. The second step is catalysed by GSH synthase (GS) which adds glycine to γ-glutamylcysteine to form the final product, γ-glutamylcysteinylglycine, or GSH. ROS species such as H_2O_2 are reduced via GSH peroxidase (GPx). In the process, 2 GSH molecules are oxidized to form glutathione disulfide (GSSG). GSH is replenished via glutathione reductase (GR), requiring nicotinamide adenine dinucleotide phosphate (NADPH) as a co-factor. **(B)** Glutathione S-transferase (GST) enzymes catalyze the conjugation of GSH to electrophiles such as 1-chloro-2,4-dinitrobenzene (CDNB).

The GSH conjugate is typically less reactive and harmful than the electrophile and is also more polar, which aids in the excretion of the electrophile-GSH conjugate[256]. Reactions between GSH and electrophiles can occur non-enzymatically, but are often facilitated by glutathione-S-transferase (GST) enzymes[257,258]. There are seven classes of cytosolic GSTs with different individual class members (**Table 1**).

GST class	Class members
Alpha (α)	A1, A2, A3, A4, A5
Mu (μ)	M1, M1L, M2, M3, M4, M5
Pi (π)	P1
Sigma (σ)	S1
Theta (θ)	T1, T2
Omega (ω)	O1, O2
Zeta (ζ)	Z1

Table 1. Class members of human cytosolic glutathione S-transferases.

Within a class, members have at least 40% sequence homology and between classes, homology is less than 25%[259]. GSTs are catalytically active as dimers, and are thus named according to class and dimerization members. The GSH binding site (G site) is highly conserved between classes and is located at the N-terminus of each protomer[259,260]. Class assignment is based on this domain, which contains a catalytically active tyrosine, cysteine, or serine residue[260]. The electrophilic substrate binding site is a more variable hydrophobic

region (H site) located at the C-terminus and is in close proximity to the G site, according to tertiary structure analysis by x-ray crystallography[259–262]. Several GSTs are catalytically redundant and have common electrophilic substrates[259]. In addition to detoxifying electrophiles, GSTs are involved in other cellular processes, including post-translational modification of proteins via S-glutathionylation and the biosynthesis of various endogenous compounds, including testosterone and progesterone[259,263]. GSTs also interact with components of the MAPK pathway[264]. GSTM1 regulates the activity of apoptosis signal-regulating kinase 1 (ASK1) by sequestering it and preventing its oligomerization and activation of downstream pro-apoptotic signaling cascades[265–267]. GSTP1 binds to and inhibits the activity of JNK. Under conditions of oxidative stress, GSTP1 oligomerizes, releasing JNK, which is able to phosphorylate and activate the transcription factor c-jun, leading to either increased cell differentiation and proliferation or apoptosis (depending on the length of exposure to stress)[260]. The overexpression of GSTP1 in many types of cancers is thought to drive cell proliferation as well as confer resistance to chemotherapeutic drugs[264,268–270]. For this reason, GSTP1 is a highly sought after anti-cancer drug target. Telintra® (ezatiostat), a structural analog of GSH designed to be a potent GSTP1-1 inhibitor, was being investigated in Phase II trials in the United States for the treatment of myelodysplastic syndrome (NCT01422486, NCT01459159) and severe neutropenia (NCT00909584, NCT00701870). In myelodysplastic syndrome, it is believed that the inhibition of GSTP1 promotes JNK-mediated phosphorylation of c-jun, leading to proliferation of normal hematopoietic progenitors and apoptosis of malignant cells[271–273].

The ability of ezatiostat to induce apoptosis in malignant cells may also be related to its ability to increase levels of ROS in these cells[274].

1.5 Rationale, hypothesis and objectives

The heterogeneous response to OVs continues to be a significant barrier that limits their use as standalone treatments for cancer patients. Combination strategies have the potential to overcome this barrier, as demonstrated by positive results emerging from clinical trials of OVs and pharmacological therapies[189,193,201]. VSe1 is a previously uncharacterized molecule that is able to robustly improve VSVΔ51 efficacy *in vitro* and in pre-clinical *in vivo* studies. In spite of this, VSe1 exhibits poor stability in aqueous environments at physiological pH and is not well tolerated by mice when administered intraperitoneally at doses over 10 mg/kg[275]. Specifically, mice treated with lethal doses of VSe1 experience irrevocable weight loss and intestinal distension, associated with tissue destruction in the abdominal cavity. This could be due to a number of factors, one of which is poor aqueous solubility and consequent compound precipitation[276]. Altogether, these factors limit VSe1's suitability for *in vivo* use. Studying the physico-chemical and pharmacological properties of VSe1 and elucidating its precise mechanism of action would aid in the development of it or related compounds into viable drug candidates. Structure-activity-relationship studies are regularly employed in the pharmaceutical industry during lead optimization to identify important pharmacophores of drug candidates. This can also lead to the generation of active and inactive probes that can be used to identify putative biomolecular targets through activity-based profiling[277–279]. Thus, we chose to combine

chemistry-based and biology-based strategies to simultaneously tackle the unknown mechanism of action of VSe1 and the need for more viable drug candidates based on this molecule.

Hypothesis

1. Structure–activity–relationship studies will allow the generation of VSe1 analogs with improved physico-chemical and pharmacological properties that can be used to enhance VSVΔ51-mediated oncolysis in vivo
2. Synthetic VSe1 derivatives can be used to identify potential targets of VSe1

Objectives

1. Characterize the structure-activity relationship (SAR) of VSe1 via high-throughput screening of VSe1 analogs.
2. Evaluate the in vivo safety and efficacy of VSe1 analogs that possess better physico-chemical and pharmacological properties.
3. Characterize the mechanism of action of VSe1.

Materials and Methods

2.1 Drugs, chemicals and cytokines

VSe1 and its analogs (compounds **2**-**53**, **57**, **58**, **10**-GSH adduct and **28**-GSH adduct) were synthesized in Dr. Christopher Boddy's lab. Synthetic methods and characterization dose response curves for VSe1 and analogs **2 – 51** are described in the Appendix. Other drugs, chemicals and cytokines used in this study are described below in **Table 2.**

Table 2. Drugs, chemicals and cytokines

Name	Abbreviation	Supplier(s)
bardoxolone methyl ester	CDDO-Me	Cayman Chemical
buthionine sulfoximine	BSO	Sigma-Aldrich (St. Louis, MO)
6-carboxy-2',7'-dichlorodihydrofluorescein diacetate	C-H_2DCFDA	Thermo Fisher Scientific
1-chloro-2,4-dinitrobenzene	CDNB	Alfa Aesar
diethyl maleate	DEM	Sigma-Aldrich (St. Louis, MO)
diethyl fumarate	DMF	Sigma-Aldrich (St. Louis, MO)
dimethyl maleate	DMM	Sigma-Aldrich (St. Louis, MO)
dimethyl fumarate	DMF	Sigma-Aldrich (St. Louis, MO)
dimethyl sulfoxide	DMSO	Fisher Scientific
dithiothreitol	DTT	Bioshop
ezatiostat hydrochloride	-	ApexBio (Houston, TX)
L-glutathione, reduced	GSH	Sigma-Aldrich (St. Louis, MO)
L-glutathione, oxidized	GSSG	Sigma-Aldrich (St. Louis, MO)
hydrogen peroxide	H_2O_2	Fisher Scientific (Fair Lawn, NJ)
interferon beta	IFN-β	PBL Interferon Source (Piscataway, NJ)
D-luciferin, potassium salt	luciferin	Biotium (Hayward, CA) and Perkin Elmer
N-[4-[2,3-Dihydro-1-(2-methylbenzoyl)-1H-indol-5-yl]-5-methyl-2-thiazolyl]-1,3-benzodioxole-5-acetamide	ML385	Sigma-Aldrich (St. Louis, MO)
monomethyl fumarate	MMF	Sigma-Aldrich (St. Louis, MO)
human tumour necrosis factor alpha	TNF-α	R&D systems (Minneapolis, MN)

2-[(aminocarbonyl)amino]-5 -(4-fluorophenyl)-3-thiophenecarboxamide	TPCA-1	Abcam

2.2 Cell lines

All cell lines were incubated at 37°C with 5% CO_2 in a humidified incubator and described below in Table 3.

Table 3. Cell lines

Cell Line	Origin	Cell Type	Growth medium	Source
786-0	human	renal clear cell adenocarcinoma	DMEM[a,#,$]	ATCC
CT26.WT	mouse	colon adenocarcinoma	DMEM[a,#]	ATCC
B16-F10	mouse	melanoma	αMEM[b,#]	ATCC
HT29	human	colorectal adenocarcinoma	DMEM[a,#]	ATCC
Vero	African green monkey	kidney	DMEM[a,#,$]	ATCC
4T1	mouse	mammary carcinoma	DMEM[a,#]	ATCC
Pan02	mouse	pancreatic adenocarcinoma	DMEM[a,#]	ATCC
MC-38	mouse	colon carcinoma	DMEM[a,#]	NIH
CT-2A	mouse	astrocytoma	DMEM[a,#]	*
S180	mouse	Sarcoma	DMEM[a,#]	ATCC
OVAC433	human	ovarian carcinoma	RPMI[c,#]	**
293T	human	embryonic kidney	DMEM[a,#]	ATCC
A549	human	lung adenocarcinoma	DMEM[a,#]	ATCC

[a] Dulbecco's Modified Eagle's Medium (Corning, Manassas, VA)
[b] Minimum Essential Medium Alpha modification (Hyclone,
[c] Roswell Park Memorial Institute medium (Hyclone, Waltham, MA)
[#] supplemented with 10% fetal bovine serum (Sigma-Aldrich, St. Louis, MO) and 30 mM Hepes (Thermo Fisher Scientific, Waltham, MA)
[$] supplemented with 10% 3:1 newborn calf serum: fetal bovine serum (Sigma-Aldrich, St. Louis, MO) and 30 mM Hepes (Thermo Fisher Scientific, Waltham, MA)
* Kindly provided by Dr. Thomas N. Seyfried (Boston College, Chestnut Hill, MA)
** Kindly provided by Dr. Barbara Vanderhyden, University of Ottawa, Ottawa, ON

2.3 Viruses

Oncolytic Rhabodviruses

VSVΔ51 is a recombinant variant of the Indiana serotype of Vesicular Stomatitis Virus (VSV) harbouring a deletion of the 51st methionine in the M protein. VSVΔ51 expressing green fluorescent protein (GFP), red fluorescent protein (RFP) or firefly luciferase (FLuc) are recombinant derivatives of VSVΔ51 that have been previously described[146]. Maraba MG1 as described was obtained from Dr. David F. Stojdl[167]. All virus stocks were propagated in Vero cells, purified on Optiprep gradient and titered on Vero cells as previously described[280].

Oncolytic Herpes simplex-1

HSV-1 N212 (an ICP0-deleted oncolytic strain) expressing GFP was obtained from Dr. Karen Mossman and has been described previously[281]. HSV-1 samples were titered on Vero cells. Vero cells (2.5×10^5 cells) were infected with serial dilutions of virus containing samples in 12-well dishes. Cells were incubated at 37° C for 1 h, after which the inoculum was removed and replaced with fresh culture media. After 48h incubation at 37° C, GFP positive plaques were visualized and counted.

Non-replicating vectors

AAV2-luciferase (adeno-associated virus serotype 2 expressing luciferase) was a gift from Dr. Sarah Wootton (University of Guelph) and Ad5-luciferase (adenovirus serotype 5 expressing luciferase) was a gift from Dr. Jack Gauldie (McMaster University).

2.4 Luciferase reporter-based viral titration assay

This assay has been described in detail by Garcia et al[282]. Cells were seeded in 96-well plates at a density of $3x10^4$ cells/100 μL/ well. Twenty-four hours later, cells were pre-treated for 4 hours with control vehicle (DMSO) or compound at various concentrations and subsequently infected with VSVΔ51-FLuc at a MOI of 0.005. Forty hours later, 25 μL of 786-0 supernatant from each well was transferred into corresponding wells of white-walled 96-well plates seeded with a confluent monolayer of Vero cells. At the same time, known amounts of virus (starting at $1x10^8$ plaque forming units (pfu) and decreasing by 1 log unit to 10 pfu) were added to two columns on the white-walled plate to generate a standard curve. Plates were centrifuged at 430xg for 5 minutes and then incubated for 5 hours at 37°C. Then, 25 μL of luciferin (2mg/mL) was added to each well and bioluminescence was measured in mean relative light units (mRLU; SynergyMx Microplate Reader, BioTek). To generate the standard curve, mRLU was plotted against known input pfu. Four-parameter non-linear regression analysis generated a Hill plot from which unknown input pfu (estimate of viral titer) was interpolated. Data transformation was conducted in R. These estimated titers are termed “viral expression units” (VEU) and strongly correlate positively with VSVΔ51 titers obtained via plaque assay on Vero cells (**Figure 4**).

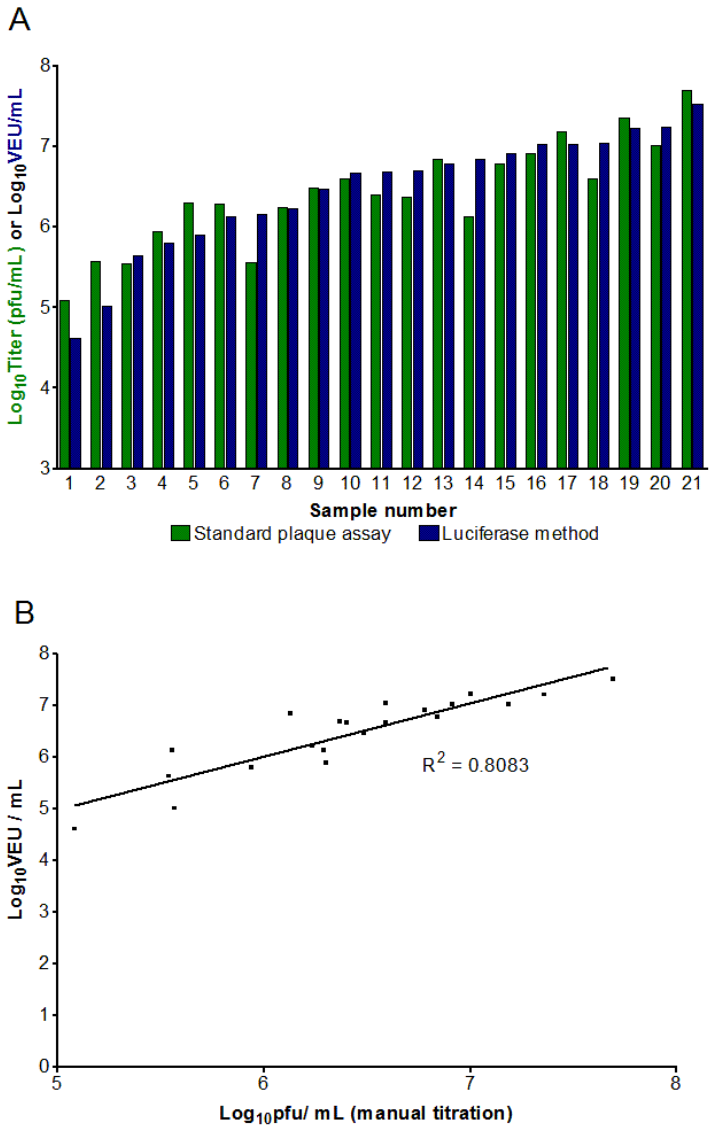

Figure 4. Comparison of standard plaque assay titers with those obtained by high-throughput method. (A) Viral titers in pfu/ml obtained by standard plaque assay on Vero cells were compared with calculated viral titers (VEU/ml) from the same samples titered using the high-throughput luciferase assay. **(B)** Linear relationship between VEU/ml and titer obtained via standard plaque assay. Linear regression curve and coefficient of determination (R^2) are shown. Reprinted with permission from Garcia V, et al *J. Vis. Exp.* (91), e51890, doi:10.3791/51890 (2014) (published under the Creative Commons License 3.0, by,nc,nd).

2.5 *In vitro* cellular cytotoxicity assay

Cellular cytotoxicity was assessed by incubating treated samples with alamarBlue® (AbD Serotec and BioRad) as per the manufacturer's instructions. After 2.5 hours, fluorescence was measured (530 nm excitation and 590 nm emission) on a Fluoroskan Ascent Microplate Fluorometer (Thermo Scientific, Hudson, NH). Emission values were normalized to that of untreated controls after subtracting background fluorescence from wells containing media without cells.

2.6 Glutathione reactivity experiment

Reactivity with glutathione was assessed using an assay adapted from a recently reported method[283]. 250 µL of a 40 mM DMSO stock solution of each compound was added to L-glutathione (15.4 mg, 5 mol equiv.) suspended in 250 µL of DMSO. The resulting mixture was placed in a 37 °C shaker. 10 µL aliquots were removed and quenched in 990 µL of water (containing 0.5% formic acid) at various time points, including at t = 0 min, for analysis by electrospray ionization- liquid chromatography-mass spectrometry (ESI-LC-MS). All ESI-LC-MS analyses were collected on an API2000 LC/MS/MS System (Applied Biosystems) equipped with a turbo-ion spray ESI probe interfaced with a Prominence UFLC (Shimadzu) equipped with a reverse phase BDS Hypersil C18 50 × 2.1 mm column, particle size 3 µm (Thermo Scientific). HPLC/LC-MS UV absorption was monitored at 254 nm and 210 nm. Both the compound and the glutathione adduct were identified by MS. Area of the UV peak was recorded for each time point.

2.7 Plasma stability assay

10 mM methanol stock solutions of each analog were prepared and diluted to 1 µM with aqueous 0.1% formic acid. 5 µL of the diluted solution was inserted into a Proxeon nanoelectrospray emitter (Thermo Scientific, Odense, Denmark) and analyzed in positive ion mode via nanoESI MS on a QStarXL hybrid quadrupole time-of-flight mass spectrometer (AB Sciex, Framingham, MA, USA). Product ion spectra were collected for each compound at varying CID collision energies using an ESI voltage of 1000 V, a declustering potential of 30 V and a focusing potential of 120 V. Two fragments were chosen as multiple reaction monitoring (MRM) transitions for each compound with optimized collision energies. The quantitative transition was used to determine the relative quantities of each compound and the confirmatory transition was used to validate the ion signal observed for the first transition (see Supporting Information).

1 mM methanol stock solutions of each analog were prepared and mixed in experimental triplicate with Balb/c mouse plasma (Innovative Research, Novi, MI, USA) that was buffered 1:1 with phosphate buffered saline (PBS, pH=7.4). The compounds were multiplexed into sets of three and added to a final concentration of 10 µM in a total volume of 400µL. Immediately upon mixing, 200µL of the sample mixture was quenched with 300µL of aqueous formic acid (5%) to prevent further analog degradation. The remaining 200µL of sample was incubated at 37°C for 3 hours and quenched in an identical fashion[284]. The quenched samples were passed through 3 kDa Amicon molecular weight cut off filters (Millipore, Billerica, MA, USA) by centrifugation at 14,000 rpm for 15 minutes. 20 µL samples of the filtrates were subjected to LC-MRM (liquid chromatography-mass

spectrometric multiple reaction monitoring) analysis using a Qtrap 4000 (AB Sciex, Framingham, MA, USA) hybrid triple quadrupole linear ion trap mass spectrometer with an ion spray voltage of 5000 V and a declustering potential of 25V. The MS was equipped with a Turbo V ion spray source coupled to a Dionex Ultimate3000 HPLC (Thermo Fisher Scientific, Waltham, MA, USA). Fritted fused silica columns (200 µm ID) (Molex, Lisle, IL, USA) were packed with 5 µm Magic C18 (MICHROM Bioresources Inc., Auburn, CA, USA) reversed-phase beads to a length of 5 cm using an in-house high-pressure vessel. Chromatographic separation employed a linear gradient using reversed phase solvents (water and acetonitrile both containing 0.1% formic acid) over 10 minutes (see Supporting Information). Automatic quantitation was achieved using MultiQuant software (AB Sciex, Framingham, MA, USA) by integrating the peak areas of the quantitative MRM transition extracted ion chromatogram. The plasma stability of each compound was calculated as a percentage of the compound ion signal detected after 3 hours of plasma incubation relative to the original amount.

2.8 *Ex vivo* studies

Balb/c mice were implanted with CT26.WT (murine colon carcinoma) cells. Mice were sacrificed 24 days later, after tumours had reached at least 10mm x 10mm in size. Tumour, lung, spleen, brain, and abdominal muscle tissue were extracted from the mice, cut into 2 mm thick slices and cored into 2mm x 2mm pieces via punch biopsy. Each tissue core was incubated in 1 mL of Dulbecco's Modified Eagle's Medium (DMEM) supplemented with 10% fetal bovine serum, 30 mM HEPES and 2.5 mg/L amphotericin B, in a 37^{o}C, 5% CO_2

humidified incubator. In order to assess the viability of each core, alamarBlue® was added to each well for a 4-hour incubation period. Viable cores were selected and treated with various concentrations of VSe1 and analogs. Four hours later, cores were infected with $1x10^4$ pfu of VSVΔ51-GFP. GFP pictures were taken for each core 24 hours post infection. Cores and supernatants were collected 36 hours post infection and titered by plaque assay. Cores were homogenized with a TissueLyser II (Qiagen) prior to titering.

2.9 *In vivo* studies

All experiments were reviewed and approved by the University of Ottawa Animal Care Committee (ACC) and were performed in accordance with the University of Ottawa Animal Care and Veterinary Services guidelines for animal care under protocols OGHRI-58, OHRI-2264 and OHRI-2265.

Dose escalation studies

Nine-week-old Balb/c mice were intraperitoneally administered various doses of VSe1, **10**, **24**, or **28** dissolved in DMSO (approximately 50 µL). The dose was adjusted for individual mice based on weight. Weight loss and other outward signs of toxicity (piloerection, lethargy, respiratory distress, quiet behaviour) were recorded over a 10 (VSe1, **10**) or 18-day (**24**, **28**) period. Mice were euthanized when more than 20% of original body weight was lost or outward signs of toxicity did not improve within 48 hours.

Pharmacokinetics

Short time course

Nine-week-old female Balb/c mice were given subcutaneous tumours by injecting ~ 3×10^5 syngeneic CT26.WT cells suspended in 100 µl serum-free DMEM. Nineteen days post-implantation, mice were intratumourally administered 50 mg/kg of compound **10** or **24** dissolved in DMSO (approximately 50 µL). Tumours were excised after 0h, 15 minutes, 1h and 3h and homogenized immediately at 30 Hz for 5 minutes with a TissueLyser II (Qiagen). At the time of tumour excision, peripheral blood was also collected and allowed to clot at room temperature for at least 30 minutes. Samples were then centrifuged (20,000 rpm, 30 s, 4°C) and tumour samples were homogenized again in 500 µL PBS. Serum was diluted 5x with 0.1% formic acid in water. After another round of centrifugation, supernatants were passed through Amicon Ultra-0.5 mL 3 kDa molecular weight cut off filters (EMD Millipore) by centrifugation, and the filtrate was quantified by LC-MRM.

Long time course

Nine-week-old female Balb/c mice were given subcutaneous tumours by injecting ~ 3×10^5 syngeneic CT26.WT cells suspended in 100 µl serum-free DMEM. Nineteen days post-implantation mice were intratumourally administered vehicle control (DMSO), or **28** dissolved in DMSO (40mg/kg of body weight, approximately 30 µL). Tumours treated with **28** were excised after 1h, 3h, 10h and 24h. Tumours treated with vehicle alone were excised after 3h and 24h. Tumour homogenization and centrifugation was conducted in an identical fashion to that described in the short time course (above). At the time of tumour

excision, peripheral blood was also collected and allowed to clot at room temperature for at least 30 minutes. Samples were centrifuged at 20,000 rpm for 10 minutes at 4°C, and the supernatant (serum) was collected. Serum was diluted 5x with 0.1% formic acid in water and centrifuged through Amicon Ultra-0.5 mL 3 kDa molecular weight cut off filters (EMD Millipore). For both tumour and serum samples, 25 µL of the filtrate was mixed with 5 µL of a 6 µM solution of caffeine in water (as a standard to allow relative quantitation) and quantified by LC-MRM.

In vivo imaging of virus replication

Twenty-four hours after treatment and infection, 200 µl of a 10 mg/mL luciferin solution in sterile PBS (Corning, Manassas, VA) was administered to mice intraperitoneally. Five minutes later, mice were anaesthetized using 3% isoflurane and imaged with an *in vivo* imaging system (IVIS; Perkin Elmer, Waltham MA) according to the manufacturer's instructions. For quantification of luminescence, bioluminescent signal intensities were measured using Living Image® v2.50.1 software. Background intensities were measured using the software and subtracted from user-defined regions of interest (ROIs) that were manually delineated around the tumour for each mouse.

CT26.WT tumour model

Compound **10** + VSVΔ51-FLuc

Six-week-old female Balb/c mice were given subcutaneous tumours by injecting 3×10^5 CT26.WT cells suspended in 100 µl serum-free DMEM. Eleven days post-implantation (when

tumours were approximately 5 mm x 5 mm), mice were treated with 50 mg/kg of **10** dissolved in DMSO or vehicle control administered intraperitoneally (approximately 30 μL; weight-adjusted for each mouse). Four hours later, mice were treated with an intratumoural injection of 1×10^8 pfu of VSVΔ51-FLuc. **10** or vehicle was re-administered on day 13 and 15 post-implantation. Tumour dimensions were measured with electronic calipers. Tumour volumes were calculated as ($width^2$ x length) / 2. Mice were euthanized when tumour volume exceeded 1600 mm^3. Initial tumour sizes measured on the first day of treatment were used to calculate relative tumour size.

Compound **28** + VSVΔ51-FLuc

CT26.WT tumours were implanted as above. When tumours were at least 5 mm x 5 mm (between 11-15 days post-implantation), mice were treated with 40 mg/kg of **28** dissolved in DMSO or vehicle control administered intratumourally (approximately 30 μL; weight-adjusted for each mouse). Four hours later, mice were treated with intratumoural injection of 1×10^8 pfu of VSVΔ51-FLuc. Twenty-four hours later, viral luciferase expression was monitored with an IVIS as described above. Tumour dimensions were measured with electronic calipers. Tumour volumes were calculated as ($width^2$ x length) / 2. Mice were euthanized when tumour volume exceeded 1600 mm^3. Initial tumour sizes measured on the first day of treatment were used to calculate relative tumour size.

HT29 tumour model

Six-week-old CD1 nude mice were given subcutaneous tumours by injecting 1×10^6 HT29 cells suspended in 100 μl serum-free DMEM. When tumours grew to at least 5 mm x 5 mm (between 18 – 25 days post-implantation), mice were treated with 40 mg/kg of **28** dissolved in DMSO or vehicle control administered intratumourally (approximately 30 μL; weight-adjusted for each mouse). Four hours later, mice were treated with an intratumoural injection of 1×10^8 pfu of VSVΔ51-FLuc. Twenty-four hours later, viral luciferase expression was monitored with an IVIS as described above. Tumour dimensions were measured every other day with electronic calipers. Tumour volumes were calculated as (width^2 x length) / 2. Mice were euthanized when tumour volume exceeded 1600 mm^3. Initial tumour sizes measured on the first day of treatment were used to calculate relative tumour size.

B16-F10 tumour model

Seven-week-old female C57/B6 mice were given subcutaneous tumours by injecting 3.5×10^5 B16-F10 cells suspended in 100 μl serum-free DMEM. When tumours grew to at least 5 mm x 5 mm (between 10-14 days post-implantation), mice were treated with 40 mg/kg of **28** dissolved in DMSO or vehicle control administered intratumourally (approximately 30 μL; weight-adjusted for each mouse). Four hours later, mice were treated with intratumoural injection of 1×10^8 pfu of VSVΔ51-FLuc. Twenty-four hours later, viral luciferase expression was monitored with an IVIS as described above. Tumour dimensions were measured with electronic calipers. Tumour volumes were calculated as (width^2 x length) / 2. Mice were euthanized when tumour volume exceeded 1600 mm^3.

Initial tumour sizes measured on the first day of treatment were used to calculate relative tumour size.

2.10 Microarray

786-0 cells seeded at a density of 1 x 10^6 cells in 6-well flat bottom plates (Costar). Twenty-four hours later, cells were treated with VSe1 (55 μM), **2** (55 μM), **6** (50 μM), **40** (55 μM), **28** (95 μM), **29** (95 μM), **25** (95 μM), **58** (150 μM), **52** (150 μM), media or vehicle (DMSO). After 28 hours, cell lysates were collected, RNA was collected using an RNA-easy kit (Qiagen, Valencia, CA, USA). Biological triplicates were subsequently pooled and RNA quality was measured using Agilent 2100 Bioanalyzer (Agilent Technologies) before hybridization to Affymetrix Human PrimeView Array. Hybridization was performed by The Centre for Applied Genomics, The Hospital for Sick Children, Toronto, Canada. Microarray datasets were processed using Transcriptome Analysis Console (TAC) 3.0 under default parameters of Gene Level Differential Expression Analysis. Fold change in gene expression was calculated for each gene in relation to uninfected, untreated control. Gene ontology (GO)-term enrichments were evaluated using GOrilla[285].

2.11 ELISA

IFN-β

786-0 cells were seeded at 3x10^5 cells per well in 12-well plates. The following day, the cells were pre-treated with 60, 50, 50 and 95 μM of VSe1, **2**, **10** and **28** respectively. Two hours later the cells were infected with VSVΔ51-GFP at MOI 3. Supernatants were collected 16

hours post infection, and an ELISA was performed using VeriKine™ Human IFN Beta ELISA Kit (PBL Assay Science, Piscataway, NJ) according to the manufacturer's protocol. IFN-β levels were interpolated from experimental standard curves.

TNF-α

786-0 cells were seeded at $2.5x10^5$ cells per well in 12-well plates. The following day, the cells were pre-treated with 60, and 80 μM of VSe1, and **28** respectively. Two hours later the cells were infected with VSVΔ51-GFP at MOI 1. Supernatants were collected 8, 16 and 24 hours post-infection and an ELISA was performed using the Human TNF-alpha Quantikine ELISA Kit (R&D Systems, Minneapolis, MN) according to the manufacturer's protocol. TNF-α levels were interpolated from experimental standard curves.

2.12 Quantitative real-time PCR

786-0 cells were seeded at $1x10^6$ cells/well in 6-well plates. The following day, the cells were pre-treated with 60, 50, 50 and 95 μM of VSe1, **2**, **10** and **28** respectively. Two hours following pre-treatments the cells were infected with VSVΔ51-GFP at MOI 3. Sixteen hours post infection the cells were lysed and RNA extraction was performed using RNeasy® Mini Kit (Qiagen, Valencia, CA). RNA (1 μg) was converted to cDNA with RevertAid H Minus First Strand cDNA Synthesis Kit (Thermo Fisher Scientific, Waltham, MA). Real-time PCR reactions with 20 ng of cDNA were performed with QuantiTect® SYBR® Green PCR Kit (Qiagen, Valencia, CA) on a 7500 Fast Real-Time PCR system (Applied Biosystems, Foster City, CA).

Gene expression was normalized to GAPDH and fold induction was calculated relative to the untreated/uninfected samples for each gene using the Pfaffl method[286].

Table 4. q-RT PCR primers

Model	Gene	Forward Primer (5'→3')	Reverse Primer (5'→3')
Human	*IFNβ*	CATTACCTGAAGGCCAAGGA	CAGCATCTGCTGGTTGAAGA
Human	*MX2*	GAACGTGCAGCGAGCTTGTC	AAGGCTTGTGGGCCTTAGAC
Human	*GBP3*	ACTGGTGGCGAATCCAGAAG	GCCCAGAGAGAAGCCCTTATT
Human	*IFI44*	CCCATCGCTGAAGGACAGAA	CACATGTACCACACCAGCGT
Human	*IFIT3*	GCACAGACCTAACAGCACCC	TTGGTGACCTCACTCATGATGGC
Human	*IL6*	ACCCCCAATAAATATAGGACTGGA	GAAGGCGCTTGTGGAGAAGG
Human	*TNFα*	GCTGCACTTTGGAGTGATCG	GAGGGTTTGCTACAACATGGG
Human	*GAPDH*	ACAGTCAGCCGCATCTTCTT	GTTAAAAGCAGCCCTGGTGA
Human	*GSTP1*	GAGACCAGATCTCCTTCGCTG	GCCATTGATGGGGAGGTTCA
Human	*HMOX1*	ACTGCGTTCCTGCTCAACAT	GGGGCAGAATCTTGCACTTT
Human	*OSGIN*	GTTCCCCTGACCCTCCTAGT	GGCCGTTACCCACAATGATG

2.13 Immunoblot analysis

Cells were lysed on ice for 10 minutes in protein extraction buffer (50mM Hepes, 150mM NaCl, 10mM EDTA, 10mM $Na_4P_2O_7$, 1% NP-40 pH 7.4) containing 1M NaF, 200mM Na_3VO_4 and protease inhibitor cocktail (Roche, Mississauga, Ontario, Canada). Lysates were centrifuged at 16,000xg for 10 minutes at 4°C. NE-PER™ nuclear and cytoplasmic extraction reagents (Pierce Biotechnology, Rockford, IL) were used as per the manufacturer's protocol for separation of nuclear and cytoplasmic fractions. Protein determination was performed by Bradford assay (Protein Assay Solution, BioRad, Mississauga, Ontario) and 20-50 μg of

protein extracts were prepared in NuPAGE LDS sample buffer (Invitrogen, Burlington, Ontario) supplemented with dithiothreitol (DTT). Lysates were separated by SDS-PAGE using 4-12% precast gradient gels (Invitrogen, Burlington, Ontario) and the XCell *SureLock*® Mini-cell (Invitrogen, Burlington, Ontario), and then transferred onto nitrocellulose membranes (GE Healthcare, Baie d'Urfe, Quebec). Membranes were blocked with 5% bovine serum albumin (BSA) or 5% non-fat dry milk in 0.1% TBS-Tween-20 for 1 hour at room temperature and then incubated overnight at 4°C with rabbit or mouse antibodies against NFκB p65 (#8242 Cell Signaling Technology, Danvers, MA), phospho-NFκB p65 (Ser536, #3033, Cell Signaling Technology, Danvers, MA), NFκB p105/p50 (#3035, Cell Signaling Technology, Danvers, MA), IRF-3 (#11904, Cell Signaling Technology, Danvers, MA), phospho-IRF-3 (Ser396, #4947, Cell Signaling Technology, Danvers, MA), c-jun (#9165, Cell Signaling Technology, Danvers, MA), phospho-c-jun (Ser63, #9261, Cell Signaling Technology, Danvers, MA), IκBα (#4814, Cell Signaling Technology, Danvers, MA), β-Actin (#4970, Cell Signaling Technology, Danvers, MA), or α-Tubulin (sc-8035, Santa Cruz Biotechnology, Dallas, Texas). The membranes were then probed with horseradish-peroxidase conjugated anti-rabbit (Jackson Immunoresearch Labs, West Grove, PA) or anti-mouse (Cell Signaling Technology, Danvers, MA) secondary antibodies for 1 hour at room temperature. Bands were imaged using Clarity™ Western ECL blotting substrates (Bio-Rad, Mississauga, Ontario) on HyBlotCL autoradiography films (Denville Scientific, Holliston, MA).

2.14 Immunoprecipitation

Cells were lysed as described above and 250 μL of lysates were pre-cleared with protein G Dynabeads (Invitrogen, Burlington, ON) for 30 minutes at room temperature. Lysates were then incubated with fresh beads and rabbit anti-NFκB p65 antibody for 1 hour at room temperature (1:250 ratio for antibody to lysate). Beads were pelleted, washed three times with protein extraction buffer and bound proteins were eluted with 100 mM glycine pH 2.8. Eluate was diluted in NuPAGE LDS sample buffer with DTT and immunoblotting was performed as described above.

2.15 Ligand-based affinity chromatography

Active and inactive probes were independently conjugated to Amino PEGA resin (dimethyl acrylamide and mono-2-acrylamidoprop-1-yl[2-aminoprop-1-yl] polyethylene glycol cross-linked with bis 2-acrylamidoprop-1-yl polyethyleneglycol; Novabiochem). Confluent 15 cm plates of 786-0s were mock-infected or infected with VSVΔ51-GFP (MOI 0.005). Twenty-four hours later, cells were then lysed on ice (in 50 mM Tris-HCl pH 7.4, 150 mM NaCl, 0.5% Triton-X, 10% glycerol, 5 mM EDTA, 1 M NaF, 200 mM Na_3VO_4 and protease inhibitor cocktail). Three mock-infected plates were pooled, 6 infected plates were pooled and both lysates were incubated with resin-bound active or inactive probe overnight at 4°C. The following day, resins were washed in lysis buffer, eluted by boiling in Laemmli buffer and resolved by SDS-PAGE on 4-12% precast gradient gels (Invitrogen, Burlington, Ontario). Proteins were stained with a 0.25% Coomassie Blue R-250 solution (in a 50% methanol, 10% acetic acid solution) and de-stained overnight in a 45% methanol, 10% acetic acid solution.

Visible bands were cut out and sent for liquid chromatography-mass spectrometry (LC-MS) analysis. A schematic is presented in **Figure 5**.

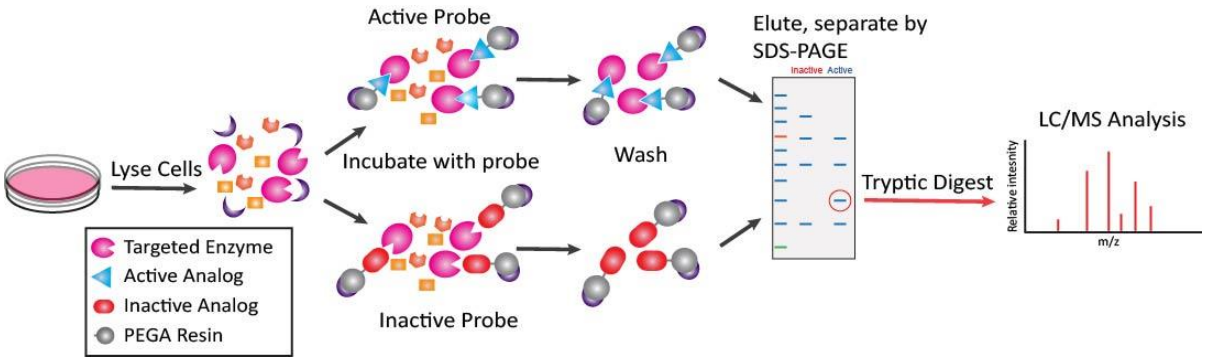

Figure 5. Schematic workflow of ligand-based affinity chromatography.

2.16 Glutathione S-transferase activity assay

Glutathione S-transferase (GST) activity was assayed as described in Groom et al[287], with 1-chloro-2,4-dinitrobenzene (CDNB) and by monitoring the formation of the dinitrophenyl-GSH adduct. Enzyme assays performed in 100 mM potassium phosphate buffer, pH 6.5. Recombinant human GST purified from *Escherichia coli* (a kind gift from Dr. Bengt Mannervik, Uppsala University, Sweden) was incubated with inhibitor and GSH for the indicated length of time. The reaction was initiated by the addition of CDNB. The final concentration of non-aqueous components in the reaction mixture was ≤ 2%. Formation of the reaction product (GSH-CDNB adduct; S-((2,4)-dinitrobenzene)glutathione) was monitored at 340 nm with an Evolution™ 60S UV-Visible Spectrophotometer (Thermo Scientific) in quartz cuvettes. The initial rate of the reaction (V_0) was calculated using the following equation:

$$Vo = absorption/(l \times \varepsilon)$$

where *l* (path length of cuvette) is 1 cm and ε for the GSH-CDNB adduct is 9.6 $mM^{-1}cm^{-1}$. IC_{50} values were measured by fitting the four-parameter logistic function[288] to each data set, using Sigma-Plot™ software.

2.17 Reversibility of GST inhibition

The reversibility of GST inhibition was tested by removing the inhibitor (VSe1) by dialysis. GSTP1-1 (25 μg) was incubated with VSe1 (0.5 mM), and GSH (1 mM) in 100 mM potassium phosphate buffer, pH 6.5. Control samples lacked VSe1. Dialysis was carried out for 3 hours at 4°C in 100 mM potassium phosphate buffer. Enzyme activity was subsequently measured as described above, with 1 mM GSH and 0.5 mM CDNB.

2.18 siRNA transfections

786-0 cells were seeded in 12-well plates at $6x10^4$ cells/well. Twenty-four hours later, cells were transfected with scrambled siRNA control (ON-TARGETplus Non-targeting Control Pool; # D-001810-10-05; Dharmacon), or SMARTpool ON-TARGETplus *GSTP1* siRNA (#L-011179-00-0005; Dharmacon) or oligofectamine (#12252011, Invitrogen) alone, according to the manufacturers' protocols. Forty-eight hours later, cell lysates were collected for immunoblot analysis with antibodies against GSTP1 (#LS-C154708; LifeSpan Biosciences, Inc.) and β-Actin (#4970, Cell Signaling Technology, Danvers, MA. A parallel set of plates was infected with VSVΔ51-GFP at MOI 0.01. Supernatants were collected 24 and 46 hours post-infection and titered by plaque assay. RNA was also collected 72 hours post-

transfection for quantification of human *GSTP1* mRNA via quantitative RT-PCR as described above.

2.19 GSH and GSSG measurement by High Performance Liquid Chromatography (HPLC)

786-0 cells were seeded in 60mm tissue culture plates and treated 24 hours later with VSe1 or **28**. At the indicated times post-treatment, cells were washed twice with ice-cold PBS and lysed on ice for 20 minutes in 125mM sucrose, 1.5mM EDTA, 5mM Tris, 0.1% TFA and 0.5% MPA in HPLC mobile phase (10% HPLC grade methanol, 0.09% TFA – 0.2 μM filtered). Lysates were centrifuged for 20 min at 14,000 g at 4°C and supernatants were collected and injected into an Agilent HPLC system[289,290]. Samples were run in duplicate on a Pursuit5 C18 column (150 × 4.6 mm, 5 μM; Agilent Technologies, Santa Clara, CA) with a 1 mL/min flow rate. GSH and GSSG were detected with an Agilent UV-Vis wavelength detector at 215 nm. Retention times were determined by injecting standard solutions prepared in the same buffer. Absolute amounts of GSH and GSSG were obtained by integrating the area under each peak using Agilent ChemStation software. Quantities in nanomoles were obtained by interpolating from GSH and GSSG standard curves. A parallel set of treated 786-0 plates were trypsinized so that GSH and GSSG levels could be calculated on a per cell basis.

2.20 Ratiometric detection of GSH and GSSG levels with cyto-Grx1-roGFP2

293T cells were seeded in poly-D-lysine coated 96-well plates at a density of $1.25x10^4$ cells/well. Twenty-four hours later, cells were transfected with cyto-Grx1-roGFP2 (a kind gift from Dr. Brett Finlay, University of British Columbia, Canada) or a GFP plasmid (pEGFP-

C3, Clonetech, Mountain View, CA, USA, Cat. PT3052-5) using Genejuice®, according to the manufacturer's protocol (EMD Millipore). Forty-eight hours later, cells were excited at 408 and 488 nm and the ratios of the emissions detected at 530 nm were calculated. Cells were then treated with H_2O_2, VSe1 or **28** and fluorescent readings were made after the indicated timepoints. After the last reading, cells were treated with 5 mM of DTT and fluorescence readings were taken after 2 minutes.

2.21 Detection of reactive oxygen species (ROS) with carboxy-H_2DCFDA

786-0 cells were seeded in 12-well plates, at $3x10^5$ cells/well. The next day, cells were treated with H_2O_2 (3 mM), DMSO or VSe1 (60 μM, 120 μM). Four hours later, cells were detached with Cellstripper® (Corning, Manassas, VA). Cells were re-suspended in fresh DMEM and incubated with 15 μM C-H_2DCFDA for 45 minutes at 37°C with 5% CO_2 in a humidified incubator. Then, samples were washed twice with FACS buffer (0.5% BSA in PBS), filtered through 40 μM cell strainers (Fisher Scientific) and stained with 7-Aminoactinomycin D (7-AAD, eBiosciences; 0.5 μL per sample). Samples were analysed within 30 minutes with a BD FACSCelesta™ (BD) and FlowJo vX.07 software (BD).

2.22 Statistics

The results shown in this study are presented as means ± standard error unless otherwise stated. For all experiments statistical significance (using indicated statistical tests) was considered to be a P value less than or equal to 0.05. Graphs and statistics were computed using GraphPad Prism 6 and Microsoft Excel.

RESULTS

3.1 Physiochemical and *in vitro* biological characterization of VSe1

3.1.1 VSe1 suffers from rapid degradation

As previously discussed, VSe1 sensitizes resistant cancer cells to infection with VSVΔ51, leading to a significant enhancement of viral titers. Upon further study, we found that pre-incubating VSe1 in an aqueous solvent prior to treating cells resulted in an abrogation of its viral sensitizing effect (**Figure 6A**). This prompted an analysis of VSe1's stability in an aqueous environment using a LC-MRM assay. When dissolved in mouse plasma, rapid degradation was observed, with a half -life of 2.1 min (**Figure 6B**).

A

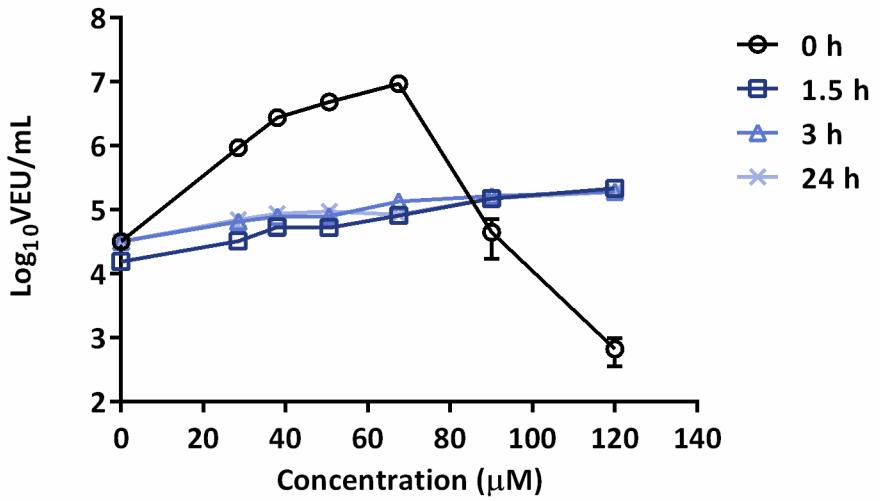
8
7
6
5
4
3
2
Log10VEU/mL
0
20
40
60
80
100
120
140
Concentration (μM)
0 h
1.5 h
3 h
24 h

B

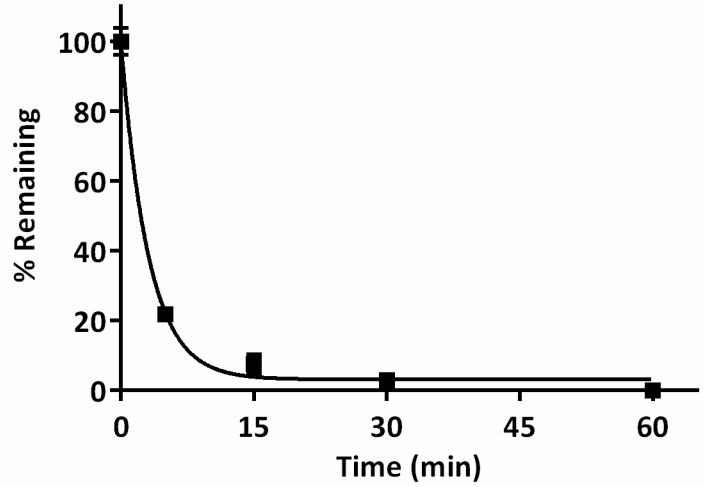
100
80
60
40
20
0
% Remaining
0
15
30
45
60
Time (min)

Figure 6. VSe1 suffers from rapid degradation. (A) VSe1 was incubated in sterile water for 0 h, 1.5 h, 3 h or 24 h before being used to treat 786-0 cells at different concentrations. Four hours post-treatment, cells were infected with VSVΔ51 expressing firefly luciferase (VSVΔ51-Fluc) at a multiplicity of infection (MOI) of 0.005. Forty hours later, virus output in viral expression units (VEUs) per millilitre was measured with a luciferase reporter assay (Materials and Methods, section 2.4)[282]. **(B)** Stability of VSe1 in mouse serum over time, measured by HPLC.

In addition to VSe1's drawbacks regarding *in vivo* administration presented earlier and the limited knowledge of VSe1's molecular target, these results provided rationale to synthesize and test derivatives of VSe1 with increased stability that could be used as tools for mechanism of action studies and that may be better suited for *in vivo* administration.

3.1.2 Structure-activity-relationship studies on VSe1

In order to study the structure-activity relationship of VSe1, chemical analogs of VSe1 were screened for their ability to augment VSVΔ51 replication in 786-0 cells, a human renal carcinoma cell line which is highly resistant to infection with VSVΔ51, but sensitive to infection after pre-treatment with VSe1[275]. A high-throughput luciferase reporter-based viral titration assay was used to assess changes in virus output 40 hours post-infection (described in detail in Materials and Methods)[282]. Viral Expression Units (VEUs) obtained from this assay correlate directly with infectious titers obtained from plaque assays (**Figure 4**)[282]. Cytotoxicity of each analog in the presence and absence of virus was also measured using the metabolic dye alamarBlue®. For each compound, the peak fold enhancement (PFE) in VEU relative to vehicle-treated infected samples is displayed, as well as the concentration at which this occurs (PFE dose). For 49 of the analogs tested, plasma stability was measured by LC-MRM, and susceptibility to nucleophilic attack was measured using a GSH challenge assay, where compounds were incubated with GSH at a supraphysiological concentration (five-fold molar excess of compound) and the quantity of unreacted parent compound was measured over time (**Table 5**). Fold-changes in viral output at 40 hours post-infection for each compound across all concentrations tested are included in **Appendix B**.

Table 5. Analog activity, toxicity and stability

ID	Structure	Peak fold enhancement[a]	PFE dose (μM)[b]	LD_{50} (μM)	LD_{50} with virus (μM)	GSH half-life (min.)	Plasma stability at 3 hours (% remaining)
1 (VSe1)	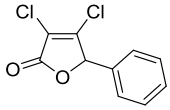	1910	60	79	16	< 5	0
2	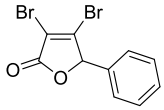	705	72	87	50	< 5	0
3	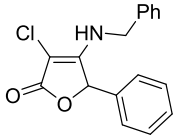	365	96	140	140	NR[c]	65.6 ± 6.5
4	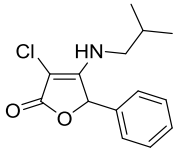	345	80	90	90	NR	0
5	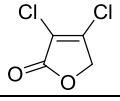	515	36	41	27	< 5	0
6	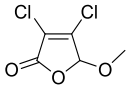	400	60	73	51	< 5	0
7	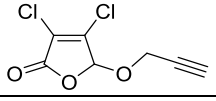	575	60	52	17	< 5	0
8	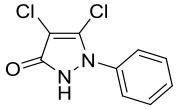	NE[d]	-	>180	>180	NR	88.3 ± 9.3
9	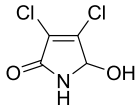	1280	120	148	87	117	0
10	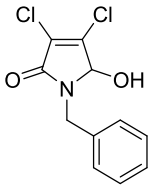	555	48	67	51	32	19.8 ± 0.4
11	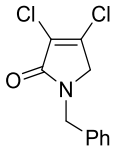	55	240	332	332	64	42.5 ± 9.6

ID	Structure	Peak fold enhancement[a]	PFE dose (μM)[b]	LD_{50} (μM)	LD_{50} with virus (μM)	GSH half-life (min.)	Plasma stability at 3 hours (% remaining)
12	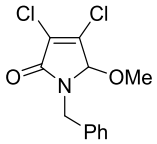	535	180	206	203	118	47.6 ± 1.4
13	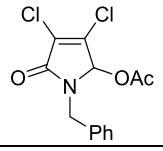	305	60	61	45	21	0
14	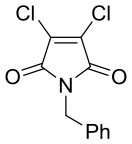	75	96	91	85	< 5	70.2 ± 8.4
15	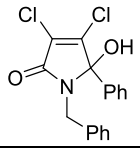	NE	-	66	66	340	14.9 ± 7.1
16	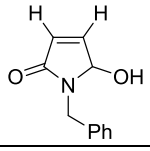	NE	-	> 360	> 360	NR	98.2 ± 3.7
17	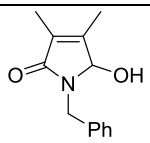	NE	-	> 360	> 360	NR	82.0 ± 10.2
18	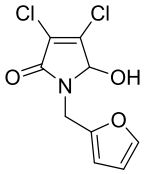	475	60	67	28	45	54.1 ± 5.1
19	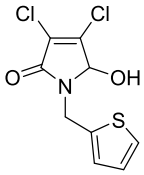	975	60	64	27	40	50.1 ± 10.5
20	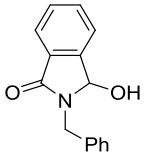	NE	-	>360	>360	NR	102.9 ± 1.6

ID	Structure	Peak fold enhancement[a]	PFE dose (μM)[b]	LD_{50} (μM)	LD_{50} with virus (μM)	GSH half-life (min.)	Plasma stability at 3 hours (% remaining)
21	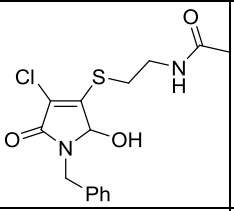	55	504	630	567	NR	102.7 ± 10.8
22	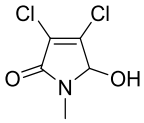	895	96	119	76	68	72.0 ± 3.0
23	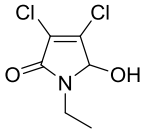	1105	120	171	89	-	ND
24	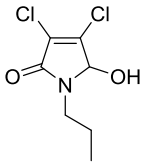	915	120	174	96	61	91.6 ± 5.2
25	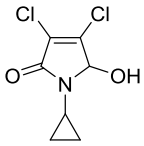	1415	80	127	51	53	54.8 ± 3.6
26	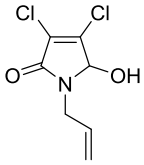	995	96	110	66	46	64.8 ± 7.7
27	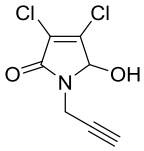	40	48	100	87	21	9.0 ± 1.4
28	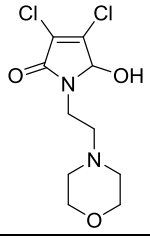	1910	80	153	55	96	38.9 ± 5.2
29	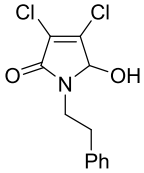	975	72	74	27	74	57.6 ± 6.6

ID	Structure	Peak fold enhancement[a]	PFE dose (μM)[b]	LD_{50} (μM)	LD_{50} with virus (μM)	GSH half-life (min.)	Plasma stability at 3 hours (% remaining)
30	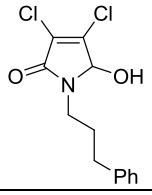	1090	32	36	20	50	42.9 ± 7.2
31	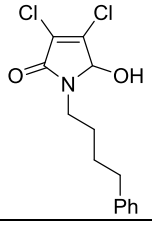	495	40	40	34	72	40.1 ± 9.8
32	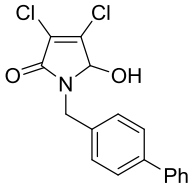	210	27	28	5	24	ND[e]
33	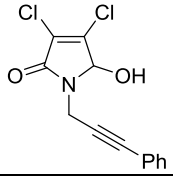	575	18	18	12	24	0
34	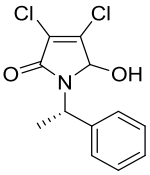	630	72	74	6	31	48.0 ± 16.5
35	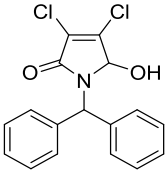	265	27	36	23	43	63.8 ± 3.2
36	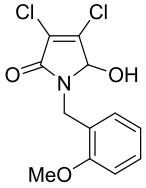	55	72	56	56	34	28.2 ± 2.6
37	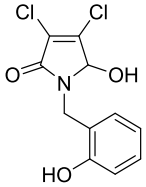	1070	48	58	38	41	0.7 ± 0.1

ID	Structure	Peak fold enhancement[a]	PFE dose (μM)[b]	LD_{50} (μM)	LD_{50} with virus (μM)	GSH half-life (min.)	Plasma stability at 3 hours (% remaining)
38	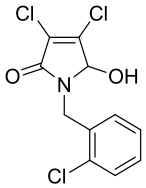	670	216	215	107	32	25.7 ± 2.9
39	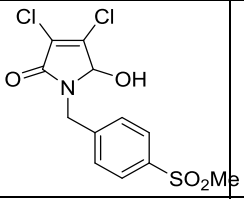	975	60	> 90	25	34	41.4 ± 5.4
40	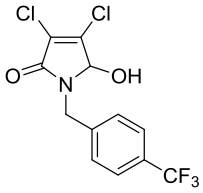	2005	27	36	13	32	15.3 ± 2.5
41	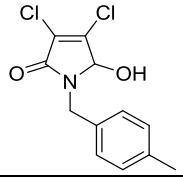	365	40	39	30	35	51.4 ± 8.2
42	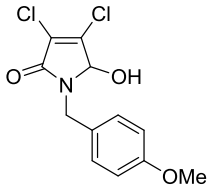	190	40	55	17	40	49.1 ± 12.4
43	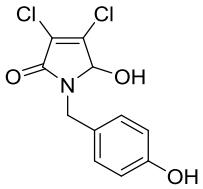	285	60	> 90	45	69	58.3 ± 0.6
44	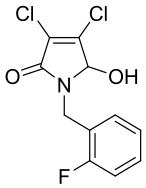	155	60	63	39	31	45.9 ± 8.1
45	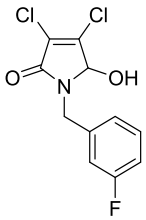	115	48	43	37	31	54.2 ± 4.2

ID	Structure	Peak fold enhancement[a]	PFE dose (μM)[b]	LD_{50} (μM)	LD_{50} with virus (μM)	GSH half-life (min.)	Plasma stability at 3 hours (% remaining)
46	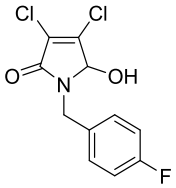	170	40	42	36	32	23.1 ± 0.8
47	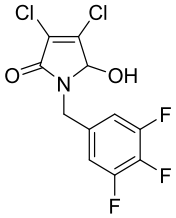	190	40	36	35	35	22.7 ± 8.4
48	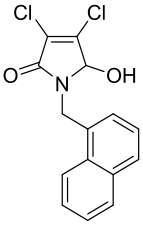	1240	32	38	24	14	36.5 ± 7.6
49	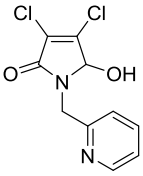	590	96	131	67	64	44.6 ± 1.2
50	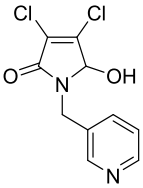	800	60	85	29	54	39.6 ± 2.6
51	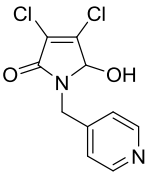	590	72	89	28	53	44.0 ± 1.0
52	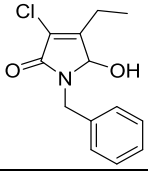	NE[d]	-	>360	>360	ND[e]	ND[e]

ID	Structure	Peak fold enhancement[a]	PFE dose (μM)[b]	LD_{50} (μM)	LD_{50} with virus (μM)	GSH half-life (min.)	Plasma stability at 3 hours (% remaining)
53	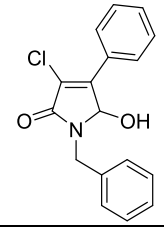	NE[d]	-	249	250	ND[e]	ND[e]
57	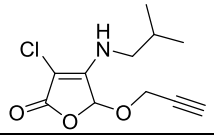	NE[d]	-	>120	120	ND[e]	ND[e]
58	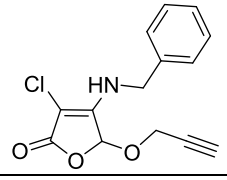	NE[d]	-	>360	>360	ND[e]	ND[e]

[a] Peak fold enhancement is the peak fold change in viral expression units (VEU) relative to vehicle-treated infected samples.
[b] PFE dose is the compound concentration cells were treated with to achieve the peak fold change in VEU.
[c] No reaction with glutathione observed.
[d] No enhancement of VEU.
[e] No data.

VSe1 was used as a reference standard every time the screen was performed, and the PFE for VSe1 is the mean from 33 separate screens. To control for minor changes in baseline VEUs and the resulting effect on PFEs, peak VEUs for each analog was normalized to those of VSe1-treated controls from that particular screen. The resulting ratio for the PFE dose was multiplied by the PFE for VSe1, and the results are displayed in column 3. Compounds that were used in additional experiments presented in this thesis following this screen are bolded.

Substitution of both chorines for bromines led to **2**, which had slightly reduced activity compared to VSe1 and similar stability and reactivity profiles. Substitution of the β-chlorine with an alkyl amine (**3** and **4**) resulted in compounds with reduced reactivity, increased stability (**3** only), but decreased viral enhancement activity. Removal of the aryl group (**5**) or replacement with a methoxide group (**6**) resulted in active compounds with poor stability, similar to VSe1. Replacing the furan scaffold with a pyrrole-based scaffold resulted in compounds (**9**, **10**) that were active but less electrophilic, as shown by the increased half-life from the GSH challenge assay. With **10**, this also resulted in increased plasma stability. The LC-MS trace observed in the GSH stability assay also showed that **10**, contrary to VSe1, cleanly reacted with GSH to form the GSH adduct as the sole detectable product (**Figure 7**).

A

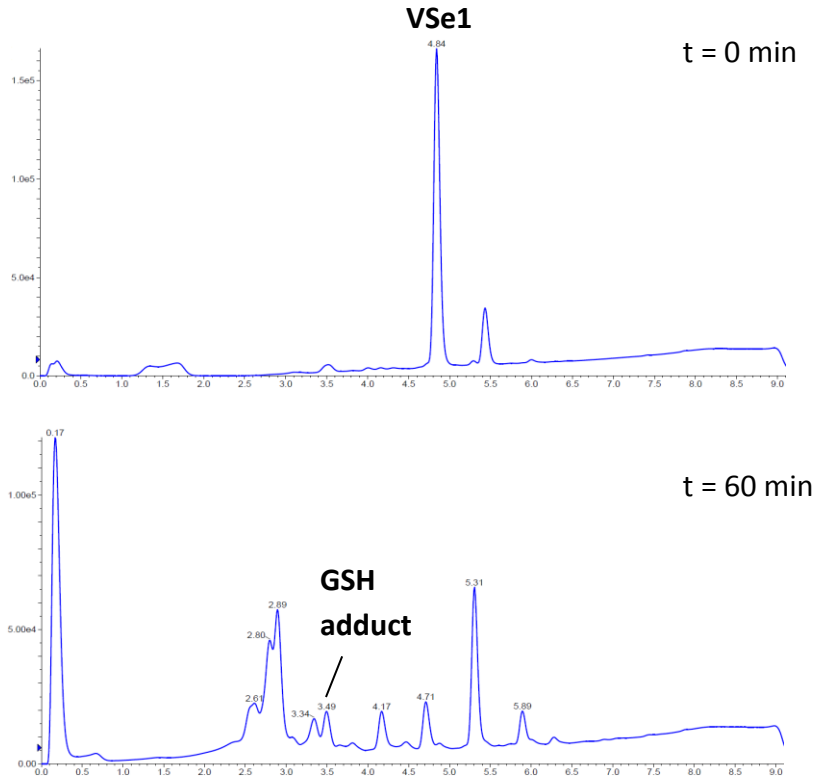
VSe1
t = 0 min
t = 60 min
GSH
adduct

B

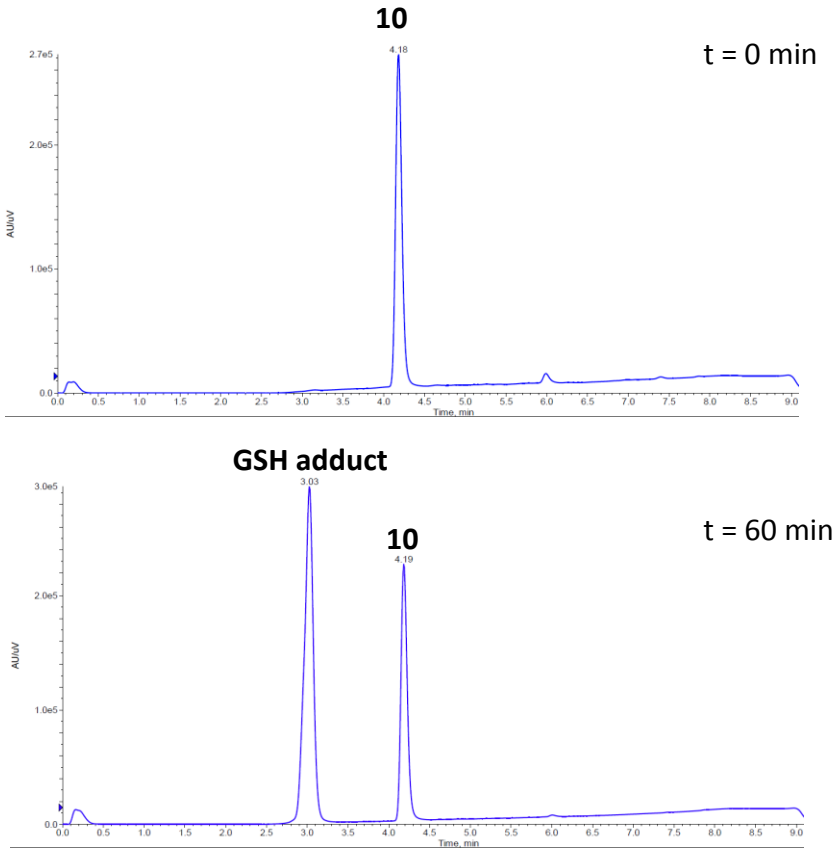
10
t = 0 min
GSH adduct
10
t = 60 min
Time, min

Figure 7. Reaction products of VSe1 and 10 from GSH stability assay. (A) 250 μL of 40 mM DMSO stock solution of VSe1 was added to L-glutathione (15.4 mg, 5 mol equiv.) suspended in 250 μ L DMSO. The resulting mixture was placed in a 37 °C shaker. 10 μL aliquots were removed and quenched in 990 μ L water (containing 0.5% formic acid) at various timepoints (t = 0 minutes and t = 60 minutes shown). Analysis by ESI-LC-MS allowed for the identification and quantification of VSe1 and the glutathione adduct by UV-Vis at 254 nm. **(B)** 250 μL of 40 mM DMSO stock solution of **10** was added to L-glutathione (15.4 mg, 5 mol equiv.) suspended in 250 μL DMSO. The resulting mixture was placed in a 37 °C shaker. 10 μL aliquots were removed and quenched in 990 μL water (containing 0.5% formic acid) at various time points (t = 0 minutes and t = 60 minutes shown). Analysis by ESI-LC-MS allowed for the identification and quantification of **10** and the glutathione adduct by UV-Vis at 254 nm. These results were generated by Mark Dornan.

Given these results, additional analogs based on the pyrrole scaffold were generated. Alterations to the hydroxyl group (**11**–**15**) considerably hindered activity, as did alterations to the dichloro- α,β-unsaturated carbonyl moiety (**16**, **17**, **20**, **21**, **52**, **53** and **57**). This suggests that the ability of these compounds to act as Michael acceptors is important for their ability to sensitize cells to VSVΔ51. Activity was maintained when the *N*-benzyl group from **10** was replaced with a furan or thiophene (**18** and **19**, respectively), indicating that substitutions at this position are tolerated. Cyclopropyl and morpholine containing analogs (**25** and **28**) retained activity and displayed remarkably improved in vitro toxicity and stability profiles. Examination of arylamine containing analogs showed that the spacer length between the amine and phenyl ring was optimal at three carbons (**10**, **29** and **31**). Testing a large set of substituted benzylamine derivatives (**36**–**51**) demonstrated that the 4-trifluoromethyl substituted system (**40**) possessed improved activity (2,000 fold enhancement, 105% of VSe1) and improved stability. A summary of the key findings from these SAR studies is presented in **Figure 8**. Overall, these results demonstrate that the activity and stability of VSe1 analogs can be readily tuned, and the capacity of VSe1 derivatives to act as Michael acceptors is likely implicated in their mechanism of action.

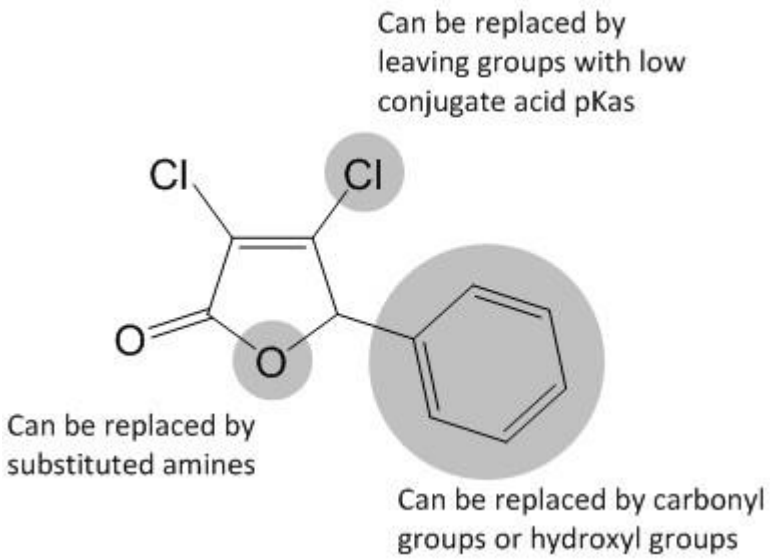

Figure 8. Key pharmacophores of VSe1

3.1.3 Activity of VSe1 and analogs in VSVΔ51-resistance cancer cell lines

Following initial analog screening studies carried out in 786-0 renal cancer cells, we tested human ovarian cancer cells (OVCA433) and various mouse cancer cell lines including B16-F10 (melanoma), CT26.WT (colon adenocarcinoma), 4T1 (mammary carcinoma), MC-38 (colon adenocarcinoma) and Pan02 (pancreatic ductal adenocarcinoma), S180 (soft tissue sarcoma) and CT-2A (glioma). These cell lines were also sensitized to VSVΔ51 by VSe1 and pyrrole-based analogs (**Figures 9-10**).

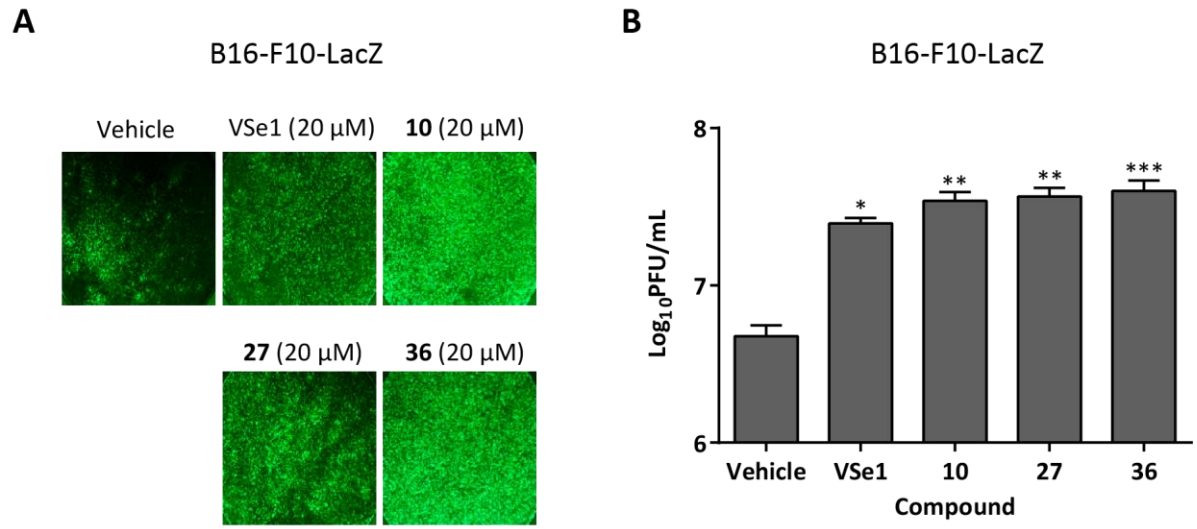
A
B16-F10-LacZ
Vehicle
VSe1 (20 μM)
10 (20 μM)
27 (20 μM)
36 (20 μM)
B
B16-F10-LacZ
Log10PFU/mL
8
7
6
*
**
**
***
Vehicle
VSe1
10
27
36
Compound

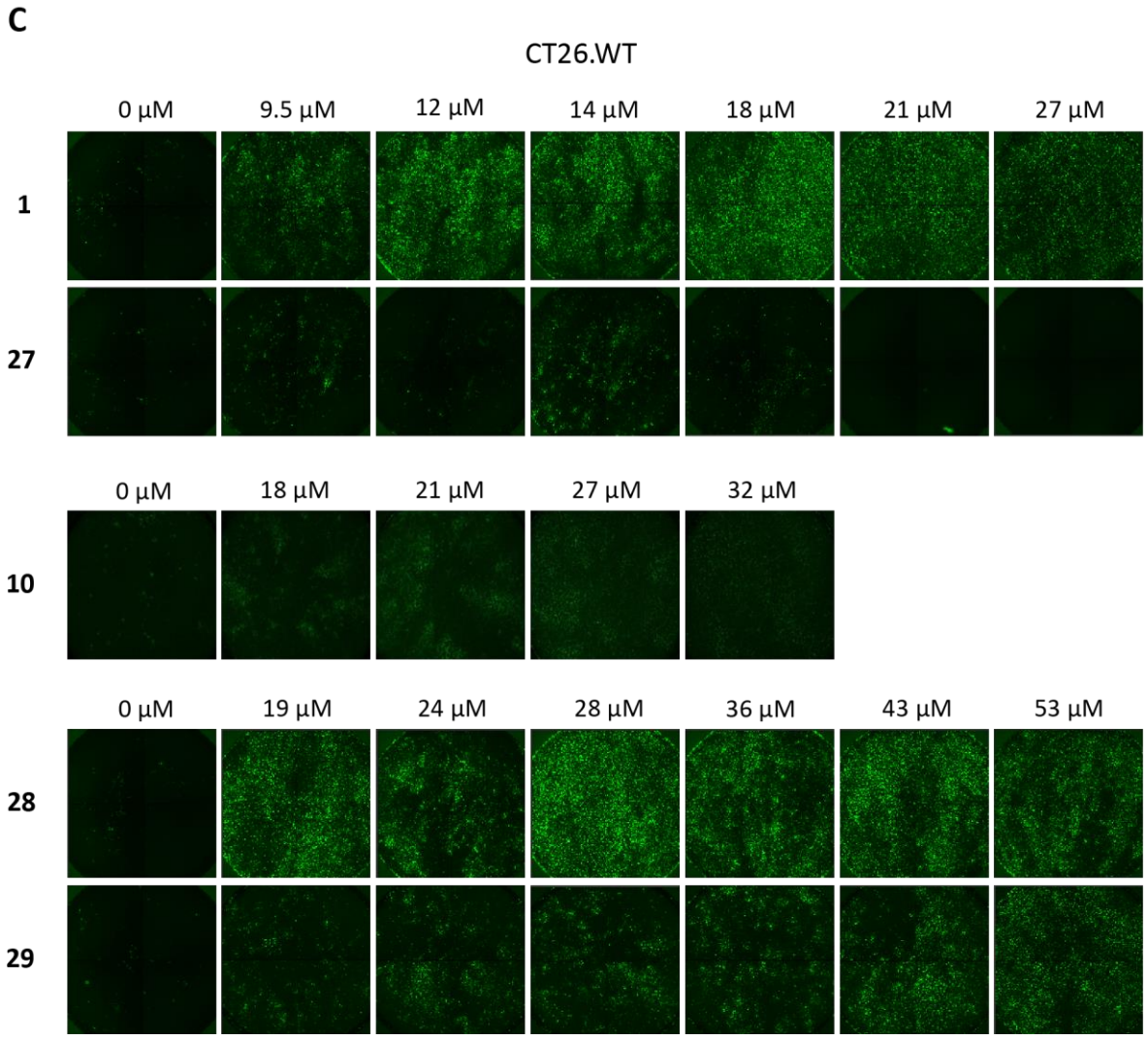
C
CT26.WT
0 μM
9.5 μM
12 μM
14 μM
18 μM
21 μM
27 μM
1
27
0 μM
18 μM
21 μM
27 μM
32 μM
10
0 μM
19 μM
24 μM
28 μM
36 μM
43 μM
53 μM
28
29

Figure 9. VSe1 and analogs enhance VSVΔ51 spread in murine melanoma and colon cancer cells. Murine melanoma (B16F10-LacZ) cells were treated with vehicle, VSe1, **10**, **27**, or **36** for 4h at the specified concentrations. Four hours later, cells were infected with VSVΔ51-GFP at MOI 0.001. **(A)** Virus replication was assessed by fluorescence microscopy 24 hours post-infection. **(B)** Samples were titered 48 hours post-infection. *p = 0.0392, **p = 0.0027 for **10** vs. vehicle and 0.0015 for **27** vs. vehicle, ***p = 0.0007 for **36** vs. vehicle (one-way ANOVA with Dunnett's multiple comparisons test), Error bars represent standard error (N =3). **(C)** Murine colon carcinoma (CT26.WT) cells were treated with vehicle, VSe1, **10**, **27**, **28**, or **29** for 4h at the specified concentrations. Four hours later, cells were infected with VSVΔ51-GFP at MOI 0.005. Virus replication was assessed by fluorescence microscopy 24 hours post-infection.

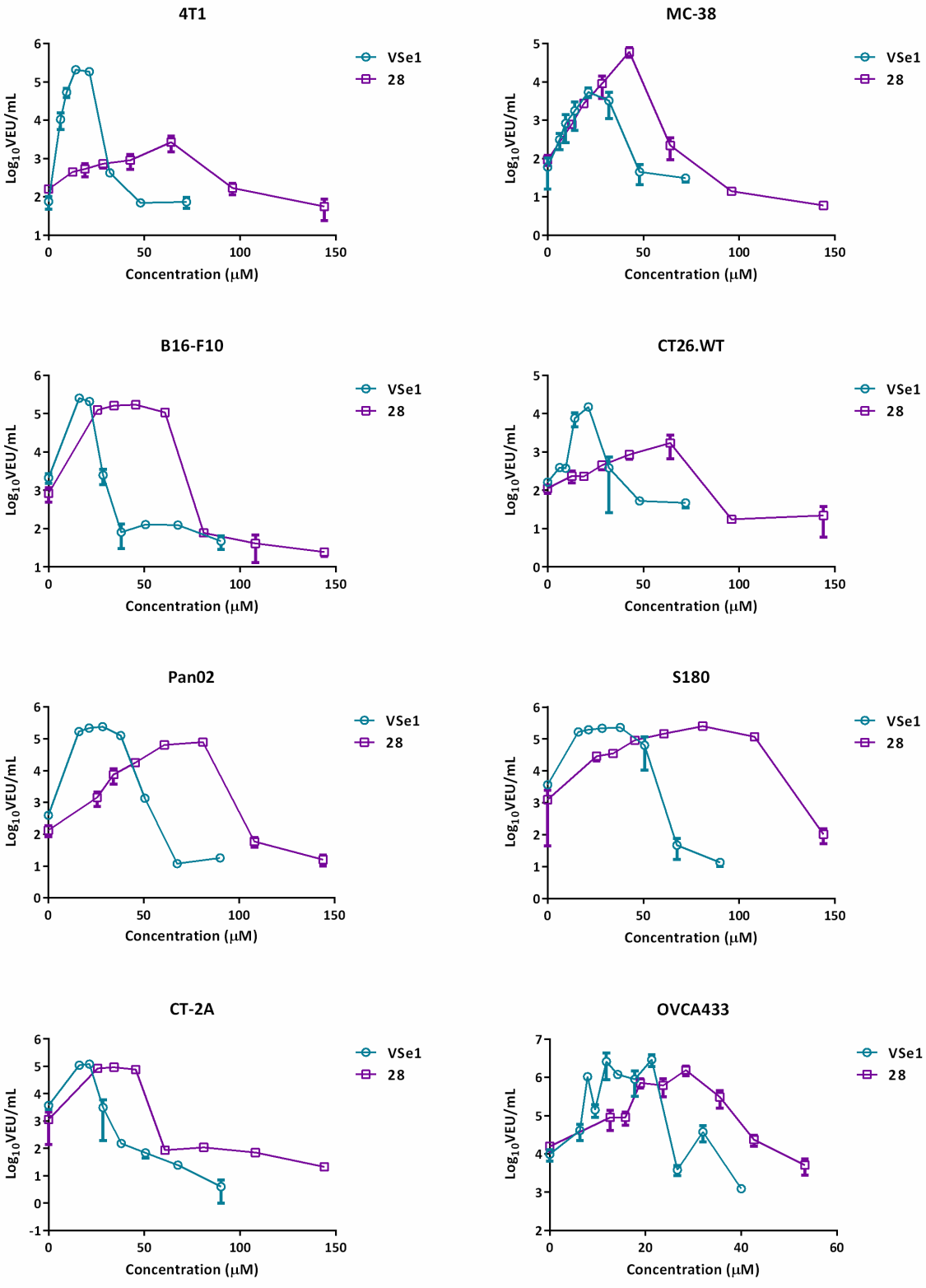
4T1
MC-38
B16-F10
CT26.WT
Pan02
S180
CT-2A
OVCA433
VSe1
28
Log10VEU/mL
Concentration (μM)

Figure 10. VSe1 and analogs enhance VSVΔ51 titers in multiple cancer cell lines. Each indicated cell line was pre-treated with VSe1 or **28** for 4 hours and then infected with infected with VSVΔ51-FLuc at MOI 0.005. Forty hours post-infection, virus output in VEUs was measured with a luciferase reporter-based viral titration assay (Materials and Methods, section 2.4)[282].

3.1.4 Activity of VSe1 and analogs with other virus platforms

VSe1, **10** and several other pyrrole analogs increased the oncolytic activity of Maraba MG1 virus[167] (**Figure 11**) as well as spread of oncolytic HSV-1 N212 (**Figure 12**) and modified Vaccinia Ankara virus (MVA; commonly used as a vaccine platform), both expressing GFP (**Figure 13**), suggesting the compounds have a broader scope of application for virus-based therapies. Luciferase transgene expression delivered to human A549 lung cancer cells by non-replicating adeno-associated virus (AAV) and adenovirus vectors (**Figures 14A** and **14B**, respectively) was also enhanced by the compounds, suggesting the potentiating effects of these compounds are not limited to replicating viruses.

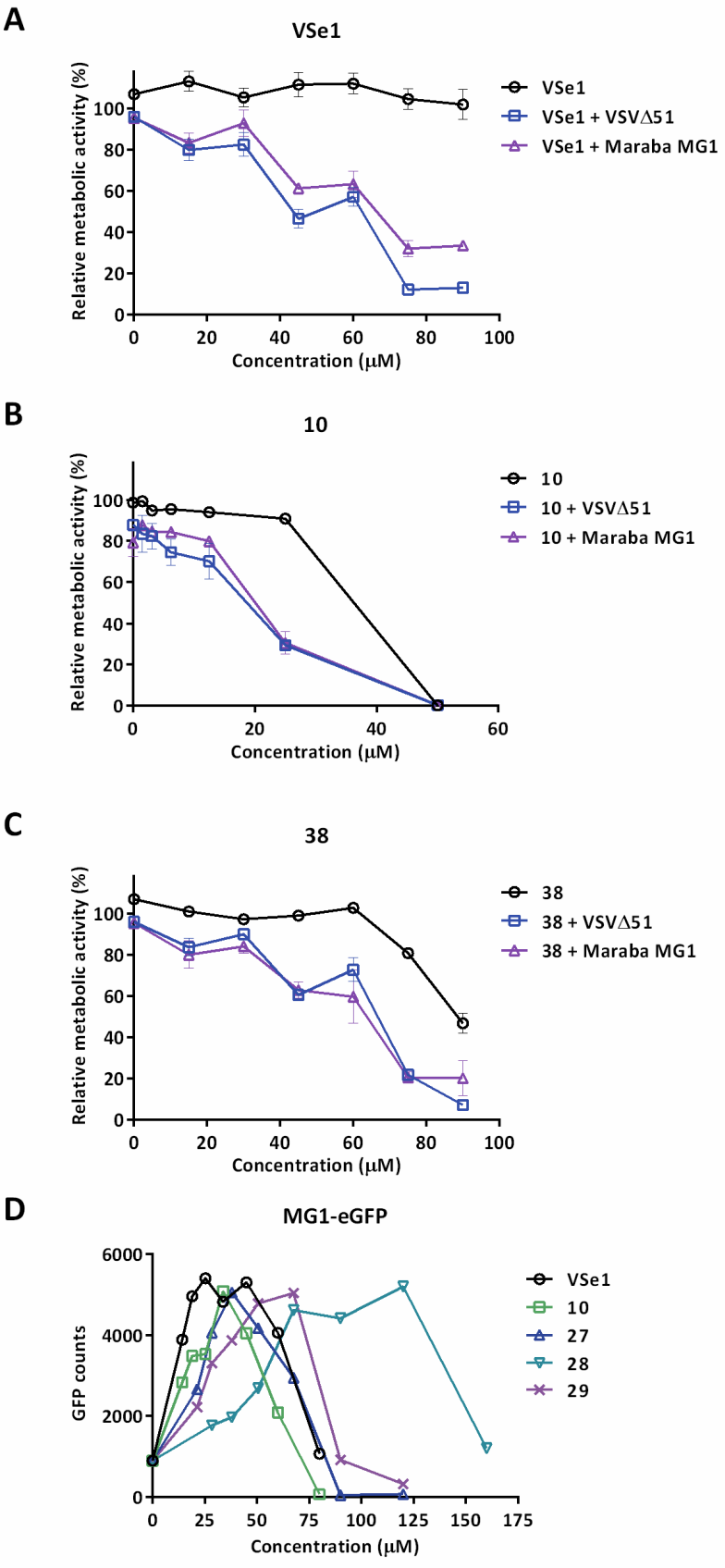
A
VSe1
Relative metabolic activity (%)
Concentration (μM)
VSe1
VSe1 + VSVΔ51
VSe1 + Maraba MG1
B
10
Relative metabolic activity (%)
Concentration (μM)
10
10 + VSVΔ51
10 + Maraba MG1
C
38
Relative metabolic activity (%)
Concentration (μM)
38
38 + VSVΔ51
38 + Maraba MG1
D
MG1-eGFP
GFP counts
Concentration (μM)
VSe1
10
27
28
29

Figure 11. VSe1 and analogs enhance oncolytic VSV and MG1 activity in cancer cells. Murine mammary carcinoma (4T1) cells were treated with vehicle, **(A)** VSe1, **(B) 10**, or **(C) 38** for 4h at the specified concentrations. Four hours later, cells were infected with VSVΔ51 or Maraba MG1 at MOI 0.005. Forty hours post-infection, cytotoxicity was assessed by incubating samples with alamarBlue® for 2 h at 37°C before measuring fluorescence (530nm excitation, 590 nm emission). Values were normalized to that of untreated controls. **(D)** 786-0 cells were pre-treated with VSe1 and analogs for 4 hours and then infected with MG1-eGFP at an MOI of 0.005. Twenty-four hours post-infection, eGFP was quantified with a Cellomics ArrayScan® VTI HCS Reader (Thermo Fisher Scientific).

A

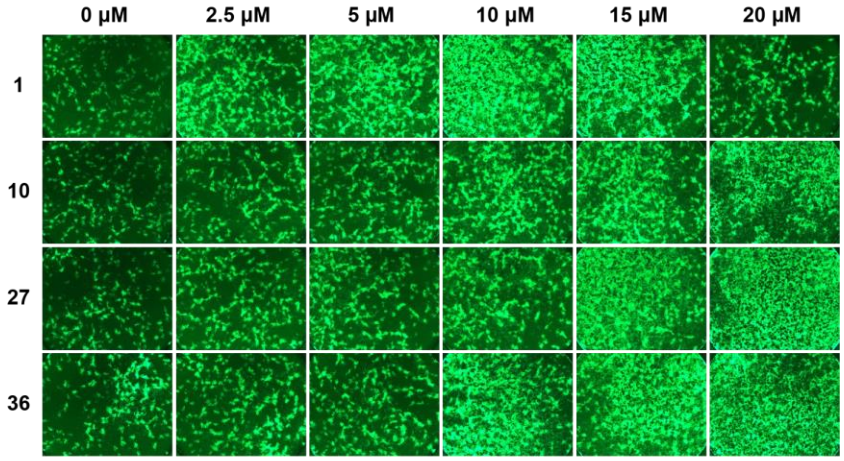
0 µM
2.5 µM
5 µM
10 µM
15 µM
20 µM
1
10
27
36

B

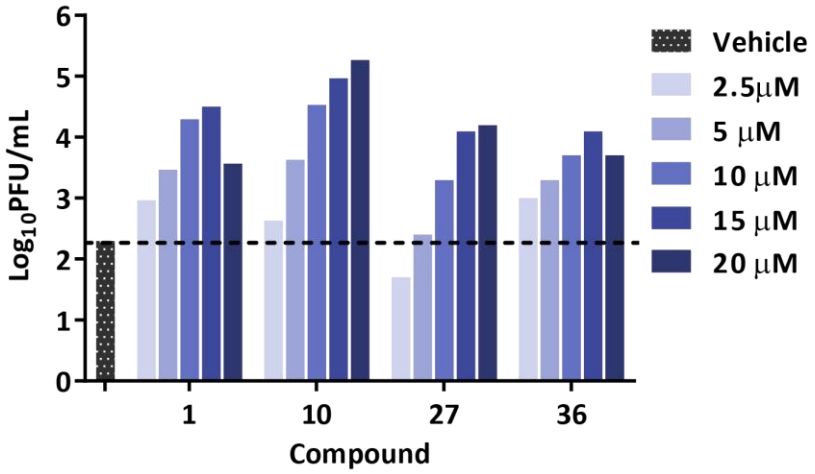
Log10PFU/mL
0
1
2
3
4
5
6
1
10
27
36
Compound
Vehicle
2.5µM
5 µM
10 µM
15 µM
20 µM

C

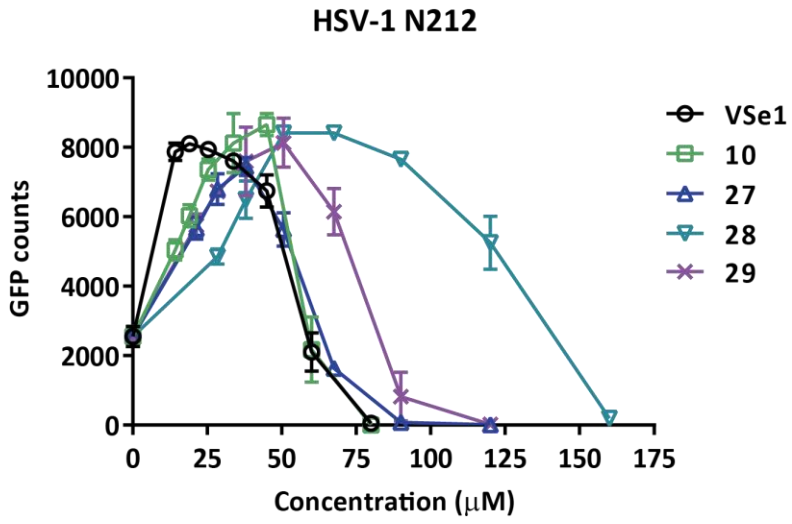
HSV-1 N212
GFP counts
0
2000
4000
6000
8000
10000
0
25
50
75
100
125
150
175
Concentration (µM)
VSe1
10
27
28
29

Figure 12. VSe1 and analogs sensitize cancer cells to oncolytic HSV-1. (A) Mouse mammary carcinoma (4T1) cells were left untreated or, treated with VSe1, **10**, **27**, or **36** for 4 h at various concentrations: 2.5 μ M, 5 μM, 10 μ M, 15 μ M or 20 μ M. ICP0-null HSV-N212eGFP was then added at MOI 0.005. eGFP fluorescence was detected 48 h after HSV infection. **(B)** HSV titers were determined 48 h after infection. **(C)** 786-0 cells were pre-treated with VSe1 and analogs for 4 hours and then infected with ICP0-null HSV-N212eGFP at an MOI of 0.01. Forty-eight hours post-infection, eGFP was quantified with a Cellomics ArrayScan® VTI HCS Reader (Thermo Fisher Scientific).

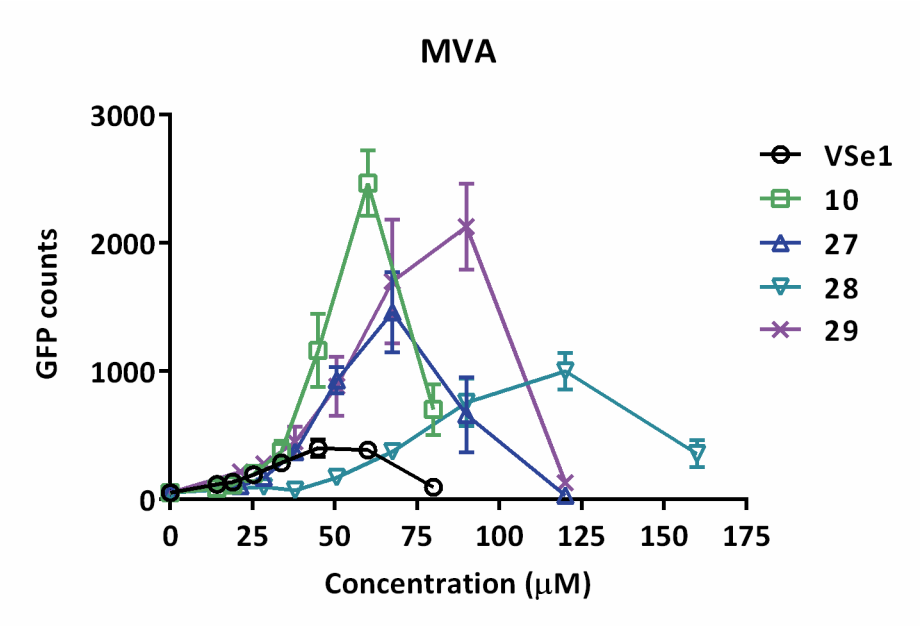
MVA
GFP counts
3000
2000
1000
0
0
25
50
75
100
125
150
175
Concentration (μM)
VSe1
10
27
28
29

Figure 13. VSe1 and analogs sensitize cancer cells to MVA virus. 786-0 cells were pre-treated with VSe1 and indicated analogs for 4 hours and then infected with MVA-eGFP at an MOI of 0.1. Forty-eight hours post-infection, eGFP expression was quantified with a Cellomics ArrayScan® VTI HCS Reader (Thermo Fisher Scientific).

A

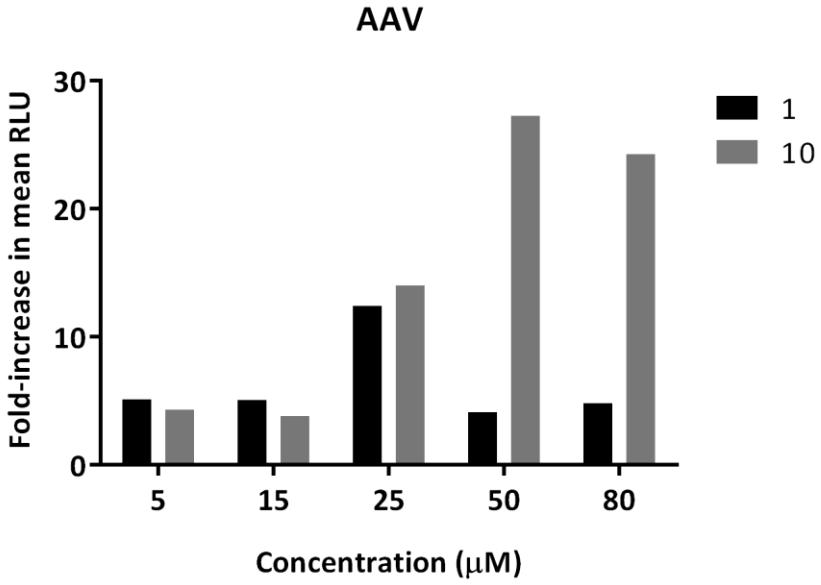
AAV
Fold-increase in mean RLU
30
20
10
0
5
15
25
50
80
Concentration (μM)
1
10

B

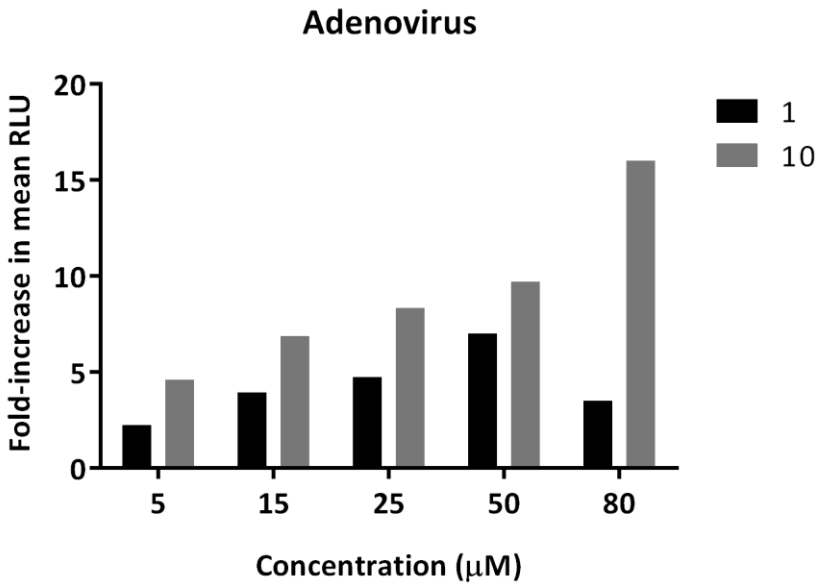
Adenovirus
Fold-increase in mean RLU
20
15
10
5
0
5
15
25
50
80
Concentration (μM)
1
10

Figure 14. VSe1 and 10 enhance transduction of non-replicating gene therapy vectors in human lung carcinoma cells. Human lung carcinoma (A549) cells were treated with VSe1 or **10** analogs at various concentrations. Four hours later, cells were infected with **(A)** replication defective adeno-associated virus expressing firefly luciferase (AAV2-luc) or **(B)** replication defective adenovirus expressing firefly luciferase (Ad5-luc) at an MOI of 1. Twenty-four hours later, luciferase activity was measured. Results are represented as the fold increase in mean relative light units (RLU) of treated samples versus untreated controls.

3.2 *Ex vivo* and *in vivo* activity of VSe1 and active analogs

3.2.1. Selective viral enhancement in ex vivo tumour specimens

A notable advantage of OV therapy over traditional cancer therapies is its selectivity for cancerous tissue and ensuing safety profile. Thus, it was necessary to confirm that this novel class of viral sensitizers does not enhance viral replication in normal tissues. To facilitate evaluation of a larger number of compounds prior to *in vivo* testing, we chose to test a subset of analogs with favourable properties (**10**, **28**, **29**, **30** and **40**) for their ability to enhance VSVΔ51 oncolysis in *ex vivo* tissue samples using an established method,[291] in comparison to VSe1 as a benchmark. Tissue samples from VSVΔ51-resistant CT26.WT murine colon cancer tumours[215,292,293] as well as normal brain, lung and spleen tissue from the same mice were excised and cored. Viable cores were selected for subsequent treatment with each compound and VSVΔ51 expressing green fluorescent protein (VSVΔ51-GFP). **Figure 15A** shows representative images of infected cores that were pre-treated with an optimized concentration of compound. Corresponding viral titers determined by plaque assay are shown in **Figure 15B**. VSe1 and analogs robustly enhanced VSVΔ51-GFP titers in CT26.WT tumour specimens. There was little to no enhancement of VSVΔ51 in normal tissue specimens, indicating that the specificity of VSVΔ51 towards tumour tissue is maintained following treatment with VSe1 and its derivatives.

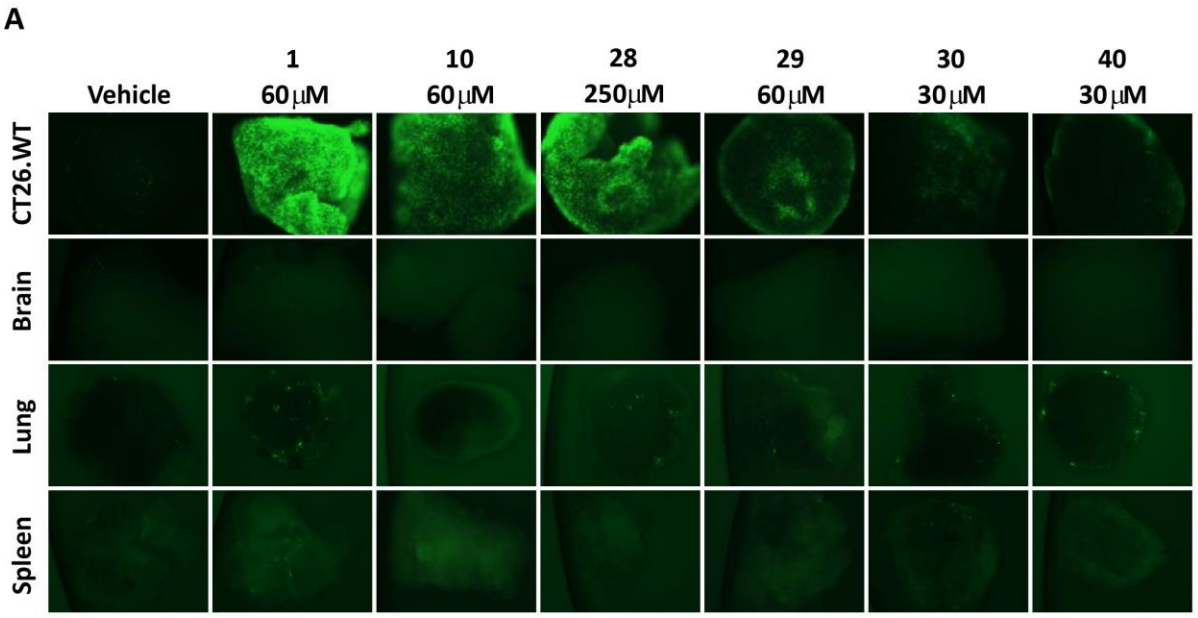
A
Vehicle
1
60 μM
10
60 μM
28
250 μM
29
60 μM
30
30 μM
40
30 μM
CT26.WT
Brain
Lung
Spleen

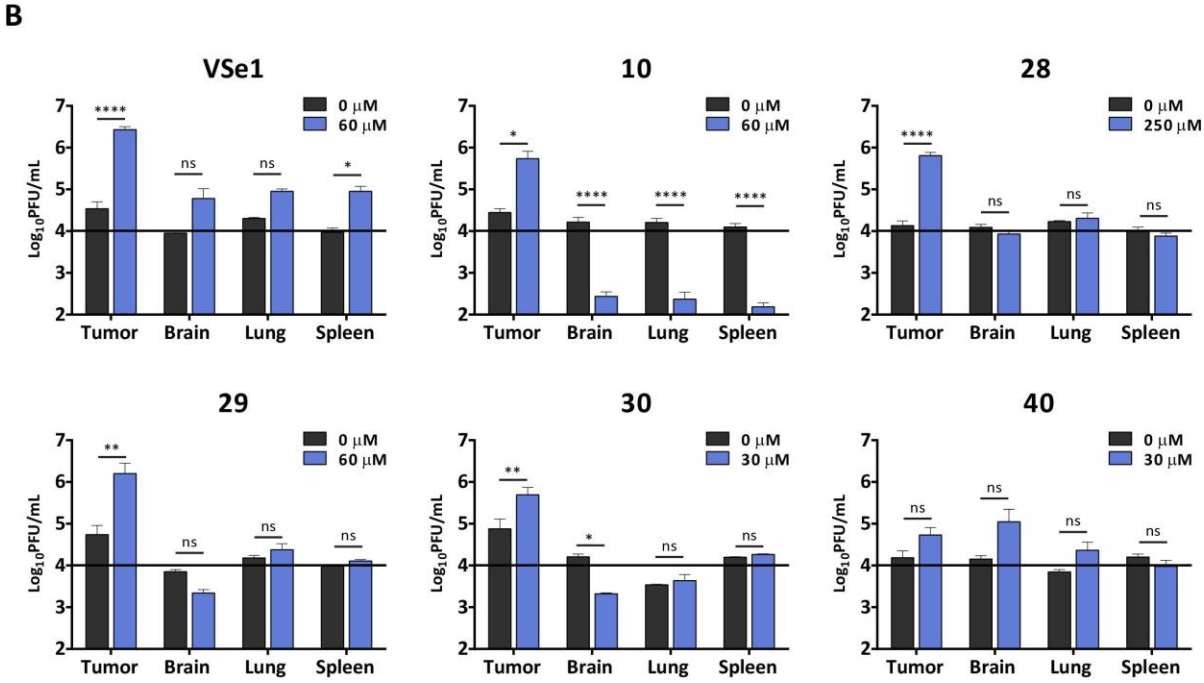
B
VSe1
10
28
29
30
40
0 μM
60 μM
250 μM
30 μM
Log10PFU/mL
Tumor
Brain
Lung
Spleen
****
**
*
ns

Figure 15. VSe1 and its analogs selectively enhance the replication of VSVΔ51-GFP in *ex vivo* tumour tissues. (A) CT26.WT (murine colon carcinoma) tumours were grown subcutaneously in Balb/c mice and subsequently excised and cored, along with normal brain, lung and spleen tissues. Tissue samples were treated in triplicate with 3 concentrations of each compound for 4 hours prior to infection with VSVΔ51-GFP. Virus replication was assessed by fluorescence microscopy 24 hours post- infection. Representative images from each triplicate set for the most effective concentration are shown. **(B)** Infected cores and corresponding supernatants were collected 36 hours post-infection. VSVΔ51-GFP titers were quantified by standard plaque assay. Graphs show the sum of infectious titer from core and supernatant for each compound in each tissue type. The horizontal black line on each graph at $1x10^4$ PFU/mL represents the amount of VSVΔ51-GFP used to initially infect each core. Error bars represent standard error from biological triplicates and statistical significance was calculated using two-way ANOVA with a Dunnett's multiple comparison test (**** $P < 0.0001$, ** $P < 0.01$, * $P < 0.05$, ns = $P > 0.05$).

3.2.2. Analogs are well tolerated in vivo

Prior to evaluating the *in vivo* efficacy of these compounds in combination with virus in mouse models of cancer, we deemed it necessary to determine the *in vivo* tolerability of the compounds alone in non-tumour bearing mice. Dose escalation studies were conducted with a subset of analogs, selected based on desirable physiochemical characteristics, *in vitro* activity and *ex vivo* activity. Compounds were administered intraperitoneally to non-tumour bearing Balb/c mice and body weight was monitored over several days. Mice were sacrificed when they reached the endpoint of 20% loss of body weight or showed significant outward signs of toxicity (piloerection, lethargy, respiratory distress, quiet behaviour) for more than 48 hours. **Figure 16** shows that VSe1 leads to toxicity starting at a dose of 10 mg/kg. In contrast **10** was well tolerated up to a dose of 50 mg/kg and **24** and **28** were well tolerated up to 100 mg/kg.

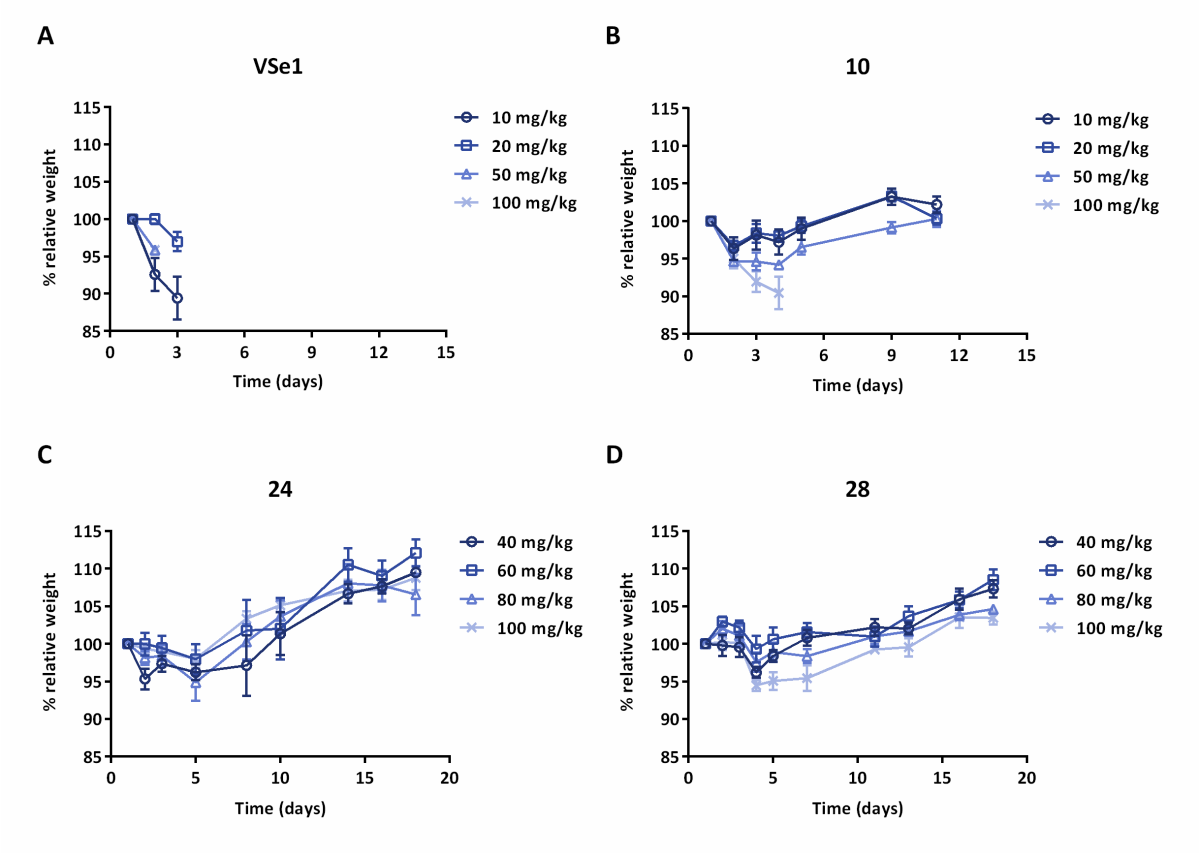
A
VSe1
% relative weight
Time (days)
10 mg/kg
20 mg/kg
50 mg/kg
100 mg/kg
B
10
% relative weight
Time (days)
10 mg/kg
20 mg/kg
50 mg/kg
100 mg/kg
C
24
% relative weight
Time (days)
40 mg/kg
60 mg/kg
80 mg/kg
100 mg/kg
D
28
% relative weight
Time (days)
40 mg/kg
60 mg/kg
80 mg/kg
100 mg/kg

Figure 16. Pyrrole-based derivatives of 1 are substantially better tolerated in mice. Balb/c mice were given **(A)** VSe1, **(B) 10**, **(C) 24** or **(D) 28** dissolved in DMSO via intraperitoneal administration. Five mice were assigned to each dose group for each compound. Graphs stop when the first mouse in the group was euthanized. For VSe1 and **10**, mice were injected on Day 1 and weights were recorded over a 10 day period. For **24** and **28**, mice were injected on Day 1, 3 and 5 and weights were recorded over an 18 day period. For all groups, weights are reported relative to initial weight on Day 1.

3.2.3. Compound 10 enhances therapeutic efficacy of VSV∆51 in CT26.WT tumours

Given its high tolerability and that it was one of the first analogs to be tested *in vivo*, initial *in vivo* studies in tumour-bearing mice were performed with compound **10**. Balb/c mice were subcutaneously engrafted with CT26.WT cells and treated eleven days post engraftment with VSV∆51-FLuc (administered intratumourally) alone or in combination with **10** (administered intraperitoneally). The combination of **10** and VSV∆51-FLuc significantly delayed tumour progression and enhanced overall survival, compared to each treatment alone or vehicle controls (**Figure 17**).

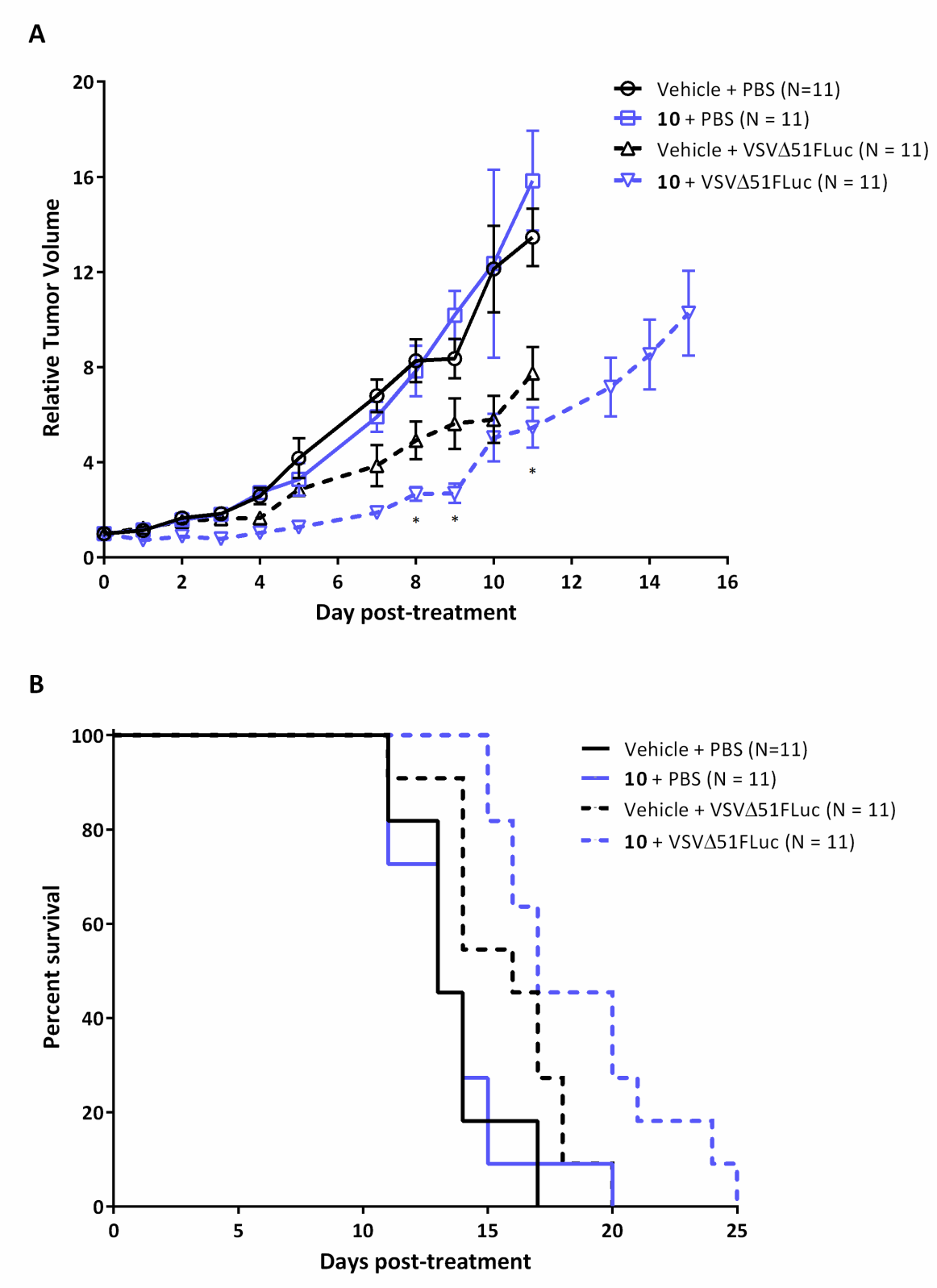
A
Relative Tumor Volume
Day post-treatment
Vehicle + PBS (N=11)
10 + PBS (N = 11)
Vehicle + VSVΔ51FLuc (N = 11)
10 + VSVΔ51FLuc (N = 11)
B
Percent survival
Days post-treatment
Vehicle + PBS (N=11)
10 + PBS (N = 11)
Vehicle + VSVΔ51FLuc (N = 11)
10 + VSVΔ51FLuc (N = 11)

Figure 17. Compound 10 enhances VSVΔ51 oncolytic activity in a resistant syngeneic tumour model. Balb/c mice bearing subcutaneous CT26.WT tumours were given 50 μL of vehicle (DMSO) or 50 mg/kg of **10** by intraperitoneal injection. Four hours later, mice were treated with $1x10^8$ plaque-forming units of VSVΔ51-Fluc by intratumoural injection. Vehicle or **10** was re-administered on day 2 and 4 post-initial treatment. Pooled results from two separate experiments are shown. Averages of relative tumour volumes (relative to volume on day 1 of treatment) for each treatment group are shown and error bars correspond to standard error. Tumour volume curves are terminated when the first mouse in each group is euthanized. Average relative tumour volumes of **10** + VSVΔ51-Fluc treated groups were compared to the other treatment groups on each day. Statistical significance was calculated by two-way ANOVA with Dunnett's multiple comparison test (for **10** + VSVΔ51 versus vehicle + VSVΔ51, * $P < 0.05$). **(B)** Survival was monitored over time. Log –rank tests indicate that treatment with **10** and virus in combination significantly improved overall survival compared to vehicle control ($p = 0.0004$), **10** alone ($p = 0.0003$) or virus alone ($p = 0.04$).

3.2.4. Detection of analogs in tumours

Despite the efficacy observed with **10** and VSVΔ51, **10** was not detectable by LC-MRM in tumour homogenates following intraperitoneal administration, up to 3 hours post-administration, although it could be detected in the serum (**Figure 18A**). We therefore decided to administer both the viral sensitizer and VSVΔ51-FLuc intratumourally. Compounds **10** and **24** were detected in the tumour up to 3 hours post-intratumoural injection into mice bearing CT26.WT tumours (**Figure 18B**). Following intratumoural injection, **28** was also detectable in the tumour and serum for up to 10 hours post-administration (**Figure 19**).

A

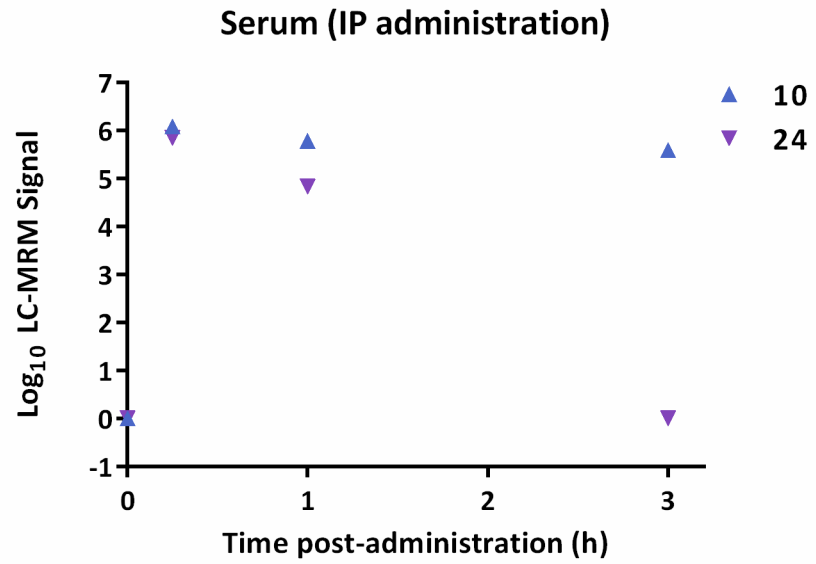
Serum (IP administration)
Log10 LC-MRM Signal
Time post-administration (h)
10
24
7
6
5
4
3
2
1
0
-1
0
1
2
3

B

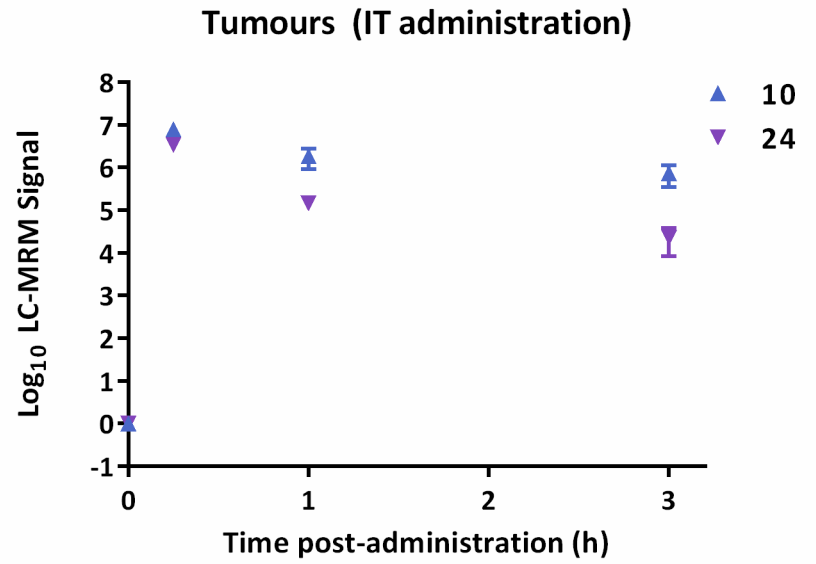
Tumours (IT administration)
Log10 LC-MRM Signal
Time post-administration (h)
10
24
8
7
6
5
4
3
2
1
0
-1
0
1
2
3

Figure 18. Compounds 10 and 24 can be detected in the tumour following intratumoural injection. Balb/c mice (N = 1 per timepoint) bearing subcutaneous CT26.WT tumours were injected **(A)** intraperitoneally (IP) or **(B)** intratumourally (IT) with 50 mg/kg of **10** or **24**. Serum was collected (IP samples) or tumours were excised (IT samples) at various times post-injection and analysed for the presence of compound by LC-MRM. Areas under the peak (AUP) for the parent compound(s) are shown. Error bars represent the standard deviation of 3 technical replicates.

A

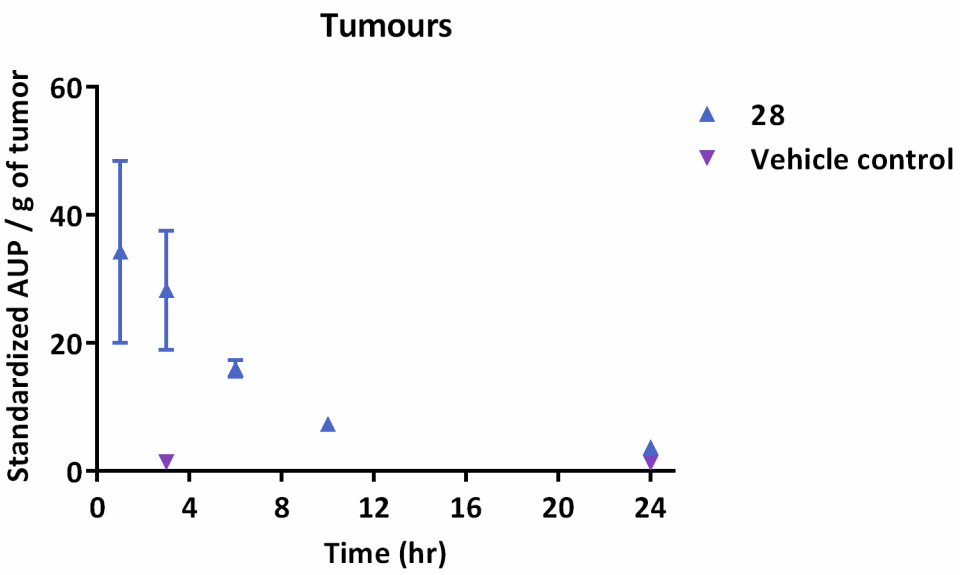
Tumours
Standardized AUP / g of tumor
60
40
20
0
0
4
8
12
16
20
24
Time (hr)
28
Vehicle control

B

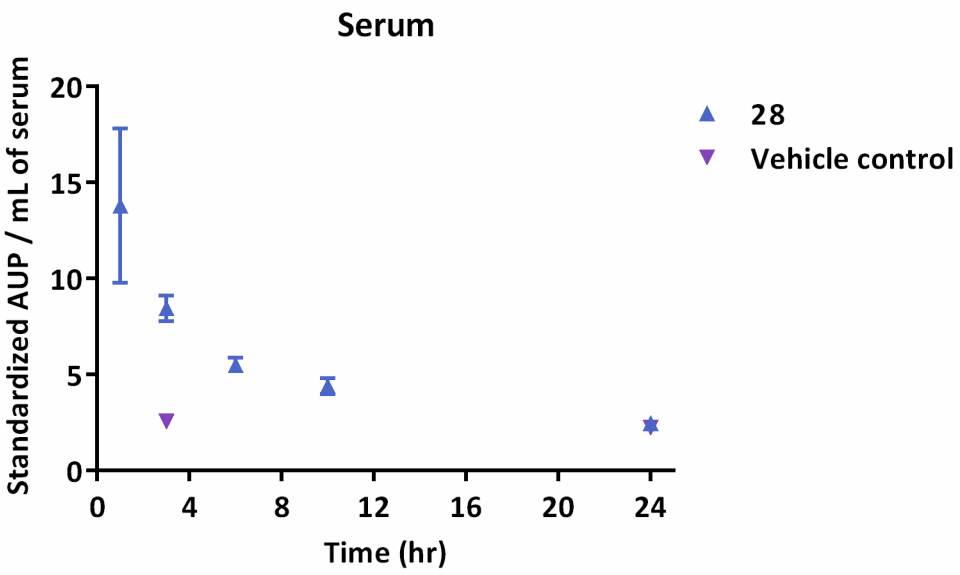
Serum
Standardized AUP / mL of serum
20
15
10
5
0
0
4
8
12
16
20
24
Time (hr)
28
Vehicle control

Figure 19. Compound 28 can be detected in the tumour and serum following intratumoural injection. Balb/c mice bearing subcutaneous CT26.WT tumours were injected intratumourally with 40 mg/kg of **28** (N = 3 per timepoint) or vehicle control (N =1 for 3h and 24h timepoints). **(A)** Tumours and were excised and **(B)** serum was collected at various times post-injection and analysed for the presence of compound by LC-MRM. Standardized areas under the peak (AUP) for the parent compound are shown. Error bars represent the standard error for 3 biological replicates.

3.2.5 Compound 28 enhances therapeutic efficacy of VSV∆51 in multiple murine tumour models

An *in vivo* imaging system (IVIS) was used to measure luciferase activity associated with virus replication 24 h post-treatment of CT26.WT tumours. Compared to VSV∆51-FLuc alone, **28** significantly enhanced virus replication-associated luciferase expression specifically in the tumour (**Figure 20**). This treatment regimen also led to a delay in tumour progression; however there was no significant improvement in overall survival compared to virus alone (**Figure 20**). When administered in a similar manner to two additional subcutaneous tumour models (B16-F10 melanoma in C57Bl/6 mice and HT29 human colon carcinoma in nude mice), the combination of **28** and VSV∆51-FLuc significantly delayed tumour progression and improved survival compared to the mono-therapies (**Figure 21**). This demonstrates the feasibility and potential of using small molecules, such as **28**, in combination with OV therapy *in vivo*.

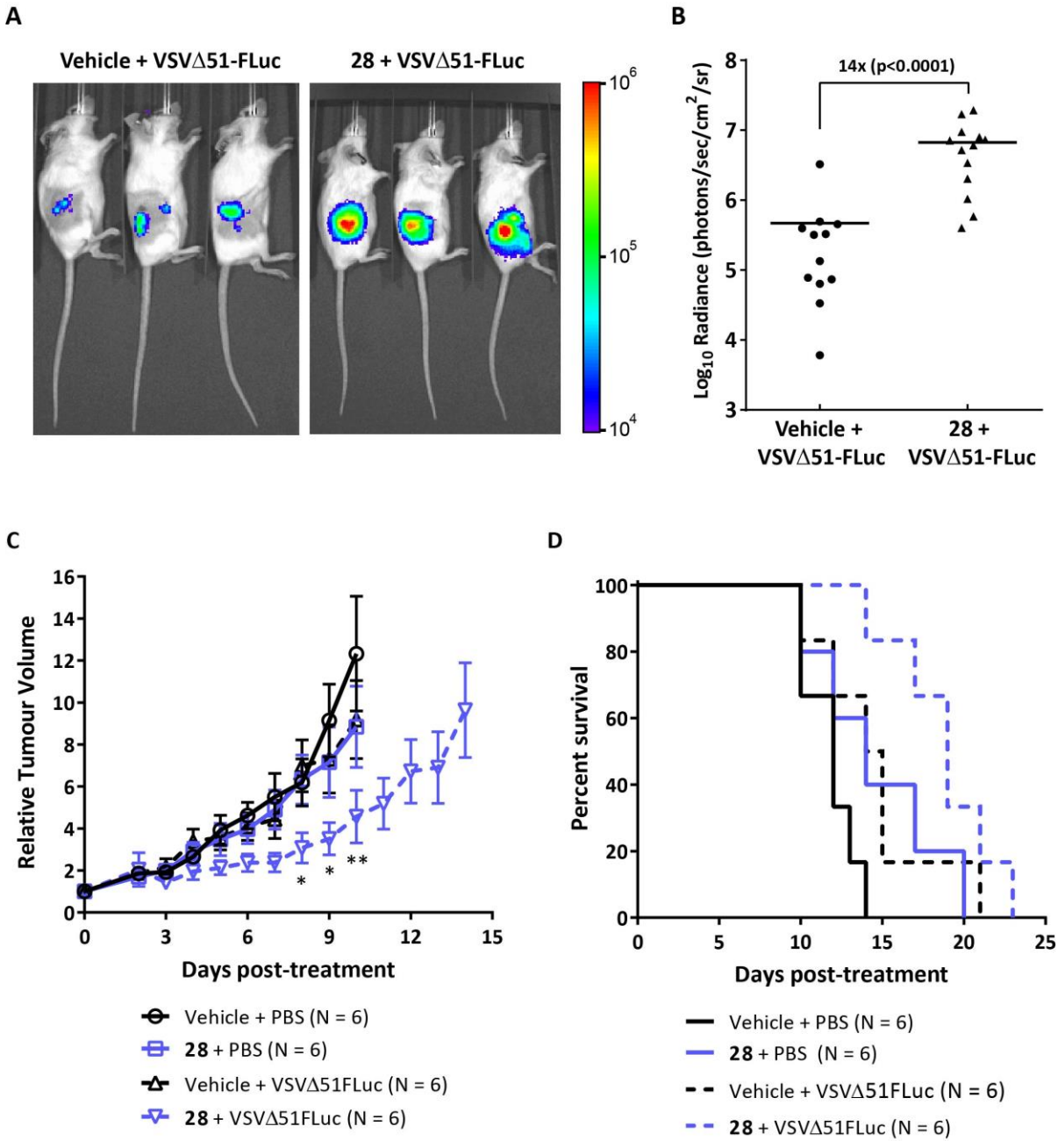
A
Vehicle + VSVΔ51-FLuc
28 + VSVΔ51-FLuc
10^6
10^5
10^4
B
14x (p<0.0001)
Log10 Radiance (photons/sec/cm2/sr)
Vehicle + VSVΔ51-FLuc
28 + VSVΔ51-FLuc
C
Relative Tumour Volume
Days post-treatment
Vehicle + PBS (N = 6)
28 + PBS (N = 6)
Vehicle + VSVΔ51FLuc (N = 6)
28 + VSVΔ51FLuc (N = 6)
D
Percent survival
Days post-treatment
Vehicle + PBS (N = 6)
28 + PBS (N = 6)
Vehicle + VSVΔ51FLuc (N = 6)
28 + VSVΔ51FLuc (N = 6)

Figure 20. Pyrrole-based compound 28 enhances VSVΔ51 oncolytic activity in a resistant syngeneic murine colon cancer model. (A) Balb/c mice bearing CT26.WT cells were treated with vehicle (DMSO) or 40 mg/kg of **28** by intratumoural injection. Four hours later, mice were treated with 1×10^8 plaque-forming units of VSVΔ51-FLuc. Virus replication was monitored twenty-four hours later by measuring luminescence using an IVIS (representative images are shown, color scale bar represents photons) and **(B)** tumour radiance was quantified. Statistical significance was determined with an unpaired t test. **(C)** Vehicle or **28** was re-administered on day 2 and 4 post-initial treatment. Tumour volumes were monitored every day and averages of relative tumour volumes (relative to volume on day 1 of treatment) for each treatment group are shown. Tumour volume curves are terminated when the first mouse in each group was euthanized. Error bars correspond to standard error. Differences between average relative tumour volumes of the **28** + VSVΔ51-Fluc group were compared to the 3 other treatment groups. Statistical significance was calculated by two-way ANOVA with Dunnett's multiple comparison test (for **28** + VSVΔ51 versus VSVΔ51 alone, * $P < 0.05$, ** $P < 0.01$). **(D)** Survival was monitored over time. Log –rank tests indicate that treatment with **28** and virus significantly improved survival compared to vehicle alone ($p = 0.0012$), but not **28** alone ($p = 0.0934$) or virus alone (0.1032).

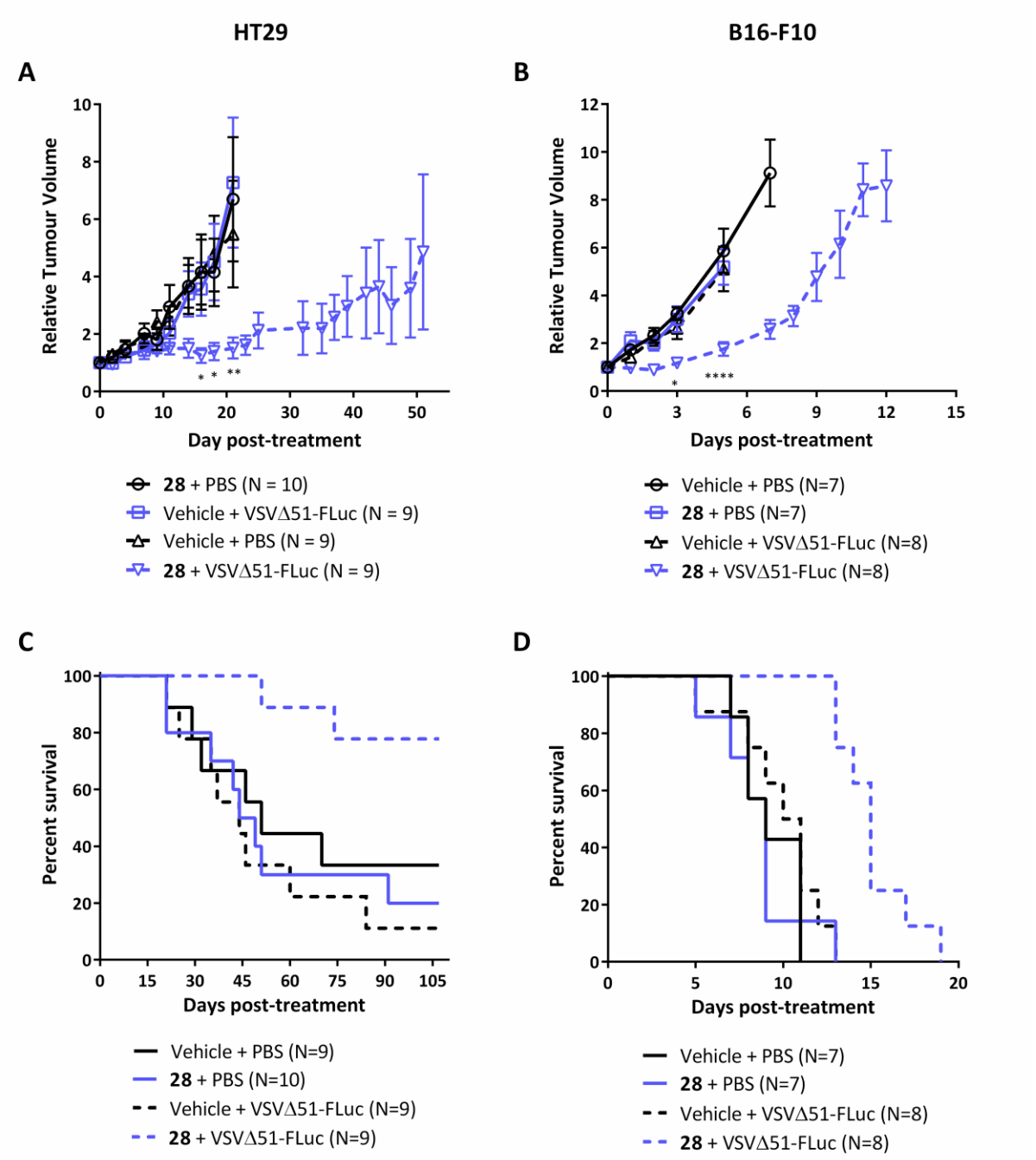
HT29
B16-F10
A
B
Relative Tumour Volume
Day post-treatment
Days post-treatment
* * **
*
****
28 + PBS (N = 10)
Vehicle + VSVΔ51-FLuc (N = 9)
Vehicle + PBS (N = 9)
28 + VSVΔ51-FLuc (N = 9)
Vehicle + PBS (N=7)
28 + PBS (N=7)
Vehicle + VSVΔ51-FLuc (N=8)
28 + VSVΔ51-FLuc (N=8)
C
D
Percent survival
Days post-treatment
Vehicle + PBS (N=9)
28 + PBS (N=10)
Vehicle + VSVΔ51-FLuc (N=9)
28 + VSVΔ51-FLuc (N=9)
Vehicle + PBS (N=7)
28 + PBS (N=7)
Vehicle + VSVΔ51-FLuc (N=8)
28 + VSVΔ51-FLuc (N=8)

Figure 21. Compound 28 enhances VSVΔ51 oncolytic activity and survival in resistant syngeneic and xenograft tumour models. (A) Nude mice bearing subcutaneous HT29 tumours and **(B)** C57/B6 mice bearing subcutaneous B16-F10 tumours were treated with vehicle (DMSO) or 40 mg/kg of **28** by intratumoural injection. Four hours later, mice were treated with $1x10^8$ plaque-forming units of VSVΔ51-FLuc. Tumour volumes were monitored daily and average tumour volumes for each treatment group are shown. Tumour volume curves are terminated when the first mouse in each group reaches endpoint (based on tumour size). Error bars represent standard error. Differences between average volumes of the **28** + VSVΔ51-Fluc group were compared to the 3 other treatment groups. Statistical significance was calculated by two-way ANOVA with Dunnett's multiple comparison test (for **28** + VSVΔ51 vs. VSVΔ51 alone, * $P < 0.05$, ** $P < 0.01$, **** $P < 0.0001$) Survival for mice bearing **(C)** HT29 and **(D)** B16-F10 tumours were monitored over time. Log –rank tests indicate that treatment with **28** and virus in HT29 tumours significantly improved survival compared to vehicle control ($p = 0.0338$), **28** alone ($p = 0.0062$) or virus alone ($p = 0.0018$). Surviving mice had static tumours that neither shrank nor grew for at least 2 weeks. Log –rank tests indicate that treatment with **28** and virus in B16-F10 tumours significantly improved survival compared to vehicle control ($p = 0.0001$), **28** alone ($p = 0.0003$) or virus alone ($p = 0.0002$).

3.3 Mechanism of action of VSe1 and its pyrrole-based analogs

3.3.1. In vitro kinetics of VSe1 activity and effects on viral growth kinetics

In spite of the rapid degradation of VSe1 described earlier, we observed that the onset of its effect on viral growth is rapid and sustained even after removal of compound from cell culture prior to infection. Treatment of 786-0 cells with VSe1 for as little as 60 min followed by replacement with fresh media (compound-free) and subsequent infection with VSVΔ51 resulted in substantial enhancement of viral titers (**Figure 22A**). The same phenomenon was observed for **10**, which is more stable and less reactive (**Figure 22B**). This suggests that these compounds irreversibly inhibit their putative target and/or change the state of the cell, increasing its sensitivity to infection.

The analog screens in 786-0 cells were conducted with a 4 hour pre-treatment period prior to infection, an arbitrary schedule based on the initial high-throughput screen where VSe1 was discovered. When this treatment schedule was altered, VSe1 and **10** were able to enhance VSVΔ51 when administered up to 30 hours before and 8 hours after infection, albeit the amount of enhancement was significantly reduced with the 30 hour pre-treatment condition (**Figure 23**). The compounds had minimal or no effect on viral growth when cells were treated 12 or 16 hours post-infection. This could indicate that the compounds are affecting cellular processes before the cells have had a chance to initiate an anti-viral response. Indeed, results from single step and multi-step growth curves demonstrate that VSe1 and its analogs increase viral replication as well as spread (**Figure 24**).

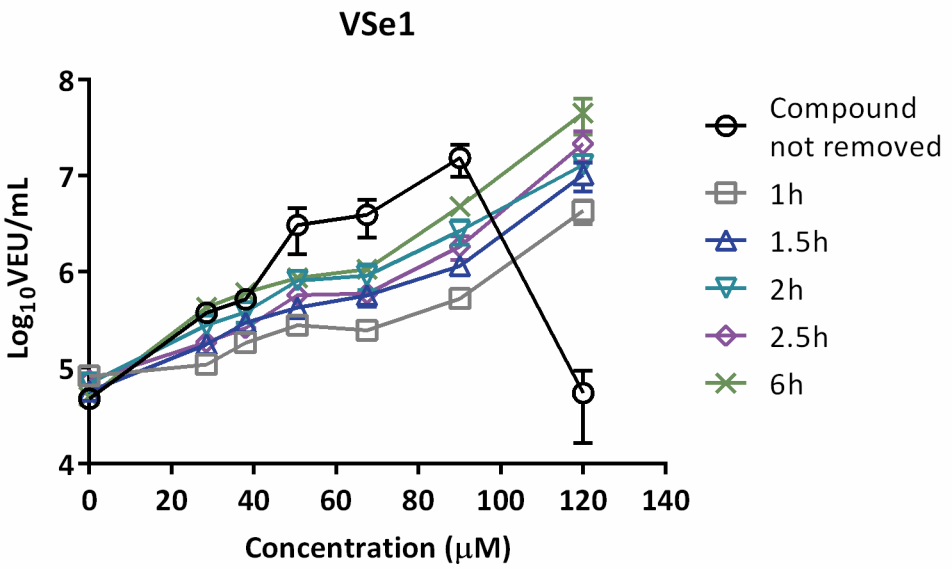
VSe1
Log10VEU/mL
8
7
6
5
4
0
20
40
60
80
100
120
140
Concentration (μM)
Compound not removed
1h
1.5h
2h
2.5h
6h

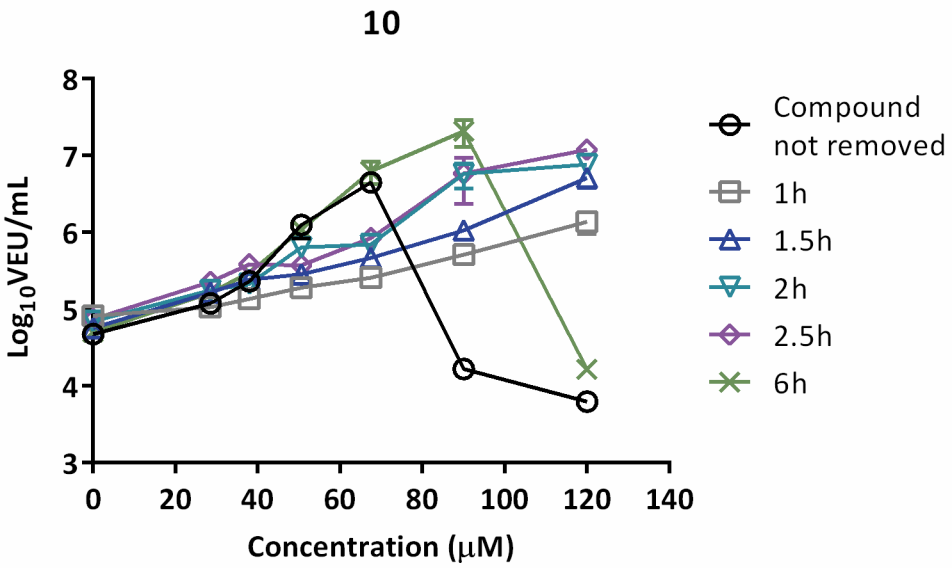
10
Log10VEU/mL
8
7
6
5
4
3
0
20
40
60
80
100
120
140
Concentration (μM)
Compound not removed
1h
1.5h
2h
2.5h
6h

Figure 22. The impact of VSe1 and analogs on viral growth is rapid and sustained. 786-0 cells were treated with VSe1 or **10** at various concentrations. Compound was removed and replaced with fresh media after 1 h, 1.5 h, 2 h, 2.5 h and 6 h. Compound was not removed in the control condition. Four hours post-treatment, cells were infected with VSVΔ51 expressing firefly luciferase VSVΔ51-FLuc at an MOI of 0.005. For the condition where compound was replaced with fresh media 6 h after treatment, infection was performed immediately following media replacement. Forty hours later, virus output in viral expression units (VEUs) per millilitre was measured with a luciferase reporter-based viral titration assay (Materials and Methods, section 2.4)[282].

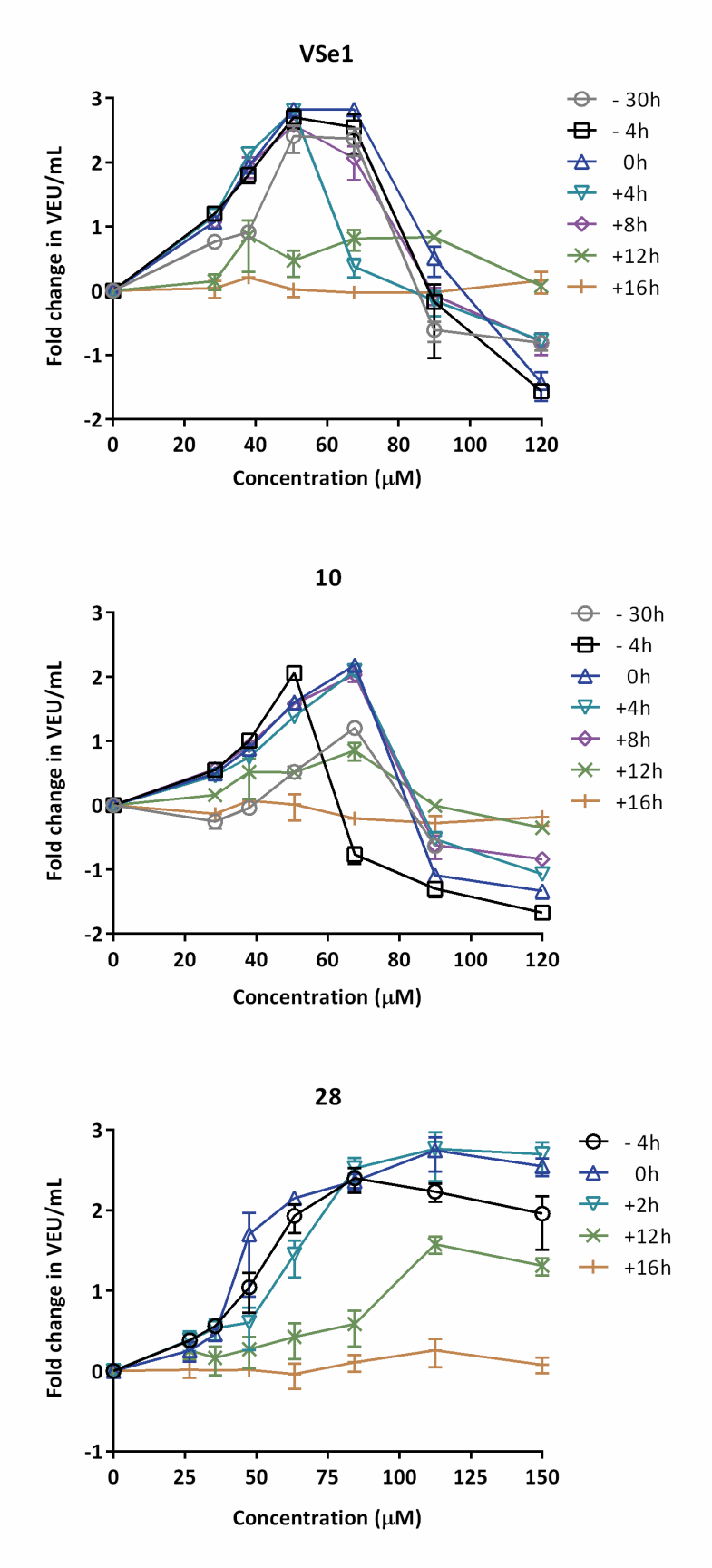
VSe1
Fold change in VEU/mL
Concentration (μM)
- 30h
- 4h
0h
+4h
+8h
+12h
+16h
10
Fold change in VEU/mL
Concentration (μM)
- 30h
- 4h
0h
+4h
+8h
+12h
+16h
28
Fold change in VEU/mL
Concentration (μM)
- 4h
0h
+2h
+12h
+16h

Figure 23. Treatment time-course with VSe1, 10 and 28. 786-0 cells were treated with VSe1, **10**, or **28** before (-30h, -4h, 0h) or after (+2h, +4h, +8h, +12h, +16h) infection with VSVΔ51-FLuc (MOI 0.005) as indicated. Forty hours later, virus output in viral expression units (VEUs) per millilitre was measured with a luciferase reporter-based viral titration assay (Materials and Methods, section 2.4)[282].

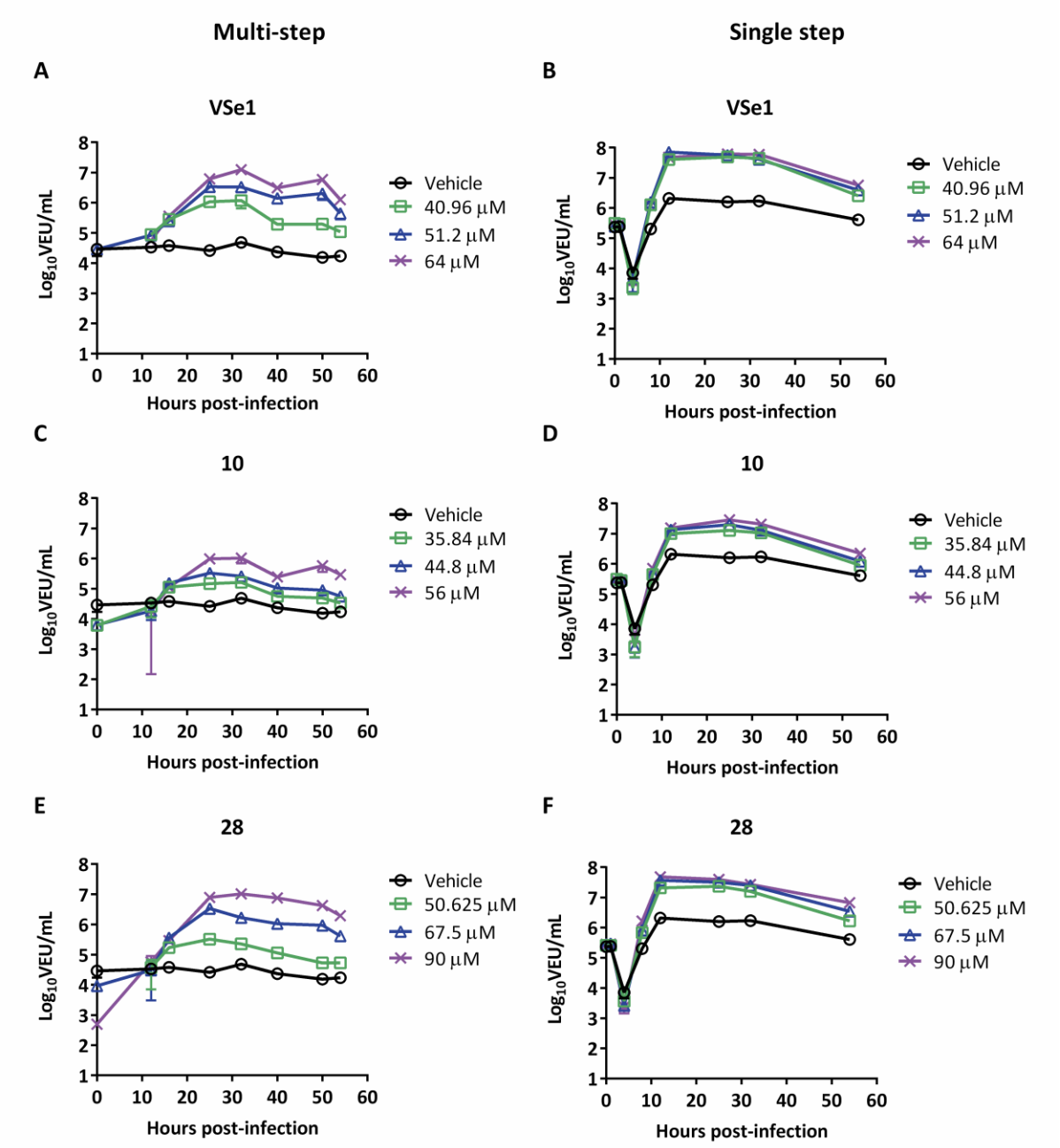
Multi-step
Single step
A
VSe1
B
VSe1
Log10VEU/mL
Hours post-infection
Vehicle
40.96 µM
51.2 µM
64 µM
C
10
D
10
Vehicle
35.84 µM
44.8 µM
56 µM
E
28
F
28
Vehicle
50.625 µM
67.5 µM
90 µM

Figure 24. VSVΔ51 growth curves with VSe1, 10 and 28. 786-0 cells were pre-treated with various concentrations of (**A – B**) (VSe1), (**C – D**) **10**, or (**E – F**) **28** for 8 hours and then infected with VSVΔ51-Fluc at MOI 3 (single step growth curves) or MOI 0.005 (multi-step growth curves). For the single step growth curves, virus inoculum was replaced with media after 1 hour. Supernatants were collected and frozen after various timepoints and virus titer was determined using a luciferase reporter-based viral titration assay (Materials and Methods, section 2.4)[282].

3.3.2. VSe1 and active analogs suppress the innate immune response to VSVΔ51

As mentioned in section 1.3.2, initial studies done with VSe1 showed that it suppressed the expression of VSVΔ51-induced mRNA transcripts in CT26.WT cells (many of which were ISGs) and pre-treatment of U251 cells with VSe1 overcame IFN-α-induced antiviral effects, resulting in recovery of viral titers[215]. When 786-0 cells were treated with exogenous IFN-β to impede viral replication and spread, a similar effect on the recovery of viral titers was observed (**Figure 25**). This prompted us to look further into the both the production and response to type I IFN. Analysis by real-time quantitative PCR and ELISA revealed that active compounds decreased overall VSVΔ51-induced levels of IFN-β protein and mRNA in 786-0 cells, as well as several ISGs that were selected from previous microarray studies (**Figure 26**).

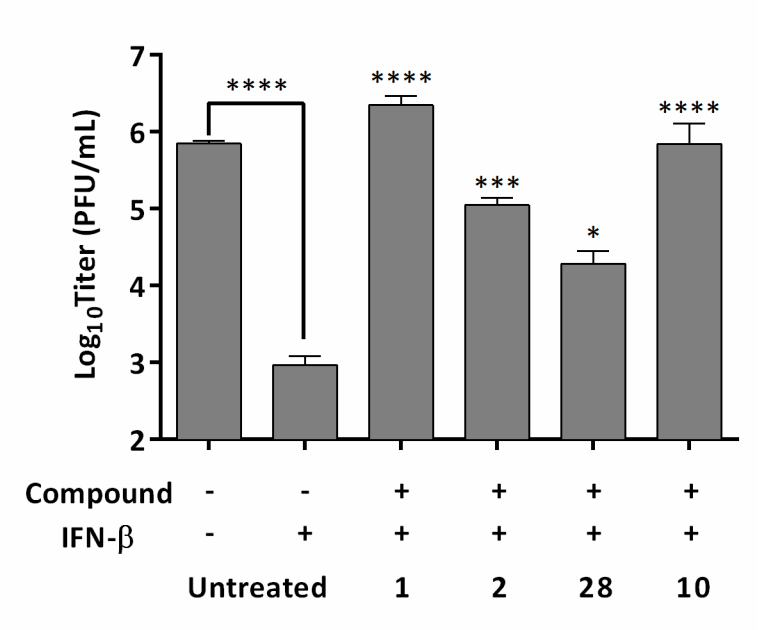
7
6
5
4
3
2
Log10Titer (PFU/mL)
****
****
***
*
****
Compound - - + + + +
IFN-β - + + + + +
Untreated 1 2 28 10

Figure 25. Interferon-induced antiviral response is overcome by VSe1 and its analogs. Human renal carcinoma (786-0) cells were co-treated with compound and IFN-β (200 U/mL) for 4 hours and then challenged with VSVΔ51-GFP at MOI 0.01. Samples were titered 48 post-infection. Values were compared to IFN-β alone and statistical significance was calculated by one-way ANOVA with Dunnett's multiple comparisons test (* P = 0.0109, *** P = 0.001, **** P < 0.0001). Error bars represent standard error. These results were generated by Nader El Sayes.

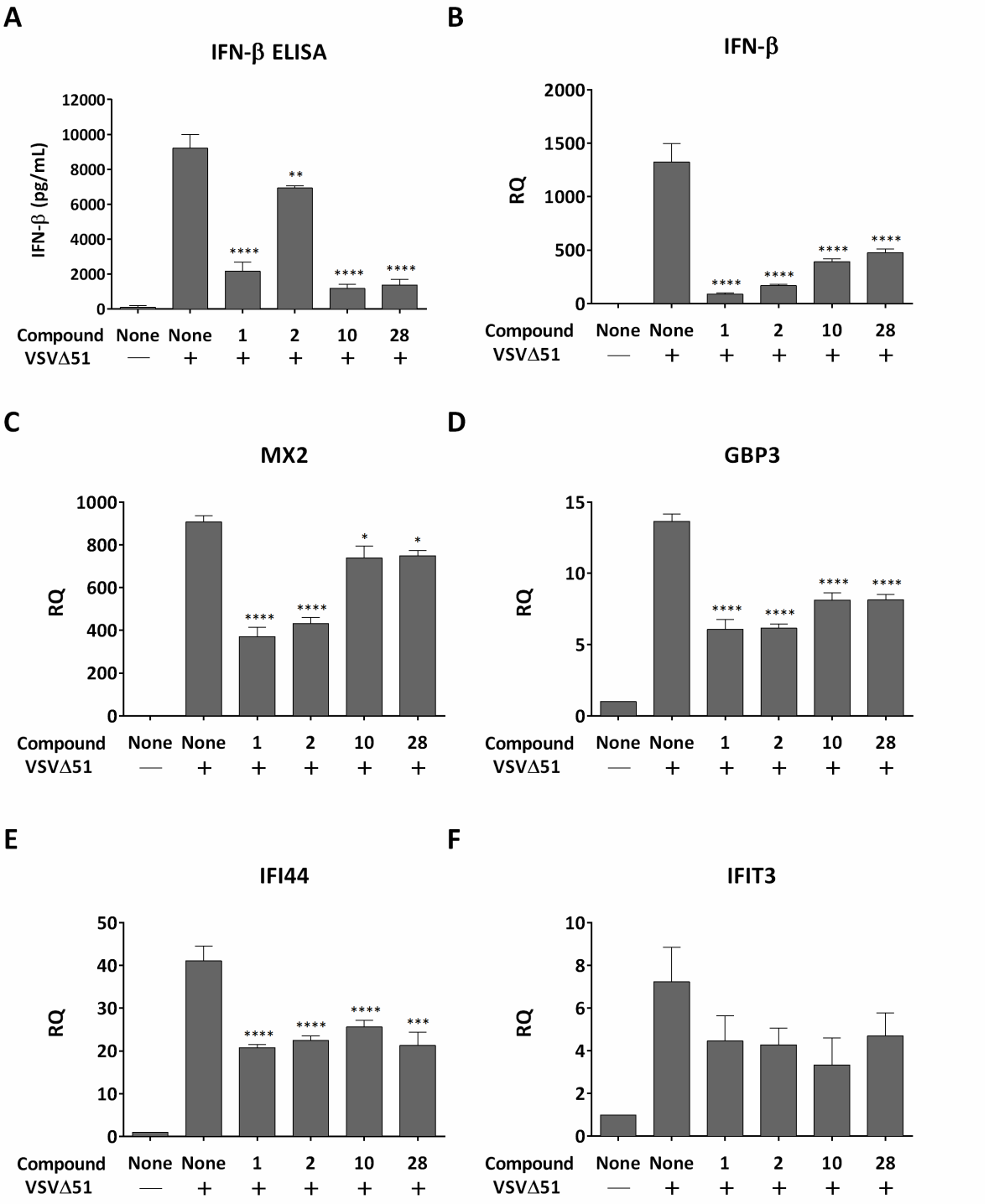
A
IFN-β ELISA
IFN-β (pg/mL)
12000
10000
8000
6000
4000
2000
0
****
**
****
****
Compound None None 1 2 10 28
VSVΔ51 — + + + + +
B
IFN-β
RQ
2000
1500
1000
500
0
****
****
****
****
Compound None None 1 2 10 28
VSVΔ51 — + + + + +
C
MX2
RQ
1000
800
600
400
200
0
****
****
*
*
Compound None None 1 2 10 28
VSVΔ51 — + + + + +
D
GBP3
RQ
15
10
5
0
****
****
****
****
Compound None None 1 2 10 28
VSVΔ51 — + + + + +
E
IFI44
RQ
50
40
30
20
10
0
****
****
****
***
Compound None None 1 2 10 28
VSVΔ51 — + + + + +
F
IFIT3
RQ
10
8
6
4
2
0
Compound None None 1 2 10 28
VSVΔ51 — + + + + +

Figure 26. VSe1 and its analogs inhibit the production of IFN-β and interferon-stimulated genes. (A) 786-0 cells were pre-treated for 2 hours with VSe1, **2**, **10** or **28** before infection with VSVΔ51-GFP (MOI 3) for 16 hours. Amount of IFN-β in the supernatant was measured by sandwich ELISA. Average values form biological triplicates were compared to VSVΔ51 alone and statistical significance was calculated using two-way ANOVA with Dunnett's multiple comparison test, (** $P < 0.01$, **** $P < 0.0001$). Error bars represent standard error. **(B-F)** Quantitative RT-PCR for *IFNB* and ISG expression in 786-0 cells pre-treated with VSe1, **2**, **10** and **28** before infection with VSVΔ51-GFP for 16 hours. Biological duplicates were pooled and the RT-qPCR was done in triplicate. Values were compared to VSVΔ51 alone and statistical significance was calculated using two-way ANOVA with Dunnett's multiple comparison test, (* $P < 0.05$, ** $P < 0.01$, *** $P < 0.001$, **** $P < 0.0001$). Error bars represent standard error. This experiment was performed twice with similar results. Representative results from one experiment are shown. The data for **(A-F)** were generated by Nader El Sayes.

3.3.3 VSe1 and 28 inhibit the activity of NFκB

Given that the compounds induced a significant reduction in IFN-β mRNA and protein, we investigated the effects of the compounds upstream of type I IFN transcription. As described in the sections 1.2.3 and 1.2.4, the *IFN-β* promoter requires a tripartite signal from NFκB p65/p50, IRF3/7 and AP-1 for maximal activation. Accordingly, we examined the effect of VSe1 and **28** on the phosphorylation and nuclear translocation of NFκB, IRF3, and c-jun. 786-0 cells were pre-treated with VSe1 and **28** for 2 hours then infected with a high MOI (MOI=1) of VSVΔ51 for 8 hours. Western blots of cell lysates show that the nuclear translocation of NFκB subunits p65 and p50 that is induced by virus alone is inhibited when the cells are pre-treated with VSe1 and **28** (**Figure 27A**). Under these conditions, the dimerization of p65 and p50, the phosphorylation and nuclear translocation of other transcription factors associated with the *IFN-β* promoter were not affected (**Figure 27A-C**). The effect on the translocation of p65 and p50 was reproduced when NFκB activation was induced by TNF-α treatment (**Figure 27D**). Interestingly, TNF-α-induced phosphorylation of p65 as well as IκBα degradation was not blocked (**Figure 27E**), suggesting that upstream signals from the IKK complex occur normally. We next investigated the effect of VSe1 and **28** on NFκB transcriptional activity by measuring the expression of *TNFA* and *IL6*, two target genes of NFκB[294–297]. Consistent with NFκB inhibition, VSVΔ51 infection-induced expression of *TNFA* and *IL6* was inhibited by both compounds as early as 8 hours and for up to 24 hours post infection (**Figure 28A**). Furthermore, significantly less TNF-α was secreted into the supernatant of VSVΔ51-infected cells treated with VSe1 and **28** at these time points as shown by ELISA (**Figure 28B**). Additionally, we observed that the compound 2-

[(aminocarbonyl)amino]-5 -(4-fluorophenyl)-3- thiophenecarboxamide (TPCA-1), an inhibitor of NFκB via inhibition of the IKK complex, was able to sensitize 786-0 cells to VSVΔ51 infection in a similar manner to VSe1 and **28** (**Figure 29A**). When cells were treated with TPCA-1, subsequent treatment with VSe1 or **28** was not able to induce a significant increase in titers (**Figure 29B-C**), supporting the fact that the targets of VSe1 and **28** are downstream of TPCA-1's targets. Altogether, these data suggest that VSe1 and **28** consistently inhibit the nuclear translocation of NFκB and its transcriptional activity, which coincides with down-regulation of virus-induced production of IFN-β and TNF-α, and enhancement of VSVΔ51 propagation.

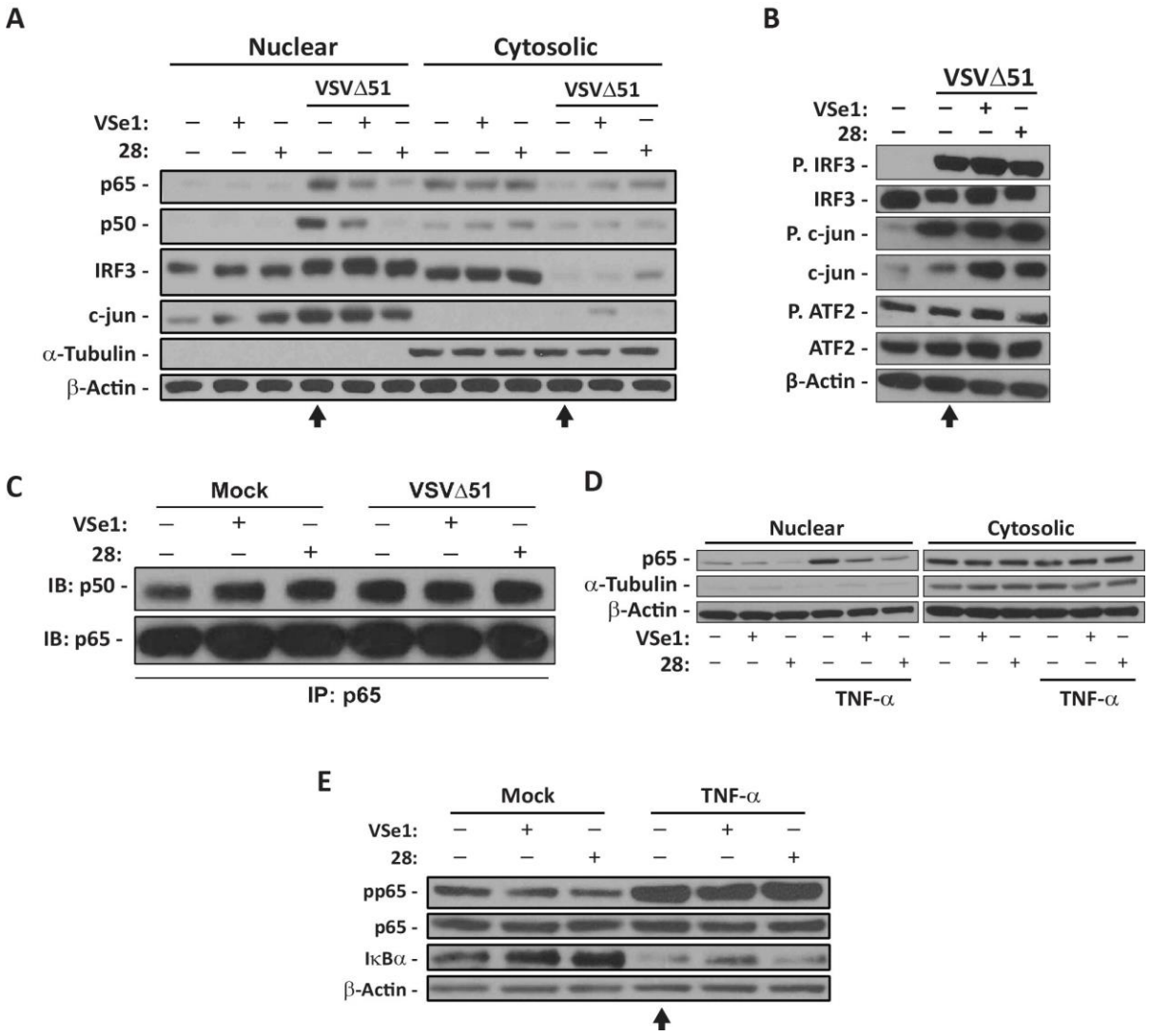
A
Nuclear
Cytosolic
VSVΔ51
VSVΔ51
VSe1:
28:
p65 -
p50 -
IRF3 -
c-jun -
α-Tubulin -
β-Actin -
B
VSVΔ51
VSe1:
28:
P. IRF3 -
IRF3 -
P. c-jun -
c-jun -
P. ATF2 -
ATF2 -
β-Actin -
C
Mock
VSVΔ51
VSe1:
28:
IB: p50 -
IB: p65 -
IP: p65
D
Nuclear
Cytosolic
p65 -
α-Tubulin -
β-Actin -
VSe1:
28:
TNF-α
TNF-α
E
Mock
TNF-α
VSe1:
28:
pp65 -
p65 -
IκBα -
β-Actin -

Figure 27. VSe1 and 28 inhibit virus and TNFα-induced NFκB nuclear translocation. (A, B, D) 786-0 cells were treated with VSe1 (60 μM) and **28** (80 μM) and then infected with VSVΔ51-GFP (MOI 1). Whole cell, cytosolic and nuclear lysate fractions were collected 8 hours post-infection, separated by SDS-PAGE and probed with the indicated antibodies. **(C)** NFκB p65 was immunoprecipitated from lysates from 786-0 cells treated with VSe1 (60 μM) or **28** (90 μM) then infected with VSVΔ51-GFP (MOI 1) for 8. Proteins were separated by SDS-PAGE then probed for p50. **(E)** 786-0 cells were treated as in **A** and then treated with TNF-α (50ng/μL). Nuclear and cytoplasmic extracts were collected 30 minutes later and were probed with the indicated antibodies. In **(A, B, and E)**, arrows indicated lanes with VSVΔ51 or TNF-α alone. The data for **(A-E)** were generated by Nader El Sayes.

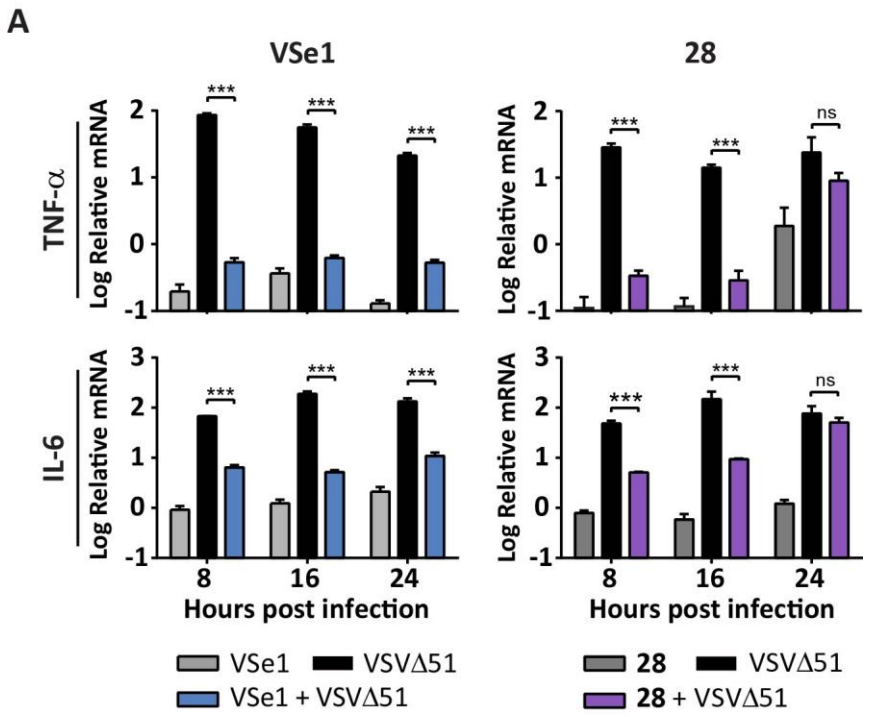
A
VSe1
28
TNF-α
IL-6
Log Relative mRNA
***
ns
8
16
24
Hours post infection
VSe1
VSVΔ51
VSe1 + VSVΔ51
28
28 + VSVΔ51

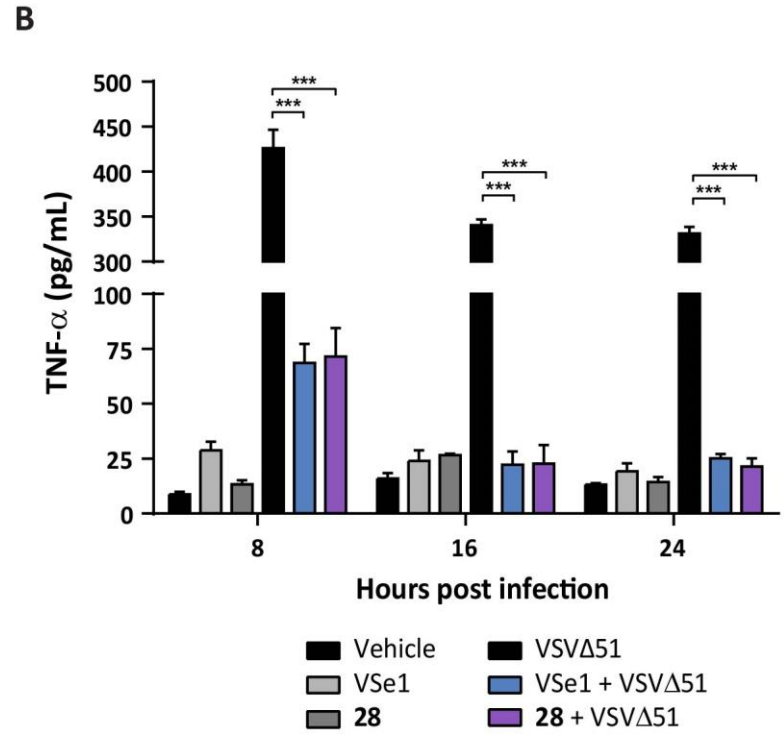
B
TNF-α (pg/mL)
500
450
400
350
300
100
75
50
25
0
***
8
16
24
Hours post infection
Vehicle
VSe1
28
VSVΔ51
VSe1 + VSVΔ51
28 + VSVΔ51

Figure 28. VSe1 and 28 inhibit the expression of NFκB targets. (A) 786-0 cells were treated with VSe1 (60 μM) and **28** (80 μM) then infected with VSVΔ51-GFP (MOI 1). RNA was extracted 8, 16 and 24 hours post-infection and quantitative RT-PCR was used to measure relative levels of *TNFA* and *IL6* mRNA Values were normalized to GAPDH and are relative to untreated control for each timepoint. **(B)** 786-0 cells were treated and infected as in A, then supernatants were collected and levels of secreted TNF-α were measured by ELISA. Error bars represent standard error from biological triplicates and statistical significance was calculated using two-way ANOVA with Dunnett's multiple comparison test (*** $P < 0.001$, ** $P < 0.01$, ns = $P > 0.05$). Values were log transformed before analysing statistical significance. The data for **(A-B)** were generated by Nader El Sayes.

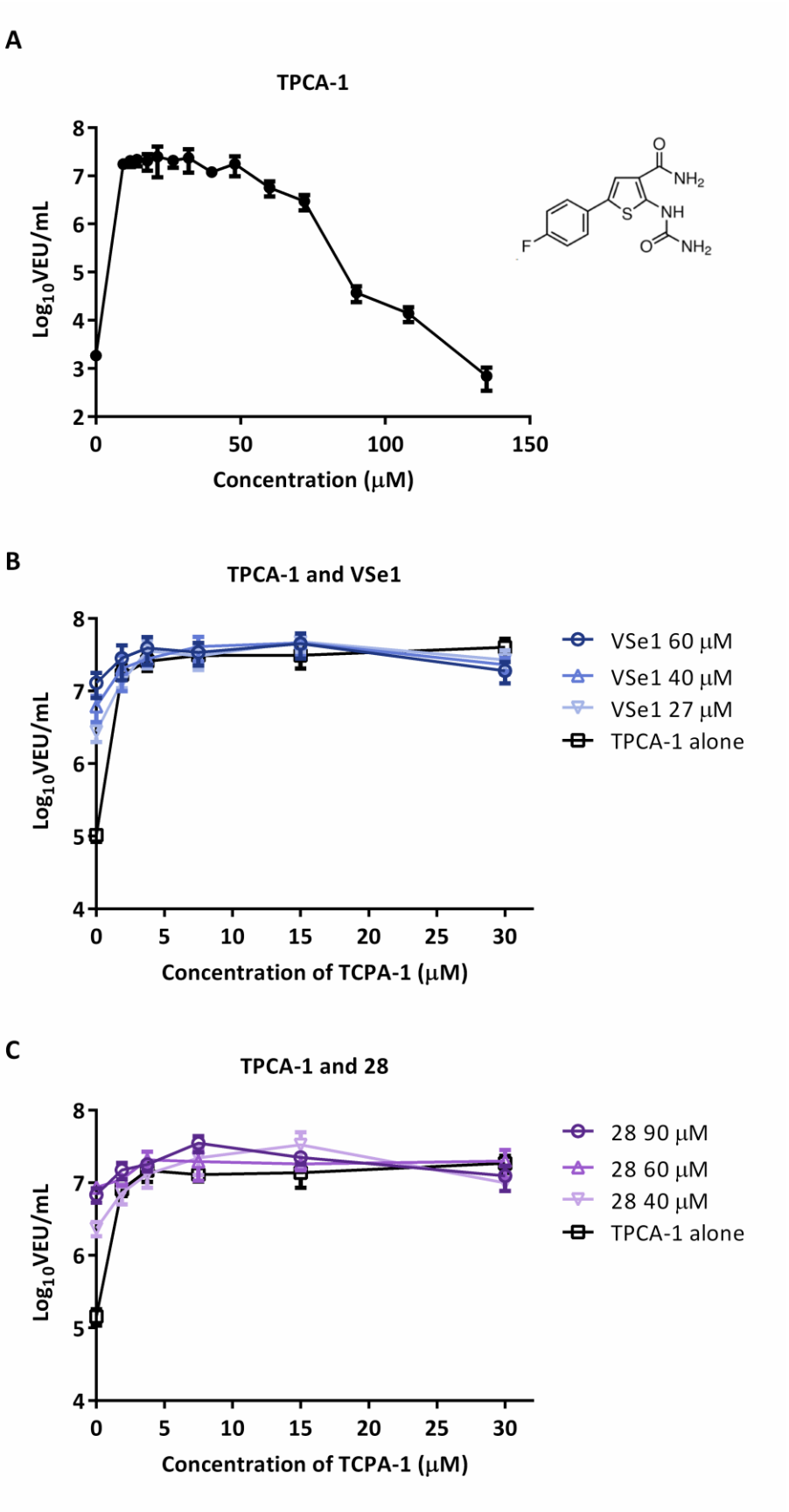
A
TPCA-1
Log10VEU/mL
Concentration (μM)
B
TPCA-1 and VSe1
VSe1 60 μM
VSe1 40 μM
VSe1 27 μM
TPCA-1 alone
Concentration of TCPA-1 (μM)
C
TPCA-1 and 28
28 90 μM
28 60 μM
28 40 μM
TPCA-1 alone
Concentration of TCPA-1 (μM)

Figure 29. The IKK inhibitor TPCA-1 enhances VSVΔ51 spread. (A) 786-0 cells were pre-treated with various concentrations of TPCA-1 for 4 hours and then infected with VSVΔ51-Fluc (MOI 0.01). Supernatants were collected 40 hours later and virus output was determined using a luciferase reporter-based viral titration assay (Materials and Methods, section 2.4). **(B)** 786-0 cells were treated with various concentrations TPCA-1 for 4 hours and then treated with VSe1 or **(C) 28** at the indicated concentrations for 2 hours prior to being infected with VSVΔ51-Fluc (MOI 0.005). Supernatants were collected 40 hours later and virus output was determined using a luciferase reporter-based viral titration assay (Materials and Methods, section 2.4)[282].

3.3.4. Active compounds interact with GSTP1

While the inhibition of NFκB translocation by VSe1 and **28** could explain their capacity to block IFN-β production and response, sensitizing cancer cells to viral infection, the molecular mechanisms leading to NFκB inhibition were unclear. As a starting point, we deemed it relevant to determine whether VSe1 and its structural analogs interact with cellular proteins. To this end, **27**, an active analog, or **57**, and inactive analog, were separately linked to Amino PEGA resins. Both probes were incubated with lysates from uninfected or VSVΔ51-infected 786-0 cells. Bound proteins were eluted and separated by gel electrophoresis. Visible bands were purified and sequenced via LC-MS/MS and are presented in **Table 6**. Of the three attempts, glutathione S-transferase π (GSTP1) was consistently identified as interacting specifically with the active probe. Peroxiredoxin-1, thioredoxin and annexin A2 were identified in only one out of three attempts and thus did not satisfy our reproducibility criteria to be considered as genuine targets. No proteins were pulled down with the inactive probe.

Table 6. Interacting proteins identified by affinity capture

Sample	Sequenced hits
Active analog, uninfected lysate	**Glutathione-S-transferase (25 kDa)**
	Peroxiredoxin-1 (25 kDa)
Active analog, infected lysate	**Glutathione-S-transferase (25 kDa)**
	Peroxiredoxin-1 (25 kDa)
	Annexin A2 isoform 2 (20 kDa)
	Thioredoxin (10 kDa)

In light of the interaction between the **27**-based probe and GSTP1, we wondered whether the parental compound VSe1 and its analogs could impact the enzymatic activity of GSTP1-1. To this end, we assayed GST enzymatic activity over short periods (5 minutes) *in vitro* using 2,4-dinitrochlorobenzene (CDNB) as a model GST-substrate as described in Groom *et al*[287]. In these assays, VSe1 was found to inhibit GSTP1-1 (IC_{50} of 2.67 μM; **Figure 30A**). The inhibitory activity of VSe1 on GSTP1-1 was further maintained following dialysis, suggesting a very strong, potentially irreversible interaction (**Figure 30B**). We also found that VSe1 inhibited the enzymatic activity of GSTM1-1 (IC_{50} of 1.74 μM; **Figure 27C**) and GSTA4-4 (IC_{50} of 46.6 μM; **Figure 30D**). Compound **2** was also found to inhibit GSTP1-1, GSTM1-1, and GSTA4-4 (**Table 7**). However, VSe1 and **2** did not inhibit GSTA1-1, GSTA2-2, and GSTM2-2 in these assays (**Table 7**). Surprisingly **28** and many other pyrroles in **Table 5** structurally related to **27** that was used to pull down GSTP1 did not inhibit GSTs at a concentration of 25 μM (**Table 7**). A prolonged incubation of a higher concentration of **10** and **28** inhibited the activity of GSTP1-1, albeit less effectively than VSe1 (**Figure 31A**).

In section 3.1, it was demonstrated that VSe1 and its analogs react with supra-physiological concentrations of free GSH with varying kinetics, with VSe1 reacting nearly instantaneously (<5 min half-life) compared to pyrrole analogs that have vastly reduced electrophilicity (e.g. **28** has a half-life of 96 minutes; **Table 5**), which may make them much better tolerated *in vivo*[298–300]. In line with this observation, we found that a high concentration of the pre-formed adduct between the **10** and GSH also inhibited GSTP1-1 (**Figure 31B**). The inhibition assay was also conducted after incubating VSe1, **10** or **28** with GSTP1-1 in the absence of GSH. GSH was added to the reaction mixture at the end of the

incubation period. Under these conditions, inhibition of enzyme activity was still observed (**Figure 31C**). This may indicate that the inhibition of enzymatic activity that was observed is partially due to direct inhibition of GSTP1-1 by the inhibitor tested, and partially due to the inhibitor-GSH adduct. Thus, VSe1 and its analogs could mediate their viral sensitizing effect indirectly through inhibition of GST activity, formation of adducts with GSH, or both. To evaluate the former, we tested the documented GSTP1 inhibitor ezatiostat, a structural analog of GSH, for its capacity to enhance VSVΔ51 growth in 786-0 cells. We found that ezatiostat hydrochloride (**Figure 32A**) enhanced VSVΔ51 growth between 75-150 μM, leading to a peak fold increase in VEU of approximately 2 logs compared to vehicle-treated controls (**Figure 32B**). In comparison, treatment with VSe1 and **28** led to nearly 4-log and 3.5 log increases in VEU respectively using the same assay (**Figure 32C-D**).

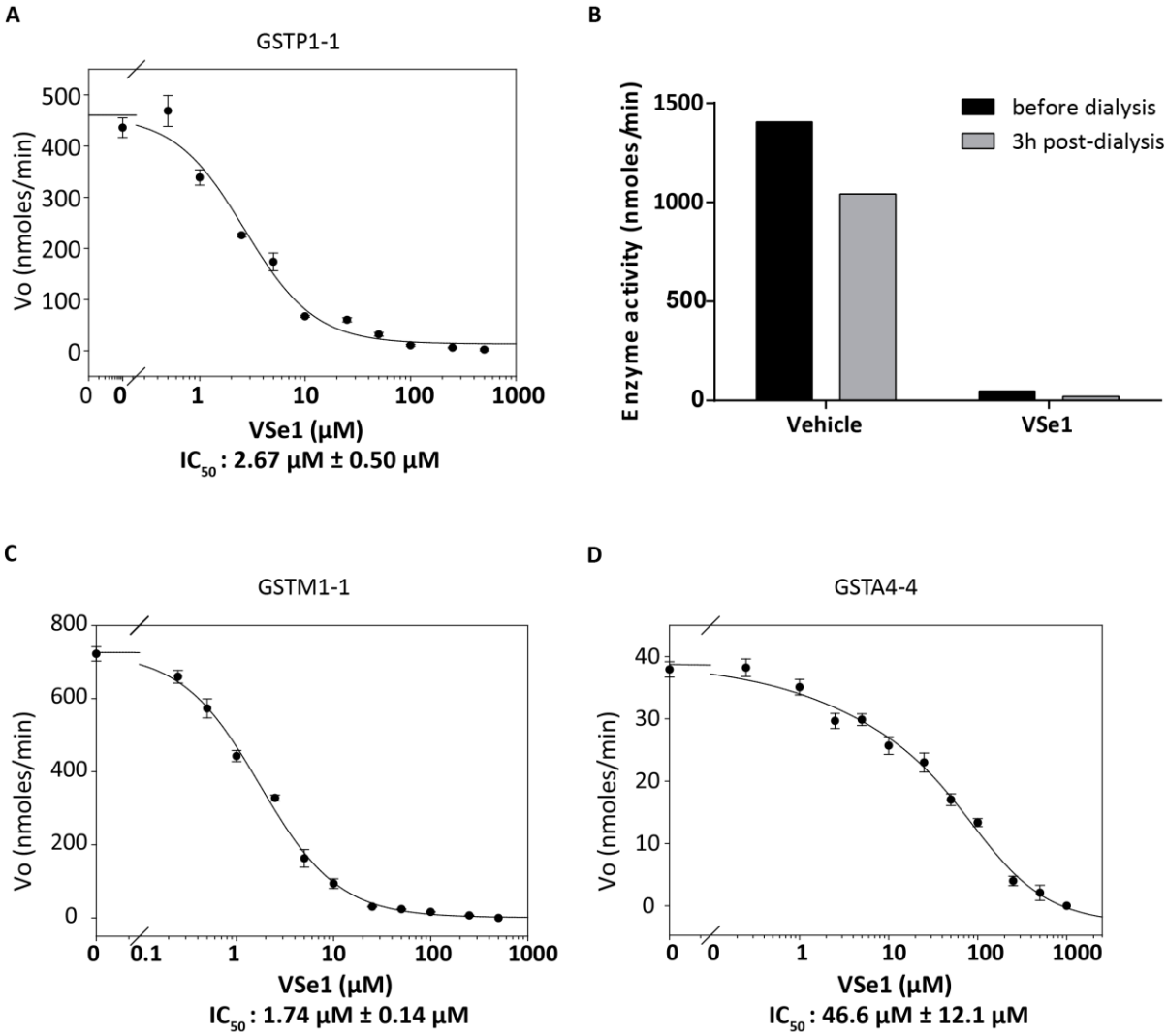
A
GSTP1-1
Vo (nmoles/min)
VSe1 (µM)
IC50 : 2.67 µM ± 0.50 µM
B
Enzyme activity (nmoles/min)
before dialysis
3h post-dialysis
Vehicle
VSe1
C
GSTM1-1
Vo (nmoles/min)
VSe1 (µM)
IC50 : 1.74 µM ± 0.14 µM
D
GSTA4-4
Vo (nmoles/min)
VSe1 (µM)
IC50 : 46.6 µM ± 12.1 µM

Figure 30. VSe1 inhibits GSTP1-1, GSTM1-1 and GSTA4-4. (A) GST P1 (5 μg) was incubated with VSe1 and GSH, 1 mM, at 37°C for 5 min. CDNB (dissolved in ethanol) was added to initiate the reaction (final concentration, 0.5 mM) and product formation was monitored at 340 nm. Final concentrations of DMSO and ethanol were 1% each. Data points represent the mean ± standard error of three biological replicates. IC50 values were determined by curve-fitting, as described in Materials and Methods. **(B)** GSTP1-1 enzymatic activity was tested pre- and post-dialysis, with and without VSe1. **(C)** GSTM1 and **(D)** GSTA4 were incubated with VSe1 as in **(A)**, and the assay was performed as described above. The data for (**A – D**) were generated by Hilary Groom.

Table 7. Summary of GST inhibition activity

	Recombinant human GST					
Compound	**A1-1**	**A2-2**	**A4-4**	**M1-1**	**M2-2**	**P1-1**
VSe1	-	-	inhibitory	inhibitory	-	inhibitory
2	-	-	inhibitory	inhibitory	-	inhibitory
10	-	-	-	-	-	-
24	-	-	-	-	-	-
25	-	-	-	-	-	-
27	-	-	-	-	-	-
28	-	-	-	-	-	-
29	-	-	-	-	-	-
30	-	-	-	-	-	-
40	-	-	-	-	-	-

Recombinant human GST enzymes were incubated with 1 mM GSH and 25 μM of inhibitor at 37°C for 5 min, in 100 mM potassium phosphate buffer, pH 6.5. CDNB was added to initiate the reaction and product formation as in Figure 26. "-" indicates that inhibition of activity was not observed. These results were generated by Hilary Groom.

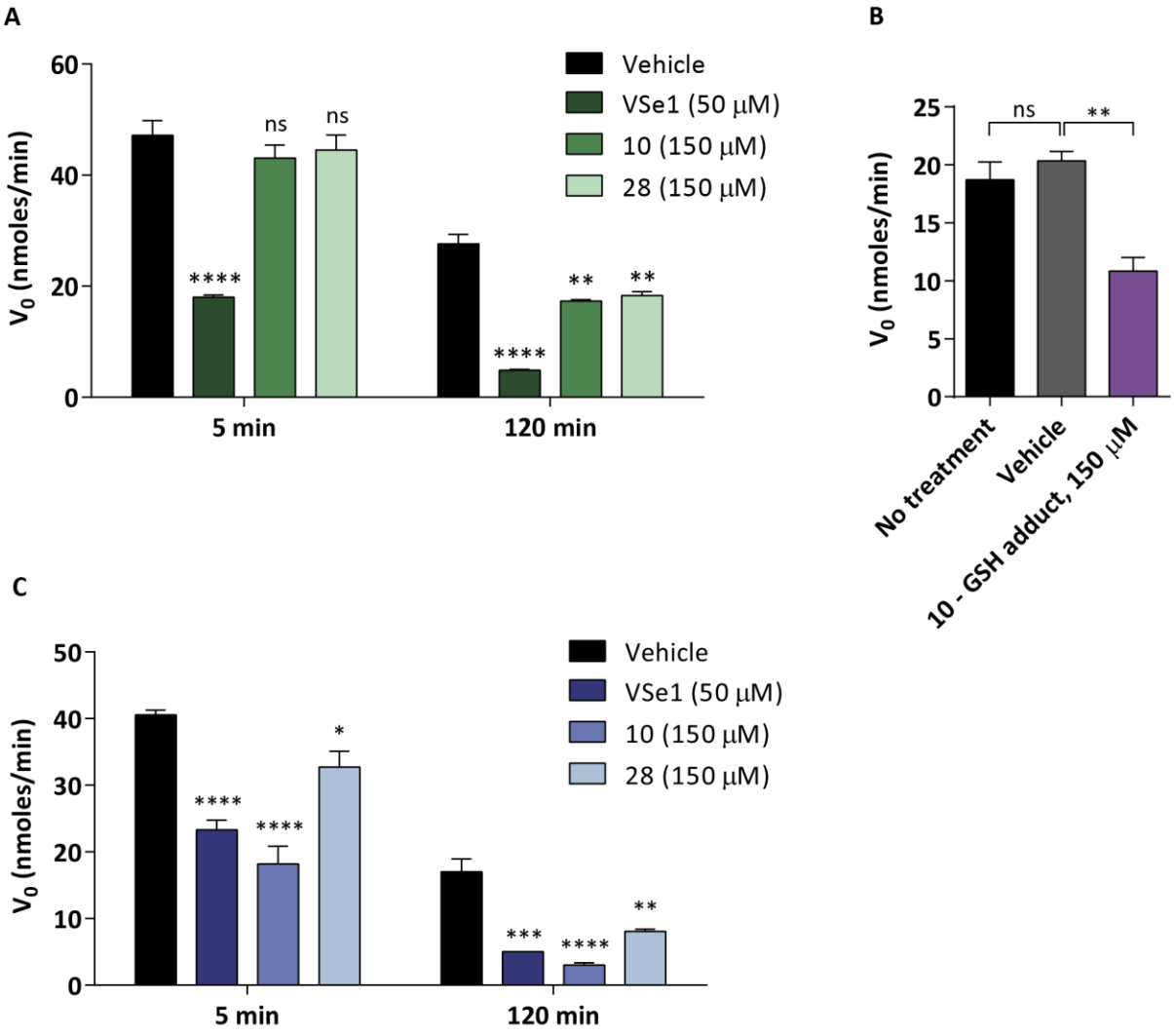
A
B
C
Vehicle
VSe1 (50 μM)
10 (150 μM)
28 (150 μM)
V0 (nmoles/min)
5 min
120 min
ns
****
**
***
*
No treatment
Vehicle
10 - GSH adduct, 150 μM

Figure 31. Pyrrole analogs are less potent inhibitors of GSTP1-1. (A) GSTP1 (1 μg) was pre-incubated with GSH (final concentration 1 mM), vehicle (DMSO), VSe1, **10** or **28**, for 5 min or 120 min at 37 °C. After the incubation period, CDNB was added to initiate the reaction, and product formation was monitored at 340 nm. Final concentration of DMSO was 2%. Bars represent the mean ± standard error of three or four biological replicates. Statistical significance was calculated using two-way ANOVA with Dunnett's multiple comparisons test (**** $P < 0.0001$, ** $P < 0.01$, ns = $P > 0.05$). **(B)** GSTP1 (1 μg) was pre-incubated with vehicle (DMSO), **10**-GSH adduct, and GSH (1 mM), for 5 min at 37 °C. The reaction with CDNB was initiated as in panel A. Bars represent the mean ± standard error of three biological replicates. Statistical significance was calculated using one-way ANOVA with Holm-Sidak's multiple comparisons test (** $P < 0.01$, ns = $P > 0.05$). **(C)** GSTP1 (1 μg) was pre-incubated with vehicle (DMSO), VSe1, **10** or **28**, for 5 min or 120 min at 37 °C. CDNB (dissolved in DMSO) and GSH was added to initiate the reaction (final concentration, 0.5 mM and 1 mM, respectively), and product formation was monitored at 340 nm. Bars represent the mean ± standard error of three or four biological replicates. Statistical significance was calculated using two-way ANOVA with Dunnett's multiple comparisons test (**** $P < 0.0001$, *** $P < 0.001$, ** $P < 0.01$, * $P < 0.05$, ns = $P > 0.05$).

A

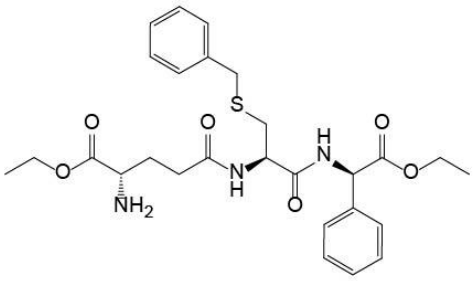
O
O
O
S
H
N
N
H
O
O
O
NH2

B

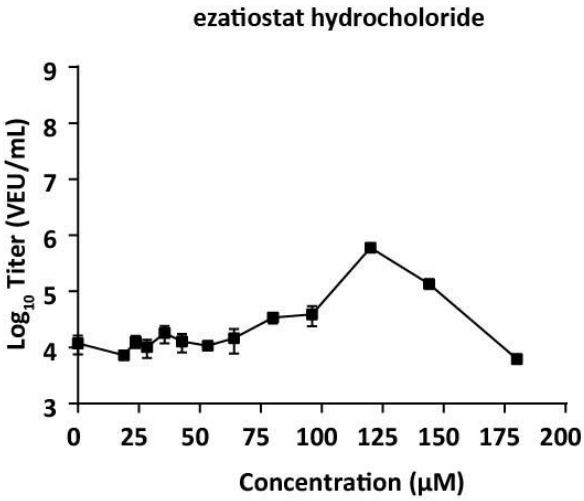
ezatiostat hydrocholoride
Log10 Titer (VEU/mL)
9
8
7
6
5
4
3
0
25
50
75
100
125
150
175
200
Concentration (μM)

C

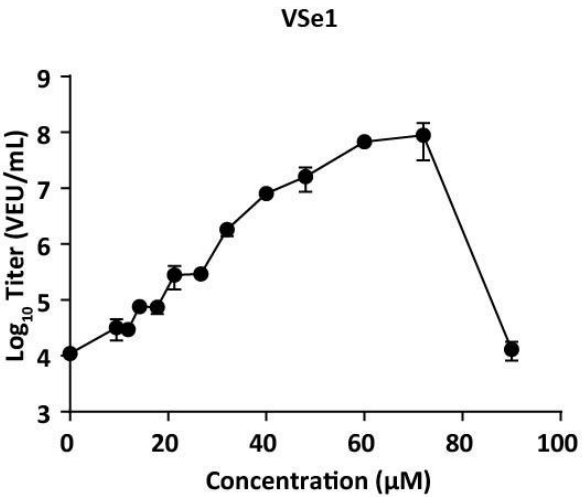
VSe1
Log10 Titer (VEU/mL)
9
8
7
6
5
4
3
0
20
40
60
80
100
Concentration (μM)

D

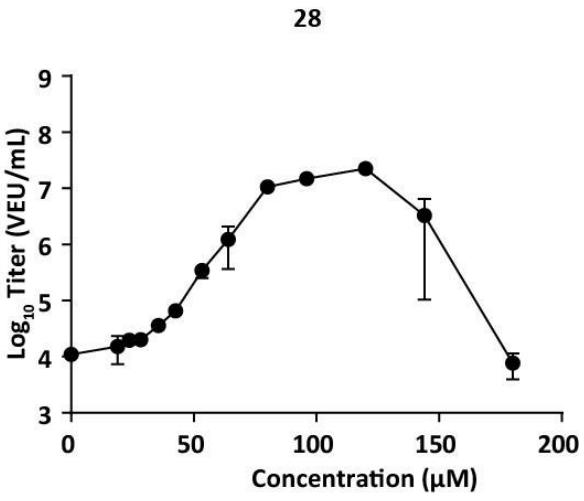
28
Log10 Titer (VEU/mL)
9
8
7
6
5
4
3
0
50
100
150
200
Concentration (μM)

Figure 32. Ezatiostat hydrochloride sensitizes 786-0 cells to VSVΔ51. (A) Structure of ezatiostat. **(B-D)** 786-0 cells were pre-treated with ezatiostat HCL, VSe1 or **28** then infected with VSVΔ51-Fluc (MOI 0.005). Supernatants were collected 40 hours later and virus output was determined using a luciferase reporter-based viral titration assay (Materials and Methods, section 2.4)[282].

3.3.5 RNAi-mediated inhibition of GSTP1-1 does not sensitize 786-0 cells to VSVΔ51

The effect of GSTP1-1 inhibition was further evaluated through targeted siRNA-mediated knock-down in 786-0 cells. Although the knock-down was successful, inhibition of *GSTP1* expression through this method did not have an effect on viral titers (**Figure 33A-D**). Furthermore, when siRNA-transfected cells were treated with VSe1, enhancement of VSVΔ51 titers was still observed, and was not significantly different from the enhancement observed in mock-transfected samples (**Figure 33E**). Altogether, this implies that inhibition of GSTP1 alone does not account for the viral enhancement induced by VSe1.

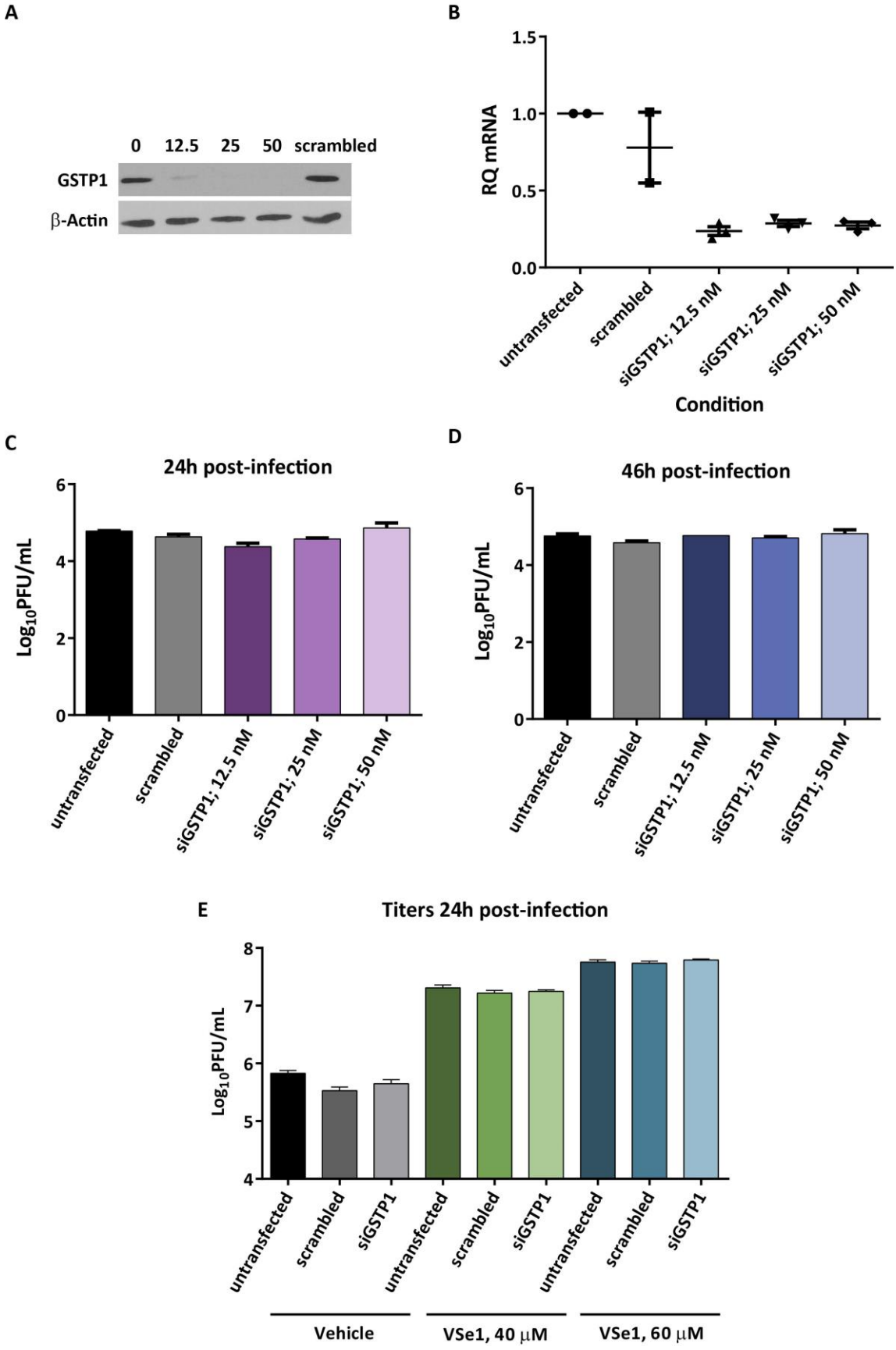
A
0
12.5
25
50
scrambled
GSTP1
β-Actin
B
RQ mRNA
1.5
1.0
0.5
0.0
untransfected
scrambled
siGSTP1; 12.5 nM
siGSTP1; 25 nM
siGSTP1; 50 nM
Condition
C
24h post-infection
Log10PFU/mL
6
4
2
0
untransfected
scrambled
siGSTP1; 12.5 nM
siGSTP1; 25 nM
siGSTP1; 50 nM
D
46h post-infection
Log10PFU/mL
6
4
2
0
untransfected
scrambled
siGSTP1; 12.5 nM
siGSTP1; 25 nM
siGSTP1; 50 nM
E
Titers 24h post-infection
Log10PFU/mL
8
7
6
5
4
untransfected
scrambled
siGSTP1
untransfected
scrambled
siGSTP1
untransfected
scrambled
siGSTP1
Vehicle
VSe1, 40 μM
VSe1, 60 μM

Figure 33. Knock-down of GSTP1 does not sensitize 786-0 cells to VSVΔ51. (A) 786-0 cells were transfected with vehicle control ("0"), scrambled siRNA control ('scrambled"; final concentration 25 nM), or various amounts of siRNA against *GSTP1* (siGSTP1) such that the final concentration of siRNA was 12.5 nM, 25 nM or 50 nM. Forty-eight hours later, samples were lysed, and triplicate protein lysates were pooled, separated by SDS-PAGE and probed for GSTP1 and β-actin by immunoblotting. **(B)** RNA from 786-0 cells exposed to the same conditions as **(A)** were collected 72 hours post-transfection and quantitative RT-PCR for *GSTP1* mRNA was performed. **(C-D)** In parallel to (A), transfected 786-0 cells and controls were infected with VSVΔ51-GFP at MOI 0.01. Supernatants were collected 24 and 46 hours post-infection and titered by plaque assay. Error bars represent standard error from biological triplicates. Any differences between conditions are statistically non-significant, by one-way ANOVA. Similar results were obtained from 2 independent experiments. Results from one experiment are shown. **(E)** 786-0 cells were transfected with vehicle control ("untransfected"), scrambled siRNA ("scrambled") or siRNA against *GSTP1* ("siGSTP1") such that the final concentration of siRNA was 25 nM. Forty-eight hours post-transfection, cells were treated with vehicle control or VSe1, and then infected 4 hours later with VSVΔ51-GFP at MOI 0.01. Supernatants were collected 24 and 46 hours post-infection and titered by plaque assay. Within each treatment group (vehicle, VSe1 40 μM, or VSe1 60 μM), differences between transfection conditions are statistically non-significant, by one-way ANOVA. Similar results were obtained from 2 independent experiments. Results from one experiment are shown. The data for **(E)** were generated by Michael Phan.

3.3.6. Depletion of cellular GSH levels sensitizes cells to VSVΔ51 infection

Given that VSe1 and its analogs react with free GSH (**Table 5**) and GSH is a substrate GSTs, I proceeded to evaluate the impact of other compounds known to modulate GSH levels. Diethyl maleate (DEM) and its structural analogs (**Figure 34A**) have been reported to deplete GSH[301–303]. All of these compounds proved to be effective viral sensitizers, leading to over 3-log increases in VEUs in 786-0 cells (**Figure 34B**). As discussed previously in section 1.4, the compound dimethyl fumarate (DMF) has been marketed as a treatment for psoriasis in Europe and for multiple sclerosis in Canada, the United States, and Europe. Once administered, DMF undergoes esterase-mediated hydrolysis to its active metabolite monomethyl fumarate (MMF). MMF also sensitized 786-0 cells to VSVΔ51, albeit at much higher concentrations, perhaps owing to the fact that it is partially hydrolyzed and thus may not diffuse across the plasma membrane as efficiently as its parent compound (**Figure 34C**).

A

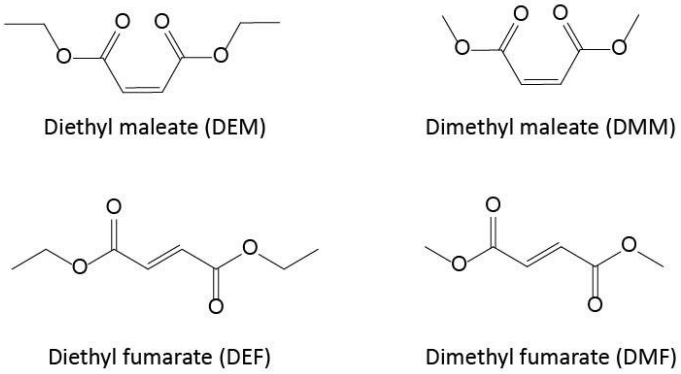
Diethyl maleate (DEM)
Dimethyl maleate (DMM)
Diethyl fumarate (DEF)
Dimethyl fumarate (DMF)

B

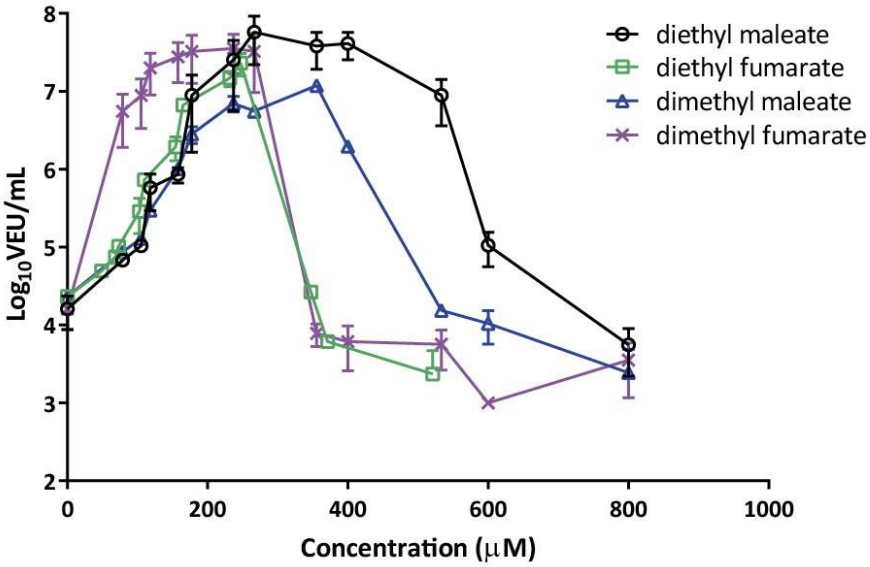
diethyl maleate
diethyl fumarate
dimethyl maleate
dimethyl fumarate
Log10VEU/mL
Concentration (μM)

C

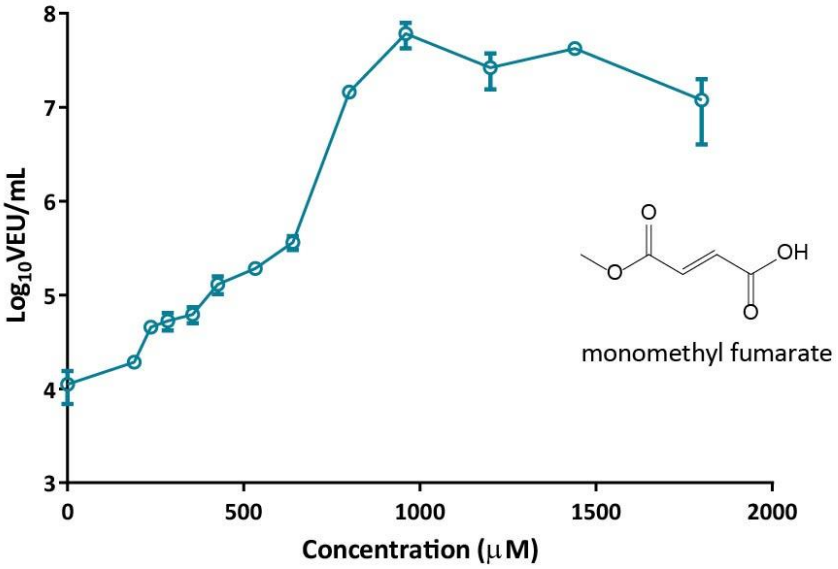
Log10VEU/mL
Concentration (μM)
monomethyl fumarate

Figure 34. Glutathione depletors sensitize 786-0 cells to VSVΔ51. (A) Structures of GSH depletors. **(B-C)** 786-0 cells were treated with various concentrations of the compounds depicted in panels A and C. Four hours later, cells were infected with VSVΔ51-FLuc (MOI 0.005). Supernatants were collected 40 hours later and virus output was determined using a luciferase reporter-based viral titration assay (Materials and Methods, section 2.4)[282].

Given the strong impact of these known GSH depletors on VSVΔ51 replication and spread and the fact that VSe1 and its active analogs react with free GSH, we proceeded to evaluate the impact of some of these compounds in cellular GSH and GSSG levels. Whole cell lysates from samples treated over a period of 12 hours were collected and used to quantify GSH and GSSG levels by HPLC-UV. Our data revealed that while GSSG levels remained stable, GSH levels decreased after 1 hour of treatment with VSe1, or **28** (**Figure 35**). Intriguingly, depletion was greater with **28** and was sustained for up to at least 4 hours post-treatment. However, GSH depletion was ultimately short-lived and was followed by recovery and accumulation of GSH above control levels by 12 hours post-treatment.

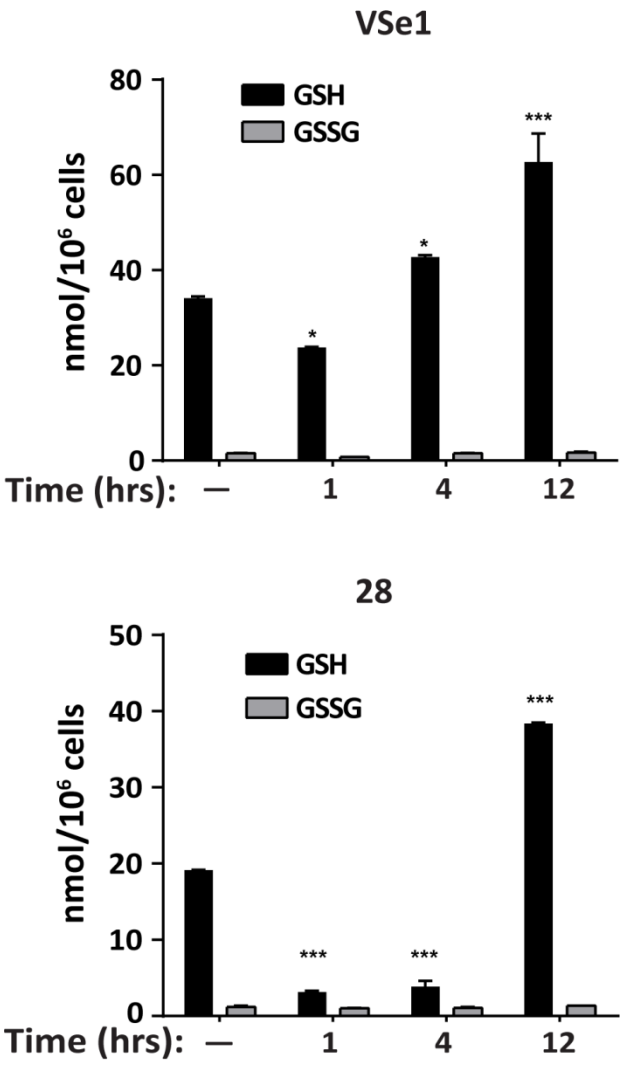
VSe1
GSH
GSSG
nmol/10^6 cells
80
60
40
20
0
*
*
***
Time (hrs):
—
1
4
12
28
GSH
GSSG
nmol/10^6 cells
50
40
30
20
10
0
***
***
***
Time (hrs):
—
1
4
12

Figure 35. VSe1 and 28 deplete intracellular glutathione. 786-0 cells were treated with VSe1 or **28** for 1, 4, and 12 hours before whole cell lysates were collected. Cellular GSH and GSSG levels were measured by HPLC-UV detection. "—" represents vehicle treated samples, collected at the same time as all other samples. Error bars represent standard error from biological duplicates and technical duplicates. Mean values for GSH or GSSG levels were compared to the respective mean values for the vehicle controls. Statistical significance was calculated using two-way ANOVA with Dunnett's multiple comparison (*** $P < 0.001$, * $P < 0.05$).

To gain a better idea of the kinetics of GSH depletion and changes in GSSG/GSH ratio caused by VSe1 and **28**, we transfected 293T cells with a redox-sensitive GFP plasmid covalently linked to the catalytic domain of glutaredoxin-1 (cyto-Grx1-roGFP2), enabling real-time monitoring of changes in the intracellular GSSG/GSH ratio[304]. Upon oxidation of cysteines in roGFP2, light emission following excitation at 408 nm increases, while emission following excitation at 488 nm decreases, resulting in an increase in the ratio of emissions (408 nm/488 nm). This is reversed upon reduction. Increases in this ratio are directly proportionate to increases in the GSSG/GSH ratio by virtue of the fused Grx1 protein. Upon treatment with H_2O_2 (a positive control for this assay) or VSe1 for 2 minutes the 408/488 ratio was increased (significantly more than vehicle controls) and subsequently decreased upon treatment with the reducing agent dithiothreitol (DTT) (**Figure 36A, B, D**). The ratio obtained from 293T cells transfected with a non-redox sensitive GFP plasmid ("ctrl GFP") did not increase to the same magnitude, indicating that the signal seen with cells expressing cyto-Grx1-roGFP2 is specific to the activity of this fusion protein. Interestingly, the increase in the 408 nm/488 nm ratio was observed within minutes of VSe1 treatment whereas the increase with **28** occurred much later and was sustained for up to 4 hours (**Figure 36 C, G**). Comparatively, the increases observed with H_2O_2 and VSe1 treatments were much shorter lived and the ratios decreased after the 2-minute timepoint without the need of a reducing agent (**Figure 36E, F**). Bearing in mind that the GSH-reaction half-lives of VSe1 and **28** are less than 5 minutes and 96 minutes respectively (**Table 5**), the changes in cyto-Grx1-roGFP2 fluorescence in this assay are consistent with the differences in electrophilicity of these two compounds.

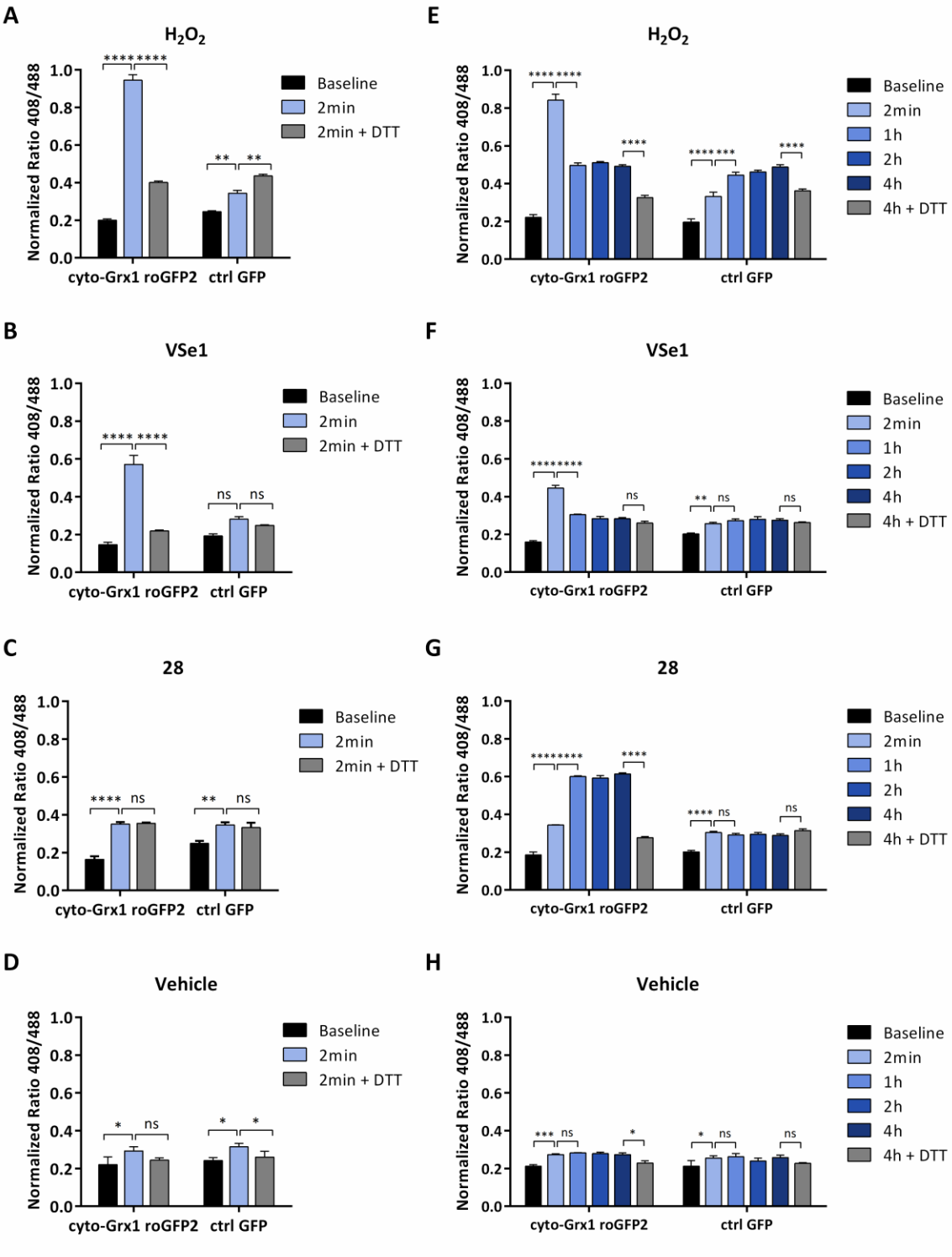
A
H_2O_2
Normalized Ratio 408/488
Baseline
2min
2min + DTT
cyto-Grx1 roGFP2
ctrl GFP
B
VSe1
C
28
D
Vehicle
E
H_2O_2
1h
2h
4h
4h + DTT
F
VSe1
G
28
H
Vehicle

Figure 36. Ratiometric detection of GSSG/GSH ratios. Transfected 293T cells were treated with VSe1 (60 μM), **28** (160 μM) or H_2O_2 (300 μM). Fluorescence readings were taken prior to treatment and post-treatment at the indicated times. 5 mM DTT was added to quench the signal. Observed ratios were normalized to a scale of 0.1 to 1.0, with 0.1 representing a fully reduced state (minimum observed ratio) and fully oxidized state (maximum observed ratio). Error bars represent standard error from biological triplicates and statistical significance was calculated using two-way ANOVA with Holm-Sidak's multiple comparison test (* $P < 0.05$, ** $P < 0.01$, **** $P < 0.0001$, ns = $P > 0.05$).

To better understand the relevance of GSH depletion on viral enhancement, 786-0 cells were cultured in buthionine sulfoximine (BSO; **Figure 37A**) to deplete endogenous GSH. BSO irreversibly inhibits γ-glutamylcysteine-synthase, the enzyme responsible for the rate-limiting step of GSH synthesis[305,306]. GSH depletion was confirmed by HPLC-UV detection. 786-0 cells cultured in BSO for 3 days were treated with VSe1 or **28** then infected with VSVΔ51 (**Figure 37B**). When cells were cultured in BSO for at least 3 days, BSO treatment alone was able to enhance VSVΔ51 titers approximately 10-fold compared to cells cultured in regular media (**Figure 37C**). When cells were treated with VSe1 or **28**, the potency of the viral sensitization was increased in BSO-cultured cells, where cellular GSH is not detectable (**Figure 37D**). This suggests that, while GSH depletion alone may have some impact on VSVΔ51 infection, depletion of GSH does not fully explain the virus sensitizing effects of VSe1 and **28**. This also argues against a key role of a viral sensitizer-GSH adduct, since this would predict an abrogation of the effects of VSe1 and **28** in the context of GSH-depleted cells, as opposed to their enhancement as we have observed.

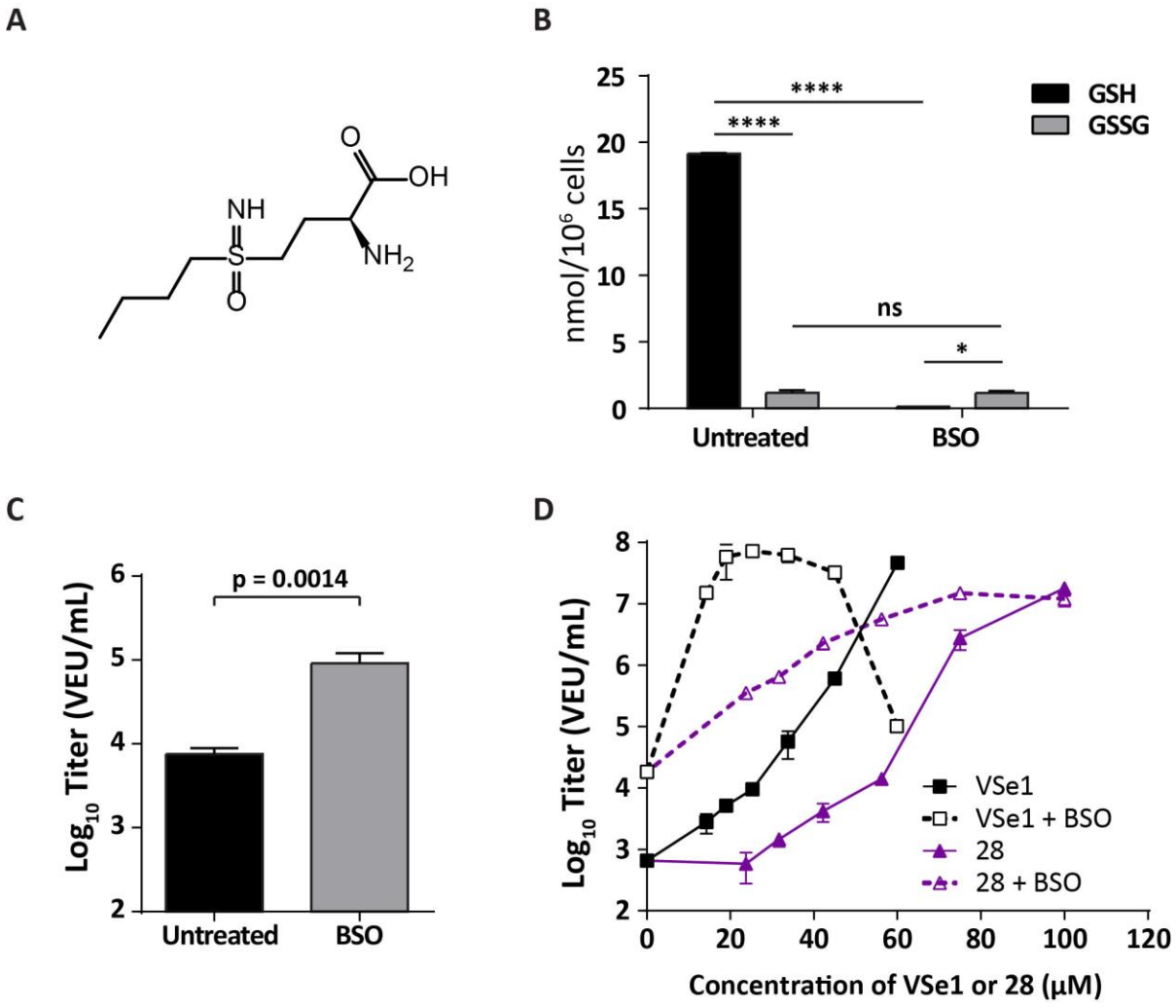
A
O
OH
NH
S
NH2
O
B
nmol/10^6 cells
25
20
15
10
5
0
****
****
ns
*
GSH
GSSG
Untreated
BSO
C
Log10 Titer (VEU/mL)
6
5
4
3
2
p = 0.0014
Untreated
BSO
D
Log10 Titer (VEU/mL)
8
7
6
5
4
3
2
0
20
40
60
80
100
120
VSe1
VSe1 + BSO
28
28 + BSO
Concentration of VSe1 or 28 (μM)

Figure 37. Glutathione depletion sensitizes 786-0s to VSVΔ51, VSe1 and 28. (A) Structure of BSO**. (B)** 786-0 cells were cultured in 2mM BSO for 3 days prior to collecting whole cell lysates. Cellular GSH and GSSG levels were measured by HPLC-UV detection. Error bars represent standard error from biological duplicates and technical duplicates. Statistical significance was calculated using a 2-way ANOVA with Holm-Sidak multiple comparisons test (****P <0.001, * P <0.05, ns = P > 0.05). **(C)** 786-0 cells were cultured as in **(B)** then infected with VSVΔ51-Fluc (MOI 0.05). Supernatants were collected 40 hours later and virus output was determined using a luciferase reporter-based viral titration assay (Materials and Methods, section 2.4)[282]. Statistical significance was calculated using unpaired t-test. **(D)** 786-0 cells were cultured in DMEM or DMEM supplemented with BSO 2mM for 10 days. Cells were then treated with VSe1 or **28** for 4 hours and then infected with VSVΔ51-Fluc (MOI 0.005). Supernatants were collected 40 hours later and virus output was determined using a luciferase reporter-based viral titration assay (Materials and Methods, section 2.4)[282].

3.3.7 VSe1 and compound 28 induce oxidative stress

A fundamental role of GSH and GSTs is the regulation of cellular redox homeostasis. We therefore questioned whether the inhibition of GST activity and GSH depletion caused by VSe1 and **28** causes a shift in cellular redox status, leading to increased viral replication.). A gene expression microarray was conducted in in 786-0 cells and a number of genes under the GO term "response to oxidative stress" were upregulated by VSe1 and the active analogs (**Figure 38A**). The microarray samples were collected 28 hours after treatment, whereas in the GSH depletion experiments and time course experiment (**Figure 20**) we observed that the onset of action of the compounds is likely earlier than 28 hours post-treatment. Thus, qPCR was used to validate a selection of these genes at earlier timepoints. VSe1 or **28** treatments alone were able to highly upregulate *HMOX-1* and *OSGIN* (**Figure 38B**). Interestingly, the maximal induction of *HMOX-1* occurred 8h post-treatment, and was further induced in combination with VSVΔ51.

A

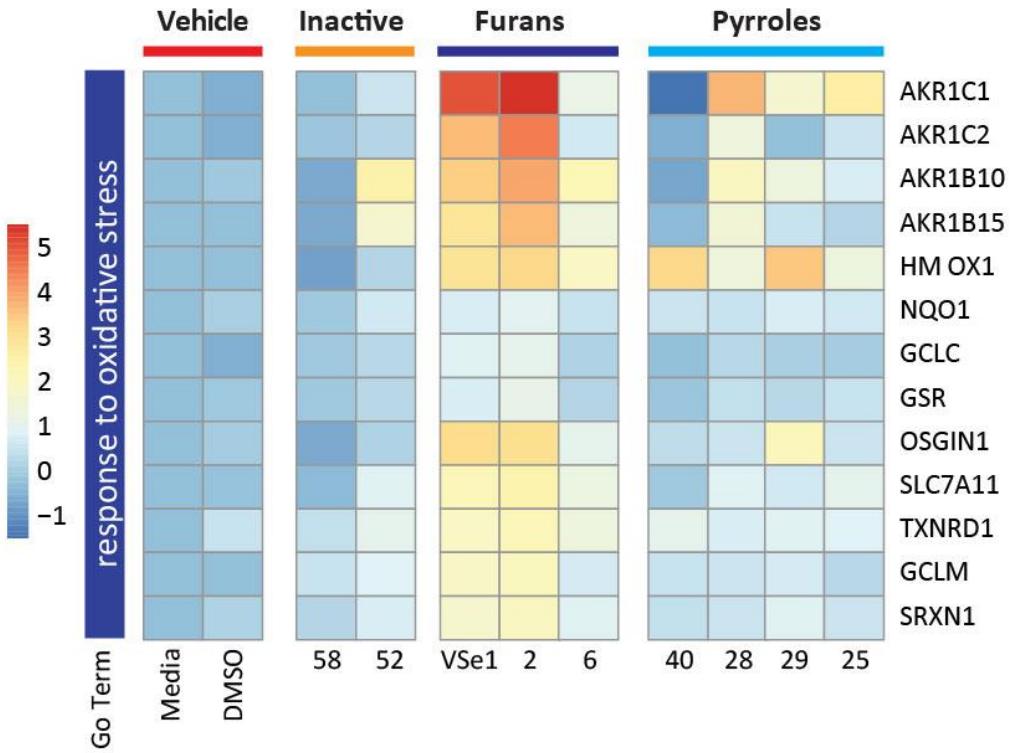
Vehicle
Inactive
Furans
Pyrroles
response to oxidative stress
5
4
3
2
1
0
−1
AKR1C1
AKR1C2
AKR1B10
AKR1B15
HM OX1
NQO1
GCLC
GSR
OSGIN1
SLC7A11
TXNRD1
GCLM
SRXN1
Go Term
Media
DMSO
58
52
VSe1
2
6
40
28
29
25

B

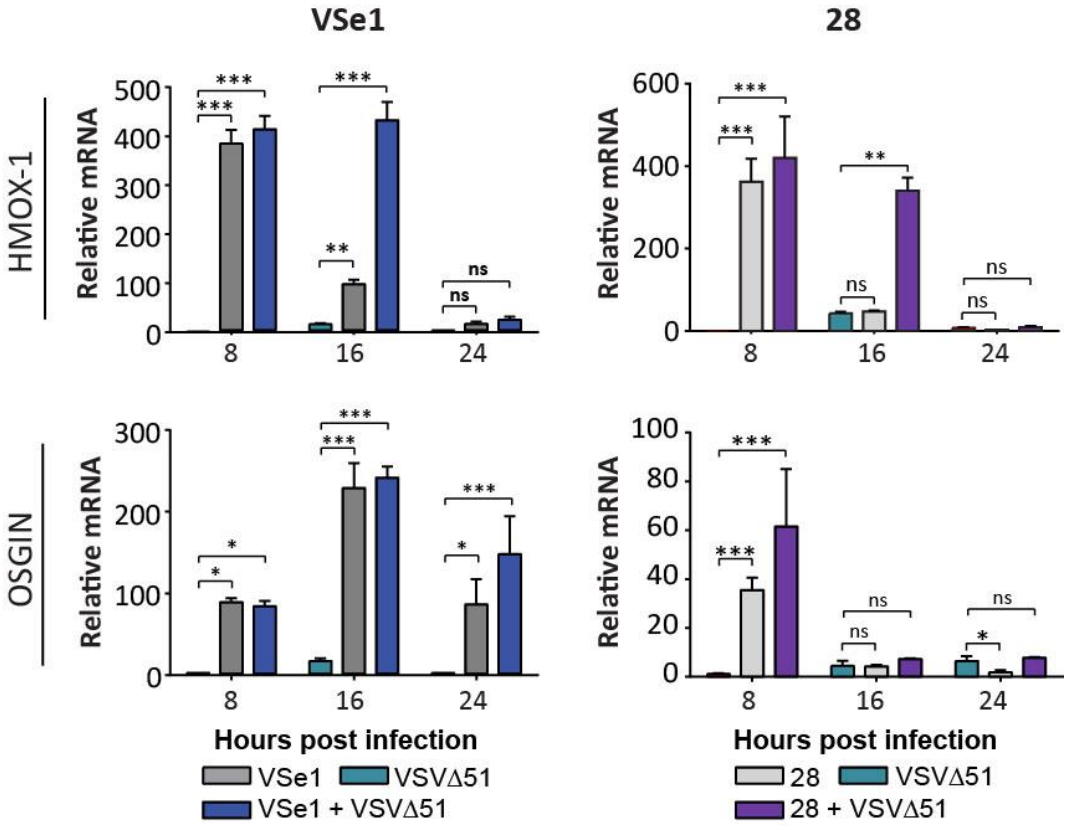
VSe1
28
HMOX-1
OSGIN
Relative mRNA
Hours post infection
VSe1
VSVΔ51
VSe1 + VSVΔ51
28
VSVΔ51
28 + VSVΔ51

Figure 38. VSe1 and compound 28 induce oxidative stress. (A) 786-0 cells were pretreated with media, vehicle (DMSO), or viral sensitizer. Twenty-eight hours later, RNA was collected, and triplicates were pooled and hybridized on Affymetrix Human PrimeView Array. Shown are heat maps of genes contained within the GO term "Response to Oxidative Stress." **(B)** 786-0 cells were treated with VSe1 (60 μM) or **28** (80 μM) for two hours prior to infection with VSVΔ51-GFP (MOI 1) and RNA was extracted at 8, 16 and 24 hours post infection. HMOX-1 and OSGIN mRNA levels were measured by quantitative RT-PCR. Values were normalized to GAPDH and are relative to untreated control for each timepoint. Values were log transformed for statistical analysis. Error bars represent standard error from biological triplicates and statistical significance was calculated using two-way ANOVA with Dunnett's multiple comparison (*** $P < 0.001$, ** $P < 0.01$, ns = $P > 0.05$). The data for B were generated by Nader El Sayes.

3.3.8 The activity of VSe1 and 28 is not likely mediated by NRF2

NRF2 is a transcription factor known to coordinate the transcriptional upregulation of antioxidant response genes, including *HMOX-1* and *OSGIN*[307–309]. Due to the coincidence between the induction of the antioxidant response and the viral sensitizing effects of VSe1 and **28**, we considered two possibilities: 1) the antioxidant response coincides with the production of reactive oxygen species (ROS) that is directly important for NFκB inhibition; or 2) an antioxidant response gene product inhibits antiviral signalling through NFκB. To assess the latter, we treated cells with ML385, a known inhibitor of NRF2 transcription that directly interacts with NRF2 and prevents DNA binding[310]. When 786-0 cells were pre-treated with ML385 prior to treatment with VSe1 or **28** and infection with VSVΔ51, titers decreased with increasing concentrations of ML385 (including samples treated with ML385 alone), however the potencies of VSe1 and **28** were not affected and at least 2-log increase in titers were still observed. Thus, while ML385 did decrease baseline infection of 786-0 cells, ML385 did not hinder the capacity of VSe1 and **28** to sensitize 786-0 cells to VSVΔ51. This suggests that while NRF2 activity may be relevant for VSV infection, NRF2 does not likely mediate the viral sensitizing effect of VSe1 or 28 (**Figure 39**).

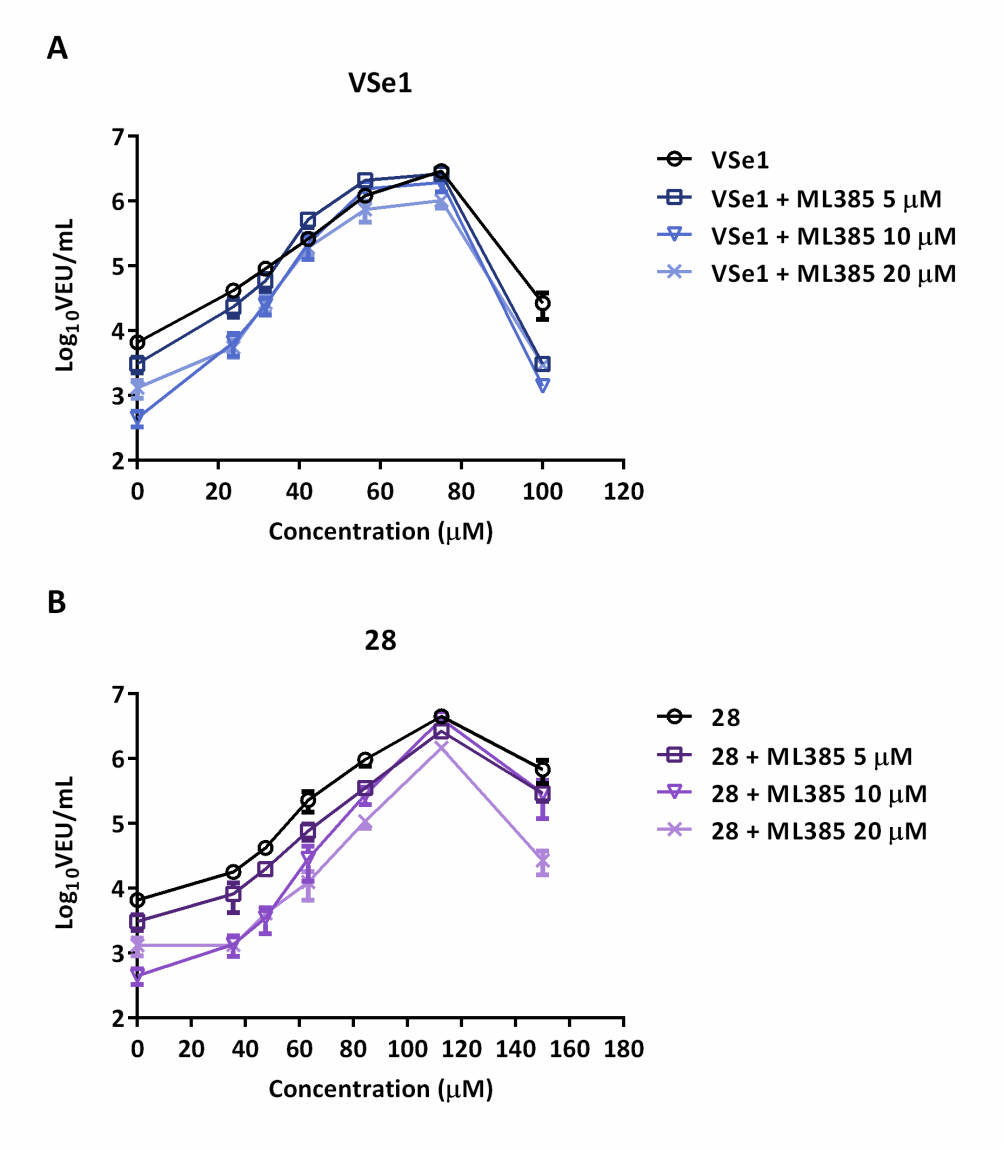
A
VSe1
Log10VEU/mL
Concentration (μM)
VSe1
VSe1 + ML385 5 μM
VSe1 + ML385 10 μM
VSe1 + ML385 20 μM
B
28
Log10VEU/mL
Concentration (μM)
28
28 + ML385 5 μM
28 + ML385 10 μM
28 + ML385 20 μM

Figure 39. NRF2 inhibitor ML385 does not significantly abrogate the activity of VSe1 or 28. 786-0 cells were treated with various concentrations of ML385. Four hours later, cells were treated with vehicle, VSe1 or **28**. Two hours later, cells were infected with VSVΔ51-Fluc (MOI 0.01). Supernatants were collected 36 hours later and virus output was determined using luciferase reporter-based viral titration assay (Materials and Methods, section 2.4)[282].

3.3.9 Reactive oxygen species sensitize cancer cells to VSV⊿51

Altogether, the data presented so far suggest that VSe1 and its analogs induce oxidative stress, which in turn may or may not contribute to increased sensitivity to VSV∆51. To confirm the potential that VSe1 and analogs increase oxidative stress, changes in reactive oxygen species (ROS) levels following VSe1 treatment were analysed using 6-carboxy-2',7'-dichlorodihydrofluorescein diacetate (C-H_2DCFDA), a non-specific indicator of intracellular ROS levels (e.g. H_2O_2, $O_2^{\bullet-}$, and $NO^{\bullet}$) that fluoresces when it is hydrolysed by intracellular esterases and then oxidized[311]. 786-0 cells were pre-treated with H_2O_2 or VSe1 for 4 hours, collected and treated with C-H_2DCFDA while in suspension. The viability indicator 7-aminoactinomycin D (7-AAD) was added 30 minutes prior to FACS analysis. Samples treated with H_2O_2 and VSe1 exhibited higher levels of fluorescence from C-H_2DCFDA, indicating higher levels of ROS (**Figure 40**).

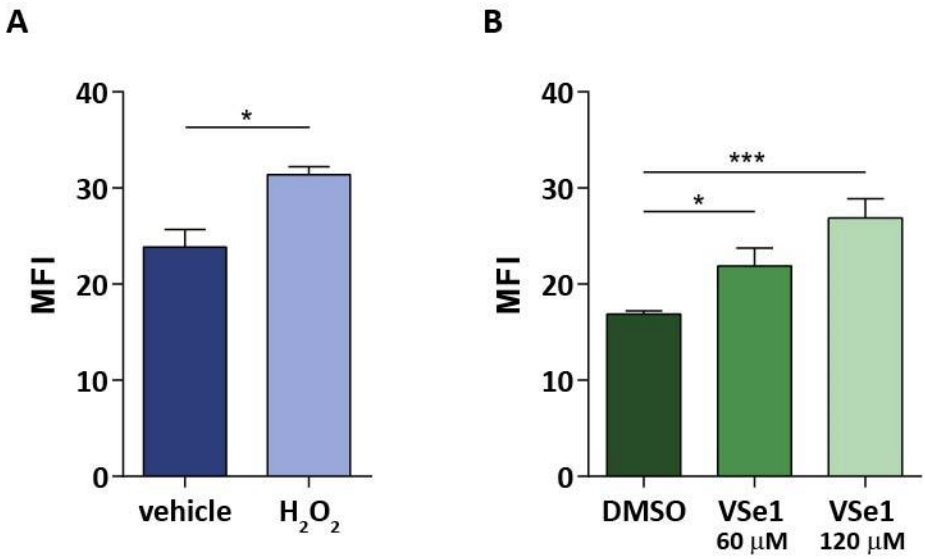
A
B
MFI
40
30
20
10
0
*
vehicle
H2O2
***
*
DMSO
VSe1
60 μM
VSe1
120 μM

Figure 40. ROS production in 786-0 cells. 786-0 cells were treated with **(A)** H_2O_2 (3 mM), **(B)** vehicle (DMSO), or VSe1. Four hours later, cells were collected and stained with C-H_2DCFDA and 7-AAD. Median fluorescence intensity (MFI) of C-H_2DCFDA in live cells (7-AAD$^-$) is presented. For **(A)**, statistical significance was determined by an unpaired t test (P = 0.0212). For **(B)**, statistical significance was determined by one-way ANOVA with Dunnett's multiple comparisons test (* P = 0.0417, *** P = 0.0007, N = 4 biological replicates for each condition).

To determine whether the exogenous administration of ROS could directly lead to viral sensitization, we pre-treated cells with H_2O_2 prior to infection with VSVΔ51. Interestingly, H_2O_2 was able to sensitize 786-0 cells to VSVΔ51 (**Figure 41A**). To functionally corroborate these results, we assessed the nuclear translocation of NFκB following co-treatment of cells with TNF-α and H_2O_2. Western blot analysis revealed that NFκB p65 and p50 nuclear translocation was hampered by H_2O_2 in the same range of concentrations that enhanced virus output (**Figure 41B**).

Given these results, we hypothesized that VSe1 may be indirectly increasing endogenous H_2O_2 via increased oxidative stress, leading to increased virus output. To test this theory, 786-0 cells were co-treated with 3-amino-1,2,4-triazole (3-ATZ), a catalase inhibitor, along with H_2O_2 or VSe1. Catalase converts H_2O_2 to water and oxygen. Thus, inhibiting this enzyme would lead to an accumulation of intracellular H_2O_2. Consistent with this mechanism, while treatment with 3-ATZ alone did not increase viral titers, when combined with H_2O_2, lower amounts of exogenous H_2O_2 were required to achieve the same increase in viral titers as H_2O_2 alone (**Figure 41C**). However, when 3-ATZ was combined with VSe1, the potency of VSe1 did not change, in contrast with what was observed for H_2O_2. When cells were pre-treated for 4 hours with (**Figure 41E**) H_2O_2 or (**Figure 41F**) VSe1 prior to treatment with 3-ATZ, the potency of neither compound was affected. Altogether this suggests that H_2O_2 levels can modulate antiviral responses in a similar fashion to VSe1 and analogs, however the activity of VSe1 and its analogs is not primarily mediated through increases of intracellular H_2O_2. Nevertheless, we cannot currently exclude the involvement of other ROS species (e.g. superoxide anion) or redox imbalance.

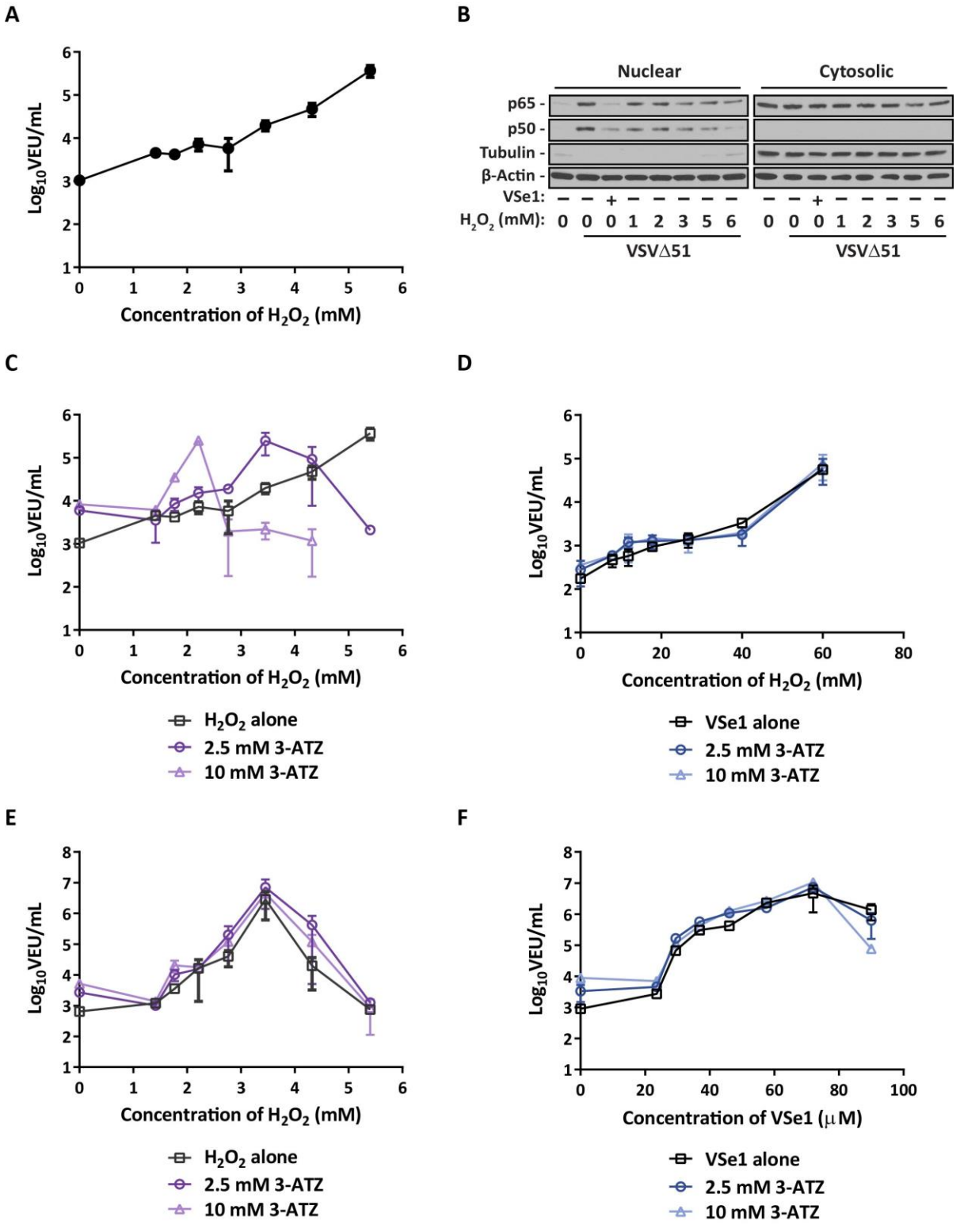
A
Log10VEU/mL
Concentration of H2O2 (mM)
B
Nuclear
Cytosolic
p65 -
p50 -
Tubulin -
β-Actin -
VSe1:
H2O2 (mM): 0 0 0 1 2 3 5 6 0 0 0 1 2 3 5 6
VSVΔ51
VSVΔ51
C
Log10VEU/mL
Concentration of H2O2 (mM)
H2O2 alone
2.5 mM 3-ATZ
10 mM 3-ATZ
D
Log10VEU/mL
Concentration of H2O2 (mM)
VSe1 alone
2.5 mM 3-ATZ
10 mM 3-ATZ
E
Log10VEU/mL
Concentration of H2O2 (mM)
H2O2 alone
2.5 mM 3-ATZ
10 mM 3-ATZ
F
Log10VEU/mL
Concentration of VSe1 (μM)
VSe1 alone
2.5 mM 3-ATZ
10 mM 3-ATZ

Figure 41. H_2O_2 treatment sensitizes 786-0 cells to VSVΔ51. (A) 786-0 cells were treated with H_2O_2 and infected 4 hours later with VSVΔ51-Fluc (MOI 0.005). Supernatants were collected 40 hours later and virus output was determined using luciferase reporter-based viral titration assay (Materials and Methods, section 2.4)[282]. **(B)** 786-0 cells were treated with the indicated concentrations of H_2O_2 for 4 hours then infected with VSVΔ51-GFP (MOI 1). Nuclear and cytoplasmic extracts were collected 8 hours post-infection then probed with the indicated antibodies. **(C)** 786-0 cells were treated concurrently with H_2O_2 and 3-ATZ or **(D)** VSe1 and 3-ATZ. Four hours later, cells were infected with VSVΔ51-Fluc (MOI 0.005). Supernatants were collected 40 hours later and virus output was determined using luciferase reporter-based viral titration assay (Materials and Methods, section 2.4)[282]. **(E)** 786-0 cells were pre-treated with H_2O_2 or **(F)** VSe1 for 4 hours and then treated with 3-ATZ. Four hours later, cells were infected with VSVΔ51-Fluc (MOI 0.005). Supernatants were collected 40 hours later and virus output was determined using luciferase reporter-based viral titration assay (Materials and Methods, section 2.4)[282]. For **(A)**, **(C-F)**, experiments were performed with biological triplicates. The data for B were generated by Nader El Sayes and Michel Phan

DISCUSSION

There is a growing list of OV clinical candidates for the treatment of cancer including VSV, vaccinia virus, reovirus, adenovirus, and herpes simplex virus-based platforms[312]. Nevertheless, it is well-recognized in the field that combination therapies will be necessary to overcome the heterogeneous response observed with these potentially curative biologics[177,178,201,313,314]. The novel agents we have developed in this study robustly increase the growth and oncolytic effects of VSVΔ51, MG1, and HSV-1-N212 in otherwise resistant cancer cells and therefore cater to an unmet need in this therapeutic area. Additionally, the enhancement in replication of the vaccine platform MVA and enhancement of transgene expression by replication-defective adenovirus and AAV vectors extends the potential of using these small molecules for co-administration with cancer gene therapies. There are numerous registered clinical trials employing gene therapy vectors expressing transgenes for the treatment of various malignancies[315,316]. It is easily foreseeable that the pharmaco-viral approach described here can be applied to therapeutically enhance attenuated viral vectors used for other types of gene therapy or for vaccines as well.

4.1 Pyrrole-based VSe1 analogs are stable and effective alternatives to VSe1

The physiochemical and *in vitro* biological characterization of structural VSe1 analogs led to the identification of compounds with enhanced aqueous stability and decreased susceptibility to nucleophilic attack, while maintaining *in vitro* efficacy of a similar order to the parent compound. Disruption of the α,β dichloro carbonyl moiety significantly abrogated efficacy, indicating that this group is central to activity. Interestingly,

the inactivity observed with compound **16** indicates that the α and β carbons must be substituted. Furthermore, the diminished activity displayed by compounds **3**, **4**, **17**, **52**, **53**, **57** and **58** implies that the substituted groups at the β carbon must be good leaving groups.

As described earlier, compounds with α,β unsaturated carbonyl act as Michael acceptors and can covalently react with nucleophilic residues on proteins, such as cysteines and lysines. Traditionally, the pharmaceutical industry has avoided the incorporation of such reactive groups in drug development due to concerns for indiscriminate reactivity. However, targeted covalent inhibitors with relatively weaker electrophilic groups such as acrylamides can be effective and potentially safer than more reactive compounds, as they need to be in close proximity to their target cysteines to form covalent bonds, thus limiting the probability of reacting non-specifically with other exposed protein thiols and GSH[218]. The reactivity of compounds containing Michael acceptors can also be finely tuned by making minor structural changes. In one study, the authors used this concept to demonstrate a correlation between the ability of their compounds to inhibit growth of ciliate protozoa and rate of reaction with GSH (an indication of compound electrophilicity by way of thiol reactivity)[298]. Similarly, with active VSe1 pyrrole analogs, a positive correlation exists between the GSH reactivity half-life and the concentration at which the peak fold-change in VEUs is observed (**Table 5**, **Appendix Figure 1**). This means that the potency of this subset of compounds inversely correlates with their susceptibility for nucleophilic attack, further supporting the fact that the reactivity of the α,β unsaturated carbonyl is a key feature of the activity of these compounds. Such a correlation may not exist with furan analogs as all of the furans tested had a GSH reaction half-life of less than 5

minutes, regardless of the peak-fold concentration. Thus, switching from a furan to a pyrrole scaffold gives us a platform that can be manipulated and refined to generate compounds with desired properties. Pyrrole derivatives possess an improved safety profile compared to VSe1 as demonstrated by selective replication in *ex vivo* tumour tissues and superior *in vivo* tolerability in dose escalation studies. Along with their enhanced plasma stability, these advantages over VSe1 and furan derivatives make the pyrrole analogs much better suited for *in vivo* use.

4.2 Effect on the type I IFN pathway and in vitro kinetics of VSe1 and analogs

VSe1 and its analogs are able to enhance the replication and cytopathic effect of VSVΔ51, Maraba MG1 and HSV-1 N212 in cancer cells. Notably, these viruses induce type I IFNs and are susceptible to type I IFN antiviral signaling[80,146,167,317–319]. Previously published data with VSe1 suggest that it dampens the type I IFN response induced by viral infection[215]. Results presented in the current study provide evidence that in 786-0 cells, VSe1 and its analogs inhibit the nuclear translocation of NFκB, leading to decreased expression of its target genes *IFNB*, *TNFA* and *IL6*, as well as ISGs. The compounds are most likely acting downstream of IκBα phosphorylation by the IKK complex, as IκBα is still being degraded after TNF-α treatment in the presence of VSe1 or **28** (**Figure 27E**). Furthermore, the IKK inhibitor TPCA-1 is also able to sensitize 786-0 cells to VSVΔ51, and co-treatment with VSe1 or **28** did not enhance infection any further. Thus, it is conceivable that the action of VSe1 and **28** are also downstream of TPCA-1's targets, namely IKKs. 786-0 cells are particularly responsive to the viral sensitizing effects of VSe1 and its active analogs. It is

worthwhile to note that the 786-0 cell line harbours a VHL mutation[320] and is unable to produce wild-type VHL[321]. This has been linked to dysfunctional regulation of antiviral signaling pathways[14] and inherent resistance of 786-0 cells to VSV[322]. 786-0 cells have also been shown to possess high basal NFκB-DNA-binding activity[323]. Thus, VSe1 derivatives may be especially effective in tumours with high basal NFκB activity. Our findings should be confirmed in other cell lines that are sensitized by VSe1 and analogs (such as B16-F10, CT26.WT and MC-38 cell lines). Repeating these assays with inactive analogs would assist in drawing a correlation between the functionally reactive pharmacophores of VSe1 and its effects on NFκB translocation and the production of IFN-β and ISGs. The effect of these compounds on NFκB could be further corroborated by seeing if the relative amount of p65 and p50 inhibition correlates with compound dose-response curves, and if it shifts in parallel with the shift in potency observed when the compounds are combined with BSO.

Further experiments are required to determine if in addition to blocking NFκB translocation, VSe1 and analogs also affect the phosphorylation and translocation of ATF-2, the dimerization partner of c-jun. The inhibition of NFκB target genes (*TNFA*, *IL6*, *IFNB*) that was observed can be corroborated by examining the effect of the compounds on the transcriptional activity and DNA binding of all components of the *IFNB* enhanceosome (NFκB, cJun/ATF-2, IRF3/7, CBP/p300) by electromobility shift assays (EMSA) and chromatin immunoprecipitation (ChIP).

It has been reported that TNF-α and IFN-β act in synergy to inhibit viral replication and spread, as well as cell proliferation in normal human fibroblasts and primary cell cultures[324,325]. However the combination failed to induce a cytostatic or antiviral state in

cancer cells, even in cell lines that were able to respond to TNF-α and IFN-β stimulation[324]. Hence, the synchronized inhibition of TNF-α and IFN-β that we observe offers a potential explanation for why VSe1 and its analogs are able to enhance viral replication and spread in cancer cells, but not in normal tissues (**Figure 15**). Even if the compounds are able to inhibit TNF-α and IFN-β in normal tissues, low levels of both cytokines may be adequate to confer a synergistic antiviral response.

The effect of VSe1 or **28**-induced cytokine depletion can be tested by transferring supernatants from cancer cells infected with VSVΔ51 alone or VSVΔ51 in combination with viral sensitizer on to new cells, and then infecting these new cells. Using a G-less version of VSVΔ51 (which is capable of replicating in cells, but incapable of producing infectious viral progeny[326]) would ensure that the effects observed are due to virus-induced cytokine production, and not the transfer of infectious virions. Cells incubated with supernatant from VSVΔ51-G-less alone would, in theory, be protected from virus challenge due to the presence of IFN-β and TNF-α in the supernatant. Cells incubated with supernatant from VSVΔ51-G-less and viral sensitizer should be more susceptible to virus infection due to diminished levels of these cytokines. Transferring supernatants on to normal cells such as GM38 fibroblasts, followed by infection with wild-type VSV, would also test the theory that low levels of TNF-α and IFN-β are still able to induce an effective antiviral response in non-cancerous cells.

Our data indicate that VSe1-derived compounds need to be administered and take effect before an anti-viral response is initiated, demonstrated by the fact that VSe1 does not significantly enhance virus replication when 786-0 cells are treated 12 hours post-

infection with a low MOI of VSVΔ51. This fits with evidence from literature showing that in 786-0 cells infected with a low MOI of VSVΔ51, very little IFN-β is secreted during the first 12 hours post-infection, and then levels spike at 24 hours post-infection[216]. The time-course experiment in **Figure 23** implies that the compounds need to be present before this spike in IFN-β occurs. Presumably, once NFκB, AP-1 and IRF3/7 have initiated the transcription of *IFNB* and downstream ISGs, treating cells with VSe1 analogs is not able to overcome their antiviral effects. The results from the IFN-β competition assay showing that VSe1 and its analogs are able to overcome the antiviral effects of IFN-β treatment (**Figure 25**) indicates that, in addition to blocking the action of NFκB, these compounds may also act downstream of IFN-β signaling. However, this experiment was performed by treating cells exogenously with IFN-β and VSe1 analogs concurrently, prior to infection with VSVΔ51. Thus, the compounds would have had a chance to bind to any targets upstream of IFN-β before an antiviral response was induced. The kinetics of antiviral ISG expression is likely specific to cell type and the nature of the stimulant. For example, in Huh7 hepatoma cells, ISG expression starts to increase 4 hours after IFN-α treatment and peaks between 6- 8 hours before rapidly decreasing[327,328]. A similar pattern has been reported in human lymphatic endothelial cells[329]. In Huh7 cells, treatment with IFN-β resulted in a similar time to peak ISG expression, but expression was sustained for up to 24 hours[328]. In the case of treatment with compounds **2** or **28** in combination with IFN-β, viral titers were only partially recovered compared to untreated controls, indicating that antiviral signaling was still effective to an extent.

Treatment with VSe1 and **28** prior to viral infection ultimately leads to decreased virus-induced ISG expression. It has also been reported that NFκB can bind to ISRE motifs on ISG promoters and drive their transcription[330]. Thus, additional experiments are required to determine if VSe1 and its analogs decrease ISG expression via NFκB, or by also affecting elements downstream of IFN-β secretion. The phosphorylation, dimerization, translocation and transcriptional activity of components of the JAK-STAT pathway (i.e. IFNAR, JAK1, TYK2, STAT1, STAT2, and IRF9) in the context of VSVΔ51 infection should be assessed. Assuming the kinetics of ISG expression in response to IFN-β treatment in 786-0 cells is similar to Huh7 cells, pre-treating cells with IFN-β for several hours prior to treatments with the compounds (and vice-versa), followed by infection with VSVΔ51, would help to verify if VSe1 and its analogs are acting upstream or downstream of IFN-β signaling. Silencing or overexpressing individual components of these pathways with CRISPR or RNAi-based strategies and then seeing if our viral sensitizers can still enhance infection would inform us if the compounds are working upstream or downstream of the altered gene.

The enhancement of viral replication, as demonstrated by the single-step growth curves, also corroborates the fact that the compounds are most effective before an anti-viral response is fully generated, i.e. earlier in VSV's life cycle. It would be valuable to further characterize the onset of action of these compounds by examining key points in the life cycle of VSV. In addition to their clear impact on antiviral defenses, some of our data suggest that the compounds may impact viral entry. Specifically, the microarray performed in 786-0 cells shows that the mRNA expression of SLC7A11 (solute carrier family 7 member 11, also known as cysteine transporter (xCT)), a factor reported to play a role in the entry of

VSV[331], is enhanced after treatment with the compounds (**Figure 38, Appendix Figure 2**). The magnitude of this observed effect is small and may be underestimated, much like it was for redox genes such as HMOX-1, given that samples for the microarray were collected 24 hours after treatment and infection. SLC7A11 has been shown to be required for the entry of Kaposi's sarcoma-associated herpesvirus (KSHV)[332] and is upregulated by the transactivator protein (Tat) encoded by human immunodeficiency virus-1 (HIV-1)[333]. With respect to VSV, SLC7A11 was found to be upregulated in monocytes as soon as 6 hours post infection with a high MOI and CRISPR-mediated knockdown abrogated viral infection[331]. The increase in intracellular GSH observed following VSe1 or **28** mediated depletion in **Figure 35** also supports the hypothesis that these compounds could upregulate SLC7A11, since SLC7A11 is a cysteine-glutamate transporter that is involved in the maintenance of intracellular GSH levels[334–337].The upregulation of SLC7A11 in response to our compounds and the effect of SLC7A11 inhibition (via CRISPR or RNAi) on VSVΔ51 titers needs be validated in our 786-0 model. It would be logical to examine changes in protein expression within 12 hours of treatment and infection with a high MOI of VSVΔ51.

Viral entry can be assessed by several methods. After a short (e.g. 1 hour) incubation to allow for virion binding and internalization, cells could be lysed and intracellular viral genomes could be quantified using RT-qPCR. There are caveats to this method, as it would not provide information on whether the genomes are from virions that are bound to the cell surface, internalized in endosomes, or in the cytoplasm after endosomal fusion. This could be explored in more detail by covalently labeling virions with a fluorophore as well as organelles of interest (e.g. plasma membrane and endosomes)[338].

Live-cell microscopy would allow us to track the progress of virions after inoculation. Altering incubation conditions (e.g. infecting at 4°C, and then warming to 37°C) could also allow us to distinguish between binding and endocytosis[339]. The localization of virions to specific sub-cellular compartments could also be analysed by labelling virions with [^{35}S]methionine and analysing fractions of infected cells separated by centrifugation.

The results from the single-step growth curves imply that the compounds are increasing viral replication. The impact on viral replication versus spread can be further teased apart by seeing if the compounds are able to enhance VSVΔ51-G-less titers. Additionally, qPCR can be used to assess increases in viral genomes over a 24-hour period, bearing in mind that this method would also quantify genomes from defective interfering particles and may not correlate with final infectious titers from fully formed virions. It would also be worthwhile to examine if VSVΔ51 itself is altered by treatment with VSe1 or analogs, or even if the compounds are incorporated into virions. Changes to VSVΔ51 virion structure, protein sequence and structure could be assessed by electron microscopy, mass spectrometry and x-ray crystallography. The presence of viral sensitizers in VSVΔ51 preparations could be identified by mass spectrometry as well.

4.3 GSH and GSTP1-1 are not direct mediators of VSe1-induced viral sensitization

Results from affinity-based chromatography studies directed us towards GSTs and GSH as possible targets of VSe1 and its derivatives. Indeed, we found that VSe1 inhibits the enzymatic activity of GSTP1-1, GSTA4 and GSTM5-5, and that high concentrations of compounds **10**, **28** and the **10**-GSH adduct inhibit GSTP1-1. VSe1, **10** and **28** were also able

to inhibit GSTP1-1 activity when incubated without GSH, indicating that the observed inhibition could be due to both the compounds alone and GSH-adducts. The dialysis experiment in **Figure 27B** also suggests that the nature of this inhibition is irreversible. IC_{50} values for irreversible inhibitors measured after a set incubation time length are largely arbitrary as these compounds interact with their targets in a time-dependent fashion, and different incubation time lengths would give different IC_{50} values[219]. Thus, if VSe1 and the analogs presented in **Table 7** are irreversible inhibitors, these inhibition data must be taken into context of the incubation lengths for these experiments, which was 5 minutes. This is supported by the fact that longer incubation times were required to see significant inhibition with **10** and **28**.

Despite the confirmation that these compounds inhibit GSTP1-1, the knockdown of *GSTP1* by siRNA transfection indicates the mechanism of action of VSe1 cannot be attributed to GSTP1-1 inhibition alone. We know that VSe1 also inhibits GSTA4-4 and GSTM5-5. It would be informative to examine the changes in VSVΔ51 titers after knocking down these GST enzymes as well. Given the redundancy between the conjugating activities of GSTs, it may be necessary to knock-down multiple GST enzymes. This could be done by co-transfecting multiple siRNAs, using a viral vector that encodes for multiple short-hairpin RNAs (shRNAs), or by designing a siRNA that targets a conserved region of the GST family, such as the G site.

While *GSTP1* knockdown did not impact VSVΔ51 growth, ezatiostat nevertheless enhanced the sensitivity to VSVΔ51. Ezatiostat is a GSH analog and is presumed to be a potent, specific inhibitor of GSTP1-1, with its active metabolite having an IC_{50} of 400 nM.

However, at the concentrations able to enhance VSVΔ51, it is likely inhibiting other classes of GSTs (specifically GSTA1-1, GSTM1-1 and GSTM2-2)[272,340], and could potentially also have off-target effects that do not relate to GST inhibition. It would be important to confirm whether ezatiostat is still capable of sensitizing cells to VSVΔ51 after *GSTP1* knockdown.

Interestingly, depletion of cellular GSH by BSO significantly increases viral titers; however, the magnitude of this effect is small in comparison to VSe1 and highly active analogs, and the potency of VSe1 and **28** actually improves in the absence of GSH. Altogether, this indicates that GSTP1-1 and its substrate GSH are not dominant players in the mechanism by which VSe1 sensitizes cells to VSVΔ51. However, their respective inhibition and depletion would cause an imbalance in redox homeostasis and oxidative stress. In this state, the cell may be more susceptible to VSVΔ51 infection. This is further supported by the increase in VSVΔ51 titers observed with H_2O_2. Oxidative stress has been known to affect protein function and signaling[341–343]. In particular, cysteine residues are prone to oxidation at the thiol group. This has been shown to affect protein-protein interactions and signal transduction[344]. Thiol oxidation is often followed by reversible, GST-catalysed, S-glutathionylation, which prevents irreversible over-oxidation and preserves redox homeostasis[344]. GSH depletion and inhibition of GSTs could theoretically lead to irreversible thiol over-oxidation which would significantly impact downstream activity. The lack of impact in viral titers when VSe1 was combined with the catalase inhibitor 3-ATZ implies that increased intracellular H_2O_2 is not implicated in VSe1's mechanism of action. If it was, we would have expected the potency of VSe1 to increase when combined with 3-ATZ, due to increased intracellular H_2O_2. However, as this was an indirect method of

assessing the impact of VSe1 on endogenous H_2O_2 levels, this should be confirmed by direct measurement of H_2O_2. This can be done using HyPer, a fluorescent probe that is transfected into cells and can be used to ratiometrically detect changes in intracellular H_2O_2[345]. To further examine the effect of H_2O_2 in 786-0 cells, catalase can also be inhibited via CRISPR or RNAi, or overexpressed following plasmid transfection. We would expect that inhibition would recapitulate the results shown in **Figure 41**, and overexpression would require higher concentrations of H_2O_2 to enhance VSVΔ51 titers. Based on our current knowledge, we would also predict that alterations in catalase expression would not affect the potency of VSe1.

4.4 VSe1 and 28 induce cellular oxidative stress

The changes in HMOX-1 and OSGIN gene expression and increase in C-H_2DCFDA fluorescence altogether strongly indicate that VSe1 and **28** increase cellular oxidative stress. The induction of HMOX-1 and OSGIN is maximal 8 hours post-infection, which is when inhibition of p65 and p50 was observed. It would be informative to examine both HMOX-1 and OSGIN gene and protein expression, as well as NFκB translocation at various timepoints within a 24 hour period to confirm if the kinetics of both phenomena is the same.

Both HMOX-1 and OSGIN are downstream targets of NRF2 signaling. It has been reported by one group that the activation of HMOX1 leads to the inhibition of p65 translocation[346]. Thus we hypothesized that inhibiting NRF2 would abrogate the effect that VSe1 and **28** have on VSVΔ51 titers. However, this was not the case. Another lab member also determined that knocking down NRF2 via siRNA did not alter VSVΔ51 titers or the

enhancement of titers after DMF treatment[347]. This observation may be unique to 786-0 cells, as another group has shown that silencing NRF2 in A549 cells, where it is constitutively active, did lead to decreased titers[348]. Although we observed a moderate, yet overall decrease in titers in 786-0 cells with the NRF2 inhibitor ML385, combinations with VSe1 or **28** still yielded titers that were comparable to VSe1 or **28** alone. To support this observation, it will be important to confirm if ML385 inhibits NRF2 transcriptional activity and HMOX-1 expression in 786-0 cells at the concentrations tested. These results do not necessarily rule out the involvement of HMOX-1 itself, as other stress-induced transcription factors such as heat shock factors and AP-1 bind to the HMOX-1 promoter[349]. Thus, the role of HMOX-1 should be definitively ruled out by gene silencing.

Increased oxidative stress has been associated with VSV infection. In Vero cells, wild-type VSV (wtVSV) infection led to the accumulation of lipid peroxidation products and treatment with the antioxidant butylated hydroxyanisole protected against VSV infection[350]. Other groups have shown that treatment with wtVSV M protein increases ROS levels and up-regulates antioxidant enzymes in MKN28 human gastric cancer cells (although the ROS were not specifically identified)[351] and that treatment of A549 cells expressing the oncogene CUG2 (cancer upregulated gene 2) with H_2O_2 enhanced wtVSV-induced apoptosis[352]. CUG2 has been associated with increased levels of STAT1 phosphorylation and confers resistance to wtVSV[353,354]. Another group has shown that ROS may have an effect on the antiviral state induced by IFN-α. HeLa cells transfected with CuZn-superoxide dismutase (CuZnSOD), the enzyme responsible for detoxifying $O_2^{\bullet-}$ by converting it to H_2O_2[241], had a biphasic effect on IFN-α-mediated control of viral infection[355]. HeLa clones

with moderate levels of CuZnSOD activity were more resistant to effects of IFN-α and susceptible to VSV,[355] whereas clones with high CuZnSOD activity were more responsive to the effects of IFN-α and were able to resist virus-induced cytoxicity[355]. The authors concluded that this implicated $O_2^{\bullet-}$ in promoting the antiviral state induced by IFN-α. However, increased CuZnSOD activity would theoretically lead to an accumulation of intracellular H_2O_2, which in our hands augments VSVΔ51 titers. Thus, it would be edifying to investigate whether VSVΔ51 increases specific types of ROS. While VSV infection in 293T cells expressing cyto-Grx1-roGFP2 did not induce a significant change in the GSSG/GSH ratio over a 24 hour period (**Appendix Figure 3**), this should be confirmed by measuring GSH and GSSG by HPLC/UV-Vis. Oxidative stress, H_2O_2 and $O_2^{\bullet-}$ levels can be measured as well.

Altogether, we have demonstrated that VSe1 and its analogs impede the activity and function of GSTs and GSH, which are key mediators of cellular redox homeostasis, and this is associated with increased oxidative stress. Furthermore, VSe1 and **28** inhibit the translocation of the NFκB subunits p65 and p50. However, we have not established a clear link or cause-and-effect relationship between these two phenomena and their impact on enhancement of VSVΔ51 titers.

4.5 Oxidative stress and NFκB activity.

The effect of oxidative stress on NFκB signaling is controversial[356,357]. There are numerous reports that reactive oxygen and nitrogen species (ROS/RNS) activate[358–360] or inhibit[361,362] NFκB activity. The diversity of reported effects could be due to cell-type specific effects, intracellular location-specific effects, differences between the upstream

pathways that are investigated, and different stimuli used to activate these pathways[356,357,363]. Despite this, it has been well established that the oxidation and/or subsequent covalent modification of specific cysteine residues of subunits p65 and p50 inhibit nuclear translocation and transcriptional activity[235,238,240]. In fact, Cys38 in p65 (located at its DNA-binding interface[364]) has been shown to be covalently modified by compounds containing α,β unsaturated carbonyls, such as DMF[235,365]. As demonstrated in **Figure 34**, DMF is an effective viral sensitizer and also decreases the nuclear translocation of p65 in a number of cell lines[235,366–368], including 786-0 cells[347]. A similar mechanism could reasonably explain many of our observations, in particular the increased potency of VSe1 and **28** in the absence of GSH, following BSO treatment.

Other proteins in the type I IFN pathway have also shown to have cysteines that are prone to electrophilic modification. For example, CBP/p300 has redox-sensitive cysteines and oxidative stress has been shown to increase complex formation between this co-activator and transcription factors[363,369]. Additionally, one of the subunits of the type I IFN receptor, IFNAR1, is palmitoylated on Cys463 and this is required for downstream STAT1 and STAT2 activation[236]. When this residue is mutated to alanine, palmitoylation does not occur and IFN-α mediated activation of STAT1 and STAT2 is inhibited[236]. If an electrophile forms an adduct with Cys463, this would theoretically block palmitoylation and also inhibit STAT1 and STAT2 activation. JAK1 also contains a reactive cysteine (Cys1077) in its kinase domain and forms adducts with the compound bardoxolone methyl ester (CDDO-Me), resulting in inhibition of downstream pathways[237]. Interestingly, CDDO-Me also inhibits NFκB activation by inhibiting the activation of the IKK complex[370] and we have found that it

sensitizes 786-0 cells to VSVΔ51 infection (**Appendix Figure 4**). In addition to blocking the translocation of NFκB, VSe1 and analogs diminish the antiviral effects of exogenously administered IFN-β (notwithstanding certain caveats, as discussed in section 4.2). If these compounds do covalently modify cysteines on the aforementioned proteins in the JAK-STAT pathway, it could offer an explanation for this observation.

Activity-based protein profiling (ABPP) would be the method of choice for assessing whether or not VSe1-based compounds covalently modify proteins. The method used to perform the affinity capture where GSTP1 was identified was not designed to detect covalent binding partners and was more likely to yield hits 35 kDa or smaller, due to the permeability of the Amino PEGA beads to which the small molecule probes (**27** and **58**) were attached. For ABPP, active and inactive VSe1 probes that are amenable to "click-chemistry" reactions would be used (**Appendix Figure 5**). After *in situ* labeling of intracellular targets or incubating probes with cell lysate, a copper(I) catalysed reaction between the alkyne group on the probe and an azide-conjugated reagent, such as biotin-azide, would be carried out, forming a triazole linker between the probe and biotin[371]. This would be followed by a pull-down of biotin-conjugated probe-protein complexes with streptavidin beads. At this point, eluted samples could be analysed by mass spectrometry or run on SDS-PAGE to compare proteins pulled down with the positive and negative probes. This technique can also be used with purified proteins of interest containing point mutations to confirm if a particular residue is covalently modified by our compounds. The relevance of hits that interact specifically with the positive probe can be verified with gene silencing/overexpression studies and x-ray crystallography of the protein-inhibitor complex.

4.6 *In vivo* mechanism of pyrrole analogs

Combination regimens of VSVΔ51 and compounds **10** or **28** led to delays in tumour progression and increased survival, particularly in the immunocompromised HT29 model, where complete cures were observed. Efficacy in the immunocompetent CT26.WT and B16-F10 models could be enhanced by incorporating these compounds into treatment strategies involving OVs that have proven to be effective. The ICV treatment strategy (described in section 1.2.5) has been used in the B16-F10 model, leading to delayed tumour progression and enhanced survival, although complete cures were not observed[157,163]. Given that the compounds are able to robustly boost viral replication *in vitro*, a potential application that could be explored is their use during preparation of the ICV when tumour cells are infected with VSV.

Curiously, despite the enhancement in efficacy conferred by combining **28** with VSVΔ51 in the B16-F10 and HT29 models, no enhancement of viral replication was detected by IVIS (**Appendix Figure 6**). This does seem to contradict the fact that these compounds are able to enhance VSVΔ51 replication *in vitro* and in the CT26.WT model. It is possible that if the mice were administered a lower dose of virus (i.e. $1x10^7$ pfu instead of $1x10^8$ pfu), a more significant difference would have been observed. Another potential caveat relates to the fact that luminescence is rapidly lost upon death of cells given that the luciferase-luciferin reaction requires ATP. This means that dead cells do not contribute to the signal, which is relevant, given that we typically observe increased cytotoxicity in the combination treatment in our *in vitro* assays. Indeed, it is for this very reason that we used a secondary infection protocol to measure viral output by VEU in the luciferase reporter-

based titration assay. It is unclear whether this effect is at play in HT29 and B16-F10 models.

Considering that VSVΔ51 has the ability to induce a strong anti-tumour immune response (as described in section 1.2.5), it may be that the observed improvement in efficacy could be due to **28** enhancing the immune stimulating properties of VSVΔ51. In particular, the improved efficacy observed in the HT29 model in athymic nude mice suggests that the compounds may be affecting processes that drive the innate immune response, as these mice are unable to produce T cells and fully functional B cells, and are thus unable to generate successful adaptive immune responses[372]. The ensuing implications are that cells involved in the innate immune response, such as NK cells, are the primary mediators of the anti-tumour immune response in this context. An examination of tumour infiltrating leukocytes (TILs) in both models suggests that the combination of **28** with VSVΔ51 is associated with enhanced infiltration of activated NK cells, which could contribute to tumour eradication (**Appendix Figure 6**). This could also explain why **10** administered intraperitoneally in combination with intra-tumoural VSVΔ51 lead to delayed tumour progression (**Figure 17**) even though **10** was not detected in the tumour. Systemic administration of the compound may have an effect on NK cell activation. The impact on NK cell activation on efficacy with this treatment regimen can be further evaluated by depleting NK cells prior to treating mice to see if we lose the benefit of the combination treatment. Furthermore, increased NK cell activity should be confirmed with functional assays, such as NK cell killing assays.

Processes that would abrogate virus-induced anti-tumour activity, such as the production of antiviral neutralizing antibodies and increased infiltration of regulatory T cells, would be at play in the immunocompetent models, but not in the HT29 model. Thus, an examination of these factors in the CT26.WT and B16-F10 models could explain the observed differences in efficacy.

Given that our compounds inhibit the translocation of NFκB and production IFN-β, the increase in activated NK cells in these models may seem contradictory, since NK cells typically require type I IFN for activation[373–376]. However, the effects of the compounds on NFκB activation and type I IFN signaling may be cell type specific[376], which is why it is critical to examine these effects in the different types of immune cells and tumours grown *in situ*. Moreover, the inhibition of type I IFN production and signaling may be temporary. In fact, in 786-0 cells treated with **28** and VSVΔ51, TNF-α and IFN-β mRNA levels are initially reduced, but start to increase 24 hours post-infection (**Figure 28**, **Appendix Figure 7**). It is conceivable that the initial inhibition of NFκB and type I IFN signaling provides the virus a head start to replicate and spread efficiently and then the cell overcompensates by up-regulating components of these pathways. Examining *in vivo* NFκB activation and type I IFN production over a period of several days could confirm this theory. The *in vivo* distribution of the compounds should also be assessed. We have demonstrated that after IT injection, the parent compound is detectable in serum, and thus could potentially accumulate in other organs and tissues. These experiments would complement the examination of the effects of VSe1 and its analogs on non-tumour tissue in an *in vivo* setting and could also allow us to predict possible off-target pharmacological and toxicological effects.

5. Concluding Remarks

Oncolytic viruses are poised to make a significant impact in the clinic and revolutionize cancer therapy. The OV field is entering a critical phase where it is crucial to establish real-world efficacy in order to obtain regulatory approval. The strategy of combining OV therapy and drug therapy is proving to be a valid approach of boosting OV efficacy in patients. The work presented here describes a new class of molecules that can be broadly utilized to enhance OV activity, and provides insight into the mechanism of action by which these electrophilic molecules inhibit innate antiviral signalling. Furthermore, this study underscores how such molecules can be tempered to maintain the safety profile of OVs such as VSVΔ51, while improving oncolytic efficacy. Thus far, our efforts have been focussed on elucidating the effects of these compounds on the type I IFN pathway. Future work should continue to identify the specific cellular and viral components involved, and establish a causal link between the actions of these compounds at a molecular level and their enhancement of the oncolytic effects of VSVΔ51 *in vivo*. Ultimately, the knowledge gained from this study contributes to the growing repertoire of combination therapy strategies to enhance OV therapy and overcome heterogeneity in clinical responses.

References

1. Canadian Cancer Sociey. Canadian Cancer Statistics Special topic : Pancreatic Cancers. *Can. Cancer Soc.* 1–132 (2017). doi:0835-2976
2. Weinstein, I. B. & Case, K. The history of Cancer Research: introducing an AACR Centennial series. *Cancer Res.* **68,** 6861–2 (2008).
3. Hanahan, D. & Weinberg, R. A. Hallmarks of Cancer: The Next Generation. *Cell* **144,** 646–674 (2011).
4. Croce, C. M. Oncogenes and Cancer. *N. Engl. J. Med.* **358,** 502–511 (2008).
5. Payne, S. R. & Kemp, C. J. Tumor suppressor genetics. *Carcinogenesis* **26,** 2031–2045 (2005).
6. Morais, C., Gobe, G., Johnson, D. W. & Healy, H. The emerging role of nuclear factor kappa B in renal cell carcinoma. *Int. J. Biochem. Cell Biol.* **43,** 1537–1549 (2011).
7. Merkhofer, E. C., Cogswell, P. & Baldwin, A. S. Her2 activates NF-κB and induces invasion through the canonical pathway involving IKKα. *Oncogene* **29,** 1238–1248 (2010).
8. Hoesel, B. & Schmid, J. A. The complexity of NF-κB signaling in inflammation and cancer. *Mol. Cancer* **12,** 86 (2013).
9. Chen, F. E. & Ghosh, G. Regulation of DNA binding by Rel/NF-kappaB transcription factors: structural views. *Oncogene* **18,** 6845–6852 (1999).
10. Verma, I. M., Stevenson, J. K., Schwarz, E. M., Van Antwerp, D. & Miyamoto, S. Rel/NF-kappa B/I kappa B family: intimate tales of association and dissociation. *Genes Dev.* **9,** 2723–35 (1995).
11. Xia, Y., Shen, S. & Verma, I. M. NF-κB, an active player in human cancers. *Cancer Immunol. Res.* **2,** 823–30 (2014).
12. Baud, V. & Karin, M. Is NF-kappaB a good target for cancer therapy? Hopes and pitfalls. *Nat. Rev. Drug Discov.* **8,** 33–40 (2009).
13. Staudt, L. M. Oncogenic Activation of NF- B. *Cold Spring Harb. Perspect. Biol.* **2,** a000109–a000109 (2010).
14. Du, J. *et al.* pVHL Negatively Regulates Antiviral Signaling by Targeting MAVS for Proteasomal Degradation. *J. Immunol.* **195,** 1782–90 (2015).
15. Peri, S., Devarajan, K., Yang, D.-H., Knudson, A. G. & Balachandran, S. Meta-analysis identifies NF-κB as a therapeutic target in renal cancer. *PLoS One* **8,** e76746 (2013).
16. Lin, Y., Bai, L., Chen, W. & Xu, S. The NF-kappaB activation pathways, emerging molecular targets for cancer prevention and therapy. *Expert Opin. Ther. Targets* **14,** 45–55 (2010).
17. Ros, J. *et al.* Induction of Mdr1b expression by tumor necrosis factor-α in rat liver cells is independent of p53 but requires NF-κB signaling. *Hepatology* **33,** 1425–1431 (2001).
18. Godwin, P. *et al.* Targeting nuclear factor-kappa B to overcome resistance to chemotherapy. *Front. Oncol.* **3,** 120 (2013).
19. Tan, C. & Waldmann, T. A. Proteasome inhibitor PS-341, a potential therapeutic agent for adult T-cell leukemia. *Cancer Res.* **62,** 1083–6 (2002).
20. Diallo, J.-S. *et al.* Enhanced killing of androgen-independent prostate cancer cells

using inositol hexakisphosphate in combination with proteasome inhibitors. *Br. J. Cancer* **99,** 1613–22 (2008).
21. Nemeth, Z. H. *et al.* Proteasome Inhibitors Induce Inhibitory B (I B) Kinase Activation, I B Degradation, and Nuclear Factor B Activation in HT-29 Cells. *Mol. Pharmacol.* **65,** 342–349 (2004).
22. Dolcet, X. *et al.* Proteasome inhibitors induce death but activate NF-kappaB on endometrial carcinoma cell lines and primary culture explants. *J. Biol. Chem.* **281,** 22118–30 (2006).
23. Bagnyukova, T. V *et al.* Chemotherapy and signaling: How can targeted therapies supercharge cytotoxic agents? *Cancer Biol. Ther.* **10,** 839–53 (2010).
24. Baudino, T. A. Targeted Cancer Therapy: The Next Generation of Cancer Treatment. *Curr. Drug Discov. Technol.* **12,** 3–20 (2015).
25. Hill, M. & Kyle, F. NHL (diffuse large B-cell lymphoma). *BMJ Clin. Evid.* **2010,** (2010).
26. Early Breast Cancer Trialists' Collaborative Group (EBCTCG), E. B. C. T. C. G. *et al.* Comparisons between different polychemotherapy regimens for early breast cancer: meta-analyses of long-term outcome among 100,000 women in 123 randomised trials. *Lancet (London, England)* **379,** 432–44 (2012).
27. DiPiro, J. T. *Pharmacotherapy : a pathophysiologic approach*. (McGraw-Hill Medical, 2008).
28. Koda-Kimble, M. A. & Alldredge, B. K. *Applied therapeutics : the clinical use of drugs.* (Wolters Kluwer/Lippincott Williams & Wilkins, 2013).
29. Livshits, Z. & Rao, R. B. An Approach to Chemotherapy-Associated Toxicity. *Emerg. Med. Clin. North Am.* **32,** 167–203 (2014).
30. Early Breast Cancer Trialists' Collaborative Group (EBCTCG). Aromatase inhibitors versus tamoxifen in early breast cancer: patient-level meta-analysis of the randomised trials. *Lancet (London, England)* **386,** 1341–1352 (2015).
31. Smith, I. E. & Dowsett, M. Aromatase Inhibitors in Breast Cancer. *N. Engl. J. Med.* **348,** 2431–2442 (2003).
32. Scott, A. M., Allison, J. P. & Wolchok, J. D. Monoclonal antibodies in cancer therapy. *Cancer Immun.* **12,** 14 (2012).
33. Diamantis, N. & Banerji, U. Antibody-drug conjugates—an emerging class of cancer treatment. *Br. J. Cancer* **114,** 362–367 (2016).
34. Gross, S., Rahal, R., Stransky, N., Lengauer, C. & Hoeflich, K. P. Targeting cancer with kinase inhibitors. *J. Clin. Invest.* **125,** 1780–1789 (2015).
35. El-Kenawi, A. E. & El-Remessy, A. B. Angiogenesis inhibitors in cancer therapy: mechanistic perspective on classification and treatment rationales. *Br. J. Pharmacol.* **170,** 712–29 (2013).
36. Comunanza, V. & Bussolino, F. Therapy for Cancer: Strategy of Combining Anti-Angiogenic and Target Therapies. *Front. cell Dev. Biol.* **5,** 101 (2017).
37. Holohan, C., Van Schaeybroeck, S., Longley, D. B. & Johnston, P. G. Cancer drug resistance: an evolving paradigm. *Nat. Rev. Cancer* **13,** 714–726 (2013).
38. Chen, H. X. & Cleck, J. N. Adverse effects of anticancer agents that target the VEGF pathway. *Nat. Rev. Clin. Oncol.* **6,** 465–477 (2009).
39. Lodish, M. B. Kinase Inhibitors: Adverse Effects Related to the Endocrine System. *J.*

Clin. Endocrinol. Metab. **98,** 1333–1342 (2013).
40. Jabbour, E., Deininger, M. & Hochhaus, A. Management of adverse events associated with tyrosine kinase inhibitors in the treatment of chronic myeloid leukemia. *Leukemia* **25,** 201–210 (2011).
41. Yang, Y. Cancer immunotherapy: harnessing the immune system to battle cancer. *J. Clin. Invest.* **125,** 3335–7 (2015).
42. Teng, M. W. L., Galon, J., Fridman, W.-H. & Smyth, M. J. From mice to humans: developments in cancer immunoediting. *J. Clin. Invest.* **125,** 3338–46 (2015).
43. Shalapour, S. & Karin, M. Immunity, inflammation, and cancer: an eternal fight between good and evil. *J. Clin. Invest.* **125,** 3347–55 (2015).
44. Schreiber, R. D., Old, L. J. & Smyth, M. J. Cancer immunoediting: integrating immunity's roles in cancer suppression and promotion. *Science* **331,** 1565–70 (2011).
45. Dunn, G. P., Koebel, C. M. & Schreiber, R. D. Interferons, immunity and cancer immunoediting. *Nat. Rev. Immunol.* **6,** 836–848 (2006).
46. Dunn, G. P., Bruce, A. T., Ikeda, H., Old, L. J. & Schreiber, R. D. Cancer immunoediting: from immunosurveillance to tumor escape. *Nat. Immunol.* **3,** 991–998 (2002).
47. Mittal, D., Gubin, M. M., Schreiber, R. D. & Smyth, M. J. New insights into cancer immunoediting and its three component phases—elimination, equilibrium and escape. *Curr. Opin. Immunol.* **27,** 16–25 (2014).
48. Medrano, R. F. V, Hunger, A., Mendonça, S. A., Barbuto, J. A. M. & Strauss, B. E. Immunomodulatory and antitumor effects of type I interferons and their application in cancer therapy. *Oncotarget* **8,** 71249–71284 (2017).
49. Saidi, R. F. *et al.* Expression of interferon receptors in pancreatic cancer: Identification of a novel prognostic factor. *Surgery* **139,** 743–748 (2006).
50. Yi, Y. *et al.* Interferon Regulatory Factor (IRF)-1 and IRF-2 are Associated with Prognosis and Tumor Invasion in HCC. *Ann. Surg. Oncol.* **20,** 267–276 (2013).
51. Gordziel, C., Bratsch, J., Moriggl, R., Knösel, T. & Friedrich, K. Both STAT1 and STAT3 are favourable prognostic determinants in colorectal carcinoma. *Br. J. Cancer* **109,** 138–46 (2013).
52. Ren, Y. *et al.* JAK1 truncating mutations in gynecologic cancer define new role of cancer-associated protein tyrosine kinase aberrations. *Sci. Rep.* **3,** 3042 (2013).
53. Behan, J. W., Sutton, A. & Wysong, A. Management of Skin Cancer in the High-Risk Patient. *Curr. Treat. Options Oncol.* **17,** 60 (2016).
54. Trinh, V. A., Zobniw, C. & Hwu, W.-J. The efficacy and safety of adjuvant interferon-alfa therapy in the evolving treatment landscape for resected high-risk melanoma. *Expert Opin. Drug Saf.* **16,** 933–940 (2017).
55. Thallinger, C. *et al.* Review of cancer treatment with immune checkpoint inhibitors. *Wien. Klin. Wochenschr.* 1–7 (2017). doi:10.1007/s00508-017-1285-9
56. Mellman, I., Coukos, G. & Dranoff, G. Cancer immunotherapy comes of age. *Nature* **480,** 480–489 (2011).
57. U. S. Food and Drug Administration. Press Announcements - FDA approval brings first gene therapy to the United States. (2017). Available at: https://www.fda.gov/NewsEvents/Newsroom/PressAnnouncements/ucm574058.htm. (Accessed: 27th December 2017)

58. U. S. Food and Drug Administration. Press Announcements - FDA approves CAR-T cell therapy to treat adults with certain types of large B-cell lymphoma. (2017). Available at: https://www.fda.gov/NewsEvents/Newsroom/PressAnnouncements/ucm581216.htm. (Accessed: 27th December 2017)
59. Ilkow, C. S., Swift, S. L., Bell, J. C. & Diallo, J. S. From Scourge to Cure: Tumour-Selective Viral Pathogenesis as a New Strategy against Cancer. *PLoS Pathog.* **10,** (2014).
60. Pikor, L. A., Bell, J. C. & Diallo, J. S. Oncolytic Viruses: Exploiting Cancer's Deal with the Devil. *Trends in Cancer* **1,** 266–277 (2015).
61. Keller, B. A. & Bell, J. C. Oncolytic viruses—immunotherapeutics on the rise. *J. Mol. Med.* **94,** 979–991 (2016).
62. Dock, G. The Influence Of Complicating Diseases Upon LeukÆmia. *Am. J. Med. Sci.* **127,** 563–592 (1904).
63. Kelly, E. & Russell, S. J. History of Oncolytic Viruses: Genesis to Genetic Engineering. *Mol. Ther.* **15,** 651–659 (2007).
64. Yu, W. & Fang, H. Clinical trials with oncolytic adenovirus in China. *Curr. Cancer Drug Targets* **7,** 141–8 (2007).
65. Andtbacka, R. H. I. *et al.* Talimogene Laherparepvec Improves Durable Response Rate in Patients With Advanced Melanoma. *J. Clin. Oncol.* **33,** 2780–2788 (2015).
66. U. S. Food and Drug Administration. Press Announcements - FDA approves first-of-its-kind product for the treatment of melanoma. Available at: https://www.fda.gov/NewsEvents/Newsroom/PressAnnouncements/ucm469571.htm. (Accessed: 28th December 2017)
67. Fukuhara, H., Ino, Y. & Todo, T. Oncolytic virus therapy: A new era of cancer treatment at dawn. *Cancer Sci.* **107,** 1373–1379 (2016).
68. Anderson, B. D., Nakamura, T., Russell, S. J. & Peng, K.-W. High CD46 Receptor Density Determines Preferential Killing of Tumor Cells by Oncolytic Measles Virus. *Cancer Res.* **64,** 4919–4926 (2004).
69. Mühlebach, M. D. *et al.* Adherens junction protein nectin-4 is the epithelial receptor for measles virus. *Nature* **480,** 530–533 (2011).
70. DeRycke, M. S. *et al.* Nectin 4 Overexpression in Ovarian Cancer Tissues and Serum. *Am. J. Clin. Pathol.* **134,** 835–845 (2010).
71. Fabre-Lafay, S. *et al.* Nectin-4, a New Serological Breast Cancer Marker, Is a Substrate for Tumor Necrosis Factor-α-converting Enzyme (TACE)/ADAM-17. *J. Biol. Chem.* **280,** 19543–19550 (2005).
72. Takano, A. *et al.* Identification of Nectin-4 Oncoprotein as a Diagnostic and Therapeutic Target for Lung Cancer. *Cancer Res.* **69,** 6694–6703 (2009).
73. Vander Heiden, M. G., Cantley, L. C. & Thompson, C. B. Understanding the Warburg effect: the metabolic requirements of cell proliferation. *Science* **324,** 1029–33 (2009).
74. Li, C. *et al.* Dichloroacetate blocks aerobic glycolytic adaptation to attenuated measles virus and promotes viral replication leading to enhanced oncolysis in glioblastoma. *Oncotarget* **6,** 1544–55 (2015).
75. He, B., Gross, M. & Roizman, B. The gamma(1)34.5 protein of herpes simplex virus 1

complexes with protein phosphatase 1alpha to dephosphorylate the alpha subunit of the eukaryotic translation initiation factor 2 and preclude the shutoff of protein synthesis by double-stranded RNA-activa. *Proc. Natl. Acad. Sci. U. S. A.* **94,** 843–8 (1997).
76. Liu, B. L. *et al.* ICP34.5 deleted herpes simplex virus with enhanced oncolytic, immune stimulating and anti-tumour properties. *Gene Ther.* **10,** 292–303 (2003).
77. Chou, J., Chen, J. J., Gross, M. & Roizman, B. Association of a M(r) 90,000 phosphoprotein with protein kinase PKR in cells exhibiting enhanced phosphorylation of translation initiation factor eIF-2 alpha and premature shutoff of protein synthesis after infection with gamma 134.5- mutants of herpes si. *Proc. Natl. Acad. Sci. U. S. A.* **92,** 10516–20 (1995).
78. Peters, C. & Rabkin, S. D. Designing Herpes Viruses as Oncolytics. *Mol. Ther. oncolytics* **2,** 15010 (2015).
79. Silvera, D., Formenti, S. C. & Schneider, R. J. Translational control in cancer. *Nat. Rev. Cancer* **10,** 254–66 (2010).
80. Mossman, K. L., Saffran, H. A. & Smiley, J. R. Herpes simplex virus ICP0 mutants are hypersensitive to interferon. *J. Virol.* **74,** 2052–6 (2000).
81. Stojdl, D. F. *et al.* Exploiting tumor-specific defects in the interferon pathway with a previously unknown oncolytic virus. *Nat. Med.* **6,** 821–825 (2000).
82. Fernandez, M., Porosnicu, M., Markovic, D. & Barber, G. N. Genetically engineered vesicular stomatitis virus in gene therapy: application for treatment of malignant disease. *J. Virol.* **76,** 895–904 (2002).
83. Hastie, E. & Grdzelishvili, V. Z. Vesicular stomatitis virus as a flexible platform for oncolytic virotherapy against cancer. *J. Gen. Virol.* **93,** 2529–45 (2012).
84. Fields, B. N., Knipe, D. M. & Howley, P. M. *Fields Virology*. (Wolters Kluwer Health/Lippincott Williams & Wilkins, 2013).
85. Finkelshtein, D., Werman, A., Novick, D., Barak, S. & Rubinstein, M. LDL receptor and its family members serve as the cellular receptors for vesicular stomatitis virus. *Proc. Natl. Acad. Sci.* **110,** 7306–7311 (2013).
86. Pan, W. *et al.* The matrix protein of vesicular stomatitis virus inhibits host-directed transcription of target genes via interaction with the TFIIH subunit p8. *Vet. Microbiol.* **208,** 82–88 (2017).
87. Quan, B., Seo, H.-S., Blobel, G. & Ren, Y. Vesiculoviral matrix (M) protein occupies nucleic acid binding site at nucleoporin pair (Rae1bulletNup98). *Proc. Natl. Acad. Sci.* **111,** 9127–9132 (2014).
88. Rajani, K. R. *et al.* Complexes of vesicular stomatitis virus matrix protein with host Rae1 and Nup98 involved in inhibition of host transcription. *PLoS Pathog.* **8,** e1002929 (2012).
89. von Kobbe C *et al.* Vesicular stomatitis virus matrix protein inhibits host cell gene expression by targeting the nucleoporin Nup98. *Mol. Cell* **6,** 1243–52 (2000).
90. Petersen, J. M., Her, L. S., Varvel, V., Lund, E. & Dahlberg, J. E. The matrix protein of vesicular stomatitis virus inhibits nucleocytoplasmic transport when it is in the nucleus and associated with nuclear pore complexes. *Mol. Cell. Biol.* **20,** 8590–601 (2000).

91. Ivashkiv, L. B. & Donlin, L. T. Regulation of type I interferon responses. *Nat. Rev. Immunol.* **14,** 36–49 (2014).
92. Chen, K. & Liu, J. Regulation of type I interferon signaling in immunity and inflammation: A comprehensive review. *J. Autoimmun.* **83,** 1–11 (2017).
93. Rönnblom, L., Eloranta, M.-L. & Alm, G. V. Role of natural interferon-alpha producing cells (plasmacytoid dendritic cells) in autoimmunity. *Autoimmunity* **36,** 463–72 (2003).
94. Barchet, W. *et al.* Virus-induced interferon alpha production by a dendritic cell subset in the absence of feedback signaling in vivo. *J. Exp. Med.* **195,** 507–16 (2002).
95. Murphy, K. P. *Janeway's immunobiology*. (Garland Science, 2012).
96. Jensen, S. & Thomsen, A. R. Sensing of RNA viruses: a review of innate immune receptors involved in recognizing RNA virus invasion. *J. Virol.* **86,** 2900–10 (2012).
97. Georgel, P. *et al.* Vesicular stomatitis virus glycoprotein G activates a specific antiviral Toll-like receptor 4-dependent pathway. *Virology* **362,** 304–313 (2007).
98. Kato, H. *et al.* Length-dependent recognition of double-stranded ribonucleic acids by retinoic acid-inducible gene-I and melanoma differentiation-associated gene 5. *J. Exp. Med.* **205,** 1601–10 (2008).
99. Pippig, D. A. *et al.* The regulatory domain of the RIG-I family ATPase LGP2 senses double-stranded RNA. *Nucleic Acids Res.* **37,** 2014–25 (2009).
100. Levy, D. E., Marié, I. J. & Durbin, J. E. Induction and function of type I and III interferon in response to viral infection. *Curr. Opin. Virol.* **1,** 476–86 (2011).
101. Maniatis, T. *et al.* Structure and function of the interferon-beta enhanceosome. *Cold Spring Harb. Symp. Quant. Biol.* **63,** 609–20 (1998).
102. Iordanov, M. S. *et al.* Activation of p38 mitogen-activated protein kinase and c-Jun NH(2)-terminal kinase by double-stranded RNA and encephalomyocarditis virus: involvement of RNase L, protein kinase R, and alternative pathways. *Mol. Cell. Biol.* **20,** 617–27 (2000).
103. Huang, Y. *et al.* MAVS-MKK7-JNK2 Defines a Novel Apoptotic Signaling Pathway during Viral Infection. *PLoS Pathog.* **10,** e1004020 (2014).
104. Marchant, D. *et al.* Toll-like receptor 4-mediated activation of p38 mitogen-activated protein kinase is a determinant of respiratory virus entry and tropism. *J. Virol.* **84,** 11359–73 (2010).
105. Honda, K., Takaoka, A. & Taniguchi, T. Type I Inteferon Gene Induction by the Interferon Regulatory Factor Family of Transcription Factors. *Immunity* **25,** 349–360 (2006).
106. Du, W., Thanos, D. & Maniatis, T. Mechanisms of transcriptional synergism between distinct virus-inducible enhancer elements. *Cell* **74,** 887–898 (1993).
107. Bergstroem, B. *et al.* Identification of a novel in vivo virus-targeted phosphorylation site in interferon regulatory factor-3 (IRF3). *J. Biol. Chem.* **285,** 24904–14 (2010).
108. Noppert, S. J., Fitzgerald, K. A. & Hertzog, P. J. The role of type I interferons in TLR responses. *Immunol. Cell Biol.* **85,** 446–457 (2007).
109. Honda, K. *et al.* Spatiotemporal regulation of MyD88–IRF-7 signalling for robust type-I interferon induction. *Nature* **434,** 1035–1040 (2005).
110. Ferreiro, D. U. & Komives, E. A. Molecular mechanisms of system control of NF-

kappaB signaling by IkappaBalpha. *Biochemistry* **49,** 1560–7 (2010).
111. Sun, S.-C. The non-canonical NF-κB pathway in immunity and inflammation. *Nat. Rev. Immunol.* **17,** 545–558 (2017).
112. Jin, J. *et al.* Noncanonical NF-κB pathway controls the production of type I interferons in antiviral innate immunity. *Immunity* **40,** 342–54 (2014).
113. Basak, S. *et al.* A fourth IkappaB protein within the NF-kappaB signaling module. *Cell* **128,** 369–81 (2007).
114. Karin, M. How NF-κB is activated: the role of the IκB kinase (IKK) complex. *Oncogene* **18,** 6867–6874 (1999).
115. Viatour, P., Merville, M.-P., Bours, V. & Chariot, A. Phosphorylation of NF-κB and IκB proteins: implications in cancer and inflammation. *Trends Biochem. Sci.* **30,** 43–52 (2005).
116. Israël, A. The IKK complex, a central regulator of NF-kappaB activation. *Cold Spring Harb. Perspect. Biol.* **2,** a000158 (2010).
117. May, M. J. *et al.* Selective inhibition of NF-kappaB activation by a peptide that blocks the interaction of NEMO with the IkappaB kinase complex. *Science* **289,** 1550–4 (2000).
118. Mathes, E., O'Dea, E. L., Hoffmann, A. & Ghosh, G. NF-kappaB dictates the degradation pathway of IkappaBalpha. *EMBO J.* **27,** 1357–67 (2008).
119. Christian, F., Smith, E. L. & Carmody, R. J. The Regulation of NF-κB Subunits by Phosphorylation. *Cells* **5,** (2016).
120. Apostolou, E. & Thanos, D. Virus Infection Induces NF-kappaB-dependent interchromosomal associations mediating monoallelic IFN-beta gene expression. *Cell* **134,** 85–96 (2008).
121. Lomvardas, S. & Thanos, D. Modifying gene expression programs by altering core promoter chromatin architecture. *Cell* **110,** 261–71 (2002).
122. Rajaiya, J., Sadeghi, N. & Chodosh, J. Specific NFkappaB subunit activation and kinetics of cytokine induction in adenoviral keratitis. *Mol. Vis.* **15,** 2879–89 (2009).
123. Yurochko, A. D. *et al.* The human cytomegalovirus UL55 (gB) and UL75 (gH) glycoprotein ligands initiate the rapid activation of Sp1 and NF-kappaB during infection. *J. Virol.* **71,** 5051–9 (1997).
124. Balachandran, S. & Beg, A. A. Defining Emerging Roles for NF-κB in Antivirus Responses: Revisiting the Interferon-β Enhanceosome Paradigm. *PLoS Pathog.* **7,** e1002165 (2011).
125. Wang, J. *et al.* NF-kappa B RelA subunit is crucial for early IFN-beta expression and resistance to RNA virus replication. *J. Immunol.* **185,** 1720–9 (2010).
126. Basagoudanavar, S. H. *et al.* Distinct roles for the NF-kappa B RelA subunit during antiviral innate immune responses. *J. Virol.* **85,** 2599–610 (2011).
127. de Weerd, N. A., Samarajiwa, S. A. & Hertzog, P. J. Type I interferon receptors: biochemistry and biological functions. *J. Biol. Chem.* **282,** 20053–7 (2007).
128. Platanias, L. C. Mechanisms of type-I- and type-II-interferon-mediated signalling. *Nat. Rev. Immunol.* **5,** 375–386 (2005).
129. Horvath, C. M., Stark, G. R., Kerr, I. M., Darnell, J. E. & Jr. Interactions between STAT and non-STAT proteins in the interferon-stimulated gene factor 3 transcription

complex. *Mol. Cell. Biol.* **16,** 6957–64 (1996).
130. Li, X., Leung, S., Burns, C. & Stark, G. R. Cooperative binding of Stat1-2 heterodimers and ISGF3 to tandem DNA elements. *Biochimie* **80,** 703–10
131. Schneider, W. M., Chevillotte, M. D. & Rice, C. M. Interferon-stimulated genes: a complex web of host defenses. *Annu. Rev. Immunol.* **32,** 513–45 (2014).
132. Kane, M. *et al.* MX2 is an interferon-induced inhibitor of HIV-1 infection. *Nature* **502,** 563–6 (2013).
133. Goujon, C. *et al.* Human MX2 is an interferon-induced post-entry inhibitor of HIV-1 infection. *Nature* **502,** 559–62 (2013).
134. Jin, H. K., Takada, A., Kon, Y., Haller, O. & Watanabe, T. Identification of the murine Mx2 gene: interferon-induced expression of the Mx2 protein from the feral mouse gene confers resistance to vesicular stomatitis virus. *J. Virol.* **73,** 4925–30 (1999).
135. Desai, T. M., Marin, M., Mason, C. & Melikyan, G. B. pH regulation in early endosomes and interferon-inducible transmembrane proteins control avian retrovirus fusion. *J. Biol. Chem.* **292,** 7817–7827 (2017).
136. Bailey, C. C., Zhong, G., Huang, I.-C. & Farzan, M. IFITM-Family Proteins: The Cell's First Line of Antiviral Defense. *Annu. Rev. Virol.* **1,** 261–283 (2014).
137. Marié, I., Durbin, J. E. & Levy, D. E. Differential viral induction of distinct interferon-alpha genes by positive feedback through interferon regulatory factor-7. *EMBO J.* **17,** 6660–9 (1998).
138. Izaguirre, A. *et al.* Comparative analysis of IRF and IFN-alpha expression in human plasmacytoid and monocyte-derived dendritic cells. *J. Leukoc. Biol.* **74,** 1125–1138 (2003).
139. Colonna, M., Trinchieri, G. & Liu, Y.-J. Plasmacytoid dendritic cells in immunity. *Nat. Immunol.* **5,** 1219–1226 (2004).
140. Li, L. & Sherry, B. IFN-α expression and antiviral effects are subtype and cell type specific in the cardiac response to viral infection. *Virology* **396,** 59–68 (2010).
141. Honda, K. *et al.* IRF-7 is the master regulator of type-I interferon-dependent immune responses. *Nature* **434,** 772–777 (2005).
142. Amirache, F. *et al.* Mystery solved: VSV-G-LVs do not allow efficient gene transfer into unstimulated T cells, B cells, and HSCs because they lack the LDL receptor. *Blood* **123,** 1422–4 (2014).
143. Johnson, J. E. *et al.* Neurovirulence properties of recombinant vesicular stomatitis virus vectors in non-human primates. *Virology* **360,** 36–49 (2007).
144. Sur, J.-H., Allende, R. & Doster, A. R. Vesicular Stomatitis Virus Infection and Neuropathogenesis in the Murine Model are Associated with Apoptosis. *Vet. Pathol.* **40,** 512–520 (2003).
145. Huneycutt, B. S., Bi, Z., Aoki, C. J. & Reiss, C. S. Central neuropathogenesis of vesicular stomatitis virus infection of immunodeficient mice. *J. Virol.* **67,** 6698–706 (1993).
146. Stojdl, D. F. *et al.* VSV strains with defects in their ability to shutdown innate immunity are potent systemic anti-cancer agents. *Cancer Cell* **4,** 263–275 (2003).
147. Breitbach, C. J., Lichty, B. D. & Bell, J. C. Oncolytic Viruses: Therapeutics With an Identity Crisis. *EBioMedicine* **9,** 31–36 (2016).
148. Breitbach, C. J. *et al.* Targeting tumor vasculature with an oncolytic virus. *Mol. Ther.*

19, 886–94 (2011).
149. Breitbach, C. J. *et al.* Targeted Inflammation During Oncolytic Virus Therapy Severely Compromises Tumor Blood Flow. *Mol. Ther.* **15,** 1686–1693 (2007).
150. Leung, D. W., Cachianes, G., Kuang, W. J., Goeddel, D. V & Ferrara, N. Vascular endothelial growth factor is a secreted angiogenic mitogen. *Science* **246,** 1306–9 (1989).
151. Hicklin, D. J. & Ellis, L. M. Role of the Vascular Endothelial Growth Factor Pathway in Tumor Growth and Angiogenesis. *J. Clin. Oncol.* **23,** 1011–1027 (2005).
152. Arulanandam, R. *et al.* VEGF-Mediated Induction of PRD1-BF1/Blimp1 Expression Sensitizes Tumor Vasculature to Oncolytic Virus Infection. *Cancer Cell* **28,** 210–224 (2015).
153. Melzer, M. K., Lopez-Martinez, A. & Altomonte, J. Oncolytic Vesicular Stomatitis Virus as a Viro-Immunotherapy: Defeating Cancer with a "Hammer" and "Anvil". *Biomedicines* **5,** (2017).
154. Janelle, V. *et al.* The Strength of the T Cell Response Against a Surrogate Tumor Antigen Induced by Oncolytic VSV Therapy Does Not Correlate With Tumor Control. *Mol. Ther.* **22,** 1198–1210 (2014).
155. Smedberg, J. R., Westcott, M. M., Ahmed, M. & Lyles, D. S. Signaling Pathways in Murine Dendritic Cells That Regulate the Response to Vesicular Stomatitis Virus Vectors That Express Flagellin. *J. Virol.* **88,** 777–785 (2014).
156. Bourgeois-Daigneault, M.-C. *et al.* Oncolytic vesicular stomatitis virus expressing interferon-γ has enhanced therapeutic activity. *Mol. Ther. oncolytics* **3,** 16001 (2016).
157. Lemay, C. G. *et al.* Harnessing oncolytic virus-mediated antitumor immunity in an infected cell vaccine. *Mol. Ther.* **20,** 1791–9 (2012).
158. Swiecki, M., Gilfillan, S., Vermi, W., Wang, Y. & Colonna, M. Plasmacytoid dendritic cell ablation impacts early interferon responses and antiviral NK and CD8(+) T cell accrual. *Immunity* **33,** 955–66 (2010).
159. Altomonte, J. *et al.* Enhanced oncolytic potency of vesicular stomatitis virus through vector-mediated inhibition of NK and NKT cells. *Cancer Gene Ther.* **16,** 266–278 (2009).
160. Simovic, B., Walsh, S. R. & Wan, Y. Mechanistic insights into the oncolytic activity of vesicular stomatitis virus in cancer immunotherapy. *Oncolytic Virotherapy* **4,** 157–167 (2015).
161. Guo, Z. S., Liu, Z. & Bartlett, D. L. Oncolytic Immunotherapy: Dying the Right Way is a Key to Eliciting Potent Antitumor Immunity. *Front. Oncol.* **4,** 74 (2014).
162. Conrad, D. P. *et al.* Leukemia cell-rhabdovirus vaccine: personalized immunotherapy for acute lymphoblastic leukemia. *Clin. Cancer Res.* **19,** 3832–43 (2013).
163. Alkayyal, A. A. *et al.* NK-Cell Recruitment Is Necessary for Eradication of Peritoneal Carcinomatosis with an IL12-Expressing Maraba Virus Cellular Vaccine. *Cancer Immunol. Res.* **5,** 211–221 (2017).
164. Bridle, B. W. *et al.* Vesicular stomatitis virus as a novel cancer vaccine vector to prime antitumor immunity amenable to rapid boosting with adenovirus. *Mol. Ther.* **17,** 1814–21 (2009).
165. Bridle, B. W. *et al.* Potentiating cancer immunotherapy using an oncolytic virus. *Mol.*

Ther. **18,** 1430–9 (2010).
166. Pol, J. G. *et al.* Maraba virus as a potent oncolytic vaccine vector. *Mol. Ther.* **22,** 420–429 (2014).
167. Brun, J. *et al.* Identification of genetically modified Maraba virus as an oncolytic rhabdovirus. *Mol. Ther.* **18,** 1440–9 (2010).
168. Miller, A. & Russell, S. J. The use of the NIS reporter gene for optimizing oncolytic virotherapy. *Expert Opin. Biol. Ther.* **16,** 15–32 (2016).
169. Goel, A. *et al.* Radioiodide imaging and radiovirotherapy of multiple myeloma using VSV(Delta51)-NIS, an attenuated vesicular stomatitis virus encoding the sodium iodide symporter gene. *Blood* **110,** 2342–50 (2007).
170. Opyrchal, M. *et al.* Effective Radiovirotherapy for Malignant Gliomas by Using Oncolytic Measles Virus Strains Encoding the Sodium Iodide Symporter (MV-NIS). *Hum. Gene Ther.* **23,** 419–427 (2012).
171. Li, H., Nakashima, H., Decklever, T. D., Nace, R. A. & Russell, S. J. HSV-NIS, an oncolytic herpes simplex virus type 1 encoding human sodium iodide symporter for preclinical prostate cancer radiovirotherapy. *Cancer Gene Ther.* **20,** 478–85 (2013).
172. Mansfield, D. C. *et al.* Oncolytic vaccinia virus as a vector for therapeutic sodium iodide symporter gene therapy in prostate cancer. *Gene Ther.* **23,** 357–68 (2016).
173. Hutzen, B. *et al.* Treatment of medulloblastoma using an oncolytic measles virus encoding the thyroidal sodium iodide symporter shows enhanced efficacy with radioiodine. *BMC Cancer* **12,** 508 (2012).
174. Le Boeuf, F. *et al.* Oncolytic Maraba Virus MG1 as a Treatment for Sarcoma. *Int. J. Cancer* **141,** 1257–1264 (2017).
175. Le Boeuf, F. *et al.* Synergistic Interaction Between Oncolytic Viruses Augments Tumor Killing. *Mol. Ther.* **18,** 888–895 (2010).
176. Breitbach, C. J. *et al.* Intravenous delivery of a multi-mechanistic cancer-targeted oncolytic poxvirus in humans. *Nature* **477,** 99–102 (2011).
177. Wakimoto, H., Johnson, P. R., Knipe, D. M. & Chiocca, E. A. Effects of innate immunity on herpes simplex virus and its ability to kill tumor cells. *Gene Ther.* **10,** 983–990 (2003).
178. Harrington, K. J. *et al.* Phase I/II Study of Oncolytic HSVGM-CSF in Combination with Radiotherapy and Cisplatin in Untreated Stage III/IV Squamous Cell Cancer of the Head and Neck. *Clin. Cancer Res.* **16,** 4005–4015 (2010).
179. Simpson, G. R. *et al.* Combination of a fusogenic glycoprotein, pro-drug activation and oncolytic HSV as an intravesical therapy for superficial bladder cancer. *Br. J. Cancer* **106,** 496–507 (2012).
180. Foloppe, J. *et al.* Targeted delivery of a suicide gene to human colorectal tumors by a conditionally replicating vaccinia virus. *Gene Ther.* **15,** 1361–1371 (2008).
181. Dias, J. D. *et al.* Targeted chemotherapy for head and neck cancer with a chimeric oncolytic adenovirus coding for bifunctional suicide protein FCU1. *Clin. Cancer Res.* **16,** 2540–9 (2010).
182. Kaur, B., Cripe, T. P. & Chiocca, E. A. "Buy one get one free": armed viruses for the treatment of cancer cells and their microenvironment. *Curr. Gene Ther.* **9,** 341–55 (2009).

183. Forbes, N. E., Krishnan, R. & Diallo, J.-S. Pharmacological Modulation of Anti-Tumor Immunity Induced by Oncolytic Viruses. *Front. Oncol.* **4,** 1–12 (2014).
184. Emadi, A., Jones, R. J. & Brodsky, R. A. Cyclophosphamide and cancer: golden anniversary. *Nat. Rev. Clin. Oncol.* **6,** 638–647 (2009).
185. Currier, M. A. *et al.* Efficacy and safety of the oncolytic herpes simplex virus rRp450 alone and combined with cyclophosphamide. *Mol. Ther.* **16,** 879–885 (2008).
186. Ikeda, K. *et al.* Oncolytic virus therapy of multiple tumors in the brain requires suppression of innate and elicited antiviral responses. *Nat. Med.* **5,** 881–887 (1999).
187. Thomas, M. A. *et al.* Immunosuppression enhances oncolytic adenovirus replication and antitumor efficacy in the Syrian hamster model. *Mol. Ther.* **16,** 1665–73 (2008).
188. Dhar, D., Spencer, J. F., Toth, K. & Wold, W. S. M. Effect of preexisting immunity on oncolytic adenovirus vector INGN 007 antitumor efficacy in immunocompetent and immunosuppressed Syrian hamsters. *J. Virol.* **83,** 2130–9 (2009).
189. Cerullo, V. *et al.* Immunological effects of low-dose cyclophosphamide in cancer patients treated with oncolytic adenovirus. *Mol. Ther.* **19,** 1737–46 (2011).
190. Hasegawa, N. *et al.* Cyclophosphamide enhances antitumor efficacy of oncolytic adenovirus expressing uracil phosphoribosyltransferase (UPRT) in immunocompetent Syrian hamsters. *Int. J. Cancer* **133,** 1479–1488 (2013).
191. Lun, X. Q. *et al.* Efficacy of systemically administered oncolytic vaccinia virotherapy for malignant gliomas is enhanced by combination therapy with rapamycin or cyclophosphamide. *Clin. Cancer Res.* **15,** 2777–88 (2009).
192. Qiao, J. *et al.* Cyclophosphamide facilitates antitumor efficacy against subcutaneous tumors following intravenous delivery of reovirus. *Clin. Cancer Res.* **14,** 259–69 (2008).
193. Peng, K.-W. *et al.* Using clinically approved cyclophosphamide regimens to control the humoral immune response to oncolytic viruses. *Gene Ther.* **20,** 255–61 (2013).
194. Ungerechts, G. *et al.* Mantle cell lymphoma salvage regimen: synergy between a reprogrammed oncolytic virus and two chemotherapeutics. *Gene Ther.* **17,** 1506–16 (2010).
195. Ungerechts, G. *et al.* An Immunocompetent Murine Model for Oncolysis with an Armed and Targeted Measles Virus. *Mol. Ther.* **15,** 1991–1997 (2007).
196. Kottke, T. *et al.* Improved systemic delivery of oncolytic reovirus to established tumors using preconditioning with cyclophosphamide-mediated Treg modulation and interleukin-2. *Clin. Cancer Res.* **15,** 561–9 (2009).
197. Liu, Z., Ravindranathan, R., Kalinski, P., Guo, Z. S. & Bartlett, D. L. Rational combination of oncolytic vaccinia virus and PD-L1 blockade works synergistically to enhance therapeutic efficacy. *Nat. Commun.* **8,** 14754 (2017).
198. Ribas, A. *et al.* Oncolytic Virotherapy Promotes Intratumoral T Cell Infiltration and Improves Anti-PD-1 Immunotherapy. *Cell* **170,** 1109–1119.e10 (2017).
199. Turnbull, S. *et al.* Evidence for Oncolytic Virotherapy: Where Have We Got to and Where Are We Going? *Viruses* **7,** 6291–312 (2015).
200. Chesney, J. *et al.* Interim safety and efficacy of a randomized (1:1), open-label phase 2 study of talimogene laherparepvec (T) and ipilimumab (I) vs I alone in unresected, stage IIIB-IV melanoma. *Ann. Oncol.* **27,** (2016).

201. Puzanov, I. *et al.* Talimogene Laherparepvec in Combination With Ipilimumab in Previously Untreated, Unresectable Stage IIIB-IV Melanoma. *J. Clin. Oncol.* **34,** 2619–2626 (2016).
202. Escobar-Zarate, D., Liu, Y.-P., Suksanpaisan, L., Russell, S. J. & Peng, K.-W. Overcoming cancer cell resistance to VSV oncolysis with JAK1/2 inhibitors. *Cancer Gene Ther.* **20,** 582–589 (2013).
203. Paglino, J. C. & van den Pol, A. N. Vesicular stomatitis virus has extensive oncolytic activity against human sarcomas: rare resistance is overcome by blocking interferon pathways. *J. Virol.* **85,** 9346–58 (2011).
204. Du, Z. *et al.* Inhibition of Type I Interferon-Mediated Antiviral Action in Human Glioma Cells by the IKK Inhibitors BMS-345541 and TPCA-1. *J. Interf. Cytokine Res.* **32,** 368–377 (2012).
205. Cataldi, M., Shah, N. R., Felt, S. A. & Grdzelishvili, V. Z. Breaking resistance of pancreatic cancer cells to an attenuated vesicular stomatitis virus through a novel activity of IKK inhibitor TPCA-1. *Virology* **485,** 340–354 (2015).
206. Jackson, J. D., Markert, J. M., Li, L., Carroll, S. L. & Cassady, K. A. STAT1 and NF- B Inhibitors Diminish Basal Interferon-Stimulated Gene Expression and Improve the Productive Infection of Oncolytic HSV in MPNST Cells. *Mol. Cancer Res.* **14,** 482–492 (2016).
207. Chang, H.-M. *et al.* Induction of interferon-stimulated gene expression and antiviral responses require protein deacetylase activity. *Proc. Natl. Acad. Sci.* **101,** 9578–9583 (2004).
208. Katsura, T. *et al.* The effects of trichostatin A on the oncolytic ability of herpes simplex virus for oral squamous cell carcinoma cells. *Cancer Gene Ther.* **16,** 237–245 (2009).
209. Liu, T.-C., Castelo-Branco, P., Rabkin, S. D. & Martuza, R. L. Trichostatin A and Oncolytic HSV Combination Therapy Shows Enhanced Antitumoral and Antiangiogenic Effects. *Mol. Ther.* **16,** 1041–1047 (2008).
210. Otsuki, A. *et al.* Histone Deacetylase Inhibitors Augment Antitumor Efficacy of Herpes-based Oncolytic Viruses. *Mol. Ther.* **16,** 1546–1555 (2008).
211. Alvarez-Breckenridge, C. A. *et al.* The Histone Deacetylase Inhibitor Valproic Acid Lessens NK Cell Action against Oncolytic Virus-Infected Glioblastoma Cells by Inhibition of STAT5/T-BET Signaling and Generation of Gamma Interferon. *J. Virol.* **86,** 4566–4577 (2012).
212. MacTavish, H. *et al.* Enhancement of vaccinia virus based oncolysis with histone deacetylase inhibitors. *PLoS One* **5,** e14462 (2010).
213. Nguyen, T. L.-A. *et al.* Chemical targeting of the innate antiviral response by histone deacetylase inhibitors renders refractory cancers sensitive to viral oncolysis. *Proc. Natl. Acad. Sci.* **105,** 14981–14986 (2008).
214. Bridle, B. W. *et al.* HDAC Inhibition Suppresses Primary Immune Responses, Enhances Secondary Immune Responses, and Abrogates Autoimmunity During Tumor Immunotherapy. *Mol. Ther.* **21,** 887–894 (2013).
215. Diallo, J.-S. *et al.* A high-throughput pharmacoviral approach identifies novel oncolytic virus sensitizers. *Mol. Ther.* **18,** 1123–1129 (2010).

216. Arulanandam, R. *et al.* Microtubule disruption synergizes with oncolytic virotherapy by inhibiting interferon translation and potentiating bystander killing. *Nat. Commun.* **6,** 6410 (2015).
217. Bourgeois-Daigneault, M.-C. *et al.* Combination of Paclitaxel and MG1 oncolytic virus as a successful strategy for breast cancer treatment. *Breast Cancer Res.* **18,** 83 (2016).
218. Jackson, P. A., Widen, J. C., Harki, D. A. & Brummond, K. M. Covalent Modifiers: A Chemical Perspective on the Reactivity of α,β-Unsaturated Carbonyls with Thiols via Hetero-Michael Addition Reactions. *J. Med. Chem.* **60,** 839–885 (2017).
219. Singh, J., Petter, R. C., Baillie, T. A. & Whitty, A. The resurgence of covalent drugs. *Nat. Rev. Drug Discov.* **10,** 307–317 (2011).
220. Cho, T. & Uetrecht, J. How Reactive Metabolites Induce an Immune Response That Sometimes Leads to an Idiosyncratic Drug Reaction. *Chem. Res. Toxicol.* **30,** 295–314 (2017).
221. Michalczyk, A. *et al.* Structural insights into how irreversible inhibitors can overcome drug resistance in EGFR. *Bioorg. Med. Chem.* **16,** 3482–3488 (2008).
222. Kwak, E. L. *et al.* Irreversible inhibitors of the EGF receptor may circumvent acquired resistance to gefitinib. *Proc. Natl. Acad. Sci.* **102,** 7665–7670 (2005).
223. Díez-Dacal, B. & Pérez-Sala, D. A-class prostaglandins: Early findings and new perspectives for overcoming tumor chemoresistance. *Cancer Lett.* **320,** 150–157 (2012).
224. Walter, A. O. *et al.* Discovery of a Mutant-Selective Covalent Inhibitor of EGFR that Overcomes T790M-Mediated Resistance in NSCLC. *Cancer Discov.* **3,** 1404–1415 (2013).
225. Barf, T. & Kaptein, A. Irreversible Protein Kinase Inhibitors: Balancing the Benefits and Risks. *J. Med. Chem.* **55,** 6243–6262 (2012).
226. Juswinder Singh, *,† *et al.* Structure-Based Design of a Potent, Selective, and Irreversible Inhibitor of the Catalytic Domain of the erbB Receptor Subfamily of Protein Tyrosine Kinases. (1997). doi:10.1021/JM960380S
227. Wissner, A. & Mansour, T. S. The Development of HKI-272 and Related Compounds for the Treatment of Cancer. *Arch. Pharm. (Weinheim).* **341,** 465–477 (2008).
228. Uckun, F. & D'Cruz, F. M. Novel Bruton's tyrosine kinase inhibitors currently in development. *Onco. Targets. Ther.* **6,** 161 (2013).
229. Lou, Y., Owens, T. D., Kuglstatter, A., Kondru, R. K. & Goldstein, D. M. Bruton's Tyrosine Kinase Inhibitors: Approaches to Potent and Selective Inhibition, Preclinical and Clinical Evaluation for Inflammatory Diseases and B Cell Malignancies. *J. Med. Chem.* **55,** 4539–4550 (2012).
230. Dargahi, N. *et al.* Multiple Sclerosis: Immunopathology and Treatment Update. *Brain Sci.* **7,** (2017).
231. Fox, R. J. *et al.* BG-12 (dimethyl fumarate): a review of mechanism of action, efficacy, and safety. *Curr. Med. Res. Opin.* **30,** 251–262 (2014).
232. A., S. & K., R. R. Role of dimethyl fumarate in oxidative stress of multiple sclerosis: A review. *J. Chromatogr. B* **1019,** 15–20 (2016).
233. Albrecht, P. *et al.* Effects of dimethyl fumarate on neuroprotection and

immunomodulation. *J. Neuroinflammation* **9,** 163 (2012).
234. Moharregh-Khiabani, D., Linker, R., Gold, R. & Stangel, M. Fumaric Acid and its Esters: An Emerging Treatment for Multiple Sclerosis. *Curr. Neuropharmacol.* **7,** 60–64 (2009).
235. Kastrati, I. *et al.* Dimethyl Fumarate Inhibits the Nuclear Factor κB Pathway in Breast Cancer Cells by Covalent Modification of p65 Protein. *J. Biol. Chem.* **291,** 3639–47 (2016).
236. Claudinon, J. *et al.* Palmitoylation of interferon-alpha (IFN-alpha) receptor subunit IFNAR1 is required for the activation of Stat1 and Stat2 by IFN-alpha. *J. Biol. Chem.* **284,** 24328–40 (2009).
237. Ahmad, R., Raina, D., Meyer, C. & Kufe, D. Triterpenoid CDDO-methyl ester inhibits the Janus-activated kinase-1 (JAK1)-->signal transducer and activator of transcription-3 (STAT3) pathway by direct inhibition of JAK1 and STAT3. *Cancer Res.* **68,** 2920–6 (2008).
238. Nishi, T. *et al.* Spatial redox regulation of a critical cysteine residue of NF-kappa B in vivo. *J. Biol. Chem.* **277,** 44548–56 (2002).
239. Kong, L.-M. *et al.* Identification and validation of p50 as the cellular target of eriocalyxin B. *Oncotarget* **5,** 11354–64 (2014).
240. Xia, Y.-F. *et al.* Andrographolide Attenuates Inflammation by Inhibition of NF- B Activation through Covalent Modification of Reduced Cysteine 62 of p50. *J. Immunol.* **173,** 4207–4217 (2004).
241. Dhawan, V. Studies on Respiratory Disorders. (2014). doi:10.1007/978-1-4939-0497-6
242. Attia, S. M. Deleterious effects of reactive metabolites. *Oxid. Med. Cell. Longev.* **3,** 238–53 (2010).
243. Vatansever, F. *et al.* Antimicrobial strategies centered around reactive oxygen species – bactericidal antibiotics, photodynamic therapy, and beyond. *FEMS Microbiol. Rev.* **37,** 955–989 (2013).
244. Winterbourn, C. C., Hampton, M. B., Livesey, J. H. & Kettle, A. J. Modeling the reactions of superoxide and myeloperoxidase in the neutrophil phagosome: implications for microbial killing. *J. Biol. Chem.* **281,** 39860–9 (2006).
245. Xu, D., Rovira, I. I. & Finkel, T. Oxidants Painting the Cysteine Chapel: Redox Regulation of PTPs. *Dev. Cell* **2,** 251–252 (2002).
246. Shukla, V., Mishra, S. K. & Pant, H. C. Oxidative stress in neurodegeneration. *Adv. Pharmacol. Sci.* **2011,** 572634 (2011).
247. Trachootham, D., Alexandre, J. & Huang, P. Targeting cancer cells by ROS-mediated mechanisms: a radical therapeutic approach? *Nat. Rev. Drug Discov.* **8,** 579–91 (2009).
248. Yang, X. *et al.* Oxidative Stress-Mediated Atherosclerosis: Mechanisms and Therapies. *Front. Physiol.* **8,** 600 (2017).
249. Ray, P. D., Huang, B.-W. & Tsuji, Y. Reactive oxygen species (ROS) homeostasis and redox regulation in cellular signaling. *Cell. Signal.* **24,** 981–90 (2012).
250. Nguyen, T., Nioi, P. & Pickett, C. B. The Nrf2-Antioxidant Response Element Signaling Pathway and Its Activation by Oxidative Stress. *J. Biol. Chem.* **284,** 13291–13295 (2009).

251. Furukawa, M. & Xiong, Y. BTB Protein Keap1 Targets Antioxidant Transcription Factor Nrf2 for Ubiquitination by the Cullin 3-Roc1 Ligase. *Mol. Cell. Biol.* **25,** 162–171 (2005).
252. Itoh, K. *et al.* Keap1 represses nuclear activation of antioxidant responsive elements by Nrf2 through binding to the amino-terminal Neh2 domain. *Genes Dev.* **13,** 76–86 (1999).
253. Lu, S. C. Glutathione synthesis. *Biochim. Biophys. Acta* **1830,** 3143–53 (2013).
254. Dalton, T. P., Dieter, M. Z., Yang, Y., Shertzer, H. G. & Nebert, D. W. Knockout of the Mouse Glutamate Cysteine Ligase Catalytic Subunit (Gclc) Gene: Embryonic Lethal When Homozygous, and Proposed Model for Moderate Glutathione Deficiency When Heterozygous. *Biochem. Biophys. Res. Commun.* **279,** 324–329 (2000).
255. Owen, J. B. & Butterfield, D. A. Measurement of Oxidized/Reduced Glutathione Ratio. in *Methods in molecular biology (Clifton, N.J.)* **648,** 269–277 (2010).
256. Goodman, L. S. (Louis S., Gilman, A., Brunton, L. L., Lazo, J. S. & Parker, K. L. *Goodman & Gilman's The Pharmacological Basis of Therapeutics.* (McGraw-Hill, 2006).
257. Galano, A. & Alvarez-Idaboy, J. R. Glutathione: mechanism and kinetics of its non-enzymatic defense action against free radicals. *RSC Adv.* **1,** 1763 (2011).
258. Wu, B. & Dong, D. Human cytosolic glutathione transferases: structure, function, and drug discovery. *Trends Pharmacol. Sci.* **33,** 656–668 (2012).
259. Hayes, J. D., Flanagan, J. U. & Jowsey, I. R. GLUTATHIONE TRANSFERASES. *Annu. Rev. Pharmacol. Toxicol.* **45,** 51–88 (2005).
260. McIlwain, C. C., Townsend, D. M. & Tew, K. D. Glutathione S-transferase polymorphisms: cancer incidence and therapy. *Oncogene* **25,** 1639–1648 (2006).
261. Dirr, H., Reinemer, P. & Huber, R. X-ray crystal structures of cytosolic glutathione S-transferases. Implications for protein architecture, substrate recognition and catalytic function. *Eur. J. Biochem.* **220,** 645–61 (1994).
262. Armstrong, R. N. Structure, Catalytic Mechanism, and Evolution of the Glutathione Transferases. (1997). doi:10.1021/TX960072X
263. Johansson, A.-S. & Mannervik, B. Human Glutathione Transferase A3-3, a Highly Efficient Catalyst of Double-bond Isomerization in the Biosynthetic Pathway of Steroid Hormones. *J. Biol. Chem.* **276,** 33061–33065 (2001).
264. Tew, K. D. & Townsend, D. M. Regulatory functions of glutathione S-transferase P1-1 unrelated to detoxification. *Drug Metab. Rev.* **43,** 179–93 (2011).
265. Tew, K. D. *et al.* The role of glutathione S-transferase P in signaling pathways and S-glutathionylation in cancer. *Free Radic. Biol. Med.* **51,** 299–313 (2011).
266. Cho, S. G. *et al.* Glutathione S-transferase mu modulates the stress-activated signals by suppressing apoptosis signal-regulating kinase 1. *J. Biol. Chem.* **276,** 12749–55 (2001).
267. Dorion, S., Lambert, H. & Landry, J. Activation of the p38 signaling pathway by heat shock involves the dissociation of glutathione S-transferase Mu from Ask1. *J. Biol. Chem.* **277,** 30792–7 (2002).
268. Sawers, L. *et al.* Glutathione S-transferase P1 (GSTP1) directly influences platinum drug chemosensitivity in ovarian tumour cell lines. *Br. J. Cancer* **111,** 1150–8 (2014).
269. Louie, S. M. *et al.* GSTP1 Is a Driver of Triple-Negative Breast Cancer Cell Metabolism

and Pathogenicity. *Cell Chem. Biol.* **23,** 567–578 (2016).
270. Hokaiwado, N. *et al.* Glutathione S-transferase Pi mediates proliferation of androgen-independent prostate cancer cells. *Carcinogenesis* **29,** 1134–8 (2008).
271. Steensma, D. P. Novel Therapies for Myelodysplastic Syndromes. *Hematol. Oncol. Clin. North Am.* **24,** 423–441 (2010).
272. Mahadevan, D. & Sutton, G. R. Ezatiostat hydrochloride for the treatment of myelodysplastic syndromes. *Expert Opin. Investig. Drugs* **24,** 725–733 (2015).
273. Ruscoe, J. E. *et al.* Pharmacologic or genetic manipulation of glutathione S-transferase P1-1 (GSTpi) influences cell proliferation pathways. *J. Pharmacol. Exp. Ther.* **298,** 339–45 (2001).
274. Stofega, M. *et al.* Induction of apoptosis by TLK199 in human leukemia cells. *Cancer Res.* **68,** 2270–2270 (2008).
275. Dornan, M. H. *et al.* First-in-class small molecule potentiators of cancer virotherapy. *Sci. Rep.* **6,** 1–12 (2016).
276. *Personal communication from Dr. Markus Vaha-Koskela, University of Helsinki*.
277. Ito, T. *et al.* Identification of a Primary Target of Thalidomide Teratogenicity. *Science (80-.).* **327,** 1345–1350 (2010).
278. Bantscheff, M. *et al.* Chemoproteomics profiling of HDAC inhibitors reveals selective targeting of HDAC complexes. *Nat. Biotechnol.* **29,** 255–265 (2011).
279. Sadaghiani, A. M., Verhelst, S. H. & Bogyo, M. Tagging and detection strategies for activity-based proteomics. *Curr. Opin. Chem. Biol.* **11,** 20–28 (2007).
280. Diallo, J.-S., Vähä-Koskela, M., Le Boeuf, F. & Bell, J. Propagation, Purification, and In Vivo Testing of Oncolytic Vesicular Stomatitis Virus Strains. in *Methods in molecular biology (Clifton, N.J.)* **797,** 127–140 (2012).
281. Jordan, R. & Schaffer, P. A. Activation of gene expression by herpes simplex virus type 1 ICP0 occurs at the level of mRNA synthesis. *J. Virol.* **71,** 6850–62 (1997).
282. Garcia, V. *et al.* High-throughput Titration of Luciferase-expressing Recombinant Viruses. *J. Vis. Exp.* 51890 (2014). doi:10.3791/51890
283. Budke, B. *et al.* An Optimized RAD51 Inhibitor That Disrupts Homologous Recombination without Requiring Michael Acceptor Reactivity. *J. Med. Chem.* **56,** 254–263 (2013).
284. Di, L., Kerns, E. H., Hong, Y. & Chen, H. Development and application of high throughput plasma stability assay for drug discovery. *Int. J. Pharm.* **297,** 110–9 (2005).
285. Eden, E., Navon, R., Steinfeld, I., Lipson, D. & Yakhini, Z. GOrilla: a tool for discovery and visualization of enriched GO terms in ranked gene lists. *BMC Bioinformatics* **10,** 48 (2009).
286. Pfaffl, M. W. A new mathematical model for relative quantification in real-time RT-PCR. *Nucleic Acids Res.* **29,** e45 (2001).
287. Groom, H., Lee, M., Patil, P. & Josephy, P. D. Inhibition of human glutathione transferases by dinitronaphthalene derivatives. *Arch. Biochem. Biophys.* **555–556,** 71–76 (2014).
288. Healy, M. J. Statistical analysis of radioimmunoassay data. *Biochem. J.* **130,** 207–10 (1972).

289. Mailloux, R. J. *et al.* Glutaredoxin-2 is required to control oxidative phosphorylation in cardiac muscle by mediating deglutathionylation reactions. *J. Biol. Chem.* **289,** 14812–28 (2014).
290. Mailloux, R. J., Adjeitey, C. N.-K., Xuan, J. Y. & Harper, M.-E. Crucial yet divergent roles of mitochondrial redox state in skeletal muscle vs. brown adipose tissue energetics. *FASEB J.* **26,** 363–375 (2012).
291. Diallo, J.-S., Roy, D., Abdelbary, H., De Silva, N. & Bell, J. C. Ex vivo infection of live tissue with oncolytic viruses. *J. Vis. Exp.* 4–7 (2011).
292. Vähä-Koskela, M. J. V, Heikkilä, J. E. & Hinkkanen, A. E. Oncolytic viruses in cancer therapy. *Cancer Lett.* **254,** 178–216 (2007).
293. Ruotsalainen, J. J. *et al.* Clonal variation in interferon response determines the outcome of oncolytic virotherapy in mouse CT26 colon carcinoma model. *Gene Ther.* **22,** 65–75 (2015).
294. Collart, M. A., Baeuerle, P. & Vassalli, P. Regulation of tumor necrosis factor alpha transcription in macrophages: involvement of four kappa B-like motifs and of constitutive and inducible forms of NF-kappa B. *Mol. Cell. Biol.* **10,** 1498–506 (1990).
295. Son, Y.-H. *et al.* Roles of MAPK and NF-κB in Interleukin-6 Induction by Lipopolysaccharide in Vascular Smooth Muscle Cells. *J. Cardiovasc. Pharmacol.* **51,** 71–77 (2008).
296. Libermann, T. A. & Baltimore, D. Activation of interleukin-6 gene expression through the NF-kappa B transcription factor. *Mol. Cell. Biol.* **10,** 2327–34 (1990).
297. Shakhov, A. N., Kuprash, D. V, Azizov, M. M., Jongeneel, C. V & Nedospasov, S. A. Structural analysis of the rabbit TNF locus, containing the genes encoding TNF-beta (lymphotoxin) and TNF-alpha (tumor necrosis factor). *Gene* **95,** 215–21 (1990).
298. Böhme, A., Thaens, D., Schramm, F., Paschke, A. & Schüürmann, G. Thiol Reactivity and Its Impact on the Ciliate Toxicity of α,β-Unsaturated Aldehydes, Ketones, and Esters. *Chem. Res. Toxicol.* **23,** 1905–1912 (2010).
299. Aptula, A. O., Patlewicz, G., Roberts, D. W. & Schultz, T. W. Non-enzymatic glutathione reactivity and in vitro toxicity: A non-animal approach to skin sensitization. *Toxicol. Vitr.* **20,** 239–247 (2006).
300. Chan, K., Jensen, N. & O'Brien, P. J. Structure–activity relationships for thiol reactivity and rat or human hepatocyte toxicity induced by substituted *p* -benzoquinone compounds. *J. Appl. Toxicol.* **28,** 608–620 (2008).
301. Weber, C. A., Duncan, C. A., Lyons, M. J. & Jenkinson, S. G. Depletion of tissue glutathione with diethyl maleate enhances hyperbaric oxygen toxicity. *Am. J. Physiol. Cell. Mol. Physiol.* **258,** L308–L312 (1990).
302. Markovic, J. *et al.* The Depletion of Nuclear Glutathione Impairs Cell Proliferation in 3t3 Fibroblasts. *PLoS One* **4,** e6413 (2009).
303. Mitchell, J. B., Russo, A., Biaglow, J. E. & McPherson, S. Cellular glutathione depletion by diethyl maleate or buthionine sulfoximine: no effect of glutathione depletion on the oxygen enhancement ratio. *Radiat. Res.* **96,** 422–8 (1983).
304. Gutscher, M. *et al.* Real-time imaging of the intracellular glutathione redox potential. *Nat. Methods* **5,** 553–559 (2008).
305. Griffith, O. W. Mechanism of action, metabolism, and toxicity of buthionine

sulfoximine and its higher homologs, potent inhibitors of glutathione synthesis. *J. Biol. Chem.* **257,** 13704–12 (1982).
306. Meister, A. Glutathione metabolism and its selective modification. *J. Biol. Chem.* **263,** 17205–8 (1988).
307. Brennan, M. S., Matos, M. F., Richter, K. E., Li, B. & Scannevin, R. H. The NRF2 transcriptional target, OSGIN1, contributes to monomethyl fumarate-mediated cytoprotection in human astrocytes. *Sci. Rep.* **7,** 42054 (2017).
308. Alam, J. *et al.* Nrf2, a Cap'n'Collar transcription factor, regulates induction of the heme oxygenase-1 gene. *J. Biol. Chem.* **274,** 26071–8 (1999).
309. Gorrini, C., Harris, I. S. & Mak, T. W. Modulation of oxidative stress as an anticancer strategy. *Nat. Rev. Drug Discov.* **12,** 931–947 (2013).
310. Singh, A. *et al.* Small Molecule Inhibitor of NRF2 Selectively Intervenes Therapeutic Resistance in KEAP1-Deficient NSCLC Tumors. *ACS Chem. Biol.* **11,** 3214–3225 (2016).
311. Eruslanov, E. & Kusmartsev, S. Identification of ROS Using Oxidized DCFDA and Flow-Cytometry. in 57–72 (Humana Press, Totowa, NJ, 2010). doi:10.1007/978-1-60761-411-1_4
312. Russell, S. J., Peng, K.-W. & Bell, J. C. Oncolytic virotherapy. *Nat. Biotechnol.* **30,** 658–670 (2012).
313. Guo, Z. S. & Bartlett, D. L. Oncolytic viruses as platform for multimodal cancer therapeutics: a promising land. *Cancer Gene Ther.* **21,** 261–3 (2014).
314. Ottolino-Perry, K., Diallo, J.-S., Lichty, B. D., Bell, J. C. & McCart, J. A. Intelligent design: combination therapy with oncolytic viruses. *Mol. Ther.* **18,** 251–63 (2010).
315. Kotterman, M. A., Chalberg, T. W. & Schaffer, D. V. Viral Vectors for Gene Therapy: Translational and Clinical Outlook. *Annu. Rev. Biomed. Eng.* **17,** 63–89 (2015).
316. Santiago-Ortiz, J. L. & Schaffer, D. V. Adeno-associated virus (AAV) vectors in cancer gene therapy. *J. Control. Release* **240,** 287–301 (2016).
317. Waibler, Z. *et al.* Vaccinia virus-mediated inhibition of type I interferon responses is a multifactorial process involving the soluble type I interferon receptor B18 and intracellular components. *J. Virol.* **83,** 1563–71 (2009).
318. Blanchard, T. J., Alcami, A., Andrea, P. & Smith, G. L. Modified vaccinia virus Ankara undergoes limited replication in human cells and lacks several immunomodulatory proteins:implications for use as a human vaccine. *J. Gen. Virol.* **79,** 1159–1167 (1998).
319. Dai, P. *et al.* Modified Vaccinia Virus Ankara Triggers Type I IFN Production in Murine Conventional Dendritic Cells via a cGAS/STING-Mediated Cytosolic DNA-Sensing Pathway. *PLoS Pathog.* **10,** e1003989 (2014).
320. Gnarra, J. R. *et al.* Mutations of the VHL tumour suppressor gene in renal carcinoma. *Nat. Genet.* **7,** 85–90 (1994).
321. Iliopoulos, O., Kibel, A., Gray, S. & Kaelin, W. G. Tumour suppression by the human von Hippel-Lindau gene product. *Nat. Med.* **1,** 822–826 (1995).
322. Hwang, I. I. L., Watson, I. R., Der, S. D. & Ohh, M. Loss of VHL confers hypoxia-inducible factor (HIF)-dependent resistance to vesicular stomatitis virus: role of HIF in antiviral response. *J. Virol.* **80,** 10712–23 (2006).
323. Tam, A. B., Mercado, E. L., Hoffmann, A. & Niwa, M. ER stress activates NF-κB by integrating functions of basal IKK activity, IRE1 and PERK. *PLoS One* **7,** e45078 (2012).

324. Bartee, E. & McFadden, G. Human cancer cells have specifically lost the ability to induce the synergistic state caused by tumor necrosis factor plus interferon-beta. *Cytokine* **47,** 199–205 (2009).
325. Bartee, E., Mohamed, M. R., Lopez, M. C., Baker, H. V & McFadden, G. The addition of tumor necrosis factor plus beta interferon induces a novel synergistic antiviral state against poxviruses in primary human fibroblasts. *J. Virol.* **83,** 498–511 (2009).
326. Roberts, A., Buonocore, L., Price, R., Forman, J. & Rose, J. K. Attenuated vesicular stomatitis viruses as vaccine vectors. *J. Virol.* **73,** 3723–32 (1999).
327. Jilg, N. *et al.* Kinetic differences in the induction of interferon stimulated genes by interferon-α and interleukin 28B are altered by infection with hepatitis C virus. *Hepatology* **59,** 1250–61 (2014).
328. Bolen, C. R., Ding, S., Robek, M. D. & Kleinstein, S. H. Dynamic expression profiling of type I and type III interferon-stimulated hepatocytes reveals a stable hierarchy of gene expression. *Hepatology* **59,** 1262–1272 (2014).
329. Moll, H. P., Maier, T., Zommer, A., Lavoie, T. & Brostjan, C. The differential activity of interferon-α subtypes is consistent among distinct target genes and cell types. *Cytokine* **53,** 52–9 (2011).
330. Wang, W. *et al.* Convergent Transcription of Interferon-stimulated Genes by TNF-α and IFN-α Augments Antiviral Activity against HCV and HEV. *Sci. Rep.* **6,** 25482 (2016).
331. Kandasamy, R. K. *et al.* A time-resolved molecular map of the macrophage response to VSV infection. *npj Syst. Biol. Appl.* **2,** 16027 (2016).
332. Kaleeba, J. A. R. & Berger, E. A. Kaposi's Sarcoma-Associated Herpesvirus Fusion-Entry Receptor: Cystine Transporter xCT. *Science (80-.).* **311,** 1921–1924 (2006).
333. Bridges, C. C. *et al.* Induction of Cystine-Glutamate Transporter x_c^- by Human Immunodeficiency Virus Type 1 Transactivator Protein Tat in Retinal Pigment Epithelium. *Investig. Opthalmology Vis. Sci.* **45,** 2906 (2004).
334. Sato, H., Tamba, M., Ishii, T. & Bannai, S. Cloning and expression of a plasma membrane cystine/glutamate exchange transporter composed of two distinct proteins. *J. Biol. Chem.* **274,** 11455–8 (1999).
335. Dai, L., Cao, Y., Chen, Y., Parsons, C. & Qin, Z. Targeting xCT, a cystine-glutamate transporter induces apoptosis and tumor regression for KSHV/HIV-associated lymphoma. *J. Hematol. Oncol.* **7,** 30 (2014).
336. Patel, S. A., Warren, B. A., Rhoderick, J. F. & Bridges, R. J. Differentiation of substrate and non-substrate inhibitors of transport system xc(-): an obligate exchanger of L-glutamate and L-cystine. *Neuropharmacology* **46,** 273–84 (2004).
337. Ju, H.-Q. *et al.* Redox Regulation of Stem-like Cells Though the CD44v-xCT Axis in Colorectal Cancer: Mechanisms and Therapeutic Implications. *Theranostics* **6,** 1160–1175 (2016).
338. Cureton, D. K., Massol, R. H., Whelan, S. P. J. & Kirchhausen, T. The Length of Vesicular Stomatitis Virus Particles Dictates a Need for Actin Assembly during Clathrin-Dependent Endocytosis. *PLoS Pathog.* **6,** e1001127 (2010).
339. Qiu, S. *et al.* Ebola virus requires phosphatidylinositol (3,5) bisphosphate production for efficient viral entry. *Virology* **513,** 17–28 (2018).
340. Morgan, A. S., Tew, K. D., Kauvar, L. M. & Ciaccio, F. J. Isozyme-specific glutathione S-

transferase inhibitors potentiate drug sensitivity in cultured human tumor cell lines. *Cancer Chemother. Pharmacol.* **37,** 363–370 (1996).
341. Na, H.-K. & Surh, Y.-J. Transcriptional Regulation via Cysteine Thiol Modification: A Novel Molecular Strategy for Chemoprevention and Cytoprotection. *Mol. Carcinog.* **45,** 368–380 (2006).
342. Gào, X. & Schöttker, B. Reduction-oxidation pathways involved in cancer development: a systematic review of literature reviews. *Oncotarget* **8,** 51888–51906 (2017).
343. Zhang, J. *et al.* ROS and ROS-Mediated Cellular Signaling. *Oxid. Med. Cell. Longev.* **2016,** 1–18 (2016).
344. Popov, D. Protein *S* -glutathionylation: from current basics to targeted modifications. *Arch. Physiol. Biochem.* **120,** 123–130 (2014).
345. Belousov, V. V *et al.* Genetically encoded fluorescent indicator for intracellular hydrogen peroxide. *Nat. Methods* **3,** 281–6 (2006).
346. Bellezza, I. *et al.* Inhibition of NF-kB nuclear translocation via HO-1 activation underlies a-tocopheryl succinate toxicity. *J. Nutr. Biochem.* **23,** 1583–1591 (2012).
347. Selman, M. *et al.* Dimethyl fumarate potentiates oncolytic virotherapy through NF-κB inhibition. *Sci. Transl. Med.* **10,** eaao1613 (2018).
348. Olagnier, D. *et al.* Activation of Nrf2 Signaling Augments Vesicular Stomatitis Virus Oncolysis via Autophagy-Driven Suppression of Antiviral Immunity. *Mol. Ther.* **25,** 1900–1916 (2017).
349. Alam, J. & Cook, J. L. How Many Transcription Factors Does It Take to Turn On the Heme Oxygenase-1 Gene? *Am. J. Respir. Cell Mol. Biol.* **36,** 166–174 (2007).
350. Riva, D. A. *et al.* Oxidative stress in vero cells infected with vesicular stomatitis virus. *Intervirology* **49,** 294–8 (2006).
351. Zeng, D. *et al.* Proteomic Analyses of Gastric Cancer Cells Treated with Vesicular Stomatitis Virus Matrix Protein. *Protein J.* **30,** 308–317 (2011).
352. Malilas, W. *et al.* Suppression of autophagic genes sensitizes CUG2-overexpressing A549 human lung cancer cells to oncolytic vesicular stomatitis virus-induced apoptosis. *Int. J. Oncol.* **44,** 1177–1184 (2014).
353. Malilas, W. *et al.* Cancer upregulated gene 2, a novel oncogene, confers resistance to oncolytic vesicular stomatitis virus through STAT1-OASL2 signaling. *Cancer Gene Ther.* **20,** 125–132 (2013).
354. Malilas, W. *et al.* Cancer upregulated gene 2, a novel oncogene, enhances migration and drug resistance of colon cancer cells via STAT1 activation. *Int. J. Oncol.* **43,** 1111–1116 (2013).
355. Huang, T. T., Carlson, E. J., Epstein, L. B. & Epstein, C. J. The role of superoxide anions in the establishment of an interferon-alpha-mediated antiviral state. *Free Radic. Res. Commun.* **17,** 59–72 (1992).
356. Morgan, M. J. & Liu, Z. Crosstalk of reactive oxygen species and NF-κB signaling. *Cell Res.* **21,** 103–15 (2011).
357. Brennan, P. & O'Neill, L. A. J. Effects of oxidants and antioxidants on nuclear factor κB activation in three different cell lines: evidence against a universal hypothesis involving oxygen radicals. *Biochim. Biophys. Acta - Gene Struct. Expr.* **1260,** 167–175

(1995).
358. Schreck, R., Rieber, P. & Baeuerle, P. A. Reactive oxygen intermediates as apparently widely used messengers in the activation of the NF-kappa B transcription factor and HIV-1. *EMBO J.* **10,** 2247–58 (1991).
359. Kamata, H., Manabe, T., Oka, S., Kamata, K. & Hirata, H. Hydrogen peroxide activates IκB kinases through phosphorylation of serine residues in the activation loops. *FEBS Lett.* **519,** 231–237 (2002).
360. Gloire, G., Legrand-Poels, S. & Piette, J. NF-κB activation by reactive oxygen species: Fifteen years later. *Biochem. Pharmacol.* **72,** 1493–1505 (2006).
361. Lou, H. & Kaplowitz, N. Glutathione depletion down-regulates tumor necrosis factor alpha-induced NF-kappaB activity via IkappaB kinase-dependent and -independent mechanisms. *J. Biol. Chem.* **282,** 29470–81 (2007).
362. Liao, B.-C., Hsieh, C.-W., Lin, Y.-C. & Wung, B.-S. The Glutaredoxin/Glutathione System Modulates NF-κB Activity by Glutathionylation of p65 in Cinnamaldehyde-Treated Endothelial Cells. *Toxicol. Sci.* **116,** 151–163 (2010).
363. Rahman, I., Marwick, J. & Kirkham, P. Redox modulation of chromatin remodeling: impact on histone acetylation and deacetylation, NF-κB and pro-inflammatory gene expression. *Biochem. Pharmacol.* **68,** 1255–1267 (2004).
364. Chen, F. E., Huang, D.-B., Chen, Y.-Q. & Ghosh, G. Crystal structure of p50/p65 heterodimer of transcription factor NF-κB bound to DNA. *Nature* **391,** 410–413 (1998).
365. Widen, J. C., Kempema, A. M., Villalta, P. W. & Harki, D. A. Targeting NF-κB p65 with a Helenalin Inspired Bis-electrophile. *ACS Chem. Biol.* **12,** 102–113 (2017).
366. Loewe, R. *et al.* Dimethylfumarate inhibits TNF-induced nuclear entry of NF-kappa B/p65 in human endothelial cells. *J. Immunol.* **168,** 4781–7 (2002).
367. Gillard, G. O. *et al.* DMF, but not other fumarates, inhibits NF-κB activity in vitro in an Nrf2-independent manner. *J. Neuroimmunol.* **283,** 74–85 (2015).
368. Tsubaki, M. *et al.* Dimethyl fumarate induces apoptosis of hematopoietic tumor cells via inhibition of NF-κB nuclear translocation and down-regulation of Bcl-xL and XIAP. *Biomed. Pharmacother.* **68,** 999–1005 (2014).
369. Dansen, T. B. *et al.* Redox-sensitive cysteines bridge p300/CBP-mediated acetylation and FoxO4 activity. *Nat. Chem. Biol.* **5,** 664–672 (2009).
370. Shishodia, S., Sethi, G., Konopleva, M., Andreeff, M. & Aggarwal, B. B. A synthetic triterpenoid, CDDO-Me, inhibits IkappaBalpha kinase and enhances apoptosis induced by TNF and chemotherapeutic agents through down-regulation of expression of nuclear factor kappaB-regulated gene products in human leukemic cells. *Clin. Cancer Res.* **12,** 1828–38 (2006).
371. Zheng, T., Rouhanifard, S. H., Jalloh, A. S. & Wu, P. Click Triazoles for Bioconjugation. *Top. Heterocycl. Chem.* **28,** 163–183 (2012).
372. Szadvari, I., Krizanova, O. & Babula, P. Athymic nude mice as an experimental model for cancer treatment. *Physiol. Res.* **65,** S441–S453 (2016).
373. Müller, L., Aigner, P. & Stoiber, D. Type I Interferons and Natural Killer Cell Regulation in Cancer. *Front. Immunol.* **8,** 304 (2017).
374. Hervas-Stubbs, S. *et al.* Direct effects of type I interferons on cells of the immune

system. *Clin. Cancer Res.* **17,** 2619–27 (2011).
375. Bukowski, J. F., Woda, B. A., Habu, S., Okumura, K. & Welsh, R. M. Natural killer cell depletion enhances virus synthesis and virus-induced hepatitis in vivo. *J. Immunol.* **131,** 1531–8 (1983).
376. Lee, A. J. *et al.* Inflammatory monocytes require type I interferon receptor signaling to activate NK cells via IL-18 during a mucosal viral infection. *J. Exp. Med.* **214,** 1153–1167 (2017).

Contributions from Collaborators

Dr. Mark Dornan and members of Dr. Christopher Boddy's lab (Department of Chemistry, University of Ottawa) synthesized VSe1 and its analogs (presented in Table 5). Mark also performed the glutathione reactivity experiments (section 2.7; results presented in Table 5 as "GSH half-life"), and generated the data for figures 6 and 7.

Andrew Macklin from Dr. Jeffrey Smith's lab (Carleton University) performed the plasma stability experiments (section 2.8; results presented in Table 5 as "Plasma stability at 3 hours"). Andrew also performed the data acquisition and analysis for figure 18 and table 6.

Nader El Sayes performed the experiments for figures 25, 26, 27, 28, 38B, 41B and Appendix figure 7. Nader also assisted with performing the experiments for figures 15, 35, 37B and 38A.

Andrew Chen assisted with all *in vivo* experiments (figures 15, 16, 17, 20, 21 and Appendix figure 6).

Hilary Groom from Dr. David Josephy's lab (University of Guelph) performed the experiments for figure 30 and table 7.

Dr. David Patten from Dr. Mary-Ellen Harper's lab (University of Ottawa) assisted with measuring GSH and GSSG levels by HPLC for figures 35 and 37B.

Carlos R. Canez from Dr. Jeffrey Smith's lab (Carleton University) performed the data acquisition for figure 19.

Dr. Rozanne Arulanandam helped perform the experiments for Table 6.

Dr. Fanny Tzelepis helped with planning and performing the experiment, data acquisition and data analysis for Appendix figure 6E-F.

Mohammed Selman performed the experiment for Appendix figure 4, assisted with performing the experiment for figures 15, 38A and analysed the microarray data for figure 38A.

Dr. Fabrice Le Boeuf performed the experiments for figures 12A, 12B and 14.

Michael Phan performed the experiment for figure 33E, the Western blot for 33A and assisted with the experiments for Appendix figure 3.

Paula Ou assisted with performing the *ex vivo* experiment for figure 15.

Johanne Mathieu assisted with the experiments for figure 10.

Appendices

Appendix A- Additional Figures

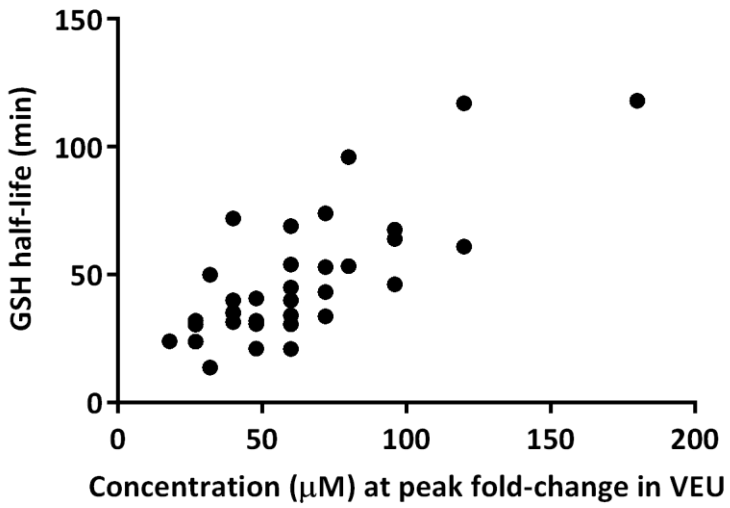

Appendix Figure 1. Correlation between a subset of pyrrole VSe1 analogs and GSH reactivity. Pyrrole analogs with a hydroxyl group substituted at C5, that are active (PFE in VEU > 10-fold) at 200 μM or lower were plotted against their GSH reactivity half-lives. Spearman correlation R^2= 0.6742, p<0.0001.

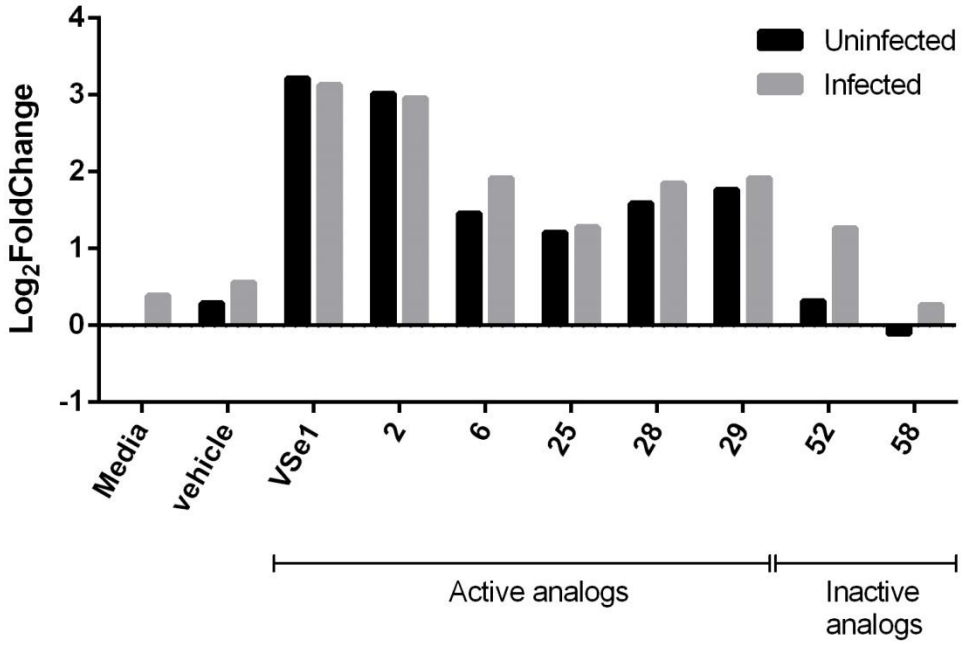

Appendix Figure 2. Fold-change in expression of SLC7A11. 786-0 cells were pre-treated with media, vehicle (DMSO), or viral sensitizer. Twenty-four hours later, RNA was collected and triplicates were pooled and hybridized on Affymetrix Human PrimeView Array. Fold-change in gene expression is shown relative to the uninfected, media control.

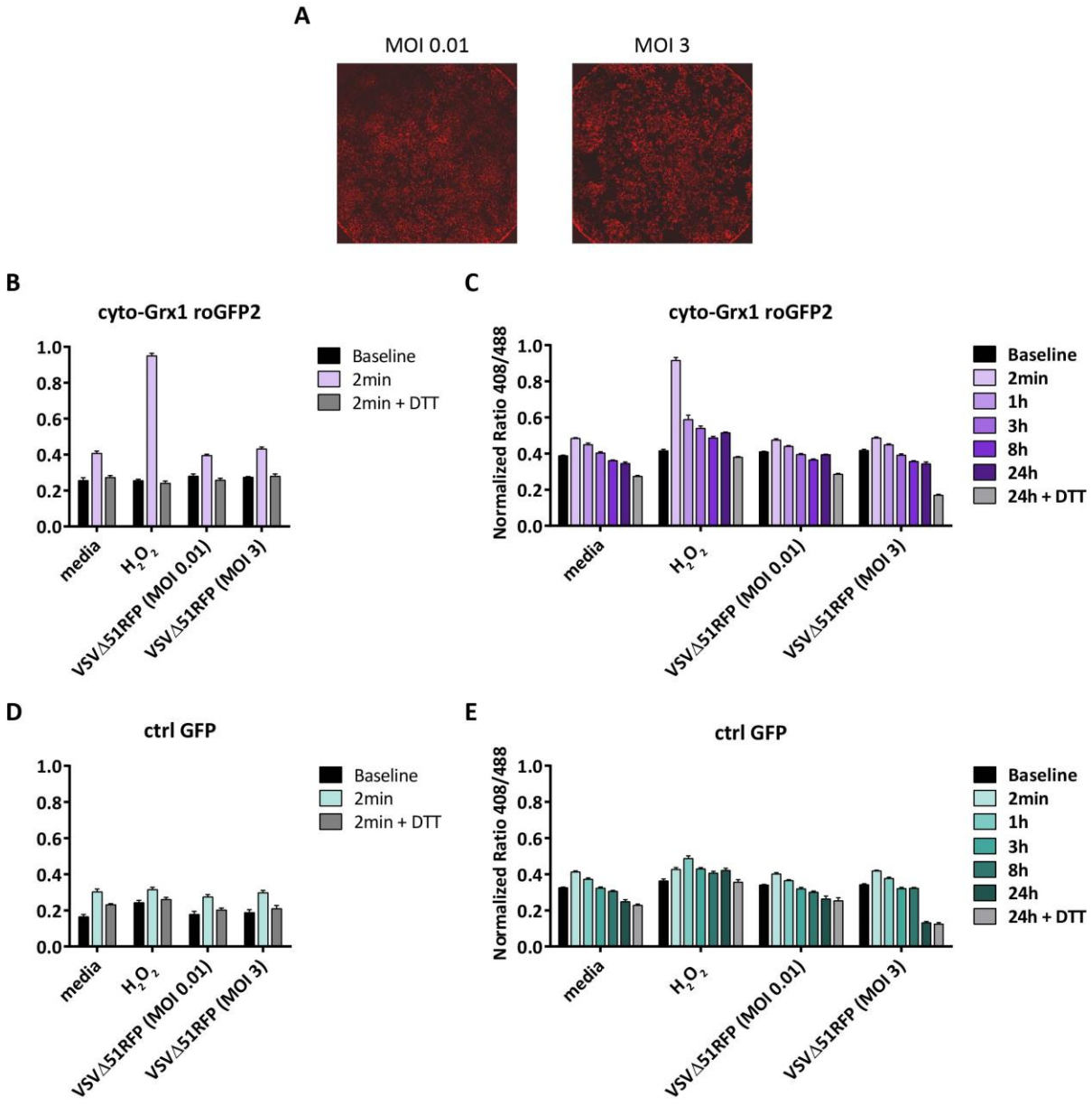

Appendix Figure 3. Ratiometric detection of GSSG/GSH after VSVΔ51 infection. (A) 293T cells were transfected with cyto-Grx1-roGFP and then infected with VSVΔ51-RFP and infection was monitored by fluorescence microscopy pictures 24 hours post-infection. **(B-E)** Transfected 293T cells were infected with VSVΔ51-RFP or treated with H_2O_2 (300 μM). Fluorescence readings were taken prior to treatment and post-treatment at the indicated times. 5 mM DTT was added to quench the signal.

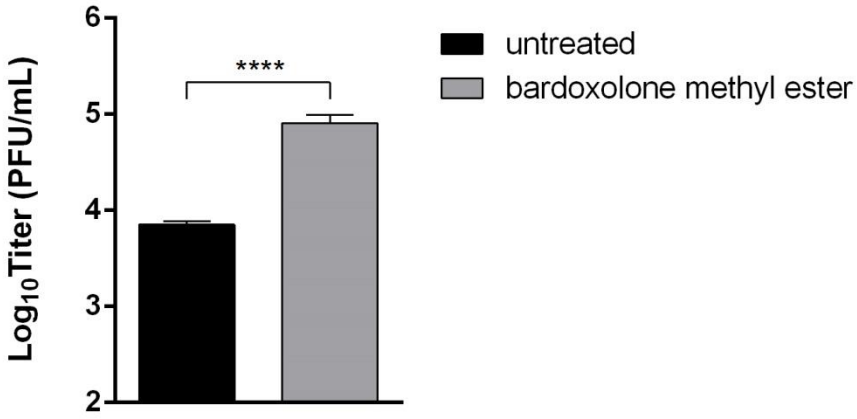

Appendix Figure 4. Bardoxolone methyl ester sensitizes 786-0 cells to VSVΔ51. 786-0 cells were pre-treated with bardoxolone methyl ester (4 μM) for 4 hours prior to infection with VSVΔ51 (MOI 0.01). Twenty-four hours later, supernatants were collected and virus titers were quantified by plaque assay. Statistical significance was calculated with an unpaired t test (****P < 0.0001). These results were generated by Mohammed Selman.

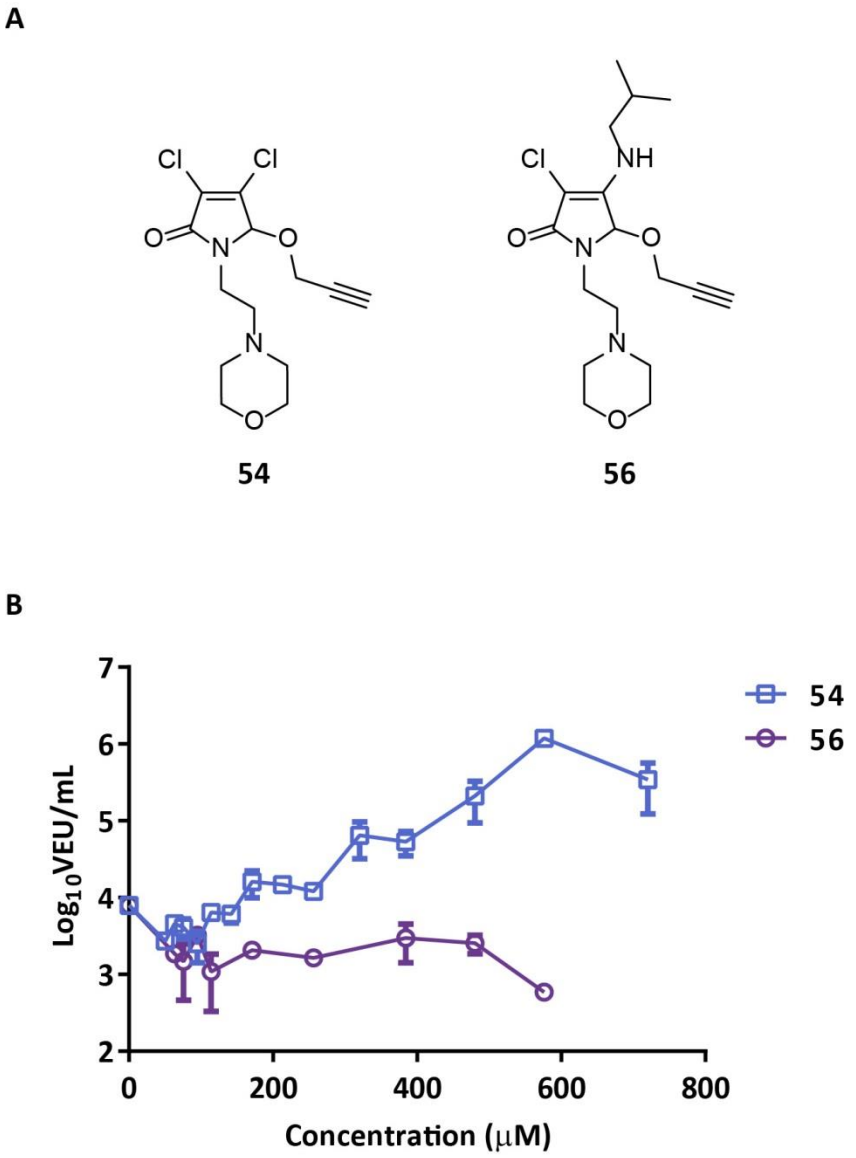

Appendix Figure 5. Structure and activity of 28-based probes for activity-based protein profiling experiments. (A) Active (**54**) and inactive (**56**) probes. **(B)** The viral-sensitizing effect of the active and inactive probes was assessed with a luciferase reporter-based viral titration assay in 786-0 cells.

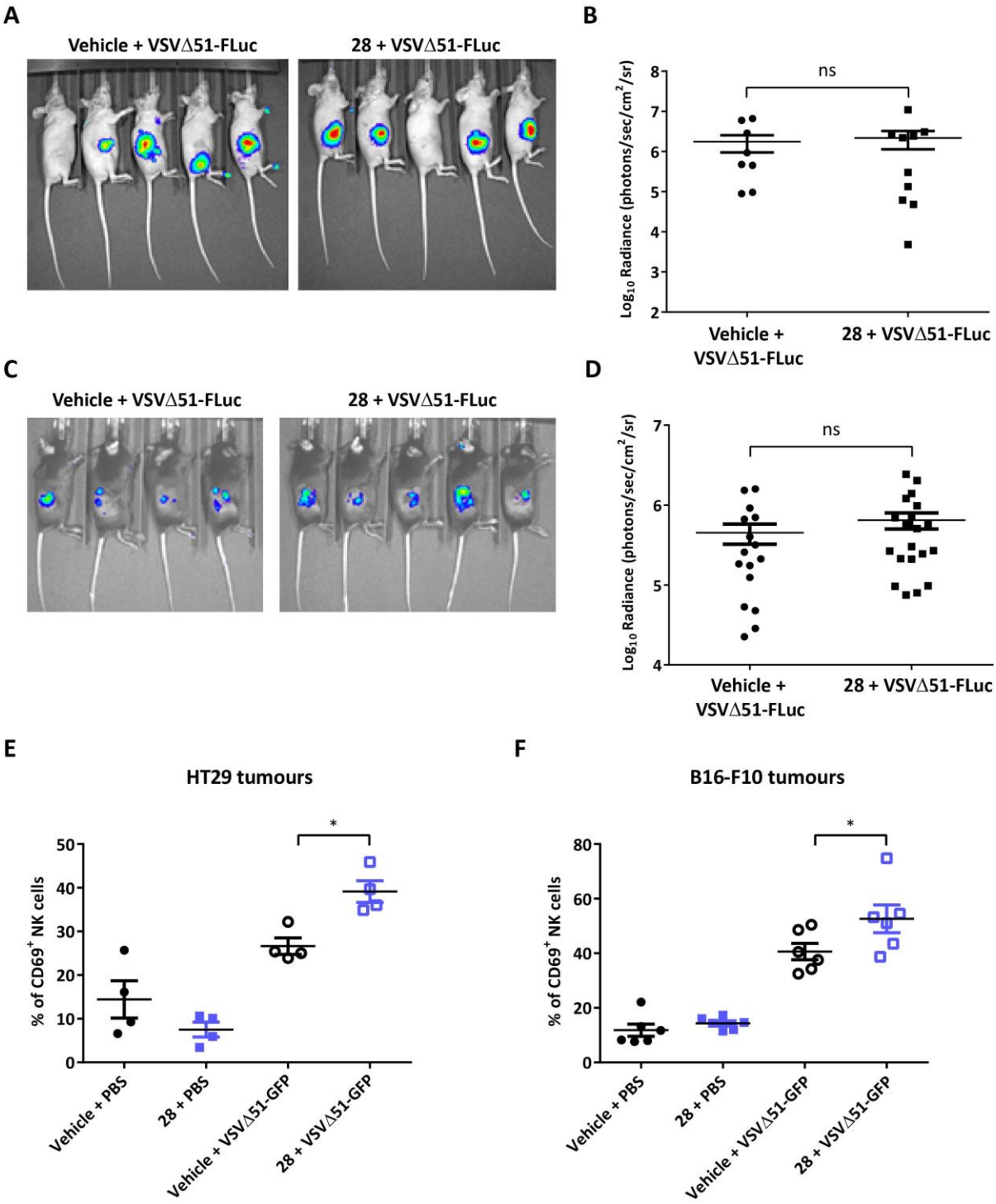
A
Vehicle + VSVΔ51-FLuc
28 + VSVΔ51-FLuc
B
ns
Log10 Radiance (photons/sec/cm2/sr)
Vehicle + VSVΔ51-FLuc
28 + VSVΔ51-FLuc
C
Vehicle + VSVΔ51-FLuc
28 + VSVΔ51-FLuc
D
ns
Log10 Radiance (photons/sec/cm2/sr)
Vehicle + VSVΔ51-FLuc
28 + VSVΔ51-FLuc
E
HT29 tumours
% of CD69+ NK cells
Vehicle + PBS
28 + PBS
Vehicle + VSVΔ51-GFP
28 + VSVΔ51-GFP
F
B16-F10 tumours
% of CD69+ NK cells
Vehicle + PBS
28 + PBS
Vehicle + VSVΔ51-GFP
28 + VSVΔ51-GFP

Appendix Figure 6. Effect of 28 on VSVΔ51-associated luminescence and on innate immune cell infiltration in HT29 and B16F10 models. (A-B) HT29 cells were subcutaneously engrafted into female CD1 nude mice and **(C-D)** B16F10 cells were subcutaneously engrafted into female C57/B6 mice. When tumors reached 5 mm x 5 mm in size, mice were given 25 µL of vehicle (DMSO) or 40 mg/kg of **28** by intratumoural injection. Four hours later, mice were treated with $1x10^8$ plaque-forming units of VSVΔ51-FLuc. Virus replication was monitored twenty-four hours later by measuring luminescence using an IVIS (representative images are shown, color scale bar represents photons) and tumor radiance was quantified. Statistical significance was determined with an unpaired t-test (ns = P > 0.05). **(E-F)** Mice were treated as described above, with vehicle, PBS, **28** and VSVΔ51-GFP. Forty hours after treatment tumours were excised, dissociated (Tumor Dissociation Kit and gentleMACS™ Dissociator, Miltenyi Biotec) and processed for analysis by flow cytometry. Each experiment was performed twice, producing similar results. Results from one experiment are shown. Samples were stained with Fixable Viability Stain 780 (#565388, BD Biosciences) and antibodies specific for mouse CD45 (#564225, BD Biosciences), CD3 (#561388, BD Biosciences), CD122 (#12-1222-81, eBioscience), CD49b (#560628, BD Biosciences) and CD69 (#563290, BD Biosciences). After gating on live cells, samples were gated as follows: $CD45^+ \rightarrow CD3^- \rightarrow CD122^+CD49b^+ \rightarrow CD69^+$. For each tumour model, average values for each group were compared to each other with a one-way ANOVA and statistical significance was calculated with Holm-Sidak's multiple comparisons test (for **(E)** * P = 0.0306; for **(F)** * P = 0.0233).

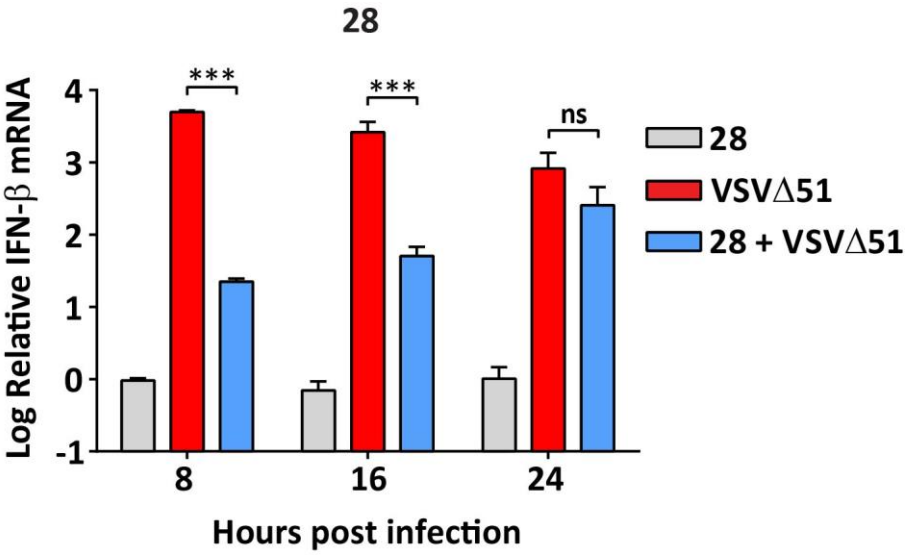

Appendix Figure 7. Expression of IFN-β over time. 786-0 cells were treated with **28** (80 μM) then infected with VSVΔ51-GFP (MOI 1). RNA was extracted 8, 16 and 24 hours post-infection and quantitative RT-PCR was used to measure relative levels of IFN-β mRNA. Values were normalized to GAPDH and are relative to untreated control for each timepoint. Error bars represent standard error from biological triplicates and statistical significance was calculated using two-way ANOVA with Dunnett's multiple comparisons test (*** $P < 0.001$, ns = $P > 0.05$). Values were log-transformed before analyzing statistical significance. These results were generated by Nader El Sayes.

Appendix B- Dose response curves for compounds in Table 5

Fold-changes in VEUs (black solid line) is to be read on the left y-axis. Relative metabolic activity (cytotoxicity) is to be read on the right y-axis. Grey solid lines represent compound alone and grey-hashed lines represent compound plus virus. Error bars represent standard error.

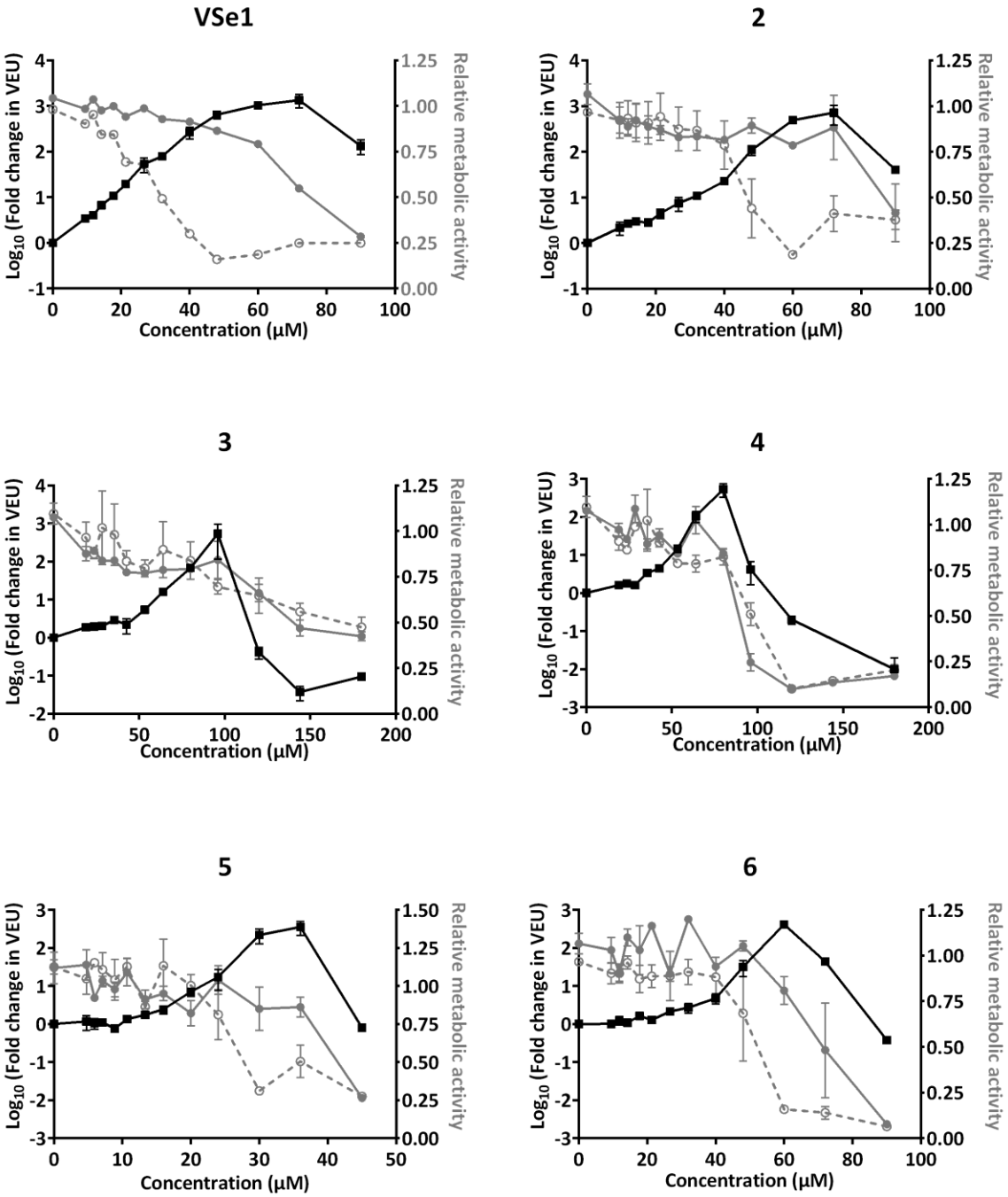

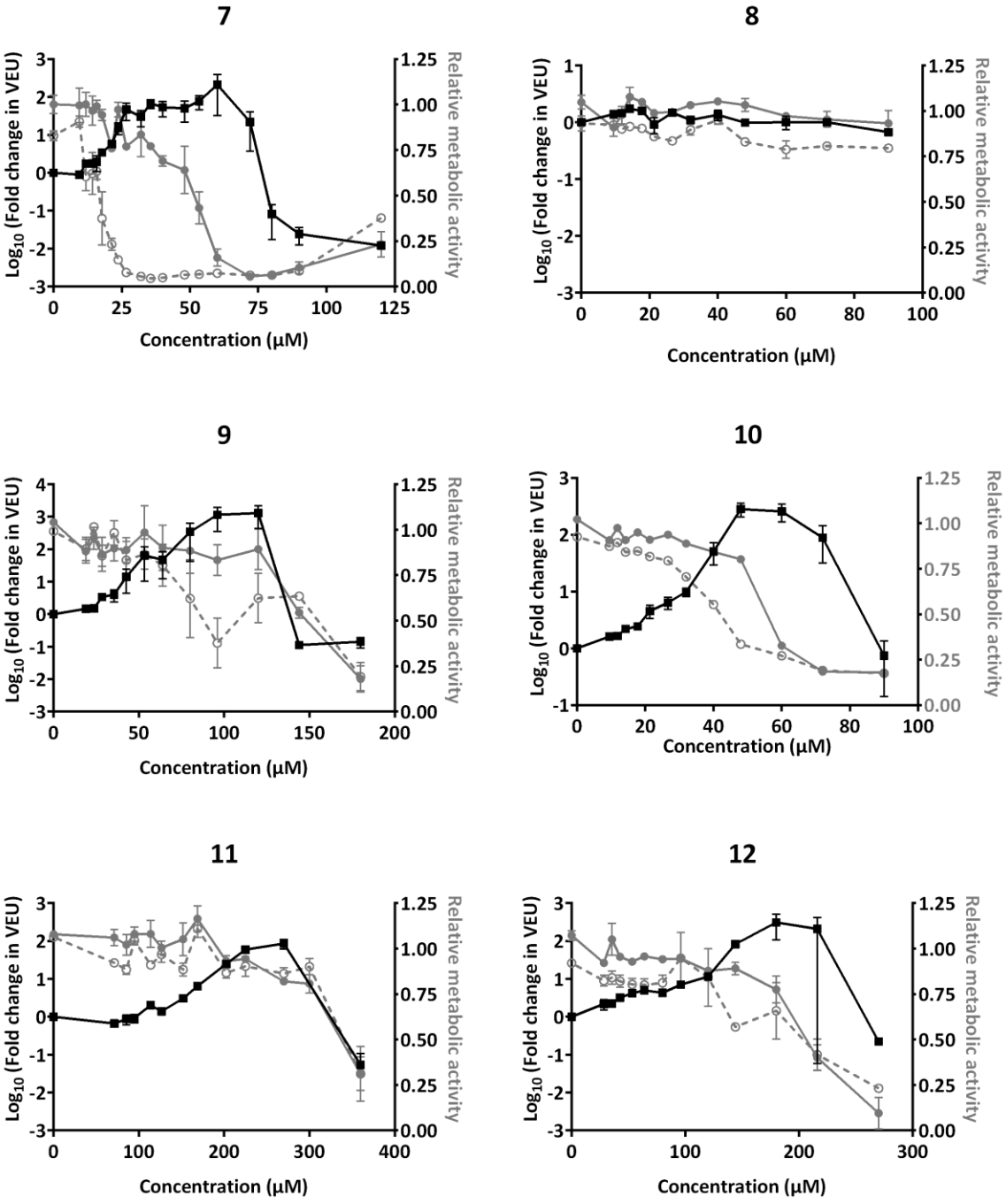
7
8
9
10
11
12
Log10 (Fold change in VEU)
Relative metabolic activity
Concentration (µM)

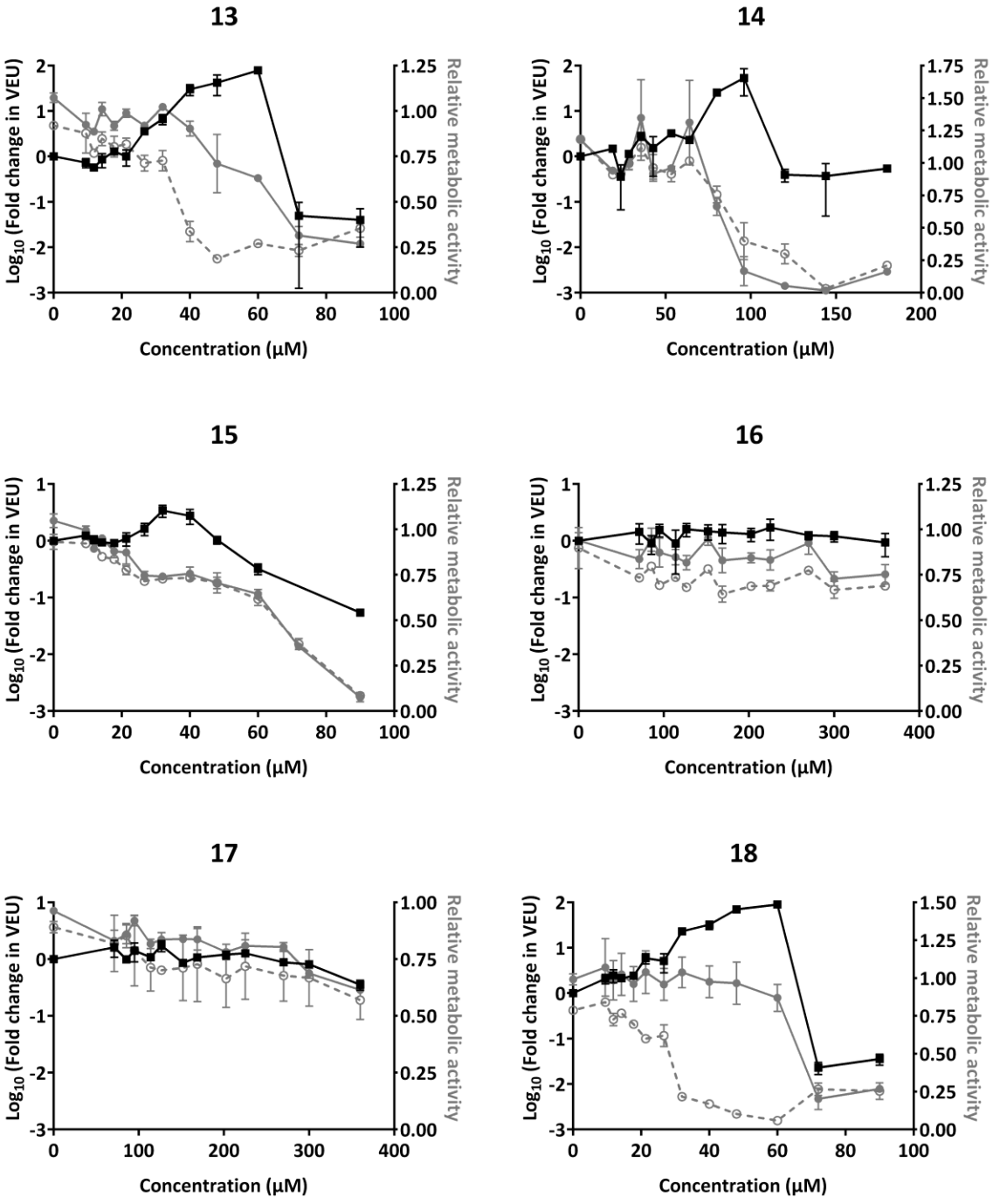
13
14
15
16
17
18
Log10 (Fold change in VEU)
Relative metabolic activity
Concentration (µM)

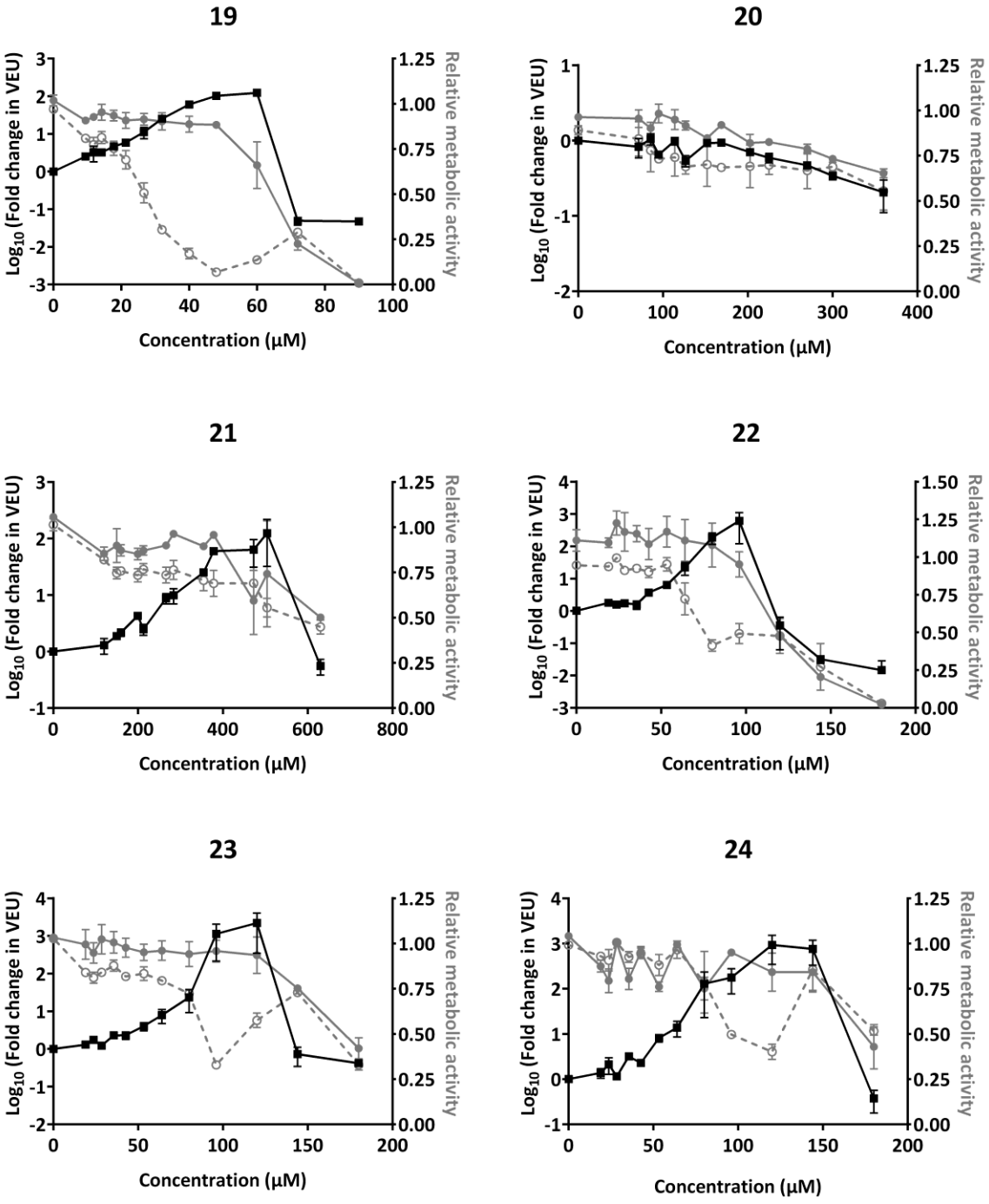
19
20
21
22
23
24
Log10 (Fold change in VEU)
Relative metabolic activity
Concentration (µM)

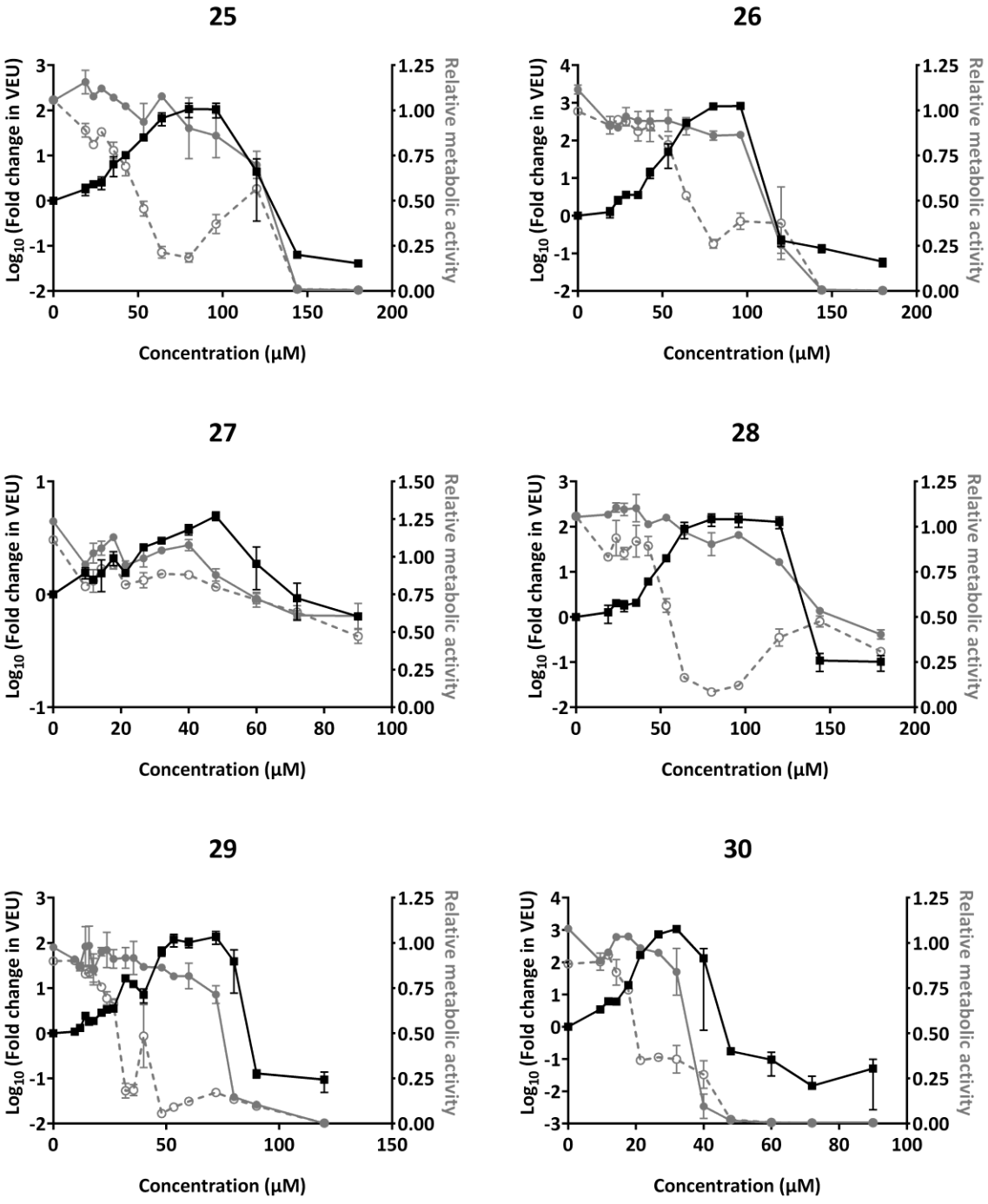
25
26
27
28
29
30
Log10 (Fold change in VEU)
Relative metabolic activity
Concentration (µM)

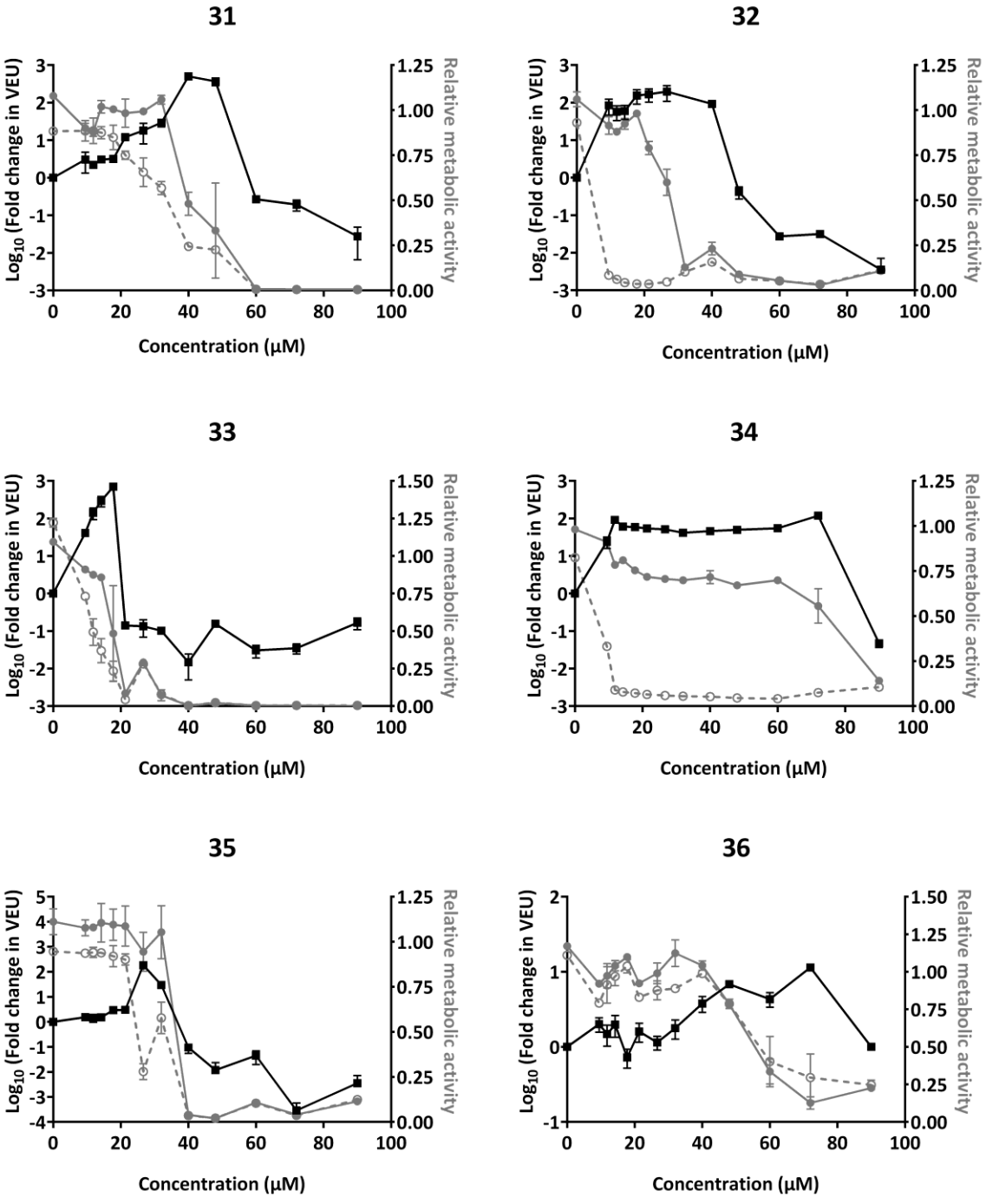
31
32
33
34
35
36
Log10 (Fold change in VEU)
Relative metabolic activity
Concentration (µM)

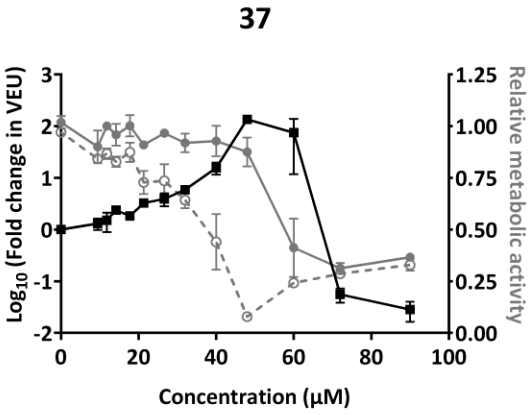
37
Log10 (Fold change in VEU)
Relative metabolic activity
Concentration (µM)

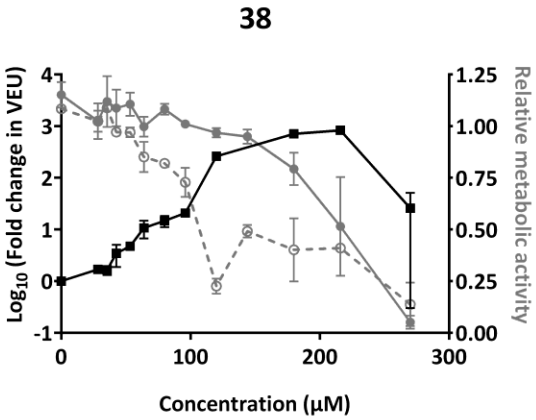
38
Log10 (Fold change in VEU)
Relative metabolic activity
Concentration (µM)

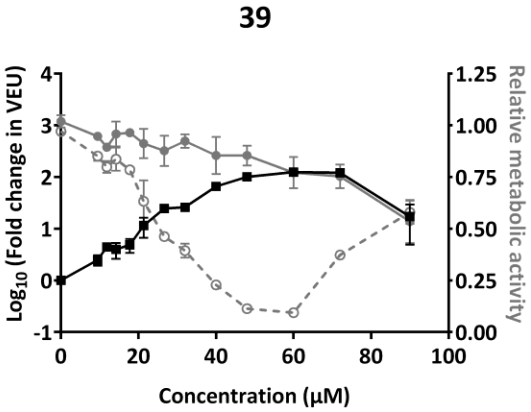
39
Log10 (Fold change in VEU)
Relative metabolic activity
Concentration (µM)

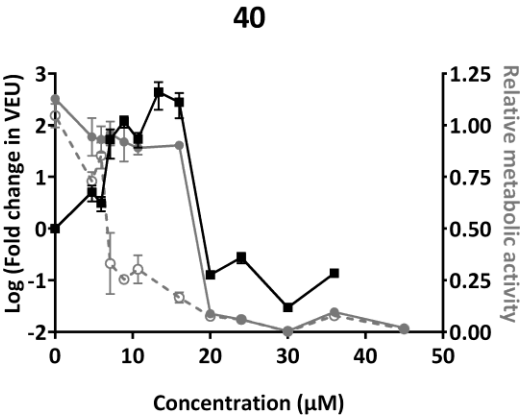
40
Log (Fold change in VEU)
Relative metabolic activity
Concentration (µM)

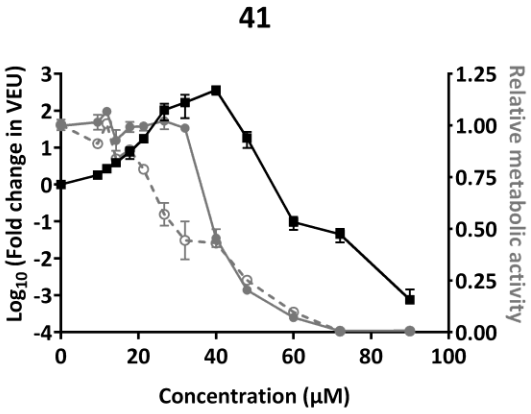
41
Log10 (Fold change in VEU)
Relative metabolic activity
Concentration (µM)

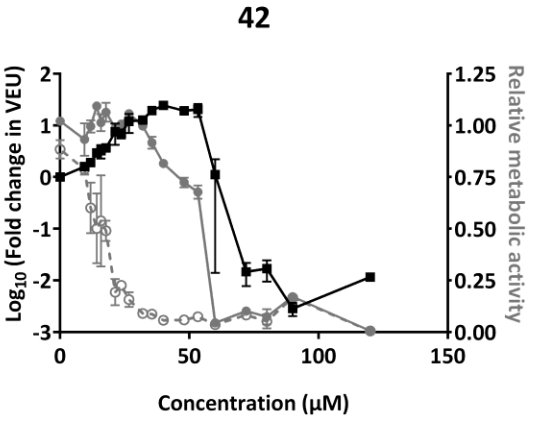
42
Log10 (Fold change in VEU)
Relative metabolic activity
Concentration (µM)

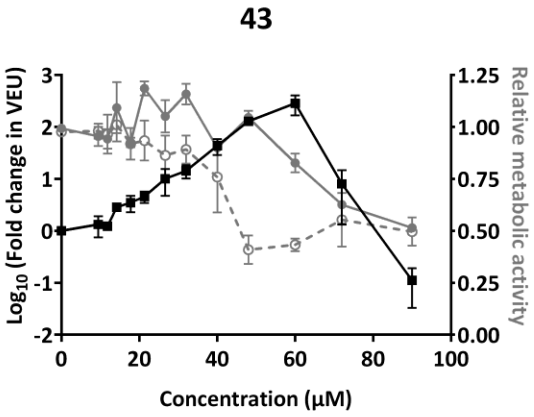
43
Log10 (Fold change in VEU)
Relative metabolic activity
Concentration (µM)

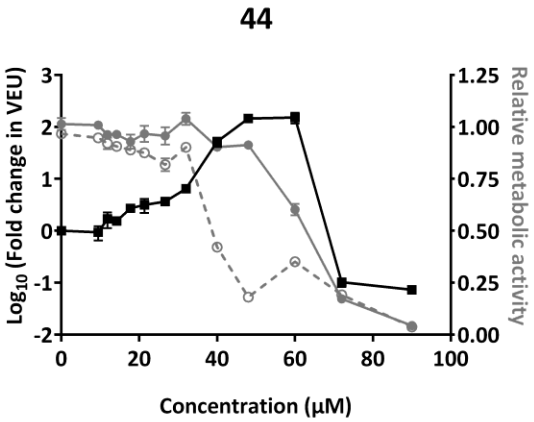
44
Log10 (Fold change in VEU)
Relative metabolic activity
Concentration (µM)

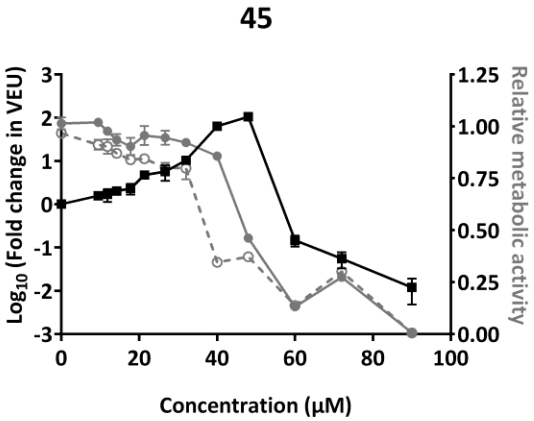
45
Log10 (Fold change in VEU)
Relative metabolic activity
Concentration (µM)

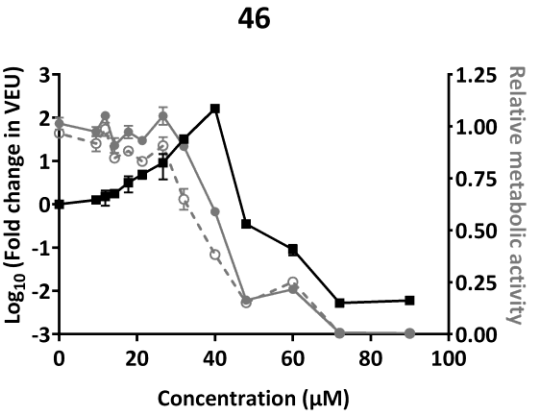
46
Log10 (Fold change in VEU)
Relative metabolic activity
Concentration (µM)

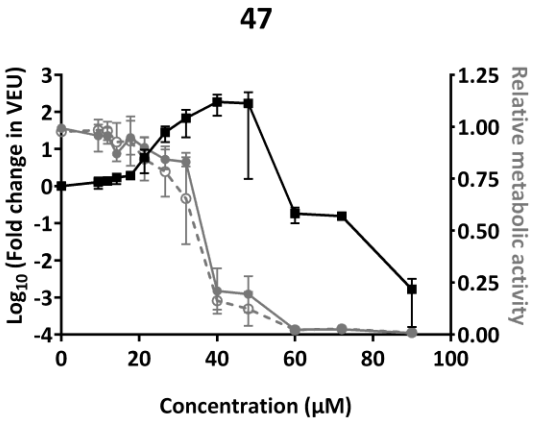
47
Log10 (Fold change in VEU)
Relative metabolic activity
Concentration (µM)

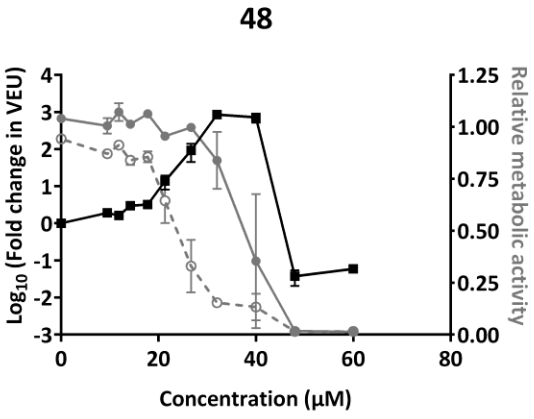
48
Log10 (Fold change in VEU)
Relative metabolic activity
Concentration (µM)

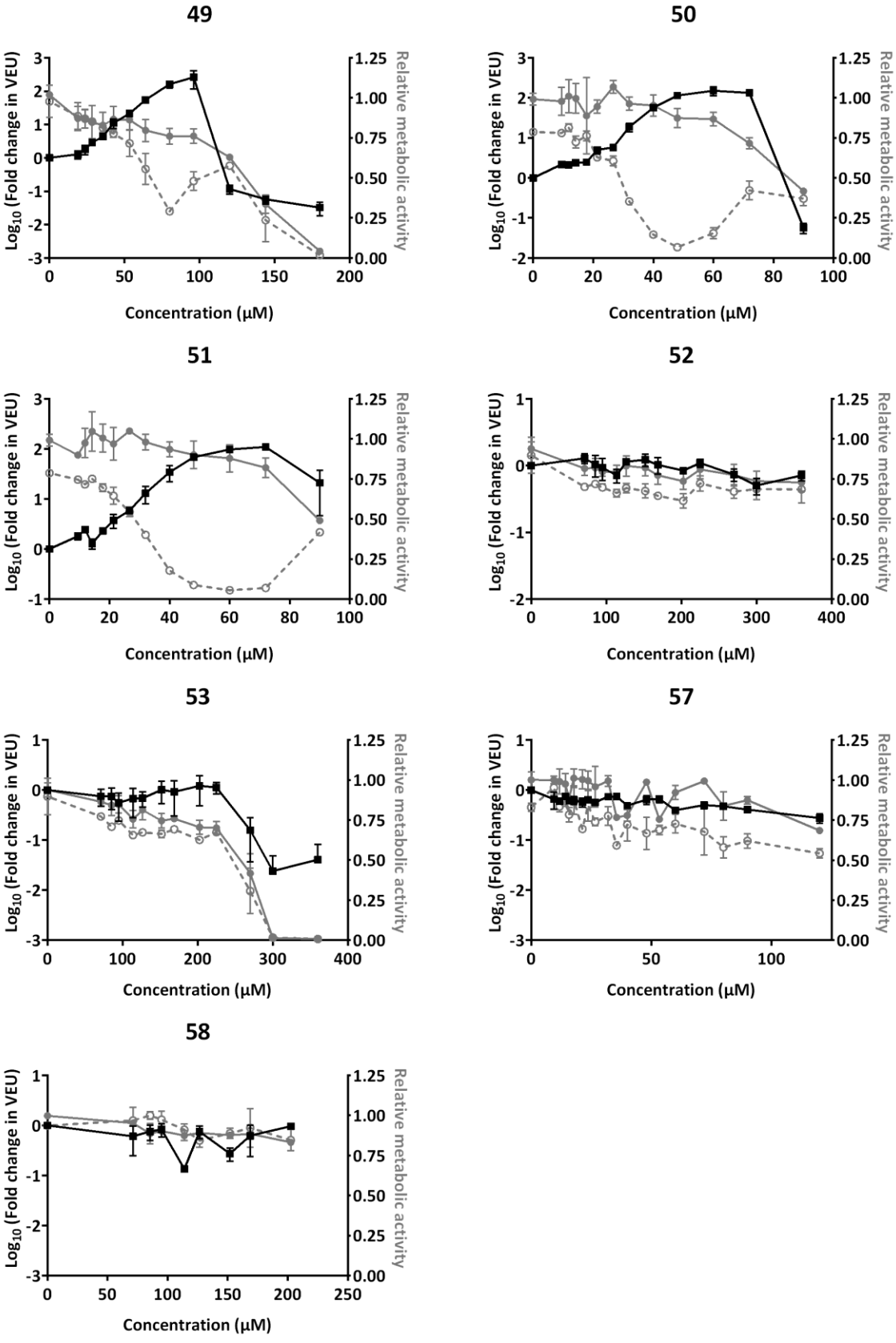
49
50
51
52
53
57
58
Log10 (Fold change in VEU)
Relative metabolic activity
Concentration (μM)

Appendix C- Licenses

Creative Commons Attribution 3.0 License (CC BY).

A copy of this license is presented below, and can also be found at https://creativecommons.org/licenses/by/3.0/legalcode.

CREATIVE COMMONS CORPORATION IS NOT A LAW FIRM AND DOES NOT PROVIDE LEGAL SERVICES. DISTRIBUTION OF THIS LICENSE DOES NOT CREATE AN ATTORNEY-CLIENT RELATIONSHIP. CREATIVE COMMONS PROVIDES THIS INFORMATION ON AN "AS-IS" BASIS. CREATIVE COMMONS MAKES NO WARRANTIES REGARDING THE INFORMATION PROVIDED, AND DISCLAIMS LIABILITY FOR DAMAGES RESULTING FROM ITS USE.

License

THE WORK (AS DEFINED BELOW) IS PROVIDED UNDER THE TERMS OF THIS CREATIVE COMMONS PUBLIC LICENSE ("CCPL" OR "LICENSE"). THE WORK IS PROTECTED BY COPYRIGHT AND/OR OTHER APPLICABLE LAW. ANY USE OF THE WORK OTHER THAN AS AUTHORIZED UNDER THIS LICENSE OR COPYRIGHT LAW IS PROHIBITED.

BY EXERCISING ANY RIGHTS TO THE WORK PROVIDED HERE, YOU ACCEPT AND AGREE TO BE BOUND BY THE TERMS OF THIS LICENSE. TO THE EXTENT THIS LICENSE MAY BE CONSIDERED TO BE A CONTRACT, THE LICENSOR GRANTS YOU THE RIGHTS CONTAINED HERE IN CONSIDERATION OF YOUR ACCEPTANCE OF SUCH TERMS AND CONDITIONS.

1. Definitions

a. **"Adaptation"** means a work based upon the Work, or upon the Work and other pre-existing works, such as a translation, adaptation, derivative work, arrangement of music or other alterations of a literary or artistic work, or phonogram or performance and includes cinematographic adaptations or any other form in which the Work may be recast, transformed, or adapted including in any form recognizably derived from the original, except that a work that constitutes a Collection will not be considered an Adaptation for the purpose of this License. For the avoidance of doubt, where the Work is a musical work, performance or phonogram, the synchronization of the Work in timed-relation with a moving image ("synching") will be considered an Adaptation for the purpose of this License.

b. **"Collection"** means a collection of literary or artistic works, such as encyclopedias and anthologies, or performances, phonograms or broadcasts, or other works or subject matter other than works listed in Section 1(f) below, which, by reason of the selection and arrangement of their contents, constitute intellectual creations, in which the Work is included in its entirety in unmodified form along with one or more other contributions, each constituting separate and independent works in themselves, which together are assembled into a collective whole. A work that constitutes a Collection will not be considered an Adaptation (as defined above) for the purposes of this License.

c. **"Distribute"** means to make available to the public the original and copies of the Work or Adaptation, as appropriate, through sale or other transfer of ownership.

d. **"Licensor"** means the individual, individuals, entity or entities that offer(s) the Work under the terms of this License.

e. **"Original Author"** means, in the case of a literary or artistic work, the individual, individuals, entity or entities who created the Work or if no individual or entity can be identified, the publisher; and in addition (i) in the case of a performance the actors, singers, musicians, dancers, and other persons who act, sing, deliver, declaim, play in, interpret or otherwise perform literary or artistic works or expressions of folklore; (ii) in the case of a phonogram the producer being the person or legal entity who first fixes the sounds of a performance or other sounds; and, (iii) in the case of broadcasts, the organization that transmits the broadcast.

f. **"Work"** means the literary and/or artistic work offered under the terms of this License including without limitation any production in the literary, scientific and artistic domain, whatever may be the mode or form of its expression including digital form, such as a book, pamphlet and other writing; a lecture, address, sermon or other work of the same nature; a dramatic or dramatico-musical work; a choreographic work or entertainment in dumb show; a musical composition with or without words; a cinematographic work to which are assimilated works expressed by a process analogous to cinematography; a work of drawing, painting, architecture, sculpture, engraving or lithography; a photographic work to which are assimilated works expressed by a process analogous to photography; a work of applied art; an illustration, map, plan, sketch or three-dimensional work relative to geography, topography, architecture or science; a performance; a broadcast; a phonogram; a compilation of data to the extent it is protected as a copyrightable work; or a work performed by a variety or circus performer to the extent it is not otherwise considered a literary or artistic work.

g. **"You"** means an individual or entity exercising rights under this License who has not previously violated the terms of this License with respect to the Work, or who has received express permission from the Licensor to exercise rights under this License despite a previous violation.

h. **"Publicly Perform"** means to perform public recitations of the Work and to communicate to the public those public recitations, by any means or process, including by wire or wireless means or public digital performances; to make available to the public Works in such a way that members of the public may access these Works from a place and at a place individually chosen by them; to perform the Work to the public by any means or process and the communication to the public of the performances of the Work, including by public digital performance; to broadcast and rebroadcast the Work by any means including signs, sounds or images.

i. **"Reproduce"** means to make copies of the Work by any means including without limitation by sound or visual recordings and the right of fixation and reproducing fixations of the Work, including storage of a protected performance or phonogram in digital form or other electronic medium.

2. Fair Dealing Rights. Nothing in this License is intended to reduce, limit, or restrict any uses free from copyright or rights arising from limitations or exceptions that are provided for in connection with the copyright protection under copyright law or other applicable laws.

3. License Grant. Subject to the terms and conditions of this License, Licensor hereby grants You a worldwide, royalty-free, non-exclusive, perpetual (for the duration of the applicable copyright) license to exercise the rights in the Work as stated below:

a. to Reproduce the Work, to incorporate the Work into one or more Collections, and to Reproduce the Work as incorporated in the Collections;

b. to create and Reproduce Adaptations provided that any such Adaptation, including any translation in any medium, takes reasonable steps to clearly label, demarcate or otherwise identify that changes were made to the original Work. For example, a translation could be marked "The original work was translated from English to Spanish," or a modification could indicate "The original work has been modified.";

c. to Distribute and Publicly Perform the Work including as incorporated in Collections; and,

d. to Distribute and Publicly Perform Adaptations.

e. For the avoidance of doubt:

i. **Non-waivable Compulsory License Schemes**. In those jurisdictions in which the right to collect royalties through any statutory or compulsory licensing scheme cannot be waived, the Licensor reserves the exclusive right to collect such royalties for any exercise by You of the rights granted under this License;

ii. **Waivable Compulsory License Schemes**. In those jurisdictions in which the right to collect royalties through any statutory or compulsory licensing scheme can be waived, the Licensor waives the exclusive right to collect such royalties for any exercise by You of the rights granted under this License; and,

iii. **Voluntary License Schemes**. The Licensor waives the right to collect royalties, whether individually or, in the event that the Licensor is a member of a collecting society that administers voluntary licensing schemes, via that society, from any exercise by You of the rights granted under this License.

The above rights may be exercised in all media and formats whether now known or hereafter devised. The above rights include the right to make such modifications as are technically necessary to exercise the rights in other media and formats. Subject to Section 8(f), all rights not expressly granted by Licensor are hereby reserved.

4. Restrictions. The license granted in Section 3 above is expressly made subject to and limited by the following restrictions:

a. You may Distribute or Publicly Perform the Work only under the terms of this License. You must include a copy of, or the Uniform Resource Identifier (URI) for, this License with every copy of the Work You Distribute or Publicly Perform. You may not offer or impose any terms on the Work that restrict the terms of this License or the ability of the recipient of the Work to exercise the rights granted to that recipient under the terms of the License. You may not sublicense the Work. You must keep intact all notices that refer to this License and to the disclaimer of warranties with every copy of the Work You Distribute or Publicly Perform. When You Distribute or Publicly Perform the Work, You may not impose any effective technological measures on the Work that restrict the ability of a recipient of the Work from You to exercise the rights granted to that recipient under the terms of the License. This Section 4(a) applies to the Work as incorporated in a Collection, but this does not require the Collection apart from the Work itself to be made subject to the terms of this License. If You create a Collection, upon notice from any Licensor You must, to the extent practicable, remove from the Collection any credit as required by Section 4(b), as requested. If You create an Adaptation, upon notice from any Licensor You must, to the extent practicable, remove from the Adaptation any credit as required by Section 4(b), as requested.

b. If You Distribute, or Publicly Perform the Work or any Adaptations or Collections, You must, unless a request has been made pursuant to Section 4(a), keep intact all copyright notices for the Work and provide, reasonable to the medium or means You are utilizing: (i) the name of the Original Author (or pseudonym, if applicable) if supplied, and/or if the Original Author and/or Licensor designate another party or parties (e.g., a sponsor institute, publishing entity, journal) for attribution ("Attribution Parties") in Licensor's copyright notice, terms of service or by other reasonable means, the name of such party or parties; (ii) the title of the Work if supplied; (iii) to the extent reasonably practicable, the URI, if any, that Licensor specifies to be associated with the Work, unless such URI does not refer to the copyright notice or licensing information for the Work; and (iv) , consistent with Section 3(b), in the case of an Adaptation, a credit identifying the use of the Work in the Adaptation (e.g., "French translation of the Work by Original Author," or "Screenplay based on original Work by Original Author"). The credit required by this Section 4 (b) may be implemented in any reasonable manner; provided, however, that in the case of a Adaptation or Collection, at a minimum such credit will appear, if a credit for all contributing authors of the Adaptation or Collection appears, then as part of these credits and in a manner at least as prominent as the credits for the other contributing authors. For the avoidance of doubt, You may only use the credit required by this Section for the purpose of attribution in the manner set out above and, by exercising Your rights under this License, You may not implicitly or explicitly assert or imply any connection with, sponsorship or endorsement by the Original Author, Licensor and/or Attribution Parties, as appropriate, of You or Your use of the Work, without the separate, express prior written permission of the Original Author, Licensor and/or Attribution Parties.

c. Except as otherwise agreed in writing by the Licensor or as may be otherwise permitted by applicable law, if You Reproduce, Distribute or Publicly Perform the Work either by itself or as part of any Adaptations or Collections, You must not distort, mutilate, modify or take other derogatory action in relation to the Work which would be prejudicial to the Original Author's honor or reputation. Licensor agrees that in those jurisdictions (e.g. Japan), in which any exercise of the right granted in Section 3(b) of this License (the right to make Adaptations) would be deemed to be a distortion, mutilation, modification or other derogatory action prejudicial to the Original Author's honor and reputation, the Licensor will waive or not assert, as appropriate, this Section, to the fullest extent permitted by the applicable national law, to enable You to reasonably exercise Your right under Section 3(b) of this License (right to make Adaptations) but not otherwise.

5. Representations, Warranties and Disclaimer

UNLESS OTHERWISE MUTUALLY AGREED TO BY THE PARTIES IN WRITING, LICENSOR OFFERS THE WORK AS-IS AND MAKES NO REPRESENTATIONS OR WARRANTIES OF ANY KIND CONCERNING THE WORK, EXPRESS, IMPLIED, STATUTORY OR OTHERWISE, INCLUDING, WITHOUT LIMITATION, WARRANTIES OF TITLE, MERCHANTIBILITY, FITNESS FOR A PARTICULAR PURPOSE, NONINFRINGEMENT, OR THE ABSENCE OF LATENT OR OTHER DEFECTS, ACCURACY, OR THE PRESENCE OF ABSENCE OF ERRORS, WHETHER OR NOT DISCOVERABLE. SOME JURISDICTIONS DO NOT ALLOW THE EXCLUSION OF IMPLIED WARRANTIES, SO SUCH EXCLUSION MAY NOT APPLY TO YOU.

6. Limitation on Liability. EXCEPT TO THE EXTENT REQUIRED BY APPLICABLE LAW, IN NO EVENT WILL LICENSOR BE LIABLE TO YOU ON ANY LEGAL THEORY FOR ANY SPECIAL, INCIDENTAL, CONSEQUENTIAL, PUNITIVE OR EXEMPLARY DAMAGES ARISING OUT OF THIS LICENSE OR THE USE OF THE WORK, EVEN IF LICENSOR HAS BEEN ADVISED OF THE POSSIBILITY OF SUCH DAMAGES.

7. Termination

a. This License and the rights granted hereunder will terminate automatically upon any breach by You of the terms of this License. Individuals or entities who have received Adaptations or Collections from You under this License, however, will not have their licenses terminated provided such individuals or entities remain in full compliance with those licenses. Sections 1, 2, 5, 6, 7, and 8 will survive any termination of this License.

b. Subject to the above terms and conditions, the license granted here is perpetual (for the duration of the applicable copyright in the Work). Notwithstanding the above, Licensor reserves the right to release the Work under different license terms or to stop distributing the Work at any time; provided, however that any such election will not serve to withdraw this License (or any other license that has been, or is required to be, granted under the terms of this License), and this License will continue in full force and effect unless terminated as stated above.

8. Miscellaneous

a. Each time You Distribute or Publicly Perform the Work or a Collection, the Licensor offers to the recipient a license to the Work on the same terms and conditions as the license granted to You under this License.

b. Each time You Distribute or Publicly Perform an Adaptation, Licensor offers to the recipient a license to the original Work on the same terms and conditions as the license granted to You under this License.

c. If any provision of this License is invalid or unenforceable under applicable law, it shall not affect the validity or enforceability of the remainder of the terms of this License, and without further action by the parties to this agreement, such provision shall be reformed to the minimum extent necessary to make such provision valid and enforceable.

d. No term or provision of this License shall be deemed waived and no breach consented to unless such waiver or consent shall be in writing and signed by the party to be charged with such waiver or consent.

e. This License constitutes the entire agreement between the parties with respect to the Work licensed here. There are no understandings, agreements or representations with respect to the Work not specified here. Licensor shall not be bound by any additional provisions that may appear in any communication from You. This License may not be modified without the mutual written agreement of the Licensor and You.

f. The rights granted under, and the subject matter referenced, in this License were drafted utilizing the terminology of the Berne Convention for the Protection of Literary and Artistic Works (as amended on September 28, 1979), the Rome Convention of 1961, the WIPO Copyright Treaty of 1996, the WIPO Performances and Phonograms Treaty of 1996 and the Universal Copyright Convention (as revised on July 24, 1971). These rights and subject matter take effect in the relevant jurisdiction in which the License terms are sought to be enforced according to the corresponding provisions of the implementation of those treaty provisions in the applicable national law. If the standard suite of rights granted under applicable copyright law includes additional rights not granted under this License, such additional rights are deemed to be included in the License; this License is not intended to restrict the license of any rights under applicable law.

Creative Commons Notice

Creative Commons is not a party to this License, and makes no warranty whatsoever in connection with the Work. Creative Commons will not be liable to You or any party on any legal theory for any damages whatsoever, including without limitation any general, special, incidental or consequential damages arising in connection to this license. Notwithstanding the foregoing two (2) sentences, if Creative Commons has expressly identified itself as the Licensor hereunder, it shall have all rights and obligations of Licensor.

Except for the limited purpose of indicating to the public that the Work is licensed under the CCPL, Creative Commons does not authorize the use by either party of the trademark "Creative Commons" or any related trademark or logo of Creative Commons without the prior written consent of Creative Commons. Any permitted use will be in compliance with Creative Commons' then-current trademark usage guidelines, as may be published on its website or otherwise made available upon request from time to time. For the avoidance of doubt, this trademark restriction does not form part of this License.

Creative Commons may be contacted at **https://creativecommons.org/**.

Creative Commons Attribution 3.0 License (CRC 3.0, by,nc,nd).

A copy of this license is presented below, and can also be found at https://creativecommons.org/licenses/by-nc-nd/3.0/legalcode

CREATIVE COMMONS CORPORATION IS NOT A LAW FIRM AND DOES NOT PROVIDE LEGAL SERVICES. DISTRIBUTION OF THIS LICENSE DOES NOT CREATE AN ATTORNEY-CLIENT RELATIONSHIP. CREATIVE COMMONS PROVIDES THIS INFORMATION ON AN "AS-IS" BASIS. CREATIVE COMMONS MAKES NO WARRANTIES REGARDING THE INFORMATION PROVIDED, AND DISCLAIMS LIABILITY FOR DAMAGES RESULTING FROM ITS USE.

License

THE WORK (AS DEFINED BELOW) IS PROVIDED UNDER THE TERMS OF THIS CREATIVE COMMONS PUBLIC LICENSE ("CCPL" OR "LICENSE"). THE WORK IS PROTECTED BY COPYRIGHT AND/OR OTHER APPLICABLE LAW. ANY USE OF THE WORK OTHER THAN AS AUTHORIZED UNDER THIS LICENSE OR COPYRIGHT LAW IS PROHIBITED.

BY EXERCISING ANY RIGHTS TO THE WORK PROVIDED HERE, YOU ACCEPT AND AGREE TO BE BOUND BY THE TERMS OF THIS LICENSE. TO THE EXTENT THIS LICENSE MAY BE CONSIDERED TO BE A CONTRACT, THE LICENSOR GRANTS YOU THE RIGHTS CONTAINED HERE IN CONSIDERATION OF YOUR ACCEPTANCE OF SUCH TERMS AND CONDITIONS.

1. Definitions

a. **"Adaptation"** means a work based upon the Work, or upon the Work and other pre-existing works, such as a translation, adaptation, derivative work, arrangement of music or other alterations of a literary or artistic work, or phonogram or performance and includes cinematographic adaptations or any other form in which the Work may be recast, transformed, or adapted including in any form recognizably derived from the original, except that a work that constitutes a Collection will not be considered an Adaptation for the purpose of this License. For the avoidance of doubt, where the Work is a musical work, performance or phonogram, the synchronization of the Work in timed-relation with a moving image ("synching") will be considered an Adaptation for the purpose of this License.

b. **"Collection"** means a collection of literary or artistic works, such as encyclopedias and anthologies, or performances, phonograms or broadcasts, or other works or subject matter other than works listed in Section 1(f) below, which, by reason of the selection and arrangement of their contents, constitute intellectual creations, in which the Work is included in its entirety in unmodified form along with one or more other contributions, each constituting separate and independent works in themselves, which together are assembled into a collective whole. A work that constitutes a Collection will not be considered an Adaptation (as defined above) for the purposes of this License.

c. **"Distribute"** means to make available to the public the original and copies of the Work through sale or other transfer of ownership.

d. **"Licensor"** means the individual, individuals, entity or entities that offer(s) the Work under the terms of this License.

e. **"Original Author"** means, in the case of a literary or artistic work, the individual, individuals, entity or entities who created the Work or if no individual or entity can be identified, the publisher; and in addition (i) in the case of a performance the actors, singers, musicians, dancers, and other persons who act, sing, deliver, declaim, play in, interpret or otherwise perform literary or artistic works or expressions of folklore; (ii) in the case of a phonogram the producer being the person or legal entity who first fixes the sounds of a performance or other sounds; and, (iii) in the case of broadcasts, the organization that transmits the broadcast.

f. **"Work"** means the literary and/or artistic work offered under the terms of this License including without limitation any production in the literary, scientific and artistic domain, whatever may be the mode or form of its expression including digital form, such as a book, pamphlet and other writing; a lecture, address, sermon or other work of the same nature; a dramatic or dramatico-musical work; a choreographic work or entertainment in dumb show; a musical composition with or without words; a cinematographic work to which are assimilated works expressed by a process analogous to cinematography; a work of drawing, painting, architecture, sculpture, engraving or lithography; a photographic work to which are assimilated works expressed by a process analogous to photography; a work of applied art; an illustration, map, plan, sketch or three-dimensional work relative to geography, topography, architecture or science; a performance; a broadcast; a phonogram; a compilation of data to the extent it is protected as a copyrightable work; or a work performed by a variety or circus performer to the extent it is not otherwise considered a literary or artistic work.

g. **"You"** means an individual or entity exercising rights under this License who has not previously violated the terms of this License with respect to the Work, or who has received express permission from the Licensor to exercise rights under this License despite a previous violation.

h. **"Publicly Perform"** means to perform public recitations of the Work and to communicate to the public those public recitations, by any means or process, including by wire or wireless means or public digital performances; to make available to the public Works in such a way that members of the public may access these Works from a place and at a place individually chosen by them; to perform the Work to the public by any means or process and the communication to the public of the performances of the Work, including by public digital performance; to broadcast and rebroadcast the Work by any means including signs, sounds or images.

i. **"Reproduce"** means to make copies of the Work by any means including without limitation by sound or visual recordings and the right of fixation and reproducing fixations of the Work, including storage of a protected performance or phonogram in digital form or other electronic medium.

2. Fair Dealing Rights. Nothing in this License is intended to reduce, limit, or restrict any uses free from copyright or rights arising from limitations or exceptions that are provided for in connection with the copyright protection under copyright law or other applicable laws.

3. License Grant. Subject to the terms and conditions of this License, Licensor hereby grants You a worldwide, royalty-free, non-exclusive, perpetual (for the duration of the applicable copyright) license to exercise the rights in the Work as stated below:

a. to Reproduce the Work, to incorporate the Work into one or more Collections, and to Reproduce the Work as incorporated in the Collections; and,

b. to Distribute and Publicly Perform the Work including as incorporated in Collections.

The above rights may be exercised in all media and formats whether now known or hereafter devised. The above rights include the right to make such modifications as are technically necessary to exercise the rights in other media and formats, but otherwise you have no rights to make Adaptations. Subject to 8(f), all rights not expressly granted by Licensor are hereby reserved, including but not limited to the rights set forth in Section 4(d).

4. Restrictions. The license granted in Section 3 above is expressly made subject to and limited by the following restrictions:

a. You may Distribute or Publicly Perform the Work only under the terms of this License. You must include a copy of, or the Uniform Resource Identifier (URI) for, this License with every copy of the Work You Distribute or Publicly Perform. You may not offer or impose any terms on the Work that restrict the terms of this License or the ability of the recipient of the Work to exercise the rights granted to that recipient under the terms of the License. You may not sublicense the Work. You must keep intact all notices that refer to this License and to the disclaimer of warranties with every copy of the Work You Distribute or Publicly Perform. When You Distribute or Publicly Perform the Work, You may not impose any effective technological measures on the Work that restrict the ability of a recipient of the Work from You to exercise the rights granted to that recipient under the terms of the License. This Section 4(a) applies to the Work as incorporated in a Collection, but this does not require the Collection apart from the Work itself to be made subject to the terms of this License. If You create a Collection, upon notice from any Licensor You must, to the extent practicable, remove from the Collection any credit as required by Section 4(c), as requested.

b. You may not exercise any of the rights granted to You in Section 3 above in any manner that is primarily intended for or directed toward commercial advantage or private monetary compensation. The exchange of the Work for other copyrighted works by means of digital file-sharing or otherwise shall not be considered to be intended for or directed toward commercial advantage or private monetary compensation, provided there is no payment of any monetary compensation in connection with the exchange of copyrighted works.

c. If You Distribute, or Publicly Perform the Work or Collections, You must, unless a request has been made pursuant to Section 4(a), keep intact all copyright notices for the Work and provide, reasonable to the medium or means You are utilizing: (i) the name of the Original Author (or pseudonym, if applicable) if supplied, and/or if the Original Author and/or Licensor designate another party or parties (e.g., a sponsor institute, publishing entity, journal) for attribution ("Attribution Parties") in Licensor's copyright notice, terms of service or by other reasonable means, the name of such party or parties; (ii) the title of the Work if supplied; (iii) to the extent reasonably practicable, the URI, if any, that Licensor specifies to be associated with the Work, unless such URI does not refer to the copyright notice or licensing information for the Work. The credit required by this Section 4(c) may be implemented in any reasonable manner; provided, however, that in the case of a Collection, at a minimum such credit will appear, if a credit for all contributing authors of Collection appears, then as part of these credits and in a manner at least as prominent as the credits for the other contributing authors. For the avoidance of doubt, You may only use the credit required by this Section for the purpose of attribution in the manner set out above and, by exercising Your rights under this License, You may not implicitly or explicitly assert or imply any connection with, sponsorship or endorsement by the Original Author, Licensor and/or Attribution Parties, as appropriate, of You or Your use of the Work, without the separate, express prior written permission of the Original Author, Licensor and/or Attribution Parties.

d. For the avoidance of doubt:

   i. **Non-waivable Compulsory License Schemes**. In those jurisdictions in which the right to collect royalties through any statutory or compulsory licensing scheme cannot be waived, the Licensor reserves the exclusive right to collect such royalties for any exercise by You of the rights granted under this License;

   ii. **Waivable Compulsory License Schemes**. In those jurisdictions in which the right to collect royalties through any statutory or compulsory licensing scheme can be waived, the Licensor reserves the exclusive right to collect such royalties for any exercise by You of the rights granted under this License if Your exercise of such rights is for a purpose or use which is otherwise than noncommercial as permitted under Section 4(b) and otherwise waives the right to collect royalties through any statutory or compulsory licensing scheme; and,

   iii. **Voluntary License Schemes**. The Licensor reserves the right to collect royalties, whether individually or, in the event that the Licensor is a member of a collecting society that administers voluntary licensing schemes, via that society, from any exercise by You of the rights granted under this License that is for a purpose or use which is otherwise than noncommercial as permitted under Section 4(b).

e. Except as otherwise agreed in writing by the Licensor or as may be otherwise permitted by applicable law, if You Reproduce, Distribute or Publicly Perform the Work either by itself or as part of any Collections, You must not distort, mutilate, modify or take other derogatory action in relation to the Work which would be prejudicial to the Original Author's honor or reputation.

5. Representations, Warranties and Disclaimer

UNLESS OTHERWISE MUTUALLY AGREED BY THE PARTIES IN WRITING, LICENSOR OFFERS THE WORK AS-IS AND MAKES NO REPRESENTATIONS OR WARRANTIES OF ANY KIND CONCERNING THE WORK, EXPRESS, IMPLIED, STATUTORY OR OTHERWISE, INCLUDING, WITHOUT LIMITATION, WARRANTIES OF TITLE, MERCHANTIBILITY, FITNESS FOR A PARTICULAR PURPOSE, NONINFRINGEMENT, OR THE ABSENCE OF LATENT OR OTHER DEFECTS, ACCURACY, OR THE PRESENCE OF ABSENCE OF ERRORS, WHETHER OR NOT DISCOVERABLE. SOME JURISDICTIONS DO NOT ALLOW THE EXCLUSION OF IMPLIED WARRANTIES, SO SUCH EXCLUSION MAY NOT APPLY TO YOU.

6. Limitation on Liability. EXCEPT TO THE EXTENT REQUIRED BY APPLICABLE LAW, IN NO EVENT WILL LICENSOR BE LIABLE TO YOU ON ANY LEGAL THEORY FOR ANY SPECIAL, INCIDENTAL, CONSEQUENTIAL, PUNITIVE OR EXEMPLARY DAMAGES ARISING OUT OF THIS LICENSE OR THE USE OF THE WORK, EVEN IF LICENSOR HAS BEEN ADVISED OF THE POSSIBILITY OF SUCH DAMAGES.

7. Termination

a. This License and the rights granted hereunder will terminate automatically upon any breach by You of the terms of this License. Individuals or entities who have received Collections from You under this License, however, will not have their licenses terminated provided such individuals or entities remain in full compliance with those licenses. Sections 1, 2, 5, 6, 7, and 8 will survive any termination of this License.

b. Subject to the above terms and conditions, the license granted here is perpetual (for the duration of the applicable copyright in the Work). Notwithstanding the above, Licensor reserves the right to release the Work under different license terms or to stop distributing the Work at any time; provided, however that any such election will not serve to withdraw this License (or any other license that has been, or is required to be, granted under the terms of this License), and this License will continue in full force and effect unless terminated as stated above.

8. Miscellaneous

a. Each time You Distribute or Publicly Perform the Work or a Collection, the Licensor offers to the recipient a license to the Work on the same terms and conditions as the license granted to You under this License.

b. If any provision of this License is invalid or unenforceable under applicable law, it shall not affect the validity or enforceability of the remainder of the terms of this License, and without further action by the parties to this agreement, such provision shall be reformed to the minimum extent necessary to make such provision valid and enforceable.

c. No term or provision of this License shall be deemed waived and no breach consented to unless such waiver or consent shall be in writing and signed by the party to be charged with such waiver or consent.

d. This License constitutes the entire agreement between the parties with respect to the Work licensed here. There are no understandings, agreements or representations with respect to the Work not specified here. Licensor shall not be bound by any additional provisions that may appear in any communication from You. This License may not be modified without the mutual written agreement of the Licensor and You.

e. The rights granted under, and the subject matter referenced, in this License were drafted utilizing the terminology of the Berne Convention for the Protection of Literary and Artistic Works (as amended on September 28, 1979), the Rome Convention of 1961, the WIPO Copyright Treaty of 1996, the WIPO Performances and Phonograms Treaty of 1996 and the Universal Copyright Convention (as revised on July 24, 1971). These rights and subject matter take effect in the relevant jurisdiction in which the License terms are sought to be enforced according to the corresponding provisions of the implementation of those treaty provisions in the applicable national law. If the standard suite of rights granted under applicable copyright law includes additional rights not granted under this License, such additional rights are deemed to be included in the License; this License is not intended to restrict the license of any rights under applicable law.

Creative Commons Notice

Creative Commons is not a party to this License, and makes no warranty whatsoever in connection with the Work. Creative Commons will not be liable to You or any party on any legal theory for any damages whatsoever, including without limitation any general, special, incidental or consequential damages arising in connection to this license. Notwithstanding the foregoing two (2) sentences, if Creative Commons has expressly identified itself as the Licensor hereunder, it shall have all rights and obligations of Licensor.

Except for the limited purpose of indicating to the public that the Work is licensed under the CCPL, Creative Commons does not authorize the use by either party of the trademark "Creative Commons" or any related trademark or logo of Creative Commons without the prior written consent of Creative Commons. Any permitted use will be in compliance with Creative Commons' then-current trademark usage guidelines, as may be published on its website or otherwise made available upon request from time to time. For the avoidance of doubt, this trademark restriction does not form part of this License.

Creative Commons may be contacted at **https://creativecommons.org/**.

Creative Commons Attribution 4.0 International License

A copy of the license is presented below, and can also be found at https://creativecommons.org/licenses/by/4.0/legalcode.

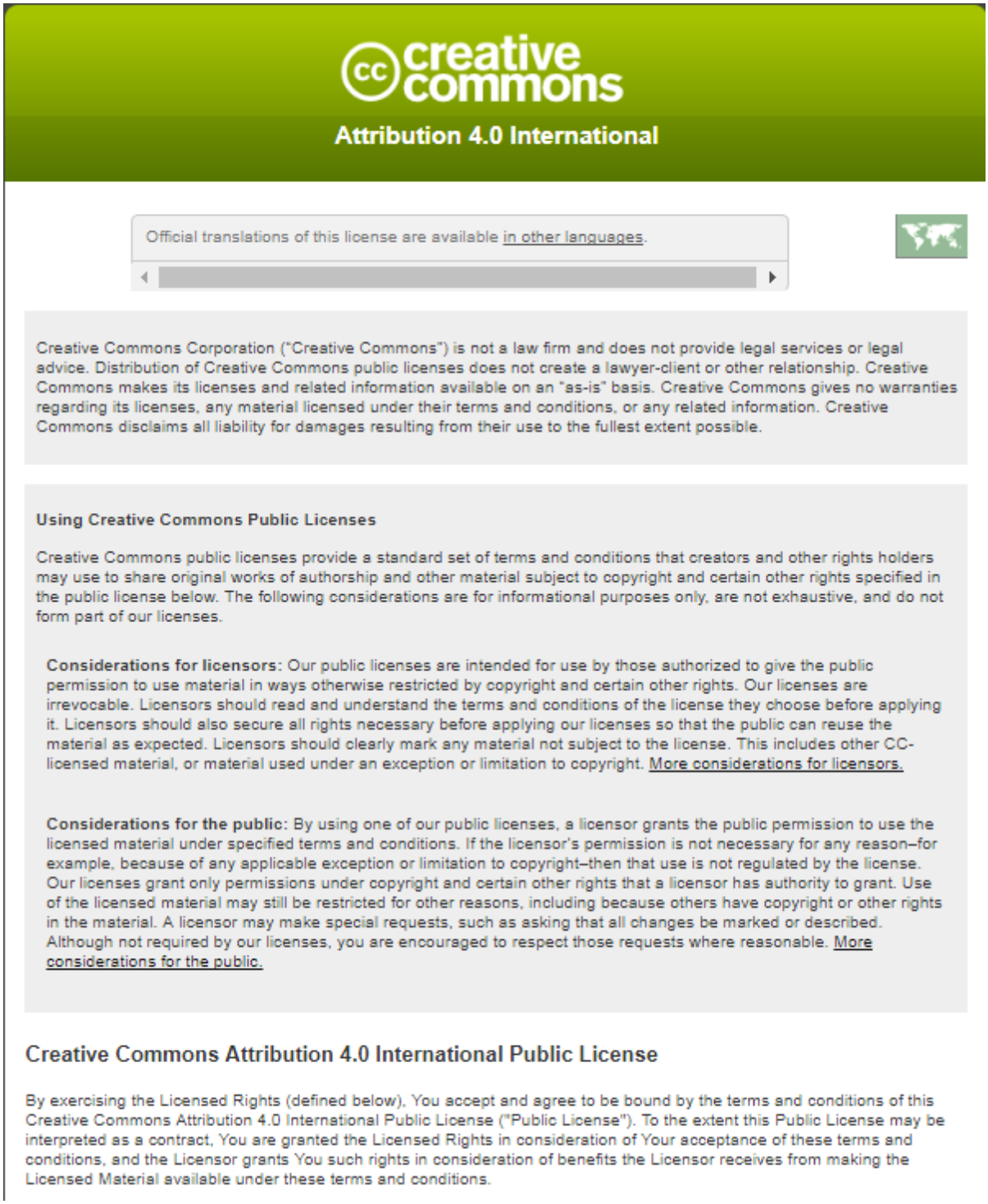

creative commons

Attribution 4.0 International

Official translations of this license are available in other languages.

Creative Commons Corporation ("Creative Commons") is not a law firm and does not provide legal services or legal advice. Distribution of Creative Commons public licenses does not create a lawyer-client or other relationship. Creative Commons makes its licenses and related information available on an "as-is" basis. Creative Commons gives no warranties regarding its licenses, any material licensed under their terms and conditions, or any related information. Creative Commons disclaims all liability for damages resulting from their use to the fullest extent possible.

Using Creative Commons Public Licenses

Creative Commons public licenses provide a standard set of terms and conditions that creators and other rights holders may use to share original works of authorship and other material subject to copyright and certain other rights specified in the public license below. The following considerations are for informational purposes only, are not exhaustive, and do not form part of our licenses.

Considerations for licensors: Our public licenses are intended for use by those authorized to give the public permission to use material in ways otherwise restricted by copyright and certain other rights. Our licenses are irrevocable. Licensors should read and understand the terms and conditions of the license they choose before applying it. Licensors should also secure all rights necessary before applying our licenses so that the public can reuse the material as expected. Licensors should clearly mark any material not subject to the license. This includes other CC-licensed material, or material used under an exception or limitation to copyright. More considerations for licensors.

Considerations for the public: By using one of our public licenses, a licensor grants the public permission to use the licensed material under specified terms and conditions. If the licensor's permission is not necessary for any reason–for example, because of any applicable exception or limitation to copyright–then that use is not regulated by the license. Our licenses grant only permissions under copyright and certain other rights that a licensor has authority to grant. Use of the licensed material may still be restricted for other reasons, including because others have copyright or other rights in the material. A licensor may make special requests, such as asking that all changes be marked or described. Although not required by our licenses, you are encouraged to respect those requests where reasonable. More considerations for the public.

Creative Commons Attribution 4.0 International Public License

By exercising the Licensed Rights (defined below), You accept and agree to be bound by the terms and conditions of this Creative Commons Attribution 4.0 International Public License ("Public License"). To the extent this Public License may be interpreted as a contract, You are granted the Licensed Rights in consideration of Your acceptance of these terms and conditions, and the Licensor grants You such rights in consideration of benefits the Licensor receives from making the Licensed Material available under these terms and conditions.

Section 1 – Definitions.

a. **Adapted Material** means material subject to Copyright and Similar Rights that is derived from or based upon the Licensed Material and in which the Licensed Material is translated, altered, arranged, transformed, or otherwise modified in a manner requiring permission under the Copyright and Similar Rights held by the Licensor. For purposes of this Public License, where the Licensed Material is a musical work, performance, or sound recording, Adapted Material is always produced where the Licensed Material is synched in timed relation with a moving image.

b. **Adapter's License** means the license You apply to Your Copyright and Similar Rights in Your contributions to Adapted Material in accordance with the terms and conditions of this Public License.

c. **Copyright and Similar Rights** means copyright and/or similar rights closely related to copyright including, without limitation, performance, broadcast, sound recording, and Sui Generis Database Rights, without regard to how the rights are labeled or categorized. For purposes of this Public License, the rights specified in Section 2(b)(1)-(2) are not Copyright and Similar Rights.

d. **Effective Technological Measures** means those measures that, in the absence of proper authority, may not be circumvented under laws fulfilling obligations under Article 11 of the WIPO Copyright Treaty adopted on December 20, 1996, and/or similar international agreements.

e. **Exceptions and Limitations** means fair use, fair dealing, and/or any other exception or limitation to Copyright and Similar Rights that applies to Your use of the Licensed Material.

f. **Licensed Material** means the artistic or literary work, database, or other material to which the Licensor applied this Public License.

g. **Licensed Rights** means the rights granted to You subject to the terms and conditions of this Public License, which are limited to all Copyright and Similar Rights that apply to Your use of the Licensed Material and that the Licensor has authority to license.

h. **Licensor** means the individual(s) or entity(ies) granting rights under this Public License.

i. **Share** means to provide material to the public by any means or process that requires permission under the Licensed Rights, such as reproduction, public display, public performance, distribution, dissemination, communication, or importation, and to make material available to the public including in ways that members of the public may access the material from a place and at a time individually chosen by them.

j. **Sui Generis Database Rights** means rights other than copyright resulting from Directive 96/9/EC of the European Parliament and of the Council of 11 March 1996 on the legal protection of databases, as amended and/or succeeded, as well as other essentially equivalent rights anywhere in the world.

k. **You** means the individual or entity exercising the Licensed Rights under this Public License. **Your** has a corresponding meaning.

Section 2 – Scope.

a. **License grant.**
   1. Subject to the terms and conditions of this Public License, the Licensor hereby grants You a worldwide, royalty-free, non-sublicensable, non-exclusive, irrevocable license to exercise the Licensed Rights in the Licensed Material to:
      A. reproduce and Share the Licensed Material, in whole or in part; and
      B. produce, reproduce, and Share Adapted Material.
   2. Exceptions and Limitations. For the avoidance of doubt, where Exceptions and Limitations apply to Your use, this Public License does not apply, and You do not need to comply with its terms and conditions.
   3. Term. The term of this Public License is specified in Section 6(a).
   4. Media and formats; technical modifications allowed. The Licensor authorizes You to exercise the Licensed Rights in all media and formats whether now known or hereafter created, and to make technical modifications necessary to do so. The Licensor waives and/or agrees not to assert any right or authority to forbid You from making technical modifications necessary to exercise the Licensed Rights, including technical modifications necessary to circumvent Effective Technological Measures. For purposes of this Public License, simply making modifications authorized by this Section 2(a)(4) never produces Adapted Material.
   5. Downstream recipients.
      A. Offer from the Licensor – Licensed Material. Every recipient of the Licensed Material automatically receives an offer from the Licensor to exercise the Licensed Rights under the terms and conditions of this Public License.

B. No downstream restrictions. You may not offer or impose any additional or different terms or conditions on, or apply any Effective Technological Measures to, the Licensed Material if doing so restricts exercise of the Licensed Rights by any recipient of the Licensed Material.

6. No endorsement. Nothing in this Public License constitutes or may be construed as permission to assert or imply that You are, or that Your use of the Licensed Material is, connected with, or sponsored, endorsed, or granted official status by, the Licensor or others designated to receive attribution as provided in Section 3(a)(1)(A)(i).

b. **Other rights**.

1. Moral rights, such as the right of integrity, are not licensed under this Public License, nor are publicity, privacy, and/or other similar personality rights; however, to the extent possible, the Licensor waives and/or agrees not to assert any such rights held by the Licensor to the limited extent necessary to allow You to exercise the Licensed Rights, but not otherwise.
2. Patent and trademark rights are not licensed under this Public License.
3. To the extent possible, the Licensor waives any right to collect royalties from You for the exercise of the Licensed Rights, whether directly or through a collecting society under any voluntary or waivable statutory or compulsory licensing scheme. In all other cases the Licensor expressly reserves any right to collect such royalties.

Section 3 – License Conditions.

Your exercise of the Licensed Rights is expressly made subject to the following conditions.

a. **Attribution**.

1. If You Share the Licensed Material (including in modified form), You must:

A. retain the following if it is supplied by the Licensor with the Licensed Material:
i. identification of the creator(s) of the Licensed Material and any others designated to receive attribution, in any reasonable manner requested by the Licensor (including by pseudonym if designated);
ii. a copyright notice;
iii. a notice that refers to this Public License;
iv. a notice that refers to the disclaimer of warranties;
v. a URI or hyperlink to the Licensed Material to the extent reasonably practicable;

B. indicate if You modified the Licensed Material and retain an indication of any previous modifications; and

C. indicate the Licensed Material is licensed under this Public License, and include the text of, or the URI or hyperlink to, this Public License.

2. You may satisfy the conditions in Section 3(a)(1) in any reasonable manner based on the medium, means, and context in which You Share the Licensed Material. For example, it may be reasonable to satisfy the conditions by providing a URI or hyperlink to a resource that includes the required information.
3. If requested by the Licensor, You must remove any of the information required by Section 3(a)(1)(A) to the extent reasonably practicable.
4. If You Share Adapted Material You produce, the Adapter's License You apply must not prevent recipients of the Adapted Material from complying with this Public License.

Section 4 – Sui Generis Database Rights.

Where the Licensed Rights include Sui Generis Database Rights that apply to Your use of the Licensed Material:

a. for the avoidance of doubt, Section 2(a)(1) grants You the right to extract, reuse, reproduce, and Share all or a substantial portion of the contents of the database;

b. if You include all or a substantial portion of the database contents in a database in which You have Sui Generis Database Rights, then the database in which You have Sui Generis Database Rights (but not its individual contents) is Adapted Material; and

c. You must comply with the conditions in Section 3(a) if You Share all or a substantial portion of the contents of the database.

For the avoidance of doubt, this Section 4 supplements and does not replace Your obligations under this Public License where the Licensed Rights include other Copyright and Similar Rights.

Section 5 – Disclaimer of Warranties and Limitation of Liability.

a. **Unless otherwise separately undertaken by the Licensor, to the extent possible, the Licensor offers the Licensed Material as-is and as-available, and makes no representations or warranties of any kind concerning the Licensed Material, whether express, implied, statutory, or other. This includes, without limitation, warranties of title, merchantability, fitness for a particular purpose, non-infringement, absence of latent or other defects, accuracy, or the presence or absence of errors, whether or not known or discoverable. Where disclaimers of warranties are not allowed in full or in part, this disclaimer may not apply to You.**

b. **To the extent possible, in no event will the Licensor be liable to You on any legal theory (including, without limitation, negligence) or otherwise for any direct, special, indirect, incidental, consequential, punitive, exemplary, or other losses, costs, expenses, or damages arising out of this Public License or use of the Licensed Material, even if the Licensor has been advised of the possibility of such losses, costs, expenses, or damages. Where a limitation of liability is not allowed in full or in part, this limitation may not apply to You.**

c. The disclaimer of warranties and limitation of liability provided above shall be interpreted in a manner that, to the extent possible, most closely approximates an absolute disclaimer and waiver of all liability.

Section 6 – Term and Termination.

a. This Public License applies for the term of the Copyright and Similar Rights licensed here. However, if You fail to comply with this Public License, then Your rights under this Public License terminate automatically.

b. Where Your right to use the Licensed Material has terminated under Section 6(a), it reinstates:

   1. automatically as of the date the violation is cured, provided it is cured within 30 days of Your discovery of the violation; or

   2. upon express reinstatement by the Licensor.

   For the avoidance of doubt, this Section 6(b) does not affect any right the Licensor may have to seek remedies for Your violations of this Public License.

c. For the avoidance of doubt, the Licensor may also offer the Licensed Material under separate terms or conditions or stop distributing the Licensed Material at any time; however, doing so will not terminate this Public License.

d. Sections 1, 5, 6, 7, and 8 survive termination of this Public License.

Section 7 – Other Terms and Conditions.

a. The Licensor shall not be bound by any additional or different terms or conditions communicated by You unless expressly agreed.

b. Any arrangements, understandings, or agreements regarding the Licensed Material not stated herein are separate from and independent of the terms and conditions of this Public License.

Section 8 – Interpretation.

a. For the avoidance of doubt, this Public License does not, and shall not be interpreted to, reduce, limit, restrict, or impose conditions on any use of the Licensed Material that could lawfully be made without permission under this Public License.

b. To the extent possible, if any provision of this Public License is deemed unenforceable, it shall be automatically reformed to the minimum extent necessary to make it enforceable. If the provision cannot be reformed, it shall be severed from this Public License without affecting the enforceability of the remaining terms and conditions.

c. No term or condition of this Public License will be waived and no failure to comply consented to unless expressly agreed to by the Licensor.

d. Nothing in this Public License constitutes or may be interpreted as a limitation upon, or waiver of, any privileges and immunities that apply to the Licensor or You, including from the legal processes of any jurisdiction or authority.

Appendix D:

Dornan MH[1], **Krishnan R[1]**, Macklin AM[1], Selman M, El Sayes N, Son HH, Davis C, Chen A, Keillor K, Le PJ, Moi C, Ou P, Pardin C, Canez CR, Le Boeuf F, Bell JC, Smith JC, Diallo JS, Boddy CN. "First-in-class small molecule potentiators of cancer virotherapy." *Scientific Reports*. 26;6:26786 (2016) doi: 10.1038/srep26786.

[1]Equal contribution

SCIENTIFIC REPORTS

OPEN

First-in-class small molecule potentiators of cancer virotherapy

Mark H. Dornan[1,*], Ramya Krishnan[2,3,*], Andrew M. Macklin[4,*], Mohammed Selman[2,3], Nader El Sayes[2,3], Hwan Hee Son[2,3], Colin Davis[2,3], Andrew Chen[2], Kerkeslin Keillor[1], Penny J. Le[1], Christina Moi[1], Paula Ou[2,3], Christophe Pardin[1], Carlos R. Canez[4], Fabrice Le Boeuf[2], John C. Bell[2,3], Jeffrey C. Smith[4], Jean-Simon Diallo[2,3] & Christopher N. Boddy[1]

Received: 09 September 2015
Accepted: 09 May 2016
Published: 26 May 2016

The use of engineered viral strains such as gene therapy vectors and oncolytic viruses (OV) to selectively destroy cancer cells is poised to make a major impact in the clinic and revolutionize cancer therapy. In particular, several studies have shown that OV therapy is safe and well tolerated in humans and can infect a broad range of cancers. Yet in clinical studies OV therapy has highly variable response rates. The heterogeneous nature of tumors is widely accepted to be a major obstacle for OV therapeutics and highlights a need for strategies to improve viral replication efficacy. Here, we describe the development of a new class of small molecules for selectively enhancing OV replication in cancer tissue. Medicinal chemistry studies led to the identification of compounds that enhance multiple OVs and gene therapy vectors. Lead compounds increase OV growth up to 2000-fold *in vitro* and demonstrate remarkable selectivity for cancer cells over normal tissue *ex vivo* and *in vivo*. These small molecules also demonstrate enhanced stability with reduced electrophilicity and are highly tolerated in animals. This pharmacoviral approach expands the scope of OVs to include resistant tumors, further potentiating this transformative therapy. It is easily foreseeable that this approach can be applied to therapeutically enhance other attenuated viral vectors.

Genetically attenuated viruses form the basis of a growing number of biotechnology and pharmaceutical platforms, including oncolytic viruses (OVs) and gene therapy vectors for the treatment of cancers. In particular, OV therapy has shown significant promise with strong clinical evidence demonstrating that OVs can lead to profound anti-tumor responses in patients[1,2] with very mild side-effects, often described as acute flu-like symptoms[2]. OVs are based on a wide range of viral backbones from small RNA viruses like rhabdoviruses, to large DNA viruses such as herpesviruses (HSV) and are currently being evaluated in clinical trials to treat a range of cancer types[3]. OV therapeutics have been explored for over 60 years and in 2005, the oncolytic adenovirus H101 was approved in China for the treatment of head and neck cancers. Oncolytic HSV-1 expressing granulocyte macrophage colony stimulating factor has been approved in North America based on favourable phase III clinical trial data in melanoma (NCT00769704).

OVs have been selectively engineered to take advantage of several hallmarks of cancer in order to preferentially replicate in tumor cells. The increased metabolism of cancers, their resistance to apoptosis, and their often defective innate antiviral response provide fertile ground for most viruses[4]. Genetic attenuation of specific virulence genes generates viruses that are selectively attenuated in normal host cells but still capable of infecting cancer cells. When effective, OVs lead to durable cures by direct lysis of cancer cells, vascular shutdown, and through generation of a strong anti-tumor immune response[4].

Heterogeneity in the clinical response to OVs remains a major hurdle to overcome, as demonstrated in several human clinical trials[2,3,5]. Because an estimated 30–35% of tumors have effective antiviral defenses[4,6,7], it is no surprise that OVs show tremendous effects in some models and patients but have minimal impact in others. Given that innate cellular antiviral responses can compromise the therapeutic efficacy of OVs, developing

[1]Departments of Chemistry and Biomolecular Sciences, University of Ottawa, Ottawa, Ontario, Canada. [2]Centre for Innovative Cancer Research, Ottawa Hospital Research Institute, Ottawa, Ontario, Canada. [3]Department of Biochemistry, Microbiology and Immunology, University of Ottawa, Ontario, Canada. [4]Department of Chemistry and Institute of Biochemistry, Carleton University, Ottawa, Ontario, Canada. *These authors contributed equally to this work. Correspondence and requests for materials should be addressed to J.C.S. (email: jeff.smith@carleton.ca) or J.-S.D. (email: jsdiallo@ohri.ca) or C.N.B. (email: cboddy@uottawa.ca)

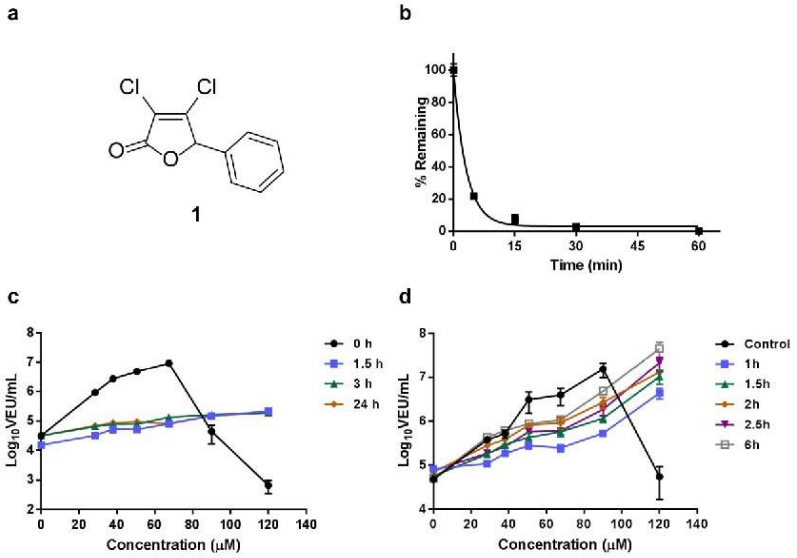

Figure 1. Compound 1 acts quickly but suffers from rapid degradation. (**a**) Structure of **1** (3,4-dichloro-5-phenyl-5H-furan-2-one). (**b**) Stability of **1** in mouse serum over time measured by HPLC (**c**) **1** was incubated in sterile water for 0 h, 1.5 h, 3 h or 24 h before being used to treat 786-0 cells at different concentrations. 4 hours post-treatment, cells were infected with VSVΔ 51 expressing firefly luciferase (VSVΔ 51-FLuc) at a multiplicity of infection (MOI) of 0.005. 40 hours later, virus output in viral expression units (VEUs) per millilitre was measured with a previously describe luciferase reporter assay[12]. (**d**) 786-0 cells were treated with **1** at various doses. **1** was removed and replaced with fresh media after 1 h, 1.5 h, 2 h, 2.5 h and 6 h. **1** was not removed in the control condition. 4 hours post-treatment, cells were infected with VSVΔ 51 expressing firefly luciferase VSVΔ 51-FLuc at an MOI of 0.005. For the condition where **1** was replaced with fresh media 6 h after treatment, infection was performed immediately following media replacement. 40 hours later, virus output in viral expression units (VEUs) per millilitre was measured with a previously describe luciferase reporter assay[12].

pharmaceuticals that target this complex cellular defense mechanism will have important clinical ramifications, improving current OV therapies and enabling the development of new therapeutic strategies[3,8,9].

We recently identified compounds from a high-throughput screen that sensitize resistant cancer cells to infection with the rhabdovirus-based OV named VSVΔ 51[10]. VSVΔ 51 is an engineered mutant of vesicular stomatitis virus (VSV) that is highly sensitive to interferon (IFN) and its antiviral effects. Much like HSV-1 and many other OVs, VSVΔ 51 faces a roadblock in tumors that retain effective cellular antiviral responses. The most active compound from this screen (**1**, Figs 1a and 2), was shown to enhance VSVΔ 51 oncolysis *in vitro* and *in vivo*, where virus output was increased by as much as 1,000-fold in cancer cells[10]. **1** has been shown to dampen the activation of antiviral responses in cancer cells, including the transcriptional response to type I IFN[10]. Given the impact of tumor heterogeneity on the clinical response to OVs, there is an unmet need and an opportunity to develop small molecule potentiators such as **1** to improve OV therapy. The electrophilic nature of **1** prompted us to investigate the scaffold to identify active analogs with more favourable physiochemical properties and explore structure-activity relationships. Herein we report the development of first-in-class small molecules with favourable pharmacological properties and demonstrate that they significantly enhance OV propagation selectively in resistant cancers *in vitro*, *ex vivo*, and *in vivo*, completing proof-of-concept studies for a pharmacoviral combination approach to enhancing OV therapy.

Results

1 suffers from rapid degradation. To gain a better understanding of the physiochemical nature of **1**, we measured the compound's stability in mouse serum with an LC/MRM assay (Fig. 1b). Degradation occurred very quickly ($t_{1/2}$ = 2.1 min). **1** showed similar degradation behaviour in a simple aqueous medium (data not shown), which resulted in reduced biological activity. Pre-incubation of **1** in aqueous media for as little as 90 min was sufficient to eliminate the robust enhancement of VSVΔ 51 titers otherwise observed (Fig. 1c). However, the effect of **1** on viral growth is rapid and sustained. Treatment of cells with **1** for as little as 60 min followed by its complete removal from cell culture media and subsequent infection with VSVΔ 51 of drug treatment resulted in substantial enhancement of viral titers (Fig. 1d).

Compound ID	Structure	Peak fold enhancement (dose (μM))	GSH half-life (min)	Plasma stab. % remaning at 3 hrs	Compound ID	Structure	Peak fold enhancement (dose (μM))	GSH half-life (min)	Plasma stab. % remaning at 3 hrs
1		1810 (60 μM)	<5	0	24		915 (120 μM)	61	91.6 ± 5.2
3		365 (96 μM)	NR	65.6 ± 6.5	25		1415 (80 μM)	53	54.8 ± 3.6
4		345 (80 μM)	NR	0	28		1810 (80 μM)	66	36.9 ± 5.2
5		515 (36 μM)	<5	0	29	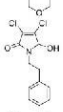	975 (72 μM)	74	57.6 ± 6.6
6		400 (60 μM)	<5	0	30	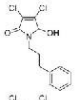	1090 (32 μM)	50	42.9 ± 7.2
9		1260 (120 μM)	117	0	38		870 (216 μM)	32	25.7 ± 2.9
10		555 (48 μM)	32	19.8 ± 0.4	40		2005 (27 μM)	32	15.3 ± 2.5

Figure 2. The structure of the analogs investigated in this study, their ability to enhance VSVΔ 51 activity, their half-life in a glutathione challenge assay, and their stability in serum.

Derivatives with improved properties and activity. These observations provided a rationale to derive novel compounds based on **1** with increased stability. Taking advantage of the versatile reactions that mucochloric acid can undergo[11], a diverse set of analogs (**1–10**) was synthesized to reveal structure-activity relationships (Supplementary Table 1). Analogs were screened for their ability to augment VSVΔ 51 activity in OV resistant 786-0 renal cancer cells using a previously described high-throughput luciferase reporter-based titration assay[12] and their maximal viral enhancing activity was compared to that of **1**. Cytotoxicity in the presence and absence of virus was also assessed using an alamarBlue® metabolic dye. Analog stability was measured with a plasma stability assay as well as a glutathione stability assay, which indicated physiochemical susceptibility to act as a Michael-acceptor.

Substitution of the β-chlorine with an alkyl amine resulted in compounds with dramatically increased stability but loss of viral enhancement activity (**3** and **4**). Removal of the aryl group (**5**) or replacement with a methoxide group (**6**) resulted in active compounds with poor stability similar to **1** (Supplementary Table 1). Encouragingly, compounds with a pyrrole-based scaffold (**9** and **10**) enhanced viral growth and showed remarkably improved stability by both the GSH and plasma stability assays. The LC/MS trace observed in the GSH stability assay also showed that **10**, contrary to **1**, cleanly reacted with the nucleophile to form the glutathione adduct as the sole detectable product (Fig. 3a,b). Similar to **1**, the impact of **10** on viral growth was found to be rapid and sustained (Fig. 3c).

Given these results, we decided to further explore the pyrrole scaffold from **10** (Supplementary Table 1). Analogs with alterations to the hydroxyl group (**11–15**) abolished activity, as did alterations to the dichloro- moiety (**16–21**). We then decided to investigate various substitutions on the pyrrole amine (Supplementary Table 1). Cyclopropyl and morpholine containing analogs (**25** and **28**) displayed retained activity and remarkably improved *in vitro* toxicity and stability profiles. Examination of arylamine containing analogs showed that the spacer length between the amine and phenyl ring was optimal at three carbons (**10**, **29**, **30** and **31**). Testing a large set of substituted benzylamine derivatives (**36–51**) demonstrated that the 4-trifluoromethyl substituted system (**40**) possessed improved activity (2,000 fold enhancement, 105% of **1**) and improved stability. Overall the activity and stability of the analogs could be readily tuned.

While initial analog screening studies were carried out in highly virus-resistant human 786-0 renal cancer cells, mouse cancer cell lines originating from skin (B16-F10), colon (CT26) and breast (4T1), were also sensitized to VSVΔ 51 by pyrrole-based analogs (Supplementary Figs 1–3). **1**, **10** and several other pyrrole analogs

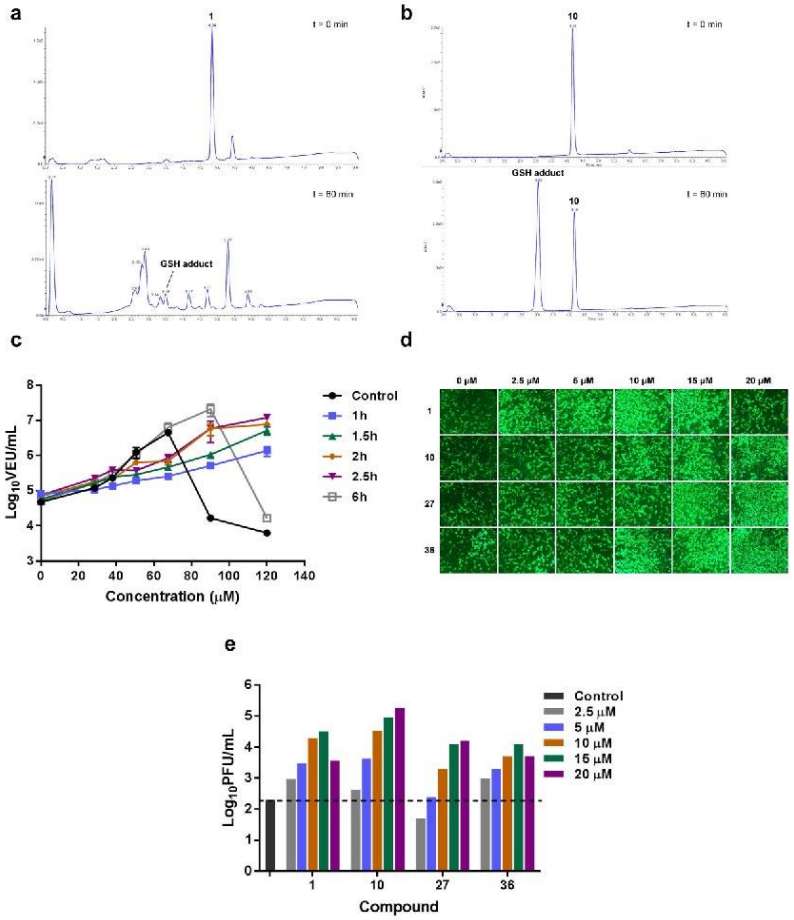

Figure 3. Pyrrole-based derivatives of 1 have improved stability but retain rapid, robust activity with oncolytic VSV and HSV-1 . (**a**) 250 μL of 40 mM DMSO stock solution of **1** was added to L-glutathione (15.4 mg, 5 mol equiv.) suspended in 250 μL DMSO. The resulting mixture was placed in a 37 °C shaker. 10 μL aliquots were removed and quenched in 990 μL water (containing 0.5% formic acid) at various time points (t = 0 minutes and t = 60 minutes shown). Analysis by ESI-LC-MS allowed for the identification and quantification of **1** and the glutathione adduct by UV-Vis at 254 nm. (**b**) 250 μL of 40 mM DMSO stock solution of **10** was added to L-glutathione (15.4 mg, 5 mol equiv.) suspended in 250 μL DMSO. The resulting mixture was placed in a 37 °C shaker. 10 μL aliquots were removed and quenched in 990 μL water (containing 0.5% formic acid) at various time points (t = 0 minutes and t = 60 minutes shown). Analysis by ESI-LC-MS allowed for the identification and quantification of **10** and the glutathione adduct by UV-Vis at 254 nm. (**c**) 786-0 cells were treated with **10** at various doses. **10** was removed and replaced with fresh media after 1 h, 1.5 h, 2 h, 2.5 h and 6 h. **10** was not removed in the control condition. 4 hours post-treatment, cells were infected with VSVΔ 51 expressing firefly luciferase (VSVΔ 51-FLuc at a multiplicity of infection (MOI) of 0.005). For the condition where **10** was replaced with fresh media 6 h after treatment, infection was performed immediately following media replacement. 40 hours later, virus output in viral expression units (VEUs) per millilitre was measured with a previously describe luciferase reporter assay[12]. (**d**) Mouse mammary carcinoma (4T1) cells were left untreated or, treated with **1**, **10**, **27**, or **36** for 4 h at various concentrations: 2.5 μM, 5 μM, 10 μM, 15 μM or 20 μM. ICP0-null HSV-N212eGFP was then added at MOI 0.005. eGFP fluorescence was detected 48 h after HSV infection. (**e**) HSV titers were determined 48 h after infection.

increased the oncolytic activity of Maraba MG-1 virus[13] (Supplementary Fig. 3) as well as spread of oncolytic HSV-1 expressing GFP[14] as observed by fluorescence microscopy and standard plaque assay (Fig. 3d,e, and Supplementary Fig. 4), suggesting the compounds have a broader scope of application for virus-based therapies. Luciferase transgene expression delivered to human A549 lung cancer cells by non-replicating adenovirus and adeno-associated virus (AAV) vectors (Supplementary Fig. 5a,b respectively) was also enhanced by the compounds, suggesting the potentiating effect of the compounds is not limited to replicating viruses.

Selective viral enhancement in *ex vivo* tumor specimens. To facilitate evaluation of a larger number of compounds prior to *in vivo* testing, we chose to test a subset of analogs (**1**, **10**, **28**–**30** and **40**, Fig. 2) for their ability to enhance VSVΔ 51 oncolysis in *ex vivo* tissue samples using an established method[15]. Tissue samples from VSVΔ 51 resistant CT26 murine colon cancer tumors[10,16,17] as well as normal mouse brain, lung and spleens were cored. Viable cores were selected for subsequent treatment with each compound and VSVΔ 51 expressing green fluorescent protein (VSVΔ 51-GFP). Figure 4a shows representative images of infected cores that were pre-treated with an optimized dose of compound. Corresponding viral titers as determined by plaque assay are shown in Fig. 4b–g and Supplementary Fig. 6. **1** and analogs robustly enhanced VSVΔ 51-GFP titers in CT26 colon cancer specimens. There was little to no enhancement of VSVΔ 51 in normal tissue specimens, indicating that the specificity of VSVΔ 51 towards tumour tissue is maintained following treatment with **1** and its derivatives.

Analogs are well-tolerated and enhance tumor specific OV replication *in vivo*. We proceeded to evaluate the *in vivo* tolerability of a subset of analogs, selected based on desirable physiochemical characteristics, *in vitro* activity and *ex vivo* activity. Compounds were administered intraperitoneally to non-tumor bearing Balb/c mice and body weight was monitored over several days. Mice were sacrificed when they reached the endpoint of 20% loss of body weight or showed significant outward signs of toxicity. Figure 5 shows that **1** leads to toxicity starting at a dose of 10 mg/kg. In contrast **10** was well tolerated up to a dose of 50 mg/kg and **24** and **28** up to 100 mg/kg.

Because it was highly active *ex vivo* and very well tolerated in mice, we proceeded to evaluate **28** for its ability to increase the infection of tumors with VSVΔ 51 expressing luciferase (VSVΔ 51-FLuc) *in vivo*. Balb/c mice were subcutaneously engrafted with CT26 cells and treated intra-tumorally with VSVΔ 51-FLuc alone or in combination with **28**. We used an *in vivo* imaging system (IVIS) to measure luciferase activity associated to virus replication 24 h post treatment. Figure 6a–c shows that compared to VSVΔ 51-FLuc alone, **28** significantly enhanced virus replication-associated luciferase expression specifically in the tumor. A similar treatment schedule was used to evaluate therapeutic efficacy in the human HT29 colon cancer xenograft model. The combination of **28** and VSVΔ 51-FLuc significantly delayed tumour progression and improved survival compared to the mono-therapies (Fig. 6d,e). This demonstrates the feasibility and potential of using small molecules, such as **28**, in combination with OV therapy *in vivo*.

Discussion

In this study, we identified a new class of pyrrole-based potentiators of tumor specific OV infection. Compared to the parent molecule **1**, these have substantially improved stability, reduced electrophilicity, and retained or improved ability to enhance growth of OVs in resistant cancer cell lines *in vitro* and *in vivo*.

There is a growing list of OV clinical candidates for the treatment of cancer including VSV, vaccinia virus, reovirus, poliovirus, adenovirus, and herpes simplex virus-based platforms[3]. Talimogene laherparepvec (T-Vec, Amgen), an intra-tumorally delivered HSV-1-based oncolytic virus expressing granulocyte-macrophage colony-stimulating factor (GM-CSF), has been recently approved for treatment of melanoma in North America. Nevertheless, it is well-recognized in the field that combination therapies will be necessary to overcome the heterogeneous response observed with these potentially curative biologics. The first-in-class agents we have developed in this study robustly increase growth of oncolytic VSV, (Fig. 2 and Supplementary Table 1), Maraba MG-1 (Supplementary Fig. 3), and HSV-1 (Fig. 3e) in otherwise resistant cancer cells and therefore cater to an unmet need in this therapeutic area. In this regard, we consider that pyrrole-based molecules have significant clinical potential due to their *in vivo* activity and high tolerability. Indeed, the combination of **28** and oncolytic VSV delivered intra-tumorally robustly improved survival in the human HT-29 colon cancer model. Enhanced therapeutic effect of the combination treatment was also observed when **10** was delivered by intra-peritoneal route in the mouse CT26 colon cancer model (Supplementary Fig. 7), suggesting systemic administration is feasible.

Further to this, we have observed that the pyrrole-based compounds derived in this study can also enhance transgene expression levels from replication-defective gene therapy vectors such as AAV and adenovirus (Supplementary Fig. 5a,b). This extends the potential of using these small molecules for co-administration with cancer gene therapies. There are numerous registered clinical trials employing gene therapy vectors expressing transgenes for the treatment of various malignancies. It is easily foreseeable that the pharmaco-viral approach described here can be applied to therapeutically enhance other attenuated viral vectors as well.

In this study, we have observed that similarly to **1**, pyrrole derivatives inhibit the production of IFNβ and various interferon-stimulated genes (ISGs) (Supplementary Fig. 8) and are able to block the antiviral effects of IFNβ (Supplementary Fig. 9). As such, it remains unclear whether this could also impact the adaptive immune response. This is relevant since in addition to viral oncolysis, generation of anti-tumor immunity is thought to contribute to the therapeutic effect of OVs[3]. Interestingly, other small molecules that dampen IFN response such as HDAC inhibitors can skew the immune response favourably in some contexts, where oncolytic virotherapy is coupled to a cancer vaccine approach[18]. Non-replicating gene therapy vectors such as adenovirus or AAV have been known to induce IFN[19,20]. Thus, dampening innate immunity is likely to be an advantage for cancer gene therapy applications where the objective is to express a therapeutic transgene, for example a pro-drug converting enzyme[21,22]. Clearly, the pyrrole derivatives described in this study lead to robust enhancement of

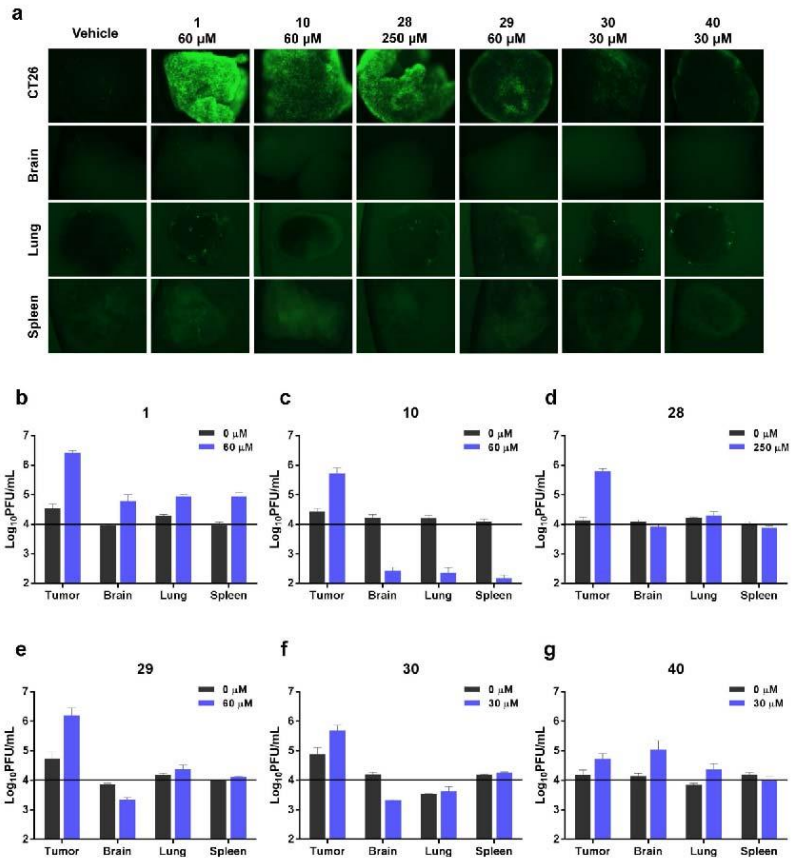

Figure 4. 1 and its analogs selectively enhance the replication of oncolytic VSV in *ex vivo* tumor tissues. (**a**) CT26 (murine colon carcinoma) tumors were grown subcutaneously in Balb/c mice for 24 days and subsequently excised and cored, along with normal brain, lung and spleen tissues. Tissue samples were treated in triplicate with various concentrations of compounds for 4 hours prior to infection with 1×10^4 plaque-forming units of vesicular stomatitis virus expressing GFP (VSVΔ 51-GFP). Virus replication was assessed by fluorescence microscopy 24 hours post- infection. Representative images from each triplicate set for the most effective concentration are shown. (**b–g**) Infected cores and corresponding supernatants were collected 36 hours post-infection. VSVΔ 51-GFP infection was quantified by standard plaque assay. Cores were homogenized prior to titering. Graphs show the sum of infectious titer from core and supernatant for each compound in each tissue type. Doses shown here are those that are depicted in panel (**a**). The horizontal black line on each graph at 1×10^4 PFU/mL represents the amount of VSVΔ 51-GFP used to initially infect each core.

luciferase transgene expressed by oncolytic VSV *in vivo* (Fig. 6) but also *in vitro* using non-replicating vectors (Supplementary Fig. 5a,b).

In addition to the broad potential therapeutic applications in combination with OVs and other virus-based therapies, the novel pyrrole-based molecules provide an arsenal of new probes to explore innate immunity. While the pyrrole-compounds described here clearly impact the antiviral IFN response as per **1** (Supplementary Figs 8,9), the precise molecular target remains elusive. The enhanced stability of the pyrrole-based analogs will provide opportunities to pursue target identification and/or activity based protein profiling. For example, the propargyl-based compound, **27**, synthesized in this study was found to be active and is amenable to click chemistry for inhibitor affinity capture or other relevant target identification strategies.

Relating to mechanism, one interesting property of the viral potentiators described in this study (including **1**) is the observed rapid and sustained activity. As little as 1 hour pre-treatment with the compounds, prior to

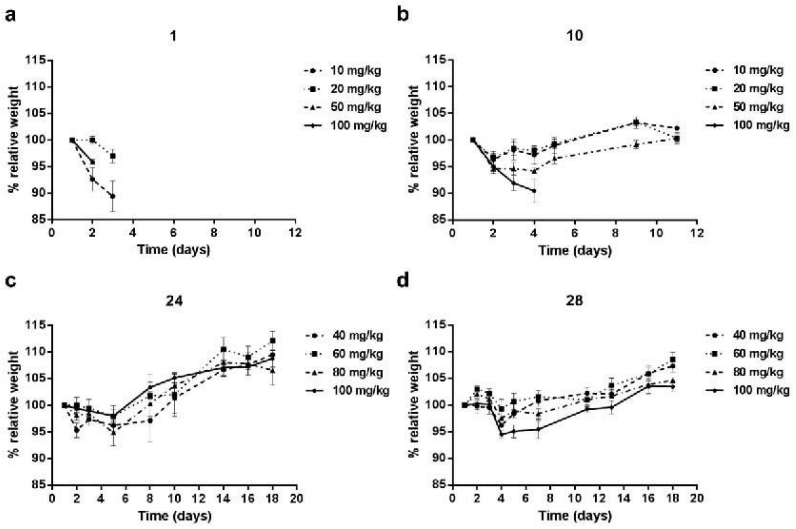

Figure 5. Pyrrole-based derivatives of 1 are substantially better tolerated in mice. Balb/c mice were given (**a**) **1**, (**b**) **10**, (**c**) **24**, or (**d**) **28** dissolved in DMSO via intraperitoneal administration. Five mice were assigned to each dose group for each compound. The dose was adjusted for individual mice based on weight. Graphs stop when the first mouse in the group was euthanized. (**a**,**b**) Mice were injected on Day 1 and weights were recorded over a 10 day period. (**c**,**d**) Mice were injected on Day 1, 3 and 5. Weights were recorded over an 18 day period. For all groups, weights are reported relative to initial weight on Day 1.

their complete removal from cell culture media, was sufficient to observe enhanced OV titers in cancer cells for up to 40 h (Figs 1d and 3c) . This suggests the possibility that these compounds irreversibly inhibit their putative target and/or change the state of the cell, increasing its sensitivity to infection. This may notably explain why we have previously observed *in vivo* activity with **1**, even though we find it is rapidly degraded in serum (Fig. 1b)[10]. While we have not been able to detect **1** in tumors (data not shown), we could detect pyrrole-based **10** and **24** by LC-MRM following intratumoral injection for up to 3 hours (Supplementary Fig. 10). Following intratumoural injection, **28** was detectable in the tumor and serum for up to 10 hours (Supplementary Fig. 11).

Importantly, the selectivity of OVs for cancer cells is generally maintained using these novel compounds. It is unclear whether this is due to the decreased susceptibility of normal cells to the small molecules, or rather, a reflection of the inherent tropism of the viruses. In particular, cancer cells have generally elevated metabolic rates and produce more virus per cell even with non-attenuated viruses[4,23]. Hence, in the context of cancer cells, dampened IFN-response may have a more significant impact as has been suggested from mathematical modeling studies[23,24].

One of the properties that has been successfully improved over parent compound **1** is the reduction of electrophilicity as determined by GSH reactivity. Highly electrophilic compounds such as **1** are susceptible to nucleophilic attack and generally less desirable from a pharmacological standpoint. While completely eliminating the electrophilicity of the compounds leads to inactive molecules (Supplementary Table 1), reducing it by employing the pyrrole scaffold does lead to biologically active molecules with substantially improved tolerability. Importantly, similar electrophilic compounds are used clinically for cancer and other applications (e.g. afatinib, mitomycin C, exemestane, esomeprazole, and orlistat)[25].

In summary, we have developed a new class of well-tolerated compounds that sensitize cancer cells to infection with attenuated viruses *in vitro* and *in vivo*. As such, these have high clinical potential for use in combination with OV and gene therapy strategies for treatment of cancer.

Experimental Section

Cell lines. 786-0 (human renal carcinoma), A549 (human lung adenocarcinoma), Vero (monkey kidney), CT26 (murine colon carcinoma), 4T1 cells (murine mammary carcinoma), B16F10-LacZ (murine melanoma) cells, and HT29 (human colon carcinoma) were obtained from the American Type Culture Collection (Manassas, VA) and maintained in Dulbecco's Modified Eagle's medium (Corning, Manassas, VA) supplemented with 10% fetal bovine serum (Sigma-Aldrich, St Louis, MO) and buffered with 30 mM Hepes (Thermo Fisher Scientific, Waltham, MA). All cell lines were incubated at 37 °C with 5% CO_2 in a humidified incubator.

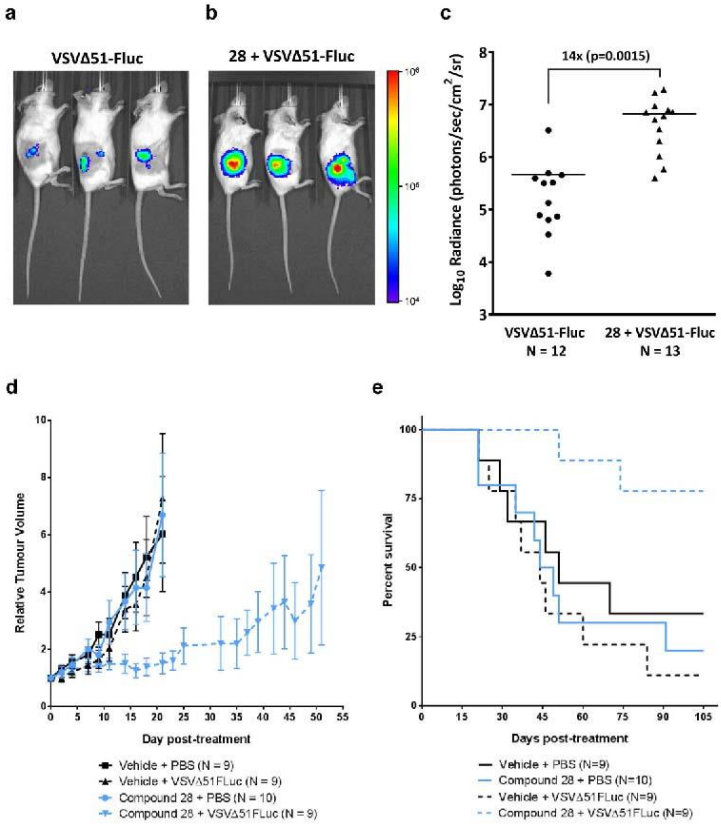

Figure 6. Pyrrole-based compound 28 enhances VSVΔ 51 oncolytic activity in resistant syngeneic and xenograft tumor models. (**a**,**b**) VSVΔ 51-resistant CT26 cells were subcutaneously engrafted into female Balb/c mice. After 11 days, mice were given 30 μL of vehicle (DMSO), or 40 mg/kg of **28** by intratumoral injection. Four hours later, mice were treated with 1×10^8 plaque-forming units of VSVΔ 51-FLuc. Virus replication was monitored twenty-four hours later by measuring luminescence using an IVIS (representative images are shown, color scale bar represents photons) and (**c**) tumor radiance was quantified. (**d**) HT29 cells were subcutaneously engrafted into female CD1 nude mice. When tumors reached 5 mm × 5 mm in size, mice were given 30 μL of vehicle (DMSO), or 40 mg/kg of **28** by intratumoral injection. Four hours later, mice were treated with 1×10^8 plaque-forming units of VSVΔ 51-FLuc. Tumor volumes were monitored every other day and average tumor volumes for each treatment group are shown. Tumor volume curves are terminated when the first mouse in each group is euthanized. Error bars correspond to standard error. (**e**) Survival was monitored over time. Log-rank tests indicated that treatment with **28** and virus significantly improved survival compared to vehicle control ($p = 0.03$), **28** alone ($p = 0.006$) or virus alone ($p = 0.002$). Surviving mice had static tumors that neither shrank nor grew for at least 2 weeks.

Viruses. *Oncolytic Rhabdoviruses.* VSVΔ 51 is a recombinant variant of the Indiana serotype of VSV harbouring a deletion of the 51st methionine in the M protein. VSVΔ 51 expressing green fluorescent protein (GFP) or firefly luciferase (FLuc) are recombinant derivatives of VSVΔ 51 that have been previously described[7]. Maraba MG-1 as described[13] was obtained from Dr David F. Stojdl. All virus stocks were propagated in Vero cells, purified on Optiprep gradient and titered on Vero cells as previously described[23].

Oncolytic Herpes simplex-1. HSV-1 N212 (an ICPO-deleted oncolytic strain) expressing GFP was obtained from Dr. Karen Mossman and has been described previously[26]. HSV-1 samples were titered on Vero cells. Vero cells (2.5×10^5 cells) were infected with serial dilutions of virus containing samples in 12-well dishes. Cell were

incubated at 37 °C for 1 h, after which the inoculum was removed and replaced with fresh culture media. After a 48 h incubation at 37 °C, GFP positive plaques were visualized and counted.

Non-replicating vectors. AAV2-luciferase (adeno-associated virus serotype 2 expressing luciferase) was obtained from Dr. Sarah Wootton (University of Guelph) and Ad5-luciferase (adenovirus serotype 5 expressing luciferase) was obtained from Dr. Jack Gauldie (McMaster University).

Luciferase reporter-based viral titration assay. This assay has previously been described in detail[12]. Briefly, 786-0 cells were seeded in 96-well plates at a density of 3×10^4 cells/100 µL/ well and allowed to adhere over a 24-hour period. Cells were then pre-treated for 4 hours with control vehicle (DMSO) or compound at various concentrations and subsequently infected with VSVΔ 51-FLuc at a multiplicity of infection (MOI) of 0.005. Forty hours later, 25 µL of 786-0 supernatant from each well was transferred into corresponding wells containing a confluent monolayer of Vero cells. At the same time, known amounts of virus (starting at 1×10^8 plaque forming units (pfu) and decreasing by 1 log unit to 10 pfu) were added to Vero cells to generate a standard curve. Plates were centrifuged at 1400 rpm for 5 minutes and then incubated for 5 hours at 37 °C. Luciferase expression was then measured and bioluminescence was expressed in mean relative light units (mRLU; SynergyMx Microplate Reader, BioTek). To generate the standard curve, mRLU was plotted against known input pfu. Four-parameter non-linear regression analysis generated a Hill plot from which unknown input pfu (estimate of viral titer) was interpolated. Data transformation was conducted in R. These estimated titers are termed "viral expression units" (VEU). After supernatant transfer as described, cytotoxicity of compounds was assessed by incubating 786-0 cells with alamarBlue® (AbD Serotec) as per the manufacturer's instructions. After 2.5 hours, fluorescence was measured (530 nm excitation and 590 nm emission) on a Fluoroskan Ascent Microplate Fluorometer (Thermo Scientific, Hudson, NH). Emission values were normalized to that of untreated controls.

Glutathione stability experiment. Glutathione stability was assessed using an assay adapted from a recently reported method[27]. 250 µL of a 40 mM DMSO stock solution of each compound was added to L-glutathione (15.4 mg, 5 mol equiv.) suspended in 250 µL of DMSO. The resulting mixture was placed in a 37 °C shaker. 10 µL aliquots were removed and quenched in 990 µL of water (containing 0.5% formic acid) at various time points, including at t = 0 min, for analysis by ESI-LC-MS. All ESI-LC-MS analyses were collected on an API2000 LC/MS/MS System (Applied Biosystems) equipped with a turbo-ion spray ESI probe interfaced with a Prominence UFLC (Shimadzu) equipped with a reverse phase BDS Hypersil C18 50 × 2.1 mm column, particle size 3 µm (Thermo Scientific). HPLC/LCMS UV absorption was monitored at 254 nm and 210 nm. Both the compound and the glutathione adduct were identified by MS. Area of the UV peak was recorded for each time point.

Plasma stability assay. 10 mM methanol stock solutions of each analog were prepared and diluted to 1 µM with aqueous 0.1% formic acid. 5 µL of the diluted solution was inserted into a Proxeon nanoelectrospray emitter (Thermo Scientific, Odense, Denmark) and analyzed in positive ion mode via nanoESI MS on a QStarXL hybrid quadrupole time-of-flight mass spectrometer (AB Sciex, Framingham, MA, USA). Product ion spectra were collected for each compound at varying CID collision energies using an ESI voltage of 1000 V, a declustering potential of 30 V and a focusing potential of 120 V. Two fragments were chosen as multiple reaction monitoring (MRM) transitions for each compound with optimized collision energies. The quantitative transition was used to determine the relative quantities of each compound and the confirmatory transition was used to validate the ion signal observed for the first transition (see Supporting Information).

1 mM methanol stock solutions of each analog were prepared and mixed in experimental triplicate with Balb/c mouse plasma (Innovative Research, Novi, MI, USA) that was buffered 1:1 with phosphate buffered saline (PBS, pH = 7.4). The compounds were multiplexed into sets of three and added to a final concentration of 10 µM in a total volume of 400 µL. Immediately upon mixing, 200 µL of the sample mixture was quenched with 300 µL of aqueous formic acid (5%) to prevent further analog degradation. The remaining 200 µL of sample was incubated at 37 °C for 3 hours and quenched in an identical fashion[28]. The quenched samples were passed through 3 kDa Amicon molecular weight cut off filters (Millipore, Billerica, MA, USA) by centrifugation at 14,000 rpm for 15 minutes. 20 µL samples of the filtrates were subjected to LC-MRM analysis using a Qtrap 4000 (AB Sciex, Framingham, MA, USA) hybrid triple quadrupole linear ion trap mass spectrometer with an ion spray voltage of 5000 V and a declustering potential of 25 V. The MS was equipped with a Turbo V ion spray source coupled to a Dionex Ultimate3000 HPLC (Thermo Fisher Scientific, Waltham, MA, USA). Fritted fused silica columns (200 µm ID) (Molex, Lisle, IL, USA) were packed with 5 µm Magic C18 (MICHROM Bioresources Inc., Auburn, CA, USA) reversed-phase beads to a length of 5 cm using an in-house high-pressure vessel. Chromatographic separation employed a linear gradient using reversed phase solvents (water and acetonitrile both containing 0.1% formic acid) over 10 minutes (see Supporting Information). Automatic quantitation was achieved using MultiQuant software (AB Sciex, Framingham, MA, USA) by integrating the peak areas of the quantitative MRM transition extracted ion chromatogram. The plasma stability of each compound was calculated as a percentage of the compound ion signal detected after 3 hours of plasma incubation relative to the original amount.

ELISA. 786-0 cells were seeded at 3.0×10^5 cells per well in 12-well plates. The following day, the cells were pre-treated with 60, 50, 50 and 95 µM of compound **1**, **2**, **10** and **28** respectively. Two hours following pre-treatments the cells were infected with VSVΔ 51-GFP at MOI 3. Supernatants were collected 16 hours post infection, and an ELISA was performed using VeriKine™ Human IFN Beta ELISA Kit (PBL assay science, Piscataway, NJ).

Quantitative real-time PCR. 786-0 cells were seeded at 1.0×10^6 cells/well in 6-well plates. The following day, the cells were pre-treated with 60, 50, 50 and 95 µM of compound **1**, **2**, **10** and **28** respectively. Two hours

following pre-treatments the cells were infected with VSVΔ 51-GFP at MOI 3. 16 hours post infection the cells were lysed and RNA extraction was performed using RNeasy® Mini Kit (Qiagen, Valencia, CA). RNA was converted to cDNA with RevertAid H Minus First Strand cDNA Synthesis Kit (Thermo Fisher Scientific, Vilnius, Lithuania). Real-time PCR reactions were performed with QuantiTect® SYBR® Green PCR Kit (Qiagen, Valencia, CA) on a 7500 Fast Real-Time PCR system (Applied Biosystems, Foster City, CA). Gene expression was normalized to GAPDH and fold induction was calculated relative to the untreated/uninfected samples for each gene using the Pfaffl method[29].

***Ex vivo* studies.** Balb/c mice were implanted with CT26-WT (murine colon carcinoma) cells. Mice were sacrificed 24 days later, after tumors had reached at least 10 mm × 10 mm in size. Tumor, lung, spleen, brain, and abdominal muscle tissue were extracted from the mice, cut into 2 mm thick slices and cored into 2 mm × 2 mm pieces via punch biopsy. Each tissue core was incubated in 1 mL of Dulbecco's Modified Eagle's Medium (DMEM) supplemented with 10% fetal bovine serum, 30 mM HEPES and 2.5 mg/L amphotericin B, in a 37 °C, 5% CO_2 humidified incubator. In order to assess the viability of each core, alamarBlue® was added to each well for a 4-hour incubation period. Viable cores were selected and treated with various concentrations of **1** and analogs. The cores were then infected with VSVΔ 51 expressing a GFP transgene (VSVΔ 51-GFP) four hours post treatment. GFP pictures were taken for each core 24 hours post infection. Cores and supernatants were collected 30 hours post infection and titered by plaque assay.

***In vivo* studies.** *Dose escalation studies.* Nine-week-old Balb/c mice were intraperitoneally administered various doses of compounds **1**, **10**, **24**, or **28** dissolved in DMSO (approximately 50 μL). Weight loss and other outward signs of toxicity (piloerection, malaise, quiet behaviour) were recorded over a 10 (**1**, **10**) or 18-day (**24**, **28**) period.

In vivo enhancement of virus replication. Nine-week-old female Balb/c mice were given subcutaneous tumors by injecting 3 × 10^5 syngeneic CT26 cells suspended in 100 μl serum-free DMEM. Eleven days post-implantation (when tumors were approximately 5 mm × 5 mm), mice were treated with 40 mg/kg of compound **28** dissolved in DMSO or vehicle control administered intratumorally (approximately 30 μL). Four hours later, mice were treated with an intratumoral injection of VSVΔ 51-FLuc (1 × 10^8 plaque-forming units). For *in vivo* imaging, an IVIS (Perkin Elmer, Waltham, MA) was used as described previously[30]. Briefly, 200 μl of a 10 mg/mL D-Luciferin (Biotium Hayward, CA) solution in PBS (Corning, Manassas, VA) was administered to mice intraperitoneally. Five minutes later, mice were anaesthetized using 3% isoflurane and imaged according to the manufacturer's instructions. For quantification of luminescence described in Fig. 6c, bioluminescent signal intensities were measured using Living Image® v2.50.1 software. Background intensities were measured using the software and subtracted from user-defined regions of interest (ROIs) that were manually delineated around the tumor for each mouse.

CT26 tumor model. Six-week-old female Balb/c mice were given subcutaneous tumors by injecting 3 × 10^5 syngeneic CT26 cells suspended in 100 μl serum-free DMEM. Eleven days post-implantation (when tumors were approximately 5 mm × 5 mm), mice were treated with 50 mg/kg of compound **10** dissolved in DMSO or vehicle control administered intraperitoneally (approximately 30 μL). Four hours later, mice were treated with an intratumoral injection of VSVΔ 51-FLuc (1 × 10^8 plaque-forming units). **10** or vehicle was readministered on day 13 and 15 post-implantation. Tumor dimensions were measured with electronic calipers. Tumor volumes were calculated as (width^2 × length)/2. Mice were euthanized when tumor volume exceeded 1600 mm^3. Initial tumor sizes measured on day 11 were used to calculate relative tumor size.

HT29 tumour model. Six-week-old CD1 nude mice were given subcutaneous tumors by injecting 1 × 10^6 syngeneic HT29 cells suspended in 100 μl serum-free DMEM. When tumors grew to approximately 5 mm × 5 mm (between 18–25 days post-implantation), mice were treated with 40 mg/kg of compound **28** dissolved in DMSO or vehicle control administered intraperitoneally (approximately 30 μL). Four hours later, mice were treated with an intratumoral injection of VSVΔ 51-FLuc (1 × 10^8 plaque-forming units). Tumor dimensions were measured every other day with electronic calipers. Tumor volumes were calculated as (width^2 × length)/2. Mice were euthanized when tumor volume exceeded 1600 mm^3. Initial tumor sizes measured on the day of treatment were used to calculate relative tumor size.

Pharmacokinetics. Short time course. Nine-week-old female Balb/c mice were given subcutaneous tumors by injecting ~3 × 10^5 syngeneic CT26 cells suspended in 100 μl serum-free DMEM. Nineteen days post-implantation, mice were intratumorally administered 50 mg/kg of compound **10** or **24** dissolved in DMSO (approximately 50 μL). Tumors were excised after 0 h, 15 minutes, 1 h and 3 h and homogenized immediately at 30 Hz for 5 minutes with a TissueLyser II (Qiagen). Samples were the centrifuged (20,000 rpm, 30 s, 4 °C) and homogenized again in 500 μL PBS. After another round of centrifugation, the supernatant was passed through Amicon Ultra– 0.5 mL 3 kDa molecular weight cut off filters (EMD Millipore) by centrifugation, and the filtrate was quantified by LC-MRM.

Long time course. Nine-week-old female Balb/c mice were given subcutaneous tumors by injecting ~3 × 10^5 syngeneic CT26 cells suspended in 100 μl serum-free DMEM. Nineteen days post-implantation, mice were intratumorally administered vehicle control (DMSO), or **28** dissolved in DMSO (approximately 30 μL). Tumors treated with **28** were excised after 1 h, 3 h, 10 h and 24 h. Tumors treated with vehicle alone were excised after 3 h and 24 h. Tumor homogenization and centrifugation was conducted in an identical fashion to that described in

the short time course (above). At the time of tumor excision, peripheral blood was also collected and allowed to clot at room temperature for at least 30 minutes. Samples were centrifuged at 20,000 rpm for 10 minutes at 4 °C, and the supernatant (serum) was collected. Serum was diluted 5x with 0.1% formic acid in water and centrifuged through Amicon Ultra− 0.5 mL 3 kDa molecular weight cut off filters (EMD Millipore). For both tumor and serum samples, 25 µL of the filtrate was mixed with 5 µL of a 6 µM solution of caffeine in water (as a standard to allow relative quantitation) and quantified by LC-MRM.

All experiments were reviewed and approved by the University of Ottawa Animal Care Committee (ACC) and were performed in accordance with the University of Ottawa Animal Care and Veterinary Services guidelines for animal care under protocols OGHRI-58 and OHRI-2265.

References

1. Park, B.-H. *et al.* Use of a targeted oncolytic poxvirus, JX-594, in patients with refractory primary or metastatic liver cancer: a phase I trial. *Lancet. Oncol.* **9,** 533–42, doi: 10.1016/S1470-2045(08)70107-4 (2008).
2. Breitbach, C. J. *et al.* Intravenous delivery of a multi-mechanistic cancer-targeted oncolytic poxvirus in humans. *Nature* **477,** 99–102, doi: 10.1038/nature10358 (2011).
3. Russell, S. J., Peng, K.-W. & Bell, J. C. Oncolytic virotherapy. *Nat. Biotechnol.* **30,** 658–670, doi: 10.1038/nbt.2287. (2012).
4. Ilkow, C. S., Swift, S. L., Bell, J. C. & Diallo, J.-S. From scourge to cure: tumour-selective viral pathogenesis as a new strategy against cancer. *Plos Pathog.* **10,** e1003836, doi: 10.1371/journal.ppat.1003836 (2014).
5. Heo, J. *et al.* Randomized dose-finding clinical trial of oncolytic immunotherapeutic vaccinia JX-594 in liver cancer. *Nat. Med.* **19,** 329–36, doi: 10.1038/nm.3089 (2013).
6. Stojdl, D. F. *et al.* Exploiting tumor-specific defects in the interferon pathway with a previously unknown oncolytic virus. *Nat. Med.* **116,** 821–825, doi: 10.1038/77558 (2000).
7. Stojdl, D. F. *et al.* VSV strains with defects in their ability to shutdown innate immunity are potent systemic anti-cancer agents. *Cancer Cell* **4,** 263–275, doi: 10.1016/S1535-6108(03)00241-1 (2003).
8. Ottolino-Perry, K., Diallo, J.-S., Lichty, B. D., Bell, J. C. & McCart, J. A. Intelligent design: combination therapy with oncolytic viruses. *Mol. Ther.* **18,** 251–63, doi: 10.1038/mt.2009.283 (2010).
9. Forbes, N. E., Krishnan, R. & Diallo, J.-S. Pharmacological modulation of anti-tumor immunity induced by oncolytic viruses. *Front. Oncol.* **4,** 191, doi: 10.3389/fonc.2014.00191 (2014).
10. Diallo, J.-S. *et al.* A high-throughput pharmacoviral approach identifies novel oncolytic virus sensitizers. *Mol. Ther.* **18,** 1123–9, doi: 10.1038/mt.2010.67 (2010).
11. Zhang, J., Sarma, K. & Curran, T. Recent Progress in the Chemistry of Mucohalic Acids: Versatile Building Blocks in Organic Synthesis. *Synlett* **24,** 550–569, doi: 10.1055/s-0032-1318138 (2013).
12. Garcia, V. *et al.* High-throughput Titration of Luciferase-expressing Recombinant Viruses. *J. Vis. Exp.* e51890, doi: 10.3791/51890 (2014).
13. Brun, J. *et al.* Identification of genetically modified Maraba virus as an oncolytic rhabdovirus. *Mol. Ther.* **18,** 1440–9, doi: 10.1038/mt.2010.103 (2010).
14. Mossman, K. L., Saffran, H. a. & Smiley, J. R. Herpes Simplex Virus ICP0 Mutants Are Hypersensitive to Interferon. *J. Virol.* **74,** 2052–2056, doi: 10.1128/JVI.74.4.2052-2056.2000 (2000).
15. Diallo, J.-S., Roy, D., Abdelbary, H., De Silva, N. & Bell, J. C. *Ex vivo* infection of live tissue with oncolytic viruses. *J. Vis. Exp.* e2854, doi: 10.3791/2854. (2011).
16. Vähä-Koskela, M. J. V., Heikkilä, J. E. & Hinkkanen, A. E. Oncolytic viruses in cancer therapy. *Cancer Lett.* **254,** 178–216, doi: 10.1016/j.canlet.2007.02.002 (2007).
17. Ruotsalainen, J. J. *et al.* Clonal variation in interferon response determines the outcome of oncolytic virotherapy in mouse CT26 colon carcinoma model. *Gene Ther.* **22,** 65–75, doi: 10.1038/gt.2014.83. (2015).
18. Bridle, B. W. *et al.* HDAC inhibition suppresses primary immune responses, enhances secondary immune responses, and abrogates autoimmunity during tumor immunotherapy. *Mol. Ther.* **21,** 887–94, doi: 10.1038/mt.2012.265 (2013).
19. Thaci, B., Ulasov, I. V., Wainwright, D. a & Lesniak, M. S. The challenge for gene therapy: innate immune response to adenoviruses. *Oncotarget* **2,** 113–121, doi: 10.18632/oncotarget.231 (2011).
20. Rogers, G. L. *et al.* Innate immune responses to AAV vectors. *Front. Microbiol.* **2,** 1–10, doi: 10.3389/fmicb.2011.00194. (2011).
21. Manome, Y. *et al.* Viral vector transduction of the human deoxycytidine kinase cDNA sensitizes glioma cells to the cytotoxic effects of cytosine arabinoside *in vitro* and *in vivo*. *Nat. Med.* **2,** 567–573, doi: 10.1038/nm0596-567 (1996).
22. Chase, M., Chung, R. Y. & Chiocca, E. A. An oncolytic viral mutant that delivers the CYP2B1 transgene and augments cyclophosphamide chemotherapy. *Nat. Biotechnol.* **16,** 444–448, doi: 10.1038/nbt0598-444 (1998).
23. Le Bœuf, F. *et al.* Model-based rational design of an oncolytic virus with improved therapeutic potential. *Nat. Commun.* **4,** 1974, doi: 10.1038/ncomms2974 (2013).
24. Arulanandam, R. *et al.* Microtubule disruption synergizes with oncolytic virotherapy by inhibiting interferon translation and potentiating bystander killing. *Nat. Commun.* **6,** 6410, doi: 10.1038/ncomms7410 (2015).
25. Singh, J., Petter, R. C., Baillie, T. & Whitty, A. The resurgence of covalent drugs. *Nat. Rev. Drug Discov.* **10,** 307–17, doi: 10.1038/nrd3410 (2011).
26. Jordan, R. & Schaffer, P. A. Activation of Gene Expression by Herpes Simplex Virus Type 1 ICP0 Occurs at the Level of mRNA Synthesis. *J. Virol.* **71,** 6850–6862 (1997).
27. Budke, B. *et al.* An optimized RAD51 inhibitor that disrupts homologous recombination without requiring Michael acceptor reactivity. *J. Med. Chem.* **56,** 254–63, doi: 10.1021/jm301565b (2013).
28. Di, L., Kerns, E. H., Hong, Y. & Chen, H. Development and application of high throughput plasma stability assay for drug discovery. *Int. J. Pharm.* **297,** 110–9, doi: 10.1016/j.ijpharm.2005.03.022 (2005).
29. Pfaffl, M. W. A new mathematical model for relative quantification in real-time RT-PCR. *Nucleic Acids Res.* **29,** e45, doi: 10.1093/nar/29.9.e45 (2001).
30. Le Boeuf, F. *et al.* Synergistic interaction between oncolytic viruses augments tumor killing. *Mol. Ther.* **18,** 888–95, doi: 10.1038/mt.2010.44. (2010).

Acknowledgements

CNB, JSD and JCS were supported from the Canadian Institutes of Health Research (CIHR) and the National Science and Engineering Research Council (NSERC) through a Collaborative Research Project Grant. Additional NSERC funding supported CB, JCS and MHD. JSD and JCB also received funding from the Terry Fox Research Institute program project grant (grant # TFF 122868) and a The Lotte & John Hecht Memorial Foundation Innovation Grant of the Canadian Cancer Society (grant #2012-701460). RK is supported by an Ontario Graduate Scholarship, MS is supported by a CIHR doctoral fellowship, and HHS is supported by a CIHR Master's Award.

We would also like to thank Dr. Karen Mossman (McMaster University), Dr. Sarah Wootton (Guelph University), and Dr. Jack Gauldie (McMaster University) for generously providing HSV-N212, AAV2-luciferase, and Ad5-Luciferase (respectively).

Author Contributions

J.S.D., J.C.B., J.C.S. and C.N.B. designed the study, M.H.D., K.K., P.L., C.M. and C.P. synthesized the compounds, M.H.D. and A.M.M. performed and analyzed the stability assays, R.K. and C.D. performed and analyzed the *in vitro* screens, R.K., M.S., N.E.S., A.C. and P.O. performed the *ex vivo* screens, R.K., A.C., H.H.S. and M.S. performed the *in vivo* studies. N.E.S. performed the *in vitro* I.F.N. inhibition assays and F.L.B. and R.K. examine *in vitro* activity with H.S.V. and G.T. vectors. A.M.M., R.K. and C.R.C. collected the pharmacokinetic data. All authors contributed to the analysis of the data and M.H.D., R.K., A.M.M., J.C.S., J.S.D. and C.N.B. wrote the manuscript.

Additional Information

Supplementary information accompanies this paper at http://www.nature.com/srep

Competing financial interests: The authors declare no competing financial interests.

How to cite this article: Dornan, M. H. *et al.* First-in-class small molecule potentiators of cancer virotherapy. *Sci. Rep.* **6**, 26786; doi: 10.1038/srep26786 (2016).

SUPPLEMENTARY INFORMATION

First-in-class small molecule potentiators of cancer virotherapy

Mark H. Dornan,[1,5] Ramya Krishnan,[2,3,5] Andrew M. Macklin,[4,5] Mohammed Selman,[2,3] Nader El Sayes,[2,3] Hwan Hee Son,[2,3] Colin Davis,[2,3] Andrew Chen,[2] Kerkeslin Keillor,[1] Penny Le,[1] Christina Moi,[1] Paula Ou,[2,3] Christophe Pardin,[1] Carlos R. Canez,[4] Fabrice Le Boeuf,[2] John C. Bell,[2,3] Jeffrey C. Smith,*[4] Jean-Simon Diallo,*[2,3] Christopher N. Boddy *[1]

[1] Departments of Chemistry and Biomolecular Sciences, University of Ottawa, Ottawa, Ontario, Canada

[2] Centre for Innovative Cancer Research, Ottawa Hospital Research Institute, Ottawa, Ontario, Canada

[3] Department of Biochemistry, Microbiology and Immunology, University of Ottawa, Ontario, Canada

[4] Department of Chemistry and Institute of Biochemistry, Carleton University, Ottawa, Ontario, Canada

[5] These authors contributed equally to this work

* email: jeff.smith@carleton.ca; jsdiallo@ohri.ca; cboddy@uottawa.ca

Table of Contents

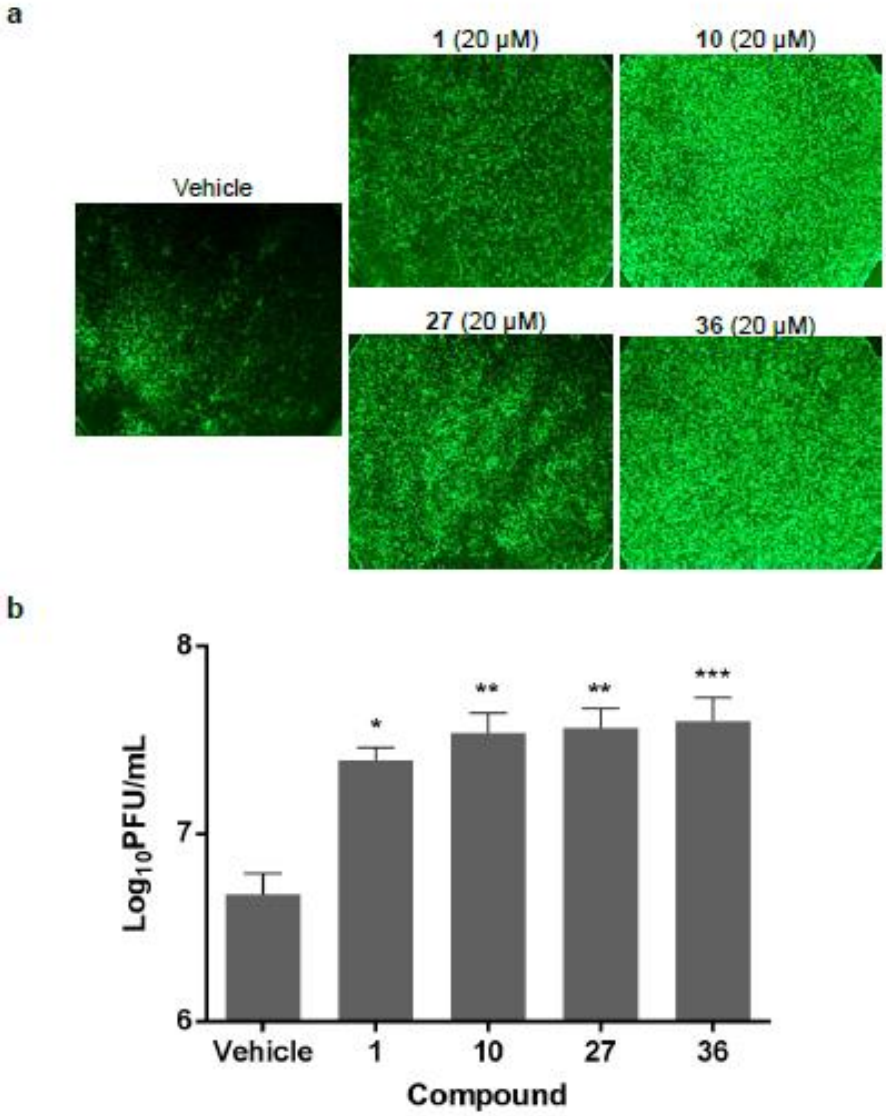

Supplementary Figure S1. Analogs of 1 enhance oncolytic VSV spread in murine melanoma cells. Murine melanoma (B16F10-LacZ) cells were treated with vehicle, **1**, **10**, **27**, or **36** for 4h at the specified concentrations. 4 hours later, cells were infected with VSVΔ51-GFP at MOI 0.001. (A) Virus replication was assessed by fluorescence microscopy 24 hours post-infection. (B) Samples were titered 48 hours post-infection. *p = 0.0392, **p = 0.0027 for 10 vs vehicle and 0.0015 for 27 vs vehicle, ***p = 0.0007 for 36 vs vehicle (one-way ANOVA with Dunnett's multiple comparisons test), Error bars represent standard error.

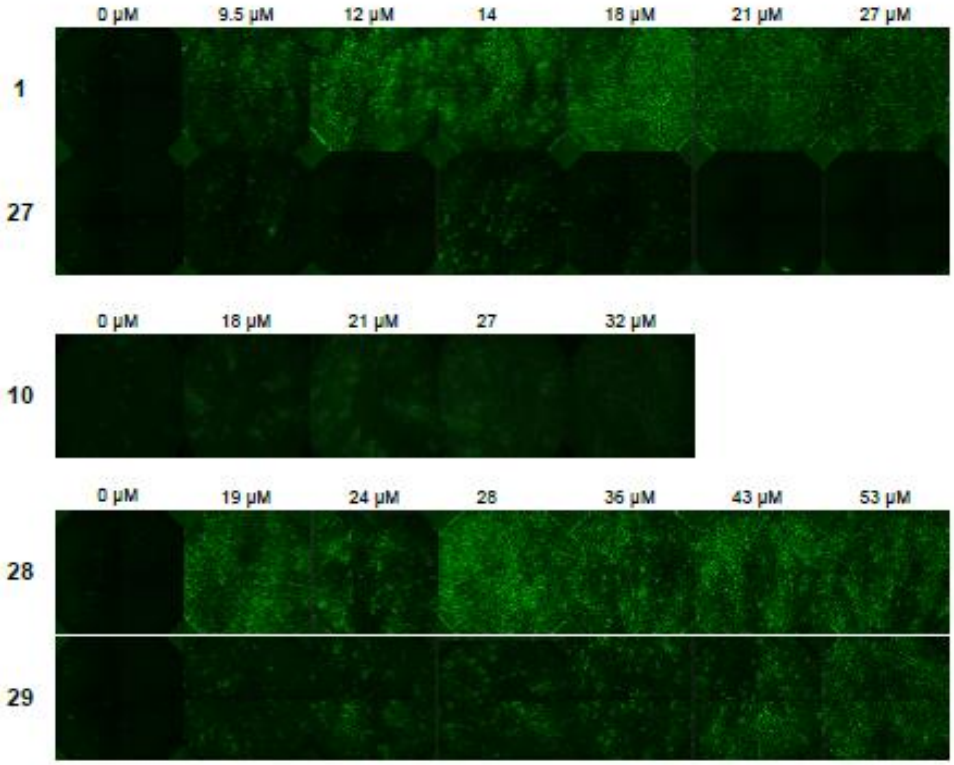

Supplementary Figure S2. Analogs of 1 enhance oncolytic VSV spread in murine colon cancer cells. Murine colon carcinoma (CT26-WT) cells were treated with vehicle, **1**, **10**, **27**, **28**, or **29** for 4h at the specified concentrations. 4 hours later, cells were infected with VSVΔ51-GFP at MOI 0.005. Virus replication was assessed by fluorescence microscopy 24 hours post-infection.

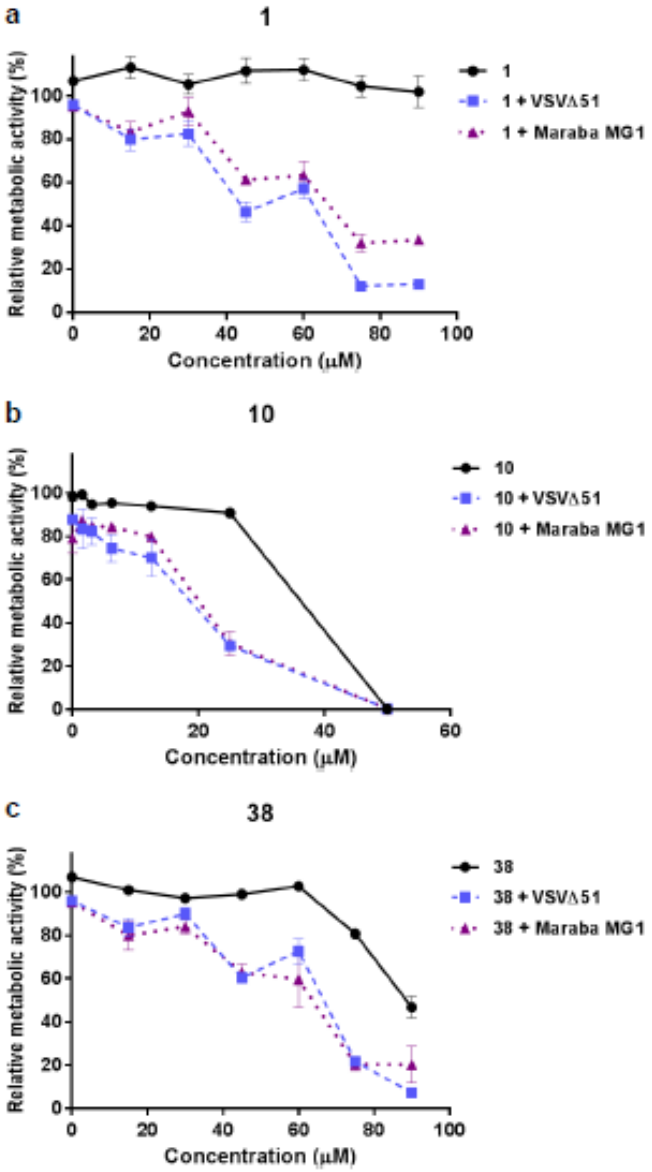

Supplementary Figure S3. Analogs of 1 enhance oncolytic VSV activity in murine breast cancer cells. Murine mammary carcinoma (4T1) cells were treated with vehicle, (A) **1**, (B) **10**, or (C) **38** for 4h at the specified concentrations. 4 hours later, cells were infected with VSVΔ51 or Maraba MG1 at MOI 0.005. 40 hours post-infection, cytotoxicity was assessed by incubating samples with alamarBlue® for 2 h at 37°C before measuring fluorescence (530nm excitation, 590 nm emission). Values were normalized to that of untreated controls.

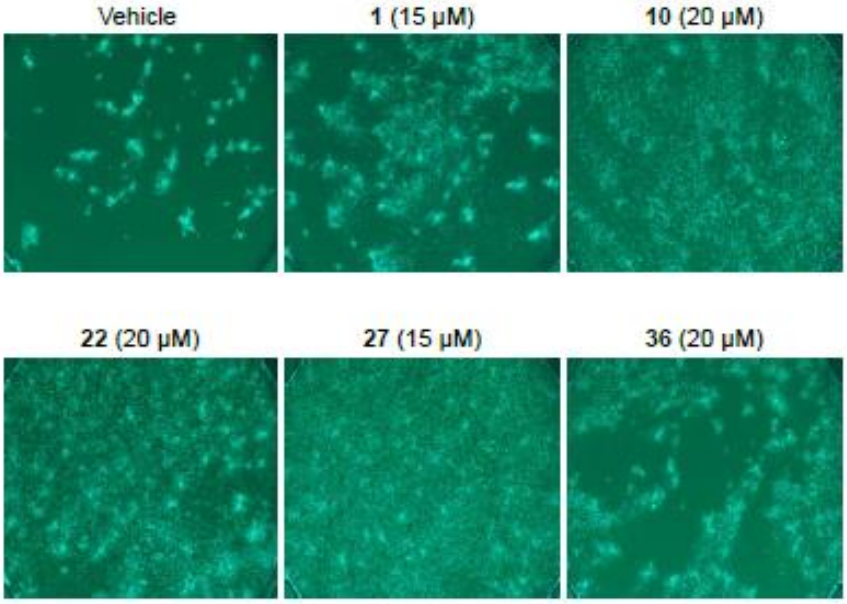

Supplementary Figure S4. Analogs of 1 enhance oncolytic HSV-1 spread in human renal carcinoma cells. Human renal carcinoma (786-0) cells were treated with vehicle, **1**, **10**, **22**, **27**, or **36** for 4h at the specified concentrations. 4 hours later, cells were infected with ICP0-null HSV-N212eGFP at MOI 0.005. eGFP fluorescence was detected 48h after HSV infection.

a

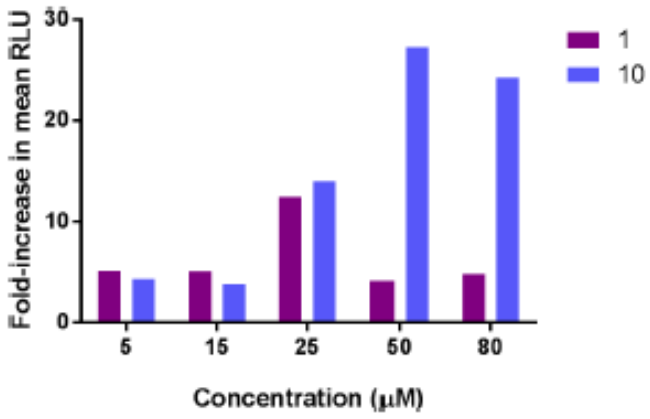

b

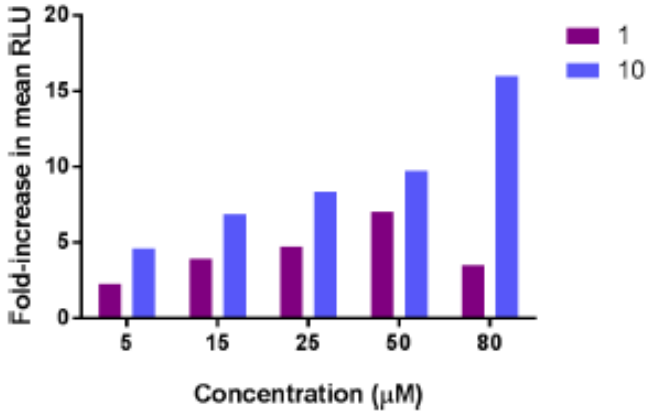

Supplementary Figure S5. 1 and Pyrrole-based analog 10 enhance transduction of non-replicating gene therapy vectors in human lung carcinoma cells. Human lung carcinoma (A549) cells were treated with **1** or **10** analogs at various concentrations. 4 hours later, cells were infected with A) replication defective adeno-associated virus expressing firefly luciferase (AAV2-luc) or B) replication defective adenovirus expressing firefly luciferase (Ad5-luc) at an MOI of 1. 24 hours later, luciferase activity was measured. Data is represented as the fold increase in mean relative light units of treated samples versus untreated controls

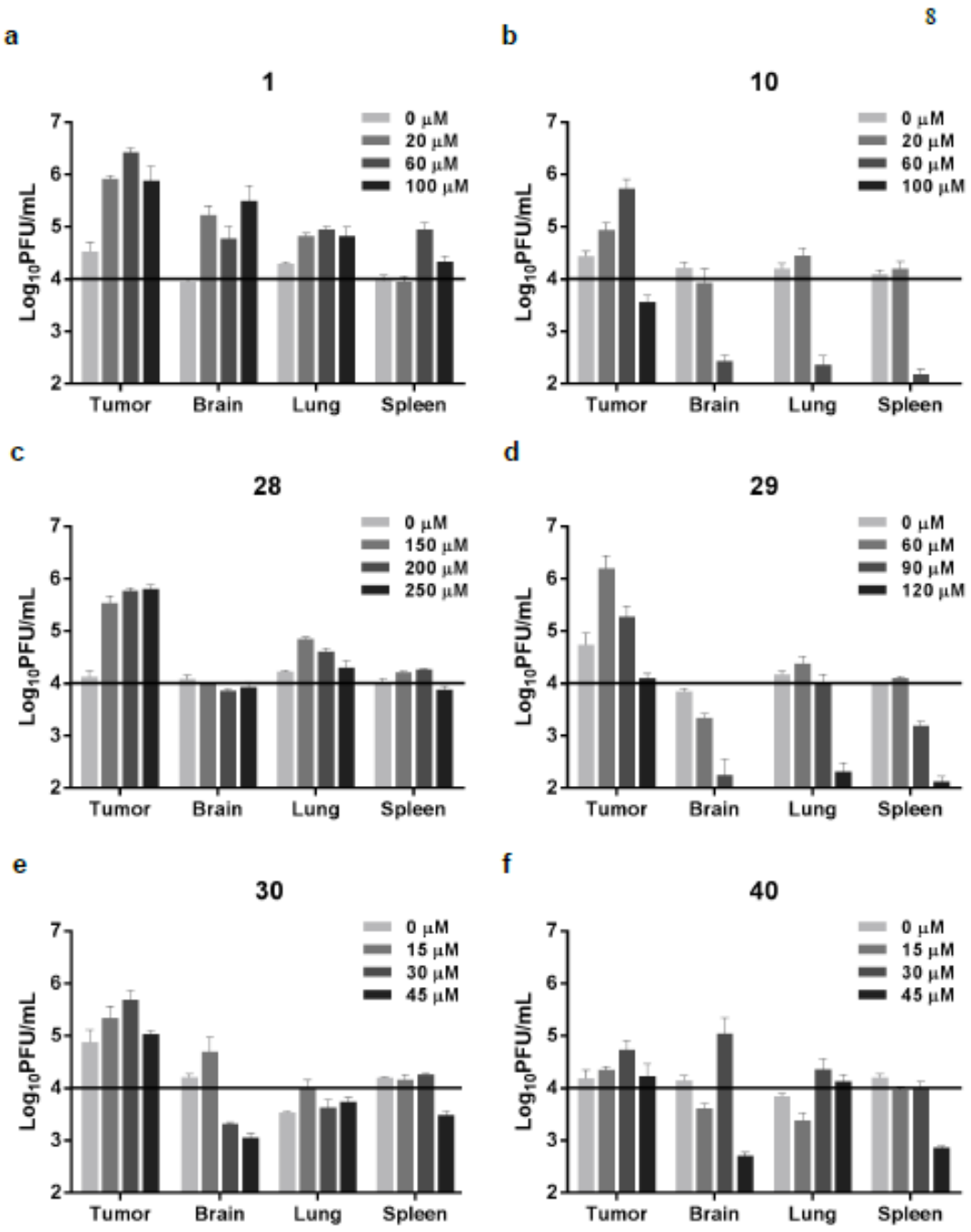

Supplementary Figure S6. VSV Titers for all concentrations tested in *ex vivo* experiment. Increasing doses of 1 and its analogs were tested as described in Figure 3, which depicts the most effective concentration in tumor tissues for each analog. See Methods section for more information.

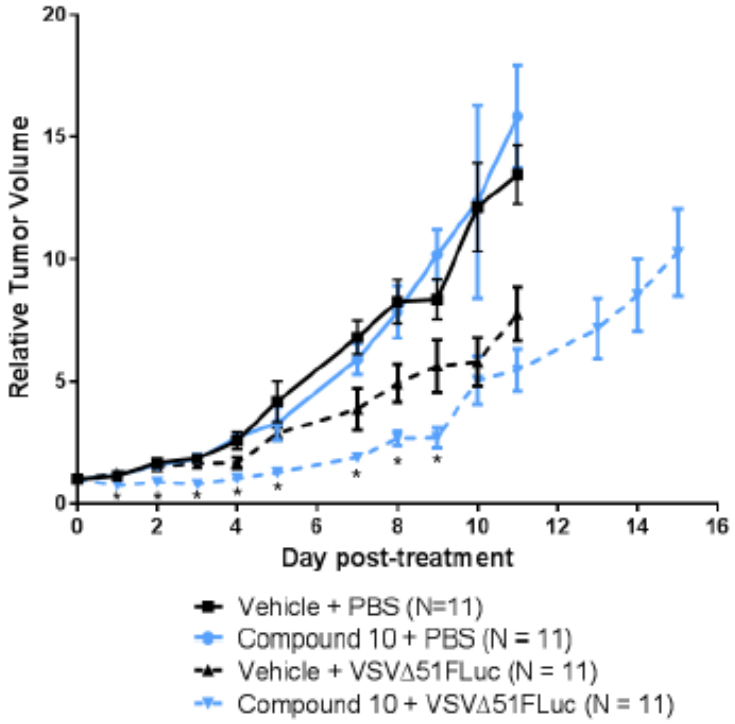

Supplementary Figure S7. Compound 10 enhances VSVΔ51 oncolytic activity in a resistant syngeneic tumor model. VSVΔ51-resistant CT26 cells were subcutaneously engrafted into female Balb/c mice. After 11 days, mice were given 50 µL of vehicle (DMSO), or 50 mg/kg of **10** by intraperitoneal injection. Four hours later, mice were treated with $1x10^8$ plaque-forming units of VSVΔ51-Fluc by intratumoral injection. Vehicle or or **10** was readministered on day 2 and 4 post-initial treatment. Pooled results from two separate experiments are shown. Average tumor volumes for each treatment group are shown and error bars correspond to standard error. Tumor volume curves are terminated when the first mouse in each group is euthanized. Average tumor volumes of vehicle + VSVΔ51-Fluc and **10** + VSVΔ51-Fluc treated groups were compared with a Student's t-test for each day. * $P < 0.05$.

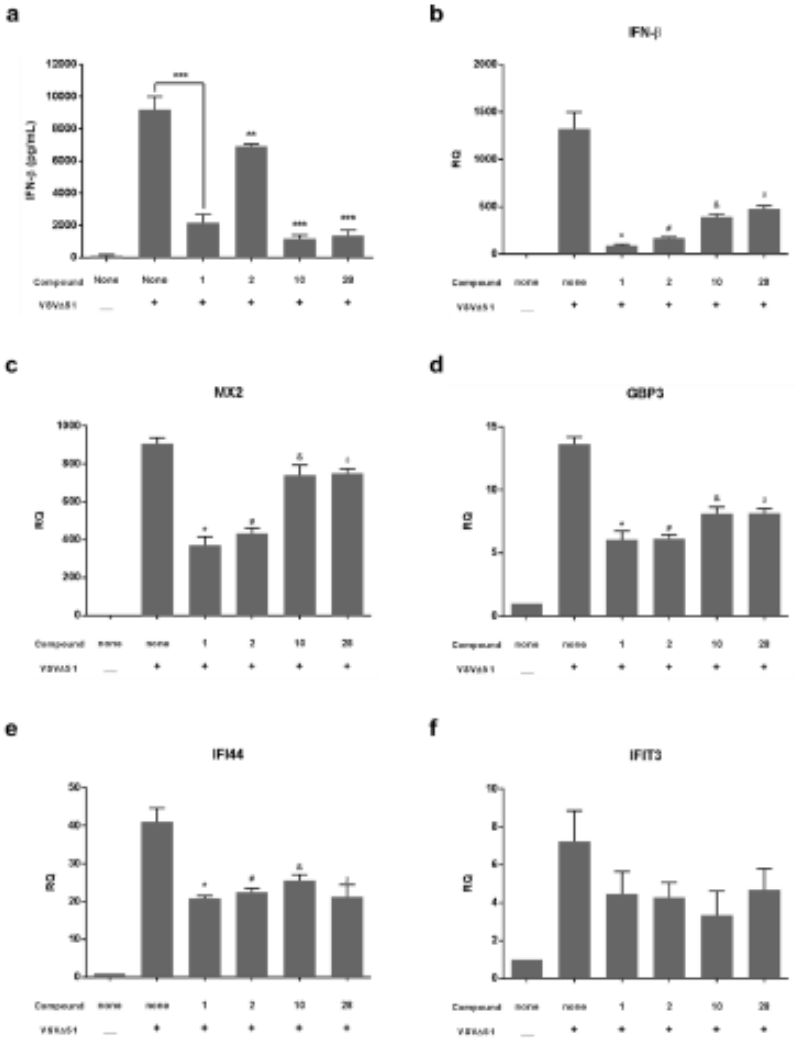

Supplementary Figure S8. Compound 1 and its analogs inhibit the production of IFNβ and interferon-stimulated genes (ISGs). (a) 786-0 cells were pre-treated with compounds 1, 2, 10 and 28 before infection with VSVΔ51-GFP for 16 hours. Amount of IFN□ in the supernatant was measured by sandwich ELISA. *** P < 0.0001, **P = 0.0091 (One-Way ANOVA), n=3 (biological replicates). (b-f) Quantitative RT-PCR for IFN□ and ISG expression in 786-0 cells pre-treated with 1, 2, 10 and 28 before infection with VSVΔ51-GFP for 16 hours. (A/IFNb) * P < 0.0001, # P < 0.0001, & P < 0.0001, □ P < 0.0001. (B/MX2) * P < 0.0001, # P < 0.0001, & P < 0.0195, □ P < 0.0290. (C/GBP3) * P < 0.0001, # P < 0.0001, & P < 0.0001, □ P < 0.0001. (D/IFI44) * P < 0.0001, # P < 0.0001, & P < 0.0001, □ P= 0.0003 (One-Way ANOVA), n=3 (biological duplicates were pooled and the RT-PCR was done in triplicate). This experiment was performed twice with similar results. Representative results from one experiment are shown.

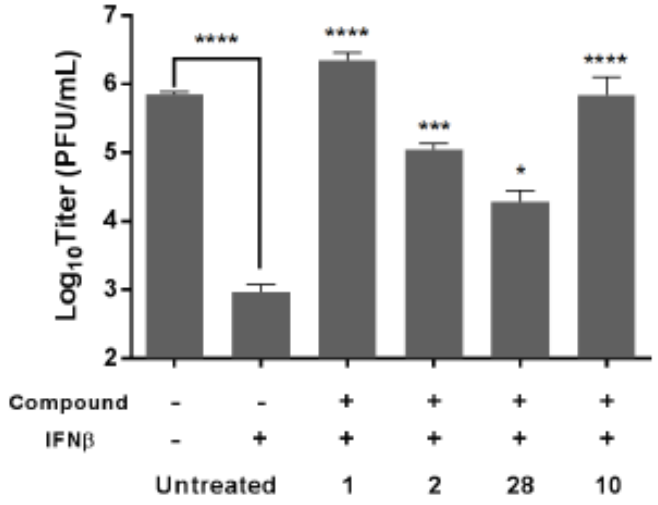

Supplementary Figure S9. Interferon-induced antiviral response is overcome by 1 and its analogs. Human renal carcinoma (786-0) cells were co-treated with compound and IFNβ for 4 hours and then challenged with VSVΔ51-GFP at MOI 0.01. Samples were titered 48 post-infection. *p = 0.0109, ***p = 0.001, ****p = <0.0001 (one-way ANOVA with Dunnett's multiple comparisons test), Error bars represent standard error.

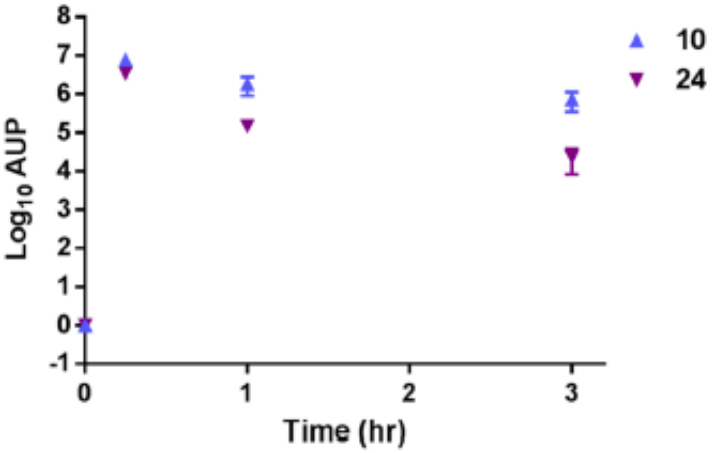

Supplementary Figure S10. Compounds 10, and 24 can be detected in the tumor following intratumoral injection. Mice (N = 1 per timepoint) bearing subcutaneous CT26 tumors were injected intratumorally with 50 mg/kg of 10 or 24. Tumors were excised at various times post-injection and analysed for the presence of compound by LC-MRM. Area under the peak (AUP) for the parent compound(s) are shown. Error bars represent the standard deviation of 3 technical replicates.

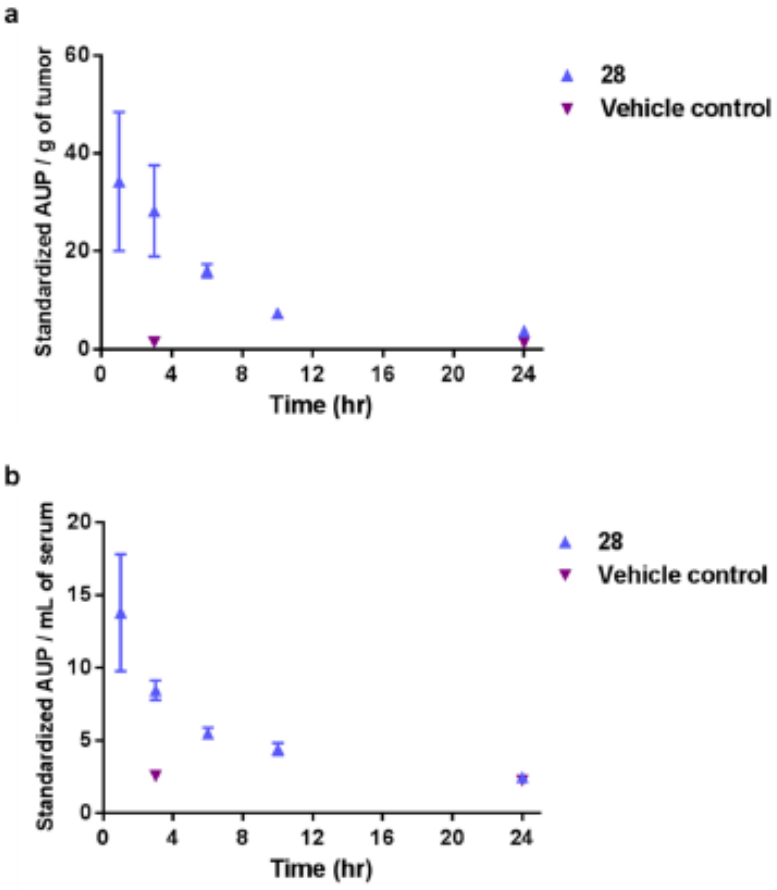

Supplementary Figure S11. Compounds 28 can be detected in the tumor and serum following intratumoral injection. Mice bearing subcutaneous CT26 tumors were injected intratumorally with 40 mg/kg of 28 (N = 3 per timepoint) or vehicle control (N =1 for 3h and 24h timepoints). (a) Tumors and were excised and (b) serum was collected at various times post-injection and analysed for the presence of compound by LC-MRM. Standardized area under the peak (AUP) for the parent compound are shown. Error bars represent the standard error for 3 biological replicates.

Appendix E:

Forbes NE, **Krishnan R**, Diallo JS. "Pharmacological modulation of anti-tumor immunity induced by oncolytic viruses." *Frontiers in Oncology* 4, 191 (2014) doi: 10.3389/fonc.2014.00191.

frontiers in ONCOLOGY

REVIEW ARTICLE
published: 23 July 2014
doi: 10.3389/fonc.2014.00191

Pharmacological modulation of anti-tumor immunity induced by oncolytic viruses

Nicole E. Forbes[1,2], Ramya Krishnan[1,2] and Jean-Simon Diallo[1,2]*

[1] Center for Innovative Cancer Research, Ottawa Hospital Research Institute, Ottawa, ON, Canada
[2] Faculty of Medicine, University of Ottawa, Ottawa, ON, Canada

Edited by:
Volker Schirrmacher, DKFZ, Germany

Reviewed by:
Pier Paolo Claudio, Marshall University, USA
Jianping Huang, University of Florida, USA

***Correspondence:**
Jean-Simon Diallo, Center for Innovative Cancer Research, Ottawa Hospital Research Institute, 501 Smyth Road, Ottawa, ON K1J 8L6, Canada
e-mail: jsdiallo@ohri.ca

Oncolytic viruses (OVs) not only kill cancer cells by direct lysis but also generate a significant anti-tumor immune response that allows for prolonged cancer control and in some cases cures. How to best stimulate this effect is a subject of intense investigation in the OV field. While pharmacological manipulation of the cellular innate anti-viral immune response has been shown by several groups to improve viral oncolysis and spread, it is increasingly clear that pharmacological agents can also impact the anti-tumor immune response generated by OVs and related tumor vaccination strategies. This review covers recent progress in using pharmacological agents to improve the activity of OVs and their ability to generate robust anti-tumor immune responses.

Keywords: Oncolytic virotherapy, anti-tumor immunity, cancer, combination therapy, pharmacological therapy, chemotherapy, immuno-modulatory therapy

INTRODUCTION: ONCOLYTIC VIRUSES: MULTI-MECHANISTIC BIOTHERAPEUTICS AGAINST CANCER

Oncolytic viruses (OVs) are self-amplifying biotherapeutics that have been selected or engineered to preferentially infect and kill cancer cells. Generated from a multitude of viral species, OVs exploit cancer-associated cellular defects arising from genetic perturbations including mutations and epigenetic reprograming [reviewed in Ref. (1)]. Among others, these cellular defects lead to dysfunctional anti-viral responses and immune evasion, increased cell proliferation and metabolism, and leaky tumor vasculature (2). These characteristics in turn provide a fertile ground for viral replication and subsequent lysis of tumor cells and permit the growth of genetically attenuated OVs that are otherwise harmless to normal cells.

In addition to the direct killing of cancer cells, OVs can also trigger a potent anti-tumor immune response. Infected tumor cells induce the release of pro-inflammatory cytokines and expose both viral and tumor-associated antigens to patrolling immune cells, promoting the differentiation of antigen-presenting cells and T-cell activation (3–5). How much tumor infection and lysis are necessary to trigger these responses remains a topic of debate; however, it is clear that the combination of direct oncolysis and activation of anti-tumor immunity can lead to durable cures in pre-clinical mouse models of cancer.

A number of OVs are currently being evaluated in clinical trials to treat a range of cancer types. For a more comprehensive overview, the reader is invited to consult an excellent review by Russell et al. (6). Of particular note, herpes simplex virus-1 (HSV-1), vaccinia virus, reovirus, and adenovirus-based OV strains have made the most progress toward approval (7–10). Shanghai Sunway Biotech's oncolytic adenovirus (H101), deleted for the viral E1B gene and thought to target p53 deficient cancer cells, was the first approved OV in China as early as 2005, indicated for head and neck cancers. (11). Profound tumor regression is common following treatment with OVs; for example, durable objective responses were observed in 3/14 patients (hepatocarcinoma, lung cancer, and melanoma) following treatment with vaccinia virus JX-594 in a phase I trial (7). This virus has been deleted for viral thymidine kinase (TK), making it dependent on cellular TK that is overexpressed in cancer cells (7). In addition to the TK deletion that provides tumor selectivity, the virus also expresses granulocyte macrophage colony-stimulating factor (GM-CSF) to stimulate anti-tumor immunity. Most recently, Amgen's HSV-1-based talimogene laherparepvec (T-VEC) led to 16% durable response in a phase III clinical trial for late-stage melanoma, and it is expected that the company will file for FDA approval in North America in the coming year (12, 13). Like JX-594, T-VEC expresses GM-CSF but has deletions in viral genes ICP34.5 and ICP47 that confer tumor selectivity and promote antigen presentation, respectively (14).

While widespread approval and clinical implementation of oncolytic virotherapy are in the foreseeable future, heterogeneity in clinical response to OVs remains a significant challenge as evidenced from a number of early and late-stage human clinical trials (6, 15, 16). This heterogeneity in response can be attributed to factors that impact OV delivery and spread within tumors, such as pre-existing immunity and remnant tumor anti-viral responses, as well as to a variably immunosuppressive tumor microenvironment that can prevent the generation of an effective anti-tumor immune response. To overcome these challenges, it has been long recognized in the OV field that improvements to therapeutic efficacy either through viral engineering or through combination therapies will be critical (6, 17). In the current review, we will focus on advances in therapeutic strategies employing small-molecule pharmacological agents that ameliorate OV treatment *in vivo* by manipulating the innate and/or adaptive immune response to virus and tumor (summarized in **Table 1**).

Table 1 | Combinations of pharmacological and oncolytic therapies with demonstrated improvements in *in vivo* treatment efficacy.

Drug	Mechanism of action/molecular target	Reported immunomodulatory effect (systemic immunomodulation or specific modulation of anti-viral response	Oncolytic virus	Reference
CLASSIC CHEMOTHERAPY AGENTS				
Cyclophosphamide	DNA alkylation	Systemic immunomodulation	HSV	Ikeda et al. (20), Ikeda et al. (21), Wakimoto et al. (22), and Currier et al. (24)
			Adenovirus	Thomas et al. (25), Dhar et al. (26), Cerullo et al. (27), and Hasegawa et al. (28)
			Vaccinia	Lun et al. (29)
			Reovirus	Qiao et al. (30) and Kottke et al. (34)
			Measles	Ungerechts et al. (31) and Ungerechts et al. (32)
Gemcitabine	Nucleoside substitution and inhibition of DNA replication, ribonucleotide reductase inhibitor	Systemic immunomodulation	Adenovirus	Leitner et al. (38), Liu et al. (39), Onimaru et al. (40), Bhattacharyya et al. (41), Cherubini et al. (42), Wang et al. (43), and Kangasniemi et al. (44)
			Parvovirus	Angelova et al. (45)
			Reovirus	Gujar et al. (46)
			VSV	Hastie et al. (48)
			HSV	Watanabe et al. (50) and Esaki et al. (51)
			Vaccinia	Yu et al. (52)
			Myxoma	Wennier et al. (53)
Bortezomib	Proteasome inhibition	Systemic immunomodulation	VSV (VSV-mIFNβ)	Yarde et al. (61)
			Reovirus	Carew et al. (62)
			Adenovirus (hTERT-Ad)	Boozari et al. (63)
Mitoxantrone	Type II topoisomerase inhibition	Systemic immunomodulation	HSV	Workenhe et al. (69)
Irinotecan	Type I topoisomerase inhibition	systemic immunomodulation	HSV	Tyminski et al. (74)
			Sindbis	Granot and Meruelo (75)
Temozolomide	DNA alkylation	Systemic immunomodulation	Adenovirus	Alonso et al. (80), Holzmuller et al. (81), Liikanen et al. (82), and Tobias et al. (83)
			HSV	Aghi et al. (84) and Kanai et al. (85)
EPIGENETIC MODULATORS				
Valproic acid	Histone deacetylase inhibition	Specific modulation of anti-viral response	HSV	Otsuki et al. (106)
Trichostatin A	Histone deacetylase inhibition	Specific modulation of anti-viral response	HSV	Liu et al. (105)
			Vaccinia	MacTavish et al. (108)
Entinostat (MS-275)	Histone deacetylase inhibition	Both	VSV	Nguyen et al. (99) and Bridle et al. (109)
5-Azacitidine	DNA methyltransferase inhibition	Specific modulation of anti-viral response	HSV	Okamoto et al. (111)
PI3K/Akt/mTOR PATHWAY INHIBITORS				
LY294002	PI3K inhibition	Specific modulation of anti-viral response	HSV	Kanai et al. (116)

(Continued)

Table 1 | Continued

Drug	Mechanism of action/molecular target	Reported immunomodulatory effect (systemic immunomodulation or specific modulation of anti-viral response	Oncolytic virus	Reference
Rapamycin	mTORC1 and mTORC2 inhibition	Both	Adenovirus HSV VSV	Jiang et al. (120) Fu et al. (121) Alain et al. (122)
Everolimus (RAD001)	mTORC1 inhibition	Both	Adenovirus	Lukashev et al. (119)
OTHER				
Viral sensitizer 1 (VSe1)	Unknown	Specific modulation of anti-viral response	VSV	Diallo et al. (125)
Triptolide	Global transcription inhibition via RNA pol II inhibition	Specific modulation of anti-viral response	VSV	Ben Yebdri et al. (130)
Sunitinib	Receptor tyrosine kinase inhibition	Specific modulation of anti-viral response	VSV Reovirus Vaccinia	Kottke et al. (87) and Jha et al. (88) Kottke et al. (87) Hou et al. (89)
Ipilimumab	CTLA-4 inhibition	Systemic immunomodulation	NDV	Zamarin et al. (138)

Numerous studies have shown that combining oncolytic virotherapy and pharmacological therapy leads to improved outcomes in vivo. This table summarizes these reports, presenting the small molecule used in the study, its main mechanism of action or molecular target, its reported immuno-modulatory effect(s), and type of oncolytic virus used. Abbreviations: HSV, herpes simplex virus; VSV, vesicular stomatitis virus; mIFNβ, murine interferon beta; hTERT-Ad, human telomerase reverse transcriptase promoter-regulated adenovirus; PI3K, phosphoinositide 3-kinase; mTOR, mammalian target of rapamycin; mTORC1, mammalian target of rapamycin complex 1; mTORC2, mammalian target of rapamycin complex 2; CTLA-4, cytotoxic Tlymphocyte antigen-4.

STANDARD CHEMOTHERAPEUTIC DRUGS THAT BOOST OV ACTIVITY THROUGH SYSTEMIC EFFECTS ON IMMUNE CELLS AND THE IMMUNE RESPONSE

Most cancer patients with advanced disease will be subjected to some form of chemotherapy. This will largely depend on the type of cancer and other salient pathophysiological characteristics. Given that most patients enrolled in clinical trials to test the efficacy of OVs suffer from advanced disease (7), a natural trend in the OV field has been to test OVs in combination with chemotherapeutics that are currently the standard of care. Classic chemotherapy drugs typically capitalize on the fact that cancer cells are continuously replicating unlike most normal cells (18). However, some normal cell types have higher replication rates, leading to significant off-target effects. Hematopoietic cells among others can be affected and this can lead to systemic immunosuppression (discussed below). While the evaluation of chemotherapeutic drugs in the context of OV therapy has been fairly empirical for the most part, their immunosuppressive effects can inherently complement OV activity by increasing OV spread within tumor beds and/or increasing anti-tumor immune responses. The following sections provide an overview of classic chemotherapy drugs that have been evaluated in combination with OVs focusing on their anti-cancer mechanism of action, examples of OVs with which they have been tested, and the mechanism by which these agents suppress immunity and co-operate with OVs to improve therapeutic outcomes.

CYCLOPHOSPHAMIDE

Cyclophosphamide (CPA) is a nitrogen mustard alkylating agent that leads to cross-linking of nucleotides. Its active metabolite, phosphoramide mustard, interferes with DNA replication by forming guanine-to-guanine intra-strand and inter-strand crosslinks (19). Aldehyde dehydrogenase (ALDH) catalyzes the conversion of the immediate precursor of phosphoramide mustard, aldophosphamide, to an inactive metabolite. Normal cells, for example intestinal epithelial cells and bone marrow stem cells, have a high level of ALDH, protecting them from the effects of CPA's toxic metabolites. In contrast, some lymphocytes have a lower level of ALDH, which makes them more susceptible to the effects of CPA. CPA has been used in combination with several OVs including HSV-1 (20–24), adenovirus (25–28), vaccinia (29), reovirus (30), measles (31–33), and vesicular stomatitis virus (VSV) (33), leading to improved anti-tumor activity *in vivo*. Several studies suggest that CPA can be efficacious in combination with OVs by preventing immune-mediated viral neutralization through inhibiting or delaying the rise of neutralizing antibodies and depleting anti-viral immune cells including natural killer (NK) cells, monocytes, macrophages, and lymphocytes (20, 22, 23, 25, 26). For example, one study showed that CPA inhibits tumor infiltration of innate phagocytes (macrophages, microglia, and NK cells) following HSV treatment in a syngeneic rat glioma model, leading to increased viral persistence and improved overall efficacy (23). Other studies suggest CPA can also enhance the generation of

anti-tumor immunity by inhibiting regulatory T-cells (Tregs) (27, 34). Results from a first in-human clinical trial using Ad-GM-CSF (CGTG-102) to treat solid tumors suggest that metronomic dosing of CPA decreases Tregs without compromising the induction of anti-tumor T-cell responses. This was found to be associated with increased cytotoxic T-cell responses and the induction of Th1 type immunity in most patients. The best progression-free survival and overall patient survival rates were seen with the combination of metronomic CPA and intratumoral infection of adenovirus (27).

GEMCITABINE

Gemcitabine is a fluorinated deoxycytidine nucleoside analog. Incorporation of this analog into DNA prevents further addition of nucleosides during DNA polymerization and thereby halts DNA replication and cell division. Gemcitabine also binds irreversibly to the active site of ribonucleotide reductase. As a result, nucleotide production is halted and DNA replication ceases, leading to apoptosis in rapidly dividing cells [reviewed in Ref. (35)]. While gemcitabine can decrease neutralizing antibodies similar to CPA (36), it is thought to promote anti-tumor immune responses by off-target elimination of myeloid derived stem cells (MDSCs), which suppress T-cell responses. Gemcitabine treatment thereby increases the activity of CD4+ and CD8+ T-cells that recognize tumor antigens (37). This drug has been shown to increase the anti-tumor activity of a wide array of OVs including adenovirus (38–44), parvovirus (45, 46), reovirus (47, 48), VSV (49), HSV (50, 51), vaccinia (52), and myxoma virus (53). In the latter example, the anti-cancer activity of oncolytic myxoma virus was improved using gemcitabine in disseminated pancreatic cancer murine models (53). Interestingly, no sensitization occurred in immunocompromised mice, supporting the requirement for a virus-triggered anti-tumor immune response in mediating the combination effect. The combination of gemcitabine and reovirus was recently evaluated in a phase I clinical trial and while anti-tumor immune responses were not measured, neutralizing antibodies against reovirus were decreased by gemcitabine treatment. In this study, 80% of evaluable patients showed either partial response or stable disease (36).

BORTEZOMIB

Bortezomib is a proteasome inhibitor approved to treat multiple myeloma and mantle cell lymphoma. It reversibly binds the catalytic site of the 26S proteasome with high affinity and specificity (54). Bortezomib has been shown to inhibit NF-κB by preventing degradation of IκB-α in some cell types (55) although the opposite effect has also been observed (56). Other mechanisms of action by which bortezomib may kill cancer cells are through ER-stress and activation of the unfolded protein response (UPR) (57) and triggering apoptosis by preventing the degradation of pro-apoptotic proteins (56, 58). Some studies have shown that treatment of cancer cells using bortezomib increases surface expression of Hsp90 and Hsp60 in cancer cells leading to their more effective phagocytosis by dendritic cells (DCs), improving tumor vaccine effects (59). Bortezomib-treated mice also exhibit increased DC maturation and phagocytic potential (59). On the other hand, one study found that bortezomib treatment leads to apoptosis of allo-reactive CD4+ T-cells. Thus the net result on anti-cancer and anti-viral immune responses is likely context-dependent (60).

Bortezomib has been tested in combination with oncolytic VSV (61), reovirus (62), and adenovirus (63). Using VSV-mIFNβ, combined treatment with bortezomib was inhibitory to virus replication in myeloma cells *in vitro* but led to improved therapeutic efficacy compared to single treatments in syngeneic murine myeloma models (61). Given no observed effect on tumor viral load, this suggests bortezomib likely increases virus-induced cell death and/or potentiates the anti-tumor response mediated by the virus. Supporting the former, in combination with the oncolytic adenovirus hTERT-Ad, bortezomib enhanced infection-induced ER-stress and activated the UPR and UPR-associated apoptotic cell death *in vitro* (63). In subcutaneous hepatocellular carcinoma (HCC) mouse models, bortezomib refocused the immune response toward tumor-associated antigens by inhibiting immune recognition of the virus. This allowed for a reduction in viral dose in the combination therapy while maintaining similar efficacy. It was further demonstrated that bortezomib's efficacy is dependent upon a functional CD8+ T-cell response, as no response was seen *in vivo* upon depletion of CD8+ T-cells.

MITOXANTRONE

Mitoxantrone is a type II topoisomerase inhibitor and a DNA intercalating agent. Thus, it disrupts DNA synthesis and DNA repair in both healthy cells and cancer cells (64). Mitoxantrone was initially developed for treatment of cancer and has been notably approved to treat leukemia and prostate cancer. However, due to its immunosuppressive effects, mitoxantrone was also approved for the treatment of multiple sclerosis over a decade ago. Similar to other immunosuppressive chemotherapies, its activity can be attributed to its effects on proliferating immune cells, but it also has additional effects on antigen-presenting cells and enhances suppressor T-cell functions. Mitoxantrone treatment notably reduces the secretion of pro-inflammatory cytokines such as IL-2, interferon-γ (IFN-γ), and tumor necrosis factor alpha (65–68). This drug has been tested in combination with oncolytic HSV-1 in syngeneic murine breast tumor models (69) but only *in vitro* with adenovirus in prostate cancer cells (70–72). In the case of the HSV-1 ICP0 null OV KM100, mitoxantrone was found to induce immunogenic cell death and whereas no enhanced cell killing was observed *in vitro*, the combination treatment improved survival compared to single treatments in a Her2/neu TUBO-derived syngeneic murine tumor model. This effect was associated with increased intratumoral infiltration of neutrophils and tumor antigen-specific CD8+ T-cells. It was also observed that CD8+ and CD4+ T-cells as well as Ly6G+ neutrophils were important in mediating the improved anti-tumor efficacy.

IRINOTECAN

Irinotecan or more accurately its active metabolite SN-38 inhibits topoisomerase I leading to a blockade in DNA replication and transcription. It is mainly used in colon cancer as part of a regimen known as FOLFIRI, which also includes folinic acid and 5-fluorouracil. This course of therapy has been found to reduce the number of Tregs in colorectal cancer patients with minimal impact on total lymphocyte and CD4+ T-cells counts (73). Few studies

have used irinotecan in combination with OVs *in vivo*. One study showed that HSV-1 expressing CYP2B1, which converts irinotecan into SN-38, leads to improved survival in combination with irinotecan as compared to virus or drug alone in an immunodeficient mouse glioma model (74). While potential immunological effects were not assessed, a likely contributor to the effect of combination therapy is the increased conversion of irinotecan to active SN-38 due to the expression of CYP2B1 by the virus. Another study used oncolytic Sindbis to treat immunodeficient mice bearing human ovarian tumors (75). In this model irinotecan improved the oncolytic efficacy of Sindbis and this effect required NK cells.

TEMOZOLOMIDE

Temozolomide (TMZ) is an alkylating agent that leads to alkylation/methylation of DNA and has demonstrated clinical benefits in patients with glioblastoma (GBM) (76) and advanced metastatic melanoma (77). At higher doses, TMZ can be myeloablative and in these conditions, CD4+ and CD8+ T-cells, as well as Tregs are markedly reduced. Vaccination using an anti-tumor peptide vaccine following TMZ-induced myeloablation leads to improved CD8+ T-cell anti-tumor responses and prolongs survival in a murine model of established intracerebral tumors (78). However, Treg depletion has also been observed following low-dose TMZ in rats (79). Oncolytic adenovirus (80–83) and HSV (84, 85) have been tested *in vivo* in combination with TMZ, albeit immune effects have not been systematically explored. In one study with Ad5/3-D24-GM-CSF ± low-dose CPA (to reduce Tregs), treatment with TMZ increased tumor cell autophagy, anti-tumor immunity, and ultimately reduced tumor burden in murine models of xenogeneic prostate cancer (82). When used in chemotherapy-refractory patients, adenovirus infusion followed by TMZ treatment was found to increase tumor-specific T-cells and immunogenic cell death as well as overall survival compared to adenovirus treatment alone.

SUNITINIB

Sunitinib is an oral, small-molecule, and multi-targeted receptor tyrosine kinase (RTK) inhibitor that was approved by the FDA for the treatment of metastatic renal cell carcinoma (RCC) and gastrointestinal stromal tumors (GIST) in 2006. Since then it has also been approved for use in neuroendocrine pancreatic cancer. Sunitinib inhibits cellular signaling by targeting multiple RTKs. These include platelet-derived growth factor receptors (PDGF-R) and vascular endothelial growth factor receptors (VEGF-R). Sunitinib also inhibits KIT (CD117), the RTK that drives the majority of GISTs. In addition, sunitinib inhibits other RTKs including RET, CSF-1R, and FLT3. Sunitinib has been recently shown to have additional off-target effects that block effector proteins of the IFN signaling pathway such as RNaseL and PKR (86).

Sunitinib has been evaluated in combination with VSV (87, 88), reovirus (87), and vaccinia virus (89). In the context of VSV oncovirotherapy, sunitinib decreased phosphorylation of the PKR substrate eIF2-α, leading to increased viral titers *in vitro*. Quite remarkably, combination therapy resulted in complete and sustained tumor regression in several immunodeficient and immunocompetent mouse tumor models (88). However, sunitinib may have additional effects on the infectivity of tumor vasculature. One study used sunitinib to transiently inhibit VEGF signaling, creating a "VEGF burst" upon treatment recovery. In combination with oncolytic VSV and reovirus, this led to increased viral infection and endothelial cell lysis as well as virus spread from blood vessels to cancerous tissues (87). A recent study looked at the combined effect of sunitinib and oncolytic vaccinia virus in syngeneic kidney and breast cancer mouse models, and found the combined treatment led to the most dramatic tumor reduction. Infection of tumors with oncolytic vaccinia as a monotherapy led to decreased VEGF expression (89), in line with the observation that vaccinia induces tumor vascular shutdown in both murine tumor models and in patients (90–92). Thereby, the combination effect in this study was attributed to enhanced tumor devascularization, although other potential effects of sunitinib on the cellular anti-viral response cannot be ruled out.

DRUGS THAT EPIGENETICALLY REPROGRAM IMMUNE RESPONSES TO ENHANCE OV THERAPY

Epigenetic changes in gene regulation and expression can lead to phenotypic heterogeneity in genetically identical cell populations. Through reversible modifications to DNA and chromatin structures by enzymes targeting DNA, histones, and the distribution pattern of nucleosomes, the ability of transcriptional factors to access their respective promoters can be deeply altered (93). Not surprisingly, many enzymes that are involved in epigenetic regulation are deregulated in cancer and manipulation of the cancer epigenome using small molecules has been explored successfully as a treatment modality for cancer. As will be discussed in the following sub-sections, modification of the cancer epigenome has also proven beneficial to improve oncolytic virotherapy through effects on the cellular anti-viral response, the anti-tumor immune response, and even viral gene expression [for a more extensive review, refer to Ref. (1)].

HDAC INHIBITORS

Transformed cells often have defective IFN signaling pathways due to the cytokine's ability to suppress cellular proliferation and stimulate immune responses, both of which cancer cells must bypass in order to evolve to full-blown malignancies (94–96). Indeed, it has been estimated that roughly three quarters of tumor cell lines within the NCI60 panel have defective IFN responses (97). Numerous reports have attributed dysfunctional IFN pathways in tumors to epigenetic silencing including DNA promoter hypermethylation and transcriptionally suppressive histone modifications [reviewed in Ref. (1)]. The extent to which interferon-stimulated genes (ISGs), the effector arsenal of the IFN-mediated anti-viral response, are epigenetically silenced can lead to differences in the sensitivity to virus infection (98–102). Importantly, transcriptional activation of ISGs has been shown to require histone deacetylase (HDAC) activity (103), which has spawned the evaluation of HDAC inhibitors (HDIs) in combination with several OVs.

HDAC inhibitors including valproic acid (VPA), trichostatin A (TSA), suberoylanilide hydroxamic acid (SAHA), and MS-275 have all been used in the context of OV therapy to effectively "reprogram" IFN-responsive tumors to become permissive to OV infection. HDIs such as VPA and TSA were found to enhance

HSV oncolysis in oral squamous carcinoma cells (SCC) (104) and glioma tumors (105–107). In one report, this was attributed to an inhibition of virally induced ISG expression, even in the presence of exogenously added IFNβ (106). The result of HDI/HSV combination therapy led to prolonged survival in several murine tumor models (105, 106). TSA also enhanced the oncolytic capacity of vaccinia virus, where the two agents synergistically increased cell killing *in vitro* in several cancer cell lines and the combination therapy led to improved survival responses in syngeneic lung metastasis and subcutaneous colorectal carcinoma mouse models (108).

Similarly, MS-275 (entinostat), SAHA (vorinostat), and other HDIs robustly sensitized resistant cells to VSV-mediated oncolysis by suppressing transcription of IFNβ and ISGs, increasing viral titers, and increasing cancer cell death. This potent synergy was cancer cell-specific and led to delayed tumor progression in xenograft models and improved viral spread within tumors in a syngeneic metastatic breast cancer model (99). While only evaluated *in vitro* in this study, HDI treatment of several cancer cell lines increased spreading of vaccinia and Semliki Forest viruses as well. This activity was ultimately linked to HDI-elicited dampening of the response to IFN (99).

In addition to the effects of HDIs on the response to IFN, evidence suggests HDIs can have additional immuno-modulatory properties. Particularly striking effects of HDIs have been observed in the context of a heterologous oncolytic prime-boost strategy, where mice with syngeneic B16 melanoma brain tumors were first primed with an oncolytic adenovirus expressing the tumor-associated antigen dopachrome tautomerase (hDCT, overexpressed in B16) then treated with oncolytic VSV expressing hDCT. MS-275 given along with VSV-hDCT potentiated the anti-tumor response to hDCT while suppressing the adaptive anti-viral response, ultimately redirecting the immune response toward the tumor. As a result, efficacy was dramatically improved, where the majority of mice given MS-275 in the prime-boost regime experienced long-lasting (>200 day) cures, compared to 100% mortality before day 50 in the mice given the same therapy minus MS-275 (109). In this study, it was also shown that MS-275 reduced virus neutralizing antibodies and memory CD8+ T-cells while maintaining prime-induced levels of humoral and cellular immunity against the tumor antigen (109).

5-AZA

DNA methylation and histone modifications are highly interdependent epigenetic processes (110). In addition to histone acetylation-mediated gene silencing, ISGs and other genes implicit in the IFN-mediated anti-viral response are often silenced in cancers by DNA hypermethylation at CpG islands in their promoter region [reviewed in Ref. (1)]. In addition to cellular genes, viral genomes can also be susceptible to direct epigenetic silencing. For example, oncolytic HSV rQNestin34.5 is transcriptionally silenced upon infection of glioma cells, due to increased DNA methylation levels at the virally encoded mammalian Nestin promoter (111). As such, some groups have investigated using OVs in combination with 5-AZA-2′-deoxycytidine (5-AZA): a DNA methyltransferase inhibitor that prevents DNA methylation and allows silenced DNA to regain accessibility to transcription factors. In the case of oncolytic HSV rQNestin34.5, treatment with 5-AZA was sufficient to de-repress transcription under control of the Nestin promoter, allowing viral gene expression, increased viral replication, and HSV-mediated glioma cell killing. This translated to increased survival in glioma bearing mice treated with both 5-AZA and the OV, compared to either treatment administered alone (111). However, it is interesting to mention that in the same study, VPA an HDAC inhibitor was sufficient to drive down DNA methylation at the Nestin promoter *in vitro* in infected glioma cells, highlighting the closely interrelated impact of DNA methylation and histone modification (111).

PI3K/Akt/mTOR PATHWAY INHIBITORS

The phosphoinositide 3-kinase (PI3K) pathway is critical to cell survival/apoptosis signaling in response to stress. Genetic mutations in the PI3K pathway frequently occur in cancers resulting in dysfunctional apoptotic responses and pro-survival signaling (112). Various growth hormones and stress signals including IFN-α activate PI3K, which triggers a signaling cascade leading to Akt phosphorylation (112, 113). This activates the kinase, which then phosphorylates a number of cellular factors involved in cell survival and proliferation such as NF-κB, which is also involved in inducing the type I IFN cascade.

Several PI3K pathway inhibitors including GDC-0941 and NVP-BEZ235 are currently being clinically evaluated for the treatment of cancer (114). Both GDC-0941 and LY294002, a common PI3K inhibitor chemical probe, inhibit PI3K activity via competitive inhibition of an ATP binding site on the p85α subunit (115). The PI3K inhibitors LY294002, GDC-0941, BEZ235, as well as the Akt inhibitor tricibine, acted synergistically with oncolytic HSV MG18L to induce apoptosis in glioma cell lines *in vitro* in a cancer cell-specific manner. Remarkably, combination therapy resulted in durable cures in mice bearing glioblastoma multiforme (GBM) tumors, surpassing the efficacy of either therapy administered alone (116). Recent findings also indicated LY294002 increased killing of multiple myeloma cells *in vitro* triggered by the oncolytic adenovirus ZD55-TRAIL (117).

Mammalian target of rapamycin (mTOR), a master regulator of cellular translation, is downstream of PI3K and Akt signaling. Indeed, both GDC-0941 and NVP-BEZ235, a PI3K inhibitor developed by Novartis, have been reported to inhibit mTOR as well as PI3K (114). While mTOR controls translation of a host of cellular mRNAs and can also impact translation of viral proteins, evidence suggests it can control the anti-viral response by regulating translation of IFN and other key mediators of the anti-viral response such as IRF-7 (118). The mTOR inhibitor rapamycin, a well-known immunosuppressant, has been tested in combination with several OVs including oncolytic adenovirus (119, 120), HSV (121), VSV (122), and myxoma (123, 124). Treatment with rapamycin or closely related mTOR inhibitors such as everolimus (RAD001) has been reported to suppress the adaptive immune response to OVs by reducing levels of antibodies generated against the viruses (120), improving OV activity in several rodent models of cancer (119–121). In one study, enhancement of OV activity was also observed *in vitro* following treatment with rapamycin (121). This may be due to the impact of rapamycin on the IFN response as determined from another study where rapamycin was shown to reduce levels of VSV-induced IFN in rats, improving VSV efficacy

in an aggressive rat glioma model (122). Interestingly, oncolytic myxoma is enhanced by rapamycin in normally resistant human tumor cells *in vitro*; however, the mechanism by which this occurs is thought to be due to rapamycin-induced increases in Akt kinase levels optimal for sustaining myxoma replication (123).

OTHER PROMISING IMMUNO-MODULATORY OV-ENHANCING DRUGS

NOVEL VIRAL SENSITIZERS

The paragraphs above have shown countless examples of empirically or rationally selected combination therapeutic approaches aiming to improve the activity of OVs using well-characterized chemotherapeutics and signaling pathway inhibitors. A high-throughput screen was performed in an effort to expand this approach in an unbiased manner to identify previously uncharacterized small molecules that enhance OV activity. This screen was performed using oncolytic VSVΔM51 in the resistant murine breast cancer cell line 4T1 (125). Several molecules were identified as novel "viral sensitizers" (VSes) that were capable of boosting VSV replication and spread *in vitro*. One of these compounds, VSe1, boosted VSVΔM51 replication by up to 1000-fold, and was found to synergistically increase tumor cell killing. The mode of action of VSe1 is not fully understood but at a minimum it involves disruption of the IFN response. More specifically, ISGs typically triggered upon VSV infection remained silenced in cells pre-treated with VSe1 (125). When used as a combination therapy to treat an aggressive mouse colon carcinoma model refractory to VSVΔM51, VSe1 potentiated OV activity leading to delayed tumor progression in the context of the combination treatment, while either VSVΔM51 or VSe1 alone had no appreciable anti-cancer effects (125).

TRIPTOLIDE

Triptolide (TPL) is a naturally derived component of the Chinese herb *Tripterygium wilfordii* and has been used for centuries as an anti-inflammatory remedy that has also been found to have anti-cancer properties (126–128). TPL is known to be a global transcription inhibitor and has multiple effects including the inhibition of RNA polymerase II and the expression of genes involved in apoptosis and NFκB signaling (129). A recent report found that TPL also suppresses IFN signaling downstream of IRF3 (130). When combined with oncolytic VSV both *in vitro* in VSV-resistant tumor cells and *in vivo* in an aggressive mouse GBM tumor model, the two therapies synergistically improved tumor-specific virus replication leading prolonged survival and delayed tumor progression compared to either therapy given alone (130).

JAK KINASE INHIBITORS

Ruxolitinib (Jakafi) is a Jak1/2 kinase inhibitor (131) approved in 2011 for the treatment of myelofibrosis (132). Patients with myeloproliferative neoplasms often possess an activating mutation in the gene encoding *Jak2* (133), resulting in aberrant inflammatory cytokine release and splenomegaly. Treatment with ruxolitinib, while not targeting the genetic determinant of the neoplasm, led to profound resolution of severe symptoms in human trials to treat myelofibrosis (splenomegaly, weight loss, fatigue), and this clinical efficacy was associated with a potent reduction in inflammatory cytokine levels (134). Given that Jak1 is required for type I IFN signaling and induction of ISGs, Jak1 inhibitors have the potential to benefit OV therapy in IFN-responsive tumors. Both ruxolitinib and Jak inhibitor 1 were sufficient to sensitize VSV-resistant squamous cell carcinoma cells *in vitro* to VSV infection, and this sensitization was associated with marked decreases in ISG expression (135). Pre-treatment with the Jak inhibitor 1 also sensitized sarcoma and bladder carcinoma cells to VSV infection *in vitro* (136).

CHECKPOINT INHIBITORS

Targeting T-cell inhibitory check point molecules, including the T-cell inhibitory receptor cytotoxic T-lymphocyte antigen 4 (CTLA-4) and programed cell death 1 (PD1), is a relatively new therapeutic approach to cancer therapy. During normal immune responses, T-cell checkpoint receptors such as PD1 and CTLA-4 prevent over-active T-cell responses, which can lead to harmful tissue damage. However in cancers, tumor infiltrating T-cells are often inhibited by both PD1 and CTLA-4 stimulation. As a result, T-cell anergy is a major barrier to immune-mediated tumor recognition and clearance. Given the ability of OVs to stimulate an anti-tumor immune response, combining OV with checkpoint inhibitors has emerged as a logical combination approach. While several groups are currently working on this approach, published studies to date have focused on ipilimumab, an anti-CTLA-4 antibody approved to treat melanoma in 2011. By targeting CTLA-4, ipilimumab blocks interaction with its ligands, CD80/CD86, leading to increases in T-cell mediated anti-tumor responses. Anti-CTLA-4 antibodies have been used in combination with oncolytic parvovirus *in vitro* (137) and Newcastle disease virus (NDV) *in vivo* to treat murine B16 melanoma (138). Remarkably, the combination therapy of NDV and anti-CTLA-4 led to nearly 70% cures in a B16 melanoma mouse model compared to 20% cures for anti-CTLA-4 antibody alone and no effect of the OV on its own (138). Notably, NDV complemented with anti-CTLA-4 led to an increase in the infiltration of activated CD8+ and CD4+ T-cells and a reduction in Tregs.

CONCLUSION

Successful therapy using OVs will ultimately depend on effectively navigating the delicate balance between the anti-viral response and the anti-tumor immune response such as to minimize the former in the short term and maximize the latter in the long term. As outlined above, several approved drugs and novel small molecules can be effective tools to dampen the innate and adaptive anti-viral responses, increase the anti-tumor immune response, or both. However, given the close interplay between the cellular anti-viral response and the adaptive immune response that is required for prolonged tumor control, OV/drug scheduling is likely to be critical. To this end, it is probable that the combination of some of the agents described above may allow for additional flexibility and more effective therapy. For example, one can easily foresee first using a drug that specifically dampens the cellular antiviral to permit robust OV replication followed with another that promotes the generation of an anti-tumor response. However, given the efficacy of each approach is undoubtedly both context-dependent (e.g., tumor type and tumor site) and OV-dependent, more preclinical and clinical studies will be necessary to identify winning

combinations that can maximize the potential for curing cancers in a clinical context.

While many studies demonstrate therapeutic benefit of combination therapies at least in animal models, we can perceive a deficit in regards to systematic head-to-head comparisons of different combination therapies coupling OVs and the immune-modulatory drugs reviewed above. While such a feat may prove daunting experimentally, this exercise seems warranted and necessary to delineate a more educated choice of combination therapies to push forward into clinical trials. One clear trend overall is that evaluation of promising combination therapies with novel immuno-modulatory agents seems to stop at the pre-clinical level. There are likely several factors that contribute to this. For example, companies developing novel small molecules may be reluctant to explore combinations with OVs that are still relatively novel themselves. Similarly, novel small molecules need to be validated clinically, which complicates clinical trial design and adds additional risk from the perspective of those spearheading clinical translation of OVs. This is particularly challenging for novel small molecules such as VSe1, which have been selected for the sole purpose of enhancing OV activity (125). This type of small-molecule/OV co-development can only be reasonably achieved by pharmaceutical companies that have experience in developing both small-molecule and biological therapies separately. Hence, from a clinical perspective, it is likely that the combination of OV therapy with a chemotherapy drug that is part of current standard of care would be the easiest to implement as demonstrated with the combination of oncolytic adenovirus and CPA (27). With promising results emerging from the clinic showing benefits combining OVs with traditional chemotherapy drugs, and as pharmaceutical companies such as Amgen begin to take heed of the potential of OV therapy for the treatment of cancer, clinical evaluation of some of the more novel OV-synergizing compounds seems likely in the near future as a means to overcome heterogeneity in clinical response.

ACKNOWLEDGMENTS

This work was supported by grants from the Terry Fox Research Institute (grant # TFF 122868) and The Lotte and John Hecht Memorial Foundation Innovation Grant of the Canadian Cancer Society (grant #2012-701460) held by Jean-Simon Diallo.

REFERENCES

1. Forbes NE, Abdelbary H, Lupien M, Bell JC, Diallo JS. Exploiting tumor epigenetics to improve oncolytic virotherapy. *Front Genet* (2013) **4**:184. doi:10.3389/fgene.2013.00184
2. Ilkow CS, Swift SL, Bell JC, Diallo JS. From scourge to cure: tumor-selective viral pathogenesis as a new strategy against cancer. *PLoS Pathog* (2014) **10**:e1003836. doi:10.1371/journal.ppat.1003836
3. Prestwich RJ, Errington F, Ilett EJ, Morgan RS, Scott KJ, Kottke T, et al. Tumor infection by oncolytic reovirus primes adaptive antitumor immunity. *Clin Cancer Res* (2008) **14**:7358–66. doi:10.1158/1078-0432.CCR-08-0831
4. Cujar SA, Pan DA, Marcato P, Garant KA, Lee PW. Oncolytic virus-initiated protective immunity against prostate cancer. *Mol Ther* (2011) **19**:797–804. doi:10.1038/mt.2010.297
5. Steele L, Errington F, Prestwich R, Ilett E, Harrington K, Pandha H, et al. Pro-inflammatory cytokine/chemokine production by reovirus treated melanoma cells is PKR/NF-kappaB mediated and supports innate and adaptive anti-tumour immune priming. *Mol Cancer* (2011) **10**:20. doi:10.1186/1476-4598-10-20
6. Russell SJ, Peng KW, Bell JC. Oncolytic virotherapy. *Nat Biotechnol* (2012) **30**:658–70. doi:10.1038/nbt.2287
7. Park BH, Hwang T, Liu TC, Sze DY, Kim JS, Kwon HC, et al. Use of a targeted oncolytic poxvirus, JX-594, in patients with refractory primary or metastatic liver cancer: a phase I trial. *Lancet Oncol* (2008) **9**:533–42. doi:10.1016/S1470-2045(08)70107-4
8. Galanis E, Markovic SN, Suman VJ, Nuovo GJ, Vile RG, Kottke TJ, et al. Phase II trial of intravenous administration of Reolysin((R)) (Reovirus Serotype-3-dearing Strain) in patients with metastatic melanoma. *Mol Ther* (2012) **20**:1998–2003. doi:10.1038/mt.2012.146
9. Kim KH, Dmitriev IP, Saddekni S, Kashentseva EA, Harris RD, Aurigemma R, et al. A phase I clinical trial of Ad5/3-Delta24, a novel serotype-chimeric, infectivity-enhanced, conditionally-replicative adenovirus (CRAd), in patients with recurrent ovarian cancer. *Gynecol Oncol* (2013) **130**:518–24. doi:10.1016/j.ygyno.2013.06.003
10. Morris DG, Feng X, Difrancesco LM, Fonseca K, Forsyth PA, Paterson AH, et al. REO-001: a phase I trial of percutaneous intralesional administration of reovirus type 3 dearing (Reolysin(R)) in patients with advanced solid tumors. *Invest New Drugs* (2013) **31**:696–706. doi:10.1007/s10637-012-9865-z
11. Garber K. China approves world's first oncolytic virus therapy for cancer treatment. *J Natl Cancer Inst* (2006) **98**:298–300. doi:10.1093/jnci/djj111
12. Andtbacka RH, Collichio FA, Amatruda T, Senzer NN, Chesney J, Delman KA, et al. OPTIM: a randomized phase III trial of talimogene laherparepvec (T-VEC) versus subcutaneous (SC) granulocyte-macrophage colony-stimulating factor (GM-CSF) for the treatment (tx) of unresected stage IIIB/C and IV melanoma. *J Clin Oncol* (2013) **31**:LBA9008.
13. Helfand C. *Amgen to Pursue T-Vec Approval Despite PhIII Survival Miss [Online]*. FierceMarkets. (2014) [cited 2014 Jun 24]. Available from: http://www.fiercevaccines.com/story/amgen-pursue-t-vec-approval-despite-phiii-survival-miss/2014-06-03?utm_medium=nl&utm_source=internal
14. Senzer NN, Kaufman HL, Amatruda T, Nemunaitis M, Reid T, Daniels G, et al. Phase II clinical trial of a granulocyte-macrophage colony-stimulating factor-encoding, second-generation oncolytic herpesvirus in patients with unresectable metastatic melanoma. *J Clin Oncol* (2009) **27**:5763–71. doi:10.1200/JCO.2009.24.3675
15. Breitbach CJ, Burke J, Jonker D, Stephenson J, Haas AR, Chow LQ, et al. Intravenous delivery of a multi-mechanistic cancer-targeted oncolytic poxvirus in humans. *Nature* (2011) **477**:99–102. doi:10.1038/nature10358
16. Heo J, Reid T, Ruo L, Breitbach CJ, Rose S, Bloomston M, et al. Randomized dose-finding clinical trial of oncolytic immunotherapeutic vaccinia JX-594 in liver cancer. *Nat Med* (2013) **19**:329–36. doi:10.1038/nm.3089
17. Ottolino-Perry K, Diallo JS, Lichty BD, Bell JC, Andrea Mccart J. Intelligent design: combination therapy with oncolytic viruses. *Mol Ther* (2010) **18**:251–63. doi:10.1038/mt.2009.283
18. Hanahan D, Weinberg RA. Hallmarks of cancer: the next generation. *Cell* (2011) **144**:646–74. doi:10.1016/j.cell.2011.02.013
19. Emadi A, Jones RJ, Brodsky RA. Cyclophosphamide and cancer: golden anniversary. *Nat Rev Clin Oncol* (2009) **6**:638–47. doi:10.1038/nrclinonc.2009.146
20. Ikeda K, Ichikawa T, Wakimoto H, Silver JS, Deisboeck TS, Finkelstein D, et al. Oncolytic virus therapy of multiple tumors in the brain requires suppression of innate and elicited antiviral responses. *Nat Med* (1999) **5**:881–7. doi:10.1038/11320
21. Ikeda K, Wakimoto H, Ichikawa T, Jhung S, Hochberg FH, Louis DN, et al. Complement depletion facilitates the infection of multiple brain tumors by an intravascular, replication-conditional herpes simplex virus mutant. *J Virol* (2000) **74**:4765–75. doi:10.1128/JVI.74.10.4765-4775.2000
22. Wakimoto H, Fulci G, Tyminski E, Chiocca EA. Altered expression of antiviral cytokine mRNAs associated with cyclophosphamide's enhancement of viral oncolysis. *Gene Ther* (2004) **11**:214–23. doi:10.1038/sj.gt.3302143
23. Fulci G, Breymann L, Gianni D, Kurozomi K, Rhee SS, Yu J, et al. Cyclophosphamide enhances glioma virotherapy by inhibiting innate immune responses. *Proc Natl Acad Sci U S A* (2006) **103**:12873–8. doi:10.1073/pnas.0605496103
24. Currier MA, Gillespie RA, Sawtell NM, Mahller YY, Stroup G, Collins MH, et al. Efficacy and safety of the oncolytic herpes simplex virus rRp450 alone and combined with cyclophosphamide. *Mol Ther* (2008) **16**:879–85. doi:10.1038/mt.2008.49
25. Thomas MA, Spencer JF, Toth K, Sagartz JE, Phillips NJ, Wold WS. Immunosuppression enhances oncolytic adenovirus replication and antitumor efficacy

in the Syrian hamster model. *Mol Ther* (2008) **16**:1665–73. doi:10.1038/mt.2008.162

26. Dhar D, Spencer JF, Toth K, Wold WS. Effect of preexisting immunity on oncolytic adenovirus vector INGN 007 antitumor efficacy in immunocompetent and immunosuppressed Syrian hamsters. *J Virol* (2009) **83**:2130–9. doi:10.1128/JVI.02127-08
27. Cerullo V, Diaconu I, Kangasniemi L, Rajecki M, Escutenaire S, Koski A, et al. Immunological effects of low-dose cyclophosphamide in cancer patients treated with oncolytic adenovirus. *Mol Ther* (2011) **19**:1737–46. doi:10.1038/mt.2011.113
28. Hasegawa N, Abei M, Yokoyama KK, Fukuda K, Seo E, Kawashima R, et al. Cyclophosphamide enhances antitumor efficacy of oncolytic adenovirus expressing uracil phosphoribosyltransferase (UPRT) in immunocompetent Syrian hamsters. *Int J Cancer* (2013) **133**:1479–88. doi:10.1002/ijc.28132
29. Inn XQ, Jang JH, Tang N, Deng H, Head R, Bell JC, et al. Efficacy of systemically administered oncolytic vaccinia virotherapy for malignant gliomas is enhanced by combination therapy with rapamycin or cyclophosphamide. *Clin Cancer Res* (2009) **15**:2777–88. doi:10.1158/1078-0432.CCR-08-2342
30. Qiao J, Wang H, Kottke T, White C, Twigger K, Diaz RM, et al. Cyclophosphamide facilitates antitumor efficacy against subcutaneous tumors following intravenous delivery of reovirus. *Clin Cancer Res* (2008) **14**:259–69. doi:10.1158/1078-0432.CCR-07-1510
31. Ungerechts G, Springfeld C, Frenzke ME, Lampe J, Parker WB, Sorscher EJ, et al. An immunocompetent murine model for oncolysis with an armed and targeted measles virus. *Mol Ther* (2007) **15**:1991–7. doi:10.1038/sj.mt.6300291
32. Ungerechts G, Frenzke ME, Yaiw KC, Miest T, Johnston PB, Cattaneo R. Mantle cell lymphoma salvage regimen: synergy between a reprogrammed oncolytic virus and two chemotherapeutics. *Gene Ther* (2010) **17**:1506–16. doi:10.1038/gt.2010.103
33. Peng KW, Myers R, Greenslade A, Mader E, Greiner S, Federspiel MJ, et al. Using clinically approved cyclophosphamide regimens to control the humoral immune response to oncolytic viruses. *Gene Ther* (2013) **20**:255–61. doi:10.1038/gt.2012.31
34. Kottke T, Thompson J, Diaz RM, Pulido J, Willmon C, Coffey M, et al. Improved systemic delivery of oncolytic reovirus to established tumors using preconditioning with cyclophosphamide-mediated Treg modulation and interleukin-2. *Clin Cancer Res* (2009) **15**:561–9. doi:10.1158/1078-0432.CCR-08-1688
35. Mini E, Nobili S, Caciagli B, Landini I, Mazzei T. Cellular pharmacology of gemcitabine. *Ann Oncol* (2006) **17**(Suppl 5):v7–12. doi:10.1093/annonc/mdj941
36. Lolkema MP, Arkenau HT, Harrington K, Roxburgh P, Morrison R, Roulstone V, et al. A phase I study of the combination of intravenous reovirus type 3 Dearing and gemcitabine in patients with advanced cancer. *Clin Cancer Res* (2011) **17**:581–8. doi:10.1158/1078-0432.CCR-10-2159
37. Gabrilovich DI, Nagaraj S. Myeloid-derived suppressor cells as regulators of the immune system. *Nat Rev Immunol* (2009) **9**:162–74. doi:10.1038/nri2506
38. Leitner S, Sweeney K, Oberg D, Davies D, Miranda E, Lemoine NR, et al. Oncolytic adenoviral mutants with E1B19K gene deletions enhance gemcitabine-induced apoptosis in pancreatic carcinoma cells and anti-tumor efficacy in vivo. *Clin Cancer Res* (2009) **15**:1730–40. doi:10.1158/1078-0432.CCR-08-2008
39. Lin D, Kojima T, Onchi M, Kuroda S, Watanabe Y, Hashimoto Y, et al. Preclinical evaluation of synergistic effect of telomerase-specific oncolytic virotherapy and gemcitabine for human lung cancer. *Mol Cancer Ther* (2009) **8**:980–7. doi:10.1158/1535-7163.MCT-08-0901
40. Onimaru M, Ohuchida K, Nagai E, Mizumoto K, Egami T, Cui L, et al. Combination with low-dose gemcitabine and hTERT-promoter-dependent conditionally replicative adenovirus enhances cytotoxicity through their crosstalk mechanisms in pancreatic cancer. *Cancer Lett* (2010) **294**:178–86. doi:10.1016/j.canlet.2010.01.034
41. Bhattacharyya M, Francis J, Eddouadi A, Lemoine NR, Halliden G. An oncolytic adenovirus defective in pRb-binding (dl922-947) can efficiently eliminate pancreatic cancer cells and tumors in vivo in combination with 5-FU or gemcitabine. *Cancer Gene Ther* (2011) **18**:734–43. doi:10.1038/cgt.2011.45
42. Cherubini G, Kallin C, Mosetic A, Hammaren-Busch K, Muller H, Lemoine NR, et al. The oncolytic adenovirus Ad5Δ enhances selective cancer cell killing in combination with DNA-damaging drugs in pancreatic cancer models. *Gene Ther* (2011) **18**:1157–65. doi:10.1038/gt.2011.141
43. Wang H, Satoh M, Chen GP, Li DC, Hamada H, Arai Y. E1A, E1B double-restricted adenovirus enhances the cytotoxicity and antitumor activity of gemcitabine to renal cell carcinoma. *Chin Med J (Engl)* (2011) **124**:1082–7.
44. Kangasniemi L, Parviainen S, Pisto T, Koskinen M, Jokinen M, Kivitanto T, et al. Effects of capsid-modified oncolytic adenoviruses and their combinations with gemcitabine or silica gel on pancreatic cancer. *Int J Cancer* (2012) **131**:253–63. doi:10.1002/ijc.26370
45. Angelova AL, Aprahamian M, Grekova SP, Hajri A, Leuchs B, Giese NA, et al. Improvement of gemcitabine-based therapy of pancreatic carcinoma by means of oncolytic parvovirus H-1PV. *Clin Cancer Res* (2009) **15**:511–9. doi:10.1158/1078-0432.CCR-08-1088
46. Angelova AL, Grekova SP, Heller A, Kithlmann O, Soyka E, Giese T, et al. Complementary induction of immunogenic cell death by oncolytic parvovirus H-1PV and gemcitabine in pancreatic cancer. *J Virol* (2014) **88**:5263–76. doi:10.1128/JVI.03688-13
47. Sei S, Mussio JK, Yang QE, Nagashima K, Parchment RE, Coffey MC, et al. Synergistic antitumor activity of oncolytic reovirus and chemotherapeutic agents in non-small cell lung cancer cells. *Mol Cancer* (2009) **8**:47. doi:10.1186/1476-4598-8-47
48. Gujar SA, Clements D, Dielschneider R, Helson E, Marcato P, Lee PW. Gemcitabine enhances the efficacy of reovirus-based oncotherapy through anti-tumour immunological mechanisms. *Br J Cancer* (2014) **110**:83–93. doi:10.1038/bjc.2013.695
49. Hastie E, Besmer DM, Shah NR, Murphy AM, Moerdyk-Schauwecker M, Molestina C, et al. Oncolytic vesicular stomatitis virus in an immunocompetent model of MUC1-positive or MUC1-null pancreatic ductal adenocarcinoma. *J Virol* (2013) **87**:10283–94. doi:10.1128/JVI.01412-13
50. Watanabe I, Kasuya H, Nomura N, Shikano T, Shirota T, Kanazumi N, et al. Effects of tumor selective replication-competent herpes viruses in combination with gemcitabine on pancreatic cancer. *Cancer Chemother Pharmacol* (2008) **61**:875–82. doi:10.1007/s00280-007-0567-8
51. Esaki S, Goshima F, Kimura H, Murakami S, Nishiyama Y. Enhanced antitumoral activity of oncolytic herpes simplex virus with gemcitabine using colorectal tumor models. *Int J Cancer* (2013) **132**:1592–601. doi:10.1002/ijc.27823
52. Yu YA, Galanis C, Woo Y, Chen N, Zhang Q, Fong Y, et al. Regression of human pancreatic tumor xenografts in mice after a single systemic injection of recombinant vaccinia virus GLV-1h68. *Mol Cancer Ther* (2009) **8**:141–51. doi:10.1158/1535-7163.MCT-08-0533
53. Wennier ST, Liu J, Li S, Rahman MM, Mona M, McFadden G. Myxoma virus sensitizes cancer cells to gemcitabine and is an effective oncolytic virotherapeutic in models of disseminated pancreatic cancer. *Mol Ther* (2012) **20**:759–68. doi:10.1038/mt.2011.293
54. Bonvini P, Zorzi E, Basso G, Rosolen A. Bortezomib-mediated 26S proteasome inhibition causes cell-cycle arrest and induces apoptosis in CD-30+ anaplastic large cell lymphoma. *Leukemia* (2007) **21**:838–42. doi:10.1038/sj.leu.2404528
55. Berenson JR, Ma HM, Vescio R. The role of nuclear factor-kappaB in the biology and treatment of multiple myeloma. *Semin Oncol* (2001) **28**:626–33. doi:10.1053/sonc.2001.29542
56. Dizillo JS, Betton B, Parent N, Peant B, Lessard L, Le Page C, et al. Enhanced killing of androgen-independent prostate cancer cells using inositol hexakisphosphate in combination with proteasome inhibitors. *Br J Cancer* (2008) **99**:1613–22. doi:10.1038/sj.bjc.6604730
57. Nawrocki ST, Carew JS, Dunner K Jr., Boise LH, Chiao PJ, Huang P, et al. Bortezomib inhibits PKR-like endoplasmic reticulum (ER) kinase and induces apoptosis via ER stress in human pancreatic cancer cells. *Cancer Res* (2005) **65**:11510–9. doi:10.1158/0008-5472.CAN-05-2370
58. Marshansky V, Wang X, Bertrand R, Lno H, Duguid W, Chinnadurai G, et al. Proteasomes modulate balance among proapoptotic and antiapoptotic Bcl-2 family members and compromise functioning of the electron transport chain in leukemic cells. *J Immunol* (2001) **166**:3130–42. doi:10.4049/jimmunol.166.5.3130
59. Chang CL, Hsu YT, Wu CC, Yang YC, Wang C, Wu TC, et al. Immune mechanism of the antitumor effects generated by bortezomib. *J Immunol* (2012) **189**:3209–20. doi:10.4049/jimmunol.1103826
60. Berges C, Haberstock H, Fuchs D, Militz M, Sadeghi M, Opelz G, et al. Proteasome inhibition suppresses essential immune functions of human CD4+ T cells. *Immunology* (2008) **124**:234–46. doi:10.1111/j.1365-2567.2007.02761.x

61. Yarde DN, Nace RA, Russell SJ. Oncolytic vesicular stomatitis virus and bortezomib are antagonistic against myeloma cells in vitro but have additive anti-myeloma activity in vivo. *Exp Hematol* (2013) **41**:1038–49. doi:10.1016/j.exphem.2013.09.005
62. Carew JS, Espitia CM, Zhao W, Kelly KR, Coffey M, Freeman JW, et al. Reolysin is a novel reovirus-based agent that induces endoplasmic reticular stress-mediated apoptosis in pancreatic cancer. *Cell Death Dis* (2013) **4**:e728. doi:10.1038/cddis.2013.259
63. Bourgeois B, Mundt B, Wolker N, Strayer N, Gurlevik E, Schache P, et al. Antitumoral immunity by virus-mediated immunogenic apoptosis inhibits metastatic growth of hepatocellular carcinoma. *Gut* (2010) **59**:1416–26. doi:10.1136/gut.2009.196519
64. Mazerski J, Martelli S, Borowski E. The geometry of intercalation complex of antitumor mitoxantrone and ametantrone with DNA: molecular dynamics simulations. *Acta Biochim Pol* (1998) **45**:1–11.
65. Fidler JM, Dejoy SQ, Smith FR III, Gibbons JJ Jr. Selective immunomodulation by the antineoplastic agent mitoxantrone. II. Nonspecific adherent suppressor cells derived from mitoxantrone-treated mice. *J Immunol* (1986) **136**:2747–54.
66. Neuhaus O, Wiendl H, Kieseier BC, Archelos JJ, Hemmer B, Stüve O, et al. Multiple sclerosis: mitoxantrone promotes differential effects on immunocompetent cells in vitro. *J Neuroimmunol* (2005) **168**:128–37. doi:10.1016/j.jneuroim.2005.01.024
67. Kopadze T, Dehmel T, Hartung HP, Stüve O, Kieseier BC. Inhibition by mitoxantrone of in vitro migration of immunocompetent cells: a possible mechanism for therapeutic efficacy in the treatment of multiple sclerosis. *Arch Neurol* (2006) **63**:1572–8. doi:10.1001/archneur.63.11.1572
68. Okuda DT. Immunosuppressive treatments in multiple sclerosis. *Handb Clin Neurol* (2014) **122**:503–11. doi:10.1016/B978-0-444-52001-2.00022-4
69. Workenhe S, Pol JG, Lichty BD, Cummings DT, Mossman KL. Combining oncolytic HSV-1 with immunogenic cell death-inducing drug mitoxantrone breaks cancer immune tolerance and improves therapeutic efficacy. *Cancer Immunol Res* (2013) **1**:1–11. doi:10.1158/2326-6066.CIR-13-0059-T
70. Oberg D, Yanover E, Adam V, Sweeney K, Costas C, Lemoine NR, et al. Improved potency and selectivity of an oncolytic E1ACR2 and E1B19K deleted adenoviral mutant in prostate and pancreatic cancers. *Clin Cancer Res* (2010) **16**:541–53. doi:10.1158/1078-0432.CCR-09-1960
71. Radhakrishnan S, Miranda E, Ekblad M, Holford A, Pizarro MT, Lemoine NR, et al. Efficacy of oncolytic mutants targeting pRb and p53 pathways is synergistically enhanced when combined with cytotoxic drugs in prostate cancer cells and tumor xenografts. *Hum Gene Ther* (2010) **21**:1311–25. doi:10.1089/hum.2010.019
72. Miranda E, Maya Pineda H, Oberg D, Cherubini G, Garate Z, Lemoine NR, et al. Adenovirus-mediated sensitization to the cytotoxic drugs docetaxel and mitoxantrone is dependent on regulatory domains in the E1ACR1 gene-region. *PLoS One* (2012) **7**:e46617. doi:10.1371/journal.pone.0046617
73. Maeda K, Hazama S, Tokuno K, Kan S, Maeda Y, Watanabe Y, et al. Impact of chemotherapy for colorectal cancer on regulatory T-cells and tumor immunity. *Anticancer Res* (2011) **31**:4569–74.
74. Tyminski E, Leroy S, Terada K, Finkelstein DM, Hyatt JL, Danks MK, et al. Brain tumor oncolysis with replication-conditional herpes simplex virus type 1 expressing the prodrug-activating genes, CYP2B1 and secreted human intestinal carboxylesterase, in combination with cyclophosphamide and irinotecan. *Cancer Res* (2005) **65**:6850–7. doi:10.1158/0008-5472.CAN-05-0154
75. Granot T, Meruelo D. The role of natural killer cells in combinatorial anticancer therapy using Sindbis viral vectors and irinotecan. *Cancer Gene Ther* (2012) **19**:588–91. doi:10.1038/cgt.2012.33
76. Stupp R, Mason WP, Van Den Bent MJ, Weller M, Fisher B, Taphoorn MJ, et al. Radiotherapy plus concomitant and adjuvant temozolomide for glioblastoma. *N Engl J Med* (2005) **352**:987–96. doi:10.1056/NEJMoa043330
77. Middleton MR, Grob JJ, Aaronson N, Fierlbeck G, Tilgen W, Seiter S, et al. Randomized phase III study of temozolomide versus dacarbazine in the treatment of patients with advanced metastatic malignant melanoma. *J Clin Oncol* (2000) **18**:158–66.
78. Sanchez-Perez LA, Choi BD, Archer GE, Cui X, Flores C, Johnson LA, et al. Myeloablative temozolomide enhances CD8(+) T-cell responses to vaccine and is required for efficacy against brain tumors in mice. *PLoS One* (2013) **8**:e59082. doi:10.1371/journal.pone.0059082
79. Banissi C, Ghiringhelli F, Chen L, Carpentier AF. Treg depletion with a low-dose metronomic temozolomide regimen in a rat glioma model. *Cancer Immunol Immunother* (2009) **58**:1627–34. doi:10.1007/s00262-009-0671-1
80. Alonso MM, Gomez-Manzano C, Jiang H, Bekele NB, Piao Y, Yung WK, et al. Combination of the oncolytic adenovirus ICOVIR-5 with chemotherapy provides enhanced anti-glioma effect in vivo. *Cancer Gene Ther* (2007) **14**:756–61. doi:10.1038/sj.cgt.7701067
81. Holzmüller R, Mantwill K, Haczek C, Rognoni E, Anton M, Kasajima A, et al. YB-1 dependent virotherapy in combination with temozolomide as a multimodal therapy approach to eradicate malignant glioma. *Int J Cancer* (2011) **129**:1265–76. doi:10.1002/ijc.25783
82. Liikanen I, Ahtiainen L, Hirvinen ML, Bramante S, Cerullo V, Nokisalmi P, et al. Oncolytic adenovirus with temozolomide induces autophagy and antitumor immune responses in cancer patients. *Mol Ther* (2013) **21**:1212–23. doi:10.1038/mt.2013.51
83. Tobias AL, Thaci B, Auffinger B, Rincon E, Balyasnikova IV, Kim CK, et al. The timing of neural stem cell-based virotherapy is critical for optimal therapeutic efficacy when applied with radiation and chemotherapy for the treatment of glioblastoma. *Stem Cells Transl Med* (2013) **2**:655–66. doi:10.5966/sctm.2013-0039
84. Aghi M, Rabkin S, Martuza RL. Effect of chemotherapy-induced DNA repair on oncolytic herpes simplex viral replication. *J Natl Cancer Inst* (2006) **98**:38–50. doi:10.1093/jnci/djj003
85. Kanai R, Rabkin SD, Yip S, Sgubin D, Zaupa CM, Hirose Y, et al. Oncolytic virus-mediated manipulation of DNA damage responses: synergy with chemotherapy in killing glioblastoma stem cells. *J Natl Cancer Inst* (2012) **104**:42–55. doi:10.1093/jnci/djr509
86. Jha BK, Polyakova I, Kessler P, Dong B, Dickerman B, Sen GC, et al. Inhibition of RNase L and RNA-dependent protein kinase (PKR) by sunitinib impairs antiviral innate immunity. *J Biol Chem* (2011) **286**:26319–26. doi:10.1074/jbc.M111.253443
87. Kottke T, Hall G, Pulido J, Diaz RM, Thompson J, Chong H, et al. Antiangiogenic cancer therapy combined with oncolytic virotherapy leads to regression of established tumors in mice. *J Clin Invest* (2010) **120**:1551–60. doi:10.1172/JCI41431
88. Jha BK, Dong B, Nguyen CT, Polyakova I, Silverman RH. Suppression of antiviral innate immunity by sunitinib enhances oncolytic virotherapy. *Mol Ther* (2013) **21**:1749–57. doi:10.1038/mt.2013.112
89. Hou W, Chen H, Rojas J, Sampath P, Thorne SH. Oncolytic vaccinia virus demonstrates antiangiogenic effects mediated by targeting of VEGF. *Int J Cancer* (2014) **135**:1238–46. doi:10.1002/ijc.28747
90. Breitbach CJ, Paterson JM, Lemay CG, Falls TJ, Mcguire A, Parato KA, et al. Targeted inflammation during oncolytic virus therapy severely compromises tumor blood flow. *Mol Ther* (2007) **15**:1686–93. doi:10.1038/sj.mt.6300215
91. Lin TC, Hwang T, Park BH, Bell J, Kirn DH. The targeted oncolytic poxvirus JX-594 demonstrates antitumoral, antivascular, and anti-HBV activities in patients with hepatocellular carcinoma. *Mol Ther* (2008) **16**:1637–42. doi:10.1038/mt.2008.143
92. Breitbach CJ, Arulanandam R, De Silva N, Thorne SH, Patt R, Daneshmand M, et al. Oncolytic vaccinia virus disrupts tumor-associated vasculature in humans. *Cancer Res* (2013) **73**:1265–75. doi:10.1158/0008-5472.CAN-12-2687
93. Magnani L, Eeckhoute J, Lupien M. Pioneer factors: directing transcriptional regulators within the chromatin environment. *Trends Genet* (2011) **27**:465–74. doi:10.1016/j.tig.2011.07.002
94. Picaud S, Bardot B, De Maeyer E, Seif I. Enhanced tumor development in mice lacking a functional type I interferon receptor. *J Interferon Cytokine Res* (2002) **22**:457–62. doi:10.1089/10799900252952244
95. Dunn GP, Koebel CM, Schreiber RD. Interferons, immunity and cancer immunoediting. *Nat Rev Immunol* (2006) **6**:836–48. doi:10.1038/nri1961
96. Uno K, Hirosaki M, Kakimi K, Tominaga M, Sugimoshita Y, Hasegawa G, et al. Impaired IFN-alpha production and the risk of cancer development. *J Interferon Cytokine Res* (2007) **27**:1013–7. doi:10.1089/jir.2007.0047
97. Stojdl DF, Lichty BD, Tenoever BR, Paterson JM, Power AT, Knowles S, et al. VSV strains with defects in their ability to shutdown innate immunity are potent systemic anti-cancer agents. *Cancer Cell* (2003) **4**:263–75. doi:10.1016/S1535-6108(03)00241-1

98. Naka K, Abe K, Takemoto K, Dansako H, Ikeda M, Shimotohno K, et al. Epigenetic silencing of interferon-inducible genes is implicated in interferon resistance of hepatitis C virus replicon-harboring cells. *J Hepatol* (2006) **44**:869–78. doi:10.1016/j.jhep.2006.01.030
99. Nguyen TL, Abdelbary H, Arguello M, Breithach C, Lewelle S, Diallo JS, et al. Chemical targeting of the innate antiviral response by histone deacetylase inhibitors renders refractory cancers sensitive to viral oncolysis. *Proc Natl Acad Sci U S A* (2008) **105**:14981–6. doi:10.1073/pnas.0803988105
100. Fang TC, Schaefer U, Mecklenbrauker I, Stienen A, Dewell S, Chen MS, et al. Histone H3 lysine 9 di-methylation as an epigenetic signature of the interferon response. *J Exp Med* (2012) **209**:661–9. doi:10.1084/jem.20112343
101. Chen Q, Denard B, Huang H, Ye J. Epigenetic silencing of antiviral genes renders clones of Huh-7 cells permissive for hepatitis C virus replication. *J Virol* (2013) **87**:659–65. doi:10.1128/JVI.01984-12
102. Cho H, Proll SC, Szretter KJ, Katze MG, Gale M Jr, Diamond MS. Differential innate immune response programs in neuronal subtypes determine susceptibility to infection in the brain by positive-stranded RNA viruses. *Nat Med* (2013) **19**:458–64. doi:10.1038/nm.3108
103. Chang HM, Paulson M, Holko M, Rice CM, Williams BR, Marie I, et al. Induction of interferon-stimulated gene expression and antiviral responses require protein deacetylase activity. *Proc Natl Acad Sci U S A* (2004) **101**:9578–83. doi:10.1073/pnas.0400567101
104. Katsura T, Iwai S, Ota Y, Shimizu H, Ikuta K, Yura Y. The effects of trichostatin A on the oncolytic ability of herpes simplex virus for oral squamous cell carcinoma cells. *Cancer Gene Ther* (2009) **16**:237–45. doi:10.1038/cgt.2008.81
105. Lin TC, Castelo-Branco P, Rabkin SD, Martuza RL. Trichostatin A and oncolytic HSV combination therapy shows enhanced antitumoral and antiangiogenic effects. *Mol Ther* (2008) **16**:1041–7. doi:10.1038/mt.2008.58
106. Otsuki A, Patel A, Kasai K, Suzuki M, Kurozumi K, Chiocca EA, et al. Histone deacetylase inhibitors augment antitumor efficacy of herpes-based oncolytic viruses. *Mol Ther* (2008) **16**:1546–55. doi:10.1038/mt.2008.155
107. Alvarez-Breckenridge CA, Yu J, Price R, Wei M, Wang Y, Nowicki MO, et al. The histone deacetylase inhibitor valproic acid lessens NK cell action against oncolytic virus-infected glioblastoma cells by inhibition of STAT5/T-BET signaling and generation of gamma interferon. *J Virol* (2012) **86**:4566–77. doi:10.1128/JVI.05545-11
108. MacTavish H, Diallo JS, Huang B, Stanford M, Le Boeuf F, De Silva N, et al. Enhancement of vaccinia virus based oncolysis with histone deacetylase inhibitors. *PLoS One* (2010) **5**:e14462. doi:10.1371/journal.pone.0014462
109. Bridle BW, Chen L, Lemay CG, Diallo JS, Pol J, Nguyen A, et al. HDAC inhibition suppresses primary immune responses, enhances secondary immune responses, and abrogates autoimmunity during tumor immunotherapy. *Mol Ther* (2013) **21**:887–94. doi:10.1038/mt.2012.265
110. Cedar H, Bergman Y. Linking DNA methylation and histone modification: patterns and paradigms. *Nat Rev Genet* (2009) **10**:295–304. doi:10.1038/nrg2540
111. Okemoto K, Kasai K, Wagner B, Haseley A, Meisen H, Bolyard C, et al. DNA demethylating agents synergize with oncolytic HSV1 against malignant gliomas. *Clin Cancer Res* (2013) **19**:5952–9. doi:10.1158/1078-0432.CCR-12-3588
112. Wong KK, Engelman JA, Cantley LC. Targeting the PI3K signaling pathway in cancer. *Curr Opin Genet Dev* (2010) **20**:87–90. doi:10.1016/j.gde.2009.11.002
113. Uddin S, Fish EN, Sher DA, Gardziola C, White MF, Platanias LC. Activation of the phosphatidylinositol 3-kinase serine kinase by IFN-alpha. *J Immunol* (1997) **158**:2390–7.
114. Martini M, Ciraolo E, Gulluni F, Hirsch E. Targeting PI3K in cancer: any good news? *Front Oncol* (2013) **3**:108. doi:10.3389/fonc.2013.00108
115. Vlahos CJ, Matter WF, Hui KY, Brown RF. A specific inhibitor of phosphatidylinositol 3-kinase, 2-(4-morpholinyl)-8-phenyl-4H-1-benzopyran-4-one (LY294002). *J Biol Chem* (1994) **269**:5241–8.
116. Kanai R, Wakimoto H, Martuza RL, Rabkin SD. A novel oncolytic herpes simplex virus that synergizes with phosphoinositide 3-kinase/Akt pathway inhibitors to target glioblastoma stem cells. *Clin Cancer Res* (2011) **17**:3686–96. doi:10.1158/1078-0432.CCR-10-3142
117. Tong Y, Zhu W, Huang X, You L, Han X, Yang C, et al. PI3K inhibitor LY294002 inhibits activation of the Akt/mTOR pathway induced by an oncolytic adenovirus expressing TRAIL and sensitizes multiple myeloma cells to the oncolytic virus. *Oncol Rep* (2014) **31**:1581–8. doi:10.3892/or.2014.3020
118. Kaur S, Lal L, Sassano A, Majchrzak-Kita B, Srikanth M, Baker DP, et al. Regulatory effects of mammalian target of rapamycin-activated pathways in type I and II interferon signaling. *J Biol Chem* (2007) **282**:1757–68. doi:10.1074/jbc.M607365200
119. Lukashev AN, Pfuerer C, Chen MJ, Searle P, Iggo R. Late expression of nitroreductase in an oncolytic adenovirus sensitizes colon cancer cells to the prodrug CB1954. *Hum Gene Ther* (2005) **16**:1473–83. doi:10.1089/hum.2005.16.1473
120. Jiang ZK, Johnson M, Monaghon DL, Kuo J, Sato M, Wu L. Rapamycin enhances adenovirus-mediated cancer imaging and therapy in pre-immunized murine hosts. *PLoS One* (2013) **8**:e73650. doi:10.1371/journal.pone.0073650
121. Fu X, Tao L, Rivera A, Zhang X. Rapamycin enhances the activity of oncolytic herpes simplex virus against tumor cells that are resistant to virus replication. *Int J Cancer* (2011) **129**:1503–10. doi:10.1002/ijc.25808
122. Alain T, Lun X, Martineau Y, Sean P, Pulendran B, Petroulakis E, et al. Vesicular stomatitis virus oncolysis is potentiated by impairing mTORC1-dependent type I IFN production. *Proc Natl Acad Sci U S A* (2010) **107**:1576–81. doi:10.1073/pnas.0912344107
123. Stanford MM, Barrett JW, Nazarian SH, Werden S, Mcfadden G. Oncolytic virotherapy synergism with signaling inhibitors: rapamycin increases myxoma virus tropism for human tumor cells. *J Virol* (2007) **81**:1251–60. doi:10.1128/JVI.01408-06
124. Zemp FJ, Lun X, Mckenzie BA, Zhou H, Maxwell L, Sun B, et al. Treating brain tumor-initiating cells using a combination of myxoma virus and rapamycin. *Neuro Oncol* (2013) **15**:904–20. doi:10.1093/neuonc/not035
125. Diallo JS, Le Boeuf F, Lai F, Cox J, Vaha-Koskela M, Abdelbary H, et al. A high-throughput pharmacoviral approach identifies novel oncolytic virus sensitizers. *Mol Ther* (2010) **18**:1123–9. doi:10.1038/mt.2010.67
126. Kiviharju TM, Lecane PS, Sellers RG, Peehl DM. Antiproliferative and proapoptotic activities of triptolide (PG490), a natural product entering clinical trials, on primary cultures of human prostatic epithelial cells. *Clin Cancer Res* (2002) **8**:2666–74.
127. Kitzen JJ, De Jonge MJ, Lamers CH, Eskens FA, Van Der Biessen D, Van Doorn L, et al. Phase I dose-escalation study of F60038, a novel apoptosis inducer, in patients with advanced solid tumours. *Eur J Cancer* (2009) **45**:1764–72. doi:10.1016/j.ejca.2009.01.026
128. Wong KF, Yuan Y, Luk JM. Tripterygium wilfordii bioactive compounds as anticancer and anti-inflammatory agents. *Clin Exp Pharmacol Physiol* (2012) **39**:311–20. doi:10.1111/j.1440-1681.2011.05586.x
129. Zhou ZL, Yang YX, Ding J, Li YC, Miao ZH. Triptolide: structural modifications, structure-activity relationships, bioactivities, clinical development and mechanisms. *Nat Prod Rep* (2012) **29**:457–75. doi:10.1039/c2np00088a
130. Ben Yebdri F, Van Grevenynghe J, Tang VA, Goulet ML, Wu JH, Stojdl DF, et al. Triptolide-mediated inhibition of interferon signaling enhances vesicular stomatitis virus-based oncolysis. *Mol Ther* (2013) **21**:2043–53. doi:10.1038/mt.2013.187
131. Quintas-Cardama A, Vaddi K, Liu P, Manshouri T, Li J, Scherle PA, et al. Preclinical characterization of the selective JAK1/2 inhibitor INCB018424: therapeutic implications for the treatment of myeloproliferative neoplasms. *Blood* (2010) **115**:3109–17. doi:10.1182/blood-2009-04-214957
132. Mesa RA, Yasothan U, Kirkpatrick P. Ruxolitinib. *Nat Rev Drug Discov* (2012) **11**:103–4. doi:10.1038/nrd3652
133. Quintas-Cardama A, Kantarjian H, Cortes J, Verstovsek S. Janus kinase inhibitors for the treatment of myeloproliferative neoplasias and beyond. *Nat Rev Drug Discov* (2011) **10**:127–40. doi:10.1038/nrd3264
134. Verstovsek S, Kantarjian H, Mesa RA, Pardanani AD, Cortes-Franco J, Thomas DA, et al. Safety and efficacy of INCB018424, a JAK1 and JAK2 inhibitor, in myelofibrosis. *N Engl J Med* (2010) **363**:1117–27. doi:10.1056/NEJMoa1002028
135. Escobar-Zarate D, Liu YP, Suksanpaisan L, Russell SJ, Peng KW. Overcoming cancer cell resistance to VSV oncolysis with JAK1/2 inhibitors. *Cancer Gene Ther* (2013) **20**:582–9. doi:10.1038/cgt.2013.55
136. Paglino JC, van den Pol AN. Vesicular stomatitis virus has extensive oncolytic activity against human sarcomas: rare resistance is overcome by blocking interferon pathways. *J Virol* (2011) **85**:9346–58. doi:10.1128/JVI.00723-11
137. Heinrich B, Goepfert K, Delic M, Galle PR, Moehler M. Influence of the oncolytic parvovirus H-1, CTLA-4 antibody tremelimumab and cytostatic drugs on the human immune system in a human in vitro model of colorectal cancer cells. *Onco Targets Ther* (2013) **6**:1119–27. doi:10.2147/OTT.S49371

138. Zamarin D, Holmgaard RB, Subudhi SK, Park JS, Mansour M, Palese P, et al. Localized oncolytic virotherapy overcomes systemic tumor resistance to immune checkpoint blockade immunotherapy. *Sci Transl Med* (2014) 6:226ra232. doi:10.1126/scitranslmed.3008095

Conflict of Interest Statement: The authors declare that the research was conducted in the absence of any commercial or financial relationships that could be construed as a potential conflict of interest.

Received: 21 May 2014; accepted: 07 July 2014; published online: 23 July 2014.

Citation: Forbes NE, Krishnan R and Diallo J-S (2014) Pharmacological modulation of anti-tumor immunity induced by oncolytic viruses. Front. Oncol. 4:191. doi: 10.3389/fonc.2014.00191

This article was submitted to Tumor Immunity, a section of the journal Frontiers in Oncology.

Appendix F:

Garcia V, **Krishnan R**, Davis C, Batenchuk C, Le Boeuf F, Abdelbary H, Diallo JS. "High-Throughput Titration of Vesicular Stomatitis Virus Using a Luciferase Reporter Assay." *Journal of Visualized Experiments*. 91, e51890 (2014) doi:10.3791/51890.

jove Journal of Visualized Experiments www.jove.com

Video Article

High-throughput Titration of Luciferase-expressing Recombinant Viruses

Vanessa Garcia[1,2], Ramya Krishnan[1,2], Colin Davis[1,2], Cory Batenchuk[1,2], Fabrice Le Boeuf[1,3], Hesham Abdelbary[1,3], Jean-Simon Diallo[1,2]

[1]Center for Innovative Cancer Research, Ottawa Hospital Research Institute

[2]Department of Biochemistry, Microbiology and Immunology, Faculty of Medicine, University of Ottawa

[3]Faculty of Medicine, University of Ottawa

Correspondence to: Jean-Simon Diallo at jsdiallo@ohri.ca

URL: https://www.jove.com/video/51890
DOI: doi:10.3791/51890

Keywords: Virology, Issue 91, titration, virus, plaque assay, high-throughput, transgene, luciferase, automated, cytotoxicity assay, Vesicular Stomatitis Virus, Herpes Simplex virus, Vaccinia virus, Adeno-Associated virus

Date Published: 9/19/2014

Citation: Garcia, V., Krishnan, R., Davis, C., Batenchuk, C., Le Boeuf, F., Abdelbary, H., Diallo, J.S. High-throughput Titration of Luciferase-expressing Recombinant Viruses. *J. Vis. Exp.* (91), e51890, doi:10.3791/51890 (2014).

Abstract

Standard plaque assays to determine infectious viral titers can be time consuming, are not amenable to a high volume of samples, and cannot be done with viruses that do not form plaques. As an alternative to plaque assays, we have developed a high-throughput titration method that allows for the simultaneous titration of a high volume of samples in a single day. This approach involves infection of the samples with a Firefly luciferase tagged virus, transfer of the infected samples onto an appropriate permissive cell line, subsequent addition of luciferin, reading of plates in order to obtain luminescence readings, and finally the conversion from luminescence to viral titers. The assessment of cytotoxicity using a metabolic viability dye can be easily incorporated in the workflow in parallel and provide valuable information in the context of a drug screen. This technique provides a reliable, high-throughput method to determine viral titers as an alternative to a standard plaque assay.

Video Link

The video component of this article can be found at https://www.jove.com/video/51890/

Introduction

Classical viral plaque assays continue to be a mainstay in virus research even though they can be notoriously time-consuming and constitute a significant bottleneck to obtaining results from experiments. More rapid indirect virus quantification methods have emerged including quantitative polymerase chain reaction (qPCR), ELISA, and flow cytometry[1-4]. Recent innovations such as the Virocyt virus counter can directly count viruses using advanced flow sorting technology and through a combination of protein and DNA/RNA dyes[5]. While all of these methods have undoubtedly quickened the pace of virus research, each method has its advantages and drawbacks. For example, qPCR can allow for quantification of specific viral genome sequence but cannot effectively discriminate infectious from defective virions[6]. ELISAs can be very specific however require a suitable antibody against the desired target viral protein and can be very expensive. While flow cytometry technology offers many advantages and has improved significantly, throughput and accessibility to highly specialized equipment nonetheless remains a hurdle. Importantly, all of these techniques are not ideally suited for high-throughput screening, for which the ease and time requirement of the virus quantification step is of critical importance.

Here we describe a high-throughput and easily automatable technique to titer viruses that express a Firefly luciferase (Fluc) transgene. This method generates approximate viral titers in a test sample based on luminescence signal reads through the parallel use of a standard curve of known amounts of virus. Samples containing unknown quantities of luciferase-expressing virus are transferred on to a permissive "plaquing" cell line in parallel with the standard virus dilution curve and virus-associated luminescence is read after a few hours incubation time. This allows for rapid, quantitative, often same-day generation of results, unlike classic plaque assay protocols which typically require several days of incubation in order to manually count visible plaques[7-9].

The protocol outlines the steps of our titration method using oncolytic Vesicular Stomatitis Virus encoding a Fluc transgene (VSVΔ51-Fluc) as an example and provides an overview of 1. Sample preparation 2. The plating of a permissive cell line for virus titration using an automated dispenser 3. The preparation of the viral standard curve 4. The transfer of the sample supernatants onto the permissive cell line using a 96-well manual pipettor 5. The assessment of sample cytotoxicity using a cell viability reagent 6. The preparation of the luciferin substrate 7. Reading of bioluminescence and 8. Data analysis.

Protocol

1. Sample Preparation

1. Obtain samples containing luciferase-expressing virus (herein VSVΔ51-Fluc as an example) for titration and transfer into 96-well plates. Alternately, perform infections in 96-well tissue culture plates and use supernatants directly.
2. Leave two columns untreated for the inclusion of standard curves. For experiments done directly in 96-well plates, titer at the end of the experiment (40 hr post-infection) or store at -80 °C and titer at a later date.

2. Preparation of Permissive Cells for Virus Titration

1. 24 hr prior to titering, prepare a suspension of Vero cells at a concentration of 2.5 x 10^5 cells/ml in Dulbecco's modified eagle medium (DMEM) containing 10% fetal bovine serum (FBS), 30 mM HEPES, and 1% penicillin/streptomycin. NOTE: Although this protocol uses Vero cells, any suitable permissive cell line for VSV infection could be used.
2. Seed 2.5 x 10^4 cells (100 µl) in 96-well white solid flat-bottom plates using a microplate dispenser.
    1. Prepare 12 ml of cell suspension per plate plus 5 ml for priming.
    2. Clean microplate dispenser cassette by flushing the tubing with 50 ml of sterile water.
    3. Fill the microplate dispenser lines with cell suspension and let 5 ml of cell suspension flow through.
    4. Select a program that will dispense 100 µl in each well of a white-walled 96-well plate. Dispense, and repeat as necessary for additional plates. Also seed a few wells in a 96-well clear flat-bottom plate if opaque-bottom white-walled plates are used for verification of cell health and density.
    5. When finished, flush cells back into original container. Clean the cassette by running 50 ml of 70% ethanol followed by 50 ml of warm sterile water through the tubing.
    6. Make sure cassette and tubing are appropriately cleaned between uses.
3. Incubate cells for 24 hr at 37 °C in a humidified 5% CO_2 incubator.

3. Preparation of Viral Standard Curve

1. Prepare a standard curve of VSVΔ51-Fluc in serum-free DMEM such that the final concentration of plaque forming units (pfu) per ml after transfer onto Vero cells is as follows: 10^8 pfu/ml, 10^7 pfu/ml, 10^6 pfu/ml, 10^5 pfu/ml, 10^4 pfu/ml, 10^3 pfu/ml, 10^2 pfu/ml, and 10^1 pfu/ml. Prepare 50 µl of each concentration per plate of Vero cells plus an extra 10%.
   NOTE: Titer of the luciferase virus stock will need to be assessed in a classical way[10] in order to generate a standard curve that will allow for absolute quantification. Otherwise relative quantification can be achieved without precise titer information by arbitrarily setting viral titer based on dilution steps. For example the first dilution of the standard curve may be set to 10^8 viral units and the following 1/10 dilution to 10^7 and so on. In this context, one should express values as a fold-change compared to a pre-determined sample as absolute quantification will not be accurate.

4. Transfer of Sample Supernatants onto Permissive Cells

1. Check Vero cells plated in the clear-bottom 96-well plate under a light microscope to confirm that monolayers are at least 95% confluent.
2. Transfer 25 µl of sample supernatant onto Vero cells seeded in white-walled plates. Do not transfer supernatants into the 2 columns designated for standard curves. NOTE: This can be done simultaneously for all wells on a single plate using a 96-channel liquid handler.
3. Using an 8- or 12-channel multi-channel pipettor, add 25 µl of each dilution of the standard curve prepared in Step 3 to the Vero cells in the 2 designated columns.
4. Centrifuge plates for 5 min at 430 x g at RT.
5. Incubate for 5 hr at 37 °C in a humidified 5% CO_2 incubator.

5. Assessment of Cell Viability

1. NOTE: When starting from supernatants obtained from infection experiments done in clear 96-well plates, sample viability can be assessed prior to quantification with a cell viability indicator dye such as resazurin.
2. Add resazurin in an amount equal to 10% of the volume in each well of the 96-well plate of samples containing virus and cells. Include cell-only controls as well as media-only control to determine values for 100% and 0% viability respectively.
3. After 2-4 hr (incubation time will vary depending on cell type and on the concentration of commercially available or reconstituted powder of the dye), read and record the signal using a fluorescence plate reader (530-560 excitation, 590 emission). Report cell viability for a sample according to the formula Relative Metabolic Activity = ((Test sample signal - negative control signal) / (Cell only control signal - negative control signal)) x 100%

6. Preparation of the Luciferin Substrate

1. 30 min before the end of the 5 hr incubation, prepare the luciferin to obtain a 2 mg/ml solution in sterile phosphate buffered saline (PBS). Prepare 2.5 ml per plate plus an extra 2 ml. Protect solution from light. NOTE: The luciferin may also be prepared earlier in the day and stored at 4 °C until use.

7. Reading Bioluminescence

1. After the 5 hr incubation period, add 25 µl of luciferin to each well of Vero cells in the white solid plates. Add luciferin manually or with an automated dispenser integrated in the luminometer. NOTE: The use of an instrument with only single and end point reads may require the addition of a luciferase compatible lysis buffer prior to adding the luciferin substrate to improve consistency.
2. Read the plates with the following parameters:
    1. Shake for 5 sec.
    2. Wait 30 sec.
    3. Read luminescence at an appropriate fixed sensitivity / exposure value. If the option is available on the instrument, use multi-point reads (*e.g.*, 3 x 3 matrix) to improve accuracy.
3. Record and save the quantified bioluminescent intensity.
4. If an automated dispenser was used to add luciferin purge the luciferin and prime the lines with warm sterile water.

8. Data Analysis

1. For accurate results, solve the non-linear regression to generate a Hill equation from the standard curves. Apply this equation to the titered samples to calculate viral expression units. Some viruses or situations may produce a standard curve with a linear relationship; in this case solve for a linear equation.

Representative Results

A summary of the workflow describing the high-throughput method is illustrated in **Figure 1**. **Figure 2** shows the results of a typical standard curve of VSVΔ51-Fluc. Four-parameter non-linear regression analysis generated a Hill plot from which unknown input pfu (estimate of viral titer) can be interpolated. These estimated titers are termed viral expression units (VEU). **Figure 3A** shows VEUs and titers obtained by performing a standard plaque assay with the same samples[16]. Samples originated from an experiment where various chemicals were used to enhance the replication and spread of VSVΔ51-Fluc in 786-0 cells. VEUs interpolated from the standard curve must be multiplied by a factor which is based on the dilution of sample supernatants being transferred on to Vero cells (in this case, the dilution factor is 5). The linear correlation between titers and VEU is shown in **Figure 3B** with an R^2 of 0.8083 and a Pearson's r score of 0.899 ($p < 0.0001$). In **Figure 4**, typical cell cytotoxicity data obtained from a metabolic assay is shown for 786-0 cells treated with chemicals prior to infection with VSVΔ51-Fluc. Finally, **Figure 5** shows typical standard curves obtained with various viruses (Herpes Simplex Virus (HSV), Vaccinia virus, and Adeno-Associated Virus (AAV), all expressing Firefly luciferase) and describes incubation times and freeze-thaw cycles, as required.

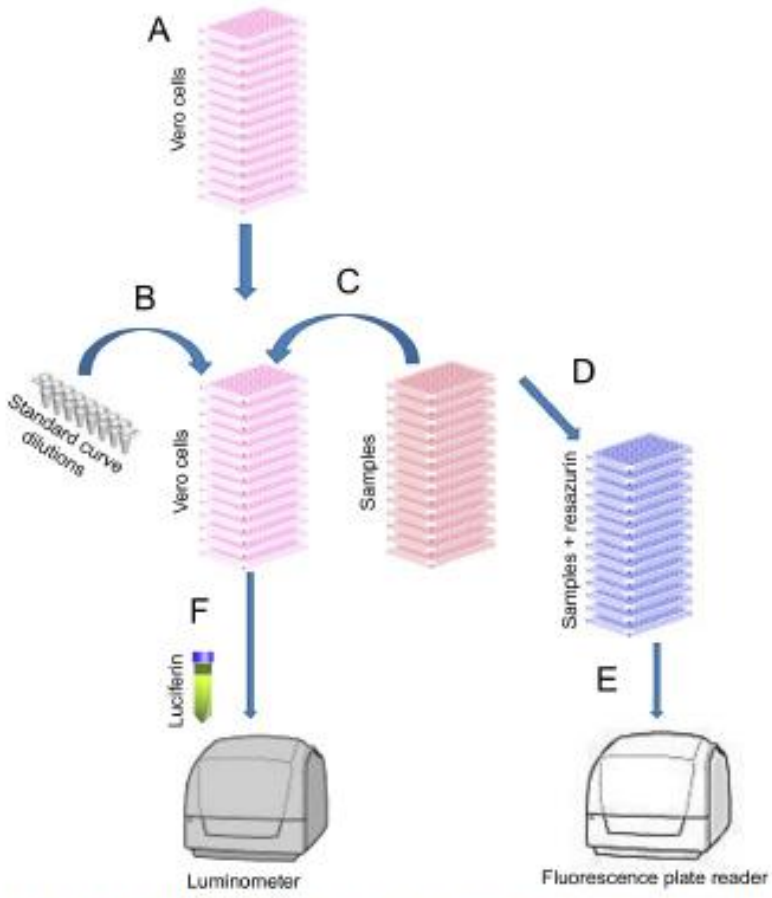

Figure 1. Workflow of high-throughput virus titering and cytotoxicity assay using VSVΔ51-Fluo. **(A)** Seed 2.5 x 10^4 Vero cells per well (100 µl) and incubate at 37 °C. **(B)** 24 hr later transfer 25 µl of standard curve on to Vero cells (2 columns per plate). **(C)** Transfer 25 µl of samples to be titered on to remaining Vero cells. Centrifuge plates and incubate at 37 °C. **(D)** In an amount equal to 10% of the volume in the well, add resazurin reagent to the plate containing the original samples. Incubate plates at 37 °C. **(E)** After 3 hr, read and record fluorescence and assess cytotoxicity. **(F)** After 5 hr, add 25 µl of 2 mg/ml solution of luciferin to each well of Vero cells. Read luminescence and calculate Viral Expression Units.

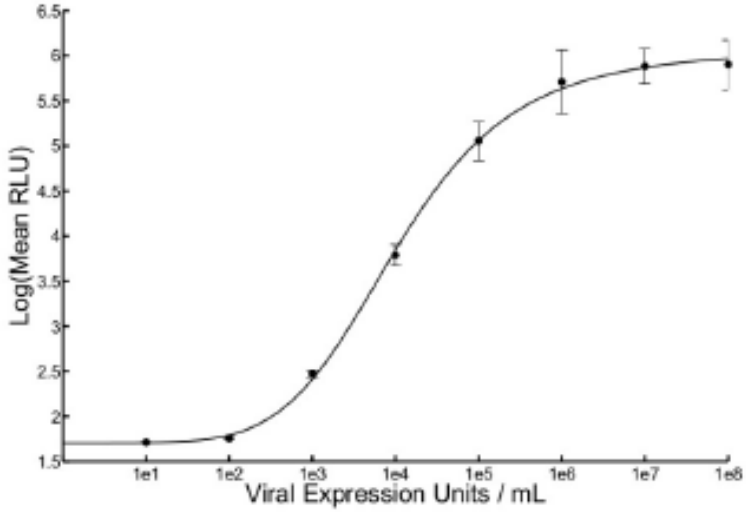

Figure 2. Expected standard curve of VSVΔ51-Fluc. Luciferase expression was measured 5 hr post supernatant transfer at five different points within a well using a luminometer and bioluminescence was expressed in mean relative light units (RLU). Mean RLU was plotted against known input pfu/ml to solve the non-linear regression and generate a Hill equation. The average of two replicate curves and standard error bars are shown (r^2 = 0.9993).

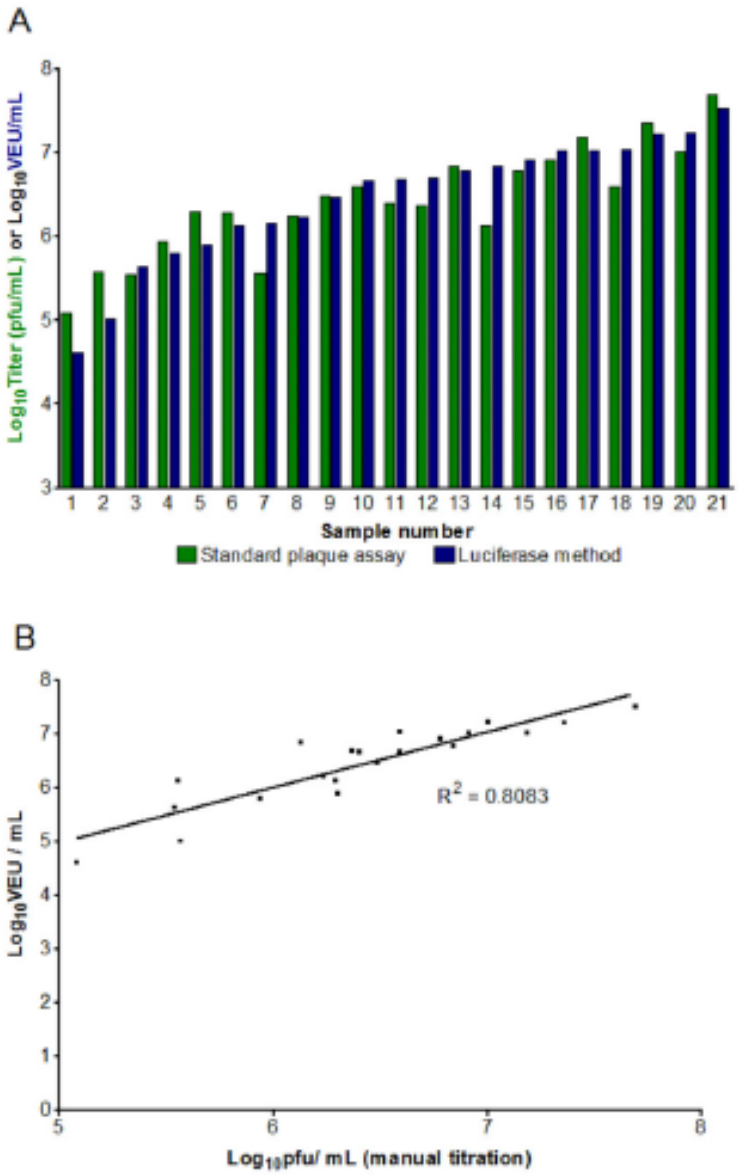

Figure 3. Comparison of standard plaque assay titers with those obtained by high-throughput method. (A) Viral titers in pfu/ml obtained by standard plaque assay on Vero cells were compared with calculated viral titers (VEU/ml) from the same samples titered using the high-throughput luciferase assay. **(B)** Linear relationship between VEU/ml and titer obtained via standard plaque assay. Linear regression curve and coefficient of determination (R^2) are shown.

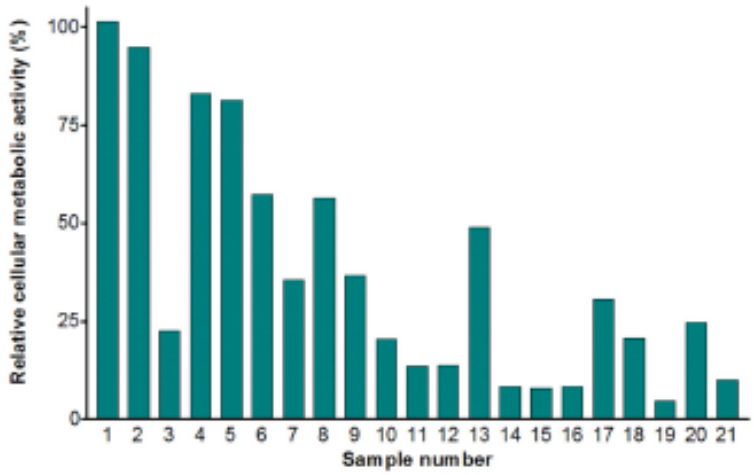

Figure 4. Sample viability. Sample viability prior to supernatant transfer onto Vero cells was determined by assessing cellular metabolic activity using a commercially available resazurin solution. Raw fluorescence values were normalized to that of untreated, uninfected wells.

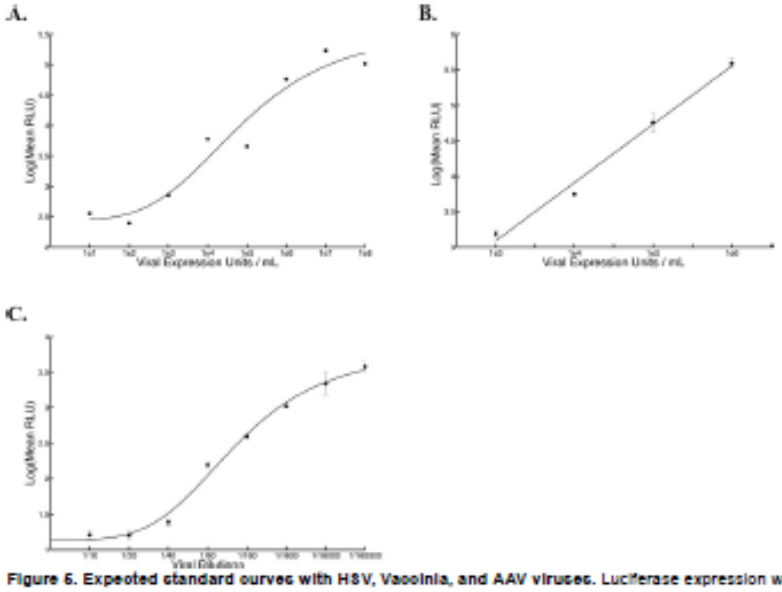

Figure 5. Expected standard curves with HSV, Vaccinia, and AAV viruses. Luciferase expression was measured at five different points within a well using a luminometer and bioluminescence was expressed in mean relative light units (RLU). **(A)** HSV standard curve was added onto Vero cells plated 24 hr earlier at a density of 2.5 x 10^4 cells per well (100 µl) and luciferase measurement was made 17 hr post supernantant transfer (R^2= 0.9489, n=1). A Hill equation was generated by solving the non-linear regression. **(B)** Vaccinia standard curve was added onto Vero cells plated 24 hr earlier a density of 2.5 x 10^4 cells per well (100 µl) and incubated for 2.5 hr at 37 °C, after which luciferase measurements were taken (R^2= 0.9892). A linear equation was generated by solving for the linear regression. **(C)** AAV standard curve was added onto human lung carcinoma cells (A549) plated 24 hr earlier at a density of 2.5 x 10^4 cells per well (100 µl) and luciferase measurement was made 24 hr post infection. A Hill equation was generated by solving the non-linear regression. The average of five replicate curves and standard error bars are shown (R^2= 0.9926).

Discussion

The luciferase-based approach described here provides a number of advantages over other existing methods including its ease, quickness, minimal equipment need, and relatively low cost. A key contributor to this is the avoidance of a serial dilution step. Nonetheless, serial dilution-based derivatives of this protocol are certainly feasible and were recently used to assess luciferase-expressing Ebola titers in a high-throughput

antiviral screen[11]. While inherently more time consuming and more expensive, such adaptations may provide greater dynamic range for viral quantification when necessary. In addition to being particularly well suited for evaluating viral titers in the context of high-throughput screens, our one-step luciferase based viral quantification method generates accurate estimates of infectious virions in the case of replicating viruses. Furthermore, readouts of luminescence along with cytotoxicity data from the same experiment give a more complete picture of the effect of the experimental conditions on target cells, which is particularly useful in the context of oncolytic viruses and drug screens.

The example illustrated here uses a replicating negative single strand RNA virus; however, this protocol can be adapted to a number of replicating and non-replicating viruses with a few minor protocol adjustments. This includes DNA viruses such as Vaccinia, HSV, and AAV (see **Figure 6**). Samples infected with intracellular viruses, such as Vaccinia virus for example, require a virus-release step prior to quantification (*e.g.*, at least one freeze-thaw cycle). When applying this technique to other viruses, it is necessary to optimize the incubation time from the transfer of the viral supernatant or lysate to the reading of the plates by the luminometer. This parameter will depend mainly on the replication cycle of the virus in the permissive cell line and the strength of the promoter driving luciferase expression. This is best done by using the full standard curve in the optimization step. To do this, one must infect the appropriate permissive cell line with various replicates of the prepared standard curve and read each replicate at a different time points post-transfer. Ideally, an incubation time point is chosen that leads to a linear relationship between LOG(RLU) and LOG(titer) spanning the expected sample titer range. For VSVΔ51-Fluc, this is typically from 10^4 pfu/ml -10^7 pfu/ml for a 5 hr incubation time. If lower or higher titers are expected from samples, one can simply increase or reduce the incubation time respectively. Alternately, samples may be diluted to fall within the range much as is done typically for ELISA.

As mentioned above, this method is well suited to perform high-throughput drug screens using drug libraries as most of the steps can be automated. Cells can be plated efficiently using an automated microplate dispenser, the drug library can be added using a 96-channel liquid handler, virus can be added using a microplate dispenser and plates read using an automated luminometer. In theory, this can also be adapted to 384-well or smaller formats; however, the limitation to this end is number of cells that can be plated, given fewer cells leads to a narrower range in the linearity of the LOG(RLU) to LOG(Titer) relationship. Finally, assessment of cell viability using resazurin or other metabolic dyes can be easily incorporated in the workflow, allowing for discrimination of cytotoxic compounds in antiviral screens or identification of compounds that lead to synergistic killing in combination with viruses[12]. Nevertheless, limitations of this method include the requirement of a luciferase transgene expressing virus, which is not always possible, and the availability of a sufficiently permissive cell line. However, it is likely possible to adapt the method for use with other reporter genes (*e.g.*, GFP) provided the reporter quantification method has a suitable linearity and signal to noise ratio. Overall, the described high-throughput method can be modified to suit many different viruses and tailored to diverse applications.

Disclosures

The authors have nothing to disclose.

Acknowledgements

Vanessa Garcia is funded by a Queen Elizabeth II Ontario Graduate Scholarship in Science and Technology and Cory Batenchuk by a Natural Sciences and Engineering Research Council fellowship.

References

1. Grigorov, B., Rabilloud, J., Lawrence, P., & Gerlier, D. Rapid titration of measles and other viruses: optimization with determination of replication cycle length. *PLoS One.* **6**, e24135, doi:10.1371/journal.pone.0024135 PONE-D-11-10153 [pii] (2011).
2. Lizee, G. *et al.* Real-time quantitative reverse transcriptase-polymerase chain reaction as a method for determining lentiviral vector titers and measuring transgene expression. *Hum Gene Ther.* **14**, 497-507, doi:10.1089/104303403764539387 (2003).
3. McGharry, J. J. Uses of flow cytometry in virology. *Clin Microbiol Rev.* **7**, 576-604 (1994).
4. Watcharatanyatip, K. *et al.* Multispecies detection of antibodies to influenza A viruses by a double-antigen sandwich ELISA. *J Virol Methods.* **163**, 238-243, doi:10.1016/j.jviromet.2009.09.027 S0166-0934(09)00439-X [pii] (2010).
5. Dawson, E. Rapid, Direct Quantification of Viruses in Solution Using the ViroCyt Virus Counter. *Journal of Biomolecular Techniques.* **23**, S10 (2012).
6. Snyder, R. O. AAV and RT-PCR: true or false? *Mol Ther.* **1**, 389-390, doi:10.1006/mthe.2000.0066 S1525-0016(00)90066-2 [pii] (2000).
7. Diallo, J. S., Roy, D., Abdelbary, H., De Silva, N., & Bell, J. C. *Ex vivo* infection of live tissue with oncolytic viruses. *J Vis Exp.* (52), doi:10.3791/2854 2854 [pii] (2011).
8. Gaush, C. R., & Smith, T. F. Replication and plaque assay of influenza virus in an established line of canine kidney cells. *Appl Microbiol.* **16**, 588-594 (1968).
9. Green, M., & Loewenstein, P. M. Human adenoviruses: propagation, purification, quantification, and storage. *Curr Protoc Microbiol.* **Chapter 14**, Unit 14C 11, doi:10.1002/9780471729259.mc14c01s00 (2006).
10. Diallo, J. S., Vaha-Koskela, M., Le Boeuf, F., & Bell, J. Propagation, purification, and *in vivo* testing of oncolytic vesicular stomatitis virus strains. *Methods Mol Biol.* **797**, 127-140, doi:10.1007/978-1-61779-340-0_10 (2012).
11. Hoenen, T., Groseth, A., Callison, J., Takada, A., & Feldmann, H. A novel Ebola virus expressing luciferase allows for rapid and quantitative testing of antivirals. *Antiviral Res.* **99**, 207-213, doi:10.1016/j.antiviral.2013.05.017 S0166-3542(13)00157-5 [pii] (2013).
12. Diallo, J. S. *et al.* A high-throughput pharmacoviral approach identifies novel oncolytic virus sensitizers. *Mol Ther.* **18**, 1123-1129, doi:10.1038/mt.2010.67 mt201067 [pii] (2010).

Appendix G:

Arulanandam R, Batenchuk C, Varette O, Zakaria C, Garcia V, Forbes NE, Davis C, **Krishnan R**, Karmacharya R, Cox J, Sinha A, Babawy A, Waite K, Weinstein E, Falls T, Chen A, Hamill J, De Silva N, Conrad DP, Atkins H, Garson K, Ilkow C, Kaern M, Vanderhyden V, Sonenberg N, Alain T, Le Boeuf F, Bell JC, Diallo JS. "Microtubule disruption synergizes with oncolytic virotherapy by inhibiting interferon translation and potentiating bystander killing." *Nature Communications*. 6:6410 (2015) doi: 10.1038/ncomms7410.

nature COMMUNICATIONS

ARTICLE

Received 26 Nov 2014 | Accepted 27 Jan 2015 | Published 30 Mar 2015

DOI: 10.1038/ncomms7410

Microtubule disruption synergizes with oncolytic virotherapy by inhibiting interferon translation and potentiating bystander killing

Rozanne Arulanandam[1], Cory Batenchuk[1], Oliver Varette[1], Chadi Zakaria[2], Vanessa Garcia[1], Nicole E. Forbes[1], Colin Davis[1], Ramya Krishnan[1], Raunak Karmacharya[1], Julie Cox[1], Anisha Sinha[1], Andrew Babawy[1], Katherine Waite[1], Erica Weinstein[1], Theresa Falls[1], Andrew Chen[1], Jeff Hamill[1], Naomi De Silva[1], David P. Conrad[1], Harold Atkins[1], Kenneth Garson[1], Carolina Ilkow[1], Mads Kærn[3], Barbara Vanderhyden[1], Nahum Sonenberg[2], Tommy Alain[4], Fabrice Le Boeuf[1], John C. Bell[1,*] & Jean-Simon Diallo[1,*]

In this study, we show that several microtubule-destabilizing agents used for decades for treatment of cancer and other diseases also sensitize cancer cells to oncolytic rhabdoviruses and improve therapeutic outcomes in resistant murine cancer models. Drug-induced microtubule destabilization leads to superior viral spread in cancer cells by disrupting type I IFN mRNA translation, leading to decreased IFN protein expression and secretion. Furthermore, microtubule-destabilizing agents specifically promote cancer cell death following stimulation by a subset of infection-induced cytokines, thereby increasing viral bystander effects. This study reveals a previously unappreciated role for microtubule structures in the regulation of the innate cellular antiviral response and demonstrates that unexpected combinations of approved chemotherapeutics and biological agents can lead to improved therapeutic outcomes.

[1] Center for Innovative Cancer Research, Ottawa Hospital Research Institute, 501 Smyth Road, Ottawa, Ontario, Canada K1H 8L6. [2] Department of Biochemistry, Goodman Cancer Center, McGill University, 1160 Pine Avenue West, Montréal, Quebec, Canada H3A 1A3. [3] Ottawa Institute of Systems Biology, University of Ottawa, 451 Smyth Road, Ottawa, Ontario, Canada K1H 8M5. [4] Children's Hospital of Eastern Ontario Research Institute, 401 Smyth Road, Ottawa, Ontario, Canada K1H 8L1. * These authors contributed equally to this work. Correspondence and requests for materials should be addressed to J.-S.D. (email: jsdiallo@ohri.ca).

Oncolytic viruses (OVs) are self-amplifying cancer biotherapeutics that destroy malignancies without harming normal tissues. Derived from a variety of viral species, OVs are often engineered to exploit well-known hallmarks of cancer, including deregulated metabolism and proliferation, evasion of cell death and inefficient antiviral signalling[1]. Within the tumour, these agents destroy the malignancy by inducing direct oncolysis, stimulating antitumour immune responses and promoting tumour-vasculature shutdown (reviewed in ref. 2). While promising early- and late-phase clinical trials employing OVs to treat cancers continue to generate great enthusiasm, heterogeneity in clinical response remains a challenge[2–4]. To this end, it has been long recognized that improvements to therapeutic efficacy either through viral engineering or through combination therapies will be critical to the success of these platforms[2,5].

Rhabdoviruses such as vesicular stomatitis virus (VSV) have been used preclinically as a backbone to generate OVs for over a decade[6–8] and are now beginning clinical evaluation (for example, NCT01628640). While wild-type rhabdoviruses such as VSV (wtVSV) preferentially replicate in cancer cells, their tumour selectivity can be greatly improved through genetic engineering, for example, by capitalizing on the frequently defective capacity of tumours to engage antiviral programmes[6–8]. One of the first characterized and widely studied oncolytic strains of VSV (VSVΔ51) harbours a deletion at methionine 51 in the matrix (M) protein, blocking its ability to interact with nuclear pore proteins and prevent the export of cellular antiviral mRNAs from the nucleus to the cytoplasm[9]. As a result, VSVΔ51 cannot replicate in normal cells that have fully functional antiviral systems but replicates robustly in tumour cells that have lost the ability to mount an effective antiviral response.

Capitalizing on cancer-specific defects in cellular immunity makes for remarkably safe and selective therapeutics; however, this can come at a significant cost in terms of efficacy. While VSVΔ51 can cure animals of some tumours incapable of producing or responding to interferon (IFN), nearly a third of cancer cell lines are essentially normal in this capacity, severely limiting viral spread and oncolysis[6]. Several genetic approaches have been explored and can be effective to overcome this roadblock. This includes using more potent viral backbones[8,10], or expressing therapeutic transgenes to impair the IFN response[11]. Enhancing potency through genetic modification, nonetheless, carries some levels of risk and could compromise the excellent safety record OVs have enjoyed to date[2].

We have explored the concept of 'conditionally enhancing' OV growth and replication by transiently complementing genetically attenuated OVs using pharmacological agents. For example in earlier work, we have shown that treatment of resistant tumour cells with histone deacetylase (HDAC) inhibitors that down-regulate IFN-responsive genes[12] leads to increased oncolysis by VSVΔ51 (ref. 13). More recently, we screened a small molecule library to discover novel enhancers of VSVΔ51-mediated oncolysis and identified distinct chemical entities that unexpectedly share the common feature of destabilizing microtubules. We report here a previously unappreciated role of microtubule structures in the control of type I IFN translation and show that microtubule-destabilizing agents (MDAs) specifically enhance the growth and spread of oncolytic rhabdoviruses in cancer cells and sensitize uninfected tumour cells to cytokine-mediated cell killing.

Results

MDAs enhance cancer-specific viral oncolysis. A high-throughput screening approach[14] identified seven approved drugs that have microtubule-destabilizing activity among 15 previously unknown compounds found to enhance VSVΔ51-mediated oncolysis. The compounds, their drug class and structures are listed in Supplementary Table 1. To validate their activity, we selected representative members of the colchicinoid (colchicine), vinka alkaloid (vinorelbine) and benzimidazole (nocodazole, albendazole and parbendazole) drug classes. These MDAs were tested across a range of concentrations on VSVΔ51-resistant 786-0 human renal carcinoma cells (Fig. 1a). Viability assays using alamarBlue metabolic dye revealed that all five drugs enhanced cell killing elicited by a low multiplicity of infection of VSVΔ51 (MOI = 0.01, Fig. 1a). Similar results were obtained in VSVΔ51-resistant mouse cancer cell lines (4T1 and CT26, Supplementary Fig. 1a,b). Treatment of cancer cells with colchicine, a drug used for autoinflammatory diseases such as gouty arthritis[15] and one of the most potent MDAs tested, led to synergistic killing in combination with both VSVΔ51 and wtVSV (Supplementary Fig. 1c). Colchicine also robustly enhanced the activity of Maraba MG-1, an IFN-sensitive oncolytic rhabdovirus strain closely related to VSVΔ51 (ref. 16; Supplementary Fig. 1d). In contrast, MDAs did not enhance VSVΔ51-mediated killing in normal human fibroblasts at any dose tested (GM-38 cells, Fig. 1b).

MDAs and rhabdovirus infection can independently have cytotoxic effects. We considered that the visible synergy between drug and rhabdoviruses could, therefore, result from improved rhabdovirus spread/oncolysis, increased sensitivity to MDAs or both. Microtubule destabilization using colchicine and other MDAs robustly increased VSVΔ51-GFP (green fluorescent protein) spread as well as viral titres in several human and mouse cancer cell lines but not in normal fibroblasts, consistent with a cancer-specific enhancement of viral growth (Fig. 1c,e and Supplementary Fig. 1e,f). In cancerous 786-0, but not in normal GM-38 cells, colchicine increased VSVΔ51-GFP spread (Fig. 1c,e) and viral protein expression (Fig. 1d). Immunofluorescence staining for β-tubulin revealed that colchicine effectively depolymerized microtubules in both cell lines at 100 nM, a dose prominently effective at enhancing rhabdovirus activity in cancer cells (Fig. 1f,g). Indeed, the increase in viral spread in 786-0 cells was observed specifically at the doses at which microtubule disruption by colchicine was visible, suggesting that the effects of MDA treatment on virus spread and cytotoxicity are dependent on destabilization of microtubule structures (Supplementary

Figure 1 | MDAs enhance VSVΔ51 spread in cancer but not normal cells. (**a**,**b**) 786-0 cancer (**a**) and GM-38 normal (**b**) cells were pretreated with MDAs (*x* axis) and then challenged with VSVΔ51, MOI 0.01. Forty-eight hours later, cell viability was assessed. (**c**) 786-0, U251 and 4T1 cancer cells as well as GM-38 were pretreated with colchicine (*x* axis) and infected as above for 48 h and supernatants titred. (**d**,**e**) 786-0 and GM-38 cells were treated with 100 nM colchicine or vehicle before infection with VSVΔ51-GFP or wtVSV, as above. At 48 h post infection, phase contrast and fluorescent images were taken (**e**, scale bar, 50 μm), and cell lysates subject to western blot, where VSV proteins are indicated by arrows (**d**). (**f**,**g**) 786-0 (**f**) and GM-38 (**g**) were treated with 0 (Control) or 100 nM colchicine for 24 h and fixed and probed for β-tubulin (yellow) and nuclei stained with DAPI (blue). Objective (×100), scale bar, 20 μm, white arrow denotes polynucleation. (**h**) 786-0s were treated as in **d** and 48 h after infection, nonpermeabilized cells were stained with PI and sorted by flow cytometry. (**i**) 786-0s were pretreated with colchicine as above (solid line/white squares) or vehicle (dotted line/black circles) and infected with MOI 0.01 (multistep) or MOI 3 (single step) of VSVΔ51 or wtVSV, and supernatants were titred by plaque assay. For **a**–**c**, **h**–**i**, error bars or numbers represent s.e. from at least three independent experiments.

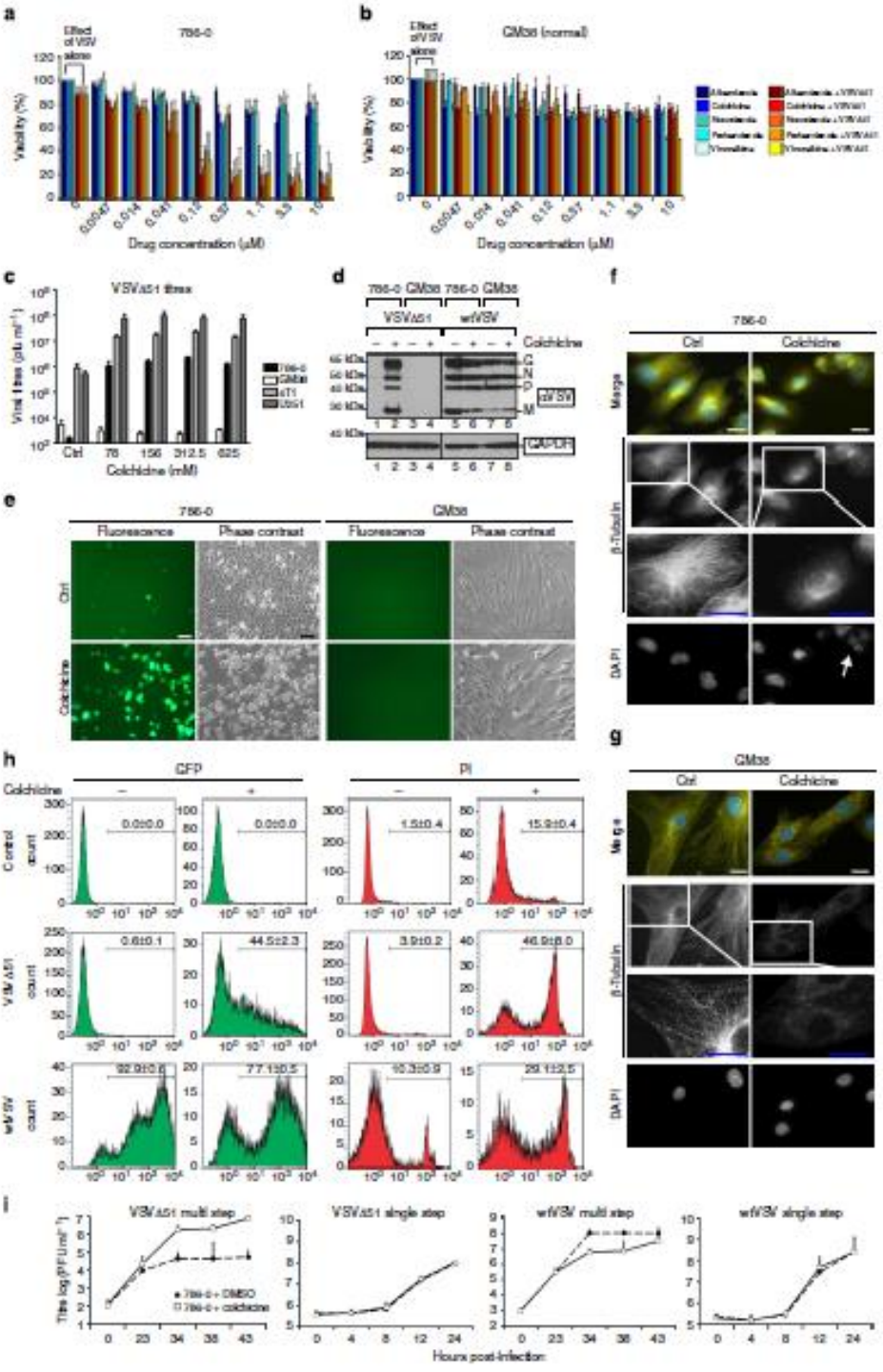

Figs 2 and 7a). Furthermore, this correlation was observed whether or not colchicine was left in or removed before VSVΔ51 infection (Supplementary Fig. 2). Colchicine treatment also led to increased numbers of polynucleate, giant cells in 786-0 but not in normal GM-38 (Fig. 1f versus Fig. 1g (arrow), Supplementary Fig. 2).

Comparing multi-step and single-step virus growth profiles suggests that in cancer cells, microtubule destabilization has an impact on the ability of VSVΔ51 to spread as opposed to its replication rate (Fig. 1i). In contrast, a slightly negative effect of the drug on virus propagation was observed using wtVSV (Fig. 1d,h,i). In parallel, we quantified cells positive for virally expressed GFP and propidium iodide (PI) staining using flow cytometry. PI staining was performed without permeabilizing the cells such as to identify dead or dying PI-positive cells. This confirmed that, while wtVSV propagation is hampered by colchicine treatment (fewer GFP-positive cells, Fig. 1h), cell death is nonetheless increased in comparison with virus or drug alone (more PI-positive cells, Fig. 1h), consistent with results from synergy assays (Supplementary Fig. 1c). The combination of VSVΔ51 and colchicine also led to substantially more PI-positive cells than either treatment alone, although this was accompanied by substantially increased GFP-positive infected cells in sharp contrast with wtVSV (Fig. 1h). Altogether, these data suggest that MDAs enhance rhabdovirus-mediated oncolysis through dual effects on viral spread and cell death. In the case of IFN-sensitive mutants such as VSVΔ51, these effects converge potently to kill resistant cancer cells while leaving normal cells unharmed.

Microtubule disruption enhances oncolytic rhabdoviruses. In order to eliminate the possibility that MDAs can synergize with rhabdoviruses in cancer cells through off-target effects, we obtained A549-T12 (AT12) and -T24 (AT24) cells, which have become resistant to the effects of Taxol through a mutation, rendering them dependent on Taxol in order for their microtubules to remain stable[17]. Indeed, tubulin staining of AT12 grown in the absence of Taxol reveals weak microtubule architecture and evidence of polynucleation compared with AT12 maintained in Taxol-containing media (Supplementary Fig. 3a). Similarly to other cancer cell lines, in parental A549 cells we observed that colchicine-induced microtubule disruption could significantly increase VSVΔ51-GFP spread and viral titres (Supplementary Fig. 3b–d). Supporting a role for microtubule destabilization, VSVΔ51-GFP spread and viral titres were significantly increased in AT12 and AT24 deprived of Taxol with destabilized microtubules compared with cells grown with Taxol where microtubule architecture was preserved (Supplementary Fig. 3e,f). To address this further, we derived three colchicine-resistant 786-0 sublines (786-0 CRV1-3),

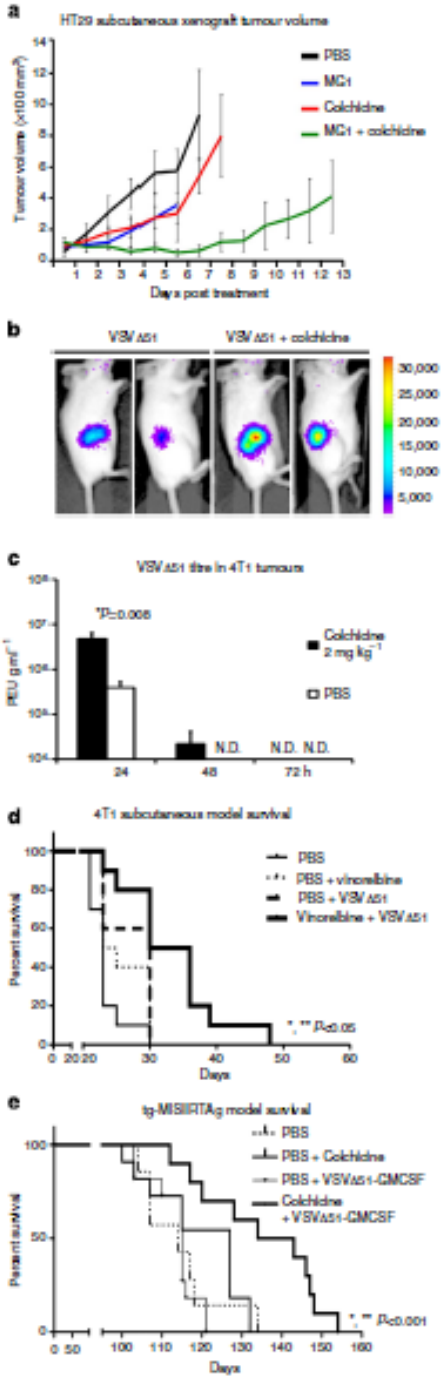

Figure 2 | Colchicine increases VSVΔ51 spread and oncolytic activity in resistant syngeneic and transgenic tumour models. (**a**) Human colon carcinoma HT29 cells were established in nude mice. Ten days later, mice were treated with colchicine, MG-1, a combination of MG-1 and colchicine or with PBS only. Tumour volume was monitored for each group and average tumour volumes are shown ($N=4$–5). Error bars correspond to the s.e. (**b**) 4T1 tumour-bearing syngeneic mice were treated with VSVΔ51-luciferase or PBS, and colchicine or vehicle and luminescence monitored after 24 h. (**c**) 4T1 tumours ($N=5$) from mice treated as in **b** were harvested at the indicated times and titred by plaque assay (*$P<0.05$, *t*test; ND = not detected). (**d**) 4T1 tumour-bearing syngeneic mice were treated with VSVΔ51, vinorelbine, a combination of VSVΔ51 and vinorelbine or PBS ($N=10$ per group). Survival was monitored over time. Log-rank test indicates that the combined treatment is significantly prolonged over virus alone (*$P=0.024$) or drug alone (**$P=0.0082$). (**e**) tgMISIIIR-TAg transgenic mice were treated with VSVΔ51-GM-CSF ($n=11$), PBS ($n=7$) colchicine ($n=11$) or VSVΔ51-GM-CSF and colchicine ($n=10$). Survival was monitored over time. Log-rank test indicates that the combined treatment is significantly prolonged over colchicine (*$P=0.0082$) and VSVΔ51-GM-CSF (**$P=0.0007$) alone.

in the presence of 10 μg ml^{-1} verapamil to prevent P-glycoprotein-mediated efflux of colchicine[18]. Correlating with visibly reduced cytotoxicity (Supplementary Fig. 4a, phase contrast), colchicine treatment of 786-0 CRV cells had no effect on viral spread determined by GFP quantification or viral titres (Supplementary Fig. 4a–c). Taken together, our data suggest that the enhancing effects of MDAs on oncolytic rhabdovirus activity are strongly linked to microtubule destabilization as opposed to off-target effects.

Efficacy of combined MDA and OV treatments in *vivo*. Since colchicine, vinorelbine and other MDAs enhanced oncolytic rhabdovirus efficacy *in vitro*, we evaluated the potential therapeutic benefit of combined MDA/oncolytic rhabdovirus *in vivo* in a series of xenograft, syngeneic and transgenic mouse tumour models. Human HT-29 colon tumour xenografts were robustly sensitized to intratumorally (i.t.) delivered oncolytic MG-1 (10^8 plaque-forming units or p.f.u.) following intraperitoneal (i.p.) administration of colchicine (2 mg kg^{-1}). In this model, combination therapy led to substantially delayed tumour progression compared with either monotherapy (Fig. 2a). Similar results were obtained using VSVΔ51 in a syngeneic mouse colon cancer model (Supplementary Fig. 5d). In a more highly virus-refractory and aggressive subcutaneous 4T1 syngeneic model of triple-negative breast cancer, co-administration of VSVΔ51 (10^8 p.f.u. i.t.) and vinorelbine (8 mg kg^{-1}) or colchicine (2 mg kg^{-1}) i.p led to delayed tumour progression and significantly prolonged survival compared with monotherapies alone (Fig. 2d, Supplementary Fig. 5a). Similar effects were observed using MG-1 in this model (Supplementary Fig. 5b). B16/F10 melanoma tumours implanted orthotopically in syngeneic B1/6 mice were analogously sensitized to VSVΔ51 oncolytic activity following co-treatment with colchicine. While neither monotherapy had any measurable impact, the combination therapy had a significant effect in prolonging survival in this highly aggressive model (Supplementary Fig. 5c).

As expected from *in vitro* evidence (Fig. 1a–i), the effects of colchicine were associated with tumour-specific increases in OV growth. Using a firefly luciferase-expressing VSVΔ51 and an *in vivo* imaging system (IVIS), we observed that 24 h post infection (i.t.), 4T1-grafted animals treated with colchicine exhibited increased luminescence specifically in tumours (Fig. 2b). Consistent with this, a significant increase in VSVΔ51 titres was observed in colchicine-treated animals (Fig. 2c). In contrast, assessment of viral titres in normal organs including the spleen, heart, liver, lungs, kidney and brain by standard plaque assay revealed no detectable VSVΔ51 in any organ at any time point in both PBS- and colchicine-treated mice.

The efficacy of combined rhabdovirus/MDA treatment was subsequently evaluated in a highly treatment-resistant tgMISIIR-TAg transgenic ovarian cancer mouse model. These mice express SV40 Large T-antigen specifically in the ovaries and develop palpable tumours at 10–11 weeks[19,20]. In these experiments, we used VSVΔ51-expressing granulocyte–macrophage colony-stimulating factor (GM-CSF) to further increase antitumour activity. Figure 2e shows that weekly treatment cycles of VSVΔ51-GM-CSF and colchicine both delivered i.p. led to significantly prolonged survival of tgMISIIR-TAg mice as compared with either monotherapy. Overall, these data suggest that combined oncolytic rhabdovirus and MDA treatment can significantly increase antitumour efficacy, prolonging survival even in highly treatment-resistant spontaneously arising tumours.

MDAs alter the type I IFN response. Combined treatment with MDAs and VSVΔ51 enhanced viral spread and oncolysis, providing therapeutic benefit in several resistant murine cancer models. We therefore used gene expression microarrays to gain insight into the possible mechanisms involved. We looked at gene expression profiles of 786-0 cells 24 h following VSVΔ51 or mock infection in presence and absence of 100 nM colchicine. In our analysis, we identified a subset of 248 genes that was either up- or down -regulated (more than twofold, $P<0.05$) in VSVΔ51-infected cells exclusively in the absence of drug (Fig. 3a). On the basis of gene set-enrichment analyses using both GOrilla and DAVID gene set databases[21–24], this group of 248 genes, and more specifically the 158 virus-induced genes dampened by colchicine, is significantly enriched in type I IFN-responsive genes (Fig. 3a, lower inset and Fig. 3b).

At first glance, our data suggested that microtubule destabilization has an impact on the transcriptional response to type I IFN normally induced following infection. However, the type I IFN response is thought to proceed in three waves. First, activation of pattern recognition receptors such as Toll-like receptor 3 and Retinoic acid-induced gene I, through signalling via Tank-binding kinase 1/IκB kinase ε (TBK-1/IKKε) and transcription factor IFN regulatory factor 3 (IRF-3) leads to increased 'first-wave' IFNβ transcription, translation, and secretion. Second, autocrine and paracrine signalling through type I IFN receptor (IFNR)/Janus kinase (JAK)/STAT (Signal Transducer and Activator of Transcription) leads to the formation of Interferon Stimulated Gene Factor 3, and to the upregulation of IFN-stimulated genes (ISGs) including IRF-7 and 'second-wave' IFNα isoforms. Third, additional ISGs are upregulated because of the combination of persistent IFN signalling and IRF-7 upregulation[7,25].

Closer inspection of the microarray data revealed that, while the induction of second-wave IFNα isoforms was dampened after treatment with colchicine, the induction of first-wave IFNβ mRNA remained similar (Fig. 3c). This was confirmed by looking at IFNβ mRNA expression in both nuclear and cytoplasmic compartments by real-time PCR (Fig. 4a). This suggested that virus-induced signalling leading to IFNβ mRNA upregulation as well as its subsequent cytoplasmic export is not affected by the MDA treatment. Further supporting this, IRF-3 nuclear shuttling and its phosphorylation status was unchanged by the colchicine treatment shortly following VSVΔ51 infection at high MOI (Fig. 4b).

We next looked for potential effects of MDAs on signalling downstream of IFNβ secretion. Colchicine treatment at 100 nM did not inhibit STAT-1 phosphorylation or alter nuclear/cytoplasmic distribution of the transcription factor following treatment with exogenous IFNβ (Fig. 4c), indicating fully functional IFN response through the (IFNR)/JAK/STAT pathway. Consistent with this, colchicine treatment (100 nM) could not overcome the antiviral effects of type I IFNs in either 786-0 or U251 cells (Supplementary Fig. 6a,b), in sharp contrast with suberoyl anilide hyroxamic acid, an HDAC inhibitor known to effectively dampen the antiviral effects of type I IFNs (Supplementary Fig. 6a and ref. 13). Overall, this suggests that MDAs severely dampen the type I IFN response without affecting signalling upstream of IFNβ mRNA induction or modulating signalling downstream of the antiviral cytokine.

MDAs inhibit translation of type I IFN mRNA. Altogether, our data suggested that microtubule destabilization decouples first- and second-wave antiviral responses without altering the intracellular signalling pathways known to be involved in their induction. We considered that this phenomenon could be explained if MDAs have an impact on type I IFN secretion, and in particular that of first-wave IFNβ. We addressed this possibility directly using enzyme-linked immunosorbent assay (ELISA).

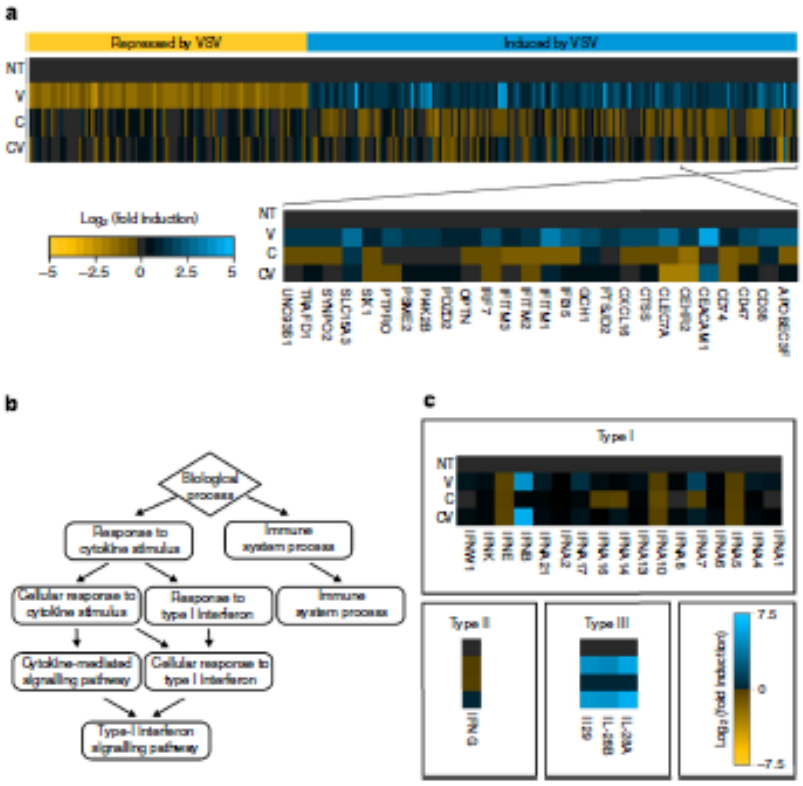

Figure 3 | Microtubule destabilization hinders the response to type I IFN-stimulated genes induced by VSVΔ51. (**a**) 786-0 cells were pretreated with 100 nM colchicine or vehicle and infected with VSVΔ51 at MOI 0.01 or were mock-infected. Twenty-four hours later, RNA was collected and pooled, and triplicate experiments were hybridized on Affymetrix human Gene ST 1.0 microarrays. Shown are heat maps of all genes found to be significantly increased (blue) or decreased (yellow) more than twofold in VSVΔ51-infected 786-0 as compared with control (NT), VSV-infected (V), colchicine-treated (C) and colchicine-treated, virus-infected (V + C) conditions ($P < 0.05$, Z-test). Inset shows a group of type I IFN-stimulated genes that are upregulated in V but not V + C conditions. (**b**) Summary of gene ontology relationships for enriched gene sets from **a**. (**c**) Microarray expression data for a subset of interferon isoforms and subtypes from **a**.

Even though mRNA levels and subcellular distribution were unaltered (Figs 3c and 4a), treatment with 100 nM colchicine caused a significant decrease in secreted IFNβ following a 24-h infection with a low MOI of VSVΔ51 (Fig. 4d). Furthermore, exposure of 786-0 to increasing doses of colchicine uncovered a correlation between microtubule disruption (Supplementary Fig. 2), inhibition of IFNβ secretion and increased virus titres (Supplementary Fig. 7a). A similar effect on IFNβ secretion was observed using other MDAs (Supplementary Fig. 8c). In contrast, VSVΔ51-induced IFNβ secretion in colchicine-resistant, 786-0 colchicine resistant variant (CRV) sublines, was not hampered by colchicine (Supplementary Fig. 7b).

A time course revealed that microtubule destabilization effectively delayed the onset of IFNβ production, which eventually accumulated over 48 h in infected cell culture supernatants (Supplementary Fig. 8a). Consistent with microarray mRNA expression data (Fig. 3c), IFNα was detected at lower concentrations than IFNβ following infection, and treatment with colchicine further reduced this (Supplementary Fig. 8b). In line with the observed decrease in type I IFN secretion, we found that the colchicine treatment reduced phosphorylation of STAT-1 24 h post infection (Fig. 4e). As was observed in 786-0 cells, IFNβ secretion was also inhibited by colchicine in U251 cancer cells (Supplementary Fig. 8d). However, the colchicine treatment also decreased IFNβ secretion in normal MRC-5 fetal lung fibroblasts (Supplementary Fig. 8d), suggesting that this effect is not restricted to cancer cells and that additional mechanisms may contribute to the cancer-specific enhancement in VSVΔ51 spread observed *in vitro* and *in vivo*.

Given that microtubules are known to play a role in vesicular transport and that microtubule destabilizers such as colchicine have been shown to have an impact on the secretion of various proteins[26–30], we considered the possibility that microtubule destabilization may simply have an impact on the ability of cells to secrete cytokines in response to virus infection. To assess this, we looked at the impact of microtubule destabilization on overall protein secretion using ^{35}S pulse-labelling following challenge with either VSVΔ51, G-less VSVΔ51 (which can infect but cannot exit the cell) or treatment with the Toll-like receptor agonist poly (I:C). Visualizing protein secretion patterns by autoradiogram, we observed a variety of responses to the colchicine treatment following viral stimulation. Whereas the secretion of some proteins 24 h post infection was increased by all three stimuli but reduced following treatment with colchicine (analogously to what was observed by ELISA for IFNβ and α), other proteins were not influenced by any viral stimulus nor affected by colchicine

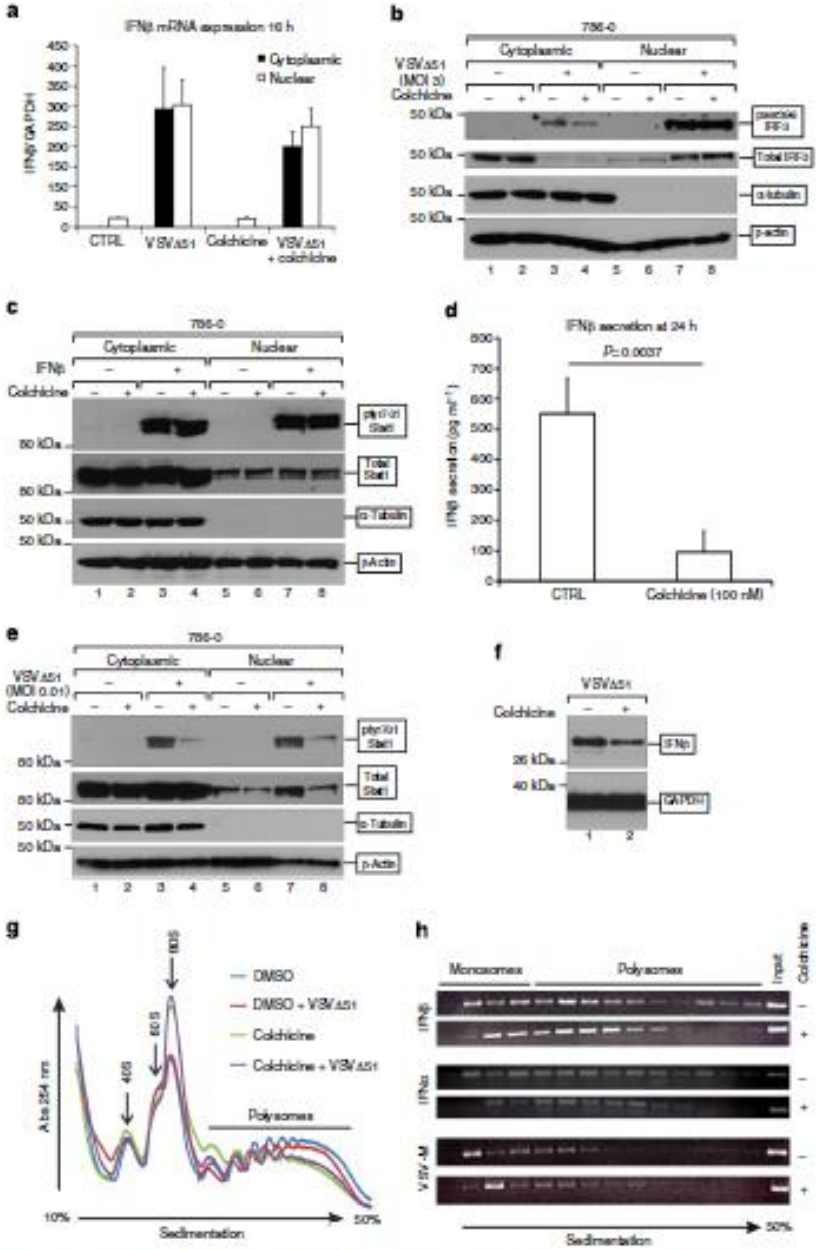

Figure 4 | Microtubule destabilization leads to a decrease in type I IFN production. (**a**) 786-0 cells were pretreated with 100 nM colchicine or vehicle and infected with VSVΔ51 at MOI 0.01 or mock. Sixteen hours later, qPCR was performed with cDNA from nuclear and cytoplasmic fractions. Data represent the fold change in IFN-β, normalized to GAPDH, relative to uninfected controls. (**b**) 786-0 were treated as above and infected at MOI 3 or mock. Eight hours later, fractionated lysates were probed with the indicated antibodies. (**c**) 786-0 cells were pretreated with colchicine and challenged with 0 or 500 U ml^{-1} IFNβ. One hour later, fractionated cell lysates were probed with the indicated antibodies. 786-0 cells were treated as in **a** and 24 h later (**d**) supernatants were collected and IFN-β quantified by ELISA, (**e**,**f**) 786-0 pretreated as in **a** and cell lysates probed for the indicated antibodies. (**g**,**h**) 786-0 cells were treated as in **a** and at 24h post infection, whole-cell lysates were collected and run on a 10–50% sedimentation gradient and absorbance measured over each fraction. (**h**) cDNA was generated from fractions and the abundance of mRNAs encoding IFNα, IFNβ and VSV M in each fraction assessed with PCR. For **a**,**d**, error bars represent s.e. from at least three replicate experiments and data analysed by analysis of variance (ANOVA) for statistical significance ($P<0.05$). For **b**,**c**,**e**,**f**, representative blots from three experiments are shown and apparent molecular sizes (kDa) of the prestained protein ladder (26616, Thermo Scientific) according to electrophoresis conditions are marked on the left.

(Supplementary Fig. 8e). This argues against a systematic negative impact of microtubule destabilization on protein secretion. To further address this, we quantified interleukin (IL)-6 secretion in cell supernatants 24 h following VSVΔ51 infection in presence and absence of colchicine, given that similarly to IFNβ this cytokine was robustly upregulated by VSVΔ51 infection at the mRNA level on the basis of microarray analyses (Fig. 3c and Supplementary Table 2). In sharp contrast with what was observed for type I IFNs, these experiments revealed no significant decrease in virus-induced IL-6 secretion following treatment with colchicine (Supplementary Fig. 8f). Further arguing against systematic inhibition of protein secretion following microtubule destabilization, secreted mouse GM-CSF encoded by the VSVΔ51-GM-CSF virus used for *in vivo* experiments shown in Fig. 2e increased proportionally to viral titres upon treatment with colchicine (Supplementary Fig. 8g).

We considered the possibility that microtubule disruption leads to decreased secretion of type I IFNs indirectly by reducing the translation of their mRNAs. Supporting this idea, western blots on whole-cell extracts of infected 786-0 cells revealed that at 24 h post infection, intracellular IFNβ protein expression levels decrease in parallel with the observed reduction in protein secretion (Fig. 4f, Supplementary Fig. 8a,d). To measure translation efficiency, we looked at RNA distribution in monoribosomes and polyribosomes using gradient sedimentation. Figure 4g shows that the colchicine treatment of 786-0 cells, irrespective of infection, led to a shift in mRNA distribution from polysome (highly translated) to monosome (poorly translated) fractions, albeit to a lesser extent than PP242, an mammalian target of rapamycin (mTOR) and translation inhibitor (see Supplementary Fig. 9a). Assessment of mRNA abundance by semiquantitative PCR further showed that both IFNβ and IFNα were less abundant in the highest-density polysomes of colchicine-treated cells (Fig. 4h). In contrast, looking at VSV M revealed a slight increase in lower-density polysomes upon treatment with colchicine (Fig. 4h). However, we failed to observe any alterations in the expression or phosphorylation of either mTOR target 4E-BP1 or downstream S6K target rpS6 (ref. 31) following treatment of 786-0 cells with colchicine (Supplementary Fig. 9a,b) arguing against a role of mTOR or 4E-BP in mediating the observed effects of MDAs on type I IFN mRNA translation efficiency. Overall, this suggests that microtubule destabilization reduces translation efficiency of cellular mRNAs such as type I IFNs, while permitting translation of viral genes.

MDAs enhance bystander death by virus-induced cytokines. While the data thus far shed light on the mechanisms leading to the enhancement of VSVΔ51 spread in cancer cells, it remained unclear why MDAs could also increase rhabdovirus infection-associated cell death (Fig. 1a,h). We therefore assessed whether viral triggers could be sufficient to elicit cytotoxic effects upon microtubule destabilization. To this end, we challenged colchicine or vehicle-treated 786-0 cells with a UV-inactivated wtVSV. As expected, even at a very high MOI (200) UV-inactivated wtVSV did not affect viability of 786-0 cells in control conditions. However, UV-inactivated virus was capable of effectively killing 786-0 cells treated with colchicine (starting at MOI 50, Fig. 5a). This was also observed in mouse 4T1 cells, albeit starting at a higher MOI of UV-inactivated virus (Supplementary Fig. 10a).

MDAs are well known to induce mitotic catastrophe and polynucleation, killing cells that divide rapidly and that have lost cell cycle checkpoints, two key hallmarks of cancer[32]. To gain a better understanding of the mechanisms leading to increased death in MDA-treated cells challenged with rhabdovirus, we looked at the frequency of polynuclear cells in the context of infection. We treated 786-0 cells with 100 nM colchicine or vehicle and infected them with VSVΔ51-GFP at low MOI (0.01). Twenty-four hours post infection, cells were fixed and stained with a nuclear dye (4′,6-diamidino-2-phenylindole, DAPI) and an anti-β-tubulin antibody. Fluorescence microscopy was then used to visualize and count GFP-positive infected cells and those exhibiting characteristic polynucleation (see Fig. 1f white arrow and Supplementary Fig. 10b). As expected, the colchicine treatment led to increased polynuclear cells, whereas infection with VSVΔ51-GFP alone did not. Importantly, upon co-treatment with VSVΔ51-GFP and colchicine, 786-0 cells exhibited a robust increase in the number of virus-associated GFP-positive cells and a near doubling in the number of polynucleated cells compared with cells treated with colchicine alone (Fig. 5b,c). Dose–response experiments revealed that this effect is observed starting at doses corresponding to those at which microtubule destabilization, decreased IFNβ secretion, and increased virus spread are also observed (Supplementary Figs 2a,b, 7a and 10c). In contrast, polynucleation remained low in normal GM-38 cells under these conditions (Fig. 5c).

Moreover, looking at the proportion of polynuclear 786-0 cells in infected (GFP+) and uninfected (GFP−) populations following the colchicine treatment further revealed that these were equally frequent in infected and uninfected cells (Fig. 5d). This distribution suggested the likely involvement of a virus-induced secreted factor in promoting polynucleation in the entire colchicine-treated 786-0 cell population. To explore this idea, we used supernatants from 786-0 cells infected with G-less VSVΔ51-GFP. As described previously, G-less VSVΔ51-GFP can infect and replicate but cannot bud from the cytoplasmic membrane[33]. We infected 786-0 cells with G-less VSVΔ51-GFP at high MOI (10) or naught and collected supernatants 24 h post infection. These supernatants were applied to virus-naive 786-0 cells treated with 100 nM colchicine or vehicle, and 24 h later cellular polynucleation was quantified. Consistent with the involvement of a secreted factor, supernatants from G-less VSVΔ51-infected but not mock-treated cells increased polynucleation and cell death in virus-naive 786-0 cells treated with colchicine (Fig. 5e,f). However, this did not occur when the same experiments were repeated using normal GM-38 supernatants and cells (Fig. 5f).

Pointing to the involvement of one or more secreted factors between 10 and 50 kDa (Fig. 5e), the polynucleation-inducing activity of G-less VSVΔ51-infected 786-0 cell supernatants was abrogated following filtration using a 10-kDa- but not 50- or 100-kDa molecular-weight cutoff filter. To generate a list of candidates, we queried the microarray data looking for secreted proteins between 10 and 50 kDa induced by VSVΔ51 in both vehicle- and colchicine-treated conditions. The short list of these candidates is shown in Supplementary Table 2. In addition to type I IFNs, this included several growth-promoting cytokines (for example, Rantes, IP-10, CXCL11, IL-8 and IL-6) as well as death-inducing cytokines (for example, tumour necrosis factor (TNF)-α and other TNF-related proteins). Type III IFNs (IL-28a, IL-28b and IL-29) also figured on this list. While it is likely that many of these factors work in concert to recapitulate the synergy observed between virus infection and colchicine treatment observed in Fig. 5a–f, we nevertheless evaluated the impact of a subset of cytokines on the frequency of polynuclear cells in 786-0 cells in presence of colchicine. We found that some cytokines such as IL-6, IL-8, IP-10 and IL-29 significantly increased the frequency of polynuclear cells in colchicine-treated 786-0 cells (Fig. 5g). In addition, colchicine treatment increased cell death induced by TNF-α in 786-0 but not GM-38 cells (Fig. 5h). Overall, this suggests that infection with rhabdoviruses in the presence of colchicine leads to cancer-specific increases in bystander polynucleation and cell death, likely through the combined action of multiple secreted factors and death-inducing cytokines.

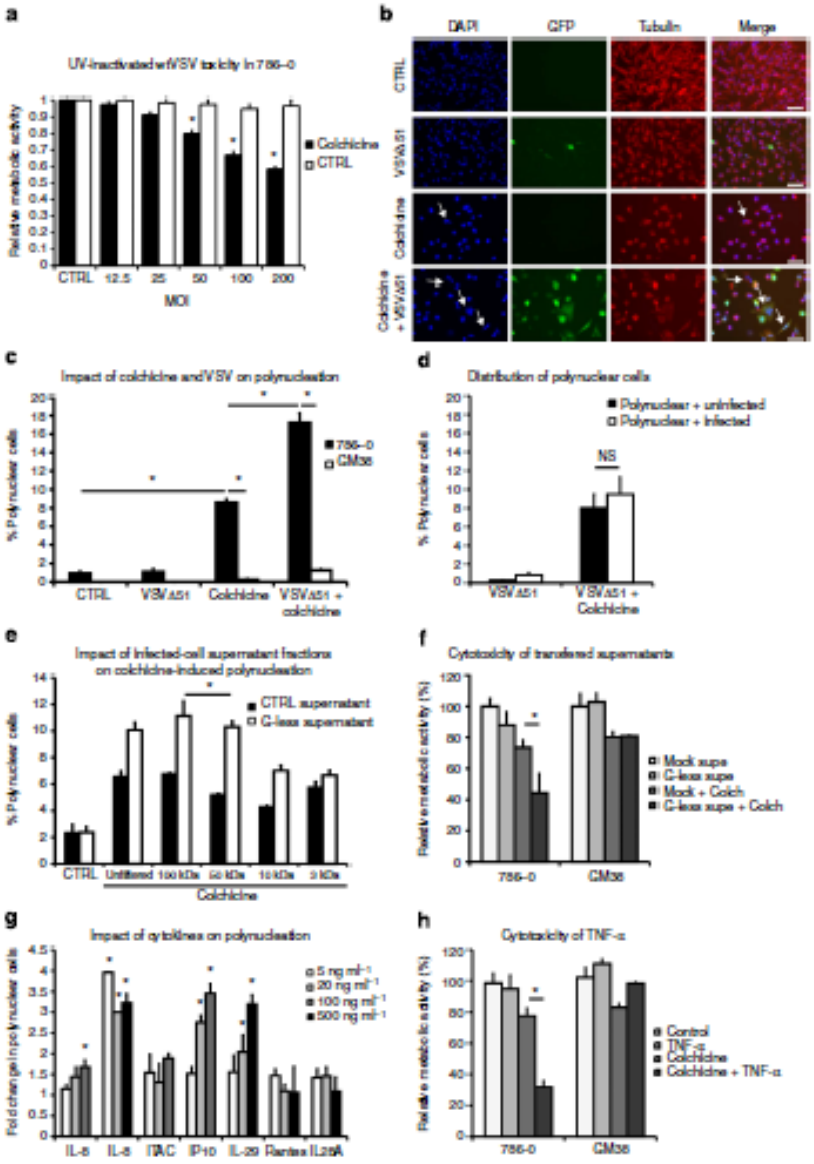

Figure 5 | VSV-induced cell death is increased by secreted factors that lead to polynucleation and death, specifically in cancer cells. (**a**) 786-0 were treated with 100 nM colchicine or vehicle and challenged with UV-inactivated virus (*x* axis). Cell viability was assessed after 48 h. (**b**–**d**) 786-0 and GM-38 were pretreated with colchicine as above and infected with VSVΔ51-GFP, MOI 0.01 or were mock-infected. After 24 h, cells were fixed and stained with DAPI and anti-β-tubulin (red). Fluorescence microscopy pictures were taken at × 40 (**b**, scale bar, 50 μm) and GFP-positive and polynuclear cells scored (yellow arrows and **c**). (**d**) 786-0 polynucleation data from **c** analysing virus-infected (GFP-positive) and uninfected cells. (**e**) 786-0 cells were infected with G-less VSVΔ51-GFP at MOI 10, and 24 h later supernatants were passed through cutoff filters (*x* axis) and applied directly to virus-naive 786-0 cells treated with colchicine or vehicle. Twenty-four hours later, cells were fixed and stained with DAPI, and β-tubulin and polynuclear cells counted. (**f**) 786-0 and GM-38 cells were treated as in **e** and cell viability was assessed. (**g**) 786-0 cells were pretreated with colchicine and recombinant cytokines (*x* axis). Twenty-four hours later, polynuclear cells were counted. (**h**) 786-0 or GM-38 treated with TNFα with colchicine or vehicle and cell viability assessed. Error bars represent s.e. from at least three replicate experiments and data analysed by ANOVA for statistical significance (*$P<0.05$).

Discussion

In this study, we reveal that MDAs can act synergistically with oncolytic rhabdoviruses by decreasing antiviral type I IFN production and increasing virus-induced cytokine-mediated bystander killing (see diagram summary in Fig. 6a,b). While we show here that MDAs elicit these two effects simultaneously, further dissecting their individual influences can provide deeper understanding on their interplay and contribution to the

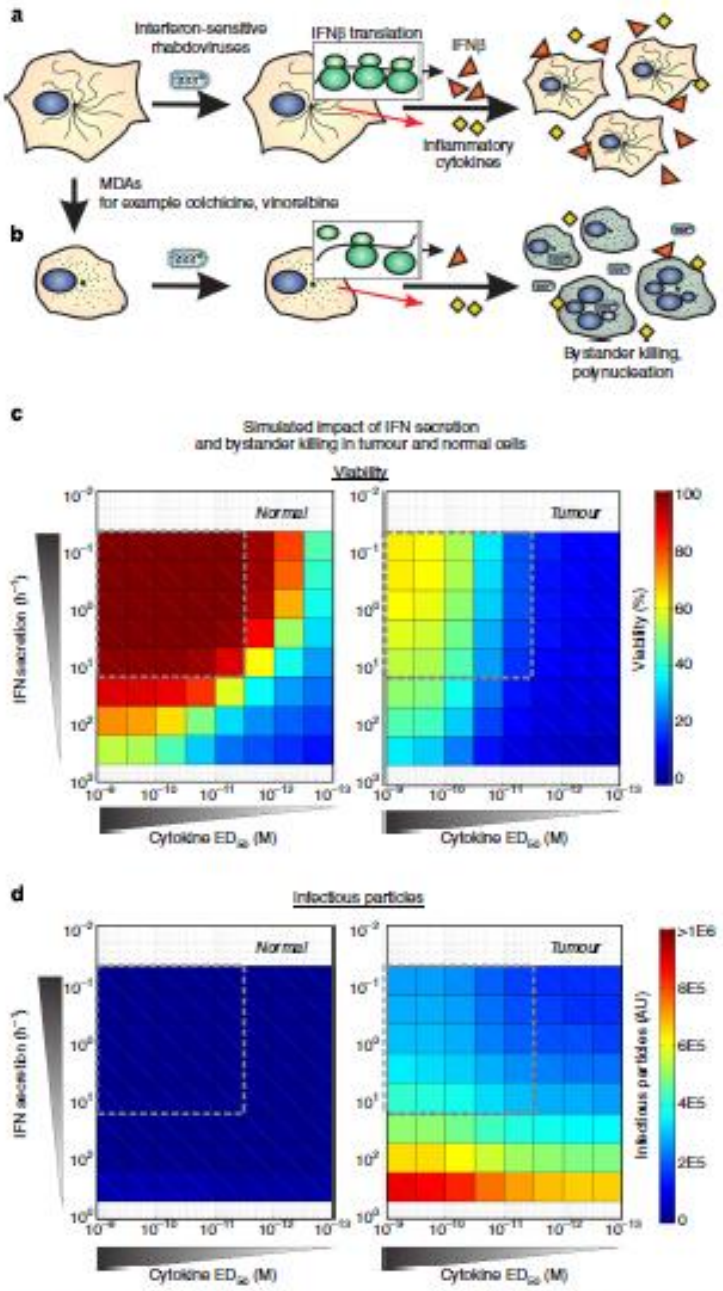

Figure 6 | Graphical and mathematical models summarizing the synergistic effects of MDAs on oncolytic virotherapy. (**a**,**b**) Graphical model. (**a**) In a subset of cancer cells that are innately resistant to oncolytic rhabdoviruses (for example, VSVΔ51 or MG-1), infection stimulates the production of type I IFN, which hampers viral replication to generate a protected population of cells. (**b**) Upon treatment with MDAs such as colchicine or vinorelbine, microtubules become destabilized, influencing the translation of cytokines such as IFNβ, by shifting its mRNA distribution from polysome to monosome fractions. This resulting lag in IFNβ secretion boosts viral spread and oncolysis. In addition, MDAs can increase bystander killing attributed to the production of virus-induced inflammatory and cytotoxic cytokines (for example, TNF-α, IL-6, IL-8, IP-10 and IL-29) through a significant increase in the proportion of polynuclear cells, a precedent to mitotic catastrophy and tumour cell destruction. (**c**,**d**) Monte Carlo simulations modelling type I IFN secretion decrease, and increased bystander effect, recapitulates the cancer-selective impact of MDAs on VSVΔ51 oncolysis. (**c**) Heat map summarizing the median viability 72 h post infection in normal or tumour cells as a function of decreasing the rate of IFN release (in a downward direction) and decreasing the ED50 of cytotoxic cytokines (in a rightward direction) in the presence of MDA. (**d**) Heat map summarizing the median number of free virus particles in the environment 72 h post infection in normal or tumour cells.

observed phenomena. Our data suggest that both effects are intimately linked to microtubule destabilization (see Supplementary Figs 2a,b, 7a and 10c), making this difficult to address this experimentally. To get around this problem, we adapted a mathematical model recently developed to investigate the impact of IFN dynamics on oncolytic rhabdovirus activity[11]. The initial framework, which we have previously shown to closely fit experimental data in normal and cancer cells[11], was modified to model separately or in combination the two effects of MDAs (Fig. 6c,d and Supplementary Fig. 11a).

In agreement with our experimental data with MDAs, this framework predicts that simultaneously decreasing IFN secretion and increasing bystander killing leads to increased viral growth and robust killing of cancer cells, but leaves normal cells unharmed (within a wide range of simulation parameters; Fig. 6c,d, Supplementary Fig. 11b). However, while decreasing IFN production boosts viral growth preferentially in cancer cells to a certain extent, simulations indicate that increasing bystander killing may be a dominant contributor to the overall cancer-selective cytopathic response when both effects are combined (Fig. 6c,d, Supplementary Fig. 11b). Nevertheless, caution must be taken in over-interpreting the results from the model, given the estimates for some of the parameters used may not adequately reflect the underlying biology.

Unlike IFN-sensitive VSVΔ51 for which both spread and bystander killing are enhanced by MDAs, wtVSV effectively overcomes the IFN response on its own[6]. This suggests that wtVSV should be mostly prone to the bystander effect of MDAs. It emerges from simulations using our model that increasing bystander killing alone comes at the cost of reducing viral output (Fig. 6c,d), corroborating our experimental observations with wtVSV (Fig. 1h). Our results altogether suggest that even though VSV has been reported to interact with microtubules in other studies[34], these cytoskeletal structures are not strictly required for rhabdovirus growth. Rather, our studies and simulations present enhanced bystander killing as an alternative explanation for the moderate inhibition of wtVSV growth measured following treatment of cells with MDAs (Fig. 1i and ref. 34).

Many viruses, such as vaccinia, are known to exploit the host cytoskeletal system to travel within the cytoplasm and to infect other cells[35]. Suggesting that MDAs may have virus-specific effects, we and others have observed that, while they enhance rhabdoviruses, microtubule destabilizers robustly inhibit vaccinia growth[36]. However, other viruses have been reported to grow at least equivalently in cells with destabilized microtubules. For example, while the mechanism was not addressed, low-dose vinblastine increased the oncolytic activity of herpes simplex virus without affecting viral titres *in vitro*[37]. It is likely that other IFN-inducing viruses could be enhanced by MDAs by taking advantage of delayed type I IFN secretion. However, our data suggest that rapidly growing viruses such as VSVΔ51 and MG-1 are more likely to benefit given this advantage is only transient (see Supplementary Fig. 8a,b). Ultimately, this may offer additional selectivity to the approach, reducing the possibility of opportunistic infections that could ensue from hindering the type I IFN system.

Somewhat controversial reports dating before the purification and sequencing of type I IFNs in the late seventies[38] noted the impact of drugs such as colchicine and vinblastine on the expression and secretion of antiviral cytokines and several other proteins[26–30]. Here we show for the first time direct evidence that several MDAs inhibit type I IFN secretion and provide data supporting the involvement of microtubule destabilization and mRNA translation in this phenomenon. Our results suggest that the incorporation of type I IFN mRNAs in polyribosome structures is compromised following disruption of microtubules. However, only a subset of secreted proteins responded analogously to type I IFNs following the MDA treatment as determined by pulse-chase experiments and by ELISA (Supplementary Fig. 8e–g). This brings forth the interesting possibility that microtubules and/or associated factors coordinate efficient translation of a subset of proteins. Supporting this idea, it has been previously reported that microtubule disruption reduces fibronectin mRNA prevalence in polyribosomes of smooth muscle cells[39]. Given these observations, it is tempting to speculate that microtubules coordinate the organization of polyribosome structures, which may be preferentially associated with a subset of mRNAs.

Overall, our study shows that MDAs can provide a significant therapeutic benefit when combined with oncolytic rhabdoviruses such as VSVΔ51 and Maraba MG-1, in several models of mouse and human cancers, from various tissue origins, including ovarian, colon, breast and skin (see Fig. 2 and Supplementary Fig. 5). While MDAs have been used for decades to treat a number of human ailments including autoimmune disorders, helminthes and cancer[15,32,40], one common characteristic is the narrow therapeutic window associated with these agents. In the case of cancer, this has led to the development of more selective biological therapies including therapeutic antibodies and OVs. Therefore, one downside of using classical MDAs in this context is their associated systemic toxicity. Notably, as a strategy to avoid overt toxicity of MDAs, these have been linked to monoclonal antibodies such as Herceptin, which retarget effects towards cancer cells[41]. It will be interesting to test oncolytic rhabdoviruses in combination with novel and recently approved antibody–MDA conjugates for the treatment of cancer in order to take full advantage of the vastly superior selectivity of these therapeutics.

Methods

Cell lines and culture conditions. 4T1 (breast), CT26 (colon), CT26-LacZ (colon) and B16 (melanoma) mouse cancer cells; 786-0 (renal); U251 (glioma), HT29 (colon) human cancer cells; Vero monkey kidney cells; MRC-5 and GM-38 normal human fibroblasts were obtained from the American Type Culture Collection (Manassas, VA). Cells were cultured in HyQ high-glucose Dulbecco's modified Eagle's medium (Hyclone, Waltham, MA) supplemented with 10 or 20% (GM-38) fetal calf serum (CanSera, Etobicoke, Ontario, Canada). A549-AT12, A549-AT24 and parental A549 lung carcinoma cells were a kind gift of Dr Susan Horwitz; cells were maintained in RPMI with 10% FBS supplemented with 12 or 24 nM paclitaxel (Taxol; Bristol-Myers Squibb, Princeton, NJ) for AT12 and AT24, respectively. 786-0 CRV were derived through passaging 786-0 cells with 0–10 nM colchicine in the presence of 10 $\mu g\,ml^{-1}$ verapamil (Sigma-Aldrich, St Louis, MO; three or more passages). All cell lines were incubated at 37 °C in a 5% CO_2-humidified incubator.

Viruses, purification and quantification. The Indiana serotype of VSV (VSVΔ51 or wild type) was used throughout this study and was propagated in Vero cells. VSVΔ51-expressing GFP, firefly luciferase or murine GM-CSF are recombinant derivatives of VSVΔ51 described previously[7,42]. Maraba MG-1 as described in ref. 16 was obtained from Dr David Stojdl. All viruses were propagated on Vero cells and purified on 5–50% Optiprep (Sigma) gradient and all virus titres were quantified by the standard plaque assay on Vero cells as described in ref. 43. For experiments described in Fig. 5a and Supplementary Fig. 6a, wtVSV was first inactivated by UV crosslinking with a total of 360 mJ cm^{-2}.

Drugs and cytokines. Colchicine, vinorelbine, nocodazole, albendazole and parbendazole were obtained from Sigma-Aldrich (St Louis, MO) and dissolved in DMSO. IFNα (Intron A) was obtained from Schering-Plough (Kenilworth, NJ). IFN-β was obtained from PBL Interferon Source (Piscataway, NJ). IL-6, IL-8, ITAC, IP-10, IL-29, IL-28a and TNF-α were obtained from ProSpec Bio (East Brunswick, NJ).

***In vitro* treatment of cells with MDAs and rhabdoviruses.** Confluent monolayers of cells were pretreated for 2–4 h with drugs, followed by infection with rhabdoviruses at indicated MOIs for the indicated times. Fluorescent images to detect virus replication were obtained using the Axiovert 5100 Fluorescence microscope (Carl Zeiss Ltd, Toronto, ON). Cell viability was assessed using an alamarBlue assay (AbD Serotec) according to the manufacturer's instructions by

measuring fluorescence (530 nm excitation and 590 nm emission) on a Fluoroskan Ascent Microplate Fluorometer (Thermo Scientific, Hudson, NH). GFP-fluorescence units were obtained using a Cellomics Arrayscan VTI HCS Reader. Virus titres were determined from cell supernatants by standard plaque assay on Vero cells[43]. Briefly, supernatants were serially diluted and incubated on confluent Vero cells for 45 min. Supernatants were removed and a 1% agarose overlay in Dulbecco's modified Eagle's medium (Gibco/BRL) with 20% FBS was immediately added. After 24-h incubation at 37 °C in a 5% CO_2-humidified incubator, cells were fixed in methanol and stained with a coomassie brilliant blue R (Sigma) solution containing 0.5 g coomassie blue, 20% methanol and 10% acetic acid. Plaques were counted and titres calculated on the basis of the dilution and reported as p.f.u. per ml.

Flow cytometry. 786-0 cells were plated in 12-well dishes, pretreated with DMSO or 100 nM colchicine for 4 h, followed by mock infection or infection with VSVΔ51-GFP or wtVSV-GFP at MOI 0.01. Forty-eight hours later, cells were collected, washed and resuspended in HBSS containing 10% FBS and 0.01% sodium azide. Non-permeabilized, single-cell suspensions were labelled with or without 50 μg ml^{-1} propidium iodide (Sigma) and subjected to flow cytometry on a Beckman Coulter FC500 (data analysed with the Kaluza v1.1 software).

Rodent tumour models. *CT26 and 4T1 models.* Six-week-old female Balb/c mice obtained from Charles River Laboratories (Wilmington, MA) were given subcutaneous tumours by injecting ~3×10^5 syngeneic 4T1 (or CT26-lacZ) cells suspended in 100 μl PBS. At the indicated times post implantation, tumours were injected with 1×10^8 p.f.u. (in 50 μl PBS) of the indicated virus. Four hours later, colchicine or vincristine was administered i.p. at the indicated dose. This was repeated a week later for a total of two treatment cycles. Tumour sizes were measured every other day using an electronic caliper. Tumour volume was calculated as $=(\text{length} \times \text{width}^2)/2$. For survival studies, mice were culled when tumours had reached 1,600 mm^3. For *in vivo* imaging, an IVIS (Perkin Elmer, Waltham, MA) was used as described previously[44]. Briefly, 100 μl of a 10-mg ml^{-1} D-luciferin solution in PBS was injected into mice i.p. Five minutes later, mice were anaesthetized using 3% isoflurane and imaged according to the manufacturer's instructions. For viral quantification described in Fig. 2b, tumours were dissected at the indicated times and homogenized in PBS using a tissue homogeniser before quantification by the standard plaque assay as described above and in ref. 43.

HT29 model. Six-week-old female Nude mice obtained from Charles River Laboratories were injected s.c. with HT29 human colon carcinoma cells (1×10^6). Ten days later, when tumours reached 5 × 5 mm size, mice were treated with MG-1 i.t. (1×10^8 p.f.u.) and/or colchicine i.p. (2 mg kg^{-1}). Tumour sizes were measured every other day using an electronic caliper.

B16 model. Six-week-old female C57B/6 mice obtained from Charles River Laboratories were injected s.c. with B16 melanoma cells (2×10^5). Two weeks later, when tumours reached 5 × 5 mm size, mice were treated with VSVΔ51 i.t. (1×10^8 p.f.u.) and/or colchicine i.p. (1.5 mg kg^{-1}). Tumour sizes were measured every other day using an electronic caliper.

Ovarian cancer model (Fig. 2c), T-Antigen-positive tgMISIIR-TAg (Tg(Amhr2-SV40TAg)1 Bcv) female transgenic mice (described previously[19]) ~10 weeks of age were treated with weekly i.p. injections of 1×10^8 p.f.u. VSVΔ51-GM-CSF and colchicine 1.5 mg kg^{-1} until end point as determined by the animal care guidelines. Doses were adjusted to body weights of individual mice to account for weight gain over time.

All experiments were performed in accordance with the University of Ottawa Animal Care and Veterinary Services guidelines for animal care under the protocol OGHRI-58. A minimum of three mice per group was considered sufficient to detect a significant difference in tumour size over time, whereas six or more mice were considered necessary to detect a meaningful difference in survival.

Microarrays and analysis. 786-O cells were plated at a density of 4×10^5 cells in six-well flat bottom plate (Costar). Following overnight growth, cells were treated with 100 nM colchicine or vehicle. Following a 4-h pretreatment, PBS or VSVΔ51 at an MOI of 0.01 was added to cell cultures. Twenty-four hours post infection, RNA was collected using an RNA-easy kit (Qiagen, Valencia, CA, USA). RNA quality was measured using Agilent 2100 Bioanalyzer (Agilent Technologies) before hybridization. Biological triplicates were subsequently pooled and hybridized to Affymetrix human gene 1.0 ST arrays. Microarray data were processed using AltAnalyze v2.0 under default parameters[45]. A detection above background score >70 and a $pV < 0.05$ were used to filter probe sets. By subsequently evaluating gene expression using constitutive probe sets shared across splice variants, our analysis focused on changes in gene transcription rates rather than alternative splicing mechanisms. Gene enrichment analyses were subsequently focused on 248 genes induced or repressed twofold by VSVΔ51 relative to all other data sets (*Z*-test $P < 0.05$, Benjamini–Hochberg correction). Gene ontology (GO)-term enrichments were evaluated using GOrilla[27] following correction for multiple hypothesis testing (Bonferroni). Pathway enrichments were evaluated using DAVID following correction for multiple hypothesis testing (Benjamini–Hochberg). Raw and processed microarray data have been deposited in the ArrayExpress database: E-MTAB-2433.

Cell lysis and western blotting. Whole-cell extracts were obtained by lysing in 50 mM HEPES, pH 7.4, 150 mM NaCl, 10 mM EDTA, 10 mM $Na_4P_2O_7$, 100 mM NaF, 2 mM Na_3VO_4, protease inhibitor cocktail (Roche) and 1% Triton X-100 as described[46]. Following protein determination by Bradford assay (Bio-Rad Protein Assay Solution, Mississauga, ON), 10–20 μg of clarified cell extract were electrophoresed on 4–12% precast gradient gels (Invitrogen) using the NuPAGE SDS–PAGE Gel system (Invitrogen) with 2-(N-morpholino) ethanesulfonic acid (MES) running buffer and transferred on nitrocellulose membranes (Hybond-C, Bio-Rad). Blots were blocked with 5% nonfat milk and probed with rabbit polyclonal antibodies specific for VSV (a gift from Dr Earl Brown, used at 1:5,000 overnight), or IFNβ (sc-20107, Santa Cruz Biotechnology, Dallas, TX, used at 1:500 overnight), with GAPDH (ab37168, Abcam, Cambridge, UK, used at 1:10,000) as a loading control, followed by horseradish peroxidase-conjugated rabbit or mouse secondary antibodies, respectively (Jackson ImmunoResearch Laboratories, West Grove, PA). Membranes were washed with Tris-buffered Saline with Tween. Bands were visualized using the Supersignal West Pico Chemiluminescent substrate (Thermo Scientific Pierce, Rockford IL). Images have been cropped for presentation and full-sized images are presented in Supplementary Fig. 12a,c.

Nuclear/cytoplasmic fractionation and western blotting. Cell fractionation experiments were performed as previously described[46]. Briefly, cells were washed with ice-cold PBS, swelled in Hypotonic buffer (0.5 M HEPES pH 7.9, 0.1 M EGTA, 0.1 M EDTA with protease and phosphatase inhibitors), lysed with 0.1% NP-40 and cytoplasmic fractions collected using low-speed centrifugation. Nuclear proteins were then extracted with hypertonic buffer (0.5 M HEPES pH 7.9, 2.5 M NaCl, 0.1 M EGTA, 0.1 M EDTA, 30% glycerol, 20 mM NaF, 1 mM Na_3VO_4, 1 mM $Na_4P_2O_5$, 1 mM dithiothreitol (DTT) and protease inhibitor cocktail) and clarified. Nuclear and cytoplasmic fractions were resolved using gel electrophoresis as above and membranes blocked with 5% BSA, cut into strips and probed for the tyrosine-701 phosphorylated (that is, activated) form of Stat-1 (9171S, Cell Signaling/New England Biolabs, Whitby, ON, 1:1,000 overnight), total Stat-1 (9172S, NEB, 1:1,000 overnight), serine-396-phosphorylated IRF-3 (4947S, NEB, 1:1,000 overnight) or total IRF-3 (FL425 SC-9082, Santa Cruz Biotechnology, 1:1,000 overnight). Antibodies against α-tubulin (sc-8035, Santa Cruz Biotechnology, 1:500 overnight) and β-actin (4970S, NEB, 1:1,000 overnight) were used as loading controls. Images have been cropped for presentation and full-sized images are presented in Supplementary Fig. 12b–d.

Quantitative real-time PCR. 786-0 cells were pretreated for 4 h with 0.1 μM colchicine or DMSO, and were infected with VSVΔ51 at MOI 0.01 or mock. Sixteen hours later, cells were collected and fractionated in nuclear and cytoplasmic fractions (Norgen Biotek Corp, ON, Canada). RNA extraction was performed using Qiagen QiaShredder columns and the Qiagen RNeasy kit (Qiagen). RNA (2 μg) was converted to cDNA with Superscript II Reverse Transcriptase (Invitrogen). Real-time PCR reactions were performed with the QuantiTect SYBR Green PCR kit (Qiagen) on a Rotor-gene RG-3000 (Corbett Research, Australia). Optimal threshold and reaction efficiency were determined using the Rotor-gene software. Melt curves for each primer exhibited a single peak, indicating specific amplification, which was also confirmed by agarose gel. C_t values were determined using the Rotor-gene software at the optimal threshold previously determined for each gene. Gene expression relative to GAPDH was calculated using the method described in ref. 47. Fold induction was calculated relative to the DMSO-treated control for each gene. Primers were designed using Primer 3 v 4.0 (sequences available upon request).

ELISA. Cells were plated in 12-well dishes, pretreated with DMSO or 100 nM colchicine for 4 h, followed by mock infection or infection with VSVΔ51-GFP (or VSVΔ51 GM-CSF) at indicated MOI. Cell supernatants were collected at different times post infection, centrifuged to remove cellular debris and protease inhibitor cocktail was added. ELISA was performed with the VeriKine Human or Mouse IFN alpha, IFN beta or mouse GM-CSF kits as appropriate (PBL Interferon Source) by following the manufacturers' instructions. Absorbance values at 450 nM were measured on a Multiskan Ascent Microplate Reader (MXT Lab Systems, Vienna, VA).

Polysome profiling. Cells were cultured in 15-cm dishes until confluent monolayers were formed and then pretreated with colchicine (100 nM) or vehicle (DMSO) for 4 h followed by infection with VSV at 0.1 MOI. Cells were washed 24 h post infection with cold PBS containing 100 μg ml^{-1} cycloheximide, collected and lysed in a hypotonic lysis buffer (5 mmol l^{-1} Tris-HCl (pH 7.5), 2.5 mmol l^{-1} $MgCl_2$, 1.5 mmol l^{-1} KCl, 100 μg ml^{-1} cycloheximide, 2 mmol l^{-1} DTT, 0.5% Triton X-100 and 0.5% sodium deoxycholate). Lysates were loaded on 10–50% sucrose density gradients (20 mmol l^{-1} HEPES-KOH (pH 7.6), 100 mmol l^{-1} KCl, 5 mmol l^{-1} $MgCl_2$) and centrifuged at 164,000 × *g* for 2 h at 4 °C. Gradients were fractionated, and the optical density (OD) at 254 nm was continuously recorded using an ISCO fractionator (Teledyne ISCO). RNA from each fraction was isolated using TRIzol (Invitrogen) and treated with DNaseTurbo (Ambion) according to the manufacturer's instructions. Reverse transcription PCR (RT–PCR) and semi-quantitative RT–PCR (qRT–PCR) reactions were carried out using SuperScript III First-Strand Synthesis System (Invitrogen) and SYBR Green Supermix (Qiagen)

according to the manufacturer's instructions using primers for human IFNβ (5′-CATTACCTGAAGGCCAAGGA-3′, 5′-CAGCATCTGCTGGTTGAAGA-3′) IFNα (5′-ACCCACAGCCTGGATAACAG-3′; 5′-ACTGGTTGCCATCAAAC TCC-3′) and VSV M (5′-CGGTATTGGCAGATCAAGGT-3′; 5′-GAGCTCAATC GTTCCCTTGT-3′).

Immunofluorescence and assessment of polynuclear cells. Human 786-0 renal carcinoma cells, A549, A549-AT12 or normal human GM-38 lung fibroblasts were plated in 12-well dishes on glass coverslips. Following a 4-h pretreatment with 0–1 μM colchicine, or 12 nM Taxol (as indicated), wells were infected with oncolytic VSVΔ51-expressing GFP at the indicated MOIs, or were mock-infected. Alternately, cells were treated with supernatants (see below) or cytokines for experiments in Fig. 5e,g. Cells were incubated for 24 h, and subsequently fixed with 4% paraformaldehyde, quenched with 50 mM ammonium chloride, permeabilized with 0.1% triton, blocked with 1% BSA and probed for β-tubulin (1:200, ab21057, Abcam) followed by treatment with donkey anti-goat AF-594 (1:400, Invitrogen). Coverslips were mounted on slides using Prolong AntiFade with DAPI (Invitrogen) and then photographed at × 40 or × 100, as indicated, using the Zeiss Imager M1 microscope equipped with the AxioCam HRm camera (Carl Zeiss Ltd) and the Axiovision software. Polynuclear/infected cells were counted from 5–15 pictures per well (at × 40) and a minimum of 100 cells in total.

Supernatant transfer and filter experiment. 786-0 or GM-38 cells were cultured and plated as described above, but were instead infected with VSVΔM51-ΔG-GFP at an MOI of 10. This virus can infect cells but cannot exit the cell because of the lack of the viral G protein, thus preventing release of viral particles in the supernatant. After overnight incubation and verification of initial infection, supernatants were filtered through a 100-, 50-, 10- or 3-kDa filter (Millipore, Billerica, MA) or left unfiltered before being transferred to fresh 786-0 (or GM-38) coverslips or 96-well plates with or without 100 nM colchicine. Coverslips or 96-well plates (as indicated) were fixed, stained and polynuclear cells counted as described above. Alternately, an alamarBlue viability assay (described above) was performed.

Mathematical modelling. The model describing OV replication dynamics in the presence of colchicine was derived from our previous work[11]. It uses four equations describing the transition between the uninfected population (UP), the infected population (IP), the activated population (AP) and the protected population (PP) depending on the concentration of virus [V], cytotoxic cytokine [Cyt] and extracellular interferon [IFN] in the environment. These equations are:

$$\frac{dUP}{dt} = -K_{VI}\times[V]\times[UP] - \left(\frac{-K_{IFN\,sti}}{1+\left(\frac{[IFN\,ext]}{EC50\;IFN}\right)^2}+K_{IFN\,sti}\right)\times[UP]+K_{IFN\,off}\times[PP]-\left(\frac{-\gamma_{C\_Cyt}}{1+\left(\frac{[Cyt]}{EC50\;Cyt}\right)^2}+\gamma_{C\_Cyt}\right)\times[UP],$$

$$\frac{dIP}{dt} = K_{VI}\times[V]\times[UP] - \left(\frac{-K_{IFN\,sti}}{1+\left(\frac{[IFN\,ext]}{EC50\;IFN}\right)^2}+K_{IFN\,sti}\right)\times[IP]-\gamma_s\times[IP]-\left(\frac{-\gamma_{C\_Cyt}}{1+\left(\frac{[Cyt]}{EC50\;Cyt}\right)^2}+\gamma_{C\_Cyt}\right)\times[IP],$$

$$\frac{dAP}{dt} = \left(\frac{-K_{IFN\,sti}}{1+\left(\frac{[IFN\,ext]}{EC50\;IFN}\right)^2}+K_{IFN\,sti}\right)[IP] - K_{VI}\times[AP]-\gamma_s\times[AP] - \left(\frac{-\gamma_{C\_Cyt}}{1+\left(\frac{[Cyt]}{EC50\;Cyt}\right)^2}+\gamma_{C\_Cyt}\right)\times[AP],$$

$$\frac{dPP}{dt} = \left(\frac{-K_{IFN\,sti}}{1+\left(\frac{[IFN\,ext]}{EC50\;IFN}\right)^2}+K_{IFN\,sti}\right)[UP] + K_{VI}\times[AP] - K_{IFN\,off}\times[PP] - \left(\frac{-\gamma_{C\_Cyt}}{1+\left(\frac{[Cyt]}{EC50\;Cyt}\right)^2}+\gamma_{C\_Cyt}\right)\times[PP].$$

The parameters used in the above equations represent the infection rate (K_{vi}), the rate of IFN signalling activation ($K_{IFN\,sti}$), the rate of IFN signalling inactivation ($K_{IFN\,off}$), the EC50 of IFN ($EC_{50\;IFN}$), the rate of virus-mediated cell death (γ_s), the EC50 of the cytotoxic cytokine ($EC_{50\;C_yt}$), the rate of cytokine-mediated cell death (γ_{C_Cyt}) and the rate viral clearance (K_{VC}).

These equations describe the concentration of virus, IFN and cytotoxic cytokine in the media. These equations are:

$$\frac{dV}{dt} = K_{bud\,IP}\times[IP] + K_{bud\,AP}\times[AP] - K_{VI}\times[V]\times[UP] - \gamma_V\times[V],$$

$$\frac{dIFN_{ext}}{dt} = K_t\times[IFN_{int}] - \gamma_{IFN}\times[IFN_{ext}]$$

$$\frac{dIFN_{int}}{dt} = K_{IFN\,IP}\times[IP] + K_{IFN\,AP}\times[AP] + K_{IFN\,AP}\times[PP] - K_t\times[IFN_{int}] - \gamma_{IFN}\times[IFN_{int}]$$

$$\frac{dCyt}{dt} = K_{Cyt}\times([IP]+[AP]) - \gamma_{Cyt}\times[Cyt]$$

The parameters described in the above equations represent the rate of virus budding from IP and AP ($K_{bud\,IP}$ and $K_{bud\,AP}$, respectively), the infection rate (K_{vi}), the rate of virus degradation (γ_V), the rate of internal IFN production on initial infection ($K_{IFN\,IP}$), the rate of internal IFN production following activation of IFN defenses ($K_{IFN\,AP}$), the rate of IFN transfer to the extracellular compartment (K_t), the rate of IFN degradation (γ_{IFN}), the rate of cytotoxic cytokine production (K_{C_Cyt}) and the rate of cytotoxic cytokine degradation (γ_{Cyt}).

A Monte Carlo simulation was generated by varying the parameters in the above model within a 10-fold range (Supplementary Table 3). These parameters were generated from literature-based evidence as described previously[11]. The difference between tumour and normal cells is assumed to be the values of $K_{bud\,IP}$ and $K_{bud\,AP}$, which are set to be 1- to 100-fold greater in tumour cells. Simulations were performed by integrating the above equations for a population containing 2.5×10^5 cells in 1 ml of media infected at an MOI = 0.001, calculating virus and viability at the 72-h time point for each $EC_{50\;Cyt}$ and K_t combination, and repeating the integration 5,000 times with novel model parameters selected within the 10-fold window. All simulations were performed in Matlab using the ODE solver ode15s under default parameters imposing a none-negativity constraint.

Statistics. Unless otherwise noted (see microarray analysis), analysis of variance was used to determine significance between all treatment conditions (Tukey's *post hoc* test). The log-rank test was used to determine significant differences in plots for survival studies. For all studies, significance was considered to mean a P value below or equal to 0.05. Graphs and Statistics were computed using Prism 5 and Excel.

References

1. Ilkow, C., Swift, S. L., Bell, J. C. & Diallo, J. S. From scourge to cure: tumour-selective viral pathogenesis as a new strategy against cancer. *PLoS Pathog.* **10**, e1003836 (2014).
2. Russell, S. J., Peng, K. W. & Bell, J. C. Oncolytic virotherapy. *Nat. Biotechnol.* **30**, 658–670 (2012).
3. Breitbach, C. J. *et al.* Intravenous delivery of a multi-mechanistic cancer-targeted oncolytic poxvirus in humans. *Nature* **477**, 99–102 (2011).
4. Heo, J. *et al.* Randomized dose-finding clinical trial of oncolytic immunotherapeutic vaccinia JX-594 in liver cancer. *Nat. Med.* **19**, 329–336 (2013).
5. Ottolino-Perry, K., Diallo, J. S., Lichty, B. D., Bell, J. C. & Andrea McCart, J. Intelligent design: combination therapy with oncolytic viruses. *Mol. Ther.* **18**, 251–263 (2009).
6. Stojdl, D. F. *et al.* Exploiting tumor-specific defects in the interferon pathway with a previously unknown oncolytic virus. *Nat. Med.* **6**, 821–825 (2000).
7. Stojdl, D. F. *et al.* VSV strains with defects in their ability to shutdown innate immunity are potent systemic anti-cancer agents. *Cancer Cell* **4**, 263–275 (2003).
8. Obuchi, M., Fernandez, M. & Barber, G. N. Development of recombinant vesicular stomatitis viruses that exploit defects in host defense to augment specific oncolytic activity. *J. Virol.* **77**, 8843–8856 (2003).
9. Faria, P. A. *et al.* VSV disrupts the Rae1/mrnp41 mRNA nuclear export pathway. *Mol. Cell* **17**, 93–102 (2005).
10. Brun, J. *et al.* Oncolytic Vaccinia virus safely and effectively treats skin tumors in mouse models of xeroderma pigmentosum. *Int. J. Cancer.* **132**, 726–731 (2013).
11. Le Boeuf, F. *et al.* Model-based rational design of an oncolytic virus with improved therapeutic potential. *Nat. Commun.* **4**, 1974 (2013).
12. Chang, H. M. *et al.* Induction of interferon-stimulated gene expression and antiviral responses require protein deacetylase activity. *Proc. Natl Acad. Sci. USA* **101**, 9578–9583 (2004).
13. Nguyen, T. L. *et al.* Chemical targeting of the innate antiviral response by histone deacetylase inhibitors renders refractory cancers sensitive to viral oncolysis. *Proc. Natl Acad. Sci. USA* **105**, 14981–14986 (2008).
14. Diallo, J. S. *et al.* A high-throughput pharmacovirial approach identifies novel oncolytic virus sensitizers. *Mol. Ther.* **18**, 1123–1129 (2010).
15. Terkeltaub, R. A. Colchicine update: 2008. *Semin. Arthritis Rheum.* **38**, 411–419 (2009).

16. Bean, J. *et al.* Identification of genetically modified Maraba virus as an oncolytic rhabdovirus. *Mol. Ther.* **18**, 1440–1449 (2010).
17. Martello, L. A. *et al.* Elevated levels of microtubule destabilizing factors in a Taxol-resistant/dependent A549 cell line with an alpha-tubulin mutation. *Cancer Res.* **63**, 1207–1213 (2003).
18. Ruiz Gomez, M. J., Gil, L., Souviron, A. & Martinez Morillo, M. Multidrug resistance increment in a human colon carcinoma cell line by colchicine. *J. Physiol. Biochem.* **56**, 33–38 (2000).
19. Connolly, D. C. *et al.* Female mice chimeric for expression of the simian virus 40 TAg under control of the MISIIR promoter develop epithelial ovarian cancer. *Cancer Res.* **63**, 1389–1397 (2003).
20. Ganson, K., Gamwell, L. F., Pitre, E. M. & Vanderhyden, B. C. Technical challenges and limitations of current mouse models of ovarian cancer. *J. Ovarian Res.* **5**, 39 (2012).
21. Eden, E., Navon, R., Steinfeld, I., Lipson, D. & Yakhini, Z. GOrilla: a tool for discovery and visualization of enriched GO terms in ranked gene lists. *BMC Bioinformatics* **10**, 48 (2009).
22. Eden, E., Lipson, D., Yogev, S. & Yakhini, Z. Discovering motifs in ranked lists of DNA sequences. *PLoS Comput. Biol.* **3**, e39 (2007).
23. Huang da, W., Sherman, B. T. & Lempicki, R. A. Systematic and integrative analysis of large gene lists using DAVID bioinformatics resources. *Nat. Protoc.* **4**, 44–57 (2009).
24. Huang da, W., Sherman, B. T. & Lempicki, R. A. Bioinformatics enrichment tools: paths toward the comprehensive functional analysis of large gene lists. *Nucleic Acids Res.* **37**, 1–13 (2009).
25. Platanias, L. C. Mechanisms of type-I- and type-II-interferon-mediated signalling. *Nat. Rev. Immunol.* **5**, 375–386 (2005).
26. Li, Z., Davis, G. S., Mohr, C., Nain, M. & Gemsa, D. Suppression of LPS-induced tumor necrosis factor-alpha gene expression by microtubule disrupting agents. *Immunobiology* **195**, 640–654 (1996).
27. Lacy, P. E., Howell, S. L., Young, D. A. & Fink, C. J. New hypothesis of insulin secretion. *Nature* **219**, 1177–1179 (1968).
28. Le Marchand, Y. *et al.* A role for the microtubular system in the release of very low density lipoproteins by perfused mouse livers. *J. Biol. Chem.* **248**, 6862–6870 (1973).
29. Zurier, R. B., Hoffstein, S. & Weissmann, G. Mechanisms of lysosomal enzyme release from human leukocytes. I. Effect of cyclic nucleotides and colchicine. *J. Cell Biol.* **58**, 27–41 (1973).
30. Williams, J. A. & Wolff, J. Colchicine-binding protein and the secretion of thyroid hormone. *J. Cell Biol.* **54**, 157–165 (1972).
31. Colina, R. *et al.* Translational control of the innate immune response through IRF-7. *Nature* **452**, 323–328 (2008).
32. Jordan, M. A. & Wilson, L. Microtubules as a target for anticancer drugs. *Nat. Rev. Cancer* **4**, 253–265 (2004).
33. Conrad, D. P. *et al.* Leukemia cell-rhabdovirus vaccine: personalized immunotherapy for acute lymphoblastic leukemia. *Clin. Cancer Res.* **19**, 3832–3843 (2013).
34. Das, S. C., Nayak, D., Zhou, Y. & Pattnaik, A. K. Visualization of intracellular transport of vesicular stomatitis virus nucleocapsids in living cells. *J. Virol.* **80**, 6368–6377 (2006).
35. Smith, G. L., Vanderplasschen, A. & Law, M. The formation and function of extracellular enveloped vaccinia virus. *J. Gen. Virol.* **83**, 2915–2931 (2002).
36. Herrero-Martinez, E., Roberts, K. L., Hollinshead, M. & Smith, G. L. Vaccinia virus intracellular enveloped virions move to the cell periphery on microtubules in the absence of the A36R protein. *J. Gen. Virol.* **86**, 2961–2968 (2005).
37. Passer, B. J. *et al.* Combination of vinblastine and oncolytic herpes simplex virus vector expressing IL-12 therapy increases antitumor and antiangiogenic effects in prostate cancer models. *Cancer Gene. Ther.* **20**, 17–24 (2013).
38. Pestka, S. The interferons: 50 years after their discovery, there is much more to learn. *J. Biol. Chem.* **282**, 20047–20051 (2007).
39. Zhou, B. & Rabinovitch, M. Microtubule involvement in translational regulation of fibronectin expression by light chain 3 of microtubule-associated protein 1 in vascular smooth muscle cells. *Circ. Res.* **83**, 481–489 (1998).
40. Havercroft, J. C., Quinlan, R. A. & Gull, K. Binding of parbendazole to tubulin and its influence on microtubules in tissue-culture cells as revealed by immunofluorescence microscopy. *J. Cell Sci.* **49**, 195–204 (1981).
41. Verma, S. *et al.* Trastuzumab emtansine for HER2-positive advanced breast cancer. *New Engl. J. Med.* **367**, 1783–1791 (2012).
42. Lemay, C. G. *et al.* Harnessing oncolytic virus-mediated antitumor immunity in an infectious cell vaccine. *Mol. Ther.* **20**, 1791–1799 (2012).
43. Diallo, J. S., Vaha-Koskela, M., Le Boeuf, F. & Bell, J. Propagation, purification, and in vivo testing of oncolytic vesicular stomatitis virus strains. *Methods Mol. Biol.* **797**, 127–140 (2012).
44. Le Boeuf, F. *et al.* Synergistic interaction between oncolytic viruses augments tumor killing. *Mol. Ther.* **18**, 888–895 (2010).
45. Ernig, D. *et al.* AltAnalyze and DomainGraph: analyzing and visualizing exon expression data. *Nucleic Acids Res.* **38**, W755–W762 (2010).
46. Vultur, A. *et al.* Cell-to-cell adhesion modulates Stat3 activity in normal and breast carcinoma cells. *Oncogene* **23**, 2600–2616 (2004).
47. Pfaffl, M. W. A new mathematical model for relative quantification in real-time RT-PCR. *Nucleic Acids Res.* **29**, e45 (2001).

Acknowledgements

This project was funded by a Terry Fox Research Institute Grant (grant no. TFF 122868; by J.C.B, J.-S.D., N.S. and T.A.) as well as a The Lotte & John Hecht Memorial Foundation Innovation Grant of the Canadian Cancer Society (grant no. 2012-701460; J.-S.D., J.C.B., M.K. and grant no. 703014 to J.-S.D. and J.C.B.) and a Cancer Research Society grant to B.V. R.A. was supported by a Mitacs Elevate Industrial Fellowship. C.B. was supported by a Natural Sciences and Engineering Research Council of Canada (NSERC) studentship. N.D. was supported by a Vanier Scholarship. V.G. is supported by an Ontario Graduate Scholarships in Science and Technology Queen Elizabeth II studentship as well as a Canadian Institutes for Health Research Frederick Banting Master's Award. J.C.B. is supported by the Ontario Institute for Cancer Research. We thank Dr Susan B. Horwitz for kindly providing the A549-AT12 and AT24 cell lines.

Author contributions

J.-S.D. and J.C.B. initiated the project. J.C.B. organized initial financial support followed by J.-S.D. who continued and led the study throughout. Additional financial support was organized by N.S. and T.A. *In vitro* experiments were performed mostly by R.A., as well as J.-S.D., C.B., O.V., C.Z., V.G., N.E.F, C.D., R.Kr., R.Ka., J.C., A.B., K.W., E.W., J.H. and C.I. *In vivo* performed experiments were performed by A.C., F.L.B., A.S., T.F, K.G., J.-S.D. C.B., F.L.B, J.-S.D., J.C.B. and M.K. were involved in developing the mathematical model, and C.B. performed the simulations. C.B. also performed the microarray analysis. The manuscript was written mostly by J.-S.D. and R.A. and editorially reviewed by N.E.F., C.B., F.L.B., D.P.C., K.G., B.V., M.K. and J.C.B. K.G. and B.V. contributed support for the tgMISIIR-Tag model. N.S., D.P.C. and H.A. contributed to experimental design through regular discussions.

Additional information

Accession codes: Microarray data have been deposited in the ArrayExpress database under the accession code E-MTAB-2433

Supplementary Information accompanies this paper at http://www.nature.com/naturecommunications.

Competing financial interests: The authors declare no competing financial interests.

Reprints and permission information is available online at http://npg.nature.com/reprintsandpermissions.

How to cite this article: Arulanandam, R. *et al.* Microtubule disruption synergizes with oncolytic virotherapy by inhibiting interferon translation and potentiating bystander killing. *Nat. Commun.* 6:6410 doi: 10.1038/ncomms7410 (2015).

Appendix H: Additional publications

1. Selman M, Rousso C, Bergeron A, Son HH, **Krishnan R**, El Sayes NA, Varette O, Chen A, Tzelepis F, Bell, JC, Crans D, Diallo JS. “Multi-modal potentiation of oncolytic virotherapy by vanadium compounds.” *Molecular Therapy*. 26(1):56-69 (2018). doi: 10.1016/j.ymthe.2017.10.014.

2. Selman M, Ou P, Rousso C, Bergeron A, **Krishnan R**, Pikor L, Chen A, Keller BA, Ilkow C, Bell JC, Diallo JS. “Dimethyl Fumarate Potentiates Oncolytic Virotherapy through NF-κB inhibition.” *Science Translational Medicine*. 10(425). pii: eaao1613 (2018). doi: 10.1126/scitranslmed.aao1613.

Curriculum Vitae

Ramya Krishnan, RPh BScPhm

POST-SECONDARY EDUCATION

January 2012- present: PhD candidate, Department of Biochemistry, Microbiology and Immunology, Faculty of Medicine, University of Ottawa (transfer from MSc to PhD program in May, 2013)

July 2007- June 2011: Completed B.Sc. Pharmacy program with first class honors, Leslie Dan Faculty of Pharmacy at the University of Toronto.

RESEARCH EXPERIENCE

2012-present: PhD Candidate in Dr. Jean-Simon Diallo's research group, Ottawa Hospital Research Institute (University of Ottawa)

Description of project: Enhancement of oncolytic viral therapy by novel small molecule viral sensitizers

Techniques: tissue culture, virus propagation, high-throughput screening, treatment of *in vivo* murine tumour models, flow cytometry, immunohistochemistry

2010: Completed 4th year research project in Dr. Carloyn L. Cummins' lab (Leslie Dan Faculty of Pharmacy, University of Toronto).

Description of project: Fluorescence-activated cell sorting (FACS) for bone marrow and peripheral blood endothelial progenitor cells in different models of liver X receptor expression.

Techniques:

- Isolation of endothelial progenitor cells (EPCs) from murine bone marrow and peripheral blood, and analysis of data acquired by flow cytometry

2010: Employed at Sunnybrook Health Sciences Centre as a pharmacy summer research student.

Description of project: clinical; consisting of retrospective chart reviews for patients with acute coronary syndromes.

Techniques:

- Database design and application using Microsoft Access 2003

Worked for three summers (2006 -2008, total of 9 months) as a summer research student in Dr. John Bell's lab in the Ottawa Regional Cancer Centre (Ottawa Hospital).

Description: Assisting post-doctoral fellows and graduate students with their projects involving oncolytic viruses (vesicular stomatitis virus and vaccinia virus derivatives).

PUBLICATIONS

1. Forbes NE, **Krishnan R**, Diallo JS. "Pharmacological modulation of anti-tumor immunity induced by oncolytic viruses." *Frontiers in Oncology* 4, 191 (2014). doi: 10.3389/fonc.2014.00191.

2. Garcia V, **Krishnan R**, Davis C, Batenchuk C, Le Boeuf F, Abdelbary H, Diallo JS. "High-Throughput Titration of Vesicular Stomatitis Virus Using a Luciferase Reporter Assay." *Journal of Visualized Experiments*. 91, e51890 (2014). doi:10.3791/51890.

3. Arulanandam R, Batenchuk C, Varette O, Zakaria C, Garcia V, Forbes NE, Davis C, **Krishnan R**, Karmacharya R, Cox J, Sinha A, Babawy A, Waite K, Weinstein E, Falls T, Chen A, Hamill J, De Silva N, Conrad DP, Atkins H, Garson K, Ilkow C, Kaern M, Vanderhyden V, Sonenberg N, Alain T, Le Boeuf F, Bell JC, Diallo JS. "Microtubule disruption synergizes with oncolytic virotherapy by inhibiting interferon translation and potentiating bystander killing." *Nature Communications*. 6:6410 (2015). doi: 10.1038/ncomms7410.

4. Dornan MH[1], **Krishnan R[1]**, Macklin AM[1], Selman M, El Sayes N, Son HH, Davis C, Chen A, Keillor K, Le PJ, Moi C, Ou P, Pardin C, Canez CR, Le Boeuf F, Bell JC, Smith JC, Diallo JS, Boddy CN. "First-in-class small molecule potentiators of cancer virotherapy." *Scientific Reports*. 26;6:26786 (2016). doi: 10.1038/srep26786.

   [1]Equal contribution

5. Selman M, Rousso C, Bergeron A, Son HH, **Krishnan R**, El Sayes NA, Varette O, Chen A, Tzelepis F, Bell, JC, Crans D, Diallo JS. "Multi-modal potentiation of oncolytic virotherapy by vanadium compounds." *Molecular Therapy*. 26(1):56-69 (2018). doi: 10.1016/j.ymthe.2017.10.014.

6. Selman M, Ou P, Rousso C, Bergeron A, **Krishnan R**, Pikor L, Chen A, Keller BA, Ilkow C, Bell JC, Diallo JS. "Dimethyl Fumarate Potentiates Oncolytic Virotherapy through NF-κB inhibition." *Science Translational Medicine*. 10(425). pii: eaao1613 (2018). doi: 10.1126/scitranslmed.aao1613.

In preparation:

7. **Krishnan R**[1], El Sayes N[1], Phan M, Mathieu J, Macklin A, Groom H, Arulanandam R, Patten D, Selman M, Lai, F, Lichty B, Harper, ME, Josephy D P, Bell JC, Smith JC, Boddy CN, Diallo JS. "Viral sensitizers suppress innate immunity to sensitize cancer cells to oncolytic virotherapy."

[1]Equal contribution

PATENTS

1. Title: Compositions and methods for enhancing oncolytic virus efficacy
   Inventors: Jean-Simon Diallo, Christopher Noyce Boddy, Mark Dornan, Ramya Krishnan, Rozanne Arulanandam, Fabrice Le Boeuf, Jeffrey Smith, Andrew Macklin
   Publication Date: August 4, 2016
   Patent offices: CA
   Patent number: CA2970954 A1

   Publication Date: September 1, 2016
   Patent offices: WO
   Patent number: WO2016119052 A8

AWARDS, SCHOLARSHIPS AND ACHIEVEMENTS

2016-2017	Ontario Graduate Scholarship
2015-2017	Excellence Scholarship from the University of Ottawa
2016	Travel award from BioCanRx for Summit for Cancer Immunotherapy, June 26-29, 2016
2016	Travel award from Terry Fox Research Institute for 7th Annual Scientific Meeting; May 11-13, 2016
2015	3rd place for seminar presented at Biochemistry, Microbiology and Immunology Seminar Day 2015
2015	Ontario Graduate Scholarship
2012-2015	Admission Scholarship from the University of Ottawa
2013	2nd place for seminar presented at Biochemistry, Microbiology and Immunology Seminar Day 2013
2007-2011	First Class honours during all four years of study, Leslie Dan Faculty of Pharmacy, University of Toronto
2010	Horace David McCord Memorial Scholarship, Leslie Dan Faculty of Pharmacy

PRESENTATIONS

Year	Venue; Date	Type	Title
2017	Summit for Cancer Immunotherapy 2017; June 25-28, 2017	Poster	First-in-class small molecule potentiators of cancer virotherapy
	Biochemistry, Microbiology and Immunology Seminar Day, University of Ottawa; March 8, 2017	Oral	First-in-class small molecule potentiators of cancer virotherapy
2016	Ottawa Hospital Research Institute Research Day 2015; November 10, 2014 (abstract accepted)	Poster	First-in-class small molecule potentiators of cancer virotherapy
	10th International Conference on Oncolytic Virus Therapeutics; October 1-4, 2016	Poster	First-in-class small molecule potentiators of cancer virotherapy
	Summit for Cancer Immunotherapy; June 26-29, 2016	Oral	First-in-class small molecule potentiators of cancer virotherapy
	Terry Fox Research Institute- 7th Annual Scientific Meeting; May 11-13, 2016	Poster + Oral	First-in-class small molecule potentiators of cancer virotherapy
2015	Ottawa Hospital Research Institute Research Day 2015; November 18, 2015	Poster	First-in-class small molecule potentiators of cancer virotherapy
	AAPS (American Association of Pharmaceutical Scientists) Annual Meeting and Exposition, October 2015.	Poster	First-in-class small molecule potentiators of cancer virotherapy
	9th International Conference on Oncolytic Virus Therapeutics	Poster	First-in-class small molecule potentiators of cancer virotherapy
	Biochemistry, Microbiology and Immunology Seminar Day, University of Ottawa; March 10, 2015	Oral	Development of a novel class of small molecules used to potentiate tumour-specific, Oncolytic Virus infection
2014	Ottawa Hospital Research Institute Research Day 2014; November 13, 2014	Oral	Development of a novel class of small molecules used to potentiate tumour-specific, Oncolytic Virus infection
	Biochemistry, Microbiology and Immunology Poster Day, University of Ottawa; May 15, 2014	Poster	Enhancement of Oncolytic Viral Efficacy by Novel Drug Candidates
2013	Ottawa Hospital Research Institute Research Day 2013; November 14, 2013	Poster	Novel VSe1 Derivatives for Improved Oncolytic Virotherapy and Drug Target Identification

	2013 Canadian Cancer Research Conference; November 3-6, 2013	Poster	Novel VSe1 Derivatives for Improved Oncolytic Virotherapy and Drug Target Identification
	7th International Meeting on Replicating Oncolytic Virus Therapeutics; June 15-18, 2013	Poster	Novel VSe1 Derivatives for Improved Oncolytic Virotherapy and Drug Target Identification
	Terry Fox Research Institute- 4th Annual Scientific Meeting; May 9-11, 2013	Poster	Enhancement of Oncolytic Viral Efficacy by Novel Drug Candidates
	Biochemistry, Microbiology and Immunology Seminar Day, University of Ottawa; March 11, 2013	Oral	Novel VSe1 Derivatives for Improved Oncolytic Viral Therapy and Identification of Drug Targets
2012	Ottawa Hospital Research Institute Research Day; November 15, 2012	Poster	Enhancement of Oncolytic Viral Efficacy by Novel Drug Candidates
	Biochemistry, Microbiology and Immunology Poster Day, University of Ottawa; May 17, 2012	Poster	Enhancement of Oncolytic Viral Efficacy by Novel Drug Candidates

OTHER VOLUNTEER AND WORK ACTIVITIES

- Supervised and mentored undergraduate (co-op and Honour's) students in the lab (2014 – present)
- Volunteer with Let's Talk Science, University of Ottawa chapter (2016-2017)
- Volunteer at Research in Science Exhibition (RISE), at the University of Ottawa, Oct 22, 2016
    - Represented the Ottawa Hospital Research Institute (OHRI) at information booth, answered questions from high-school and undergraduate students about the research at the OHRI
- Volunteer for Terry Fox Run – organizing fundraisers for Canadian Oncolytic Virus Consortium Team in Ottawa, (2013 – present)

CERTIFICATIONS

- Trained in Standard First Aid & Adult/Child/Infant CPR, level C
- Animal Care Training
- Radiation Training
- WHMIS

LANGUAGE SKILLS

Proficient in reading, writing and speaking English